AGGREGATION AND DISAGGREGATION OF SOIL MOISTURE MEASUREMENTS

by

HERBERT MANJULASISI HEMAKUMARA

BSc Agric (Hons)
PgDip (Computer Tech)
MSc (Agric Eng)

A thesis submitted as partial requirement for the

Degree of Doctor of Philosophy

in the field of Environmental Engineering, to the

Faculty of Engineering and Built Environment,

The University of Newcastle, New South Wales, Australia.

March 2007

I hereby certify that the work embodied in this thesis is the result of original research and has not been submitted for a higher degree to any other University or Institution.

H. M. Hemakumara

This thesis is dedicated
to

My father
late Mr. T. S. Hemakumara
and my mother
Mrs. K. M. C. Fernando

ACKNOWLEDGEMENTS

The time has come to gratefully acknowledge all those who have provided me with support and encouragement in the preparation of this thesis.

My dissertation committee deserves a special thanks for their guidance in this research endeavour. Firstly, I wish to sincerely thank my principal supervisor, Professor Jetse Kalma. I appreciate his patient, inspiring suggestions, and deep knowledge. Without his guidance, patience and professional input I would not be at this most memorable and happy occasion, of submitting my PhD. I equally thank my co-supervisors, Associate Professor Jeffrey Walker and Professor Garry Willgoose, for their support and encouragement of excellence in all phases of my research.

I would also like to thank all those who have contributed time and effort to make this research effort a reality. Special recognition is given to Barry Jacobs, Riki Davidson and Christoph Rüdiger for their assistance, humour, and friendships and Greg Hancock for helping in the Stanley topographic survey. Thanks are also due to the many people who helped during the three field campaigns at the Goulburn River catchment.

I wish to thanks all nineteen property owners of our monitoring sites for allowing the use of their property for this experiment. A very special thanks is given to Robert & Maree Goodear at Illogan and to Doc & Fiona Strahan at Stanley, for allowing the use of their houses during data downloading trips and also for their wonderful support.

Also I extended my sincere thanks to Ian Jeans, Roger Reece, Laurie Walker, Shaun Manning, Josh Kautto, Cristina Martinez, Patricia Saco, Cherie Pilgrim, Katherine Harrison and Anne Ramsey for their various supports.

I wish to extend a special thanks to Frank Rijsberman, Director General, International Water Management Institute, Colombo, Sri Lanka for his support and encouragement.

Finally, I would especially like to thank my wife Ama, son Prasad and daughter Mindya for their unwavering support and encouragement. Without their constant encouragement and faith in me, I could have never finished this thesis.

The research described in this thesis was supported by the International Postgraduate Research Scholarship, University of Newcastle Research Scholarship, and Australian Research Council Discovery Project Grant DP0209724. This support is gratefully acknowledged.

Table of contents

Chapter Three

Chapter Four

Chapter Five

Chapter Six

Chapter Seven

Chapter Eight

Chapter Nine

SYNOPSIS

Point-scale and remotely sensed large-scale soil moisture measurements do not provide data at the scale required for most environmental applications. Techniques are therefore needed for predicting soil moisture distributions from point-scale measurements and disaggregating large-area measurements.

This thesis discusses methodologies for soil moisture scaling in open non-forested area. These include: bucket-type water balance modelling, identification of representative monitoring sites, wetness characterization with a new topographic wetness index, and the use of wetness indices computed from land surface temperature and vegetation indices

A bucket-type water balance model was used to predict soil moisture with intermittent measurements. These models have limited usefulness for hillslope-scale although direct insertion of measurements into the model can reduce some prediction errors.

Temporal stability analysis of a network of measuring stations demonstrated that locations can be identified that are representative of the mean moisture content. It was found that 12-15 months are required to identify representative sites. Sandy soils are associated with higher temporal stability and clayey soil show less temporal stability.

A Soil-adjusted Topographic Wetness Index (STWI) was developed from limited soil moisture measurements to derive hillslope scale soil moisture distributions from topographic position and soil properties.

Point-scale measurements and remotely sensed land surface temperature (LST) and vegetation index (VI) data were used in developing methods for generating soil moisture patterns. The first approach used relationships between land surface temperature and soil moisture content. The second approach investigated the relationship between a Regionally Normalised Temperature Index (RNTI) and a Normalised Water Deficit Index (NWDI). The third, and most promising, approach used LST and VI values to develop a Vegetation-Temperature Condition Index (VTCI) to characterise the surface wetness conditions.

Large-scale AMSR-E soil moisture measurements were evaluated with two approaches. The first approach was based on many point scale soil moisture measurements collected during three intensive field campaigns. The second approach examined the temporal evolution of AMSR-E measurements against pixel-scale root-zone soil moisture measurements. Both approaches indicated that AMSR-E data can satisfactorily mimic ground-based soil moisture content.

Finally, a new methodology has been presented for disaggregating large-scale AMSR-E soil moisture values into fields with 1.1km pixels. This method used the VTCI index to describe actual soil moisture variations within AMSR-E pixels.

List of Acronyms and Abbreviations

ADEOS	Advanced Earth Observing Satellite II
AMI	Active Microwave Instrument
AMSR-E	Advanced Microwave Scanning Radiometer-Earth observing system
ASAR	Advanced Synthetic Aperture Radar
ASTER	Advanced Spaceborne Thermal Emission and Reflection radiometer
AVHRR	Advanced Very High Resolution Radiometer
AWC	Available water content
BoM	Bureau of Meteorology
CASMM	Catchment Average Soil Moisture Measurement
CSI	Campbell Scientific Inc.
CWSI	Crop Water Stress Index
DD	Deep Drainage
DIPNR	Department of Infrastructure, Planning and Natural Resources
DLWC	Department of Land and Water Conservation
EASE-Grid	Equal-Area Scalable Earth Grid
ERS	European Remote sensing Satellites
ET	Evapotranspiration
ET_a	Actual evapotranspiration
ET_o	Potential evapotranspiration
EVI	Enhanced Vegetation Index
FC	Field Capacity
FDR	Frequency domain reflectometry
GRC	Goulburn River Catchment
HDF	Hierarchical Data Format
IDW	Inverse Distance Weighting
IFOV	Instantaneous Field Of View
IR	Infra Red
LST	Land Surface Temperature
mrd	mean relative difference

MODIS	MODerate resolution Imaging Spectroradiometer
MPDI	Microwave Polarization Difference Index
MSAVI	Modified Soil Adjusted Vegetation Index
NASDA	National Space Development Agency of Japan
NASA	National Aeronautics and Space Administration
NCDC	National Climate Data Center
NDVI	Normalized Difference Vegetation Index
NIR	Near Infra Red
NOAA	National Oceanic and Atmospheric Administration
NSIDC	National Snow and Ice Data Center
NWDI	Normalized Water Deficit Index
PD	Polarization Difference
PWP	Permanent Wilting Point
REA	Representative Elementary Area
RF	Radio Frequency
rms	root mean square
RNTI	Regionally Normalized Temperature Index
RVI	Ratio Vegetation Index
SAR	Synthetic Aperture Radar
SASMAS	Scaling and Assimilation of Soil Moisture And Streamflow
SAVI	Soil Adjusted Vegetation Index
SD	Standard Deviation
SMMR	Scanning Multichannel Microwave Radiometer
SMOS	Soil Moisture and Ocean Salinity Mission
SRO	Surface Runoff
SSE	Sum of Squared Error
SSRO	Subsurface Runoff
SSM/I	Special Sensor Microwave Imager
STWI	Soil-adjusted Topographic Wetness Index
SWC	Soil Water Content
SWP	Soil Water Potential
TDR	Time Domain Reflectometry
TM	Thematic Mapper

TMI	TRMM Microwave Imager
TRMM	Tropical Rainfall Measuring Mission
TVDI	Temperature Vegetation Dryness Index
TVX	Temperature Vegetation index
TWI	Topographic Wetness Index
VI	Vegetation Indices
VP	Vapour Pressure
VPD	Vapour Pressure Deficit
VTCI	Vegetation Temperature Condition Index
VWC	Vegetation Water Content
WCR	Water Content Reflectometer
WDI	Water Deficit Index
WI	Wetness Index

List of Symbols

A	-	empirical constant
a	-	constant parameter in CS616 calibration
a	-	parameter defining the dry edge ($T_{Smax} = a + b$NDVI)
B	-	empirical constant
B_I	Wm^{-2} Hz^{-1} $steradian^{-1}$	Blackbody radiation
B		Plank function
b	-	coefficient in CS616 calibration
b		vegetation parameter
b		parameter defining the dry edge ($T_{Smax} = a + b$NDVI)
c	-	coefficient in CS616 calibration
c	$cm.nsec^{-1}$	speed of light
c		specific heat capacity
c_p	J kg^{-1} $^oC^{-1}$	heat capacity of air
C_1	-	correction coefficient for atmospheric resistance in red channel
C_2	-	correction coefficient for atmospheric resistance in blue channel
C_v	$J^oC^{-1}m^{-3}$	volumetric heat capacity of air
dT	K	measured difference between crop canopy and air temperature
dT_l	K	lower limit of canopy temperature - air temperature
dT_u	K	upper limit of canopy temperature - air temperature
EC	dS m^{-1}	electrical conductivity
ET	mm	evapotranspiration
ET_{a_DAY}	mm	daily actual evapotranspiration
$e_{r(l)}$		rough surface emissivity
e_s		smooth surface emissivity
f	Hz	frequency
G	Wm^{-2}	soil heat flux density
G		gain factor
g		combined vegetation-roughness
H	Wm^{-2}	sensible heat flux
h	-	horizontal polarization
h		empirical roughness parameter
I	cal cm^{-2} $^oC^{-1}$ $s^{-1/2}$	thermal inertia
I		Infrared spectral radiance
I_a		thermal path radiance
I_d		solar radiance at the top of atmosphere
I_r		solar diffuse radiation and atmospheric thermal radiation reflected by the surface

I_s		radiance resulting from scattering of solar radiation
K↑		up-welling solar (short-wave) radiation
K↓		down-welling solar (short-wave) radiation
K_a		apparent dielectric constant
k		thermal diffusivity
k_λ	-	absorption coefficient
L	-	canopy background brightness correction factor
L	cm	length of the waveguides
l	m	optical path-length
LST_i	K	measured temperature in pixel i
LST_{max}	K	maximum LST over given region
LST_{min}	K	minimum LST over given region
$LST_{NDVI\,i}$	K	LST of the pixel whose NDVI value is $NDVI_i$
$LST_{NDVI\,i\,max}$	-	maximum LST of the pixel $NDVI_i$
$LST_{NDVI\,i\,min}$	-	minimum LST of the pixel $NDVI_i$
n	-	total number of days
n	-	total number of pixels
P	mm	rainfall
Q	mm	outflow
Q^*	Wm^{-2}	net all-wave radiation flux
R		surface roughness term
R	μsec	CS616 period
R_n	Wm^{-2}	net radiation heat flux density
R_{ij}	-	rank of the soil moisture S_{ij} at location i on day j
$R_{ij'}$	-	rank of the location i for day j'
R_{nDAY}	Wm^{-2}	daily net radiation
$RNTI_i$	–	RNTI for high-resolution pixel i
r_a	$s\,m^{-1}$	aerodynamic resistance
r_c	$s\,m^{-1}$	canopy resistance to vapour transport
S_{ij}		i^{th} sample of n samples at the j^{th} site
$\overline{S}_{i,*}$		computed average among all sites for a given date and time, i
T	C, K	physical (thermodynamic) temperature
T_{11}	K	brightness temperatures at 10.8 μm band
T_{12}	K	brightness temperatures at 12 μm band
T_{15}	C	soil temperature at 15cm depth
T_{45}	C	soil temperature at 45cm depth
T_{75}	C	soil temperature at 75cm depth
T_S	C, K	land surface temperature
T_{Smin}	C, K	minimum LST in the triangle

T_o	C, K	Soil temperature
T_a	C, K	Air temperature
T_B	K	surface temperature
T_{Bv}		microwave brightness temperature – vertically polarized
T_{Bh}		microwave brightness temperature – horizontally polarized
$T_{b(p)}$	K	microwave brightness temperature at 'p' polarization
T_c	C, K	crop foliage temperature
T_p	K	plant surface temperature
t	nanoseconds	transit time
u	degrees	incidence angle of the observation
$VP_{sat}(T_a)$	pascal	saturation vapour pressure at air temperature
$VTCI_i$	–	VTCI for high-resolution pixel *i*
v	-	vertical polarization
υ		transmissivity
υ_0		transmittance near the Earth's surface
W_c	$cm^3\ cm^{-3}$	vegetation water content
WC_{vol}	$cm^3\ cm^{-3}$	volumetric water content
α	m	up slope area per unit contour length
α		soil moisture sensitivity term in $\sigma^o = \alpha\theta_v + \beta$
α		coefficient used in vegetation roughness estimate
β		local slope of the ground surface
β		constant parameter in $\sigma^o = \alpha\theta_v + \beta$
Γ		reflectivity of the surface
$\Gamma(l)$		transmissivity of the canopy at *l* (vertical or horizontal polarization)
γ	Pa $^oC^{-1}$	psychometric constant
Δ	Pa $^oC^{-1}$	slope of the saturated vapour pressure-temperature relation
$\bar{\delta}_{*,j}$		mean relative difference at the j^{th} site
ε	farad m^{-1}	complex dielectric constant, $\varepsilon = \varepsilon' + i\,\varepsilon''$
ε'	farad m^{-1}	real part of dielectric constant ε
ε''	farad m^{-1}	imaginary part of dielectric constant ε
ε		surface spectral emissivity
ε_o		spectral emissivity near the Earth's surface
ε_{11}		emissivities in the 10.8 µm bands
ε_{12}		emissivities in the 12 µm bands
ε_r	farad m^{-1}	relative dielectric constant, $\varepsilon_r = \varepsilon_r' + i\,\varepsilon_r''$
ε_r'	farad m^{-1}	real part of relative dielectric constant
ε_r''	farad m^{-1}	imaginary part of relative dielectric constant

$\mathrm{\theta}$	$cm^3\ cm^{-3}$	measured water content
θ	degrees	incidence angle of the sensor
$\mathrm{\theta}^*$	-	normalized water content
$\mathrm{\theta}^*$		baseline value of $\mathrm{\theta}$
θ^*	$cm^3\ cm^{-3}$	soil water storage capacity
$\mathrm{\theta}_{0\text{-}1}$	$cm^3\ cm^{-3}$	0-1 cm soil water content
$\theta_{AMSR\text{-}Ej}$	$cm^3\ cm^{-3}$	soil water content in the j^{th} AMSR-E pixel
θ_{max}	$cm^3\ cm^{-3}$	maximum soil water content
θ_{min}	$cm^3\ cm^{-3}$	residual soil water content
θ_{RNTIi}	$cm^3\ cm^{-3}$	soil moisture content computed for a given high-resolution pixel of RNTI
θ_v	$cm^3\ cm^{-3}$	volumetric soil water content
θ_{VTCIi}	$cm^3\ cm^{-3}$	soil moisture content computed from a given high-resolution pixel of VTCI
λ	*µm, mm,* cm, m	wavelength
λE	Wm^{-2}	latent heat flux
μ	Hz	frequency
ξ		microwave polarization ratio
ξ^*		baseline value of ξ
$\xi_{10.7}$		microwave polarization ratio at 10.7 GHz channel
$\xi_{18.7}$		microwave polarization ratio at 18.7 GHz channel
ρ	$kg\ m^{-3}$	density of air
ρ_{Blue}		blue reflectance
ρ_b	$g\ cm^{-3}$	soil bulk density
ρ_s	$g\ cm^{-3}$	soil particle density
ρ_{NIR}		NIR reflectance
ρ_{Red}		red reflectance
σ^o	dB	backscatter coefficient or radar cross section
τ		opacity
φ	$v\ v^{-1}$	porosity
ω		single scattering albedo

List of Figures

Chapter – 2

Chapter - 3

Chapter - 4

Chapter - 5

Chapter - 6

Chapter - 7

Chapter - 8

List of Tables

Chapter - 2

Chapter - 3

Chapter - 4

Chapter - 6

Chapter - 7

Chapter - 8

CHAPTER ONE

1. INTRODUCTION

This thesis studies the development and field application of soil moisture scaling techniques. The thesis develops methodologies for: (a) upscaling point-scale soil moisture measurements to 1.1 km scale and (b) downscaling of low resolution passive microwave soil moisture observations to 1.1 km scale, for deriving spatial patterns. This chapter presents an introduction to the soil moisture scaling and the development of the thesis. The importance of having soil moisture information at different scales is outlined and some recent efforts to confront the problems of scale issues in soil moisture for hydrological applications are discussed. Next, the framework within which this research is undertaken is developed, with a summary of the research motivations and objectives. Lastly, the structural organisation of this thesis is detailed with a brief description of each Chapter.

1.1 RATIONALE

The primary objective of the present study is to develop methodologies for using the measured soil moisture data at various scales for the prediction of moisture contents at other scales by adopting appropriate scaling techniques. Two extremes of soil moisture measurements are considered viz. small scale or point-scale *in-situ* measurements and remotely sensed soil moisture measurements of the Advanced Microwave Scanning Radiometer for EOS (AMSR-E) at the 25km scale. One important question is how to relate these two extreme moisture content measurements in a meaningful way, i.e. how to scale up the point-scale measurements and how to disaggregate the large-area measurements. It is anticipated that these methodologies should be general, in such a way that they do not require a substantial number of point scale measurements or land surface biophysical properties for calibration purposes, and that they can be used with remotely sensed land surface observations such as the land surface (skin) temperature.

The transfer of information across scales is known as scaling. Upscaling (or aggregation) involves using small scale (or point) measurements and estimating spatial averages at a larger scale. Downscaling (or disaggregation) involves estimating small scale (or point) values from larger scale average measurements. Interpolation describes the process of taking spatially distributed point (or small-scale) measurements and determining how soil moisture status varies between those points. In order to transfer information accurately, it is important to understand the functional dependence of fine scale processes and their non-linear spatial and temporal variation with respect to functional changes. Soil moisture scaling deals with the transformation of measured or estimated soil moisture information because, often soil moisture information required for hydrological models is different from the measured or estimated scales. Essentially, scaling consists of measuring and comparing objects in some meaningful way. Therefore, clear understanding of fundamental scaling principles is very important in any study that uses theory or models developed at one particular scale to assess conditions or processes at other scales. This is particularly important for hydrological studies. The procedures used to measure spatial and temporal variability of environmental parameters such as soil moisture, rainfall, evaporation or other model input parameters may not necessarily be appropriate or optimal for the scale of model used. As such, in order to have better model outputs, it may require changing the scale of original data or scaling the inputs suitable for match with the modelling scale, for example to match with the 1.1 km scale of some satellite radiometers. Often this is complex and the use of simple averages does not necessarily give better results. For example, due to the highly variable nature of soil moisture and the technical difficulty of measuring soil moisture, point-scale soil moisture measurements are often the only available soil moisture inputs. Therefore, depending on the complexity or the scale of the model, these available soil moisture fields need to be scaled up or scaled down. Thus clear understanding of fundamental scaling principles as well as technically sound scaling methods are needed.

The definition of scaling is complex. Singh (1995) defines spatial scale as the size of a grid cell or subcatchment area within which the hydrologic response can be treated as homogeneous. If the selected scale is too small, it is dominated by local physical features. On the other hand, if it is too large, it ignores significant hydrologic heterogeneity caused by spatial variability. This definition however, is incomplete and focuses only at the model application level. Because of the complexity of providing a proper definition of scaling, Blöschl and Sivapalan (1995) have proposed a conceptual framework to define the scale and the required transformation of information in modelling real environmental processes. According to Blöschl and Sivapalan (1995), the term scale refers to a characteristic time or length of a process, observation, or model. This definition is better than the previous definition by Singh (1995) since it includes both spatial and temporal aspects of processes, data or measurements and model outputs. Therefore, it helps to analyse and understand the scale issues in a more holistic manner.

Scale can be used either as a qualitative term (e.g. a small-scale or large-scale process) or as quantitative measure in space dimensions. The spatial dimension, represented as co-ordinates in x, y, z directions, varies temporally along a time domain. Thus, scaling is a change in either spatial or temporal scale and has a certain direction and magnitude. The direction of scale change is described as up-scaling and down-scaling. To change the scale from one level to another, it requires methods such as interpolation and extrapolation or aggregation and disaggregation. Aggregation may be viewed as weighted summation of sub-grid processes. Determination of the weighting function is the most important feature in aggregation. Whether this is to be done by lumping many small-scale features into a much smaller number of categories, or whether some statistical technique should be used is an unresolved question. Disaggregation of large scale data down to the regional or plot scale would require histories of each parameter for each region or plot. These methods may be based entirely on simple statistical techniques, geo-statistical techniques, process-based techniques or a combination of these techniques. Selection of an appropriate method however, is very difficult due to the complex nature of soil moisture distribution patterns.

Soil moisture is correlated in space and time due to a variety of processes. A clear understanding of soil moisture correlations for a range of scales is difficult mainly due to lack of data and the technological limitations of collecting soil moisture at variable scales. Spatial and temporal variability of soil moisture is ubiquitous (Western *et al*., 2002). As many soil moisture–dependent processes are nonlinear, this variability leads to significant scale effects. The current knowledge of soil moisture scaling is mostly limited to small catchments (<200 ha) and there is a gap in understanding for intermediate scales due to a lack of data (Western *et al*., 2002). Therefore, more studies are needed in large catchments to better understand soil moisture scaling behaviour.

1.2 IMPORTANCE OF SOIL MOISTURE AND SCALING

Soil moisture is one of the most important environmental variables in land surface climatology, hydrology, and ecology. Although soil moisture represents a small proportion (only 0.15%) of the liquid freshwater on Earth (Dingman, 1994), it is an important sink in the hydrologic cycle. It plays a significant role in temporally and spatially distributed environmental processes such as surface and subsurface runoff, evapotranspiration, infiltration capacity and climate among others. For example, soil water exerts a strong control on the rates of evaporation and transpiration, resulting in a major impact on the partitioning of incoming solar radiation which, in turn, provides an important feedback between the land surface and the atmosphere (Avissar, 1995). Hence, it influences climate and weather (Entekhabi, 1995). Also, it is important in determining the rainfall-runoff response of catchments, particularly where saturation excess runoff processes are dominant (Dunne *et al*., 1975). Further, soil moisture is important for maintaining crop and vegetation health and hence ecological patterns (Rodriguez-Iturbe, 2000) and agricultural production. Therefore its monitoring on a routine basis would allow precise irrigation planning and mapping of drought severity. Many other benefits are associated with the proper knowledge of soil moisture and these include;

- Better estimates of evapotranspiration from vegetated surfaces (Entekhabi *et al*., 1993; Grayson *et al*., 1997)
- Determining the energy balance at the soil surface (Grayson *et al*., 1997; Schmugge, 1998)
- Improved weather predictions (Engman, 1992; Su *et al.*, 1995)
- Improved flood forecasting (Entekhabi *et al*., 1993; Su *et al.*, 1995)
- Saving on irrigation water (Jackson, T. J. *et al.*, 1981b; Jackson, R. D. *et al.*, 1988).
- Co-determine plant biomass responses to CO2 enrichment (Acock and Allen, 1985; Gifford, 1992; Field *et al*., 1995)
- Increased crop yields through maintaining optimum moisture levels (Jackson, T. J. *et al.*, 1981b)
- Early drought prediction (Engman, 1990; Wang *et al*., 2001; Sandholt *et al*., 2002)
- Improved bushfire warning systems (McVicar *et al*., 2002; Sandholt *et al.*, 2002)
- Improved erosion prediction (Walker, 1999; Moore *et al.*, 1988 as cited by Western *et al*., 1998a)

Therefore, information of surface and sub-surface soil moisture over a range of time and space scales is obviously of benefit for hydrology, meteorology and agronomy related studies. Furthermore, moisture content in the soil is one of the few directly observable variables in the hydrological cycle. However, such soil moisture information is usually not available at the appropriate time-space scales.

1.3 SOIL MOISTURE VARIABILITY

Soils in their natural state exhibit considerable spatial and temporal variability of moisture content due to heterogeneity of soil properties, topography, land cover, evapotranspiration, precipitation, etc. This variability is more dominant in the surface layers than in the subsurface layers. Furthermore, it is due to inherent physical properties and is the effect of many processes acting on a range of scales. Among the inherent physical properties, factors such as soil type, soil depth, topography and vegetation play an important role in soil moisture distribution (Qiu *et al.*, 2001). Soil heterogeneity affects the distribution of soil moisture through variation in texture, organic matter content, porosity, structure and macro-porosity (Mohanty and Skaggs, 2001). The variability in soil hydraulic properties and soil water retention characteristics greatly influences the vertical and lateral transmission properties. Further, variations in soil particle and pore sizes may cause significant soil moisture variations even over very small distances. The influence of soil colour caused by moisture on albedo may also influence the rate of evaporative drying.

Topography plays a dominant role in the spatial structure of soil moisture both during and after rainfall. Results from hillslope scale studies indicate that significant variability in soil moisture content exists along the length of transects (Famiglietti *et al.*, 1998; Kim and Barros, 2002a). This variability decreases with decreasing transect-mean moisture content as the hillslope dries down following rain events. Studying the spatial organization of soil moisture in a small catchment, Grayson *et al.* (1997) have found that the moisture variation is related to the processes controlling the spatial pattern. Accordingly, spatial organization is strongest when there is lateral flow occurring (at high soil moisture content) or when the soil moisture is influenced significantly by up-slope processes (also known as non-local control). Little organization is present when the soil moisture is locally controlled (at low soil moisture content) and the main fluxes of water are vertical. Further, detailed event simulations indicate that spatial organization has a significant effect on the rainfall-runoff behaviour (Grayson *et al.*, 2002). Therefore, during inter-storm periods, topographic and soil attributes operate jointly to redistribute soil water. Under wet conditions, variability in surface moisture content is strongly influenced by porosity and hydraulic conductivity, and under dry conditions, correlations of soil moisture are strongest to soil properties such as residual moisture content and vegetation properties such as root density. Thus, during inter-storm periods, the dominant influence on soil moisture variability gradually changes from soil heterogeneity to joint control by topographic, soil and vegetation properties. This may lead to temporal stability in the spatial pattern of soil water distribution at the transect scale (Gómez-Plaza *et al.*, 2000). Studies confirm that at the point scale spatial patterns of soil moisture are determined by topographical position, as high locations, or steep areas, are usually the driest points, whereas locations in valley zones tend to be the wettest points despite the presence of vegetation.

Vegetation is another critical consideration for understanding the soil moisture regimes as it affects infiltration, runoff, and evapotranspiration. Further, the seasonal demands of soil water by plants alter the redistribution pattern of soil moisture. The key vegetation characteristics that influence soil moisture are vegetation type, density and uniformity (Reynolds, 1970). The influence of vegetation on soil moisture is more dynamic (Gómez-Plaza *et al*., 2000) as compared to the role of soil and topographic factors. The variability of soil moisture is lowest with full canopy cover and highest with partial coverage (Mohanty and Skaggs, 2001). Hawley *et al.* (1983) have suggested that the presence of vegetation tends to diminish the soil moisture variations caused by topography. On the other hand, vertical and lateral redistribution of soil moisture over scales from centimetres to tens or hundreds of meters together with spatial variation in evaporation and precipitation (Western *et al*., 1998b) cause variation in soil moisture distribution.

Knowledge of the above-mentioned causes for the variation of soil moisture is very important in describing the hydrological processes. Variations in soil moisture produce significant changes in the surface energy balance, vegetation productivity, and shape and volume of the observed hydrograph (Blöschl and Sivapalan, 1995). Therefore, knowledge of the characteristics of this variability is important for modelling purposes. However, the accurate assessment of this variability is difficult because field methods are complex and expensive. In addition, local scale variations in soil properties, terrain, and vegetation cover make selection of representative field sites difficult if not impossible (Engman and Chauhan, 1995; Wood, 1997). Consequently, its measurement is a difficult task, particularly for large spatial extents and time periods. Therefore, the best choice to estimate grid scale soil moisture is the combined use of ground based measurements, remote sensing observations and proper scaling techniques.

1.4 SCALE ISSUES AND MODELLING PROBLEMS IN HYDROLOGY

According to Gupta *et al.* (1986) the mathematical relationships describing a physical phenomenon are scale dependent. This is particularly important for hydrological studies. The procedures used to measure spatial and temporal variability of environmental parameters such as soil moisture, rainfall, evaporation or other model input parameters, and to predict processes which are represented by models may not necessarily be appropriate or optimal for the scale of interest. It is also possible that model parameters may change according to the level of disaggregation. Because of these reasons, a model developed at one scale may not be applicable at another scale. Therefore, if model results are blindly applied without considering how they might be affected by the scales used in model development and data collection, it can introduce significant problems in the final outputs.

Scaling may happen whenever a measurement technique is used to quantify the behaviour of a natural process at a particular scale of interest. Another type of scaling involves the development of process-based models using the observed data. Modelling includes the development, testing, evaluation, validation and application of a model consisting of mathematical assumptions and logical relationships to describe natural processes (Steyaert, 1993). Here, the aim of scaling procedure is to represent natural process patterns and their variance through models and then forecast or assess events. Consequently, the pattern produced by model results has to be evaluated in terms of natural patterns. The evaluation of models is essentially a scaling procedure in reverse. Through a continuous evaluation of the model approach, inappropriate assumptions and errors can be eliminated.

1.5 OBJECTIVES AND SCOPE

This thesis studies upscaling and downscaling techniques to improve the estimates of spatial and temporal distributions of soil moisture fields at three levels: hillslope scale, subcatchment scale and catchment scale (~6540 km^2). Knowledge of the variation of soil moisture is very important in describing the hydrological processes. The accurate assessment of this variability is however, difficult because field methods are complex and expensive and not representing large areas. Also, local scale variations in soil properties, terrain, and vegetation cover make selection of representative field sites difficult. Therefore, the best choice to estimate spatial patterns of soil moisture is the combined use of ground based measurements, remote sensing observations and proper scaling techniques.

The purpose of this study is to develop methodologies to upscale point measurements of soil moisture data into representative averages over larger spatial scales (e.g. 1.1 km satellite pixel scale) and to downscale area averaged soil moisture estimates over a large coverage into range of sub grid scales (1.1 km scale) to meaningfully represent the actual spatial distribution. The study mainly focuses on open, non-forested catchments. Further, hydrological modelling techniques such as simple bucket type water balance modelling and identification of catchment average soil moisture monitoring (CASMM) sites are assessed for predicting the temporal and spatial variability in catchment soil moisture status. This is done in order to establish functional relationships that can be used to estimate the soil moisture distribution at a range of scales.

This study is part of a larger project addressing Scaling and Assimilation of Soil Moisture And Streanflow (SASMAS) in a subhumid catchment. Being a dominant landscape pattern on the Australian continent it is therefore important to study the areal distribution of soil water contents in subhumid (and semiarid) catchments over a range of scales. This research focuses on the spatial and temporal variability of soil moisture status in a large catchment in the Upper Hunter region in New South Wales. This thesis' contribution to the SASMAS project is to study the spatial variability in soil moisture by developing techniques for upscaling, downscaling and interpolation of soil moisture measurements. For each of these scaling processes a range of tools have been developed and tested with the results obtained in a field experimental program which extends over several years, thus addressing seasonal differences and temporal variability in soil moisture status.

Furthermore, passive microwave technology is an emerging trend of remote sensing application to measure near-surface soil moisture in routine basis. This technique, however, is not yet widely accepted by the scientific community due to insufficient evidence of the validity of data. Thus, studies are needed to validate remotely measured soil moisture such as from AMSR-E.

The specific objectives of the research are as follows:

- To develop interpolation tools which are based on relationships between *in-situ* soil moisture measurements and remotely sensed thermal and visible imagery from different remote sensing platforms. These relationships will then be used for upscaling and interpolating soil moisture observations obtained with a network of permanent monitoring sites.
- To test terrain based hydrological modelling concepts for predicting the spatial variability in soil moisture status at local (hill slope) scale.
- To evaluate simple bucket type water balance modelling for predicting soil moisture
- To explore the potential of the temporal stability theory (see Grayson and Western, 1998) as an upscaling methodology and a solution to the problem of validating satellite based soil moisture estimation.
- To validate passive microwave remotely sensed large area AMSR-E soil moisture estimates with several intensive field campaigns based on many point-scale soil moisture and vegetation observations.

- To develop a methodology to validate AMSR-E measurements with ground-based permanent monitoring stations.
- To develop methodologies to disaggregate large-area soil moisture estimates obtained with passive microwave observations.
- To validate the above scaling methodologies and interpolation tools with *in-situ* soil moisture measurements.

1.6 OUTLINE OF APPROACH

The study starts by first analysing climatic conditions in the study region and soil moisture behaviour for different land use regimes. Then, relationships between field measured soil moisture and various other parameters such as: (a) indices derived from topographic data, (b) remotely sensed land surface temperature, (c) wetness indices derived from remotely sensed data, and (d) soil physical properties are studied. These analyses results in the development of simple physically based soil moisture scaling models at hill slope scale, sub catchment scale and large catchment scale. The hill slope scale upscaling model is tested on a 168 ha small catchment. The catchment scale model is used to upscale a limited number of point scale soil moisture observations on to a subcatchment of about 1200 - 6540 km^2. The third (large catchment) model is aiming at downscaling of 25 km scale passive microwave soil moisture observations into 1 km scale soil moisture estimates. These upscaling and downscaling models are then evaluated with field measured soil moisture measurements. Finally the models are used on the SASMAS data set and various applications of the upscaled and downscaled soil moisture estimates are discussed.

1.7 ORGANISATION OF THESIS

This thesis consists of nine chapters. Chapter 2 gives a literature review of soil moisture measurement techniques and scaling methodologies. It concludes with researchable issues and knowledge gaps in soil moisture scaling procedures.

Chapter 3 presents the field research program in the Goulburn River experimental catchment. It also describes the calibration of field instruments. Analysing the field data collected during the study period, climatic and hydrological characteristics of the catchment are also presented.

From the insight gained in Chapter 3, a simple one-dimensional bucket type water balance modelling is applied in Chapter 4 to study the hillslope-scale hydrological behaviour. Chapter 4 also investigates the control of topography and soil characteristics upon soil moisture distribution at the hillslope scale.

Chapter 5 describes an attempt to extend the soil moisture scaling relationships to an entire catchment. This chapter studies the prediction of catchment average soil moisture from the catchment average soil moisture measurement (CASMM) sites.

Chapter 6 studies the prediction of soil moisture from combined use of ground based measurements and remotely sensed land surface temperature and vegetation observations.

Chapter 7 presents results of field validation of AMSR-E soil moisture observations.

With the availability of routinely measured large area soil moisture measurements (25km x 25 km) the scientific community needs methodologies to disaggregate these large area soil moisture measurements for wider practical applications. Therefore, a soil moisture disaggregation method is developed in Chapter 8.

Chapter 9 presents the conclusions of this research. It also discusses future directions for predicting catchment scale soil moisture distribution patterns from ground-based point scale measurements and near-surface or skin soil moisture measurements from satellite-based passive microwave sensors.

CHAPTER TWO

2. LITERATURE REVIEW – MEASUREMENT, ESTIMATION AND SCALING OF SOIL MOISTURE

This chapter deals with soil moisture measurement and estimation techniques. The theoretical basis of soil moisture measurement techniques is discussed and some common *in-situ* methods and remote sensing techniques are presented. The chapter also includes approaches for soil moisture estimation. Next, the importance of soil moisture scaling is outlined and a review is presented of some recent efforts to address the problems of soil moisture scaling for hydrological applications.

2.1 INTRODUCTION

Information on the temporal and spatial distribution of soil moisture is central to many hydrological and climatic models as soil moisture provides the most direct link to water balance equation. It is widely accepted that reliable, robust and automated methods for the measurement of soil moisture content will be extremely useful, if not essential. Soil moisture however, unlike other environment variables such as rainfall, solar radiation, wind velocity and air temperature, varies over a very narrow range within a day particularly during non-rainy days. Furthermore, minimum and maximum field capacities of soils vary from approximately 0.6 mm to 4.5 mm in 1cm depth of soil for coarse sands and clay soils respectively. Small variations of soil moisture within these lower and upper boundaries therefore are difficult to measure and require very accurate techniques.

There are three common ways to describe the wetness of soil: gravimetric soil water content (SWC), volumetric soil water content and soil water potential (SWP). Gravimetric SWC refers to how much water is in the soil on a weight basis, for example 0.20 g water per 1 g of oven dried soil. Volumetric SWC refers to how much water is in the soil on a volume basis, for example 0.20 cm^3 water per 1 cm^3 of soil. This is the most useful way to express SWC because it allows comparing the water contents of different soils. Volumetric measurements are convenient for measuring how wet the soil is, but they give no indication how strongly the water is attached to the soil particles. When the soil is wet, the water is not so strongly attached to the soil particles and hence is more readily available to plants. However, as the soil becomes drier, the water is held more strongly and more energy is needed to extract it. The soil water potential is a measure of how strongly water is attached to the soil particles and is expressed in kilopascals (kPa) or in millibars (mbar). Potential is also known as soil water suction.

It is possible to use all three methods for the same purpose but which description is used depends on how the information will be used. For example, an irrigator would prefer to know the volumetric SWC as it gives an idea of water deficit in the soil on a volumetric basis and hence, it is easier to compute the diversion requirement. On the other hand, plant physiologists may prefer using SWP as it gives an indication of how easily roots can absorb soil water. Similarly, a hydrological modeller may require soil moisture information in the form of a grid pattern across the whole catchment of interest. For some applications, it may need continuous soil moisture information over a certain period. To meet these diverse requirements, a range of measuring techniques is available. The knowledge of moisture measurement techniques is important for a better insight into the scaling properties of the soil moisture fields.

Many field procedures have been employed to measure soil moisture *in-situ* as well as remotely. Each procedure has advantages and disadvantages stemming from the complexity of the instrumentation, difficulty of instrument calibration, and the cost of the data acquisition and analysis. Therefore, the selection of a procedure should be based on how the soil moisture information is to be used.

2.2 GROUND BASED TECHNIQUES FOR MEASURING SOIL MOISTURE

In a broad sense, all current *in-situ* techniques can be categorised into three groups: direct methods, indirect methods, and suction methods. Direct methods measure the water content directly, whereas in indirect methods SWC is determined by measuring another strongly related property. The suction methods, a kind of indirect approach, measure the soil water potential. A brief account of these techniques is provided in the following sections.

2.2.1 THE DIRECT METHOD

Of the scientific methods, the oldest and still most widely used method is the thermo-gravimetric method. It is the only direct way to measure SWC. Measurement of gravimetric SWC is straightforward. A soil sample is collected, weighed, dried in an oven (at $105^{o}C$ – $110^{o}C$) for 16-24 hours or more (until it reached to a constant weight) and then weighed again (AS 1289.2.1.1-2005). The weight difference between before and after drying the soil is the water content of the soil sample, which is usually expressed as a percentage of the dry soil mass. If the bulk density value is known, multiplying the mass based moisture content value by bulk density gives the volumetric moisture content. This approach requires careful sample collection and handling to minimize water loss between the time a sample is collected and processed. Replicated samples should be taken to reduce the inherent sampling variability that results from small volumes of soil.

Apart from being the most reliable method, it has the advantage of simplicity in equipment requirement, an easy calculation procedure, and it is not dependent on salinity and soil type. These factors balance the obvious drawback of destructive and tedious sampling, the time required and the inapplicability to automatic control. One problem with the gravimetric SWC measurement is that the densities of different soils vary so that a unit weight of different soils may occupy different volumes. Therefore, it limits the practical value of the gravimetric measurements. However, gravimetry is the only direct way to measure the water content in the soil. All other techniques rely on indirect methods that measure other properties of the soil that vary with water content. The calibration of all other methods, therefore, relies on gravimetric method.

2.2.2 INDIRECT METHODS

Most physical properties such as electrical conductivity, water potential, and water vapour in soils vary systematically with changes in water content. Many of these properties have been used for indirect estimation of soil water content. In an ideal situation, any property selected for such use should depend uniquely on water content but this rarely happens. A range of techniques such as based on nuclear techniques, electrical properties of porous media, and the relative humidity of the immediate atmosphere can be used for water content determination. Among the indirect methods, two approaches are widely used. One approach adopts nuclear methods and the other uses the electrical conductivity property in porous media.

In the past, the neutron scattering technique was the most accurate method widely used for *in-situ* SWC measurement. This method estimates the amount of water in a volume of soil by measuring the amount of hydrogen present by using a neutron probe. A neutron probe consists of a source of fast or high energy neutrons and a detector, both housed in a unit which is lowered into an access tube installed in the soil. Fast neutrons, emitted radially from the radioactive source and passing through the access tube into the surrounding soil, gradually lose their energy though collisions with other atomic nuclei. Hydrogen molecules in the soil are particularly effective in slowing the fast neutrons since they are of near equal mass. The result is a cloud of slow, thermalized neutrons, some of which diffuse back to the detector. This cloud is normally spherical in shape and the size and density depends mainly upon soil type and soil water content. The sphere of influence varies from 10 cm in wet soil to 25 cm or more in dry soil. Thermalized neutrons which pass through the detector create a small electrical impulse and these pulses are amplified and counted. The number of slow neutrons counted in a specified interval of time is linearly related to the SWC. A higher count indicates higher SWC and vice versa. The main advantages of this technique are that SWC can be determined with depth, that the method is temperature independent, and can accommodate automatic reading at the same site. However, this technique requires constant re-calibration which is often a difficult task. In addition, the technique is not suitable for measuring near-surface SWC. The method involves safety concerns due to potential health risks from exposure to radioactive materials and therefore, limitations on legal use exist in most locations (Zegelin, 1996).

Among the many electrical properties, measuring the dielectric constant or relative permittivity or specific inductive capacity of soil and relating it to the soil water content has become virtually a new standard technique. The dielectric technique estimates the soil moisture content by measuring the dielectric constant (K_a) in the soil. Soil is a composite mixture of air, mineral and organic particles, and water. Air, mineral particles and water have dielectric constants of 1, 2-4, and 80 respectively at frequencies between 30 MHz and 1 GHz. Because of the great difference in dielectric constant between water and other constitutes in the soil, relatively small changes in the quantity of free water in the soil have large effects on the electromagnetic properties of the soil water media. K_a is inversely related to the propagation velocity, i.e., a faster propagation velocity indicates a lower dielectric constant and thus a lower soil water content. Or, as soil water content increases, the propagation velocity decreases, and dielectric constant increases.

Two approaches have been developed for measuring the dielectric constant of the soil water media. These are categorized as time domain reflectometry and frequency domain reflectometry.

The speed with which an electromagnetic pulse of energy travels down a parallel transmission line depends on K_a of the material in contact with and surrounding the waveguide. Time Domain Reflectometry (TDR) instruments measure this wave transit time along the waveguide using sophisticated electronic circuits. The 'apparent' dielectric constant, K_a, of the air-soil-water complex can then be related by the formula:

$$K_a = \left(\frac{tc}{L}\right)^2 \qquad [-] \qquad (2.1)$$

where L is the length of the waveguides (in cm), t is the transit time (in nanoseconds) or time required for pulse to travel along a whole length of the waveguide in one direction, and c is the speed of light (in $cm.nsec^{-1}$). If the soil is completely dry, K_a will be 2 to 4. If the 25% of the volume of the soil is water, K_a will be approximately 11-12 (Soil Moisture Equipment Corporation, 1996). Based on a relationship between K_a and actual soil moisture, it is possible to measure *in-situ* soil moisture content very conveniently.

Most TDR instruments measure directly the wave guide signal reflection time. Some cheaper instruments, however measure frequency of state changes. For example, waveguides of the CS616 water content reflectometers (manufactured by Campbell Scientific Inc.) are connected to a bistable multivibrator. The signal return from the waveguides causes the bistable multivibrator to change states between two discrete values. Hence, the output of the sensor is a frequency that reflects the number of states changes per second.

Once properly calibrated and installed, the TDR technique is highly accurate and measurements may be made near the surface, an important advantage compared to the neutron probe. Other advantages include: (i) K_a depends primarily on the VWC of soil, hence facilitates measurement of VWC; (ii) K_a is largely independent of the soil type and relatively unaffected by low to moderate soil salinity and therefore may be use in a range of soil types; and (iii) portability of the techniques. The main disadvantages of the system include: (i) its poor performance in high saline soils and soils with high clay contents; (ii) sensitivity to the air gaps along the probes; and (iii) the relatively small zone of influence, up to 2 cm from the probe.

Frequency Domain Reflectometry (FDR) approaches are also known as the radio frequency (RF) capacitance technique. This technique measures the capacitance of the soil using a pair of electrodes. The soil acts as the dielectric medium completing a capacitance circuit, which is part of a feedback loop of a high frequency transistor oscillator. As high frequency radio waves (about 150 Mhz) are pulsed through the capacitance circuitry, a natural resonant frequency is established which is dependent on the soil capacitance. The soil capacitance is related to the dielectric constant by the geometry of the electric field established around the electrodes. The strengths of this technique include: (i) it is rapid and easy to use; (ii) higher sensitivity to small changes of soil moisture, particularly in dry soils; and (iii) it allows automatic logging. However, the relatively small zone of influence, its sensitivity to the soil layer immediately adjacent to the probe, and the sensitivity to air gaps surrounding the probe are weaknesses of this technique.

2.2.3 SUCTION METHODS

Soil water suction, soil water tension, or soil water potential are all concepts describing the energy status of soil water. Movement of water occurs within the soil profile, between the soil and plant roots, and between soil and atmosphere. The rate of water movement is dependent on the energy gradient such as expressed by a gradient in soil water potential. The fundamental forces acting on soil water are gravitational, matric, and osmotic. Similar to all matter, water molecules in the soil have a potential energy by virtue of their position in the gravitational force field. The matrix arrangement of soil solid particles results in capillary and electrostatic forces and determines the soil water matric potential. The magnitude of those forces depends on the texture and the physical and chemical properties of the soil particles. Soil water is a solution of soluble salts, organic solutes, and some suspended colloids. The polar nature of the water molecules results in interaction with other electrostatic poles present in the solution as free ions. This component of the energy status is the osmotic potential. Most methods for measuring soil water potential are sensitive only to the matric potential.

There is a unique relationship between water content and water potential for each soil type. Such a relationship is known as the soil water characteristic curve (or water release curve). For a given water potential, the finer the soil texture the more water is held in the soil. Fine texture soils have a broader pore size distribution and larger particle surface area; hence water molecules strongly adhere to the soil particles due to electrostatics forces. In contrast, coarse texture soils like sand comprise mostly large pores which empty of water when a relatively small force is applied. Methods for measuring soil water potential include tensiometry, thermocouple psychrometry, electrical conduction methods and heat dissipation methods.

2.2.4 REMARKS – *IN-SITU* TECHNIQUES

Several well-established methodologies are available to measure soil moisture on the ground. Successful implementation of any of the methods however, requires careful attention to the installation, operation, field calibration, and maintenance requirements.

The ability to measure soil moisture *in-situ* is important in all water resources disciplines. *In-situ* techniques are capable of providing accurate soil moisture content at any time and are therefore the best way of studying the temporal evolution of soil moisture patterns. Furthermore, *in-situ* techniques are the only way of assessing moisture status at deeper soil layers. The very small volume represented by *in-situ* measurement is however, an unavoidable obstacle. For this reason, use of measured soil moisture data for modelling applications from plot to catchment scale requires some type of scaling in order to obtain an average soil moisture value for the area concerned. Obtaining an average soil moisture value over an area is often difficult due to the spatial in-homogeneity of a soil system, both horizontally and vertically. The number of measurements needed to obtain a representative soil moisture value is difficult to determine, as is the optimal location of the measurements. In addition, these measurements are in general expensive and tedious to collect.

2.3 REMOTE SENSING FOR MEASUREMENT OF LAND SURFACE PARAMETERS

An alternative to ground based measurement networks are remote sensing techniques based on air-borne or space-borne sensors. One of the advantages of remote sensing techniques is the ability of obtaining a true spatial average soil moisture value over a large area. It is impracticable if not impossible to obtain such a spatial average soil moisture value from *in-situ* techniques. In-depth study of remote sensing techniques and their applications to infer soil moisture content is therefore indispensable for any study leading to soil moisture scaling.

The term remote sensing refers to methods that employ electromagnetic energy, such as light, heat and radio waves, as a means of detecting and measuring target characteristics (Sabin, 1997). The development and deployment of various sensors has provided an orbital vantage point for acquiring images of the earth. The large numbers of satellites in orbit around planet Earth act as platforms for a range of remote sensing instruments, which provide valuable information for atmospheric, oceanic and land surface studies.

One of the major advantages of satellites is their ability to acquire information at regional and global scales as opposed to the point scale estimation of conventional ground-based data collection techniques. In addition, the use of satellite measurements appears to be very attractive since they can give uniform estimates (i.e., with the same sensor and measurement characteristics). Remote sensing therefore offers the best practical method for determining land surface processes at various scales. Another advantage of the remotely sensed imagery is that some imagery such as from NOAA and MODIS may be downloaded almost on real-time basis from internet sites (for e.g. http://www.ga.gov.au/acres/) at no cost.

Remote sensing instruments use various windows of the electromagnetic spectrum to record the reflectance properties of the land surfaces. Figure 2.1 shows the electromagnetic spectrum, which is divided on the basis of wavelength into regions listed in Table 2-1. While the most popular remote sensing instruments such as Multi-Spectral Scanner (MSS), Advanced Very High Resolution Radiometer (AVHRR), Thematic Mapper (TM) and MODerate resolution Imaging Spectroradiometer (MODIS) use visible and infrared (IR) regions, radiometers such as Synthetic Aperture Radar (SAR), Advanced Microwave Sounding Unit (AMSU), Advanced Microwave Scanning Radiometer for Earth Observing System (AMSR-E) use microwave regions of the spectrum.

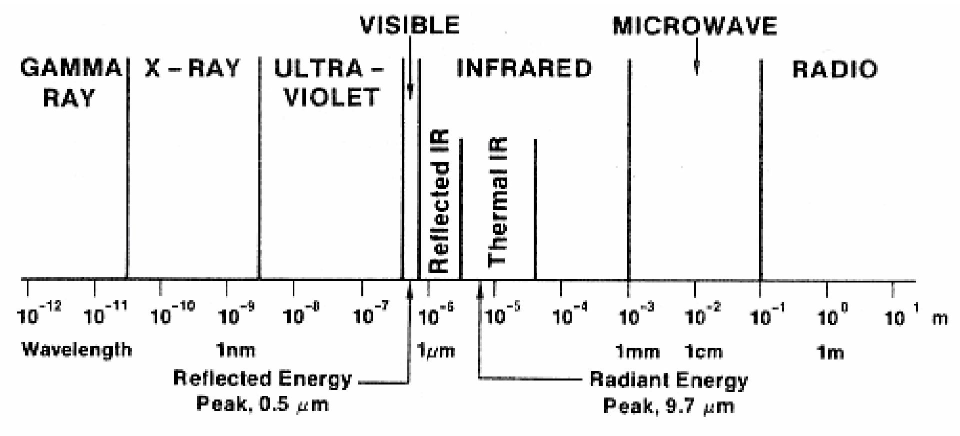

Figure 2.1: Electromagnetic spectrum (from Sabins, 1997).

Table 2-1: Electromagnetic spectral regions

Region	Wavelength	Remarks
Gamma-ray region	< 0.03 nm	Incoming radiation completely absorbed by the upper atmosphere and not available for remote sensing.
X-ray region	0.03 to 30 nm	Completely absorbed by the atmosphere. Not employed in remote sensing.
Ultraviolet region	0.03 to 0.4 μm	Incoming wavelengths less than 0.3 μm completely absorbed by ozone in the upper atmosphere.
Photographic UV band	0.3 to 0.4 μm	Transmitted through the atmosphere. Detectable with film and photo detectors, but atmospheric scattering is severe.
Visible region	0.4 to 0.7 μm	Imaged with film and photo detectors. Includes reflected energy peak of earth at 0.5 μm.
Infrared region	0.7 to 100 μm	Interaction with matter varies with wavelength. Atmospheric transmission windows are separated by absorption bands.
Reflected IR band	0.7 to 3.0 μm	Reflected solar radiation that contains no information about thermal properties of materials. The interval from 0.7 to 0.9 p-m is detectable with film and is called the photographic IR band.
Thermal IR band	3 to 5 μm, 8 to 14 μm	Principal atmospheric windows in the thermal region. Emitted radiation from the earth and atmosphere is prevalent. Images at these wavelengths are acquired by optical-mechanical scanners and special vidicon systems but not by film.
Microwave region	0.1 to 100 cm	Longer wavelengths that can penetrate clouds, fog, and rain. Images may be acquired in the active or passive mode.
Radar	0.1 to 100 cm	Active form of microwave remote sensing. Radar images are acquired at various wavelength bands.
Radio	> 100 cm	Longest-wavelength portion of electro-magnetic spectrum.

(source: F. F. Sabins (1997), Remote sensing- Principles and Interpretation)

2.3.1 GLOBAL INTEREST IN MAPPING LAND SURFACE SOIL MOISTURE

Recent advances in remote sensing have shown that soil moisture can be measured by a variety of techniques. Different parts of the electromagnetic spectrum facilitate remote observation of soil moisture on a routine basis with aircraft or satellite based sensor platforms. As shown in Table 2-2, each of these techniques has several advantages as well as some disadvantages. Among the various techniques, especially microwave remote sensing (active and passive) provides the opportunity to collect truly quantitative near-surface soil moisture information moisture under a variety of topographic and vegetation cover conditions (Engman, 1990). Like many *in-situ* measuring techniques, the microwave technique exploits the strong relationship between the moisture content and the dielectric constant of the soil. Technological and methodological progress in the past two decades has resulted in dedicated soil moisture missions such as NASA's Hydrosphere State mission (HYDROS) and European Space Agency's (ESA) Soil Moisture and Ocean Salinity Mission (SMOS). These missions are expected to provide a flow of high quality coarse resolution soil moisture data covering the entire globe.

Table 2-2: Some advantages and disadvantages of remote measurement of soil moisture using different parts of the electromagnetic spectrum.

Spectrum	Advantages	Disadvantages
Visible	• Simple to operate • Applicable at a range of spatial and temporal scales	• Cloud free conditions required • Strong empirical character
Thermal infrared	• Provides an integrated soil moisture value for the root zone • Deals with temperature which is linked to complicated surface energy balance processes • Applicable at a range of spatial and temporal scale • Cost effective technique	• Cloud free conditions required • Depth of the root zone is variable across an image
Active microwave	• All weather conditions technique • Good physical basis • Can change the polarisation	• Moisture estimates affected by surface roughness • Aircraft based measurements have a penetration depth limited to a few decimetres • Satellite based measurements are expensive
Passive microwave	• All weather conditions technique • Good physical basis • Daily basis images are currently available	• Soil moisture only retrievable from the top layer and for sparse vegetation • Large pixel size from satellites • Aircraft acquisitions are expensive

In the past, the major factor preventing wide spread use of remotely sensed soil moisture data in hydrology was the lack of data sets and optimal satellite systems. As such, studies have been restricted to data from short duration aircraft campaigns, or analysis of the SMMR and SSM/I passive microwave satellites. At present, daily soil moisture observation data such as from AMSR-E is readily and freely available. The availability of remotely sensed soil moisture data provides an opportunity to study the soil moisture status at catchment and regional scale. In fact, remote sensing technology has introduced a new type of spatially averaged soil moisture information which is not obtainable from *in-situ* techniques.

2.3.2 INSTRUMENTS FOR REMOTE OBSERVATION OF LAND SURFACE PARAMETERS

A wide range of radiometers are currently operational in space which may be used to derive the information on land surface moisture characteristics. In a broad sense, radiometers which may be used to derive soil moisture information are categorised into two types based on the part of the electromagnetic spectrum used by them; (a) visible and thermal radiometers and (b) microwave radiometers. A brief review of the most widely used radiometers under each type is presented in the following sections.

2.3.2.1 Radiometers for visible and thermal remote sensing

2.3.2.1.1 Advanced Very High Resolution Radiometer (AVHRR)

One of the most widely used remote sensing instruments is the Advanced Very High Resolution Radiometer (AVHRR) on board the NOAA satellites. The National Oceanic and Atmospheric Administration (NOAA) in the United State operates a series of polar orbiting satellites that circle the Earth in nearly sun-synchronous orbits. NOAA is currently operating four satellites; NOAA-15 (or NOAA-K, May 1998), NOAA-16 (or NOAA-L, September 2000), NOAA-17 (or NOAA-M June 2002), and NOAA-18 (or NOAA-N, May 2005). While NOAA-17 is the prime morning satellite, both NOAA-15 and NOAA-18 are prime afternoon satellites. At present, NOAA-16 has been reclassified as standby, and is transmitting a low-gain signal. The AVHRR records one visible band, two reflected IR bands, and three thermal IR bands, which are listed in Table 3.2. Band 4 and 5 together span the same spectral range as TM band 6. The average AVHRR field of view is of ± 55^{o} from nadir, which enables the system to view almost any point of the Earth's surface twice a day (on ascending and descending orbits). It must be noted however, that each point will be viewed at different viewing angles on subsequent days, with the viewing conditions being approximately repeated only every 9 days. The major advantage of the NOAA-AVHRR is the accessibility to near real-time images through the World Wide Web such as from the Geoscience Australia Internet site (http://www.ga.gov.au/acres/noaa).

Table 2-3: Characteristics of the NOAA-AVHRR

Orbit	Near polar, sun synchronous
Repeat rate	~10 hours
Spectral bands	5
Channels	
Visible-1	0.58 to 0.68 μm
Visible-2	0.725 to 1.10 μm
IR-3	3.55 to 3.93 μm
IR-4	10.3 to 11.3 μm
IR-5	11.5 to 12.5 μm
Swath width	2399 km
Instantaneous field of view (IFOV)	1.3 x 1.3 mrad
Spatial resolution	1100 m (nadir)

(Source: NOAA KLM User's guide available at http://www2.ncdc.noaa.gov/docs/klm/html/c3/sec3-1.htm)

2.3.2.1.2 MODerate resolution Imaging Spectroradiometer (MODIS)

The Moderate Resolution Imaging Spectroradiometer (MODIS) instrument has been designed to provide improved monitoring for land, ocean, and atmospheric research (Justice *et al*., 1998). The MODIS sensor is gaining much attention due to its multi-spectral capabilities with high spatial and temporal characteristics (see Table 2-4). The first MODIS instrument was launched in July 1998 on the morning platform (AM1) of the Earth Observing System (EOS), the Terra satellite. It follows a polar, sun-synchronous, 705 kilometre orbit with a morning equatorial crossing time. The second MODIS sensor is on board the Aqua satellite launched in May 2002. Aqua follows its orbital path with an afternoon equatorial crossing and is hence known as EOS PM1. The afternoon overpass of Aqua-MODIS gives more drier conditions than in the morning overpass due to evaporation from the land surface and is therefore, more suitable for soil moisture related studies.

These two MODIS instruments view the entire earth's surface at least twice a day and acquire data in 36 spectral bands. These provide high radiometric sensitivity (12-bit quantisation) ranging in wavelength from 0.4 μm to 14.4 μm. The first two bands are imaged at a nominal 250 m resolution at nadir, the next five bands at 500 m resolution and the remaining 29 bands at 1000 m resolution. MODIS acquisitions across Australia over the last seven days are available from the Geoscience Australia Internet site (http://www.ga.gov.au/acres/modis).

MODIS products such as land surface reflectance and temperature, vegetation indices, fire products, and snow products are available for free downloading from the EOS data gateway (http://nsidc.org/~imswww/pub /imswelcome/index.html).

Table 2-4: MODIS Sensor Characteristics

Primary Use	Band	Bandwidth[1]	Spectral Radiance[2]	Required SNR[3]
Land/Cloud/Aerosols Boundaries	1	620 - 670	21.8	128
	2	841 - 876	24.7	201
Land/Cloud/Aerosols Properties	3	459 - 479	35.3	243
	4	545 - 565	29.0	228
	5	1230 - 1250	5.4	74
	6	1628 - 1652	7.3	275
	7	2105 - 2155	1.0	110
Ocean Colour Phytoplankton Biogeochemistry	8	405 - 420	44.9	880
	9	438 - 448	41.9	838
	10	483 - 493	32.1	802
	11	526 - 536	27.9	754
	12	546 - 556	21.0	750
	13	662 - 672	9.5	910
	14	673 - 683	8.7	1087
	15	743 - 753	10.2	586
	16	862 - 877	6.2	516
Atmospheric Water Vapour	17	890 - 920	10.0	167
	18	931 - 941	3.6	57
	19	915 - 965	15.0	250
Surface/Cloud Temperature	20	3.660 - 3.840	0.45 (300K)	0.05
	21	3.929 - 3.989	2.38 (335K)	2.00
	22	3.929 - 3.989	0.67 (300K)	0.07
	23	4.020 - 4.080	0.79 (300K)	0.07
Atmospheric Temperature	24	4.433 - 4.498	0.17 (250K)	0.25
	25	4.482 - 4.549	0.59 (275K)	0.25
Cirrus Clouds Water Vapour	26	1.360 - 1.390	6.00	150(SNR)
	27	6.535 - 6.895	1.16 (240K)	0.25
	28	7.175 - 7.475	2.18 (250K)	0.25
Cloud Properties	29	8.400 - 8.700	9.58 (300K)	0.05
Ozone	30	9.580 - 9.880	3.69 (250K)	0.25
Surface/Cloud Temperature	31	10.780 - 11.280	9.55 (300K)	0.05
	32	11.770 - 12.270	8.94 (300K)	0.05
Cloud Top Altitude	33	13.185 - 13.485	4.52 (260K)	0.25
	34	13.485 - 13.785	3.76 (250K)	0.25
	35	13.785 - 14.085	3.11 (240K)	0.25
	36	14.085 - 14.385	2.08 (220K)	0.35

[1] Bands 1 to 19 are in nm; Bands 20 to 36 are in µm
[2] Spectral Radiance values are ($Wm^{-2}.\mu m.sr$)
[3] SNR = Signal-to-Noise Ratio
[4] NE(delta)T = Noise-equivalent temperature difference
IFOV of Bands 1-2 is 250m, Bands 3-7 is 500m and Bands 8-36 is 1.1 km

Source: http://www.ga.gov.au/acres/prod_ser/modisdata.htm (2003).

2.3.2.1.3 Other radiometers

There are number of other space borne radiometers currently available for varying temporal and ground resolution. The sensitivity of these radiometers also varies from radiometer to radiometer. For example, one of the widely used radiometers is LANDSAT 7 ETM+ which has 30m by 30m ground resolution cells similar to Thematic Mapper (TM) sensor with additional two bands, a panchromatic band with 15 m resolution and a higher resolution thermal band of 60 m. The sensitivity of visible and reflected IR of LANDSAT 7 ETM is between 0.45 μm to 2.35 μm. The nominal temporal resolution of LANDSAT data is 15 days.

Another radiometer, the Along Track Scanning Radiometer (ASTR) has the same space resolution as MODIS and AVHRR but with a 3-day repeat cycle. It also has 7 spectral bands. Other radiometers cover wide spectral regions with high spatial, spectral and radiometric resolution. For example, the Advanced Spaceborne Thermal Emission and Reflection radiometer (ASTER) has 14 bands from the visible to the thermal infrared. In the visible and near-infrared regions it has three bands with a spatial resolution of 15 m. The shortwave infrared region has 6 bands with a spatial resolution of 30 m, and the thermal infrared region has 5 bands with a spatial resolution of 90 m.

It is evident that a range of data is available from visible and thermal radiometers. The use of such data however is determined by many factors including the spatial resolution and cost involved with obtaining the data. Deriving soil moisture from visible and thermal remote sensing data is always complex and requires indirect approaches. Such approaches are based first on deriving land surface temperatures and vegetation indices and then on relating soil moisture to these computed parameters.

2.3.2.2 Radiometers for microwave remote sensing

Although numerous radiometers (e.g. SMMR, SSM/I, TMI, AMSU etc.) and scatterometers (e.g. Active Microwave Instrument in European remote sensing satellites) are in existence and have been used for measurement of passive and active microwave radiation, only the Advanced Microwave Scanning Radiometer for soil moisture measurement is discussed below.

2.3.2.2.1 Advanced Microwave Scanning Radiometer for EOS (AMSR-E)

The Advanced Microwave Scanning Radiometer - Earth Observing System (AMSR-E) is a passive microwave radiometer, launched aboard NASA's Aqua Satellite (Figure 2.2) on 4 May 2002. It is a 12-channel conically scanning radiometer measuring vertically and horizontally polarized radiation at the microwave frequencies of 6.9, 10.7, 18.7, 23.8, 36.5, and 89.0 GHz (Kawanishi *et al.,* 2003; Parkinson, 2003). Detailed AMSR-E performance characteristics are shown in Table 2-5. A modified version of AMSR was launched in December 2002 aboard the Advanced Earth Observing Satellite-II (ADEOS-II). The instrument is designed and provided to NASA by the National Space Development Agency of Japan (NASDA). Further information about the AMSR-E can be found in Kawanishi *et al.* (2003).

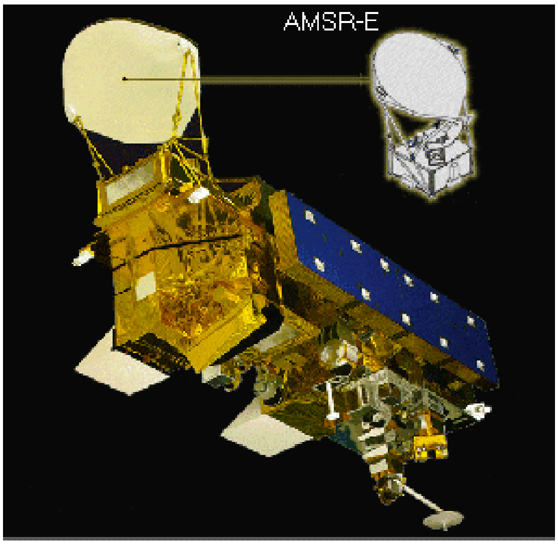

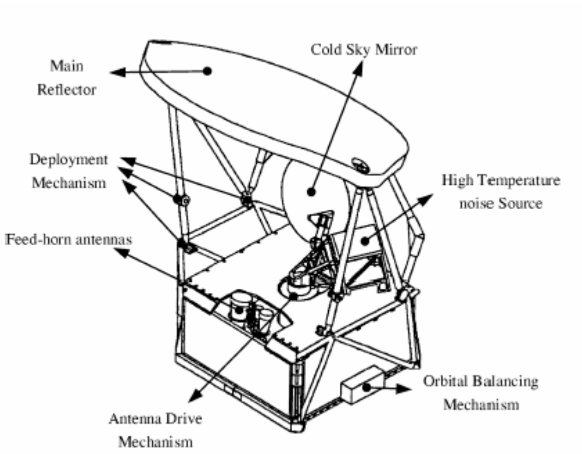

(a) (b)

Figure 2.2: (a) Aqua platform and AMSR-E position (source: National Snow and Ice Data Centre (NSIDC) web site at http://nsidc.org) and (b) overview of AMSR-E (source: Kawanishi et al., 2003).

Table 2-5: AMSR-E Instrument characteristics

Centre frequencies (GHz)	6.92	10.56	18.7	23.8	36.5	89.0
Bandwidth (MHz)	350	100	200	400	1000	3000
Sensitivity (K)	0.3	0.6	0.6	0.6	0.6	1.1
IFOV (km)	76 x 44	49 x 28	28 x 16	31 x 18	14 x 8	6 x 4
Sample spacing (km)	10 x 10	10 x 10	10 x 10	10 x 10	10 x 10	5 x 5
Integration time (ms)	2.6	2.6	2.6	2.6	2.6	1.3
Mean-beam efficiency (%)	95.3	95.0	96.3	96.4	95.3	96.0
Beamwidth (deg)	2.2	1.4	0.8	0.9	0.4	0.18
Antenna diameter (m)	1.6					
Scan period (s)	1.5					
Antenna offset angle (deg)	47.4					
Earth-incidence angle (deg)	54.8					
Orbit altitude (km)	705					
Swath width (km)	1445					
Orbit type	Sun-synchronous, 98.2^{o} inclination, 1:30 pm equator crossing					
Orbit period (min)	98.8					
Sub-spacecraft velocity (km s^{-1})	6.76					

(Source: Kawanishi *et al.,* 2003)

It is important to understand the physics behind the microwave remote sensing because it is the only remote sensing technique that is capable of providing the quantitative measure of soil moisture. The validation of microwave soil moisture data therefore needs in-depth understanding of deriving soil moisture from measured brightness temperatures. In this thesis, details of microwave techniques for soil moisture estimation are discussed in Chapter 7.

2.3.3 SATELLITE DERIVED LAND SURFACE TEMPERATURE

Undoubtedly, the most useful land surface variable that can be derived from thermal remote sensing is the land surface temperature (LST). Land surface temperatures play an important role in land-surface processes. They are of fundamental importance to the net radiation budget at the Earth's surface and to monitoring the state of crops. Except for solar irradiance components, most of the energy fluxes at the surface/atmosphere interface can only be parameterised through the use of LST (Kerr *et al*., 2004). It can play either a direct role (e.g. when estimating long-wave fluxes) or an indirect role as when estimating latent and sensible heat fluxes. Furthermore, many other modelling applications such as in hydrology, geology, vegetation monitoring, and global circulation models rely on the knowledge of land surface temperature. Remotely sensed LST have been used in number of applications including moisture availability to vegetation (Bastiaanssen *et al*., 1997; McVicar and Jupp, 1999; Moran *et al*., 1994; Wan *et al*., 2004). Other LST applications include modelling of regional scale evapotranspiration (McCabe and Wood, 2006) and land surface turbulent flux prediction (Diak and Stewart, 1989).

Soil temperature has a strong relationship with the soil moisture content. For example, dry soil shows greater day-night temperature fluctuations than wet soil under similar environmental conditions. Similarly, during mid-day, while dry areas appear as ‘hot spots’, wet areas appear as ‘cool spots’ due to the greater specific heat of water molecules. The availability of spatially averaged LST over large areas derived from remotely sensed data and the strong relationship between LST and soil moisture content provide an ideal opportunity to use remotely sensed LST data for soil moisture scaling studies. This can be done by using remotely sensed LST as a surrogate variable to derive spatial soil moisture patterns. However, due to the narrow range of temperature variations and soil moisture content, accurate estimation of LST is very important.

When inferring LST from remotely sensed data, the first problem to be solved is the translation of observed radiance into surface brightness temperature. After calibration and conversion of radiance into temperature, using an inverse Plank’s law, it is necessary to account for the atmospheric contribution. Next the surface brightness temperature must be transformed into surface temperature, taking into account emissivity and directional effects. Actually, the problem is more complicated because atmospheric, emissivity and directional effects are coupled and these modulating factors cannot be approached independently (Kerr *et al.,* 2004).

A practical way for accurately estimating spectral emissivity is from multiple thermal channels. Fortunately, several sensors have multiple thermal infrared bands that allow LST and emissivity to be estimated simultaneously, such as found in MODIS and in ASTER. The MODIS has multiple thermal bands in the 3.5–4.2 μm and the 8–13.5 μm ranges, and the ASTER has five thermal bands in the 8–12 μm range.

2.3.3.1 Theoretical basis for land surface temperature estimation

In clear sky situations, the outgoing infrared spectral radiance ($I(\lambda,\mu)$) can be represented as follows (see Wan, 1999; Sikorski and Kealy, 2002):

$$
\begin{aligned}
I(\lambda,\mu) = \upsilon(\lambda,\mu)\varepsilon(\lambda,\mu)B(\lambda,T_s) + I_a(\lambda,\mu) + I_s(\lambda,\mu,\mu_0,\varphi_0) \\
+ I_d(\lambda,\mu,\mu_0,\varphi_0) + I_r(\lambda,\mu,\mu_0,\varphi_0)
\end{aligned}
\tag{2.2}
$$

where υ is the transmissivity, $\varepsilon(\lambda,\mu)$ is the surface spectral emissivity, $B(\lambda,T_s)$ is the radiance emitted by a blackbody at surface temperature T_s, $I_a(\lambda,\mu)$ is the thermal path radiance, and $I_s(\lambda,\mu,\mu_o,\varphi_o)$ is the path radiance resulting from scattering of solar radiation. $I_d(\lambda,\mu,\mu_o,\varphi_o)$ is the solar radiance and $I_r(\lambda,\mu,\mu_o,\varphi_o)$ the solar diffuse radiation and atmospheric thermal radiation reflected by the surface. λ is the wavelength. μ is the cosine of the satellite zenith angle and μ_o is the cosine of the solar zenith angle. φ_o is the azimuth angle.

Equation 2.2 can be used in the 3–14 μm wavelength range. To compute the values of all terms on the right side, it requires complete calculations of the atmospheric radiative transfer. As cited by Sikorski and Kealy (2002) similar equations have been used in many atmospheric radiation models including the Low Resolution Transmittance Model (LOWTRAN) by Kneizys *et al*. (1988), the Moderate Resolution Atmospheric Radiance and Transmittance Model (MODTRAN) by Berk *et al*. (1987), and the Moderate Spectral Atmospheric Radiance and Transmittance (MOSART) by Cornette *et al*. (1994).

Equation 2.2 also indicates that it is necessary to take into account the atmospheric effects and it is advantageous therefore to make measurements in a spectral region where the atmospheric contribution is as small as possible. In most cases, the satellite-borne sensors are designed to work in atmospheric windows of the thermal region. According to Sikorski and Kealy (2002), the components I_d, I_s, and I_r are negligible for Long Wave Infra Red (LWIR) bands. Thus, only the first two terms on the right side of the above equation 2.2 are important. The first term represents the surface contribution term, and it is the grey-body radiance emitted by the earth's surface. The second term is the atmospheric contribution term, and is the vertically integrated effect of emission from every atmospheric layer modulated by the transmittance of the air above that emitting layer.

$$I(\lambda,\mu) = \varepsilon_0(\lambda,\mu)B(\lambda,T_s)\nu_0(\lambda,\mu) + \int_{\nu_0}^{1} b(\lambda,T_p)d\nu(\lambda,\mu,p) \qquad (2.3)$$

where υ_0 is the transmittance between the surface and the observing platform.

In order to infer the surface information, we must choose window channels with small atmospheric contributions. As shown in Figure 2.3 the wavelength between 3.5–4.2 µm, 8–9 µm, and 10–13 µm are typical atmospheric windows, with less atmospheric absorption. For a perfect window, the total atmospheric transmittance *υ_0 (λ,μ)* should be 1.0, and the transmittance weighting function should be 0. But as we see from Figure 2.3, the transmittances at these windows are not unity. This is mainly the result of the water vapor absorption and carbon dioxide absorption at wavelengths longer than 12 microns.

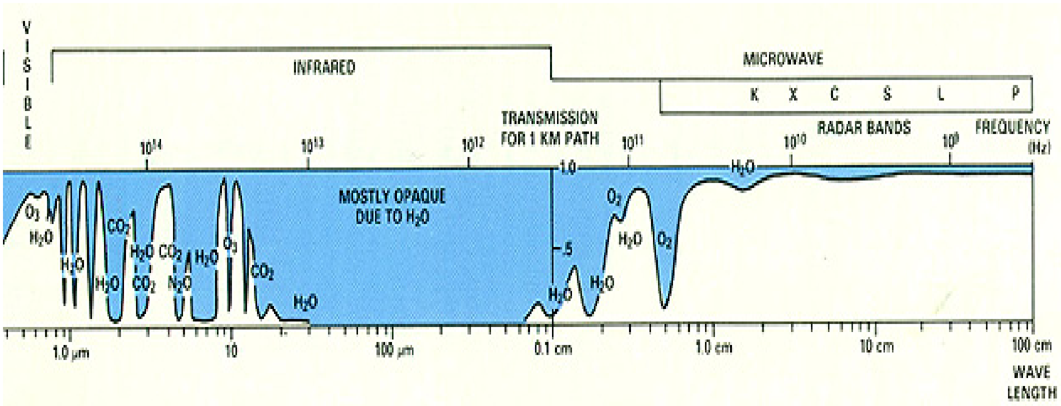

Figure 2.3: Atmospheric absorption patterns of various wavelengths (source: Sabins, 1997)

One of the major concerns in the development of LST algorithms is the considerable spectral variation in emissivities for different land surface types. Observation of emissivity spectra shows that in general, emissivity spectra with high values exhibit little variation of emissivities, while those with lower values exhibit a greater variation of emissivities, such as grass (Sikorski and Kealy, 2002). Considering brightness temperature in the window channels, it is possible to derive a true surface temperature based on Split window approach.

Assuming constant surface emissivity, these brightness temperatures approximate the true temperature and allow certain approximations to be performed. To show the fact that the true surface temperature may be represented as a *linear combination* of the two brightness bands, an expression is developed for the radiance errors introduced by the atmosphere (ΔI).

$$\begin{aligned}\Delta I &= B(\lambda,T_s) - I(\lambda,\mu) = B(\lambda,T_s) - \nu(\lambda,\mu)B(\lambda,T_s) - I_a(\lambda,\mu)\\ &= -\int_1^{\nu(\lambda,\mu)} B(\lambda,T_s)d\nu(\lambda,\mu,p) + \int_1^{\nu(\lambda,\mu)} B(\lambda,T_p)d\nu(\lambda,\mu,p)\\ &= -\int_1^{\nu(\lambda,\mu)} (B(\lambda,T_s) - B(\lambda,T_p))d\nu(\lambda,\mu,p)\end{aligned} \tag{2.4}$$

According to the Planck function we find:

$$\Delta I = \frac{\partial B}{\partial T}\Delta T = \frac{\partial B}{\partial T}(T_s - T_\lambda) \tag{2.5}$$

According to Sikorski and Kealy (2002), for an optically thin gas the following approximations can be made:

$$d\nu = d\{\exp(-k_\lambda I)\} = -k_\lambda dl \tag{2.6}$$

where k_λ is the absorption coefficient and l is the optical path-length.

Assuming that the Planck function is adequately represented by a first order Taylor series expansion in each channel window:

$$B(\lambda,T_s) - B(\lambda,T_p) = \left.\frac{\partial B(\lambda,T_p)}{\partial T}\right|_{T_s} (T_p - T_s) \tag{2.7}$$

where T_p is some arbitrary temperature close to but not equal to T_s. Substituting Equations 2.5, 2.6 and 2.7 into Equation 2.4, can obtain:

$$T_s - T_\lambda = k_\lambda \int_1^{\nu} (T_s - T_p)dl \tag{2.8}$$

where T_λ is the brightness temperature in the window band and T_s is the true temperature. Therefore, Equation 2.8 tells that the difference between the true and brightness temperature is that integral times the absorption coefficient (k_λ) for that band.

Therefore, if we select two spectral bands, we obtain two linear equations with different k_λ values to be solved simultaneously. For example, if we consider the two channels as λ=1 and λ=2, then we get:

$$T_s = \frac{k_2}{k_2 - k_1} T_1 + \frac{k_1}{k_2 + k_1} T_2 \tag{2.9}$$

showing that T_s may be expressed as a linear combination of T_1 and T_2. Because k_1 and k_2 are largely unknown or difficult to calculate, in some applications, as over the oceans, they are obtained as coefficients in regression analyses involving satellite estimates of T_1 and T_2 and surface measurements of Ts. The Equation 2.9 is similar to the Sea Surface Temperature (SST) equation derived from the split window algorithm, but can only be used for one land type, assuming the band emissivity does not vary within this land type. Sikorski and Kealy (2002) showed that for a particular land type the linear split window algorithm used in SST retrieval can be adopted for LST.

2.3.3.2 Brief review of existing algorithms

Many algorithms have been proposed and implemented for the retrieval of LST and emissivity from thermal infrared data. These methods include the two-temperature method (Watson, 1992), the temperature emissivity separation method (Kealy and Hook, 1993), the day/night method (Wan and Dozier, 1996), and the land cover regression method (Sikorski and Kealy, 2002). In particular, much research has focused on methods that use two thermal channels of the AVHRR sensor (Price, 1984; Wan and Dozier, 1989; Kerr *et al.*, 2004).

Currently, most existing LST algorithms are variants based on Becker and Li's (1990) split window technique (SWT) expressed by:

$$\begin{aligned} T_s = &\left[A1 + A2\left(\frac{1-\varepsilon}{\varepsilon}\right) + A3\left(\frac{\Delta\varepsilon}{\varepsilon^2}\right)\right]\left(\frac{T_{11}+T_{12}}{2}\right) \\ &+ \left[B1 + B2\left(\frac{1-\varepsilon}{\varepsilon^2}\right) + B3\left(\frac{\Delta\varepsilon}{\varepsilon^2}\right)\right]\left(T_{11}-T_{12}\right) + C \end{aligned} \tag{2.10}$$

where $\varepsilon = (\varepsilon_{11} + \varepsilon_{12})/2$ and $\Delta\varepsilon = \varepsilon_{11} - \varepsilon_{12}$. ε_{11} and ε_{12} are the emissivities in the 10.8 μm and 12 μm bands respectively. T_{11} and T_{12} are the brightness temperatures at 10.8 μm and 12 μm bands respectively. A1, A2, A3, B1, B2 and B3 are regression constants.

The SWT method relies on number of assumptions such as:

1) the surface is Lambertian
2) the surface temperature is close to the temperature of the lower layers of the atmosphere
3) the surface temperature remains below 305 K
4) absorption in the atmosphere is very small
5) the surface emissivity is close to unity and its spatially distribution is uniform
6) the emissivities of ε_{11} and ε_{12} (i.e. in the 10.8 μm and 12 μm bands respectively) are almost identical and $\varepsilon_{11} > \varepsilon_{12}$

The SWT method has been used successfully for sea surface temperature retrievals. However, the temperature derivation over land is more difficult than over the ocean because some of the required conditions are not usually met over land surfaces. For example, the high spatial and temporal variability of surface emissivity over land and the atmospheric water vapour (which absorbs thermal energy) significantly affect the thermal radiance reaching the sensor, thus making the LST computation error prone. The fundamental part of most split-window algorithms is based on the assumption that LST is linearly related to the brightness temperatures of two thermal channels (Liang, 2001). With the assumption that surface emissivities for these two channels are known, the split-window method can eliminate atmospheric effects for LST estimation. Other studies have revealed that when the atmosphere is moist, the traditional split-window algorithm cannot remove the atmospheric effects completely. Many efforts (e.g., Sobrino *et al.*, 1994) therefore have been made to incorporate the column water vapour content of the atmosphere into split-window formulae.

2.3.3.3 Difficulties in determining the land surface temperature

The accuracy of satellite LST measurement is limited mainly by the complexity of land surface types, the atmospheric correction, and sensor performance. It is clear from the above discussion, that the effects of LST and emissivity on thermal radiance are so closely coupled that their separation from thermal radiance measurements alone is quite difficult. In order to retrieve the LST physically from the satellite derived data, it is required to know the atmospheric profile for each pixel, and also the surface emissivity for each band. Because the surface emissivity for each band is different, the number of unknowns is always larger than the number of equations. Without any additional information, it is impossible to recover both LST and emissivity exactly. Most LST-emissivity separation studies use one additional empirical equation so that measurements plus this additional equation can be solved for one unknown. For example, the Alpha-derived emissivity (ADE) method makes use of the relation between the weighted logarithm values of spectral emissivity and the variance of spectral emissivities (see Kealy and Hook (1993) for details). The reference channel method assumes that the value of the emissivity for one of the image channels is constant and known a priori, reducing the number of unknowns to the number of equations (Liang, 2000).

The comparisons among different LST/emissivity separation algorithms have been well discussed by Gillespie *et al*. (1998) and Li *et al*. (1999). The published satellite multi-channel LST algorithms permit global LST retrievals up to 3 K measurement accuracy (Becker and Li, 1990; Dozier and Wan, 1994; Li and Becker, 1993; Wan, 1999). Therefore, satellite derived LST may be used for scientific applications with a degree of confidence.

A major limitation of LST retrieval is that it can only be done under clear sky conditions. Furthermore, it is difficult to obtain true skin LST values over the full range of land surface types. Typically, LST varies significantly on a sub-pixel scale, and over short timescales, so that the satellite retrieved LST necessarily represents a snap-shot pixel-averaged measurement at a point in time. Due to these difficulties, application of LST for soil moisture determination has been limited to few attempts. The availability of MODIS LST products however has paved the way to use LST data for broader applications including soil wetness studies.

2.3.3.4 MODIS land surface temperature products

The MODIS Land Surface Temperature and Emissivity (LST/E) product from Aqua-MODIS (e.g. MYD11A1 products) and Terra-MODIS (e.g. MOD11A1 products) provide per-pixel temperature and emissivity values on a daily basis. Temperatures are extracted in Kelvin (K) with a view-angle dependent algorithm applied to direct observations. MODIS LST algorithm claims yielding 1 K accuracy for materials with known emissivities (Wan, 1999). The view angle information is included in each LST/E product. Emissivities are estimates which are derived from applying algorithm output to database information. The LST/E algorithms use MODIS data as input, including geolocation, radiance, cloud masking, atmospheric temperature, water vapour, snow, and land cover. The theoretical basis of MODIS LST is discussed in detail by Wan (1999). Both Aqua-MODIS and Terra-MODIS LST/E products are provided daily as a gridded level-3 product in the sinusoidal projection.

The availability of daily LST as a MODIS product is very useful for soil moisture scaling studies for at least two main reasons. First, the LST inversion algorithm used by MODIS has been well documented and the methodology is available for review. Second, the data is freely accessible through the internet.

2.3.4 SATELLITE DERIVED LAND SURFACE VEGETATION INDICES

The status of vegetation gives important information on soil moisture condition and vegetation indices (VIs) may be used to describe the vegetation health. Vegetation indices are dimensionless, radiometric measures that serve as indicators of the relative abundance and activity of green vegetation. Remotely sensed spectral vegetation indices are widely used and have been of benefit for numerous disciplines interested in the assessment of vegetation biomass, water use, plant stress, plant health, crop production, and identification of biome types. VIs are also useful in estimating emissivities from space (Van de Griend and Owe, 1994b; Valor and Caselles, 1996). In order to use these vegetation indices successfully, one needs to understand the input variables used to form the indices. Furthermore, understanding of the manner in which the external environmental factors and the architectural aspects of the vegetation canopy influence and alter the computed index values is also required. The main thrust of the vegetation index (VI) is its ability to respond to subtle changes in plant health status for variable view, illumination and atmospheric conditions.

VIs can be calculated from sensor voltage outputs, radiance values, reflectance values and satellite digital numbers. Each method therefore, will yield a different VI value for the same surface conditions. Similarly, a VI calculated from data obtained over the same target, but with different instruments, may not be the same because of differences in the detector and filter characteristics of the instruments. Despite the fact that VIs were developed to extract only plant signals, other parameters such as the soil background, moisture conditions, solar zenith angle, and the atmosphere alter the index values in complex ways. Hence, any study concerned with the soil moisture status needs to carefully analyse and interpret the signatures of vegetation indices to better understand the moisture distribution pattern. Examination of spatial distribution and temporal trends of the vegetation indices over longer periods (such as the two years of the current study period) is useful and provides significant insight into regional scale vegetation water stresses across a catchment.

2.3.4.1 Theoretical basis for vegetation indices

The theoretical basis for the VI lies with the red (wavelength = 0.60-0.70 µm) and NIR or reflected IR (wavelength = 1.35-2.10 µm) contrast of the vegetation spectral reflectance signatures. When light strikes the vegetation surface, part is reflected, part is transmitted and the remainder is absorbed. The relative amounts of reflected, transmitted and absorbed light are a function of the surface and vary with the wavelength of the light. For example, most of the light in the NIR wavelengths is transmitted and reflected, with little absorbed. In contrast, light in the visible wave lengths (e.g. red) is predominantly absorbed, with some reflected and little transmitted. The decrease of red reflectance due to increase of live, green vegetation within a pixel is due to the absorption by chlorophyll. The majority of light striking the soil however is either reflected or absorbed, with minute changes with wavelength.

The amount of radiation reflected from a vegetation surface is determined by the amount and composition of solar irradiance that strikes the vegetation, and the reflectance properties of the vegetation surface. Solar irradiance varies with time and atmospheric conditions. A simple measure of reflected light is therefore not sufficient to characterize the surface in a repeatable manner. For this reason, data from two or more spectral bands are often used to form a vegetation index. VI can be calculated by ratioing, differencing, ratioing differences and sums, and by forming linear combinations of spectral band data. These techniques are intended to enhance the vegetation signal, while minimizing solar irradiance and soil background effects. Details of selected VIs are described in the Section 2.3.4.2

2.3.4.2 Review of existing indices

There are two general classes of vegetation indices: ratios and linear combinations. A Ratio VI may be the simple ratio of any two spectral bands, or the ratio of sums, differences or products of any numbers of bands. Some of these ratio vegetation indices are described in this section. Linear combinations, on the other hand, are sets of *n* linear equations calculated using data from *n* spectral bands. Details of these linear combinations may be found in Jackson and Huete (1991).

The Ratio Vegetation Index (RVI) is formed by dividing the NIR (1.35-2.10 μm) radiance by the Red (0.60-0.70 μm) radiance as shown below.

$$RVI = \frac{\rho_{NIR}}{\rho_{\mathrm{Re}d}} \qquad \textbf{(2.11)}$$

where ρ_{NIR} is NIR reflectance and ρ_{Red} is Red reflectance

To obtain an insight into the range of RVI values, for example, a healthy wheat crop has a RVI value of about 12.9 whereas dry bare soil has a value of 1.21 and bare wet soil has a value of 1.33 (Jackson and Huete, 1991). For dense green vegetation, the amount of red light reflected from the canopy is very small. As can be seen in equation 2.11, as the red band reflectance approaches zero, the ratio increases to infinity. Therefore, RVI may be useful if red reflectance light is measured with sufficient precision. However, RVI is not a very good index when the vegetation cover is sparse due to low dynamic range of the NIR/Red ratio. This low sensitivity over sparse vegetation could be enhanced by ratioing the difference between the NIR and the red band to the sum of the two bands.

The Normalized Difference Vegetation Index (NDVI) is the difference between near-infrared and red reflectance values normalized over the sum of the two (Eidenshink and Faundeen, 1994). In equation form the NDVI is given by,

$$NDVI = \frac{\rho_{NIR} - \rho_{\mathrm{Re}d}}{\rho_{NIR} + \rho_{\mathrm{Re}d}} \qquad \textbf{(2.12)}$$

The upper bound of the NDVI is one, while the lower bound is usually close to zero. Depending on the sensor characteristics and the units of the input variables (such as radiance, digital numbers, etc) the lower bound value may be slightly positive or slightly negative.

When considering the RVI and NDVI indices, Perry and Lautenschlager (1984) showed that one index can be readily transformed into the other. From the mathematical point of view, these two indices are functionally equivalent and contain the same information. Thus dividing both the numerator and the denominator of equation 2.12 by 'Red', we have

$$NDVI = \frac{RVI - 1}{RVI + 1} \qquad \textbf{(2.13)}$$

Equation 2.13 helps with better interpretation and visualization of the indices. It is evident that the NDVI is more sensitive to sparse vegetation densities than is the RVI, but is less sensitive at higher vegetation densities. Conversely, RVI is quite sensitive to the vegetation changes during the time of peak growth. Therefore, the use of same information (i.e. Red and NIR reflectance) through equation 2.13 assists in better interpretation of the index.

The strength of the NDVI is in its ratioing concept, which reduces the multiplicative noise present in multiple bands. The NDVI is sufficiently stable to permit meaningful comparisons of seasonal and inter-annual changes in vegetation growth and activity. It is a good measure of landscape patterns of green biomass and can be used to estimate landscape patterns of primary productivity (Sellers *et al*., 1992). It can also be used to predict crop yields, crop phenology (Lee *et al*., 2000), and to evaluate leaf area index. NDVI has been shown to be a good predictor of evaporation (ET) over grassland (Kondoh and Higuchi, 2001) and a good estimator of vegetation water stresses (Sandholt *et al*., 2002). However, NDVI exhibits scaling problems, and saturated signals over high biomass conditions, and it is very sensitive to canopy background variations, with NDVI values particularly high with darker canopy backgrounds. Some of these problems have been addressed by developing indices such as the soil adjusted vegetation index and the enhanced vegetation index.

The Soil Adjusted Vegetation Index (SAVI) involves the incorporation of a soil background coefficient, L, in order to remove the dependency of the NDVI on the brightness of the material underlying a vegetated canopy as follows;

$$SAVI = \frac{\rho_{NIR} - \rho_{\mathrm{Re}d}}{\rho_{NIR} + \rho_{\mathrm{Re}d} + L}(1 + L) \qquad \textbf{(2.14)}$$

The '*L*' adjustment term is based upon differential Red and NIR transmission through a canopy (Beer's law). The value of '*L*' is assumed to be 0.5 for a wide variety of leaf area index values (Huete, 1988). Later, instead of using a constant *L* factor, Qi *et al*. (1994) proposed a Modified Soil Adjusted Vegetation Index (MSAVI) with a variable *L* in order to increase the vegetation sensitivity.

The Enhanced Vegetation Index (EVI) (Liu and Huete, 1995) was developed to optimize the vegetation signal with improved sensitivity in high biomass regions and improved vegetation monitoring through de-coupling of the canopy background signal and a reduction in atmosphere influences. EVI is one of the vegetation products available from MODIS and is defined as:

$$EVI = G\frac{\rho_{NIR} - \rho_{\mathrm{Re}d}}{\rho_{NIR} + C_1\rho_{\mathrm{Re}d} - C_2\rho_{Blue} + L} \qquad \textbf{(2.15)}$$

where: ρ_{Blue} is Blue (0.44-0.50 µm) reflectance, ρ_{Red} is Red (0.60-0.70 µm) reflectance, C_1 is the correction coefficient for atmospheric resistance in Red channel, C_2 is the correction coefficient for atmospheric resistance in Blue channel, L is canopy background brightness correction factor, and G is gain factor. The C1 and C2 coefficients reflect the "atmospheric resistance" concept which is based on the wavelength dependency of aerosol effects, utilizing the more atmosphere-sensitive blue band to correct the red band for aerosol influences. The atmospheric resistance coefficient values adopted in the MODIS EVI algorithm are C_1=6 and C_2=7.5 (found to best minimize aerosol influences). Other terms in above equation are L=1 (works best for global applications) and G = 2.5. The removal of the background soil effect in EVI is similar to that of SAVI. Therefore, EVI may be considered as an improved version of the NDVI.

2.3.4.3 MODIS vegetation indices

The MODIS vegetation indices (VIs) provide consistent, spatial and temporal comparisons of global vegetation conditions. The level 3 gridded vegetation indices are standard products available to the science community. The level 3, spatial and temporal gridded vegetation index products are composites of daily bidirectional reflectances. The gridded VIs are 16- and 30-day spatial and temporal, re-sampled products designed to provide cloud-free, atmospherically corrected, and nadir-adjusted vegetation maps at nominal resolutions of 250 m, 1 km, and 28 km.

Standard MODIS products include two vegetation indices; a) the standard NDVI, which is to continue the traditional NOAA-AVHRR derived NDVI, and b) the EVI with improved sensitivity to differences in vegetation from sparse to dense vegetation conditions. Gridded VI products are also in the Sinusoidal projection.

As with MODIS LST products, the availability of MODIS vegetation indices is potentially very useful for soil moisture scaling studies.

2.3.5 SATELLITE DERIVED LAND SURFACE WETNESS INDICES

Over the last few decades, substantial research has been dedicated to the use of remotely sensed observations for evaluating soil moisture conditions at the surface, firstly by using visible and thermal infrared imagery and secondly by using active and passive microwave imagery (as discussed in Chapter 7). Studies, which employ solar reflectance measurements (e.g. Weidong *et al*., 2002) thermal infrared wavelengths (see for example Carlson *et al*., 1981; Carlson *et al*., 1995; Czajkowski *et al*., 2002; Li and Lyons, 2002), and microwave radiation (Engman and Chauhan, 1995; Ragab, 1995; Schmugge, 1998; Njoku and Li, 1999), have all shown some potential for estimating soil moisture content. Except for microwave based approaches, the other methods rely broadly on deriving soil moisture contents using land surface temperatures and/or vegetation conditions which are known to relate with soil moisture. Remotely observed land surface parameters such as LST and vegetation indices are computed from surface reflectance properties. Soil reflectance is influenced by organic matter, soil texture, surface roughness, angle of incidence, plant cover and colour, which limits the utility of such measurements for actual soil moisture content determination. Therefore, many attempts have been made to developing wetness indices rather than measuring actual soil moisture contents.

Based on thermal infrared observations, investigators have explored combinations of surface temperatures (T_s) and Spectral Vegetation Index measurements as a means to account for the variable influence of vegetation cover in soil moisture assessments (Smith and Choudhury, 1991; Carlson *et al*., 1994; Moran *et al*., 1994; Gillies *et al*., 1997; Goetz, 1997; McVicar and Jupp, 1999; Wang *et al.,* 2001; Goward *et al*., 2002, Sandholt *et al*., 2002). In most cases, there is a strong negative correlation exhibited in NDVI-T_s plots, which has been found to exist across a variety of vegetation types and sensors. A number of explanations for the negative correlation between NDVI and T_s have been given, including that it is related to the amount of energy partitioned into latent heat (Goward *et al*., 2002) and that it is driven by variations in transpiration due to differences in canopy structures (Nemani and Running, 1989), surface resistance (Goward and Hope, 1989) and soil moisture (Gillies and Carlson, 1995).

T_s and NDVI in combination can provide information on vegetation and moisture conditions at the surface. Several studies focus on the slope of the T_s/NDVI curve for vegetation/soil moisture estimation (Nemani and Running, 1989; Smith and Choudhury, 1991; Friedl and Davis, 1994). The T_s/NDVI slope is related to the evapotranspiration rate of the surface, and has also been used to estimate air temperature (Prihodko and Goward, 1997; Boegh *et al*., 1998) and areal averaged soil moisture conditions (Goetz, 1997; Goward *et al*., 2002). A scatter plot of remotely sensed LST and a VI often results in a triangular shape (Price, 1990; Carlson *et al*., 1994) or a trapezoidal shape (Moran *et al*., 1994). The location of a pixel in the T_s-NDVI space is influenced by a range of factors and many attempts have been made to furnish interpretations. While some of these attempts had a theoretical basis (Moran *et al*., 1994), others relied on simulations based on Soil-Vegetation-Atmosphere Transfer models (Gillies *et al*., 1997). Also, while some interpretations were based on *in-situ* measurements (Friedl and Davis, 1994) others were based on analysis of remotely sensed data. Consideration of the T_s-NDVI space helps the development of more meaningful indices for soil moisture status such as the Temperature-Vegetation Index (TVX; Prihodko and Goward, 1997), Temperature-Vegetation Dryness Index (TVDI; Sandholt *et al*., 2002), Water Deficit Index (WDI) and Vegetation Temperature Condition Index (VTCI). Chen *et al*. (2002) proposed the use of Diurnal Surface Temperature Variation (DSTV) together with NDVI to develop a NDVI-DSTV index which could also be used to estimate the soil moisture.

All these wetness indices may be computed at a range of scales with images from various platforms. Following is an introduction to the underlying physics of wetness indices and an overview of the wetness indices selected for the present study.

2.3.5.1 Theoretical basis for land surface wetness indices

The most widely established method for detecting vegetation water stress remotely is through the measurement of surface temperature of the vegetation.

The correlation between surface temperature and water stress is based on the assumption that as a crop transpires evaporative cooling cools the leaves below that of air temperature. As the crop becomes water stressed, transpiration will decrease, and the leaf temperature will increase. Other factors need to be accounted for in order to get a good measure of actual stress levels, but leaf temperature is one of the most important and it is easily measured with remote observations. Wetness indices therefore, aim at combining water status of the plants and ambient meteorological conditions and will yield a measure of plant water stress. Furthermore, one has to keep in mind that such wetness indices reflect the soil moisture status across the entire root zone depth rather than a particular soil layer.

It is easy to understand the underlying physics of the wetness indices by analysing the derivation of a known index. For instance, one method used to apply crop surface temperature data to irrigated agriculture is the Crop Water Stress Index (CWSI) (Jackson *et al.*, 1988):

$$CWSI = (dT - dTl) / (dTu - dTl) \quad \textbf{(2.16)}$$

where, dT is the measured difference between crop canopy and air temperature, dT_u is the upper limit of canopy minus air temperature (for a non-transpiring crop), and dT_l is the lower limit of canopy minus air temperature (for a well-watered crop).

A CWSI of 0 indicates no water stress, and a value of 1 represents maximum water stress. There are several methods to determine the upper (dT_u) and lower (dT_l) limits in the equation 2.16. One method developed by Idso *et al*. (1981) accounts for changes in the upper and lower limits due to variation in Vapour Pressure Deficit (VPD), which is calculated as the difference between saturation vapour pressure and actual vapour pressure. The lower limit in the CWSI will change as a function of vapour pressure because at lower VPDs, moisture is removed from the crop at a lower rate, so that the magnitude of cooling is decreased. Idso (1982) demonstrated that the lower limit of the CWSI is a linear function of VPD for a number of crops and locations. Using the intercepts and slopes between VPD and dT_l (or dT_u) plots for a particular crop type, dT_l and dT_u may be computed for a variety of crops as follows:

$$dT_l = \text{Intercept} + \text{Slope (VPD)} \quad \textbf{(2.17)}$$

$$dT_u = \text{Intercept} + \text{Slope } [VP_{sat}(T_a) - VP_{sat}(T_a + \text{Intercept})] \quad \textbf{(2.18)}$$

where VP and VPD have units of Pascal, $VP_{sat}(T_a)$ is the saturation vapour pressure at air temperature, and $VP_{sat}(T_a\text{+Intercept})$ is the saturation vapour pressure at air temperature plus the Intercept value for the crop of interest.

Thus, with a measure of air humidity (e.g. relative humidity, wet bulb temperature), air temperature, and canopy temperature, it is possible to determine the CWSI empirically. However, the CWSI is very sensitive to measurement error at low VPDs and should be applied with caution under such conditions. This empirical approach however has received some criticism concerning its inability to account for temperature changes due to radiation and wind speed changes. Therefore, in order to account for differences in radiation and wind speed, a theoretical method was proposed.

The CWSI may be explained by rearranging terms of the surface energy balance. Jackson *et al*. (1986 and 1988) developed an equation to predict the canopy minus air temperature difference (T_c - T_a):

$$T_c - T_a = X_1 X_2 - X_3 \quad \textbf{(2.19)}$$

where;

$$X_1 = r_a (R_n - G) / (C_v) \quad \textbf{(2.20)}$$

$$X_2 = [\gamma (1+r_c/r_a)] / [\Delta + \gamma (1 + r_c/r_a)] \quad \textbf{(2.21)}$$

$$X_3 = VPD / [\Delta + \gamma (1 + r_c/r_a)] \quad \textbf{(2.22)}$$

T_c is the crop foliage temperature (°C), T_a the air temperature (°C), r_a the aerodynamic resistance (s m^{-1}), R_n the net radiation heat flux density (Wm^{-2}), G the soil heat flux density (Wm^{-2}), C_v the volumetric heat capacity of air ($J^oC^{-1}m^{-3}$), r_c the canopy resistance (s m^{-1}) to vapour transport, γ the psychometric constant (Pa $^oC^{-1}$), and Δ is the slope of the saturated vapour pressure-temperature relation (Pa $^oC^{-1}$).

Equation 2.20 was used to obtain the upper and lower bounds for the CWSI. In the case of the upper limit (non-transpiring crop), the canopy resistance will approach infinity, so equation 2.20 reduces to

$$dT_u = r_a (R_n - G) / (C_v) \quad \textbf{(2.23)}$$

In the case of a non-stressed crop, r_c is assumed to be essentially 0:

$$dT_l = [r_a (R_n - G) / (C_v)]\ [\gamma / (\Delta + \gamma)] - [VPD /(\Delta + \gamma)] \quad \textbf{(2.24)}$$

Equations 2.23 and 2.24 can be used to determine the CWSI as given in equation 2.16. When measurements of soil heat flux are not available, under conditions of complete canopy closure, 10 percent of net radiation is assumed to be transferred to the soil or $(R_n - G) = 0.9Rn$.

The T_c-T_a approach in equation 2.19 is an attempt to use the Penman-Monteith equation with remotely sensed data and basic meteorological data. The use of the above equations to compute extreme foliage temperatures and comparison of those computed values with measured actual foliage temperatures makes it possible to estimate the ratio of actual (ET_a) to potential ET (ET_o) and infer plant water stress.

$$CWSI = 1 - \frac{ET_a}{ET_p} = \left[\gamma\left(1 + \frac{r_c}{r_a}\right) - \gamma\right] \Big/ \left[\Delta + \gamma\left(1 + \frac{r_c}{r_a}\right)\right] \quad (2.25)$$

Moran *et al*. (1994) further developed this approach to develop a concept know as Vegetation Index / Temperature (VIT) trapezoid. They found a trapezoidal shape for the scatter plot of LST and vegetation index. By interpreting the LST (composite of both the soil and plant temperatures) and spectral vegetation index space, they determined the field water deficit condition for crops with partial cover. This method is explained in section 2.3.5.2.2.

The details of CWSI reveal the strong physical principles behind the wetness indices. Thus, computation of wetness indices using spatial data should provide a reasonable assessment of soil wetness condition in a given region at a certain time. Such information is important to understand the relative soil wetness conditions at each pixel. Understanding of relative wetness conditions provides an acceptable way of scaling measured soil moisture. Particularly, when disaggregating areal average soil moisture values, wetness indices computed at higher resolution may be used as covariates.

2.3.5.2 Review of existing indices

2.3.5.2.1 Thermal inertia approach

Methods for inferring near-surface soil moisture content from soil surface temperatures derived from thermal infra-red data have shown some success, as soil moisture influences the thermal properties of the soil. The amplitude of the day-night temperature difference has been found to have a good correlation with soil moisture content in the 0 - 2 cm and the 0 - 4 cm layers of the soil (Schmugge *et al*., 1980).

Soil surface temperature is primarily dependent on the thermal inertia of the soil, which is a measure of the soil's resistance to temperature changes. Many studies have demonstrated the use of thermal inertia to retrieve surface moisture from remote measurements of surface temperature and numerous ancillary measurements combined within an appropriate model (Price, 1980; Van de Griend *et al*., 1985; Carlson, 1986; Flores and Carlson, 1987; Norman *et al*., 1995; Czajkowski *et al*., 2002). For example, the analytical approach of Price (1980) requires satellite based data such as surface albedo, surface emissivity and routine meteorological observations such as air temperature, vapour pressure, wind speed etc. Because the thermal-inertia models are based on thermal properties, they are expected to work best on bare soils where heat conduction dominates (Norman *et al*., 1995). Thermal-inertia moisture-availability methods have been applied to vegetated surfaces by several investigators including Carlson (1986). Norman *et al*. (1995) viewed the thermal inertia as an empirical parameter because vegetation tends to decouple the atmosphere from the soil substrate.

However, present understanding of the thermal-inertia moisture-availability methods is limited for vegetated surfaces, particularly in how it is affected by different vegetation types, densities etc. An error analysis by Carlson (1986) suggested an error of about ±20% in thermal inertia and estimated moisture availability from these types of models. For this reason the thermal inertia approach appears less promising for use in scaling applications.

2.3.5.2.2 Water Deficit Index

Moran *et al*. (1996) further developed the concept of CWSI for application to partially-vegetated surfaces by incorporating measurements of surface reflectance in addition to surface temperature. By computing the maximum and minimum soil temperatures associated with minimum and maximum evaporation rates, respectively and plotting these four temperatures against a spectral vegetation index (e.g. SAVI), they formed a trapezoidal shape. They noted that all possible values of surface temperature for both full-cover and partially vegetated surfaces at a particular time are enclosed within the trapezoid as shown in Figure 2.4. The X-axis shows the difference between surface (T_s) and air temperature (T_a) and Y-axis shows the percentage of vegetation cover (approximated by a VI). Whilst the top side of the trapezoid represents full vegetation cover, top left and right vertices represent well-watered and non-transpiring conditions respectively. The lower side of the trapezoid represents bare soil conditions. The lower left and right vertices reflect wet soils and dry soils respectively. Thus the trapezoid encompasses all possible situations under field conditions. With the measurement of surface composite temperature (T_s) at point C in the Figure 2.4, they showed that it was possible to equate the ratio of actual to potential evaporation with the ratio of distances CB and AB. Moran *et al*. (1996) defined this ratio as the Water Deficit Index (WDI).

To justify the approach, they used certain assumptions to describe the trapezoidal shape scatter diagram. They assumed that measurements of vegetation cover are linearly related to VI. Also they considered that T_s-T_a as a linear function of vegetation cover, the canopy (T_c) - air temperature difference (T_c-T_a) and the soil (T_o) – air temperature (T_o-T_a) difference. This assumption helps defining the left and right boundaries of the trapezoid. Further, they assumed that for a given net radiation R_n, VPD and r_a the variations in T_c-T_a and T_o-T_a are linearly correlated with variations in evapotranspiration (ET).

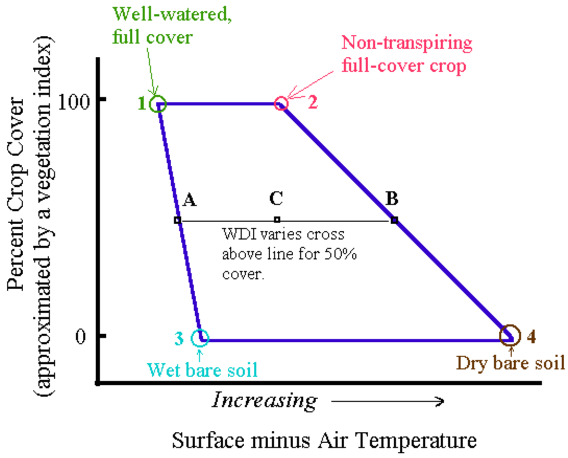

Figure 2.4: Illustration of the water deficit index trapezoid.

The main strengths of this approach appear to be its strong physical basis and its ability to map water deficit characteristics in heterogeneous landscapes. Therefore, this concept is potentially suitable for local and regional scale applications. However, the need for additional ground based measurements to define the four vertices of the trapezoid may have some implications for its practical use.

2.3.5.2.3 Vegetation Temperature Condition Index

Based on the triangular space of LST and VI, Wang *et al.* (2001) has proposed the Vegetation Temperature Condition Index (VTCI). It is defined as:

$$VTCI = \frac{LST_{NDVIi\,\max} - LST_{NDVIi}}{LST_{NDVIi\,\max} - LST_{NDVIi\,\min}} \qquad \textbf{(2.26)}$$

where: $LST_{NDVI\,i\,max}$- LST_{NDVIi} = ***A***, and $LST_{NDVI\,i\,max}$- $LST_{NDVI\,i\,min}$ = ***B*** in Figure 2.5. $LST_{NDVI\,i\,max}$ and $LST_{NDVI\,i\,min}$ are the maximum and minimum LSTs of pixels which have the same $NDVI_i$ values respectively. LST_{NDVIi} denotes LST of a chosen pixel whose NDVI value is $NDVI_i$.

The significance of VTCI is its relationship with the LST changes of pixels with a specific NDVI value. According to Wan *et al.* (2004) it can be physically explained as the ratio of temperature variations among the pixels. Thus, the numerator of equation 2.26 gives the difference between the maximum LST and the LST of one pixel. Similarly, the denominator of the equation 2.26 gives the difference between maximum and minimum LSTs across all pixels.

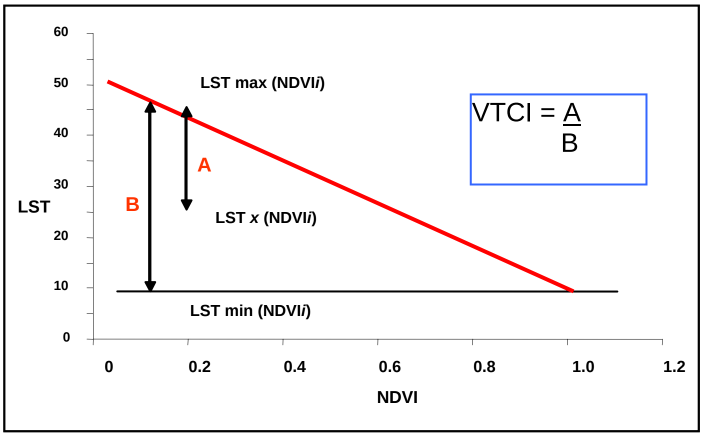

Figure 2.5: Schematic representation of the computation of Vegetation Temperature Condition Index.

The LST_{max} line in Figure 2.5 is the 'warm edge' of the triangular space of LST-VI combinations. Physically it is characterized by dry conditions with little soil moisture available to plants (i.e. plants are under stress). On the other hand, LST_{min} can be regarded as the 'cold edge' where there is no limitation of water for plant growth (Gillies *et al*., 1997; Wang *et al*., 2004). The values of VTIC range from 0 to 1; lower values indicate less soil moisture and, higher values indicate high soil moisture values.

The main thrust of the VTCI is two-fold. First, it involves a simple computational procedure and it does not depend on any ancillary data. Second, it has a strong physical background. The difficulty faced in the computations of other moisture indices such as the defining of the four vertices of the WDI trapezoid is not relevant to the VTCI approach. Land surface moisture indicators such as VTCI are therefore potentially very useful for soil moisture scaling applications and can readily be computed from remotely sensed images.

2.3.5.2.4 Vegetation Temperature Dryness Index

Sandholt *et al.* (2002) have proposed the Temperature Vegetation Dryness Index (TVDI). They defined TVDI as:

$$TVDI = \frac{T_S - T_{S_{\min}}}{a + bNDVI - T_{S_{\min}}} \tag{2.27}$$

where T_{Smin} is the minimum LST in the triangle, defining the wet edge, T_S is the observed LST at the given pixel, NDVI is the observed NDVI at the given pixel, and *a* and *b* are parameters defining the dry edge modelled as a linear fit to data ($T_{Smax} = a + b$NDVI) as shown in Figure 2.6. T_{Smax} denotes the maximum LST for a given NDVI. The parameters *a* and *b* are derived from pixels from an area large enough to represent the entire range of surface soil moisture contents from wet to dry as well as the entire range of surface vegetation conditions from bare to fully vegetated surfaces.

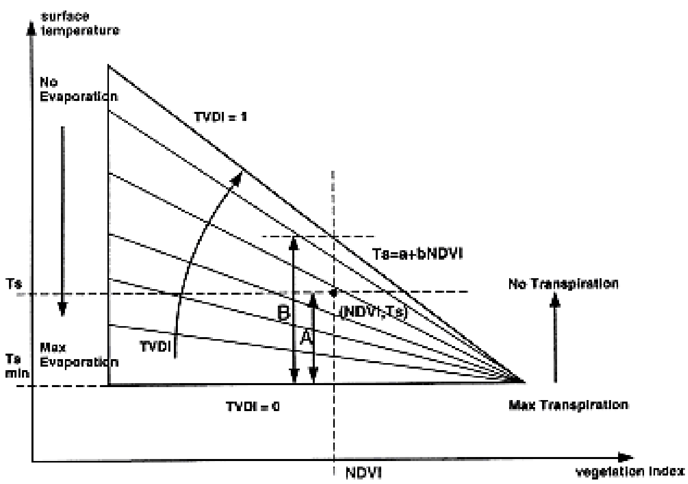

Figure 2.6: Schematic representation of the TVDI. For a given pixel, TVDI is estimated as the proportion between A and B as given in Equation 2.27 (from Sandholt *et al.*, 2002).

The main advantage of the TVDI method is the independency of ancillary data, similar to the VTCI method. This method, however, requires a large number of remotely sensed observations to define the boundaries accurately. Application of this method is therefore, more time consuming and requires more data processing.

2.3.6 REMARKS – REMOTE SENSING TECHNIQUES FOR SOIL MOISTURE MEASUREMENTS

From the above discussion, it is clear that remote sensing techniques may be applied to gain information on soil moisture conditions. While visual and thermal techniques are useful in collecting information on wetness characteristics of land surface, microwave based techniques provide quantitative measurement of soil moisture. It is therefore important to consider both measured near surface moisture (i.e. 0-1 cm from microwave sensors) and the computed wetness indices (from visual and thermal remote sensing) for catchment scale soil moisture studies. However, one has to keep in mind the differences of moisture representation. While microwave measurements provide true quantitative measures of moisture at 0-1 cm top soil layer, wetness indices provide an indication of moisture over the entire depth of the root zone.

Microwave techniques however are associated with two major concerns. First, the measurement represents very large areas (for e.g. AMSR-E 6.9GHz channel has Instantaneous Field Of View (IFOV) of 76 km x 44 km) and the scale is not suitable for catchment scale hydrological applications. In order to use these measurements for catchment scale studies it is required to disaggregate the pixel level measurements. Second, the microwave-based soil moisture measurements are limited to the 0-1 cm near surface soil layer. The moisture content of top 0-1 cm soil layer, however, does not always accurately represent the soil moisture status at the deeper layers, for example, for the 0-30 cm layer (or root-zone depth), which is more important to hydrologists as well as to farmers. For this reason, visual and thermal techniques seem very useful, as they are capable of representing the soil moisture content at deeper layers through vegetation indices.

Vegetation indices are useful in obtaining information on soil moisture status because non-water stressed crops usually show a higher vegetation index value than water stressed crops. Particularly for large land areas with a few dominant crops such as in natural pasture lands, vegetation indices may be considered as reflecting the soil moisture status of a uniform root zone depth. Vegetation indices also reflect the historical rainfall distribution and therefore indicate recent soil moisture status. For a given situation however, vegetation index alone may not sufficiently explain the soil wetness condition. When combined with LST, vegetation indices provide a much better assessment of soil wetness than when used on its own. Therefore, indices such as VTCI, WDI and TVDI are very useful in describing the land surface wetness conditions.

Wetness indices are aimed at combining water status of the plants and ambient meteorological conditions and yield a measure of plant water stress which represents soil moisture availability. Wetness indices therefore reflect the soil moisture status across the entire root zone depth rather than for a particular soil layer. Thus, computation of wetness indices using spatial data should provide a reasonable assessment of soil wetness conditions in a given region. Such information is important to understand the soil wetness conditions at each pixel. The main advantages of wetness indices computed from visual remote sensing are the higher resolution and ease of computation (e.g. VTCI). High-resolution relative wetness conditions provide an opportunity to use the indices as surrogate variables for scaling of measured soil moisture. For example, when disaggregating areal average soil moisture values, wetness indices computed at higher resolution may be used as covariates.

It can therefore be concluded that integration of wetness indices and microwave measurements may potentially provide the best solution towards estimation of areal average soil moisture contents at various scales.

2.4 SOIL MOISTURE ESTIMATION TECHNIQUES

From previous sections, it is clear there are no methods to measure soil moisture directly on the required time and space scales for hydrological studies. Point measurements of soil moisture yield information on the temporal variation of moisture content in the soil profile at a specific point. However, accurate estimation of the spatial variation in soil moisture profiles from these point measurements is difficult. In contrast, remote sensing observations provide information on the spatial distribution of soil moisture at a range of scales. Nevertheless, they do not provide timely information on the temporal variations of the moisture content or direct information on soil moisture content beyond the top few centimetres of the soil profile. Therefore, soil moisture is often inferred from hydrological models which have sufficiently sophisticated land-surface parameterizations.

A wide variety of hydrological models for predicting soil moisture have been used over the past decades, ranging from simple conceptual models to complex systems of partial differential equations that require sophisticated numerical algorithms and powerful computers. There are essentially three different approaches that can be used: lumped models, semi-distributed models and distributed models. Lumped models do not represent spatial variability and are therefore less useful in soil moisture predicting studies. Distributed models represent the spatial variability of soil moisture using a moisture distribution function. This distribution function can be derived from the catchment topography, as in the case of the TOPMODEL (Beven and Kirkby, 1979) or it can be a theoretical distribution function as in the case of the Variable Infiltration Capacity (VIC) model (Wood *et al*., 1992). When the distribution function is based on the catchment topography, theoretically, it is possible to map simulated soil moisture across the catchment to produce a catchment scale soil moisture distribution pattern. According to Western and Grayson (2001), there has not been any detailed testing of soil moisture patterns actually simulated by models such as TOPMODEL. However, a number of studies have compared various terrain index patterns with soil moisture patterns based on the TOPMODEL approach (Western *et al*., 1999; Sulebak *et al*., 2000; Pellenq *et al*., 2003). Models with distribution functions that are not related to the topography do not allow mapping the computed soil moisture patterns. However, the statistical distribution functions used in these models can be compared to the equivalent distributions derived from measurements (Western *et al*., 1999). The common feature of distributed models is that they can incorporate the spatial distribution of various inputs and boundary conditions, such as topography, vegetation, land use, soil characteristics, rainfall, and evaporation, and produce spatially detailed outputs such as soil moisture fields. One of the major problems of using distributed modelling is parameter identification, owing to a mismatch between model complexity and the scale of data which is available to parameterize, initialize, and calibrate models, and to uncertainty and error in both models and observation data.

The ability to accurately describe large-scale variations in soil moisture is severely restricted by process uncertainty in model physics and the limited availability of appropriate soil moisture data. Hence, to improve the model predictions of soil moisture status in both spatial and temporal scales, data assimilation approaches are being used (Reichle *et al*., 2001b; Walker *et al*., 2001a). Data assimilation is the incorporation of observations into a numerical model with the view of providing the model with the best estimate of the current status of the modelled system. Two major types of data assimilation techniques, intermittent initialising of model process and continuous dynamic assimilation, are currently used. It is expected that the use of data assimilation techniques should give better estimates of the soil moisture status than which can be achieved from either the numerical modelling approaches or observations alone. Methods for soil moisture data assimilation include direct insertion, Kalman filter (Walker *et al*., 2001a), extended and ensemble Kalman filters (Reichle *et al*., 2002) and optimum interpolation. Many studies have used data assimilation techniques to estimate soil moisture, particularly to address the profile soil moisture estimation (Walker, 1999; Walker *et al*., 2001a; Li and Islam, 2002). The combined use of hydrological modelling and sequential assimilation of intermittent soil moisture measurements appears to be a most promising approach to solve the problem of soil moisture estimation. Another extension to data assimilation are the downscaling techniques. It has been shown that a data assimilation technique such as the four-dimensional variational approach is a promising methodology to downscale passive microwave measurements for sub-pixel soil moisture estimation (Reichle *et al*, 2001a).

Hydrological models can provide timely information on the spatial soil moisture distribution without the necessity of field visits. However, the error associated with their estimates is a critical disadvantage. Thus, Walker (1999) suggested that integration of modelling and measurements would provide the best solution towards estimation of soil moisture content.

2.5 PROBLEMS WITH CURRENT MEASUREMENT / ESTIMATION TECHNIQUES

Current ground based soil water measuring techniques such as TDR, neutron scattering, or thermo-gravimetric methods can provide very accurate information of SWC with depth over time. However, the measurement volume is a fraction of a square meter. Many point scale observations are therefore needed to ‘upscale’ to hillslope or regional scales and to derive true moisture patterns across a catchment. Up-scaling of point scale soil moisture measurements is always difficult and requires a well-articulated model to capture the spatial variability of soil properties and topographic parameters.

On the other hand, soil moisture estimation using passive microwave remote sensing data is limited by several factors, with one of the most important being the large footprint of microwave radiometers. Hence, low-resolution soil moisture estimates from passive microwave data need to be disaggregated to produce a representative sub-pixel pattern of soil moisture. Disaggregation of large-area soil moisture estimates also requires an appropriate model. Currently, there is no such acceptable model available and more research is required to implement such an approach in various agro-ecological regions. Furthermore, the poor vertical representation (e.g. 0-1 cm) of top soil layer in soil moisture estimation from microwave data is another major problem. Often, the derivation of profile moisture patterns from the near surface estimates must rely on hydrological models. This is always difficult and often, derived profile soil moisture values may not represent the true pattern due to mismatch between modelling scale and the input data scales.

Most soil water models have been developed to describe one-dimensional soil water dynamics at a point, and are often applied to experimental plots, over time. Application of these models to larger areas requires that they be extended or extrapolated, which has been described as ‘upscaling’ by Blöschl and Sivapalan (1995). Upscaling soil water models will never be straightforward, due to large spatial variability of relevant soil properties observed in nature. The combined effect of high spatial variability and small-area representation of actual measurements (i.e. smaller measurement support) affects model input values, such as soil texture or depth, as well as model outputs such as soil water content

(SWC). As a result, model outputs are known only with considerable uncertainty. Seyfried (1998) believes that the model uncertainty is due to more attention being directed toward determining how processes should be represented in soil water models than to how the spatial variability and distribution of those processes should be represented, although both are critical. Uncertainty in parameter values is transmitted throughout the model to the final output. Hence, uncertainty in SWC limits model calibration and verification accuracy. Finally, the quality of soil water model output is compromised by these two uncertainties. Poor model output may be partly due to lack of information concerning the effect of scale on spatial variability of soil moisture.

2.6 SOIL MOISTURE SCALING

According to Blöschl and Sivapalan (1995), scale refers to a characteristic time or length of a process, observation, or model. When large-scale hydrological models are used to make predictions at small-scale, or vice versa, unacceptable results may be found due to scale differences. Thus scale issues in hydrology stem from the fact that the mathematical relationships describing a physical phenomenon are scale dependent (Gupta *et al*., 1986). Similarly, use of point scale measurement of state variables such as soil moisture in hydrologic models introduces a serious error component into the final output.

Two extreme choices of soil moisture measurements are available, i.e. accurate *in-situ* point-scale continuous measurements and large area-average discrete measurements. Many catchment scale hydrological applications however, require some in-between scale (e.g. 1 km^2) of soil moisture content preferably over the entire root zone depth of the dominant plant type. Often, this preferred scale of soil moisture is either not available or not measurable. Such information therefore has to be generated from the collected field data. The most appropriate method of extracting such preferred scale soil moisture data is by adopting a suitable scaling technique. The availability of areal average estimates of soil moisture together with point scale observations has therefore opened up new science questions such as how to relate soil moisture observations obtained at different scales, and how to disaggregate large-area observations.

2.6.1 WHY SOIL MOISTURE SCALING?

Soil moisture scaling has been the focus of numerous investigations since the early 90s. There has been increased interest in modeling and measuring SWC across the landscape for a variety of applications. Because SWC has a major impact on hydrologic processes such as infiltration, groundwater recharge, and overland flow, there is great interest in catchment–scale SWC estimates (Wood, 1995). Most of these applications involve modeling and measurement of SWC at varying spatial scales. Because the interactions between soil, vegetation and atmosphere vary both spatially and temporally, the scale at which the soil moisture information is collected may not be necessarily immediately usable for hydrological models. Often, it may require disaggregation of the moisture information down to sub pixel levels or aggregate point observations to derive large scales average moisture values. Thus, similar to other environmental variables, measured soil moisture data often require some scaling. Before implementing any scaling technique however, it is important to understand how scaling affects our initial measurements and the final results.

Hydrological processes occur at a wide range of scales and span about eight orders of magnitude in space and time (Klemes, 1983). For example, precipitation occurs at scales ranging from 1 m (cumulus convection) to 1000 km (frontal systems). Many hydrologic processes have similar length scales as precipitation but have delayed time scales. The time scale increases from infiltration excess to saturation excess to subsurface flow to groundwater controlled flows. From a hydrological perspective at least six causes of scale problems may be identified (Buggman 1997; Schulze, 2000; Wallender and Grismer, 2002). These are described below.

(1) ***Spatial heterogeneity in surface/subsurface processes***

Natural and human-affected landscapes exhibit considerable heterogeneity (or patchiness). This heterogeneity is due to a range of processes and the rates at which they occur. These include the spatial and/or temporal variability of:

- topography (altitude, aspect, slope, position in the landscape etc)
- soils (infiltration rate, water holding capacity, dependent inter alia on geology , topographic position etc)
- rainfall and irrigation (frequency of occurrence and seasonal pattern, persistence of wet or dry days, duration, intensity, average amount, etc)
- evaporation (dependent on atmospheric factors such as solar radiation, water vapour deficit, wind etc)
- land use (affects factors such as leaf area index, canopy interception of rainfall, canopy height, structure and root distribution, the degree of imperviousness, effects of tillage practices, drainage etc).

(2) ***Surface responses are non-linear at different scales***

Clear distinctions in responses may be found between hillslope processes (both on and below the surface) and channel processes. Some processes occur in an episodic manner (e.g. rainfall), others in a cyclic way (e.g. evaporation, wetting and drying of soil), still others in an ephemeral way (e.g. lateral flows) or in a continuous way (e.g. groundwater movement). Furthermore, it may be observed that certain responses are rapid (e.g. surface runoff), others are at the time scales of days (e.g. lateral flows) or months (e.g. groundwater movement). As a result of these different rates of process responses, the system shows a high degree of non-linearity. When a natural system is affected by land use changes or construction of new reservoirs / irrigation canals, the extent of this non-linearity increases.

(3) ***Processes may require threshold scales to occur***

Processes such as surface runoff generation involve two distinct processes. Each of these two processes has a different threshold in order to occur. For example, overland flow on high ground is a process which occurs at a point in the landscape when rainfall intensity exceeds the infiltration capacity of the soil (i.e. Hortonian flow). Saturated overland flow, alternatively, is an areal process which requires a minimum upslope area over which lateral flows can accumulate and move down-slope to saturate the area around the channel, with any rain then falling on the variably-sized saturated zone being converted to overland flow.

Similar to the surface flow generation process, subsurface flow consists of two components (i.e. interflow and base flow) as well as two distinct thresholds. In this case, the threshold for interflow (i.e. subsurface lateral flow down a hillslope) to occur will depend, inter alia, on soil horizonation, and different hydraulic conductivities along a hillslope toposequence (e.g. the crest, scarp, mid-slope, or foot-slope). The slope shape (e.g. concave, convex, or uniform) also influences this. On the other hand, the threshold for base flow is determined by aquifer properties, the amount of recharge to groundwater, and whether or not the groundwater level is “connected” or “disconnected” to the channel.

(4) ***Dominant processes of concern may change with scale***

In small catchments, hillslope processes are influenced by slope, soil and/or land use properties. The shape of the hydrograph of these small catchments is determined by these factors together with the occurrences and characteristics of localised small-scale storm events. Often, the hydrograph shape of large catchments is determined largely by hydraulic characteristics of channels and reservoirs. In addition, occurrences and properties of large-scale regional rains of frontal and cyclonic origin also affect the shape.

(5) ***Development of emerging properties***

New properties may emerge due to mutual interaction of small-scale properties among themselves. The edge effects between landscape patches are due to this. These show different properties at a large scale compared to the small scale. For example, the enhancement of evaporation at the edge of a well-irrigated field surrounded by a dry environment is an emerging property. Similarly, in a large irrigated area, evaporation would be suppressed by a vapour blanket of air with a reduced vapour pressure deficit. This is due to the development of so called ‘oasis effect’ or the emergence of a new situation.

(6) ***Disturbance regimes***

Scaling problems immediately arise as a consequence of disturbance regimes being superimposed over a natural system, for example by the construction of dams or contour bunds, draining of fields, drastic changes in land use etc.

Apart from these hydrological concerns, scaling problems also appear due to the scale chosen for the measurements and the technique used (i.e. *in-situ* or remote techniques). For example, use of satellite data for the characterisation of land surface parameters is associated with at least two fundamental concerns. First, land surface parameters exhibit important spatial and temporal variability at scales smaller than the scale of measurement (Hu and Islam, 1997; Hu *et al.*, 1997). Several studies have provided substantial information on the spatial variability of vegetation, soil moisture and other terrain attributes at scales smaller than 100m. Second, large-scale models that use remotely sensed land parameters or ground based observations do not require them at the same spatial resolution at which sensors are required to operate. In such a situation, an aggregation methodology is needed to ensure the incorporation of spatial heterogeneity. In addition, interpreting soil moisture patterns obtained from microwave images may be complicated due to poorly defined penetration depth which can vary across the pixel. Therefore, with both remote sensing and field monitoring, difficulties arise because the scale at which the data are collected is different from their intended usage (Western and Blöschl, 1999).

2.6.2 SPATIAL VARIABILITY

In a broad sense, spatial variability may be categorized into two types: deterministic and stochastic (Seyfried and Wilcox, 1995). Deterministic variability has also been called systematic (Wilding and Drees, 1983) or organizational (Blöschl and Sivapalan, 1995). It implies that spatial variability is known and may be related to geographical position or expressed in the form of a mathematical relationship, such as the elevation along hillslope.

In contrast, stochastic variability conveys the existence of random variability. Stochastic variability may be further subdivided into two categories based on spatially dependency: spatially dependent and spatially independent. Spatial dependency is quantifiable and generally uses variogram techniques to estimate the dependency. Accordingly, it indicates that samples spatially closer to one another are more similar than those further apart. Spatially independent variability may include small-scale variability and other ‘unexplained’ variability. It is possible to relate these parameters in a form of equation:

$$Z(q) = m(q) + \varepsilon'(q) + \varepsilon''(q) \tag{2.28}$$

where q is the position in x, y or z dimensions, $Z(q)$ is the parameter value (e.g., SWC), $m(q)$ is the deterministic component, $\varepsilon'(q)$ is the spatially dependent component, and $\varepsilon''(q)$ is the spatially independent component (Burrough, 1993).

Despite the fact that the spatial variability of soil properties increases with scale (Beckett and Webster, 1971; Wilding and Drees, 1983) neither the amount of increase nor how it is partitioned among the three terms in above equation (Eq. 2.27) has been widely reported in the literature. In general, it is expected that $\varepsilon''(x)$ will increase with scale. This may be due to increased number of interactions or unexplained processes (Wilding and Drees, 1983). It has been proposed that, at some scale, this term is dominant, and spatial variability may be viewed as strictly random. Wood *et al*. (1990) defined this scale as representative elementary area (REA). At this scale, spatial data (data tied to specific geographic locations) is not required, and spatial variability may be portrayed by statistical parameters such as the mean and standard deviation (Seyfried, 1998).

The magnitude of $\varepsilon'(x)$ is also expected to increase with scale. This however, will be highly dependent on the description of $m(x)$ and the sample spacing (Russo and Jury, 1987). In addition, considerable change may appear in the deterministic component with scale and location (Seyfried and Wilcox, 1995). In general, when this component is comparatively large, spatial data is required, and distributed modelling approaches are more appropriate.

2.6.3 THEORY OF SCALING

Clear understanding of fundamental scaling principles is very important in any study that uses theory or models developed at one particular scale to assess conditions or processes at other scales. These scale issues stem from the fact that the mathematical relationships describing a physical phenomenon are scale dependent (Gupta *et al*., 1986). This is particularly important for hydrological studies. The methods used to measure spatially and temporally variable environmental properties such as soil moisture, to obtain model input parameters, and to predict the processes represented by models may not necessarily be appropriate for the scale of interest. Therefore, if model results are used blindly, without any consideration of how they might be affected by the scales used in model development and data collection, it can introduce significant problems in the final outputs. For example, when large-scale models are used to make small-scale predictions, or vice versa, problems may arise. Furthermore, model parameters may change as the degree of watershed disaggregation changes, and thus are scale-dependent.

The transfer of information across scales is known as scaling. Scaling and its effects on hydrological modelling are linked to the land surface heterogeneity. This heterogeneity is small at small scales and large at large scales. The greater the degree of heterogeneity, the smaller the scale would have to be to represent such variability. Hydrologic models use parameters to represent entire watersheds, whereas data on watershed characteristics is collected only at a limited number of field locations (Singh, 1995). This field data is difficult to transform into a collective representation of the entire watershed. This leads to the question of what scale enables the best hydrologic simulation. As the spatial scale of model application increases from a small area to a large area, the hydrologic response becomes less sensitive to the spatial variability of the inputs.

The term 'scale' has been used differently in cartography, hydrology and soil science. Singh (1995) defines scale as the size of a grid cell or subcatchment within which the hydrologic response can be treated as homogeneous. If this scale is too small, it will be dominated by local physical features, if it is too large, it will ignore significant hydrologic heterogeneity caused by spatial variability. This definition is incomplete and focuses only at the model application level.

Blöschl and Sivapalan (1995) have proposed a conceptual framework to define scale and the required transformation of information in modelling real environmental process patterns. According to Blöschl and Sivapalan (1995), the term *scale* refers to a characteristic time or length of a process, observation, or model. Hence, scale can be used either as a qualitative term (e.g. a small-scale process) or as quantitative measure in space dimensions. The spatial dimension, represented as co-ordinates in *x, y, z* directions, varies temporally along a time domain. Therefore, scaling is a change in either spatial or temporal scale and has a certain direction and magnitude. Up and down scaling describes the direction of scale change. The scale change requires methods such as interpolation and extrapolation or aggregation and disaggregation. To describe actual properties transformed in a change in scale, it is needed to uniquely specify the space dimension of a measurement or model application. In order to do this, a *scale triplet* concept is introduced. (Figure 2.7) The space triplet in a time domain is limited to its *spacing* (e.g. distance and/or time step between single samples), *extent* (overall coverage and duration of sampling) and *support* (integration volume or area and also time increment of each sample). When measurements are taken to produce the space triplets of data that represent a true pattern of a natural process, scaling appears automatically and inherently as an issue (Figure 2.8).

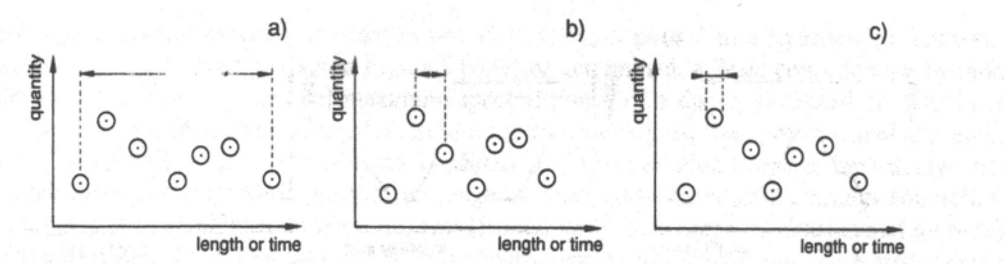

Figure 2.7: Scale triplet concept: (a) Spatial (or temporal) extent; (b) spacing (or resolution); and (c) integration volume (or time constant). The figure is taken from Blöschl and Sivapalan (1995).

It is important to further understand the types of scales and their characteristics as well as the interactions between the types of scales. Concepts described below are taken primarily from Blöschl and Sivapalan (1995) and from Schulze (2000).

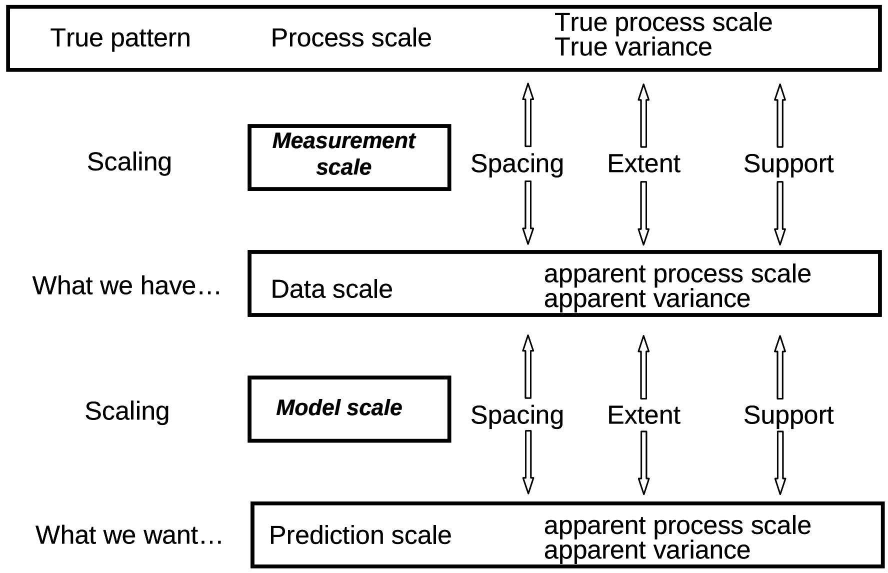

Figure 2.8: Occurrences of scaling in measuring and modelling. Transfer of information is indicated as arrow (→) and biases in model prediction happen during the transformations. The figure is adapted from Blöschl and Sivapalan (1995).

Process scales may be defined as the scales at which natural phenomena occur. These scales are not fixed, but vary with the process. Assessment of a given process for a particular scale of interest requires an understanding of land surface processes and their spatial and temporal dimensions. For example hydrological processes occur at a wide range of scales. Space scale and time scale relationships of these hydrological processes are shown in Figure 2.9, which is adapted from Blöschl and Sivapalan (1995). Processes at the lower left of the Figure 2.9 show short characteristics space and time scales. Because of the short space and time characteristics features, the processes at this part of the figure lead to patterns that are very patchy. On the other hand, slower and large scale processes (top right of the figure) shows spatially more coherent patterns which vary slowly. In order to analyse the situation with soil moisture processes, the original figure proposed by Blöschl and Sivapalan (1995) has been slightly modified by adding a space-time relationship of soil moisture by Skøien *et al.* (2003). Accordingly, as far as time is concerned, soil moisture is close to stationary with characteristic scales of the order of 2 weeks. In space however, soil moisture shows non-stationary behaviour and ‘patchy’ patterns. Skøien *et al.* (2003) noted that soil moisture characteristics in space were close to fractal over the extent sampled, about 1 km in their study.

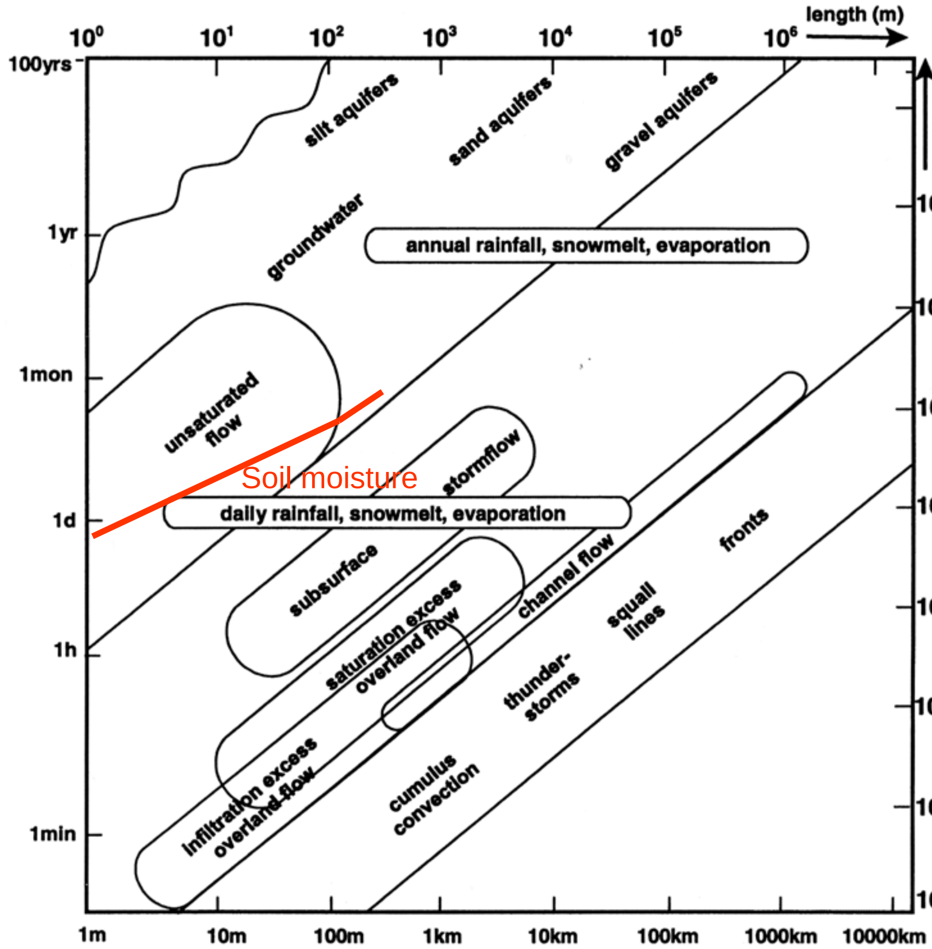

Figure 2.9: Schematic representation of relationships between spatial and temporal scales of hydrological processes (from Blöschl and Sivapalan, 1995) shown together with soil moisture (Skøien *et al.*, 2003).

Data or observation scale is that scale at which one has chosen to collect samples or observations and to study phenomena. Observation scales are determined by constraints such as: (1) logistics; (2) technology; and (3) perception. Usually, observation or measurement scale is quite inflexible in a given circumstance. The most suitable way of using scaling methods to analyse, understand and predict natural processes has its basis first in accurate and precise measurements. In reality, scaling happens inherently whenever a measurement technique is used to observe the behaviour of a natural process at a particular scale of interest. A well-designed measurement program therefore considers the scale triplet of spacing, extent and support at the very inception of the measurement program. This helps accurate representation of the dynamics of the natural process in space and time based on the intended use of the data. Measurement instruments are designed to record some characteristic of an object to certain accuracy and a precision. One has to realise that any measurement method is by its nature inexact.

It is possible to describe the relationship between process and observation scales using a diagram such as Figure 2.10 proposed by Blöschl and Sivapalan (1995). In this figure curved lines represent actual processes, circles represent the observation resolution, and squares represent the observation area (or observational grain) of the samples. The curve (a) represents situations when observational resolution is less than the process scale. This situation may present when too frequent observations are made and thus representing 'noise' rather than 'signal'. The result therefore, is an underestimation of variance. The curve (b) shows the situation of making too many observations or adoption of smaller observational resolution than the process scale. The true processes are therefore, not identified as they are shown as trends in the data. In addition, variance of the process may be underestimated. The last curve (c) shows the situation of the observational grain or coarseness exceeding the process scale. If the squares are visualised as AMSR-E soil moisture estimates, the actual soil moisture processes (e.g. redistribution) occurring within the pixel have been excessively smoothed and the information has been largely aggregated. One does not, for example, know the distribution of wet areas and dry areas within the pixel.

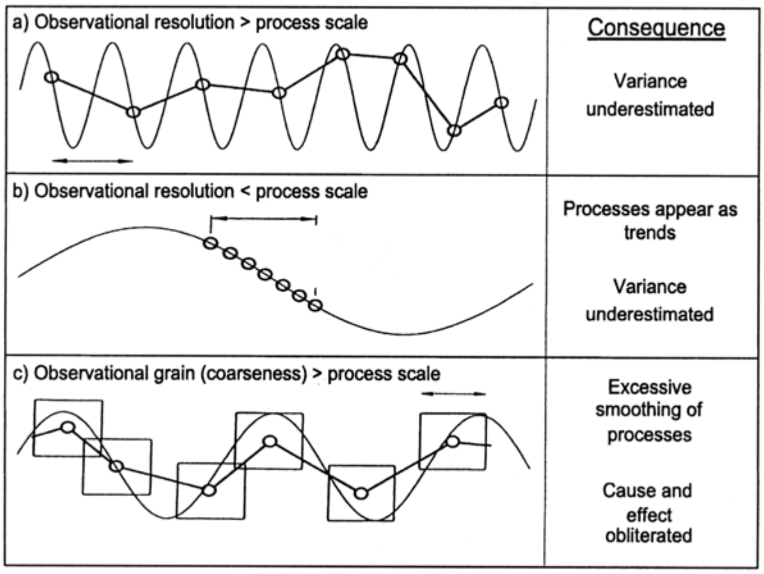

Figure 2.10: Observation (shows as small circle) vs. process (represents as a wavy line) scale relationships: (a) Greater observation resolution than the process scale; (b) smaller observation resolution than the process scale; and (c) larger observational grain than the process scale (from Blöschl and Sivapalan (1995).

Prediction or modelling scale: As discussed above, scaling occurs automatically at the initial measurement or data collection stage. Then a further scaling step occurs in modelling. The space triplet of predictions is based on model input consisting of already scaled measured data as well as data modified by model functions at the chosen scale. Hence, the predictions inherit a multiple transformation when representing a natural process. As a result, although the true pattern of a natural process at the true process scale has a true variance, both measured data and predictions have different process scales and variances. The ratios of measurement to process scales and model to process scales are important because they provide an indication of the degree of impact of the scale effect (Blöschl and Sivapalan, 1995). This scaling theory appears very logical and therefore, fundamental ideas of this theory guide the steps required to successfully address scaling issues in soil moisture.

Due to strong dependence, each scaling step affects the apparent representation of a true process in space and time. Most *in-situ* measurement techniques are typically designed to record soil moisture at the smallest possible spatial and temporal increments, in accordance with the objectives of the measurement program. Decisions taken in designing a measurement program, such as whether to collect spatial data to the nearest 1 mm, 1cm, 1m or 1000m and to temporal scales of 1 second, 1 minute, 1 day or 1 month, are based on the availability of measurement techniques at each level, economic capacity, and the expected details required meeting the research objectives.

Processes occur in natural landscapes which usually consist of spatially heterogeneous areas with structure, function, and temporal changes that are also scale-dependent (Turner, 1989). Because of this reason, the observed processes are the outcome of a combined effect of processes and controls at a range of scales. These complex geographical phenomena may be simplified into distinct aerial units by adopting regionalization procedures (Bernert *et al.*, 1997). Similar to discretization, regionalization procedures include inherent scale decisions, which in turn impact later stages of the analysis. Therefore all discretization techniques used in measuring natural properties and all regionalization decisions should be formulated and implemented properly. This ensures supply of information in an optimum way for the specific scale of interest.

2.6.4 REVIEW OF SELECTED IDEAS ON SOIL MOISTURE SCALING

The importance of soil moisture for hydrological applications and the availability of affordable measuring methodologies have triggered many field studies and provided soil moisture data sets at various scales. This has paved the way to address new science questions and to introduce new procedures for analysis of soil moisture data. A number of soil moisture studies have been conducted across the globe using actual field data as well as synthetic data. Some selected studies are presented in following sections.

2.6.4.1 Representative Elementary Area concept

Statistical self-similarity as well as the threshold scale at which a statistical representation can be considered an adequate replacement for the actual pattern of variability may be used to understand the scale issues. Wood *et al*., (1988, 1990) proposed the 'representative elementary area' (REA) concept. They defined REA as: "*the critical scale at which implicit continuum assumptions can be used without explicit knowledge of the actual patterns of topographic, soil, or rainfall fields. It is sufficient to represent these fields by their statistical characterization"*. Thus, REA is the scale at which the variance in some characteristic response variable between areas of a given scale stabilises with increasing scale. The REA concept assumes that the aggregation of those sub-REA responses will be a linear integration, even though the responses themselves may be nonlinear. At an early stage, modelling studies reported that the REA threshold level of about 1 km represented a 'fixed type' scale. However, working on a scaling of surface soil moisture in the 525 km^2 catchment in Oklahoma, Wood (1995) reported a REA threshold level of 5-10 km with multiscaling behaviour. Many argued that there is no *a priori* reason why a fixed REA scale should exist (Blöschl *et al*., 1995; Beven, 1995). In fact, process considerations suggest that REA may be expected to vary between storms with the correlation length scale of the inputs. This concept suggests that an area can be represented by the statistical distribution properties of the responses within it rather than detailed consideration of every individual point in space. The REA concept seems interesting for applications in hydrological modelling. However, there are no clear guidelines on which models are appropriate for use at the REA scale. This thesis therefore does not study the REA concept further.

2.6.4.2 Application of temporal stability

It would be an advantage to find a way to predict large scale soil moisture averages from only a few sensors located at representative sites. The question is how to find such representative sites. The representativeness of a soil moisture monitoring site may be established by analysing the temporal stability characteristics of measured data (Vachaud *et al*., 1985; Grayson and Western, 1998; Cosh *et al*., 2003). The primary method for determining the temporal stability of a soil moisture field is the mean relative difference plot. This plot represents the ability of a particular soil moisture sensor location to estimate the average over the catchment. Based on the approach by Grayson and Western (1998) and Cosh *et al*. (2003) the mean relative difference is defined as:

$$\bar{\delta}_{*,j} = \frac{1}{n}\sum_{i=1}^{n}\frac{S_{i,j} - \bar{S}_{i,*}}{\bar{S}_{i,*}} \quad \textbf{(2.29)}$$

where,

$\bar{\delta}_{*,j}$ = mean relative difference at the j^{th} site

S_{ij} = i^{th} sample of n samples at the j^{th} site within the study region

$\bar{S}_{i,*}$ = computed average among all sites for a given date and time, i

Grayson and Western (1998) argued that if temporal stability could be established in a catchment, a small number of permanent soil moisture monitoring sites could be used to predict catchment averages in a reliable way. Temporal stability can be used to assess how well any point in a population represents the average. For example, this technique may be used to investigate the idea that a soil moisture field maintains its spatial pattern over time. For a specific site, the value of soil moisture for a day is compared to the average of all sites (without that site) to compute the relative difference. Then a mean relative difference for that site is determined. This variable gives a direct measure of how a particular site compares to the average of a larger region, whether it is consistently greater or less than the mean and how variable is that relationship. Good sites are characterised by zero mean relative difference and small standard deviations. Therefore, the best sites and the worst sites may be identified to represent the catchment behaviour.

This approach helps to estimate the catchment average moisture content with good accuracy using a single point, if one can determine this point *a priori*. In addition, if they exist, identification of such individual locations facilitates validating large footprint satellite estimates of soil moisture.

It is also important to assess the spatial stability of the soil moisture fields. This may be described with the Spearman rank coefficient. Spearman's Rank Correlation is a technique to test the direction and strength of the relationship between two variables. It shows whether any on set of numbers is related to another set of numbers. For measured soil moisture fields, this coefficient may be used to calculate the correlation of site ranking from one day to the next. Therefore it is possible to assess the spatial stability of the soil moisture distribution over the entire catchment or study area. Cosh *et al*. (2003) have applied the Spearman rank coefficient (r_i) to assess the spatial stability of measured soil moisture at any location (see S_{ij} in equation 2.29) as follows.

$$r_i = 1 - \frac{6 \times \sum_{i=1}^{n} (R_{i,j} - R_{i,j'})^2}{n(n^2 - 1)} \qquad \textbf{(2.30)}$$

where,

R_{ij} = rank of the soil moisture S_{ij} at location i on day j
$R_{ij'}$ = rank of the same location i for day j'
n = total number of days

Negative values of computed Spearman rank coefficient indicate negative correlation, and positive values indicate positive correlation.

The idea of temporal stability is very useful in identifying a representative soil moisture site from a monitoring network within a catchment or at a subcatchment level. The main advantage of this concept is the confidence of using soil moisture measurement from a single site in a catchment for catchment scale applications such as water balance studies. Also, this concept may be used in long-term field studies to minimize the site maintenance cost by continuing the measurement only at the representative sites. However, the recently developed temporal stability concept requires further studies with long-term data sets.

This thesis is based on a soil moisture data collected from a network of monitoring stations and therefore provides an opportunity to study the applicability of temporal stability characteristics. The Chapter 5 of the thesis will investigate the application of temporal stability concept for various subcatchments. In addition, Section 7.7.3 will investigate the applicability of this concept for the validation of satellite-based AMSR-E soil moisture measurements.

2.6.4.3 Statistical and geo-spatial applications

Geostatistics is a set of techniques for the analysis of spatial data (Atkinson and Lewis, 2000). Many studies have attempted to develop soil moisture scaling methods using simple geostatistical methods with varying success (Bardossy and Lehmann, 1998; Western *et al*., 1998a; Western *et al.*, 1998b; Anctl *et al*., 2002). In general standard geostatistical techniques such as regularization and variogram analysis have studied by those researchers and have confirmed that these techniques are indeed applicable for organized soil moisture fields. Variograms help to characterise spatial variance as a function of the separation (lag) of the data points. The sills in the variogram, if they exist indicate that the process is stationary. In addition, correlation length measures spatial continuity of the variable of interest. Nevertheless, such methods based on multi-normal random fields cannot be used to bridge the scales over which the measurements are made and if used, may lead to systematic biases (Western *et al.*, 1998a; Blöschl *et al.*, 1995). The implications of a particular choice of interpolation method for soil moisture have been studied by Bardossy and Lehmann (1998). Their use of techniques like co-kriging and external drift kriging shows that with sparse data the interpolated patterns vary enormously depending on which method is used.

Central to geostatistical techniques is the assumption that the variable under consideration is a spatially correlated random variable. In the case of soil moisture however, this is not necessarily a valid assumption. Many studies have revealed that soil moisture is spatially organized (Western *et al*., 1998a; Blöschl and Grayson, 2001). For example, soil moisture is often organized topographically and this can be seen as wet areas in valley bottoms and near the streams.

Therefore, geostatistical techniques may not always provide the ideal solution. However, at present, these are the best techniques available for the purpose.

In an another study, Sulebak *et al*. (2000) investigated the relationship between measured soil moisture and the primary and secondary topographical parameters within two small drainage basins. Two different models were established, with the primary topographic parameters slope, aspect, and profile curvature as regression variables yielding the best results. However, the study did not include the potentially dominant attributes such as soil texture, distribution of vegetation type and elevation, which generally influence the soil moisture distribution, particularly for non-homogeneous land cover and soil texture regions and/or regions with large elevation differences. Moreover, the soil moisture distribution model was not related back to average soil moisture content for the area of interest, meaning that the relationship would not hold for other soil moisture conditions.

It appears that the geostatistical techniques are promising for soil moisture scaling applications. Implementation and evaluation of these techniques however, require large amount of spatially-distributed soil moisture data which is far beyond the scope of the field monitoring program of this thesis.

2.6.4.4 Process-based scaling concepts

Many scaling studies have been performed using data from three-dimensional water and energy models. Fully distributed, lumped and semi distributed models have been tested for a wide range of conditions. Among the simplest methods the Variable Infiltration Capacity (VIC) model (Wood *et al.*, 1992; Kalma *et al.*, 1995) and TOPMODEL (Beven and Kirkby, 1979) approach are widely used. The VIC model is very simple because it only provides a statistical explanation of the subscale soil moisture variability. The VIC model in its original form is based on saturation excess and is less suitable for applications where overland or Hortonian flow dominates over the saturation excess condition. However, there are extensions to the original model which take care of this issue (Liang *et al*., 2003). Conversely, the TOPMODEL concept uses saturation excess flow conditions and offers the possibility of interpreting the variability of soil moisture in terms of the topography. Pellenq *et al.* (2003) studied the application of TOPMODEL concepts for the disaggregation of soil moisture. By considering the topography and soil depth, they noted that topography alone could not explain the variability in near-surface soil moisture. This was particularly true for the lower reaches of their small study catchment. However, inclusion of soil depth information such as storage capacity improved the retrieval of local moisture patterns. It may be also useful to study the applicability of important modelling parameters such as the wetness index in the TOPMODEL rather than the complete model for soil moisture scaling applications. Chapter 4 of this thesis will therefore investigate the application of wetness indices for soil moisture scaling.

2.6.4.5 Spatial organizations and patterns

Studies of spatial distributions of soil moisture have reported organization of moisture field to form patterns (Western *et al.*, 1998a; D'Odorico *et al.*, 2000; Grayson and Blöschl, 2000). These patterns are not permanent and the characteristics of a pattern may change over time. Also, these patterns have a special meaning and attempts have been made to characterise them in terms of continuity and connectivity features. According to Western *et al.* (1998a) "*continuity relates to the smoothness of a spatial pattern while connectivity relates to interconnected paths through the spatial pattern*". For instance, soil moisture study in the Tarrawarra catchment (10.5 ha) in south-eastern Australia has revealed occurrence of both continuity and connectivity during wet periods but only continuity during dry periods (Western *et al.*, 1998a). According to Grayson and Blöschl (2000), during wet periods (winter in this example) surface and subsurface lateral flows occurs, particularly in gullies, which produces a topographically organised pattern highlighting the continuity and connectivity feature. In dry periods (summer in this example), however, there is a minimum of lateral redistribution and fluxes are essentially in a vertical plane, which produces a pattern that is not related to topography. As a result, the connectivity feature disappears and a random moisture pattern is present. This is very important observation where one can use this approach to evaluate the field representativeness of upscaled or disaggregated soil moisture estimates. In the absence of area average measured soil moisture data to validate the scaled soil moisture estimates, interpretation of soil moisture patterns based on continuity or randomness properties provides an indirect way of validating the results. Analysis and interpretation of soil moisture patterns are therefore essential ingredients in soil moisture scaling.

It is worth further analysing the continuity and the connectivity properties to better understand the soil moisture patterns in a catchment. In general, geostatistics tools such as semivariogram analysis are used to describe the continuity feature. Traditional semivariogram approaches however do not capture the connectivity property because it is a structural feature. Approaches such as indicator geostatistics may be applied to characterise connectivity (Western *et al.*, 1998a). The term connectivity indicates the extent to which connected features such as mosaics or arbitrary bands having similar values are present in a spatial soil moisture patterns (Western *et al.*, 2001). Understanding of continuity and connectivity features of soil moisture fields are important for soil moisture scaling studies. It is clear that simple statistical techniques are not adequate for describing continuity and connectivity features of soil moisture fields.

Another important characteristic of soil moisture spatial patterns is that they span a wide range of space and time scales (Grayson and Blöschl, 2000). According to Grayson and Blöschl (2000) different types of patterns are encountered at different temporal and spatial scales and these are associated with different processes.

Furthermore, soil moisture patterns may take either unimodal or bimodal distributions whenever the system is forced by important interannual fluctuations in the rainfall regime (D'Odorico *et al.*, 2000). The presence of two modes is the signature of a dynamic switching between two preferential states, characterized by either wet or dry average soil moisture conditions. The dry mode seems to correspond to soil moisture status close to the permanent wilting point of some vegetation species. Proper scaling studies thus need to consider the probability distributions of moisture fields. This is useful observation for validating predicted soil moisture patterns in a given catchment.

2.6.5 OUTSTANDING ISSUES TO BE ADDRESSED

Soil moisture scaling approaches such as REA, temporal stability, geostatistical methods, and process-based methods have not been tested over a wide range of soil moisture, soil texture, and land cover conditions. Because the interactions between soil, vegetation and atmosphere vary both spatially and temporally, the scale at which the soil moisture information is collected may not be directly converted to a different scale. Thus, it is important to understand the performance of these scaling approaches in various catchments with a range of soil moisture, soil texture, and land cover conditions.

In addition, none of the scaling methods presented in Section 2.6.4 include the near-surface average soil moisture measurements from very large footprints such as those from the 25km passive microwave AMSR-E footprints. Passive microwave data from AMSR-E hold great promise for estimating soil water content for two reasons: the strong physical basis and the high temporal resolution. This type of large area averaged soil moisture estimates may be used in catchment scale lumped models or models run at a coarse resolution, but may not be suitable for distributed or semi-distributed models. Often, distributed hydrologic models require sub-grid scale average soil moisture estimates. As the passive AMSR-E is the most recent addition to the earth observation system, neither sub-grid scale surface moisture data nor acceptable downscaling methods exist. Therefore, methods need to be developed for downscaling these large-scale measurements to the appropriate scale. This may be possible with the wetness indices such as VTCI derived from space-borne sensors NOAA or MODIS. Chapter 8 will therefore investigate the disaggregation of AMSR-E with wetness indices.

There, are at least two other fundamental problems associated with soil moisture scaling. First, there is the issue of inadequate field measurements. This is particularly true for the point-scale ground-based soil moisture data and leads to attempts to develop an upscaled soil moisture product from a limited number of field measurements in large catchments. Because of the higher cost involved with field data collection, the number of sites will often be determined by available funds and not by the actual number of sites actually required. Second, there is the lack of data at appropriate scale to check the validity of scaled moisture estimates.

For example, when evaluating the results of up-scaled small area measurements of 0-30cm soil moisture to 10m or 100m or 1km scale, based on current soil moisture measurement technology there is no physical method with which one can measure the area-average soil moisture of 0-30cm depth over 10m or 100m or 1km area. Thus in this situation we need better ways to assess spatial soil moisture predictions. Perhaps by establishing multiple scaling relationships from point scale to hillslope scale, sub catchment and catchment level, one may obtain new insight into the assessment of soil moisture predictions. Studies are therefore needed to explore the multi-scale behaviour of soil moisture in a catchment.

There are many unanswered questions related to upscaling and downscaling. Some of these questions are listed below:

- When is a simple linear model sufficiently accurate for upscaling?
- Are soil moisture fields obtained from point scale measurements transferable to large scales? When is this possible and how should it be done?
- How do averages vary with scale?
- How does soil moisture variability change with scale?
- How can observations made at two scales be reconciled?
- How does one validate large area soil moisture measurements with point data?
- How many sites are required to characterise area average soil moisture?
- Can we use the soil moisture from a catchment average soil moisture measurement site with confidence to represent soil moisture at different scales?
- What length of records is required to identify a catchment average soil moisture measurement (CASMM) site?

This thesis will attempt to address these questions.

2.7 CONCLUDING REMARKS

Measurement of soil moisture seems very simple, yet, at the same time soil moisture measurements are not easy to obtain at the required temporal and spatial scales and their interpretation is subject to spatial and temporal variability. For this reason, soil moisture measurement often needs to undergo some form of scaling to match the data with the intended modelling application. Thus, relationships are required to develop between soil moisture indicators with respect to different spatial and temporal scales, to extrapolate data to larger scales, and to disaggregate large-area measurements.

It is clear that none of the existing soil moisture measuring/estimation techniques is ideal for catchment scale modelling applications. Further, there is no standard method for either upscaling point measurements of soil moisture or downscaling spatially averaged or lumped observations of soil moisture. Moreover, most of the studies mentioned in Section 2.6.4 have been conducted in small catchments of < $1km^2$ with very few studies for areas over $1km^2$, and no studies for very large catchments (e.g. >1000 km^2). Therefore, there are significant problems in relating a limited number of point scale soil moisture measurements across a large catchment. Similarly, problems exist in the transferring of remotely sensed large-area soil moisture measurements from the scale of the footprint to a smaller scale. New techniques are therefore required for disaggregation of large-area soil moisture measurements.

The absence of a well established field procedure to measure soil moisture in a large area is another major concern. Because of this, it is difficult to validate the upscaled or downscaled moisture estimates. In case of passive microwave measurements, airborne data collected at various scales may be used to validate the satellite derived large area measurements such as those from AMSR-E. In the absence of *in-situ* data at the required scale, it may be possible to explain the soil moisture patterns across the catchment with reference to land surface characteristics such as terrain, soil type and land use.

Scaling methods need to be developed to produce soil moisture grids of about $5x5m^2$ resolution for detailed hillslope-scale studies and of about $1km^2$ pixels for catchment-scale studies. These methods should cover a range of soil moisture, soil texture, and land cover conditions in order to better understand the soil moisture scaling behaviour under natural conditions. Furthermore, such studies should include the recently introduced large-area soil moisture estimates such as the recent 25km passive microwave AMSR-E data. Supplanting current ground based soil moisture measurements techniques with passive microwave radiometry in future will require improved understanding of soil moisture scaling methods.

In summary, our understanding of scaling methods is not yet adequate to establish standard methods for aggregation/disaggregation of soil moisture estimates over large catchments. Hence, there is a need for further study of the scaling methods between soil moisture estimates at various scales. This thesis addresses soil moisture scaling methods at the larger catchment scale (about 6540 km^2). This thesis attempts to develop techniques to upscale ground-based point-scale soil moisture measurements up to 1 km^2 scale. This thesis also studies the prediction of catchment average soil moisture from CASMM sites. This study further explores the application of terrain based concepts for soil moisture scaling at hill slopes. Finally, it also focuses on developing new methods to disaggregate large area soil moisture measurements.

Soil moisture scaling essentially leads to generation of new soil moisture patterns. Development, assessment and interpretation of these new soil moisture patterns require new methodologies and new insights. This thesis therefore attempts to interpret catchment scale soil moisture patterns in Chapters 4, 6, and 8.

CHAPTER THREE

3. EXPERIMENTAL PROGRAM IN THE GOULBURN RIVER CATCHMENT

This chapter presents an overview of the experimental program in the Goulburn River Catchment. It summarises the key variables that were measured between January 2003 and December 2004. The collection of an adequate data set for characterising the soil moisture behaviour at each site for applications of scaling studies was the primary motivation behind this field investigation. Additionally, ground based soil moisture data were collected for the AMSR-E soil moisture validation study described in Chapter 7 and the disaggregation study of large area soil moisture measurements discussed in Chapter 8.

3.1 INTRODUCTION

Despite the importance of soil moisture, it is not a variable routinely measured in climate stations. Measurement of soil moisture is more expensive than the measurement of environmental variables such as rainfall or air temperature and soil moisture measuring sensors often require site specific calibrations. Furthermore, field measured soil moisture is not a variable which can be readily applied over a large area as is done with rainfall or air temperature. Because of these reasons, soil moisture is not considered as a priority measurement at many climate stations.

Recent advances in soil moisture measuring technology and in understanding the importance of soil moisture in water resources management and water conservation and for modelling studies have led to introduce a new trend: many farmers and researchers are now concerned with obtaining soil moisture information on a routine basis.

There have been several studies across the globe on the spatial and temporal variability of soil moisture. However, soil moisture studies in Australia are very limited. Australia is a dry continent and a considerable proportion of the population benefits directly or indirectly from agricultural or farm based activities. The scientific value and the diversity of the flora and fauna in Australia are unique. In this context, adequate scientific knowledge on spatial and temporal soil moisture behaviour is indispensable. However, the knowledge of soil moisture behaviour across Australia is very limited and most published studies have been confined to small catchments (for e.g. Tarrawarra – 10.5 ha, Nerrigundah – about 10 ha). Furthermore, most of the reported studies were conducted over a limited period and long-term soil moisture trends are therefore difficult to predict. Hence, to fill this gap in knowledge of soil moisture behaviour in Australia, a number of well-planned and dedicated soil moisture studies are required.

3.2 RESEARCH PROGRAM ON SCALING AND ASSIMILATION OF SOIL MOISTURE AND STREAM FLOW

The Scaling and Assimilation of Soil Moisture And Streamflow (SASMAS) project in south eastern Australia is a research program dedicated to develop new methodologies for meaningful estimation of spatial distribution and temporal variations of soil moisture content through a combination of modelling, field observations and data assimilation (see Rüdiger *et al*., 2003). The program has been supported by the Australian Research Council (Discovery Project DP 0209724). NASA assisted in the establishment of half of the monitoring sites by providing data loggers and sensors.

The SASMAS project area is located in the Goulburn River Catchment (GRC) in South-East Australia. There are several factors that influenced the selection of GRC as the study region, with the most important reasons being its distance from the ocean and its vegetation cover. A field site too close to the ocean or other large water bodies would experience a mixed pixel response within the satellite footprint. This is particularly important for remotely sensed passive microwave data such as data from the Advanced Microwave Scanning Radiometer for Earth observing system (AMSR-E) due to its large instantaneous field of view (~70 km). Water surfaces and saturated air masses near the water bodies have significantly different radio-brightness responses to that of soil. As a result, affected pixels generally indicate much higher soil moisture levels than exist in reality. The GRC is more than 100km away from the coast, and is not affected by coastal influences. Furthermore, there are no large water bodies within the catchment. Secondly, the relative large area of predominantly low to moderate vegetation cover in the northern half of the catchment makes it ideal for soil moisture studies based on remote sensing techniques and the validation of AMSR-E footprints. Finally, the locations of the majority of monitoring sites of the GRC are less than about 200 km from the University of Newcastle. The selection of GRC is therefore, a good compromise for a long-term soil moisture related study.

The GRC has been instrumented since September 2002 and monitoring will continue at least till late 2007. The catchment monitoring includes surface and root zone soil moisture, soil temperature, rainfall, and standard meteorological information including temperature, humidity and radiation, and streamflow measurements.

3.3 LOCATION OF STUDY AREA AND HYDROLOGIC IMPORTANCE

The GRC is located in south-eastern Australia. The Goulburn River is one of the main tributaries of the Hunter River which reaches the sea at Newcastle (see Figure 3.1). The Goulburn catchment is important as it takes in over 30% of the Hunter River catchment and contributes 23% of the Hunter river flow (HVRF, 2005). The 6,540 square kilometres of the catchment extend from 31° 46'S to 32°51'S and 149°40'E to 150°36'E, with elevations ranging from 106m in the floodplains to 1257m in the northern and southern mountain ranges.

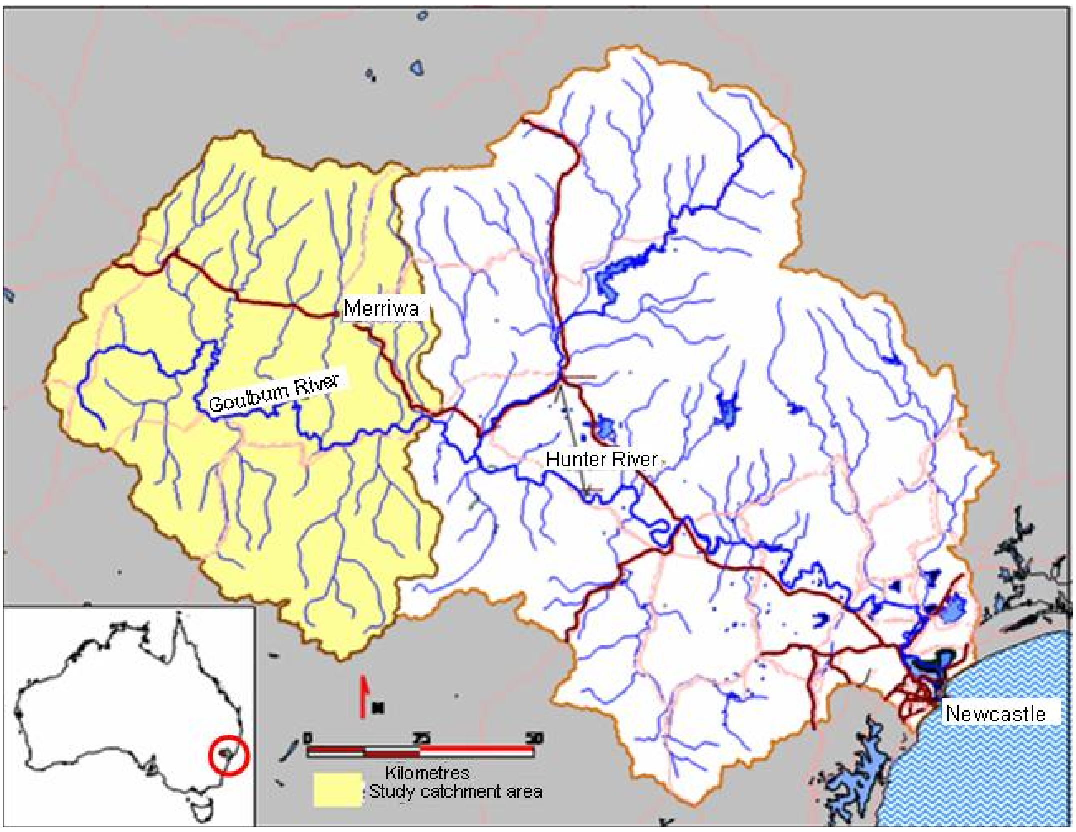

Figure 3.1: Map of the Goulburn River Catchment of the Hunter River.

Located within a subhumid area, GRC is vulnerable to frequent and prolonged droughts. To gain an insight into the severity and the duration of past droughts for the study area, Table 3-1 shows drought declarations for the Merriwa area by the Rural Lands Protection Board (RLPB) from 1952 to 1994. The catchment has also been seriously affected by the severe drought that prevailed in the region from 2002 to mid 2003. Table 3-1 gives an indication of the critical importance of soil moisture information to the farming community and for regional planning purposes. Therefore, a comprehensive study of soil moisture behaviour within the GRC is essential for better understanding of droughts in the region.

Table 3-1: Drought declarations for Merriwa area by the Rural Lands Protection Board from 1952 to 1994.

Year	Jan	Feb	Mar	Apr	May	Jun	Jul	Aug	Sep	Oct	Nov	Dec
1952-56												
1957												
1958												
1959-64												
1965												
1966												
1967-69												
1970												
1971												
1972												
1973-74												
1975												
1976-79												
1980												
1981												
1982												
1983												
1984												
1985												
1986												
1987-90												
1991												
1992												
1993												
1994												
Occurrences	9	6	8	10	10	12	13	14	10	11	8	6
No of years	42	42	42	42	42	42	42	42	42	42	41	41
As a %	21%	14%	19%	24%	24%	29%	31%	33%	24%	26%	20%	15%

Source: http://www.agric.nsw.gov.au/reader/drought-climate

Note: Light grey areas indicate that only part of the area was drought declared for that period.

3.3.1 THE GOULBURN RIVER CATCHMENT

The GRC has two distinct parts. Whilst the northern part of the catchment has rolling topography and is mainly cleared for cropping and grazing purposes, the southern part of the catchment is largely covered by woodlands and forests. As seen in Figure 3.1, the Goulburn River runs in an easterly direction while its tributaries are aligned in a north- south direction. Thus, the catchment is dominated by easterly and westerly aspects as seen in Figure 3.2. The main tributaries in the northern part include Halls Creek, and Merriwa, Krui, Bow and Munmurra Rivers, whereas tributaries in the southern area include Widden Brook, Baerami Creek, and Wollar and Bylong Rivers.

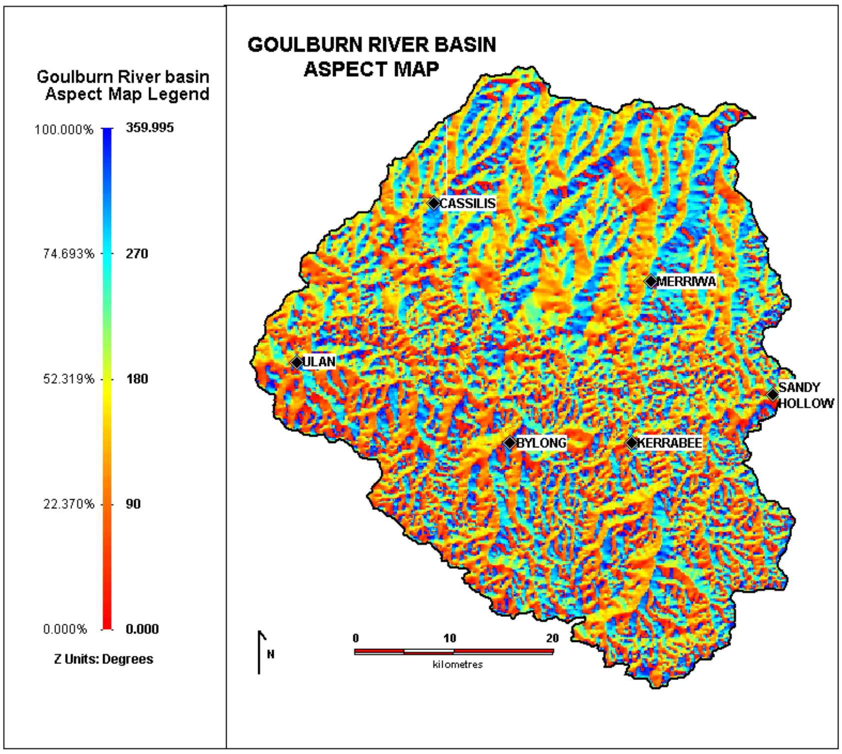

Figure 3.2: Aspect map for the Goulburn River Catchment (legend – degrees measured in clockwise direction from north).

3.3.2 CLIMATE

The general climate within the region can be described as subhumid with significant variation in the annual rainfall throughout the catchment. While the average annual rainfall in most of the catchment is approximately 700mm, it varies from 500mm to 1100mm depending on altitude. Major rainfall events generally occur in October and November with an average precipitation of 50mm, while the monthly average precipitation in July is 40mm. As indicated in Table 3-1**,** temporal variability of rainfall is generally high in GRC. The average annual Class A pan evaporation for the study region is about 1800mm. The minimum monthly pan evaporation is reached in July with an average of 75mm and the maximum can be observed in January reaching 250mm. Monthly mean maximum temperatures reach approximately 30°C in summer and 14°C in winter, with minimum values of 16°C and 2°C, respectively. Except for elevated areas, frost is unlikely to occur during daytime in winter, but night-time minimum temperatures in winter are frequently less than 0°C.

3.3.3 TOPOGRAPHY, LANDFORMS AND SOIL PROPERTIES

The geology of the Goulburn River Catchment comprises two main types: the northern half which is predominantly Tertiary basalt and the southern half which is dominated by rocks of the Triassic age laid down as sediments in lagoons and consisting of sandstone, conglomerate and shale. The region's land forms show a close relationship to geology and climatic history. Four main types of country can be identified: the northern boundary of the Liverpool Ranges, Merriwa Plateau, the Central Goulburn Valley, and the sandstone country in the southern half of the catchment (Story *et al*., 1963). The Liverpool Ranges are characterized by a rugged and basaltic landscape. The area rises over 1200m above sea level, and localized plateaus exist despite the characteristic rugged topography. The Merriwa Plateau is located between the Liverpool Ranges and the Central Goulburn Valley, comprising rolling country and hill country on basaltic topography (see Figure 3.3). Its elevation ranges between 450m to the north and 300m to the south. The hilly parts with savannah woodland on rather shallow cracking clays constitute the Ant Hill land system and the undulating parts in the more open valleys with eucalypt tree savannah and deep cracking clays forms the Bow land system. The Central Goulburn Valley is located between the Merriwa Plateau and the sandstone country as a belt about 30 km wide with irregular plateaux and ridges. The Greenhills and Roscommon land systems occur in this region. The southern part of the catchment consists of rugged mountains on Triassic sandstone. The dominant land system in the sandstone country is the Lee's Pinch land system with rugged ridges and deep cliff-walled valleys. The distribution of soils within the GRC is shown in Figure 3.4.

A detailed soil landscape map for the catchment can be found at http://www.dlwc.nsw. gov.au/care/soil/ssu/pubstat/hunter_central_rivers_index.htm.

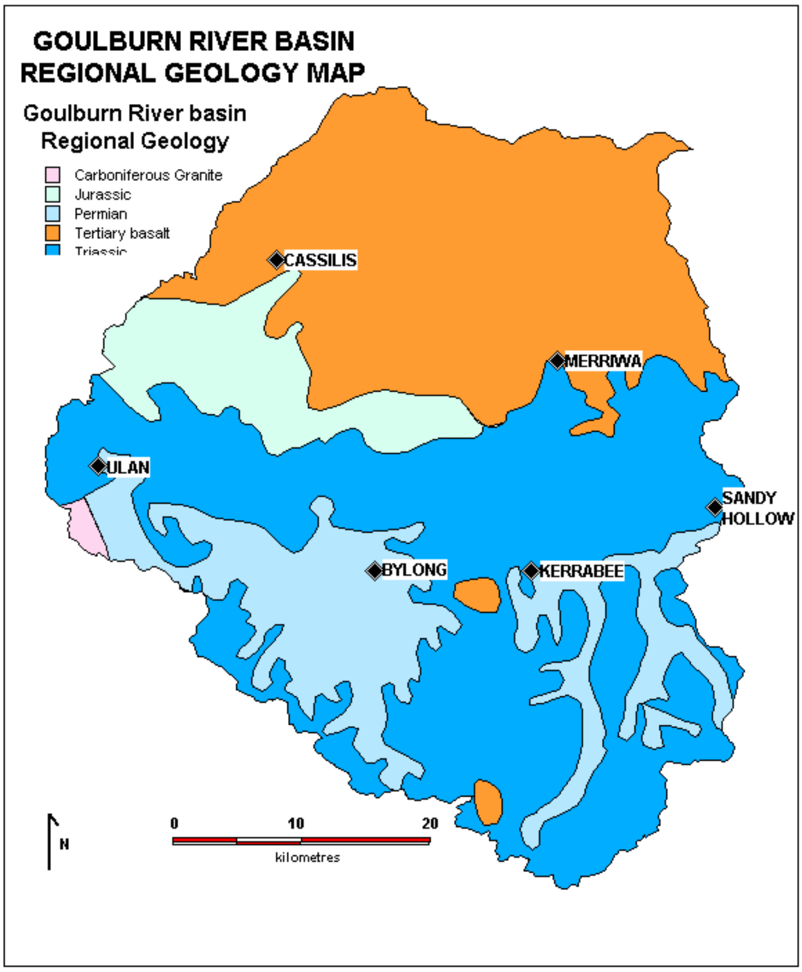

Figure 3.3: Main geological regions of the Goulburn River Catchment.

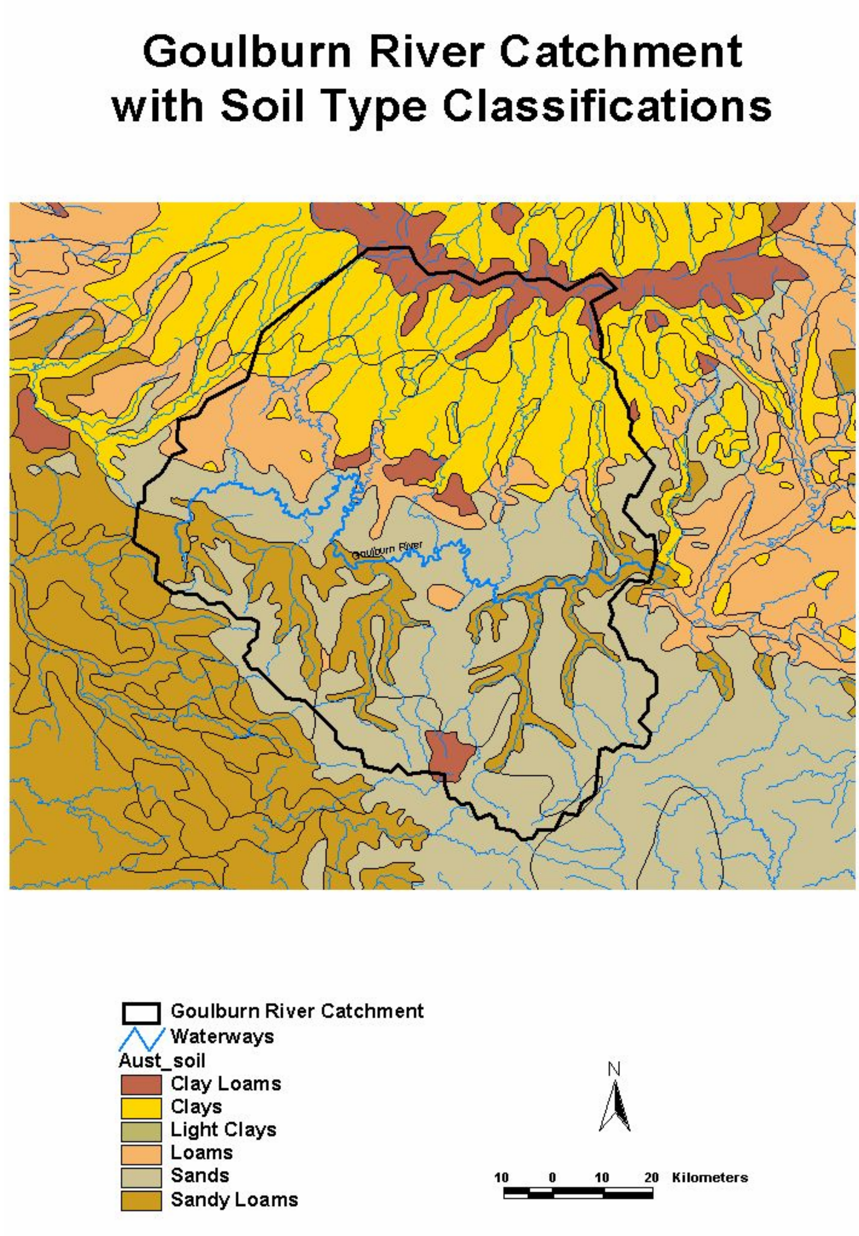

Figure 3.4: Distribution of soils within the Goulburn River Catchment.

3.3.4 VEGETATION AND LAND-USE

The natural vegetation of the area includes open grasslands, woodlands and eucalypt forests. Much of the original vegetation in the northern part of the Goulburn catchment has been cleared, the extent of which has largely been influenced by topography and soil type (Figure 3.5). At the northern boundary where the terrain is rugged (i.e. the Liverpool Range), accessibility is limited and the area has thus remained highly vegetated. In parts of the Merriwa Plateau, clearing has been more extensive due to the rolling to hilly terrain ensuring greater accessibility. Grazing and cropping activities dominate cleared areas, due to the high fertility of basaltic soils. This part of the catchment is an appropriate region for remote sensing studies. For example, remote sensing of near-surface soil moisture based on passive microwave radiation requires less vegetation cover as vegetation can attenuate the emitted microwave signal from the land surface. The substantial less vegetation cover on the Merriwa Plateau is therefore creating an ideal situation for soil moisture monitoring with remote sensing approaches. The sandstone derived soils to the far south are largely uncleared as they are less fertile and productive. Because of the denser vegetation, the southern part of the GRC is not suitable for soil moisture remote sensing studies.

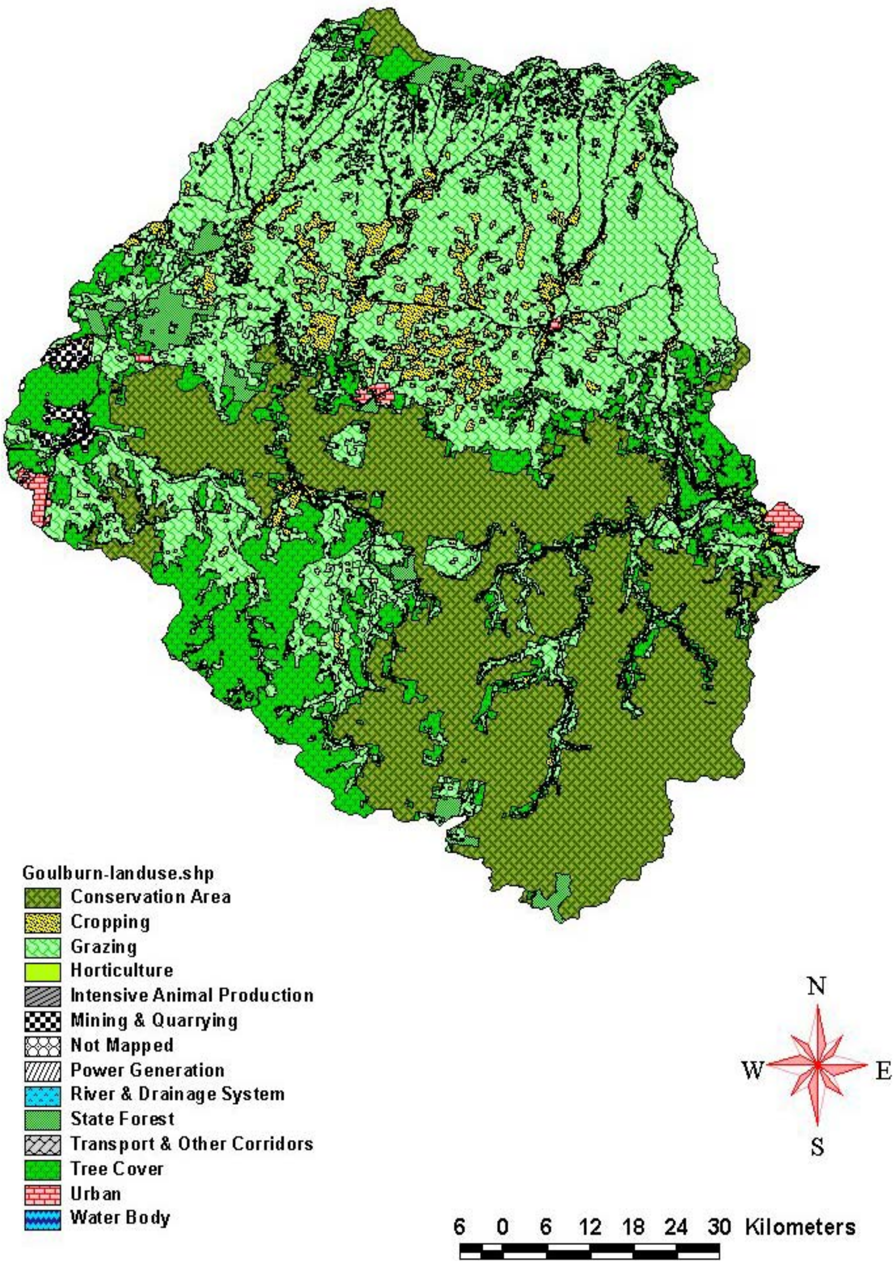

Figure 3.5: Land use pattern of the Goulburn River Catchment.

The Goulburn river catchment is also important for the conservation of native vegetation species. The catchment includes two national parks: the Goulburn River National Park and the Wollemi National Park. At present the Hunter Catchment Management Trust is undertaking the Hunter Remnant Vegetation Project, which aims to map remnants, identify potential corridors and encourage proper management of remnant native vegetation. Knowledge of soil moisture behaviour in the Goulburn catchment is therefore very useful for the current attempts of conserving the native vegetation.

Important land-uses in the catchment include: beef cattle, dairy, vineyards, wheat, sheep, thoroughbred horses, forestry, lucernes, coal mining, quarrying, recreation, conservation and rural-residential land use (HCMT, 2003). Most of these land uses may benefit from good knowledge of soil moisture behaviour within the catchment.

Due to the highly erosive nature of the common soil types in the region, the Goulburn Catchment experiences continuing erosion problems. For example, the cracking clays in northern half are exhibiting widespread signs of tunnel erosion. Extensive sheet, rill and gully erosion is also evident on undulating land and is widespread on agricultural lands. Stream bank erosion occurs along the Goulburn River and its tributaries. The Integrated Catchment Management Plan for the Hunter Catchment (HCMT, 2003) has identified many soil conservation priority areas, particularly within the northern half of the catchment. Furthermore, soil structural decline is recognised as a significant issue in the region by the Department of Environment and Conservation, NSW, but its extent is undetermined (http://www.epa.nsw.gov.au/soe/97/ch2/9_1.htm). Detailed knowledge of soil moisture behaviour will also benefit the adoption and implementation of appropriate soil conservation measures.

3.4 FIELD INSTRUMENTATION

3.4.1 LOCATION AND LAYOUT OF MONITORING SITES

A total of 26 soil moisture and soil temperature monitoring sites (Figure 3.6) were chosen on the basis of i) spatial representativeness, ii) the spatial distribution across the experimental catchment, and iii) accessibility. The representativeness objective was addressed by choosing mid-slope locations with typical vegetation, soil, and aspect, so that they represent catchment average soil moisture locations. The spatial distribution was chosen to give a concentration of measurements in the open cropping and grazing land in the north for application to remote sensing measurements, while achieving a good distribution for model verification within the chosen focus catchments and the broader Goulburn River catchment. Two focus catchments were created by establishing 7 soil moisture monitoring sites in each of the major subcatchments (6 sites in the Krui River catchment in addition to the Stanley micro-catchment (with 7 sites) and 7 sites in the Merriwa Creek catchment), with a further 6 sites installed in the remaining Goulburn River catchment (Figure 3.6). The intensively monitored Stanley micro-catchment was chosen to study hillslope-scale soil moisture distributions and sites were located along two hillslopes (Figure 3.7). Moreover, the higher density of soil moisture monitoring sites in the Krui and Merriwa catchments allows for study of the spatial organisation of soil moisture throughout the northern part of the catchment and supports work undertaken in the validation and scaling of satellite measurements.

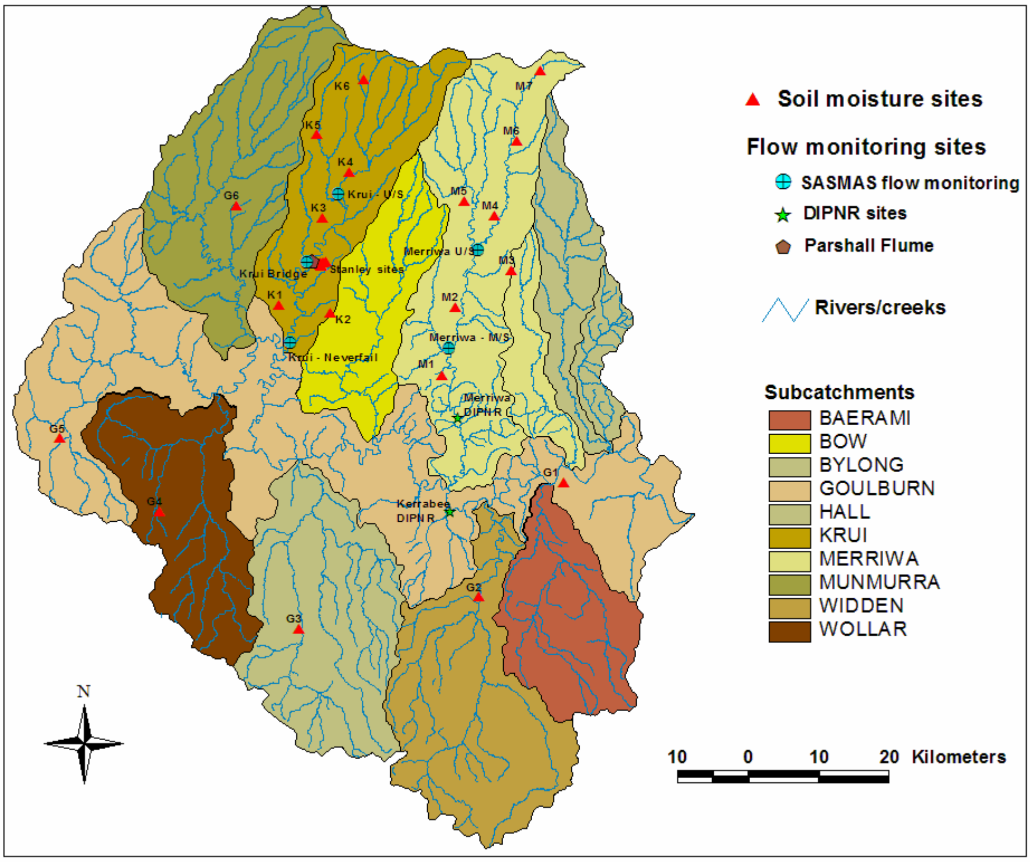

Figure 3.6: Location of soil moisture and stream flow monitoring sites in the Goulburn River Catchment. Main sub-catchments within the GRC are also shown in the figure.

(a)

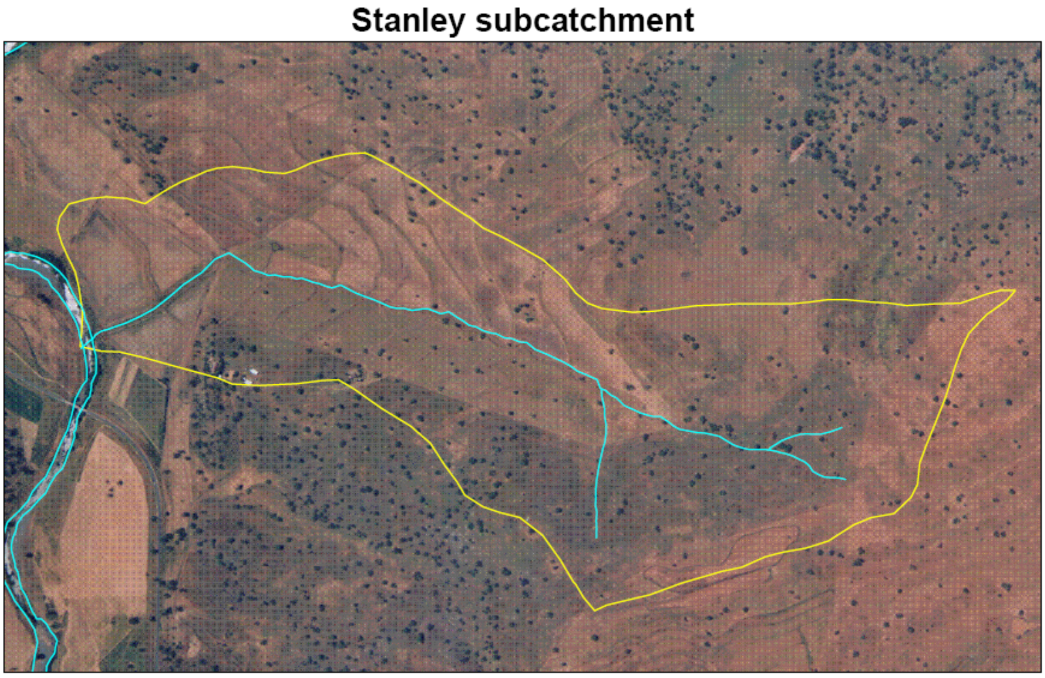

(b)

Error! Objects cannot be created from editing field codes.

Figure 3.7: (a) Areal view of Stanley micro-catchment and (b) location of monitoring sites.

Geographic locations and the physical characteristics of the selected monitoring sites are summarised in Table 3-2. The monitoring sites represent at least six tributaries of the Goulburn River Catchment. Most are in pasture and represent near-natural conditions without any disturbances to the soil moisture patterns due to irrigation.

Table 3-2: Geographic locations, topography, land use and soils of the selected monitoring sites.

Code	Property name	Sub-catchment	Longitude (East)	Latitude (South)	Topography	Land use	Soils
K1	Illogan	Krui	150.0700	-32.1486	Flat	Cropping	RBC
K2	Roscommon	Krui	150.1461	-32.1606	Flat	Grazing	RBS /SS
K3	Pembroke	Krui	150.1381	-32.0394	Flat	Cropping	BBC
K4	Pembroke	Krui	150.1800	-31.9817	Flat/gently slope	Grazing	BBC

K5	Burnbrae	Krui	150.1336	-31.9331	Flat		Grazing	BBC
K6	Spring Hill	Krui	150.2061	-31.8644	Hilly		Grazing	BBC
S1	Stanley	Krui	150.1244	-32.0922	Flat		Grazing	BBC
S2	Stanley	Krui	150.1369	-32.0958	Flat		Grazing	BBC
S3	Stanley	Krui	150.1394	-32.0956	Hilly		Grazing	RBC
S4	Stanley	Krui	150.1425	-32.0950	Hilly		Grazing	RBC
S5	Stanley	Krui	150.1339	-32.0964	Flat		Grazing	BBC
S6	Stanley	Krui	150.1344	-32.0986	Hilly		Grazing	RBC
S7	Stanley	Krui	150.1353	-32.1003	Hilly		Grazing	RBC
M1	Maram Park	Merriwa	150.3114	-32.2417	Hilly		Grazing	SS
M2	Cullingral	Merriwa	150.3336	-32.1578	Flat/gently slope		Grazing	SS
M3	Merriwa Park	Merriwa	150.4198	-32.1124	Gently rolling		Grazing	BBC
M4	Kilwirrin	Merriwa	150.3964	-32.0419	Hilly		Grazing	BBC
M5	Midlothian	Merriwa	150.3511	-32.0222	Flat/gently slope		Grazing	BBC
M6	Dales	Merriwa	150.4317	-31.9469	Gently rolling		Grazing	BBC
M7	The Echo	Merriwa	150.4672	-31.8586	Hilly		Grazing	BBC
G1	Blue Wren Park	Goulburn	150.4894	-32.3828	Flat/gently slope		Grazing	
G2	Widden Stud	Widden	150.3592	-32.5258	Flat		Stud	
G3	Talooby	Bylong	150.0875	-32.5600	Hilly		Grazing	BBC
G4	Cumbo	Wollar	149.8822	-32.4061	Flat		Grazing	SS
G5	Glenmoor	Goulburn	149.7372	-32.3092	Flat		Grazing	SS
G6	Nagolli	Munmurra	150.0106	-32.0203	Gently rolling		Grazing	BBC

BBC - Black basaltic clay, RBC - Red basaltic clay, SS – Sandy soil

The GRC has been permanently instrumented since September 2002 for soil moisture, soil temperature, soil heat flux, and a range of climate variables. Setting up of all monitoring sites and the installation of sensors were done in two dedicated field campaigns. A typical soil moisture monitoring site consists of three CS616 reflectometers, T107 temperature sensor, CR510 data logger and power supply system (solar panel and a battery). CS616 sensors were installed 30 cm apart and about 75 cm from the logger mast as shown in Figure 3.8. While the installation of surface sensors did not require special attention, the installation of deeper sensors required special care. When installing the CS616 sensors at 30-60cm and 60-90cm depths, the soil was carefully removed layer by layer with an auger and placed in distinct heaps on the ground. After installation of the sensors, the soil was returned to the access hole in a reverse order to ensure minimum disturbance (see Figure 3.9). To avoid possible damage to the CS616 sensors during installation a guide probe was used to make two narrow holes to facilitate sensor insertion. A soil temperature sensor was installed at the mid point of the top CS616 sensor, i.e. at 15 cm from the surface.

Setting up the climate stations was more complex because it involved more soil temperature measurements and a range of other sensors for measuring radiation, humidity, air temperature, pressure and wind. Figure 3.10 illustrates the steps involved in setting up a climate station. A comprehensive summary of instrumentation at each monitoring site is given in Table 3-3.

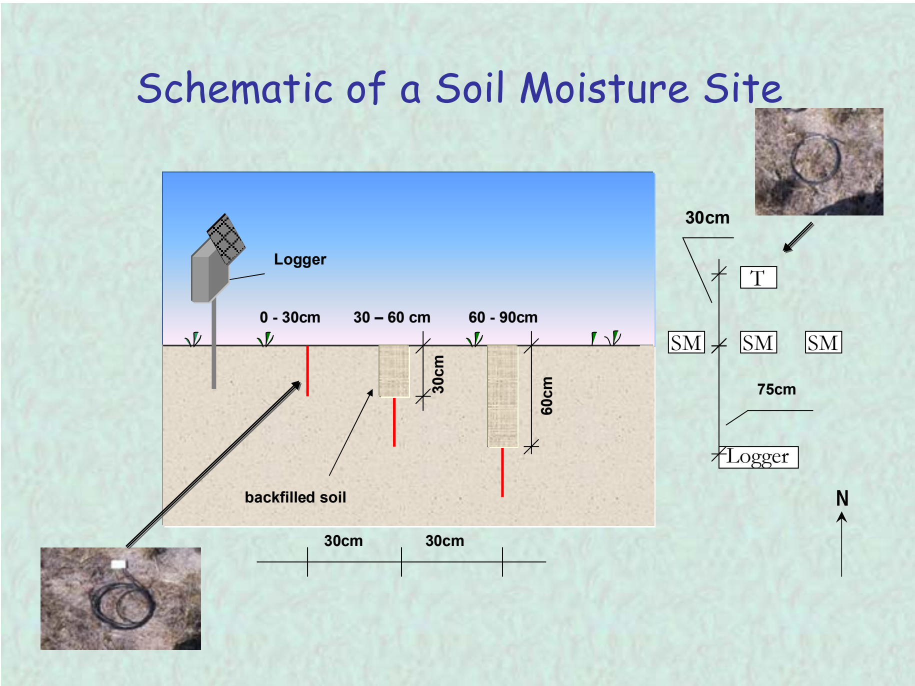

Figure 3.8: Diagrammatic illustration of a typical soil moisture measurement site with three CS616 Reflectometers (lower left image) and one T107 temperature sensor (upper right image).

Figure 3.9: Installation of CS616 sensors at 30-60cm and 60-90cm depths.

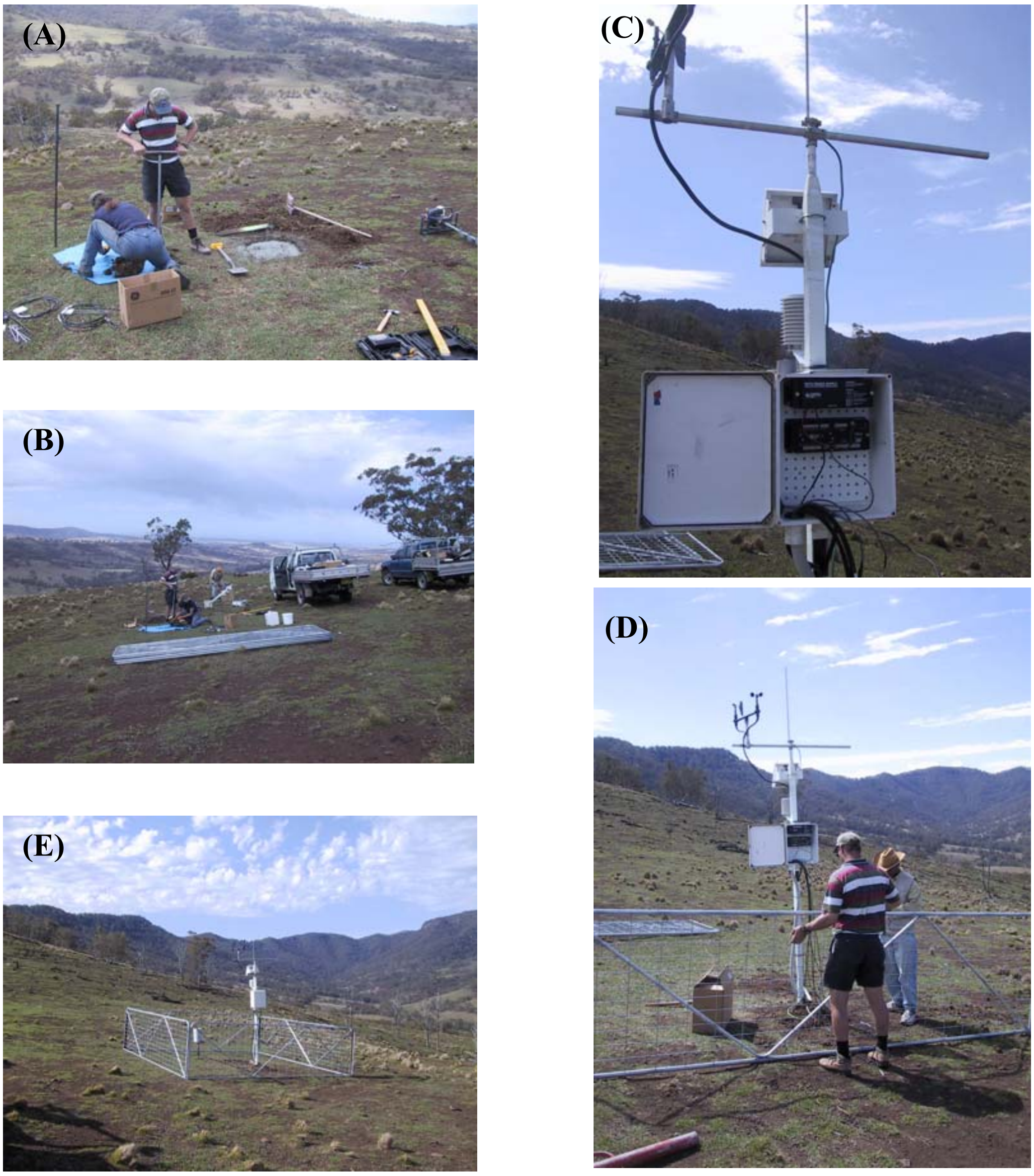

Figure 3.10: Different stages of setting up the climate station at K6 (Spring Hill): A) foundation for the mast and augering access holes for sensors, B) installation of ground sensors, C) connecting sensors to the data logger, D) fencing, and E) complete climate station.

Table 3-3: Characteristics of the instrumentation at monitoring sites

Code	Soil depth (cm)	Date Established	CS616	T107	Other sensors
K1	>100	01/10/2002	3	1	
K2	>100	30/09/2002	3	1	
K3	>100	27/09/2002	3	1	
K4	>100	26/09/2002	3	1	RF-A
K5	>100	27/09/2002	3	1	
K6	>100	26/09/2002	3	3	RF-A, Climate station-2
S1	>100	23/09/2002	3	1	RF-N
S2	>100	24/09/2002	3	8	RF-A and RF-N, Climate station-1
S3	75	25/09/2002	2	1	RF-N
S4	40	25/09/2002	1	1	
S5	>100	25/09/2002	3	1	RF-N
S6	70	23/10/2002	2	1	RF-N
S7	40	28/01/2003	1	1	
M1	67	03/10/2002	2	1	RF-A
M2	>100	01/10/2002	3	1	
M3	75	03/10/2002	2	1	
M4	45	01/10/2002	1	1	RF-A
M5	70	03/10/2002	2	1	
M6	78	22/07/2003	2	1	
M7	>100	01/10/2002	3	1	RF-A
G1	>100	04/10/2002	3	1	
G2	>100	04/10/2002	3	1	RF-A
G3	>100	02/10/2002	3	1	
G4	70	02/10/2002	2	1	
G5	>100	02/10/2002	3	1	RF-A
G6	52	30/09/2002	1	1	

Note: RF-A = Automatic Rainfall recorder, RF-N = Non-recording or collecting rain gauge

3.4.2 WATER CONTENT REFLECTOMETERS AND DATA LOGGERS

Continuous measurement of soil moisture was based on the Campbell Scientific Inc. (CSI, 2002) CS616 Water Content Reflectometers (WCR). The WCR is designed to measure volumetric water content of a porous medium such as soil. It is an improved version of CS615 WCR introduced in 1996. The water content information is derived from the probe's ability to measure the dielectric constant of the medium being measured. The probe consists of two 30 cm long stainless steel rods of 32 mm diameter with a spacing of 32mm. These two rods or wave guides are connected to a head piece which is the housing of the measurement electronic components. High-speed electronic components inside the probe head are configured as a bistable multivibrator. The output of the multivibrator is connected to the steel rods which act as a wave guide. The signal return from the guides causes the bistable multivibrator to change states between two discrete values. The output of the sensor is a frequency that reflects the number of states changes per second. For this reason CS616 is not a 'true Time Domain Reflectometry (TDR)' instrument because TDR equipment directly measures the wave guide signal reflection time and uses ultra high speed electronic circuit to make measurements in nanoseconds. The travel time of the signal along the probe rods depends on the dielectric permittivity of the material surrounding the rods. The dielectric permittivity depends on the water content of the medium. Therefore, the oscillation frequency of the multivibrator is determined by the water content of the medium being measured. As with all TDR sensors, a wetter soil will cause a longer signal return time, and will cause the CS616 circuit to vibrate at a lower frequency. The probe output is a period measurement which ranges from about 14 microseconds when the rods are in air to about 42 microseconds (μs) when the rods are completely immersed in normal tap water (Campbell Scientific Inc, 2002). Once installed the CS616 requires no maintenance. However, the CS616 has the disadvantage of being affected by salinity in soils of salinity >2 dS m^{-1}. In addition, high clay content, high quartz content and high organic matter content all affect the probe readings. Therefore, custom re-calibration is required for such soils. In addition, the CS616 is sensitive to temperature and hence requires a temperature correction. A detailed sensor calibration was therefore undertaken for each site using both laboratory and field measurements (see Section 3.8.1).

Each of the monitoring sites has up to three vertically inserted WCRs over depths of 0-300mm, 300-600mm and 600-900mm, respectively (Figure 3.8). The number of soil moisture sensors installed was determined by the depth of the top soil layer. These sensors ensured a continuous observation of the soil moisture profile, with sensors read every minute and the average values logged once every 20 minutes. The WCRs have been connected to the single-ended analogue input channel on a Campbell Scientific Inc (CSI) CR510 data logger for continuous monitoring. Six types of logger programs have been used and a sample logger program is shown in Annex-I (a). PC208W software from CSI was used for programming the data logger and for downloading of the data to a laptop computer. Table 3-4 shows the logger programs used at each site together with the logger capacities at each site. As seen in Table 3-4, loggers at the climate stations were just sufficient to store data for 6 weeks period. All routine site visits were therefore planned to occur at 6 weeks intervals.

Table 3-4: Data logging properties at monitoring sites

Site code	Data logger	Logger program	Scanning rate (Seconds)	Logger capacity (weeks)
K1	CR510	MC_3S	60	15.4
K2	CR510	MC_3S	60	15.4
K3	CR510	MC_3S	60	15.4
K4	CR510	MC_3S_RF	60	13.7
K5	CR510	MC_3S	60	15.4
K6	CR10	WEATHER	60	6.6
S1	CR510	MC_3S	60	15.4
S2	CR510	MC_3S	60	15.4
	CR10	SC_WETHR	60	6.2
S3	CR510	MC_2S	60	17.7
S4	CR510	MC_1S	60	20.6
S5	CR510	MC_3S	60	15.4
S6	CR510	MC_2S	60	17.7
S7	CR510	MC_1S	60	20.6
M1	CR510	MC_2S_RF	60	15.9
M2	CR510	MC_3S	60	15.4
M3	CR510	MC_2S	60	17.7
M4	CR510	MC_1S_RF	60	18.4
M5	CR510	MC_2S	60	17.7
M6	CR510	MC_2S	60	17.7
M7	CR510	MC_3S_RF	60	13.7
G1	CR510	MC_3S	60	15.4
G2	CR510	MC_3S_RF	60	13.7
G3	CR510	MC_3S	60	15.4
G4	CR510	MC_2S	60	17.7
G5	CR510	MC_3S_RF	60	13.7
G6	CR510	MC_1S	60	20.6

3.4.3 OTHER SOIL MOISTURE MEASUREMENTS

Two types of additional soil moisture measurements were made at all field sites on a six-weekly basis during routine data downloading visits. These additional soil moisture measurements were collected between June 2003 and August 2004. First, five 0-6 cm soil moisture measurements were made using a ThetaProbe soil moisture sensor ML-2 around the permanent site to assess local differences in surface moisture status. The ThetaProbe is a portable instrument designed to measure volumetric soil water content using a simplified standing wave measurement technique. The ThetaProbe consists of an input/output cable, probe body and a sensing head. The cable provides connection for a power supply and to a data logger such as the Moisture Meter type HH2 used in this study. The probe body contains an oscillator, a specially designed internal transmission line and measuring circuitry within a waterproof housing. The sensing head has an array of four rods (each 6 cm long), the outer three of which, connected to instrument ground, form an electrical shield around the central, signal rod. This behaves as an additional section of transmission line having an impedance that depends on the dielectric constant of the soil into which it is inserted. If this impedance differs from that of the internal transmission line, then a proportion of the signal is reflected back from the junction between the probe array and the transmission line. The output signal is 0 – 1 V DC for a range of soil dielectric constants from 1 to 32, that is for a range of 0 to approximately 0.5 cm^3cm^{-3} volumetric soil water content for a generalised mineral soil (i.e. bulk density between 1.25 – 1.5 $g.cm^{-3}$ and organic carbon < 7%). The main advantages of the ThetaProbe include: a portable device, fast measurement time of 1-5 seconds, and direct measurement of VWC in standard soil types. (More information on ThetaProbe can be found at http://www.delta-t.co.uk).

Second, soil moisture measurements were made closer to CS616 sensors (approximately 1 m away) using vertically inserted connecter TDR probes (see Figure 3.11). The connector TDR probes gave an average soil moisture measurement over depths of 0-30, 0-60 and 0-90 cm (depending on the number of SC616 sensors installed at the site). The TDR system used for these manual TDR measurements was the Soil Moisture Equipment Corporation TRASE instrument (Soil Moisture Equipment Corporation, 1996). Standard TRASE calibration was used to determine the volumetric moisture content. The main objective of TDR readings was to check the water contents measured with the CS616 sensors.

Figure 3.11: Measurement of soil moisture with TRASE instrument at site M1.

3.4.4 SOIL TEMPERATURE MEASUREMENTS

Continuous measurement of soil temperature was based on the Campbell Scientific Model 107 Temperature Probe (T107) (http://www.campbellsci.com /107-l). The T107 probe uses a thermistor to measure temperature and it is designed for measuring air, soil or water temperatures between -35^{o}C and 50^{o}C. At each soil moisture monitoring site a T107 has been installed vertically with its midpoint at 15cm below the soil surface, providing a continuous record of soil temperature at the midpoint of the 0-30cm top soil layer.

At the climate station sites, more temperature sensors have been used in order to better understand the soil temperature profile. For instance, at Stanley-S2 and Spring Hill (K6) a total of 8 and 3 temperature sensors have been installed, respectively. The main objective of measuring temperature profiles at deeper layers was to develop a methodology to infer soil temperatures at 45cm and 75cm from temperature measurement at 15cm depth. Such data are needed in order to apply a temperature correction to the CS616 readings for 30-60cm and 60-90cm depths.

In addition, 0-1 cm soil temperature and air temperature measurements were made at all field sites with a portable temperature probe on a six-weekly basis during routine data downloading visits. These additional temperature measurements were collected between June 2003 and August 2004.

3.4.5 WEATHER STATIONS

The automatic weather stations were sited with regard to existing infrastructure and expected spatial variability, resulting in one station in the Stanley catchment (at S2) and a second station in an elevated position at the northern end of the Krui catchment (Spring Hill – K6). In this way automatic weather stations were located in both the upper and lower reaches of the Krui focus catchment and in the centre of the Stanley micro-catchment. Both weather stations consisted of Campbell Scientific automatic weather stations. The Stanley weather station monitored relative humidity and air temperature; soil temperatures at 2.5, 5, 10, 15, 30, 45, 60 and 75 cm depths using T107 sensors; soil heat flux at 5 cm depth using a soil heat flux plate; atmospheric pressure; rainfall; wind speed; net radiation; total incoming radiation using a pyranometer; in-coming and out-going short-wave and long-wave radiation using a 4-channel radiometer and soil moisture content at depths 0-30, 30-60 and 60-90 cm using CS616 WCR. The Spring Hill weather station monitored relative humidity and air temperature; soil temperatures at 15, 45 and 75 cm depths; rainfall; wind speed and soil moisture content at depths 0-30, 30-60 and 60-90 cm. A summary of the instrument configuration at these weather stations is presented in Table 3.5. Apart from precipitation, all measurements were made at 1-minute intervals, and the average was logged every twenty minutes. Rainfall was recorded for each tip of the 0.2 mm tipping bucket. A sample data logger programme as used at S2 is given in Annex -I (b).

Table 3-5: Configuration of sensors at the climate stations

Sensor	No of units	Sensor height, depth etc
Stanley (S2)		
CS 616 Reflectometers	3	0-30, 30-60 and 60-90 cm depths
107 Temperature probe	8	2.5,5,10,15,30, 45, 60 & 75 cm depths
HMP35C - Temperature and relative humidity	1	200 cm above ground
Young Wind Sentry set	1	300 cm above ground
L1200X -Pyranometer (spectral range 400 to 1100 nm)	1	289 cm above ground
Q 7.1 - Net Radiometer	1	98 cm above ground
Tipping bucket rain gauge	1	Funnel top at 50 cm above ground
CS105 -Barometric pressure	1	200 cm above ground
HFT3 - Soil Heat Flux plates	2	Both at 5 cm below ground surface
Kipp CNR-1 Radiometer (spectral range 0.3 to 50 μm)	1	110 cm above ground
Spring Hill (K6)		
CS 616 Reflectometers	3	0-30, 30-60 and 60-90 cm depths
T107 temperature probe	3	15, 45 and 75 cm depths
HMP35C - Temperature and relative humidity	1	200 mm above ground
Anemometer	1	300 mm above ground
Tipping bucket rain gauge	1	Funnel top at 50 cm above ground

3.4.6 RAINFALL MEASUREMENTS

Rainfall measurements at climate stations S2 and K6 commenced in late 2002. Towards the end of 2003, another 6 rain gauges were installed at selected soil moisture monitoring sites (see Table 3-3). Rainfall is measured at these sites on a continuing basis using Hydrological Services model TB3 tipping bucket rain gauges. This device has a receiver of 200 mm diameter to collect rainfall and facilitates the recording at 0.2 mm accuracy. As for the climate stations, rainfall was recorded for each tip of the 0.2 mm tipping bucket. In addition, five collecting rain gauges were distributed throughout the Stanley micro-catchment to check on the spatial variability of rainfall. These collecting rain gauges were located at S2 (weather station), S1, S3, S5 and S6. The gauges were read during routine data downloading visits at approximately 6 weeks intervals.

The Bureau of Meteorology (BoM) collects rainfall data from a number of sites within and surrounding the GRC as shown in Figure 3.11 and in Table 3-6. Daily rainfall data were obtained for 52 BoM rainfall monitoring sites (of which 18 sites are within the GRC) for the years 2003-2004. The primary objective of collecting these rainfall data was to use the data with SASMAS rainfall data in generating monthly rainfall distribution maps as the rainfall patterns are essential in interpreting soil moisture distributions within the GRC.

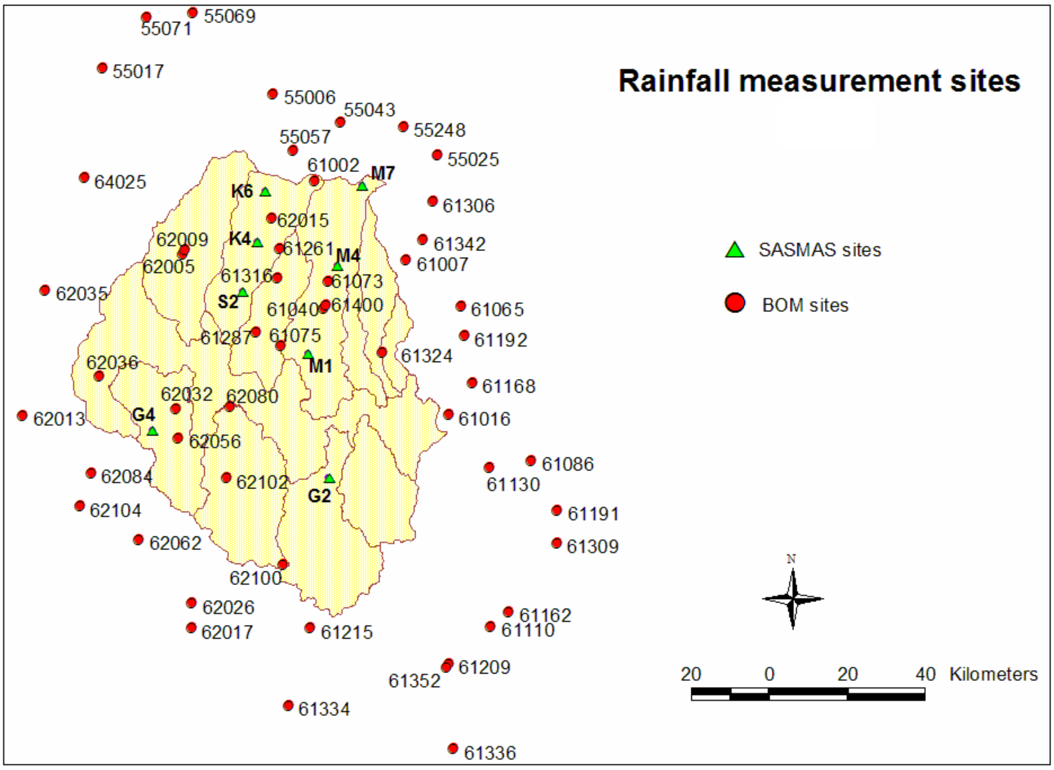

Figure 3.12: Distribution of rainfall measurement sites within and surrounding the Goulburn River Catchment. (The number indicates the BoM location code)

Table 3-6: Summary of rainfall measurement sites by the SASMAS and Bureau of Meteorology (BoM) within and in the vicinity of the Goulburn River Catchment.

	Number of rain gauges	
Sub catchment	**SASMAS**	**BOM**
Krui	3	3
Merriwa	3	3
Wollar	1	2
Widden	1	-
Bow	-	3
Bylong	-	3
Goulburn	-	1
Hall	-	1
Munmurra	-	2
No. of rain gauges within GRC	8	18
No. of rain gauges outside GRC	-	34
Total number of rain gauges	8	52

3.4.7 STREAMFLOW MEASUREMENTS

Streamflow measurement is another important component of the SASMAS monitoring network. The SASMAS streamflow measurement network was based on a miniature flow measurement and logging device called the Levelogger. Five such devices have been installed in the Krui and Merriwa focus catchments. The selection of measurement sites was done on the basis of the upper, mid and lower reaches along the river to facilitate runoff modelling for smaller modelling units. It was also expected that access would be provided to the streamflow data being collected at three other locations within the Goulburn catchment by the Department of Infrastructure, Planning and Natural Resources (DIPNR). Further, with the aim of getting better insight into the streamflow behaviour at first-order stream level, a Parshall flume (throat width = 455 mm) and an automatic water level pressure sensor have been installed at the Stanley micro-catchment.

3.5 SOIL CHARACTERISATION AT MONITORING SITES

3.5.1 SOIL PARTICLE SIZE DISTRIBUTION

The soil consists of an assembly of soil particles of various shapes and sizes. The objective of a particle size analysis is to group these particles into separate ranges of sizes. Particle size analysis data are required for correct identification of soil texture and hence estimation of soil hydraulic properties such as soil water holding capacity, soil water tension etc.

The particle size analysis of all monitoring sites except at S3 and S4 was performed by collecting soil samples from the top 0-30 cm layer. It was assumed that the soil properties at S3 and S4 sites are comparable with site S7 and therefore no soil samples were collected from these two sites. The sub-sample used for the particle size analysis was derived from three soil cores collected within 3m from the CS616 WCRs at each site. The particle size analysis was then performed following AS 1289 3.6.1 and AS 1289 3.6.3 test procedures.

Soil texture was determined from the relative proportions of clay, silt and sand using the soil texture triangle. A summary of the results are given in Table 3-7. It is clear from the results that the monitoring sites south of the Goulburn River (i.e. G1, G4 and G5) are predominantly on sandy soils with the exception of G2 and G3 where G2 has silty soil and G3 is primarily a clay soil. As discussed in section 3.3.3 and in Figure 3.4, the catchment north of the Goulburn River area comprises predominantly clay soils. It is also evident from the Table 3-7 that many sites within Krui (including Stanley catchment) and Merriwa catchments are on clayey soils. For example, sites S1, S2, S5, S6, K3, K4, K5 and K6 in Krui sub-catchment and M3, M5, M6 and M7 have a clay content of more than 30%. The two southern sites in the Merriwa catchment, M1 and M2, are located in a sandstone country with sandy soils. M4 is located within the transition zone and has loam soil.

Table 3-7: Results of the particle size soil analysis for monitoring sites

Site	Catchment	Clay %	Silt %	Sand %	Soil texture
G1	Goulburn-south	8	15	77	Sandy loam
G2	"	21	56	23	Silt loam
G3	"	64	25	11	Clay
G4	"	11	13	76	Sandy loam
G5	"	9	17	74	Sandy loam
G6	Goulburn-north	33	35	32	Clay loam
K1	Krui	23	51	26	Silt loam
K2	"	6.5	8.5	85	Loamy sand
K3	"	71	23	6	Clay
K4	"	54	36	10	Clay
K5	"	62	26	12	Clay
K6	"	35	44	21	Clay loam
M1	Merriwa	6.5	21.5	72	Sandy loam
M2	"	0	6	94	Sand
M3	"	36	43	21	Clay loam
M4	"	25	49.5	25.5	Loam
M5	"	69	21	10	Clay
M6	"	51	17.5	31.5	Clay
M7	"	35	40	25	Clay loam
S1	Krui	54	40	6	Clay
S2	"	39	35	26	Clay loam
S3	"	n/a	n/a	n/a	
S4	"	n/a	n/a	n/a	
S5	"	46	42	12	Silty clay
S6	"	41	28	31	Clay
S7	"	16	52	32	Silt loam

(Note: S3 and S4 sites are comparable with site S7)

3.5.2 SOIL BULK DENSITY AND POROSITY

Soil bulk density (ρ_b), similar to all other density measurements, is an expression of the mass to volume relationship. Measurement of soil bulk density involves the determination of the mass (oven dried, at 105 ^oC) and the volume of a given amount of soil material. Soil bulk density is computed using the total soil volume and it is best measured with an undisturbed sample. Soils that are loose, porous, or well-aggregated will have lower bulk densities than soils that are compacted or non-aggregated. Sandy soils have less total pore space than clayey soils, so generally they have higher bulk densities. Bulk densities of sandy soils vary between 1.2 to 1.8 g cm^{-3}. Fine-textured soils, such as clays, silty clays, or clay loams, have bulk densities between 1.0 and 1.6 g cm^{-3}. Bulk density is an indirect measure of pore space and is affected primarily by texture and structure.

Soil particle density (ρ_s), on the other hand, is a measure of the mass per unit volume of the soil solids only. Texture and structure do not affect particle density. Organic matter however, readily influences particle density. In general, soils high in organic matter have lower particle densities. Soil particle density generally increases with soil depth because of the concurrent decrease in organic matter. The particle density of most mineral soils is in the range of 2.60 to 2.75 g cm^{-3}.

Porosity (φ) or total pore space of soil is a measure of water holding capacity of a soil. Thus, measurement of bulk densities is important in soil moisture studies. Soil porosity can be computed with bulk density and particle density using the following relationship.

$$\varphi = 1 - \frac{\rho_b}{\rho_s} \qquad (3\text{-}1)$$

Bulk densities of all sites were estimated from the soil cores (approximately 30cm long and 15 cm in diameter) collected at each site for the purpose of calibrating the CS616 WCRs. The soil porosities were then computed by assuming a particle density of 2.65 g cm^{-3}. A summary of the results are given in Table 3-8.

Table 3-8: Measured bulk densities and computed porosities for monitoring sites.

Site	Bulk density (ρ_b), g cm^{-3}	Porosity (φ), %
G1	1.8276	31
G2	1.1783	56
G3	1.2194	54
G4	1.9168	28
G5	1.6896	36
G6	1.2429	53
K1	1.1503	57
K2	1.6772	37
K3	1.2829	52
K4	1.1307	57
K5	1.2632	52
K6	1.2403	53
M1	1.6772	37
M2	1.7030	36
M3	1.2686	52
M4	1.3146	50
M5	1.3283	50
M6	1.2126	54
M7	1.1843	55
S1	1.1907	55
S2	1.2593	52
S3	1.2350	53
S4	1.4512	45
S6	1.3460	49

As shown in Table 3-8 the computed bulk densities vary from 1.1307 (at K4) to 1.9168 (at G4) g cm^{-3}. However, due to possible inaccuracies of actual soil volume used in the calculation, some error may be associated with these computed bulk densities.

3.5.3 SOIL SALINITY

In the context of the present study, information on soil salinity was required to assess the suitability of CS616 WCRs for each monitoring site and to determine the calibration parameters. Salinity measures include electrical conductivity of a solution or a soil and water mixture. When measuring, soil samples can be measured by the '*1:5 w/v method*' - one part by weight (g) air dried soil to five parts by volume (ml) distilled water, which is agitated and then allowed to settle, after which the solution is measured for electrical conductivity (EC 1:5). The electrical conductivity of a saturated soil extract (ECe) however is the most useful and reliable measure of salinity for comparing between soil types.

Soil salinity of all sites was estimated from the same 0-30 cm soil cores collected at each site for the purpose of calibrating the CS616 WCRs. A summary of the measured salinity levels is given in Table 3-9.

Table 3-9: Measured salinity levels (dS m^{-1}) for the monitoring sites.

Site	Salinity	Site	Salinity
G1	0.026	M1	0.030
G2	0.081	M2	0.065
G3	0.095	M3	0.092
G4	0.024	M4	0.062
G5	0.040	M5	0.129
G6	0.077	M6	0.064
K1	n/a	M7	0.109
K2	0.022	S1	0.071
K3	0.119	S2	0.062
K4	0.095	S3	0.092
K5	0.104	S4	0.171
K6	0.592	S6	n/a

It was found that the measured salinity levels did not exceed the maximum salinity level of 2 dS m^{-1}. Therefore, salinity was not an issue in using CS616s for accurate estimation of water contents at all monitoring sites.

3.6 ENVIRONMENTAL MONITORING RESULTS

3.6.1 PRECIPITATION

Precipitation is the most important variable in terms of recharging the surface soil moisture levels, and it plays a critical role in soil moisture studies. However, there is much uncertainty associated with measuring this variable across a large catchment. As can be seen in Figure 3.12 the distribution of rain gauges is not uniform across the GRC. Approximately 26 rain gauges (8 SASMAS + 18 BoM) were identified within the GRC (Table 3-6). It is clear that these rain gauges are concentrated in the northern half and the south-western part of the GRC. G2 is the only rain gauge located within the south-eastern quarter of the catchment. Because of this heterogeneity in the distribution of rain gauges within the GRC, it was necessary to take into account all available rain gauges in the vicinity of GRC to better understand the rainfall distribution patterns. Therefore, rainfall measurements from another 34 locations surrounding the GRC were also considered in the analysis (see Annex –II for details).

The use of rainfall measurements from various sources and from various origins requires detailed analysis of their accuracies for scientific applications. All rainfall measurements during this research are considered reliable. There were periods however with missing rain data due to data logging problems. Furthermore, considerable rainfall variation was found to exist across the catchment. In order to ascertain the consistency of data, rainfall trends among the measurement locations needed to be compared. S2 (Stanley climate station) is considered the most reliable and the accurate rainfall measurement, all SASMAS rainfall data and selected BoM rainfall data were analysed for their temporal evolution pattern against the temporal evolution pattern of S2. The double mass curves were generated for the periods of continuous data in 2004 for all SASMAS sites (Figure 3.13) and for selected BoM rainfall sites within GRC for 2003 and 2004 (Figure 3.14). The double mass curves clearly demonstrate that there were considerable systematic differences between all rain gauges. For example, site K6 and M7 (in Figure 3.13) have much higher rainfall than other sites. A similar pattern exists at the BoM site 61002 (Figure 3.14). All these sites are located towards the northern boundary of the catchment (i.e. Liverpool Ranges) (see Figure 3.12) and they illustrate that this part of the catchment receives much higher rainfall than other parts of the catchment. Other locations however, receive less rain and the rainfall pattern is closer to that of S2. Rainfall data therefore confirm that there is a significant spatial variation of rainfall within the catchment. The catchment scale rainfall distribution needs to be assessed in order to interpret the catchment scale soil moisture distributions. Double mass curve analysis does not provide the spatial variations of rainfall across the catchment. More detailed rainfall analysis is required to understand the rainfall distribution within the catchment.

Based on daily rainfall measurements at 52 sites, monthly rainfall distribution maps were developed to help the interpretation of soil moisture distributions across the GRC. First all daily rainfall values were combined into monthly values. These monthly rainfall totals were then introduced into the ArcView (ESRI, 1996a) based Geographic Information System (GIS). Using the Spatial Analyst (ESRI, 1996b) component of the ArcView, monthly rainfall surfaces were developed with the Inverse Distance Weighted (IDW) interpolation technique. The output value for each location was determined with 12 neighbourhood values. Use of IDW interpolation assumes that the variable being mapped decreases in influence with distance from its sampled location. It was assumed that a similar condition would apply to rainfall observations. The derived monthly rainfall distributions for 2003 and 2004 in the GRC are shown in Figure 3.15 and Figure 3.16 respectively. The distribution of total rainfall in 2003 and 2004 is given in Figure 3.17.

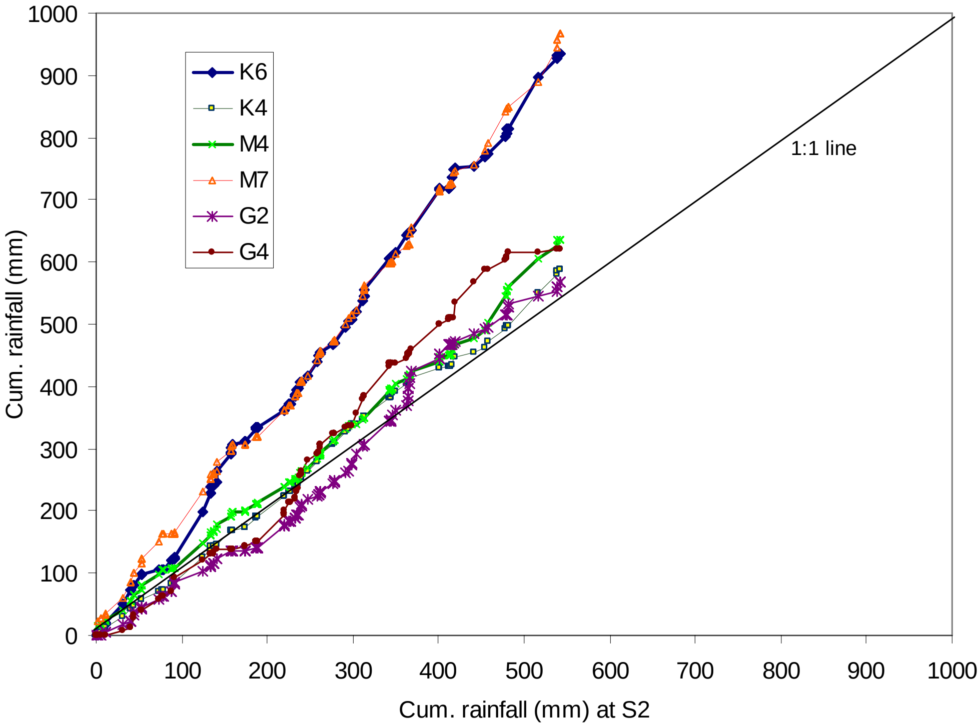

Figure 3.13: Comparison between cumulative rainfall at S2 and the cumulative rainfall of six other SASMAS sites within GRC during 2004.

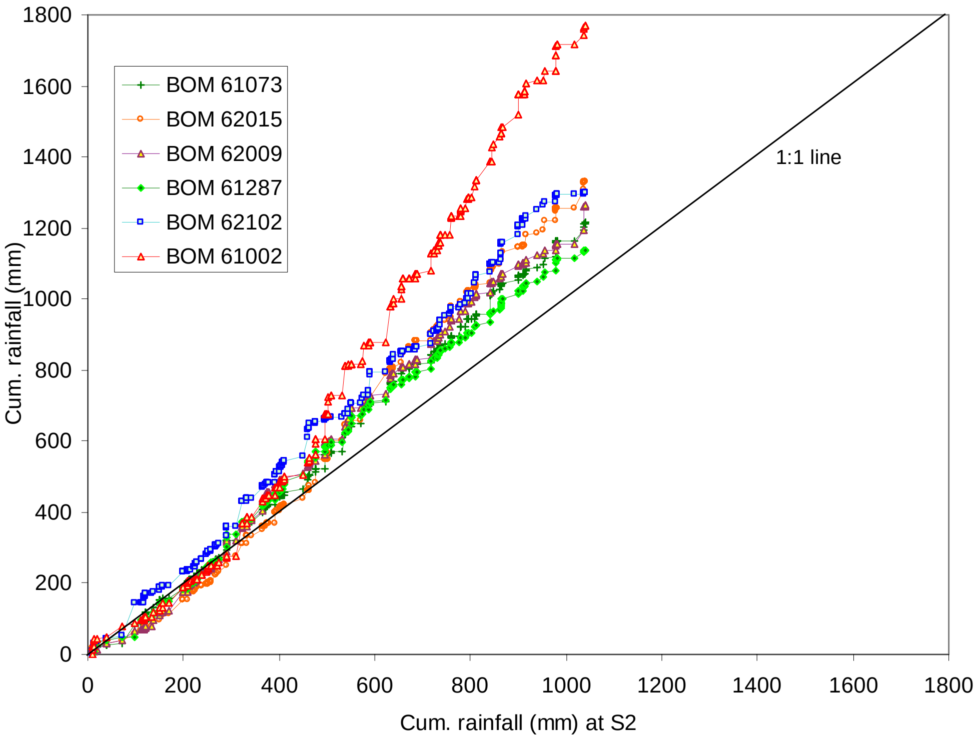

Figure 3.14: Comparison between cumulative rainfall at S2 and the cumulative rainfall of six BOM sites within GRC during 2003-2004.

According to Figure 3.15 and Figure 3.16, rainfall in GRC in 2003 and 2004 mainly occurred in mid to late spring and during summer months. Rainfall during 2003 was not normal due to the prolonged drought which continued from 2002. About five months during the year 2003 (January, March, May, July and September), the northern half of the catchment received less than 25mm of rain. The main wet month during 2003 was February. In 2004, April and June months were relatively dry (rainfall was < 25 mm) May, July and August were slightly wetter (rainfall between 25-50 mm). December was the wettest month in 2004.

Distribution of total annual rainfall across the catchment showed contrasting differences between 2003 and 2004 (Figure 3.17). In 2003, more rainfall occurred in the southern part of the catchment (> 670 mm) and the northern part of the catchment received rainfall of 550-670 mm. The annual average rainfall over the catchment was 634 mm in 2003. In contrast, whilst more rainfall (> 750 mm) was experienced towards the northern part of the catchment during 2004, the majority of the catchment gained less rainfall (<670 mm) (Figure 3.17 (b)). The annual average rainfall over the catchment was about 700 mm in 2004. It is also evident that a steep rainfall gradient is evident in the northern part of the GRC in 2004. As seen in Figure 3.17 (b), the northern most area (about 20 km wide strip) of the catchment has a significant variation in total rainfall. Some rainfall gradient is also visible in 2003 (Figure 3.17 (a)).

The spatial distributions in the rainfall pattern within GRC provide background to understanding the observed soil moisture distributions in the catchment. As seen in Figure 3.15 and Figure 3.16, monthly rainfall distributions during 2003 and 2004 were significantly different from month to month. Monthly rainfall patterns therefore should reflect the possible soil moisture distributions during each month across the catchment.

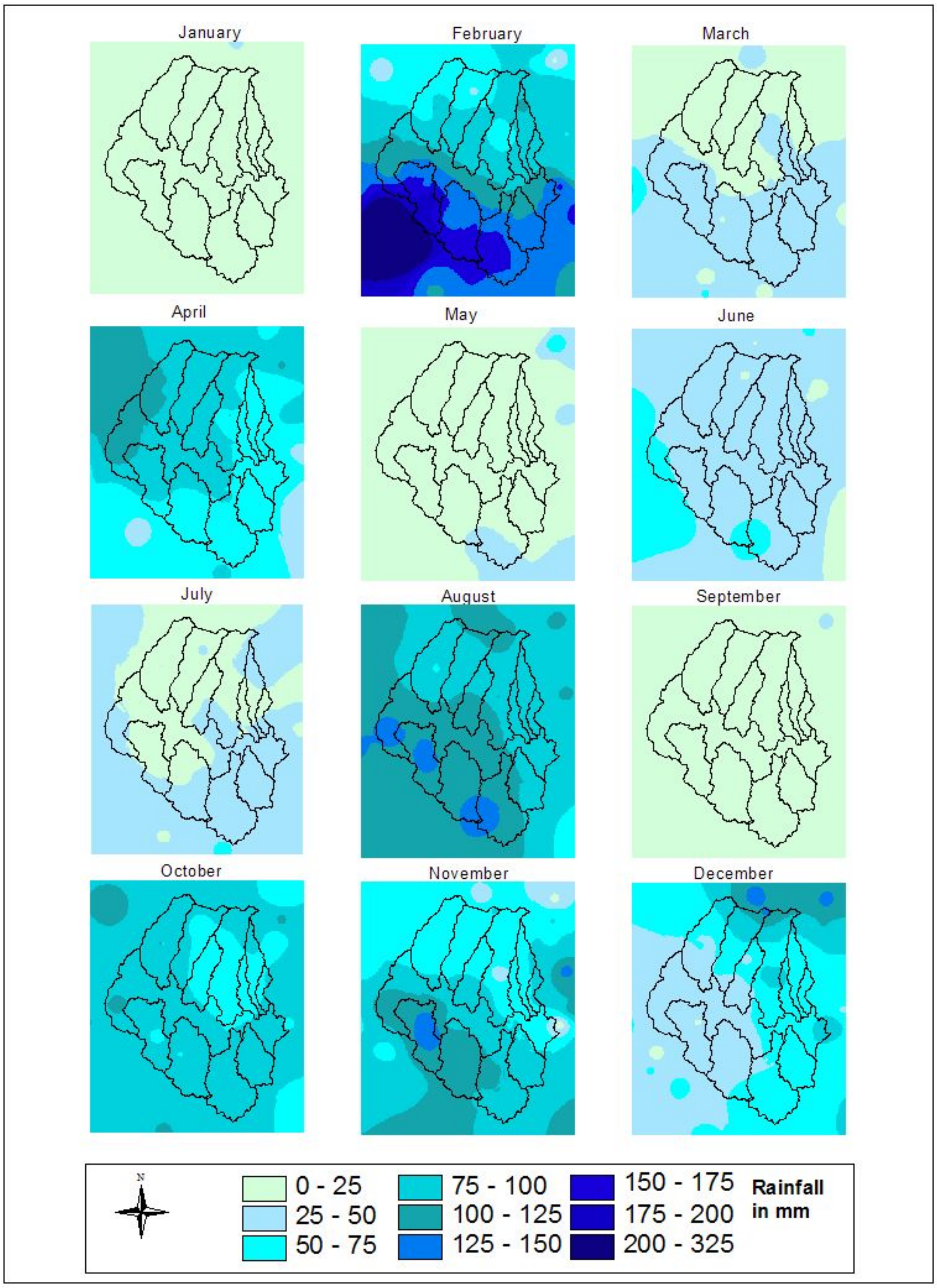

Figure 3.15: Derived monthly rainfall distributions in the Goulburn River Catchment in 2003.

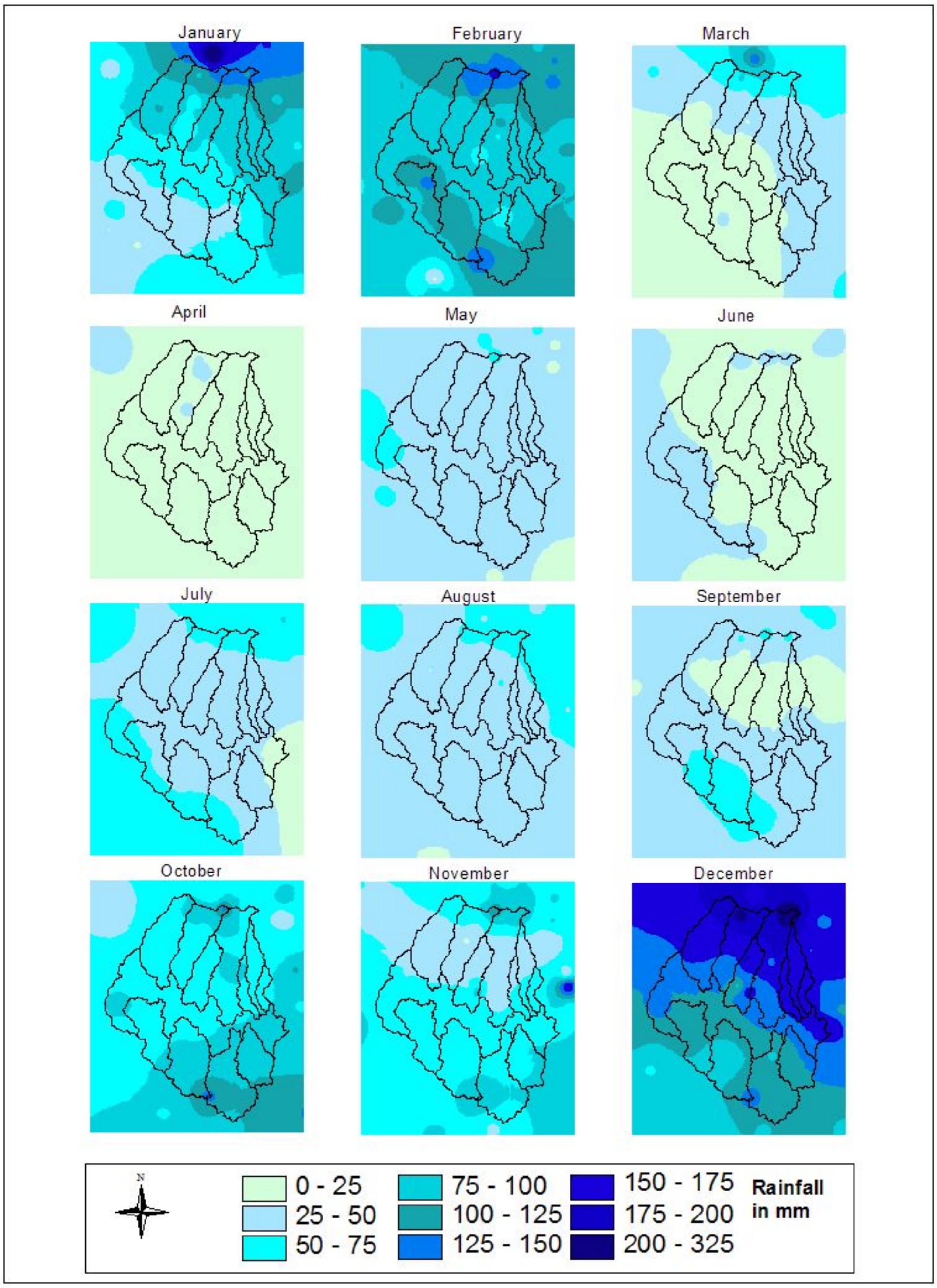

Figure 3.16: Derived monthly rainfall distributions in the Goulburn River Catchment in 2004.

(a)

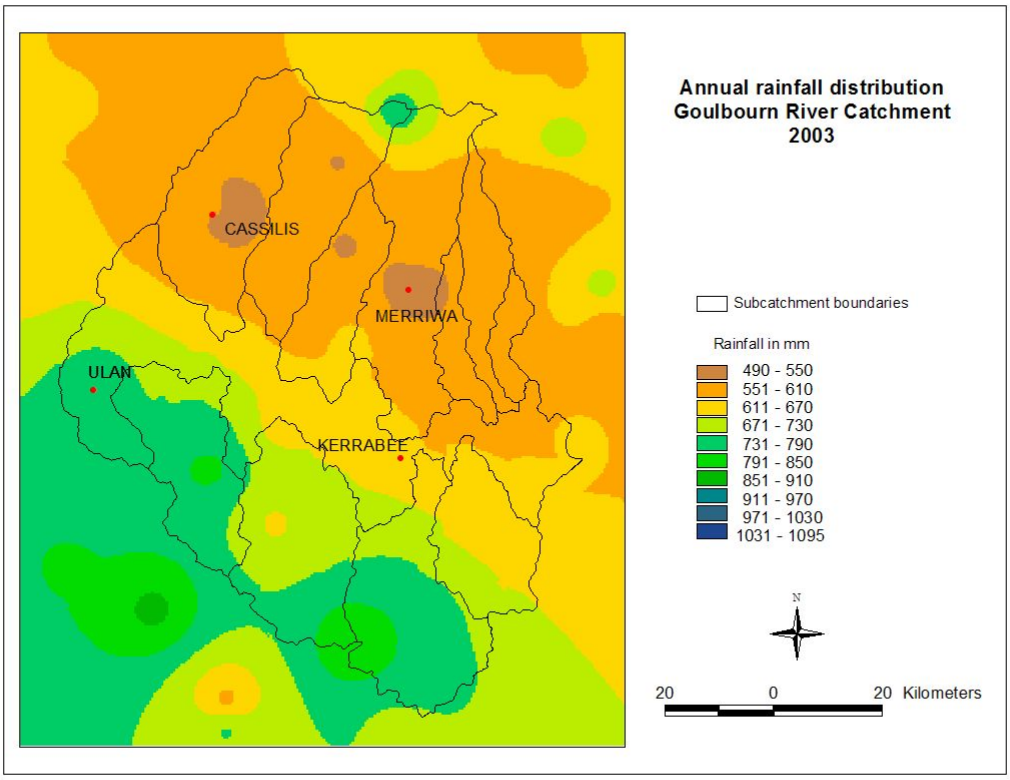

(b)

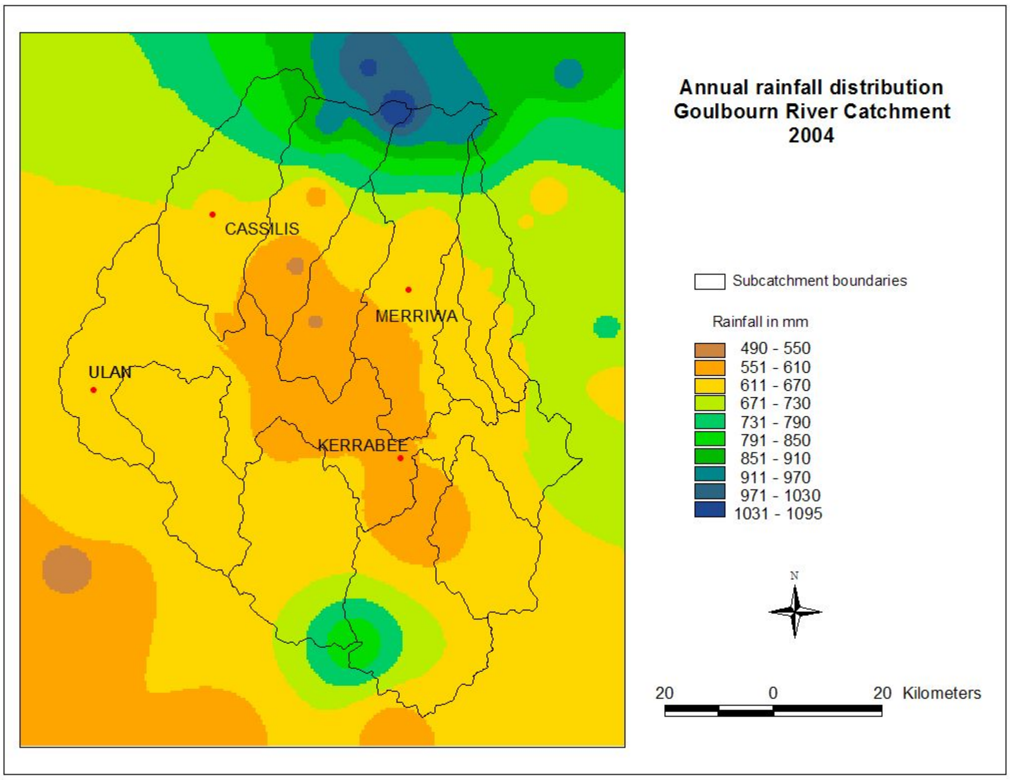

Figure 3.17: Inferred total annual rainfall distribution in the Goulburn River Catchment: (a) 2003, (b) 2004.

Additionally, the four collecting rain gauges at Stanley catchment provided an opportunity to assess the rainfall variability at the micro-catchment (~170 ha) scale. Table 3.10 shows the rainfall measurements made during field visits. This comparison shows that there were negligible differences between the collecting rain gauges at S2, S5 and S6. The gauge at S1 however, showed approximately 5 percent lower values than the other rain gauges. The collecting rain gauge data were recorded approximately once every six weeks. Due to this long recording interval, one needs to account for the loss of rainfall collected in the gauges due to evaporation, particularly during summer months. However, since all four collecting rain gauges are affected in a similar manner such evaporation loss may be ignored and it may be concluded that negligible spatial variation of rainfall occurred across the Stanley micro-catchment.

Table 3-10: Comparison of collecting rain gauge data (mm) measured between May 2003 and August 2004 at Stanley.

Date measured	S1	S2	S5	S6
8/05/2003	83.6	87.2	86.4	87.3
11/06/2003	14.6	14.5	16.0	15.0
23/07/2003	31.6	34.2	36.4	35.0
5/09/2003	105.2	104.3	103.8	96.8
16/10/2003	49.0	53.6	52.0	58.0
28/11/2003	69.6	84.3	86.8	79.0
22/01/2004	n/a	n/a	n/a	n/a
11/03/2004	92.0	91.2	88.2	95.8
22/04/2004	23.5	31.2	31.6	36.2
2/06/2004	44.6	45.6	43.4	45.0
16/07/2004	21.4	22.4	21.2	21.4
28/08/2004	40.7	39.9	37.2	37.8
Total	575.8	608.4	603.0	607.3

3.6.2 RADIATION

Measurement of total down-welling solar (short-wave) radiation (K↓) and the net all-wave radiation flux (Q^*) were undertaken at the Stanley climate station (S2). The instrument used to measure the total down-welling short-wave radiation in this field experiment is the CM3 pyranometer part of the Kipp & Zonen CNR-1

Radiometer (see Instruction manual available at www.kippzonen.com). The CM3 pyranometer consists of a thermopile sensor which generates an electric signal proportional to the radiation level. The CM3 pyranometer is sensitive to the spectral range between 0.3 – 2.8 µm. Net all-wave radiation was measured using a Radiation and Energy Balance Systems (REBS) model Q7-1 radiometer. Similar to CM3, REBS Q7-1 also uses a thermopile sensor for radiation measurement. Its spectral sensitivity is 0.25 – 60 µm.

The temporal variation of incoming solar radiation is given in Figure 3.18 and

Figure 3.19. The gaps in the plots are due to missing data. The trends in the radiation offer a clear estimation of radiation fluxes during each day. In general, daily totals of down-welling solar radiation (K↓) during summer months (25-35 $MJm^{-2}D^{-1}$) were significantly higher than those during the winter months (5-15 $MJm^{-2}D^{-1}$). Similarly, the 24-hour net radiation all-wave fluxes (Q^*) during summer months (15-20 $MJm^{-2}D^{-1}$) were much higher than the net radiation fluxes during winter months (3-6 $MJm^{-2}D^{-1}$).

The purpose of the radiation measurement was two-fold. First, radiation data are required to evaluate the available energy at the land surface. Second, radiation data are needed to compute the potential evapotranspiration (ET_o) fluxes based on Penman-Monteith approach. ET_o is needed in the estimation of the actual evapotranspiration (ET_a) component of the water balance equation and this will be presented in Section 3.6.5. Closing the water balance equation with the measured components such as rainfall, runoff and ET_a leaves one missing component, i.e. soil moisture changes. Thus, daily variations of soil moisture content may be estimated from balancing the water fluxes on a daily basis and this will be presented in Section 4.2.1. This is important because it provides a methodology to evaluate the measured and estimated soil moisture contents and thus a way of checking the validity of CS616 calibration equations which is discussed in Section 3.8.2.

Daily radiation also helps to characterize the climatic conditions during the AMSR-E validation study discussed in Chapter 7.

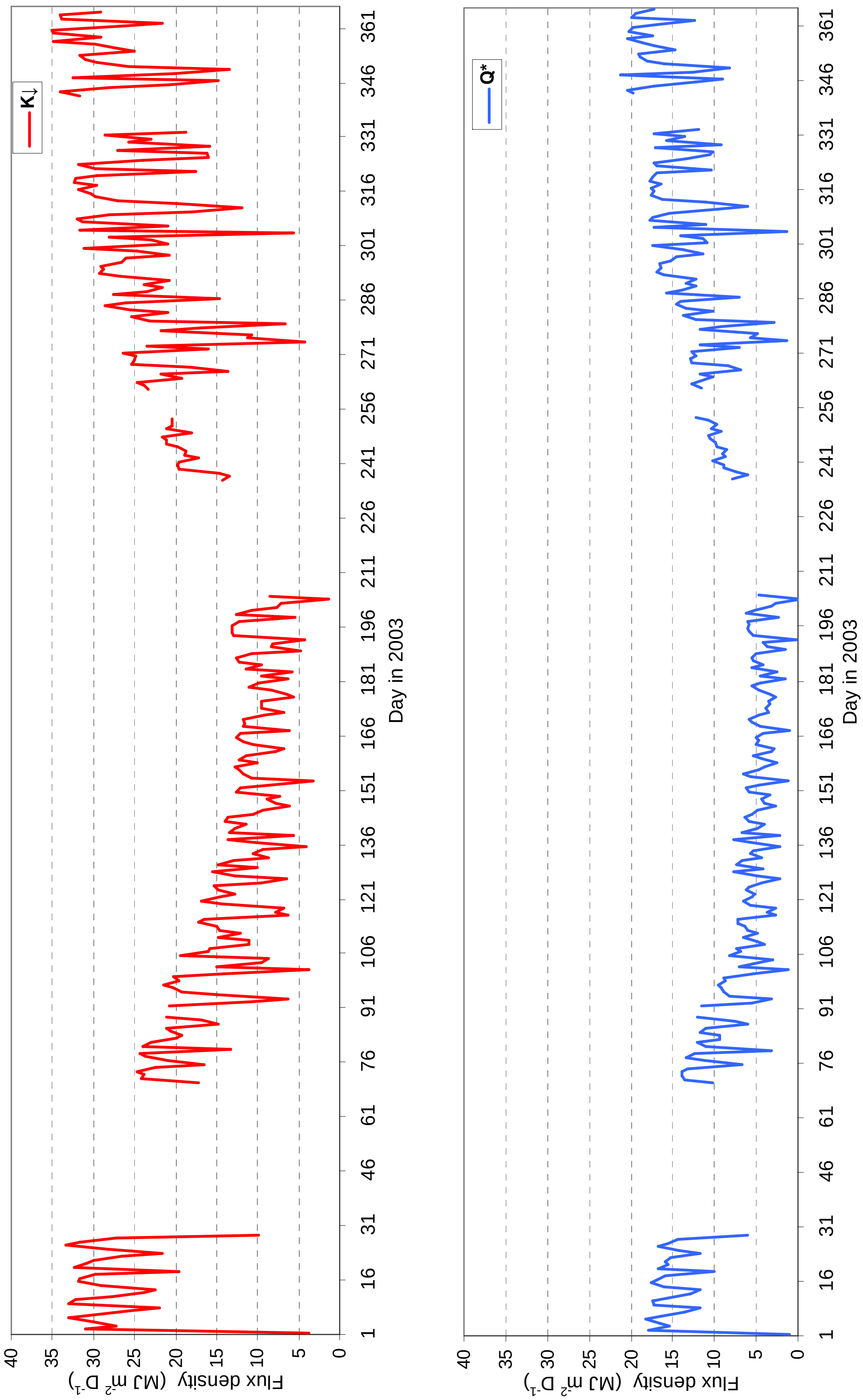

Figure 3.18: Total down-welling solar (short-wave) radiation (K↓) and net all-wave radiation (Q*) (in MJm^{-2}D^{-1}) as measured with Pyranometer and REBS Q7-1 Net Radiometer respectively, at the S2 climate station during 2003.

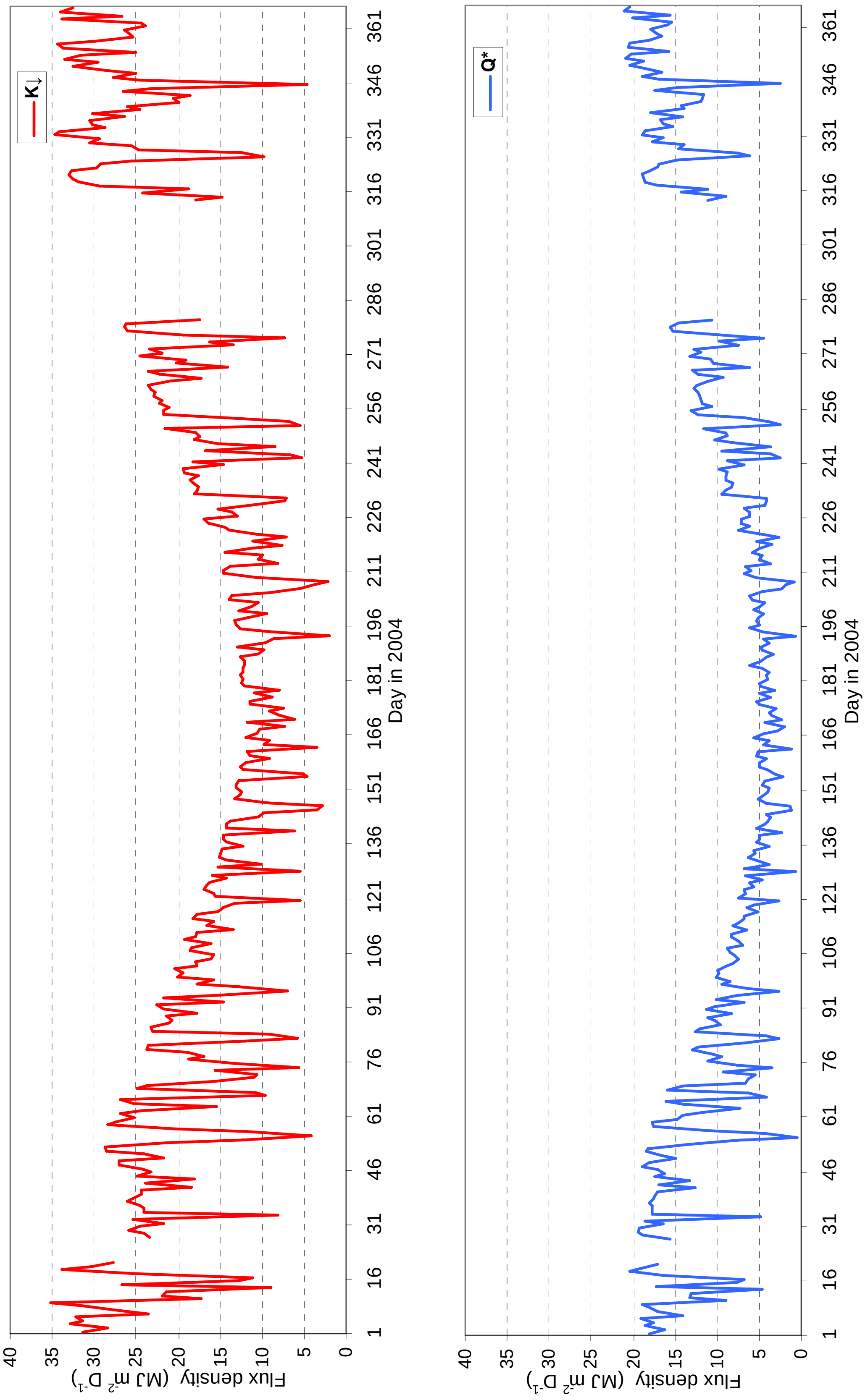

Figure 3.19: Total down-welling solar (short-wave) radiation (K↓) and net all-wave radiation (Q*) (in MJm^{-2}D^{-1}) as measured with Pyranometer and REBS Q7-1 Net Radiometer respectively, at the S2 climate station during 2004.

The installation of a 4-channel CNR-1 radiometer on Julian day 118 in 2004 allowed analysis of radiation data in another dimension. The down-welling (K↓) and up-welling (K↑) short-wave radiation components are important for many remote sensing studies such as for the validation of remotely observed land surface albedo (reflection coefficient) values. The temporal variation of up- and down-welling short-wave radiation and the computed albedo values for the same period are shown in Figure 3.20 and Figure 3.21 respectively. It can be concluded that the field measured albedo values for the land surface conditions at Stanley are in the 0.12 – 0.16 range with lowest values during winter months. The surface soil moisture is somewhat higher in winter months due to lower evaporative demand prevailing during winter. The albedo values are therefore lower during the winter season.

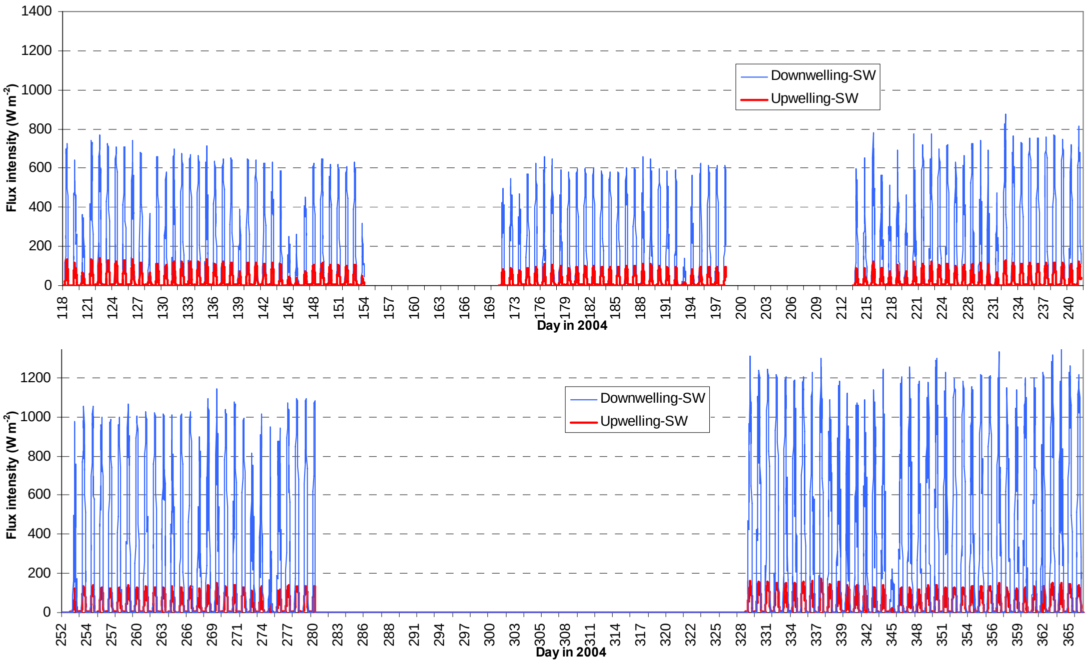

Figure 3.20: In-coming and out-going short wave radiation (Wm^{-2}) as measured from the CNR-1 radiometer at the S2 climate station from day 118 to 365 during year 2004.

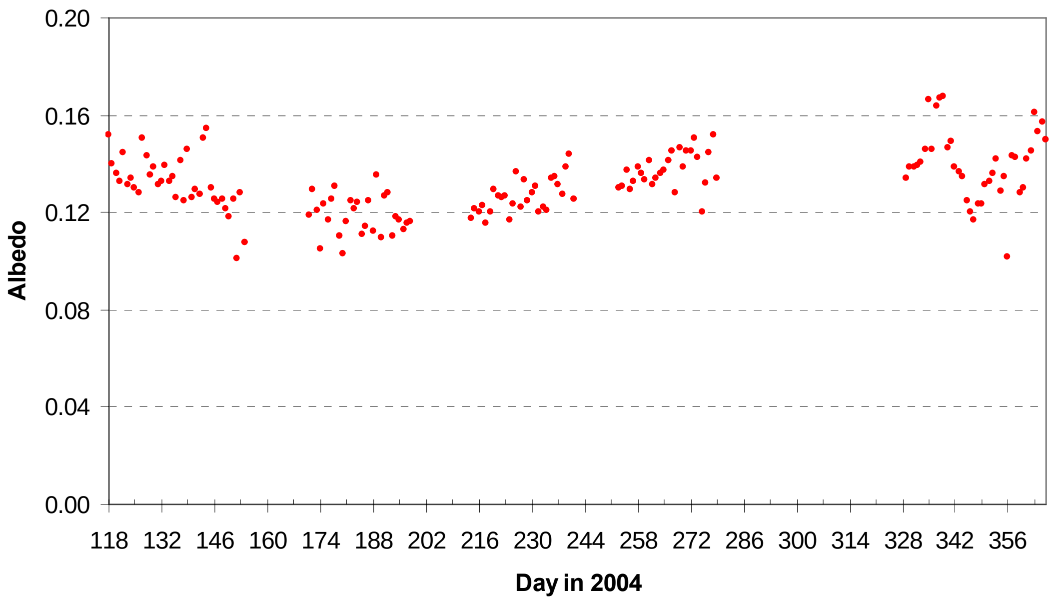

Figure 3.21: Computed albedo values for the land surface at the S2 climate station from day 118 to 365 during year 2004.

3.6.3 SOIL HEAT FLUX

The exchange processes at the land surface are important for the redistribution of moisture and heat in the near-surface soil layer and in the lower atmosphere. The thermodynamic equilibrium at the interface between atmosphere and soil can be demonstrated in the energy balance equation which for land surfaces (ignoring the energy required for photosynthesis and the heat storage in the vegetation) is represented by:

$$Q^* = G_o + H + \lambda E \qquad (\mathrm{W\ m^{-2}}) \qquad (3\text{-}2)$$

where

Q^* = net radiation flux

G_o = soil heat flux at the land surface

H = sensible heat flux

λE = latent heat flux

The sign convention in Equation 3.2 is that Q^* is considered positive if the radiation is directed towards the land surface, while the other three terms G_o, H and λE are taken as positive when directed away from the land surface. The component H is responsible for heating of air (generating a thermal gradient in the air) and the component λE is associated with evaporating water (creating a humidity gradient in the air). The component G_o heats (or cools) the soil surface. Usually the first two components on the right hand side are the most important ones and the third, soil heat flux is measured to close the equation. The partitioning between G_o, H and λE is forced by the transpiration process through stomata, evaporation from bare soil and open water surfaces.

Theoretically, the soil heat flux can be derived from temperature depth profiles. In practice it is difficult to do this as simplifications such as the assumption of uniform soil physical properties with depth makes flux estimation with this technique inherently uncertain. In this field experiment, Campbell Scientific Inc. HFT-3 soil heat flux plates were installed at climate station S2 and connected to the data logger. The HFT-3 sensor consists of a thin plate containing a thermopile which measures the temperature differences between the top and bottom surfaces from which a measure of the soil heat flux can be derived.

There are some concerns associated with installation of, and measurements with, heat flux plates. The flux plates need to be inserted into the soil surface layer, but the presence of plates very close to the surface can obstruct water vapour transport through the soil layer above the plate. This may occur in moist soils that are rapidly drying and may introduce errors in the heat flux measurements. Conversely, installation at depth gives a larger column of soil above which the vapour transport issue is minimized, but at the same time introduces a time lag into the soil heat flux measurements. The problem with measurements using soil heat flux plates may be minimised by measuring the temperature in the middle of the soil layer considered. In this experiment, soil heat flux plates were installed at the depth of about 5 cm from the surface. Soil heat flux sensors offer a local view of the soil heat flux at the level at which they are installed. Figure 3.22 details the course of the soil heat flux over 2004.

Figure 3.22: Temporal pattern of daily soil heat flux (W m^{-2}) values based on data logged at 20-minute intervals measured during 2004 at S2 climate station.

Measured daily soil heat flux intensities and the distribution over a year offer insight into the behaviour of soil heat flux intensities. During the summer months, the maximum day-time soil heat flux intensities were between 60-80 W m^{-2} which represents approximately 7.5 % - 10% of the net all-wave radiation. The night-time losses during summer months were between 10 -30 W m^{-2}, approximately 17% – 37% of the soil heat fluxes received during day-time. This situation results in gradual increase in soil temperature. In contrast, during winter months, the day-time soil heat flux intensities were less than 30 Wm^{-2} and this heat flux was approximately 7.5 % of the net all-wave radiation fluxes received during day-time (400 Wm^{-2}). The night-time soil heat losses from the soil (approximately 20 Wm^{-2}) were much higher (66 %) compared to day-time flux intensities. This situation results in gradual cooling of soil.

Field measured soil heat fluxes were used in the ET_o calculation outlined in Section 3.6.5.

3.6.4 AIR TEMPERATURE, HUMIDITY, AIR PRESSURE, AND WIND VELOCITY

Measurements of daily air temperature, humidity, air pressure and wind together with radiation are important for estimation of the potential evapotranspiration. Figure 3.23 and Figure 3.24 tracks the variation in daily temperature during 2003 and 2004 at the Stanley climate station (S2) and at the Spring Hills climate station (K6). The evolution of daily mean temperature shows a regular progression from month to month with a slightly asymmetric curve. In general, temperatures observed in K6 were slightly lower and more stable than the temperatures at S2. Minimum values at both stations were in July and maxima in January/February. Mean daily temperatures (computed from all temperature measurements collected in 20 minutes intervals during 24 hour period) in the three summer months, December, January, and February, exceed 25^{o}C for both stations, and in the three winter months are less than 11^{o}C. The trends in air temperature give an insight into the drying characteristics of the near surface soil layer and should be considered during the validation of remotely sensed near-surface soil moisture measurements as discussed further in Chapter 6. Measured air temperatures at both stations were used to compute ET_o as outlined in Section 3.6.5.

(a)

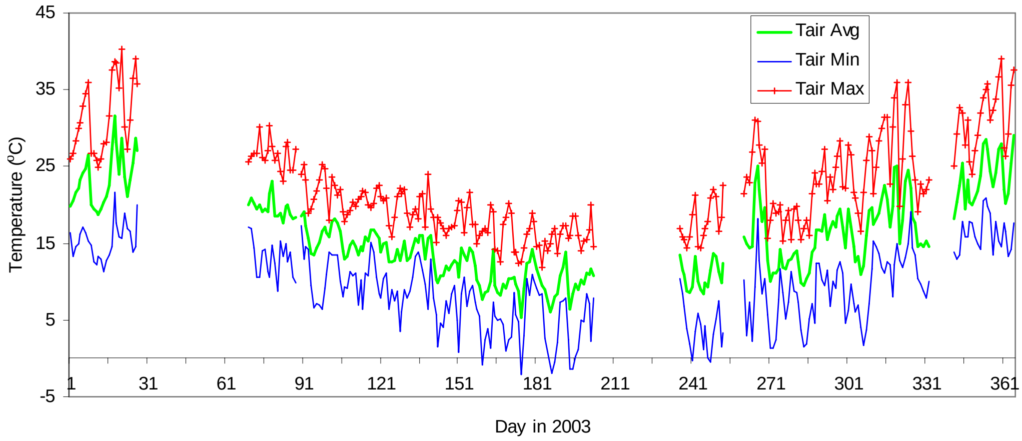

(b)

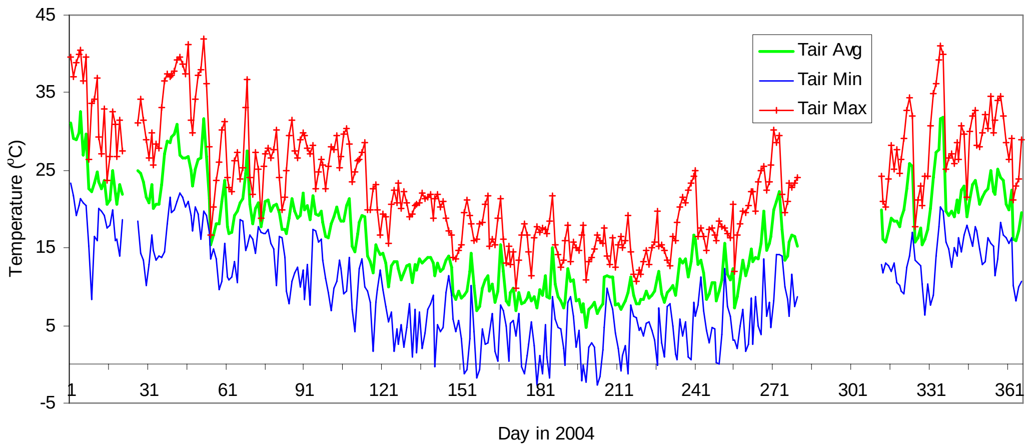

Figure 3.23: Measured daily minimum and maximum temperatures and computed average air temperature during a) 2003 and b) 2004 at Stanley-S2 (Note: gaps in the data due to data logger problems).

(a)

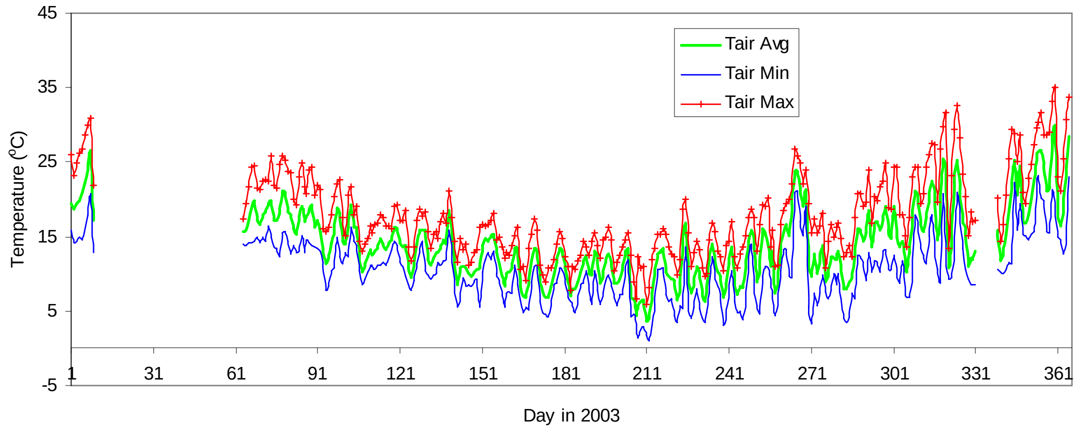

(b)

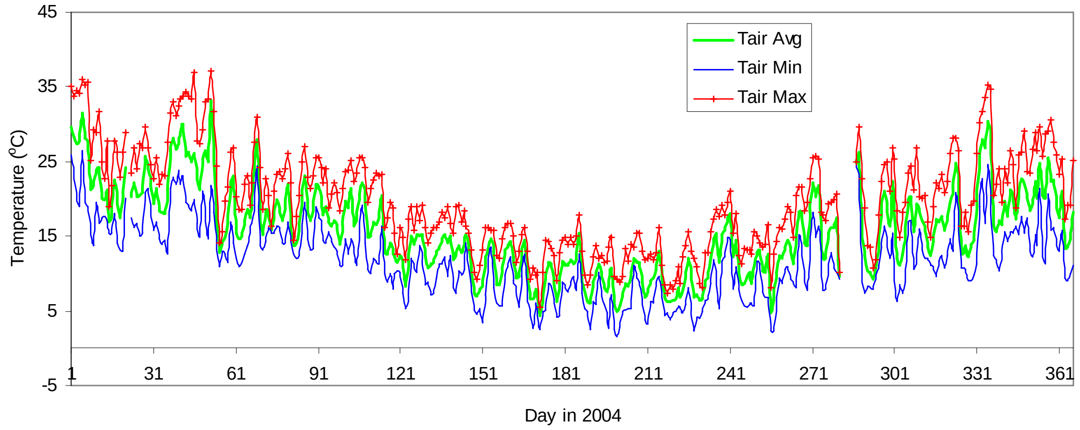

Figure 3.24: Measured daily minimum and maximum temperatures and computed average air temperature during a) 2003 and b) 2004 at Spring Hill (K6) (Note: gaps in the data due to data logger problems).

Relative humidity was also measured during this field experiment as this variable is required for the ETo computation. The instrument used to measure humidity was a Vaisala capacitive polymer-H chip sensor (Campbell Scientific Inc., 1999). Figure 3.25 and Figure 3.26 track the variation in daily average relative humidity during 2003 and 2004 at the Stanley climate station (S2) and at Spring Hill (K6) respectively. The annual patterns indicate that relative humidity at S2 was slightly higher than the humidity at K6. Generally, higher humidity values (> 80%) were associated with the winter period and lower humidity values (< 60 %) with summer months. Accordingly, the lower humidity values during summer months resulted in faster drying of the surface soil layers than during winter months.

(a)

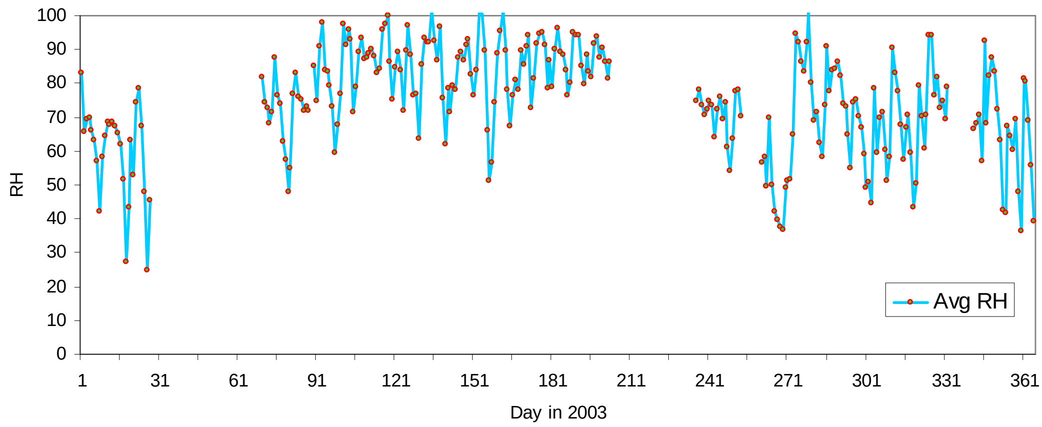

(b)

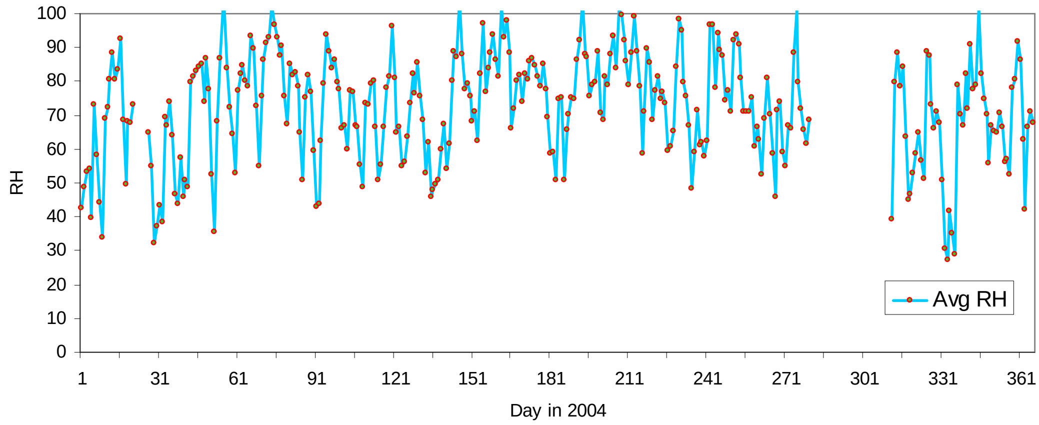

Figure 3.25: Measured daily average relative humidity during: a) 2003, and b) 2004 at Stanley S2.

(a)

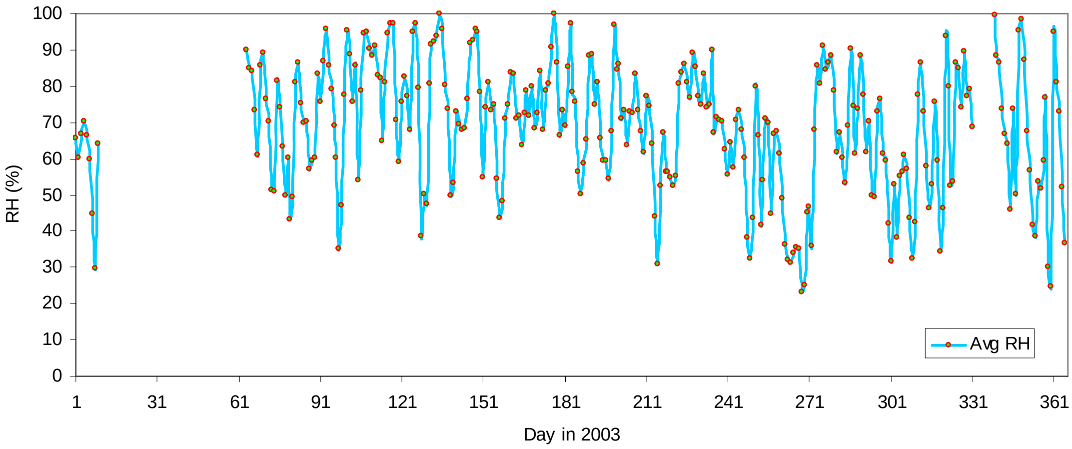

(b)

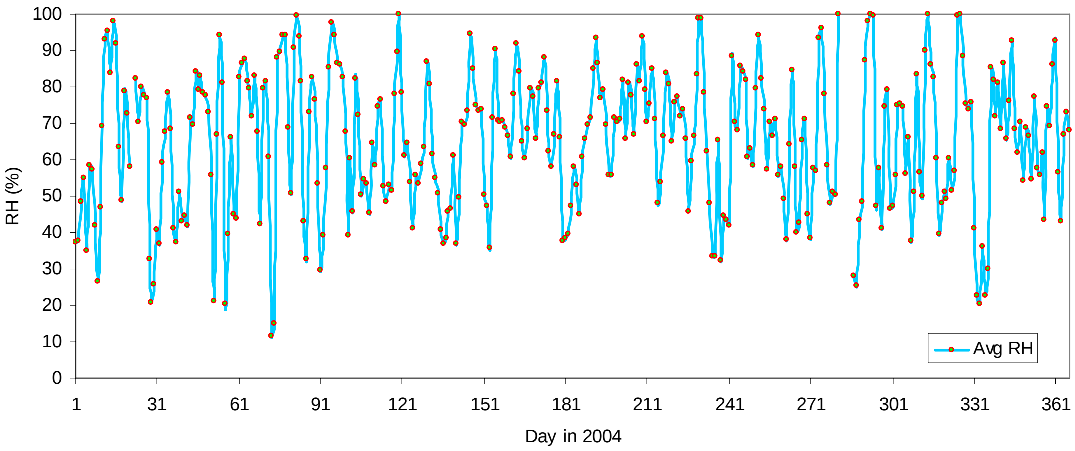

Figure 3.26: Measured daily average relative humidity during: a) 2003, and b) 2004 at Spring Hill (K6).

Daily wind speed was also measured at both S2 and K6 climate stations. Stronger wind can increase the soil drying rate, particularly of the near-surface layer. Figure 3.27 and Figure 3.28 show the daily average wind speed and 7-day average wind speed measured at S2 and K6 respectively. It is clear that there is no consistent pattern in the wind measured during 2003 and 2004 at both climate stations. Wind measurements at K6 however showed comparatively stronger wind velocities than at S2 as would be expected because of the higher elevation of K6. Wind increases the soil drying. Higher wind speed at K6, therefore should contributed to faster drying of the top soil layer.

a)

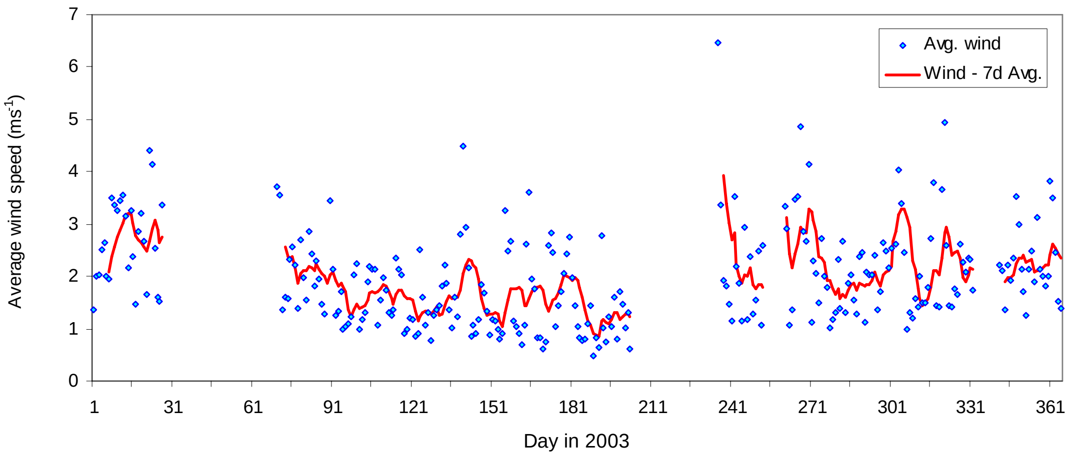

b)

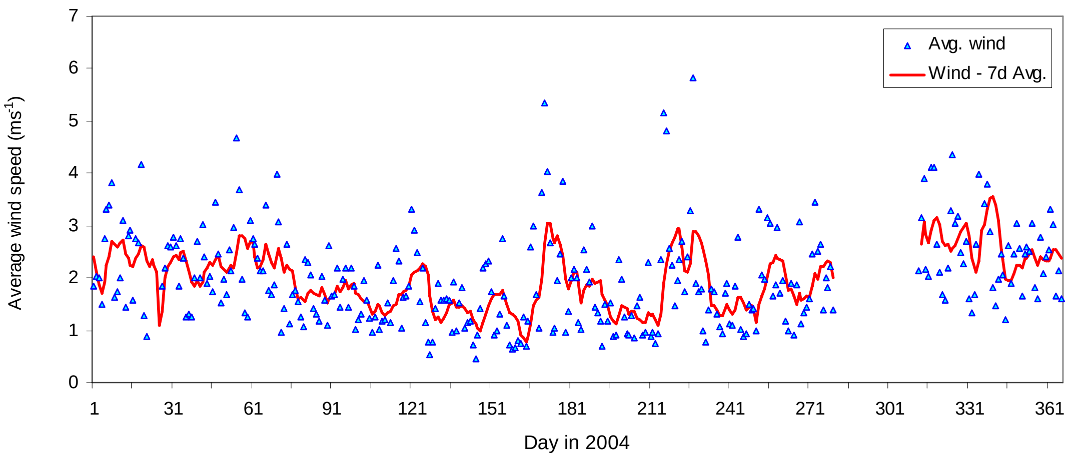

Figure 3.27: Measured daily average wind speed during: a) 2003, and b) 2004 at Stanley S2.

(a)

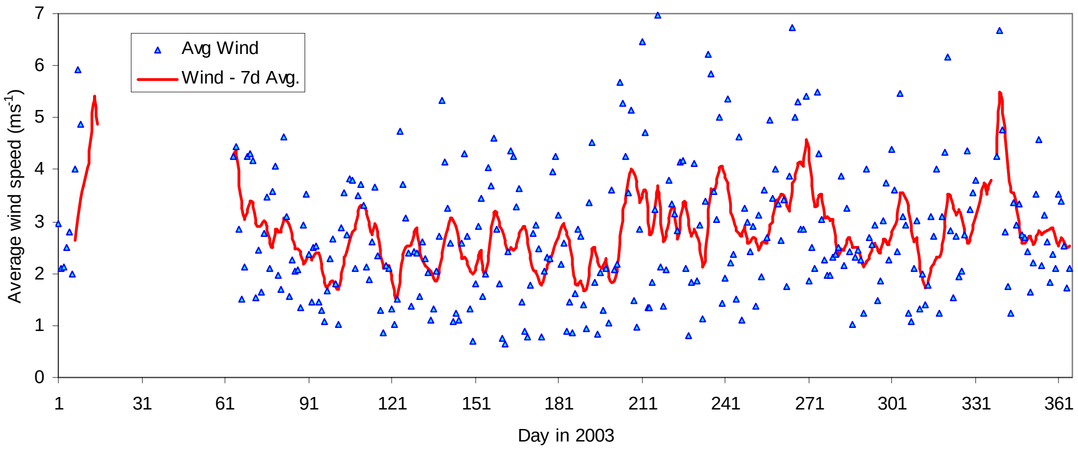

(b)

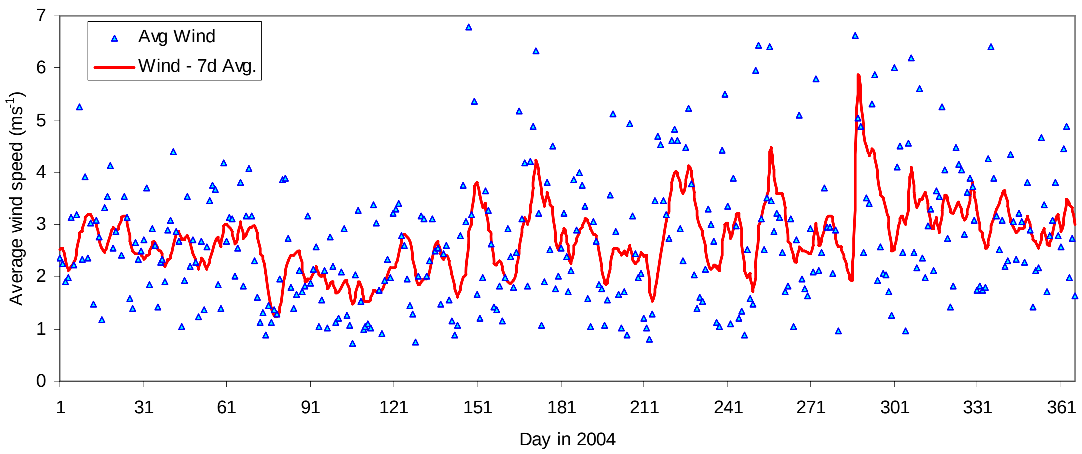

Figure 3.28: Measured daily average wind speed during: a) 2003, and b) 2004 at Spring Hill (K6).

The CS105 barometric pressure gauge at climate station S2 provides an insight into the temporal evolution of total atmospheric pressure during the study period. Measured atmospheric pressure during 2003 and 2004 is shown in Figure 3.29. While summer months were associated with slightly lower pressure conditions, winter months generally showed slightly higher pressure conditions.

(a)

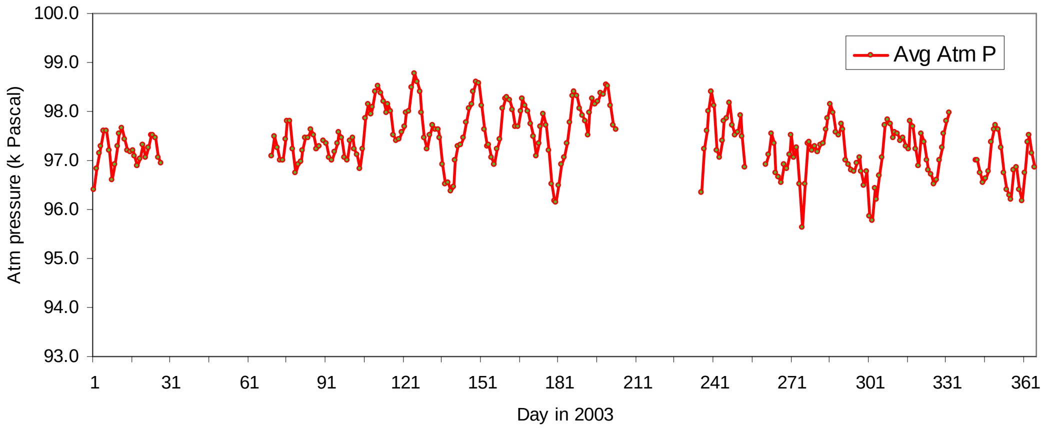

(b)

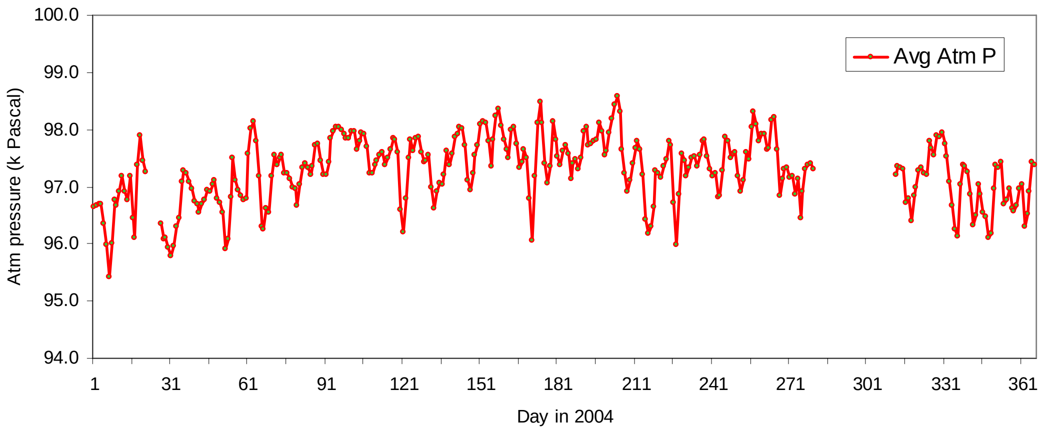

Figure 3.29: Measured daily average atmospheric pressure during: a) 2003, and b) 2004 at Stanley S2.

3.6.5 POTENTIAL EVAPOTRANSPIRATION

Actual evapotranspiration (ET_a) is an important input for the water balance study presented in Section 4.2. ET_a is one of the components of the water balance equation (see Section 2.4). When measured quantities such as rainfall and runoff and estimated quantities such as ET_a are used to close the water balance equation, the remaining component of soil moisture changes can be computed. ET_a however, is difficult to estimate directly and it is often derived from the potential evapotranspiration (ET_o). Potential evapotranspiration (ET_o), which is the actual plant water consumption at the given field situation when the soil is not under moisture stress, can be estimated using ET_o models.

Measurement of air temperature, humidity, wind, soil heat fluxes and radiation at the S2 offered an opportunity to estimate the ET_o based on the Penman-Monteith method as presented in the FAO reference evapotranspiration computation procedure (Allen *et al.*, 1998). At K6, the measured environmental variables (air temperature, humidity and wind velocity) were used with the radiation, soil heat flux and atmospheric pressure (after correcting pressure for elevation variations) at S2 to determine the ET_o because both stations are at nearly the same latitude. Therefore, there is no significant difference of incident solar radiation between these two stations. Figure 3.30 and Figure 3.31 show the trends of computed ET_o at S2 and K6 respectively. The trends in ET_o offer clear identification of low evaporation days during the winter months (< 2.5 mm d^{-1}) and high evaporation days (>9 mm d^{-1}) during the summer months.

a)

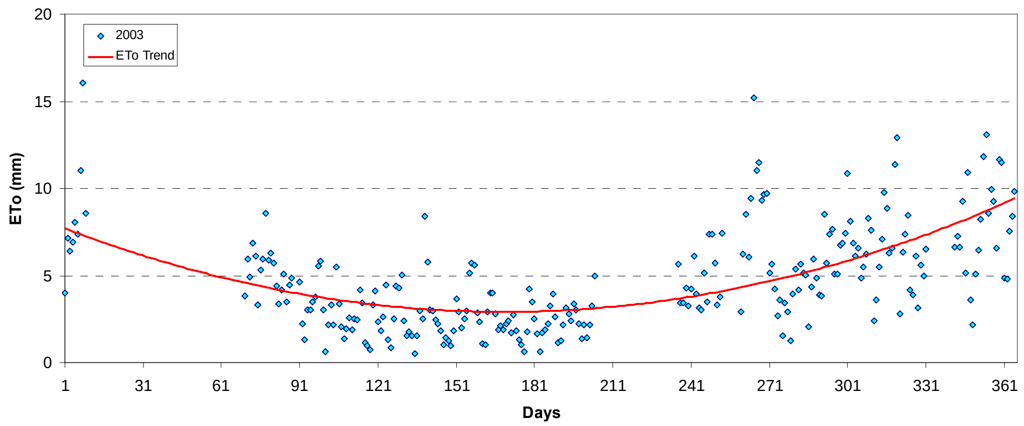

b)

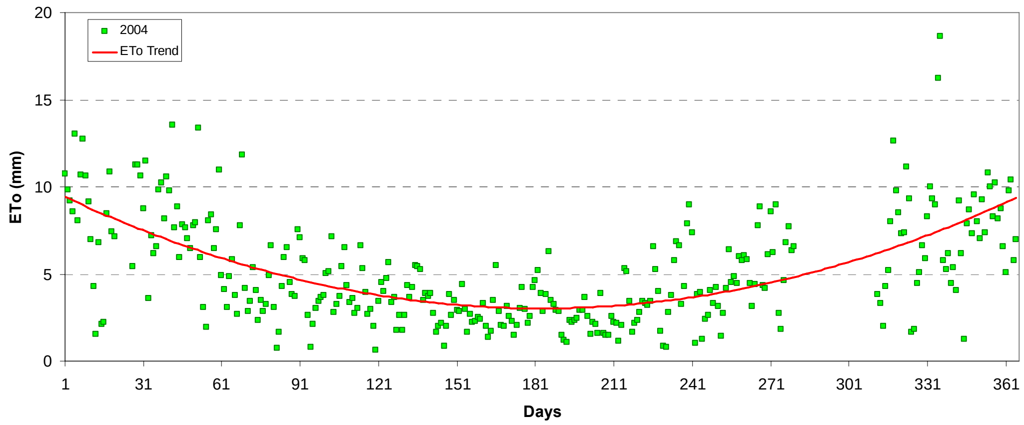

Figure 3.30: Daily ET_o at Stanley-S2 computed with the Penman-Monteith method: a) 2003, and b) 2004.

(a)

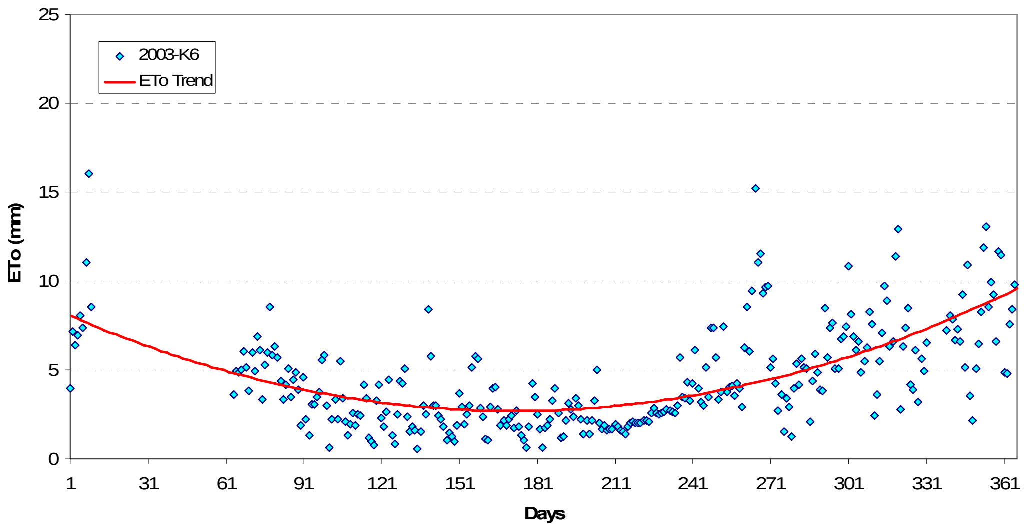

(b)

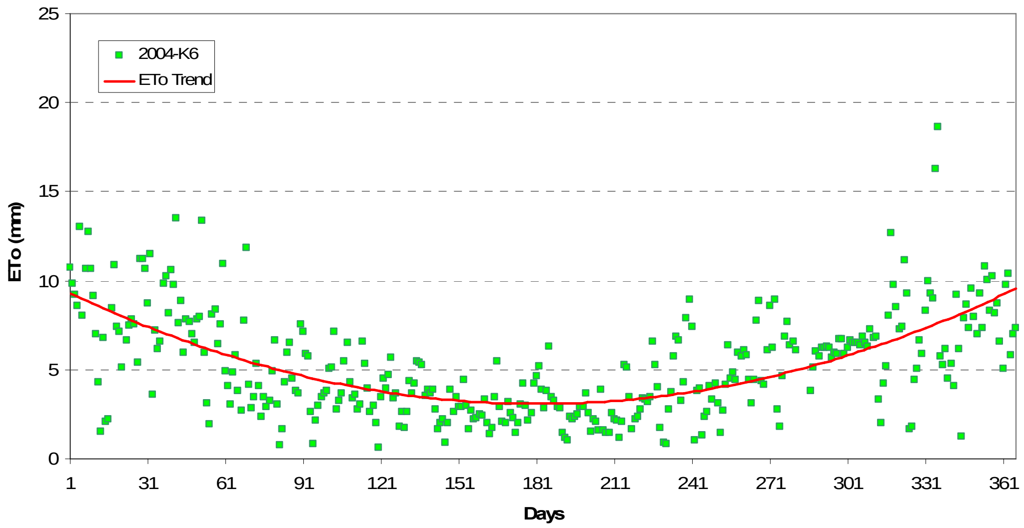

Figure 3.31: Daily ET_o at Spring Hill (K6) computed with the Penman-Monteith method: a) 2003, and b) 2004.

The comparison of computed ET_o at S2 and K6 helps to understand the potential ET (ET_o) at both stations as shown in Figure 3.32. It is clear that the ET_o values at both S2 and K6 compared well. While the total average ET_o at S2 was 1804 mm, ET_o at K6 was found to be slightly higher at 1854 mm. This may be partly attributed to the more favourable drying conditions (e.g. higher wind velocities) at K6. ET_o at K6 however does not represent the average ET_o throughout the GRC due its location. K6 is located at 741m above sea level whereas most of the catchment is positioned between 400-500m above mean sea level. For this reason, ET_o computed at S2 was considered as the ETo for the GRC. The computed ET_o values will be used in Section 4.2 to estimate the actual ET values and close the water balance equation to predict soil moisture from a single layer bucket model.

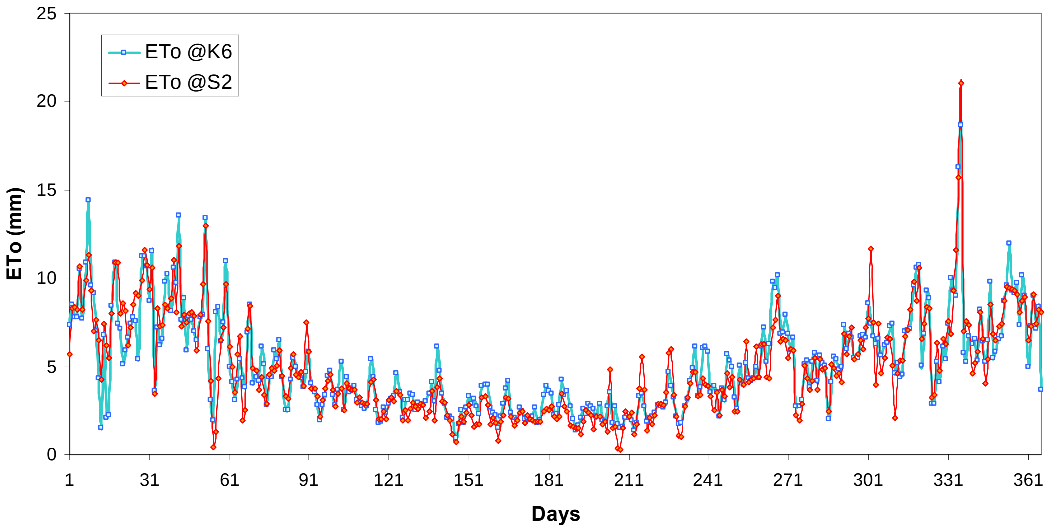

Figure 3.32: Comparison of daily ETo between K6 and S2.

3.7 SOIL TEMPERATURE

Soil temperature also gives an indication of moisture status of the soil because wet soils are generally cooler during daytime and warmer during the night. In the present study, continuous measurement of soil temperature at 15, 45 and 75 cm depths was undertaken mainly to correct the soil moisture measurements obtained from CS616 WCRs.

Near-surface (0-1 cm) soil temperature has a strong relationship with the air temperature. Figure 3.33 shows the relationship between air temperature and near-surface soil temperature based on the day-time measurements collected during field visits between June 2003 and August 2004. In general, near surface soil temperature is slightly higher than the air temperature. This suggests that in the absence of measured near surface soil temperature data, measured air temperature may be used with a degree of confidence.

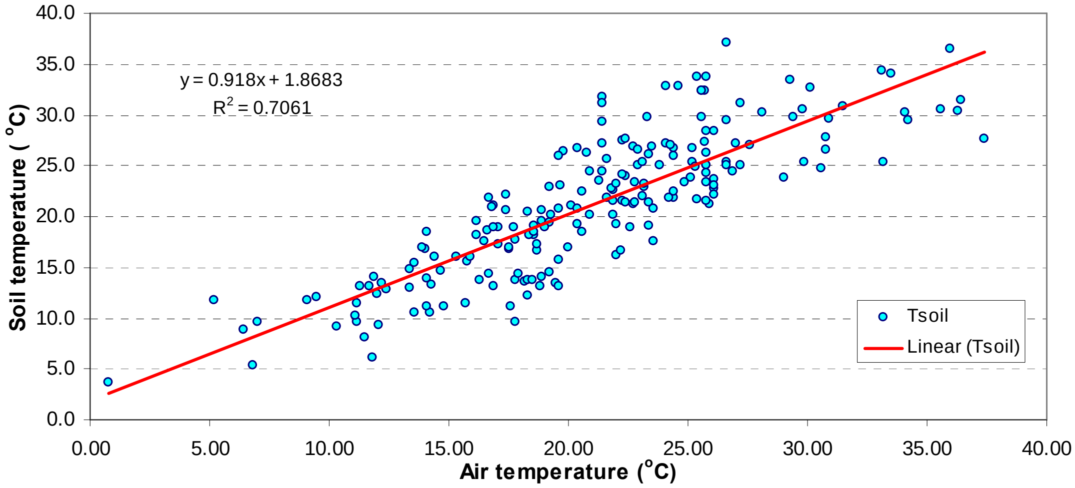

Figure 3.33: Near-surface soil temperature and air temperature measured during field visits between June 2003 and April 2004.

3.7.1 TEMPERATURE CORRECTION FOR CS616

The CS616 sensor is sensitive to the temperature of the medium being used. The original calibration of CS616 was done under constant temperature of 20°C and therefore, CSI provides the following equation to correct the readings for temperature effects:

$$R_c(T_s) = R_{uc}+(20-T_s)*(0.526-0.052*R_{uc} + 0.00136*R_{uc}^2) \qquad (3\text{-}3)$$

where R_c = corrected readings, R_{uc} = uncorrected readings, T_s = soil temperature

However, some authors do not agree with the CSI recommended equation for the temperature correction and have been proposed new equations. Stenger *et al.* (2005) found that CSI temperature correction results in higher corrected VWCs when the measurement temperature is below the reference temperature of 20°C and the uncorrected VWC is < 40%. On the other hand, it results in a lower corrected VWC if the uncorrected VWC is >40%. Western and Seyfried (2005) also identified the inaccuracies of the CSI temperature correction and have recommended a new equation. However, all these studies used CS615 WCRs, (the previous version of the CS616) and their findings may not be entirely valid for CS616s. Therefore, the CSI recommended temperature correction has been used in the current study.

3.7.2 SOIL TEMPERATURE PROFILE ESTIMATION FROM MEASURED SOIL TEMPERATURE AT 15CM DEPTH

Soil temperature follows a diurnal cycle as well as an annual cycle. Both cycles are closely linked to air temperature and solar radiation. The amplitude of these cycles is generally greater for surface layers than for the deeper soil layers. For example, Figure 3.34 shows the measured temperature profiles at different times during a selected early summer day. It is clear that the temperature measured at 15cm depth does not represent the temperature at deeper depths such as 45cm or 75cm which are important for the present study. Soil temperatures at the mid-points of CS616 WCR at 30-60 cm and 60-90 cm depths are required for the temperature correction of the sensor readings (see Section 3.7.1). Temperatures at these depths however, may be derived from the measured temperature at 15cm depth due to propagation of heat from surface layers to subsurface layers and *vice-versa*. It is also evident from Figure 3.34 that the range of temperature variations at deeper layers is much narrower than the range of temperature variations at the surface. This suggests that the computation of daily average temperature values is sufficient for soil temperatures at 45cm and 75cm depths.

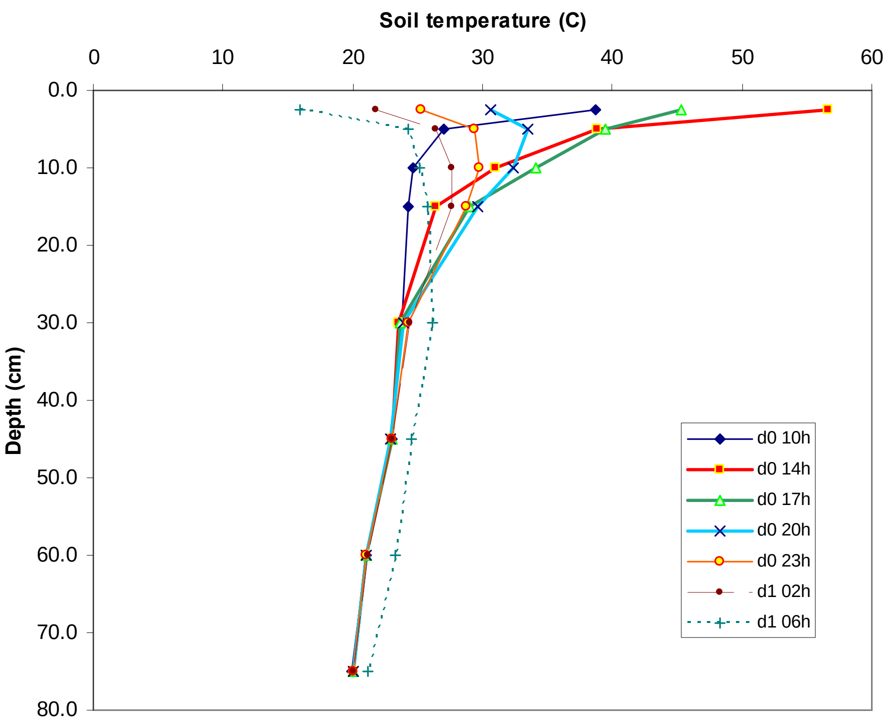

Figure 3.34: Measured soil temperature profiles at 10, 14, 17, 20 and 23 hrs on the first day (d0) and 2 and 6 hrs on the following day (d1) at S2 on day 316/317 in 2002.

Measurement of soil profile temperatures at Spring Hill (K6) and Stanley S2 provided an opportunity for establishing a methodology to derive soil temperatures at 45cm and 75 cm depths based on the measured temperature at 15cm depth. Daily soil temperature measurements at Spring Hill (K6) at 15, 45 and 75cm depths have been used to establish regression relationships between soil temperatures at 15cm and soil temperatures at 45 and 75 cm depths.

Derived soil temperatures at 45cm depth and 75 cm depth at K6 were:

1) T_{soil} at 45 cm depth is derived from (R^2 = 0.913, correlation coefficient = 0.956):

$$T_{45} = 3.8199 + 0.776 * T_{15} \quad (3\text{-}4)$$

2) T_{soil} at 75 cm depth is derived from (R^2 = 0.818, correlation coefficient = 0.904 and 95% confidence interval for intercept and T_{15} slope is 6.094-6.179 and 0.640-0.646 respectively):

$$T_{75} = 6.1366 + 0.643 * T_{15} \quad (3\text{-}5)$$

Similarly, at Stanley S2, daily soil temperature at 15, 45 and 75cm depths have used to establish regression relationships between soil temperatures at 15cm and soil temperatures at 45 and 75 cm depths.

The derived soil temperatures at 45cm depth and 75 cm depth at S2:

1) T_{soil} at 45 cm depth is derived from (R^2 = 0.906,):

$$T_{45} = 0.954 + 0.973 * T_{15} \quad (3\text{-}6)$$

2) T_{soil} at 75 cm depth is derived from (R^2 = 0.864 and 95% confidence interval for intercept and T_{15} slope is 5.981-6.071 and 0.649-0.654 respectively)):

$$T_{75} = 6.026 + 0.652 * T_{15} \quad (3\text{-}7)$$

Equation 3.6 was derived from a limited data set obtained between day 299 and 318 during 2002. The temperature sensor at 45cm depth became inoperative after this period and it was therefore impossible to collect a sufficient data set to establish a reliable relationship between soil temperatures at 15cm and 45cm depths. This is clearly evident from Figure 3.35 which shows a comparison of derived soil temperatures at 45cm and 75cm depths. Computed temperatures at 45cm depth from equation 3.6 (i.e. S2-equation) show very high temperature values compared to computed temperatures at 45cm depth from equation 3.4 (i.e. K6-equation). At 75cm depth however both equations 3.5 (K6) and 3.7 (S2) predicted very similar temperatures. Therefore, it was decided to use only the equation 3.4 and 3.5 for predicting soil temperatures at 45cm and 75cm depths, respectively. The predicted soil temperatures at 45 cm and 75 cm depths were then used for the temperature correction of 616 readings in calculating water contents in the 30-60 cm and 60-90 cm soil depths for the water balance study discussed in Section 4.2.

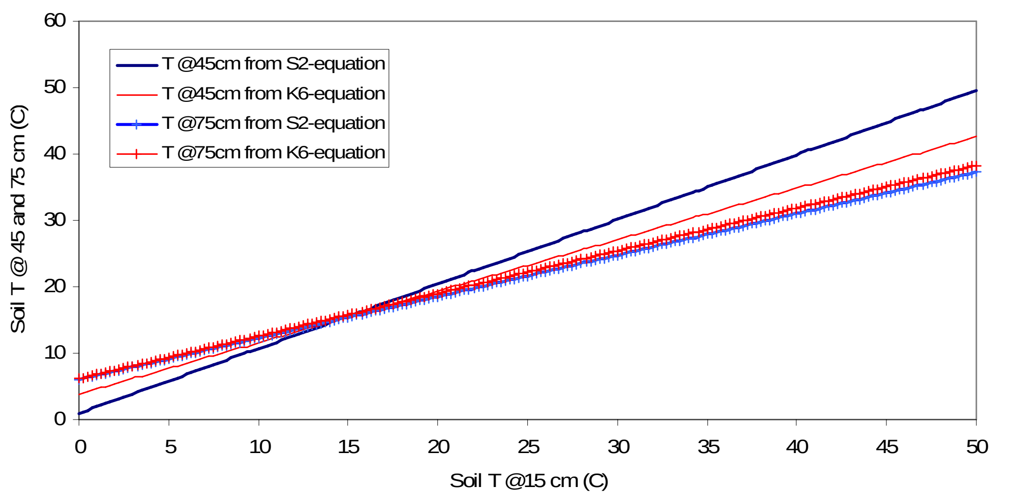

Figure 3.35: Comparison of derived soil temperatures at 45cm and 75 cm depths.

3.8 SOIL MOISTURE

3.8.1 CALIBRATION OF CS616 WCR

Despite the fact that volumetric water content measurements form both TDR and WCR are based on soil dielectric properties, the two instruments use different measurement frequencies (Chandler *et al*., 2004). While TDR instruments use up to about 1 GHz of effective measurement frequencies (Or and Wraith, 1999) the WCRs use generally between 15 and 45 MHz (Seyfried and Murdock, 2001). As a result, WCRs are more sensitive to variations in soil solution concentration or composition and variation in clay content and type, because these affect electrical conductivity and therefore, have a greater effect on soil dielectric properties at low measurement frequencies than at high frequencies (Seyfried and Murdock, 2004). Therefore, VWC calibration of a WCR will tend to be more sensitive to soil type than for TDR (Chandler *et al.*, 2004). This suggests that site specific calibration may be required for WCR. Several attempts have already been published (Seyfried and Murdock, 2001; Chandler *et al.*, 2004; Seyfried and Murdock, 2004; and Stenger *et al.*, 2005).

Calibration relates the output signal frequency to the volumetric water content. Two types of calibration equations are possible; one in the linear form and other in the quadratic form and the latter is recommended. The product literature provides standard calibration equations in linear and quadratic forms for loamy fine sand. CSI claims an accuracy of about ± 2.5% volumetric water content using standard calibration with low EC ($\leq$0.5 dS m^{-1}) and bulk density $\leq$1.55 $g.cm^{-3}$ in measurement range 0% to 50% VWC. It also provides two additional equations for sandy clay loam soils.

The CSI calibration equations are as follows:

1. Standard equation for loamy find sand:

$$WC_{vol} = -0.0663 - 0.0063 * \mathbf{R} + 0.0007 * \mathbf{R}^2 \quad (3\text{-}8)$$

2. For sandy clay loam: (BD=1.6 $g.cm^{-3}$, EC 0.4 dS m^{-1})

$$WC_{vol} = 0.0950 - 0.0211 * \mathbf{R} + 0.0010 * \mathbf{R}^2 \quad (3\text{-}9)$$

3. For sandy clay loam: (BD=1.6 $g.cm^{-3}$, EC 0.75 dS m^{-1})

$$WC_{vol} = -0.0180 - 0.0070 * \mathbf{R} + 0.0006 * \mathbf{R}^2 \quad (3\text{-}10)$$

where WC_{vol} is the volumetric water content and **R** is the period measurement in microsecond.

SASMAS soil moisture monitoring sites were located in a range of soil types with different physical and chemical properties (see Table 3-7, Table 3-8 and Table 3-9). The soil characteristics of most of these sites did not closely representing the standard soil types used for the sensor calibration by CSI. Therefore, in order to estimate the soil water content accurately and to obtain the maximum benefit of the sensor's high accuracy and precision, site specific calibrations were required.

The best method of calibrating CS616 is the laboratory based procedure where one can measure the actual weight of the soil water content using an accurate weighing device. Furthermore, the laboratory method facilitates conducting the calibration procedure under controlled environmental conditions including maintaining constant temperature. This is very important as the CS616 readings are sensitive to the temperature of the medium being measured. The University of Melbourne (UM) had such facilities and site specific calibrations of CS616 for each soil moisture monitoring site were carried out in the UM laboratory.

A total of 28 soil samples were collected for use in CS616 calibration at UM. These samples represented all SASMAS sites except S5 and S7. Three samples each were collected from G1 and G3 to represent 0-30, 30-60 and 60-90 cm depths. All other 22 soil samples were for the top 30 cm layer of the other SASMAS sites. When collecting soil samples, a cylindrical shape sample of diameter of approximately 22 cm and length of 30 cm was removed using a post-hole auger. However, collecting a clean cylindrical shape sample was often found to be difficult due to the stony nature of soil.

Twenty-three calibration equations, all in quadratic form, have been established at UM to produce volumetric water content (VWC) from CS616 measurements. (For the details of calibration procedures see Rüdiger *et al*., in review). A summary of the UM-calibration parameters is given in Table 3-11.

Before applying these calibration parameters to compute actual soil moisture content at each site, an evaluation study was conducted with the maximum and minimum field-measured CS616 readings which were assumed to represent the minimum and maximum soil moisture levels encountered over the two years of measurements. Using the UM calibration parameters minimum and maximum SWCs were computed for all sites (see Table 3-12). The soil water characteristics of 14 study sites in the Goulburn River Catchment have been previously studied (King, 2004). The results of that study provided a basis for evaluating the computed SWC from the UM calibrations. The minimum water content measured with the Tempe cell was based on air-dried soils (suction of about 1 bar) and the maximum water content was based on saturated soils (suction of about 0 bar). These boundaries of measured water contents can therefore be considered as reliable data to compare with the water contents derived from CS616 using the

UM calibrations. Table 3-12 shows the comparison of minimum and maximum water contents computed from the UM calibrations and measured from the Tempe cell. As seen in the table, anomalous low and high values in minimum and maximum values were observed at a number of sites. For example, computed maximum water contents of some sites (e.g. K5) were unacceptably high (0.67 $cm^3\ cm^{-3}$), whilst other sites gave extremely low values (e.g. the minimum SWC at G5 was 0.002 $cm^3\ cm^{-3}$). Although it is known that the CS616 WCR is not very sensitive to extremely low water contents, such very low or very high SWC are unlikely under natural conditions. Based on water-saturated and air-dried samples, significant uncertainties arose about the reliability and appropriateness of the UM calibrations.

Table 3-11: UM-calibration parameters for SASMAS sites. All calibration equations are in the form of: VWC = *a* + *b* * (Reading) + *c* * (Reading)^2 where Reading is in microseconds.

	Calibration Parameters – UM		
Site	***a***	***b***	***c***
G1	-0.39282	0.02069	0.00017
G2	-0.03994	-0.00537	0.00053
G3	0.00451	-0.00559	0.00038
G4	-0.54648	0.03493	-0.00010
G5	-0.21474	0.00124	0.00072
G6	0.29300	-0.03306	0.00094
K1	-0.12655	0.00813	0.00022
K2	0.57058	-0.06531	0.00191
K3	0.15826	-0.02060	0.00067
K4	4.72563	-0.30352	0.00499
K5	0.50111	-0.05386	0.00144
K6	0.31587	-0.03062	0.00075
M1	-0.32325	0.01338	0.00040
M2	-0.20074	0.00166	0.00069
M3	-0.01498	-0.00778	0.00051
M4	0.38908	-0.04108	0.00107
M5	0.05510	-0.01031	0.00046
M6	0.28649	-0.03067	0.00087
M7	-0.13166	0.00543	0.00017
S1	-0.06826	-0.00148	0.00034
S2	-0.02509	-0.00606	0.00047
S3		n/a	
S4	0.09427	-0.01629	0.00069
S5		n/a	
S6	-0.01380	-0.00649	0.00047
S7		n/a	

Table 3-12: Recorded minimum and maximum CS616 readings, corresponding VWCs computed with the UM calibration parameters (without using temperature correction) and Tempe cell based measured minimum and maximum VWC values (When the computed value differ by more than 0.02 cm^3 cm^{-3} of the measured (or expected) value, it is shown in bold letters).

Site	CS616 readings (microseconds)		Computed VWC ($cm^3.cm^{-3}$)		Measured VWC ($cm^3.cm^{-3}$)	
	min	max	min	max	min	max
G1	18.63	27.61	0.052	**0.308**	0.07	0.40
G2	21.57	30.87	0.091	**0.299**	0.07	0.34
G3	30.4	41.2	**0.186**	**0.419**	0.30	0.53
G4	17.55	26.76	0.036	0.317	0.06	0.34
G5	16.53	26.55	**0.002**	0.326	0.05	0.31
G6	27.3	40.16	**0.091**	**0.481**	0.20	0.56
K1	26.58	34.66	**0.245**	**0.420**	0.15	0.45
K2	18.74	26.87	**0.017**	**0.195**		
K3	28.89	41.67	0.122	**0.463**		
K4	28.02	40.03	0.139	**0.572**		
K5	25.91	40.32	0.072	**0.670**		
K6	27.46	37.72	**0.041**	**0.228**	0.12	0.40
M1	17.96	25.84	0.046	**0.290**	0.06	0.34
M2	16.84	23.42	**0.023**	**0.217**	0.10	0.34
M3	23.83	39.41	0.089	**0.471**	0.11	0.41
M4	26.59	40.48	**0.053**	0.479		
M5	20.54	41.46	**0.037**	**0.418**		
M6	23.98	40.99	**0.051**	0.491		
M7	28.54	40.33	**0.162**	0.364	0.23	0.36
S1	28.97	38.84	0.174	**0.387**	0.16	0.53
S2	29.59	39.47	**0.207**	**0.468**	0.27	0.59
S3	29.21	38.32	n/a			
S4	26.17	37.51	**0.141**	0.454		
S5	24.8	38.54	n/a			
S6	30.25	54.32	0.220	**1.020**		
S7	24.44	36.58	n/a			

To reject the UM calibration results solely on the basis of the minimum and maximum SWC values obtained from the Tempe cell measurements by King (2004), is not acceptable. This is because the Tempe cell measurements provided only indicative SWC values for air dry and saturation conditions. Thus, it was decided to use TDR measurements to adjust the UM calibrations. This was possible since 0-30 cm SWCs were collected with a portable TRASE TDR instrument during data down loading visits (see Section 3.4.3). TDR data sets have been obtained on 5 occasions at all site have been used for correcting the UM calibration equations.

When adjusting calibration parameters, CS616 readings were extracted for the dates when TDR measured values were available at each site. After applying a temperature correction for the CS616 readings, SWC values were computed for these selected days with the UM-calibration parameters. Measured soil water contents from the TDR were then compared with these computed SWC values. If the computed SWC values were within ±0.0025 of the TDR measured SWC, then those values were considered as the correct SWC values for the corresponding CS616 readings. In cases where computed SWC values deviated more than 0.0025 from the TDR readings, the TDR measured values were considered as the actual SWC values for those CS616 readings. Finally, second-order polynomial type regression equations were developed using CS616 readings against these water contents. It was assumed that this approach sufficiently adjusted the UM calibration parameters. These new calibration parameters are shown in Table 3-13 and significant differences can be seen compared to the standard calibration parameters of CSI. Reader may refer Annex – III for detailed information.

Table 3-13: New-calibration parameters for soil moisture sites and associated R^2 values. All calibration equations are in the form of: VMC = *a* + *b* * (Reading) + *c* * $(\text{Reading})^2$ where Reading is in microseconds.

Site	*a*	*b*	*c*	R^2	*S*
G1	0.2237	-0.0418	0.0018	0.8586	0.0303
G2	0.0344	-0.0138	0.0008	0.8809	0.0347
G3	0.1896	-0.0241	0.0008	0.9256	0.0453
G4	1.0001	-0.1278	0.0041	0.8489	0.0655
G5	0.7427	-0.1045	0.0037	0.8719	0.0295
G6	-0.0996	0.0009	0.0003	0.7509	0.1037
K1	-0.1589	0.0047	0.0004	0.8142	0.0760
K2	0.2453	-0.0372	0.0014	0.5536	0.0446
K3	-0.0014	-0.0071	0.0005	0.6425	0.0926
K4	-0.0536	-0.0007	0.0004	0.3512	0.1454
K5	0.1956	-0.0278	0.001	0.8660	0.0320
K6	0.0375	-0.0078	0.0004	0.5747	0.0634
M1	-0.1874	0.0066	0.0004	0.8469	0.0227
M2	0.9892	-0.1359	0.0047	0.9689	0.0057
M3	-0.0123	-0.0062	0.0005	0.9783	0.0262
M4	0.1823	-0.0229	0.0007	0.9647	0.0271
M5	0.1676	-0.0221	0.0007	0.9110	0.0517
M6	-0.1424	0.0051	0.0003	0.7591	0.0744
M7	-0.0329	-0.0043	0.0004	0.7135	0.1084
S1	0.4997	-0.0565	0.0016	0.7724	0.0503
S2	0.3460	-0.041	0.0012	0.9251	0.0246
S3	0.2252	-0.0295	0.001	0.9713	0.0311
S4	0.0676	-0.0145	0.0007	0.9957	0.0114
S5	0.1806	-0.0255	0.0009	0.9521	0.0168
S6	-0.0043	-0.0053	0.0004	0.9078	0.0659
S7	0.1955	-0.0265	0.0009	0.9063	0.0533

(Note: *S* = Estimated standard deviation about the regression line)

3.8.2 TEMPORAL PATTERNS OF SOIL MOISTURE

Computed soil moisture for S5 is shown as an example for year 2003 (Figure 3.36(a) and 2004 Figure 3.36(b). From Figure 3.36 it is clear that the new calibration parameters produce a reasonable range in view of extreme SWC values for silty clay type soil at S5. Also, computed SWCs respond well to the amount and frequency of rainfall. Therefore, it was assumed that the SWC computations based on the adjusted calibration parameters would produce correct SWC values for the present study.

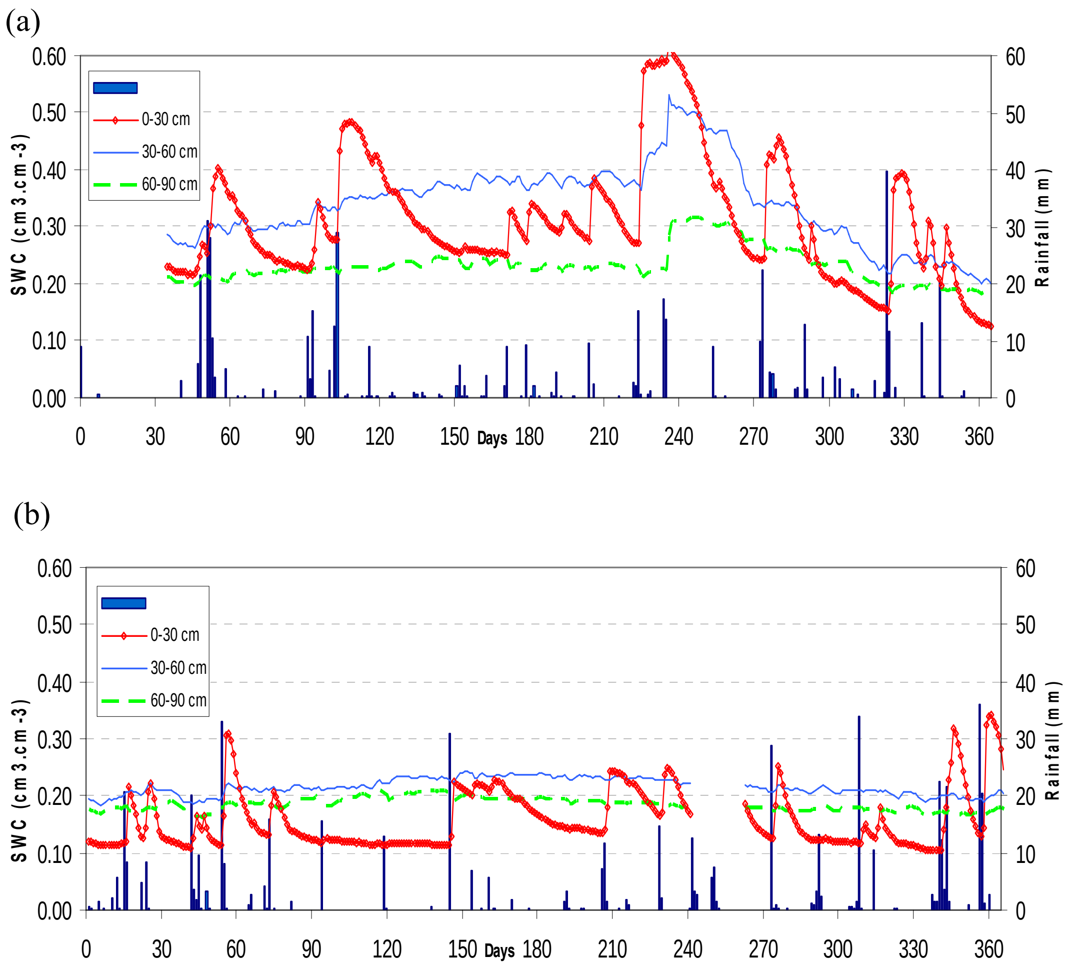

Figure 3.36: Field measured soil moisture at S5 and rainfall for (a) 2003 and (b) 2004.

However, when considering the approach used for calibrating the CS616 sensors, it would be better to use a relative moisture index than the actual computed amounts for comparing the soil moisture pattern among all monitoring sites. For this reason, all computed SWCs were divided by the maximum SWC value at each site. These standardized SWC index values for 2003 and 2004 for all sites are shown in Figure 3.37 for the Stanley, Krui, Merriwa and Goulburn catchments respectively.

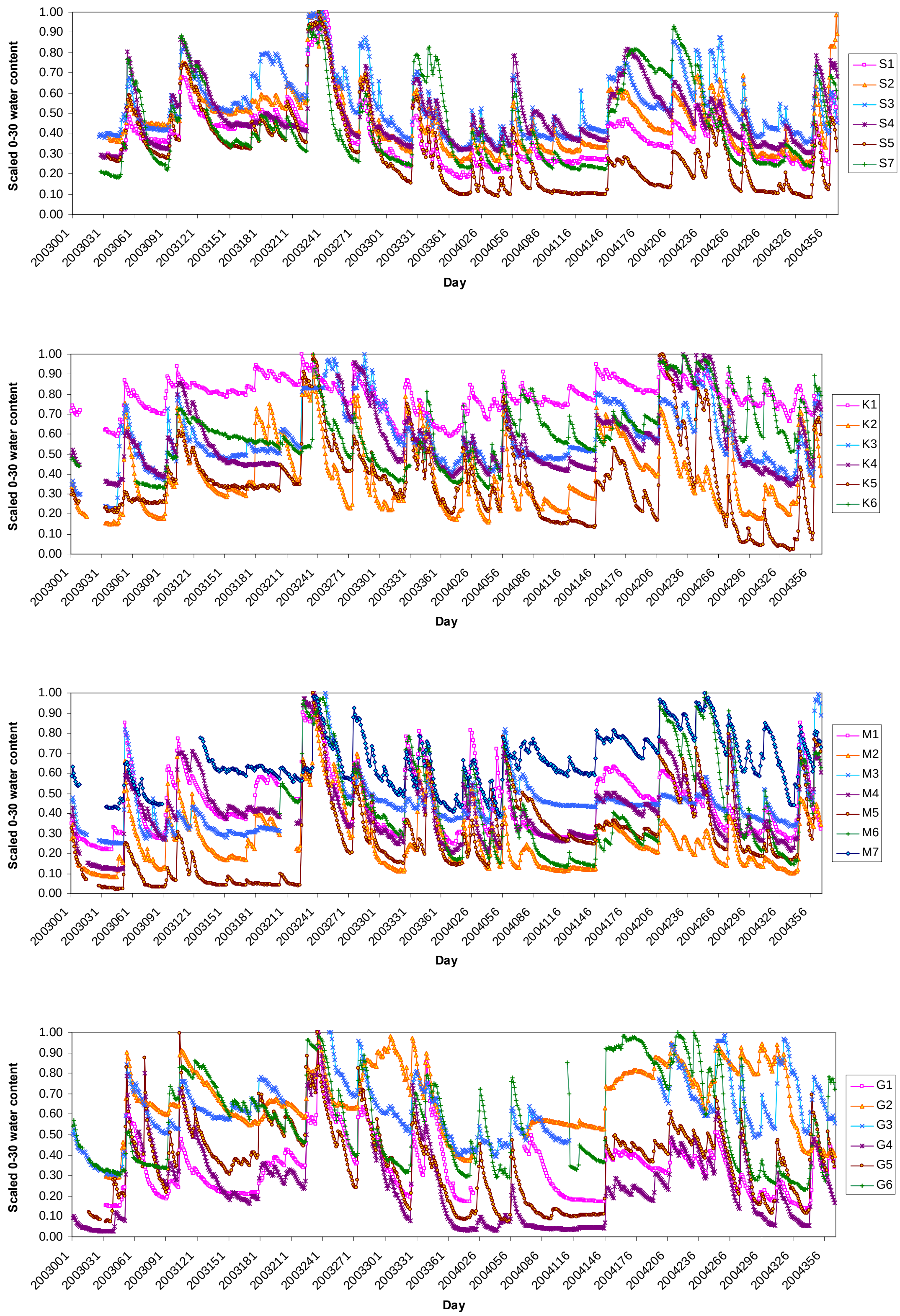

Figure 3.37: Standardized soil water contents for 2003 and 2004: (a) Stanley, (b) Krui, (c) Merriwa, and (d) Goulburn catchment.

Fluctuations of SWCs at all sites were due to rain as no site was under irrigation. It is obvious from Figure 3.37 that all sites responded well to rain events. Cropping sites such as K1 often showed higher SWC values due to farm activities (see Figure 3.37 (b)). The following broad observations can be made from Figure 3.37. First, during higher rainfall events, most sites showed saturated water contents. Second, during extended dry events most sites showed similar SWC values. Third, behaviour of SWCs during drying cycles varies from one cycle to another as well as from site to site. This may be due to variations of climatic conditions, soil physical properties at each site, land use characteristics etc. It can therefore be concluded that use of a relative moisture index is useful for comparing the soil moisture patterns at monitoring sites.

For scaling applications, it is often necessary to consider the actual SWC values rather than a relative moisture index. Therefore, all other chapters of this thesis use the actual SWC values computed with adjusted calibration parameters.

Furthermore, based on the measurements, it was found that less variation exists for deeper soil moisture contents such as at 30-60 and 60-90cm depths. Also, due to shallow depths at some monitoring sites and in order to use data from all sites in a consistent manner, it was decided to consider only 0-30cm data for the analyses presented in subsequent chapters.

3.9 CHAPTER SUMMARY

This chapter has presented an overview of the experimental program in the Goulburn River Catchment and has summarised the key variables measured between January 2003 and December 2004. The chapter has also provided an overview of the weather conditions throughout 2003 and 2004 in the study catchment. Finally, it has addressed the calibration of the CS616 WCR and has presented measured SWCs.

List of Figures – Chapter 3

List of Tables – Chapter 3

CHAPTER FOUR

4. FROM POINT OBSERVATIONS TO HILLSLOPES

The hillslope is the basic hydrological unit in a catchment. Soil moisture scaling methods at the hillslope scale therefore need to be studied. The purpose of this chapter is firstly, to examine local-scale soil moisture behaviour during the study period. Such an examination requires the application of a simple water balance approach and demands accurate field data coverage if theory and observation are to be matched. Secondly, the chapter investigates the control of topography and soil characteristics upon soil moisture distribution at the hillslope scale. From a scaling point of view, the first part of the chapter deals with the interpolation of point scale soil moisture measurements collected over 0-30 cm to 0-90 cm depths in the temporal domain. The second part, in contrast, explores the up-scaling of 0-30 cm point-scale soil moisture measurements to the scale of the hillslope catchment.

4.1 INTRODUCTION

Hillslopes are the most convenient hydrological unit used to understand the complex hydrological processes in a catchment. Any catchment can be subdivided into a number of hillslopes with manageable sizes. By doing so, it allows one to study the complex hydrological processes in a catchment, at least at the scale of hillslope level, in some detail and to develop soil moisture scaling methods at that scale.

The role of surface topography in controlling hillslope runoff processes has received much attention in recent decades. Topography plays a dominant role in the spatial structure of soil moisture both during and after rainfall. Results from hillslope scale studies indicate significant variability in soil moisture content along transects (Famiglietti *et al*., 1998; Kim and Barros, 2002b). This variability decreases with decreasing transect-mean moisture content as the hillslope dries down following rain events. Studying the spatial organization of soil moisture in a small catchment, Grayson *et al.* (1997) found that the moisture variation is related to the processes controlling the spatial pattern of soil moisture contents. Accordingly, spatial organization is strongest when there is lateral flow occurring (i.e. at high soil moisture content) or when the soil moisture is influenced significantly by up-slope processes (also known as non-local control). Little organization is present when the soil moisture is locally controlled (i.e. at low soil moisture content) and the main fluxes of water are vertical. Further, detailed event simulations indicate that spatial organization has a significant effect on the rainfall-runoff behaviour (Grayson *et al.*, 2002). Therefore, during inter-storm periods, the topographic and soil factors operate jointly to redistribute soil water. Under wet conditions, variability in surface moisture content is most strongly influenced by porosity and hydraulic conductivity, and under dry conditions, correlations are strongest to soil properties such as the residual moisture content and vegetation properties such as root density and wilting point. Thus, during inter-storm periods, the dominant influence on soil moisture variability gradually changes from soil heterogeneity to joint control by topographic, soil and vegetation properties. This may lead to temporal stability in the spatial pattern of soil water distribution at the transect scale (Gómez-Plaza *et al*., 2000). The above studies confirm that at the local scale spatial patterns of soil moisture are determined by topographical position, as high locations, or steep areas, are usually the driest points, whereas those sited in valley zones tend to be the wettest points despite the presence of vegetation. It can therefore be concluded that relative position within a catchment must be considered in any soil moisture scaling application.

Soil in field conditions exhibits strong spatial variability of moisture content. This variability is more dominant in the surface layers than in the subsurface layers. Furthermore, it is due to inherent physical properties and is the effect of many processes acting on a range of scales. Factors such as soil type, soil depth, topography and vegetation play an important role in soil moisture distribution (Qiu *et al*., 2001). Soil heterogeneity affects the distribution of soil moisture through variation in texture, organic matter content, porosity, structure and macro-porosity (Mohanty and Skaggs, 2001). The variability in soil hydraulic properties and soil water retention characteristics greatly influences the vertical and lateral transmission properties. Further, variations in soil particle and pore sizes may cause significant soil moisture variations even over very small distances. The influence of soil colour on albedo may influence the rate of evaporative drying. Thus, the soil characteristics in a given location within a catchment are important to consider for any soil moisture scaling application.

This chapter has multiple objectives. First, field measured soil moisture values are needed to evaluate for possible errors due to sensor calibration issues. Simple hydrological models such as the single layer bucket model are also useful for identifying systematic measurement errors due to poor calibration parameters of the sensors as well as any random errors. Application of bucket type water balance models also provides a methodology for the scaling of soil moisture in the temporal domain. Second objective of this chapter therefore is to investigate the prediction of soil moisture content with intermittent field observations and addresses interpolation of soil moisture in temporal domain. Finally, the chapter studies the application of topographic data and soil specific properties for soil moisture scaling at the hillslope scale. This section introduces a new method of deriving hillslope scale 0-30cm soil moisture distributions from limited field measurements.

4.2 HILLSLOPE SCALE WATER BALANCE

Hydrological relationships can sometimes be described by simple bucket models which use upper and lower limits to soil water storage. These models can be applied at a point but they are often used to represent soil moisture storage averaged over an entire catchment. In these models a bucket represents the soil water storage of the root-zone or any other specified depth. This concept is easy to understand with a schematic diagram as shown in Figure 4.1 which illustrates a single layer bucket model for soil water balance. The bucket fills with rainfall and empties due to evapotranspiration and deep drainage. The simplest form of bucket model assumes mass balance in a one direction, usually in a vertical plane, and assumes that all excess water leaves the bucket as deep-drainage. The complete three-dimensional water balance can be represented over a fixed time interval as:

$$\Delta S = P - ET - Q \quad \textbf{(4-1)}$$

$$Q = SRO + SSRO + DD \quad \textbf{(4-2)}$$

where ΔS represents the change in moisture stored in the bucket, P the rainfall input to the bucket, ET loss of water due to evapotranspiration from the bucket and Q the outflow from the bucket comprising surface runoff (SRO), subsurface runoff ($SSRO$), and deep drainage (DD) (see Figure 4.1).

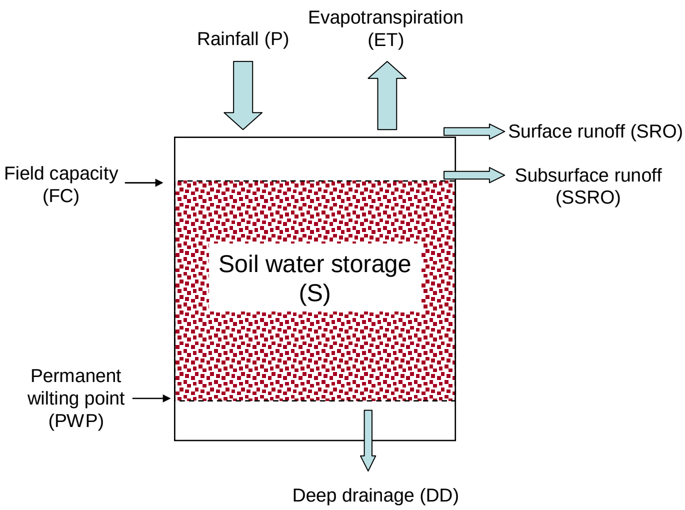

Figure 4.1: Schematic representation of the single layer bucket model.

The model calculates the difference between rainfall and evapotranspiration on a daily basis. For a given day, if there is rain excess, it is added to the available soil-water storage. If the available soil-water storage becomes full, i.e. when rainfall exceeds the total loss due to evapotranspiration, then the bucket overflows causing deep-drainage and/or runoff which are simply considered as loss. If the evapotranspiration requirement cannot be satisfied by the daily rainfall, then it is taken from the soil-water storage. The only input data required by the Equation 4.1 are daily rainfall, daily actual evapotranspiration (ET_a), the available storage capacity of the bucket (or the soil layer considered), and the soil water deficit at the start of the period being studied. Using a simple spreadsheet program, one can compute the day-to-day changes of soil moisture content within the bucket. For accurate water balance computations, the above model can be improved by adding more buckets or soil layers with different soil physical properties. This water balance model is valid at all scales considered in hydrological modelling and only through the parameterization of individual terms does the water balance become a 'distributed' or 'lumped' model (Wood, 1995). In the case of a 'distributed' model, the spatial variability of all individual terms in the above equation is considered separately. In a 'lumped' model, the catchment is considered as spatially homogeneous with regard to inputs and soil parameters.

The single-layer bucket-type water balance model requires measurements of rainfall and estimates of ET_a and the water storage capacity of different soil types. Rainfall data are usually available for many regions from a variety of sources. Measurements of soil water content at field capacity (*FC*) and permanent wilting point (*PWP*) provide information on the capacity of the bucket. The total losses due to deep-drainage and/or runoff from the bucket therefore can be computed if the other components of the Equation 4.1 are known. The most difficult component is the accurate estimation of ET_a. As reported by Lewis and Walker (2002), ET_a is proportional to the potential evapotranspiration (*ETo*). Accordingly, ET_a can be computed from the *ETo* using a proportionality coefficient called the 'actual evapotranspiration coefficient' (*AETCo*). As cited by Walker and Zhang (2002), Cook and Walker (1990) and Kennett-Smith *et al*. (1994) have reported that the magnitude of *AETCo* depends on the amount of water stored in the soil and a soil parameter (*SP*). This can be represented in an exponential relationship as:

$$AETCo = \frac{1 - e^{(-SP \times FMS)}}{1 - e^{(-SP)}} \quad \textbf{(4-3)}$$

where FMS is the amount of water storage as a fraction of the maximum available soil-water storage and can be represented as:

$$FMS = \frac{AW}{FC - PWP} \quad \textbf{(4-4)}$$

where AW is the available water, FC is the soil water content at field capacity and PWP is the soil water content at permanent wilting point. The field capacity or the upper level of soil water storage is defined as the water content at which internal drainage ceases. The PWP or the lower limit can be measured following a long dry period when plants suffer serious water stress.

The $AETCo$ therefore, ranges from a value of 1 at field capacity to 0 at wilting point. The soil parameter in the equation 4.2 (SP) determines how the $AETCo$ changes with changes in the amount of stored water between these two end points. Thus, correct determination of SP is also important for ET_a computations. Water balance modelling over a long period offers a good opportunity to objectively determine the SP for a given soil type. The value of SP can be estimated with an objective function of minimizing the difference between the total inputs and total outputs in the water balance modelling over a long period such as one or two years.

The main advantage of the simple bucket models is that it can provide timely information on the soil moisture content within a bucket without the necessity of field visits. This approach therefore can be used to assess the reliability of field measured soil moisture data if doubts exist about the measurement approaches or the sensor calibration procedures. However, one has to keep in the mind the underlying assumptions of simple water balance approaches. The error associated with estimates of individual components in the water balance is a critical disadvantage for an accurate comparison of measured and predicted soil water contents. However, this is not a serious issue for water balance modelling because the assimilation of measurements may provide the best approach towards estimation of soil moisture content over a longer period.

4.2.1 APPLICATION OF WATER BALANCE MODEL TO THE STANLEY HILLSLOPE CATCHMENT

The study domain for the water balance modelling is the small 170 ha 'Stanley' catchment in the Krui River catchment (Figure 4.2). The locations of soil moisture monitoring sites and elevation of the catchment are shown in Figure 4.3. As seen in Figures 4.2 and 4.3 the catchment consists of two peaks, hence two hill slopes. Figure 4.4 shows the local topography of the six monitoring sites used for the present study. Note that site S6 is not considered for analysis due to unreliable and incomplete data. As seen in Figure 4.4, sites S1 and S7 are located along a gentle slope, and S2 and S3 are located along a moderate slope. In contrast, site S4 is located in a steep area, especially along the West-East direction. Sites S1, S2, S3 and S5 have over 90 cm deep soil layers. Sites S4 and S7 however, located in shallow area and the soil depths are less than 40 cm. For convenience, this catchment is called hereinafter the Stanley hillslope catchment (SHC). During the two-year study period, the measured stream flow at the lowest part of the catchment was found to be negligible. Thus, for the period 2003 to 2004, from a hydrological point of view, this hillslope catchment can be considered as a closed catchment.

Stanley subcatchment

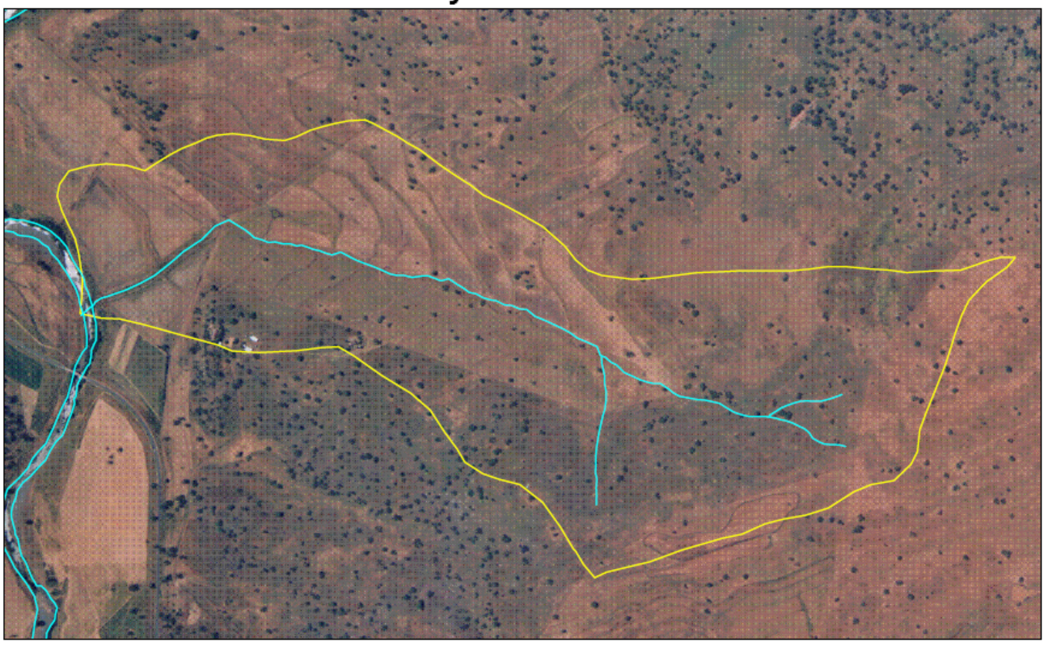

Figure 4.2 : Aerial view of Stanley hillslope catchment. Blue line shows the main drainage system. Top of the figure is pointing North.

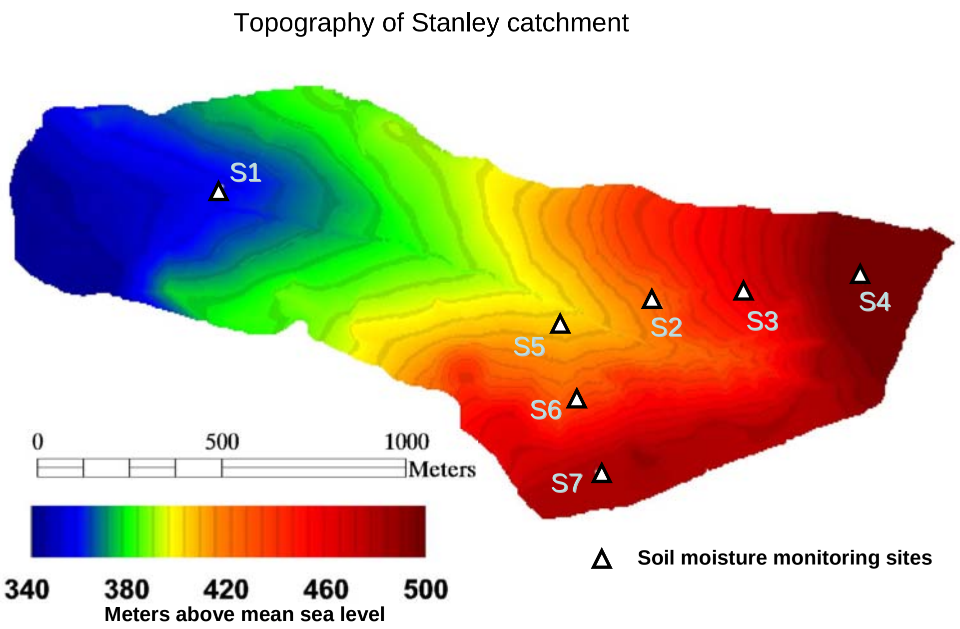

Figure 4.3: Locations of soil moisture monitoring sites within Stanley catchment. Background colours represent elevations in the catchment taken from a 5m digital elevation model. While S7 and S4 sites are located in the highest points, S1 is located in the valley bottom.

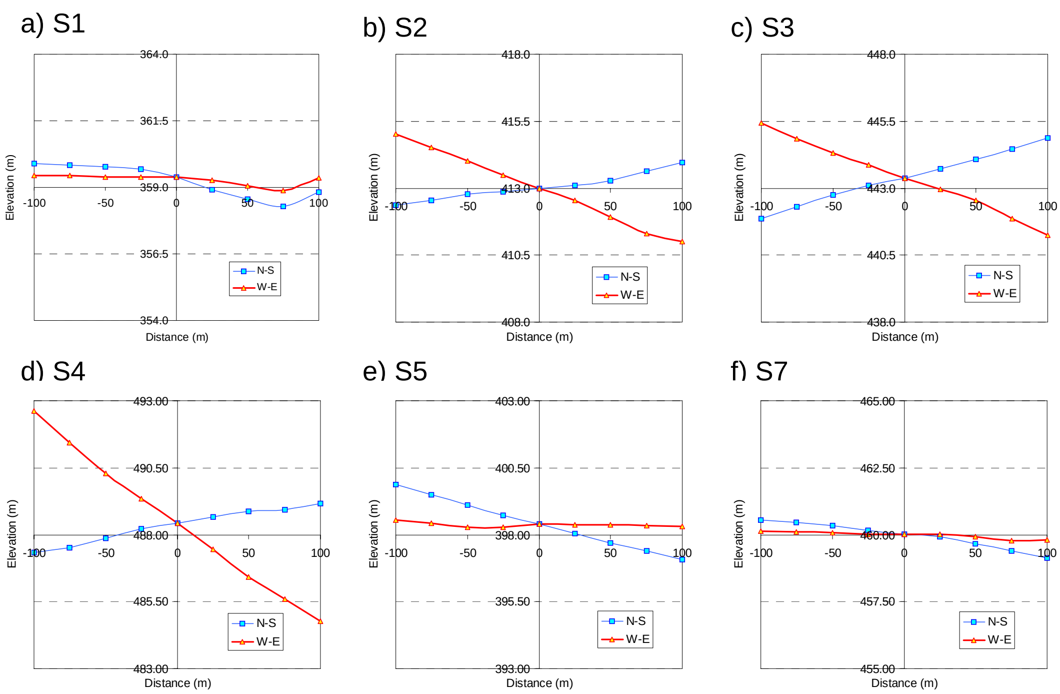

Figure 4.4: Local elevation (m) along North-South and West-East direction at: a) S1, b) S2, c) S3, d) S4, e) S5, and f) S7. (Note: North and West directions are shown as (-) distances (in metres) from the origin '0' at each monitoring site)

4.2.1.1 Derivation of water balance components

a. Rainfall estimation

As discussed in Section 3.4.6 rainfall within the Stanley hillslope catchment was monitored with a tipping bucket rain gauge located at S2 and five other collecting rain gauges. The collecting rain gauges were located at S2 (weather station), S1, S3, S5 and S6 and were read during routine data downloading visits at approximately 6 weeks intervals. As discussed in Section 3.6.1 the spatial variation of rainfall within the catchment was found to be very small (see Table 3-10). Therefore, the daily rainfall measured at S2 was considered as the rainfall input for the bucket models used for the catchment.

b. Evapotranspiration

Daily ET_o values have been computed with the Penman-Monteith method (see Section 3.6.5). Daily ET_a values have been estimated from Equations 4.2 and 4.3. The following assumptions were made in the ET_a computation.

- The measured maximum soil moisture content during the two-year study period was taken as the moisture content at *FC*.
- Measured minimum soil moisture content during the two-year study period was taken as the moisture content at *PWP*.
- The values of *SP* were estimated with an objective function for minimizing the difference between the total inputs (e.g. P) and total outputs (e.g. ET, DD, SRO, etc.) in the water balance modelling over a sixteen-month period. The value of *SP* for all study sites except S5 was found to be 2. In the case of S5, the value of the derived *SP* was 3.

c. Starting day of the water balance modelling

In the present study, the first observed day with maximum soil moisture content was selected as the starting day of the water balance modelling. This assured starting the soil-water accounting with a full-bucket condition. Accordingly, day 236 in 2003 was used as the first day of the water balance modelling and daily computations have been carried out up to 31 December 2004. Day 236 is the last day of a three-day rainfall event and soil moisture levels reached a maximum level.

4.2.1.2 Results of the water balance modelling

The simple bucket model has been applied to the six soil moisture monitoring sites in the Stanley hillslope catchment for the period August 2003 - December 2004. All the simulations initially assume that $Q = SRO + SSR + DD$ is negligible. Daily estimated and measured soil moisture values together with the observed rainfall amounts are shown in Figure 4.5 and in Figure 4.6 for study sites S1, S2, S3 and S4, S5, S7 respectively. It is clear from the figures that in general, the predicted moisture follows the same trajectory as the measured soil moisture in all six cases. This is clearly evident for all 0-90 cm deep sites (i.e. S1, S2, S3 and S5) particularly between day 236 in 2003 and day 100 in 2004. For the 0-30cm depth at S4, the predicted soil moisture pattern appears to be similar to the measured pattern over a slightly longer period up to day 141 in 2004. Again, after day 270 in 2004 all these sites show near-identical patterns of measured and predicted soil moisture. The predicted moisture patterns for 0-30 cm at site S7 appear slightly underestimated for the same period but follow the general pattern of the measured values. The highest deviations between measured and predicted moisture values can be seen for the period day 140 - day 270 in 2004. Sites S1, S2 and S3 (see Figure 4.5) show some moderate to high deviations for this period. For the same period, while the deviations found for the 0-30 cm sites of S4 and S7 were considerable, the 0-90 cm S5 site showed almost no deviations (see Figure 4.6).

In general, it appears that the difference between the predicted values and the measured values takes a negative value, indicating some water inputs other than the rainfall (i.e. run-on sites). This indicates that the Q term must be included in the water balance study. Results presented in Figure 4.5 and Figure 4.6 are based on ignoring the Q term. Therefore, if some runoff water is considered (i.e. a positive Q term) in the water balance as for run-on sites, the difference between the predicted and measured values would have been even lower. As no surface runoff was detected at the flume suggesting that runoff occurred only within the catchment. Run-off water not necessarily comes as the surface runoff from upslope area. For example, S1 is receiving water from the neighbouring area, particularly from a depression located in the down-slope along the North-South direction (Figure 4.4 (c)). As this depression acts as a water collecting pond, it saturates the soil in nearby areas. This type of water input is therefore important to consider.

(a) S1

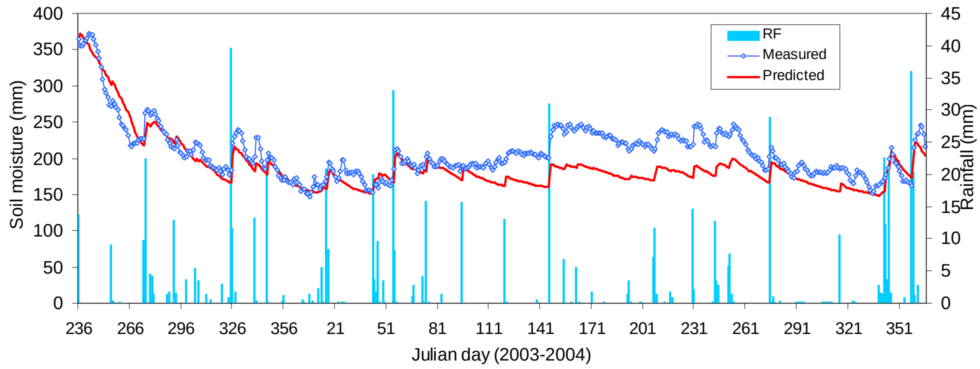

(b) S2

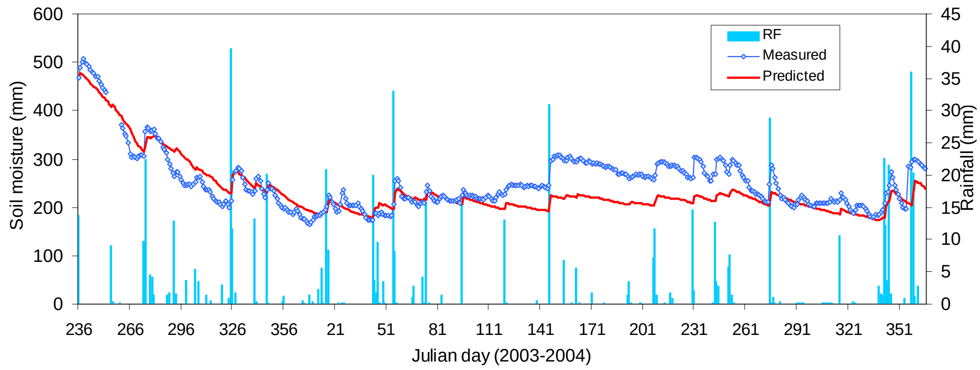

(c) S3

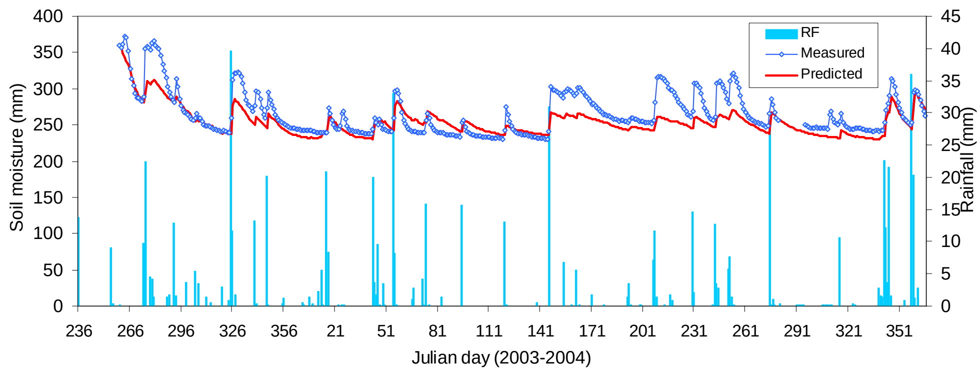

Figure 4.5: Daily rainfall (mm), measured soil moisture (mm), and predicted soil moisture contents from a simple bucket type water balance model for: (a) 0-90 cm at S1, (b) 0-90 cm at S2, and (c) 0-90 cm at S3.

(a) S4

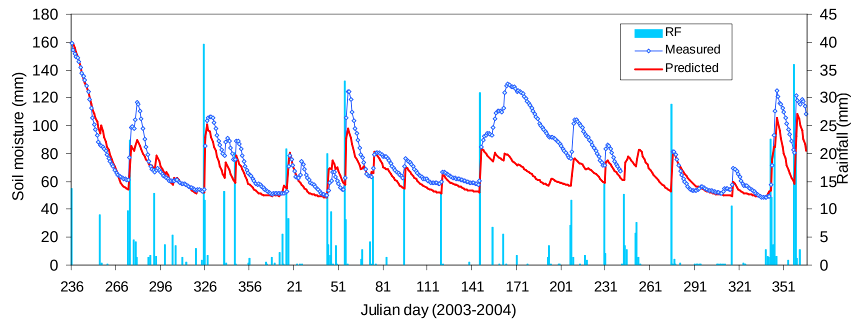

(b) S5

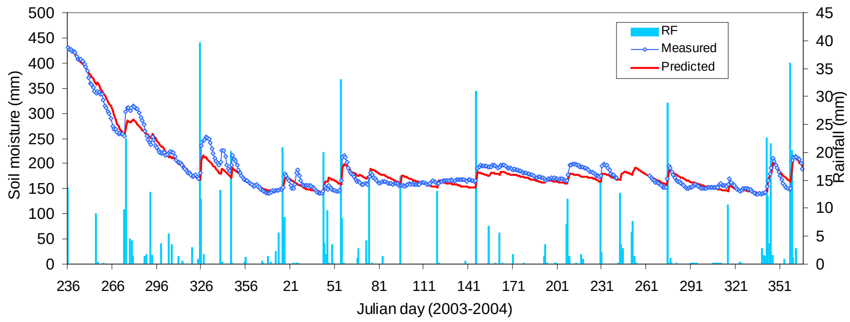

(c) S7

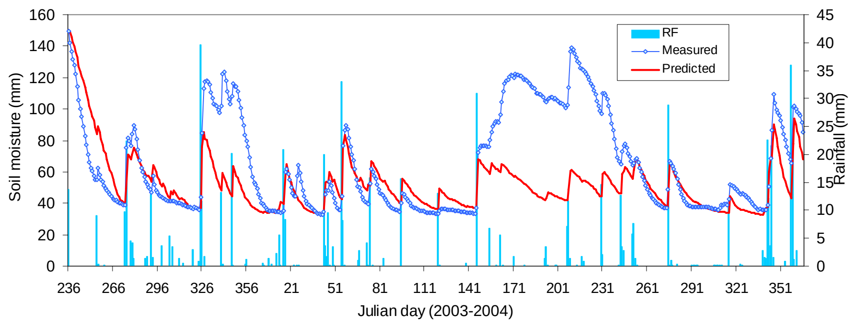

Figure 4.6: Daily rainfall (mm), measured soil moisture (mm), and predicted soil moisture contents from a simple bucket type water balance model for: (a) 0-30 cm at S4, (b) 0-90 cm at S5, and (c) 0-30 cm at S7.

On the other hand, a positive difference between the predicted values and the measured values indicates that water outputs need to be considered (i.e. run-off sites). As seen in Figure 4.5 (c), during certain periods a site may behave as a run-off site and during some other period it behaves as a run-on site. In a long-term, due to cancellation of these under- and over-estimations, predicted soil moisture value will be close to measured value (see day 2003-250 and day 2004-

365 in Figure 4.5). It appears that consideration of Q term is important in the sites considered for the present water balance modelling. Accurate measurement of the Q term under field conditions is very complicated and other approaches such as to mechanistic models therefore need to be considered.

4.2.1.3 Assimilation of field measured soil moisture in water balance modelling

Generally, because of assumptions such as $Q = 0$, the errors associated with simple bucket type water balance models are considerable. It is impossible to represent the complex interactions of soil-plant-water system in a simple bucket type modelling approach. Thus, it is obvious that the predicted soil moisture values can deviate from the measured moisture values. Furthermore, such deviations can take very large values over a longer time scales as observed in Figure 4.5 and 4.6. One way of overcoming this problem is the assimilation of measured moisture values into the water balance model at regular or irregular intervals. For example, the direct insertion of measured moisture values into the model can bring the predicted trajectory back to the actual trajectory.

The assimilation of measured soil moisture values into the model has also been studied during the soil water accounting study. Two scenarios of regular updating at two-week and one-week intervals have been considered. As expected, the assimilation of measured moisture values into the water balance model significantly reduces the difference between the predicted and the measured soil moisture contents. For example, Figure 4.7 shows predicted - measured soil moisture values for a 0-90 cm soil depth at S1 (a) without assimilation of measured data (b), with assimilation of measured data at two-week intervals and (c) with assimilation of measured data at weekly intervals. It is clear that the assimilation of measured soil moisture data on a regular basis and at closer intervals reduces the prediction errors significantly. Sum of squared error (SSE) values computed on a monthly basis also help to gain a quantitative measure of the improvement in the model predictions. As summarized in Table 4-1, the assimilation of measured soil moisture values into the simple bucket model with a

0-90 cm soil depth can reduce the model prediction errors by 77% and 88% for the two-week and one-week intervals, respectively.

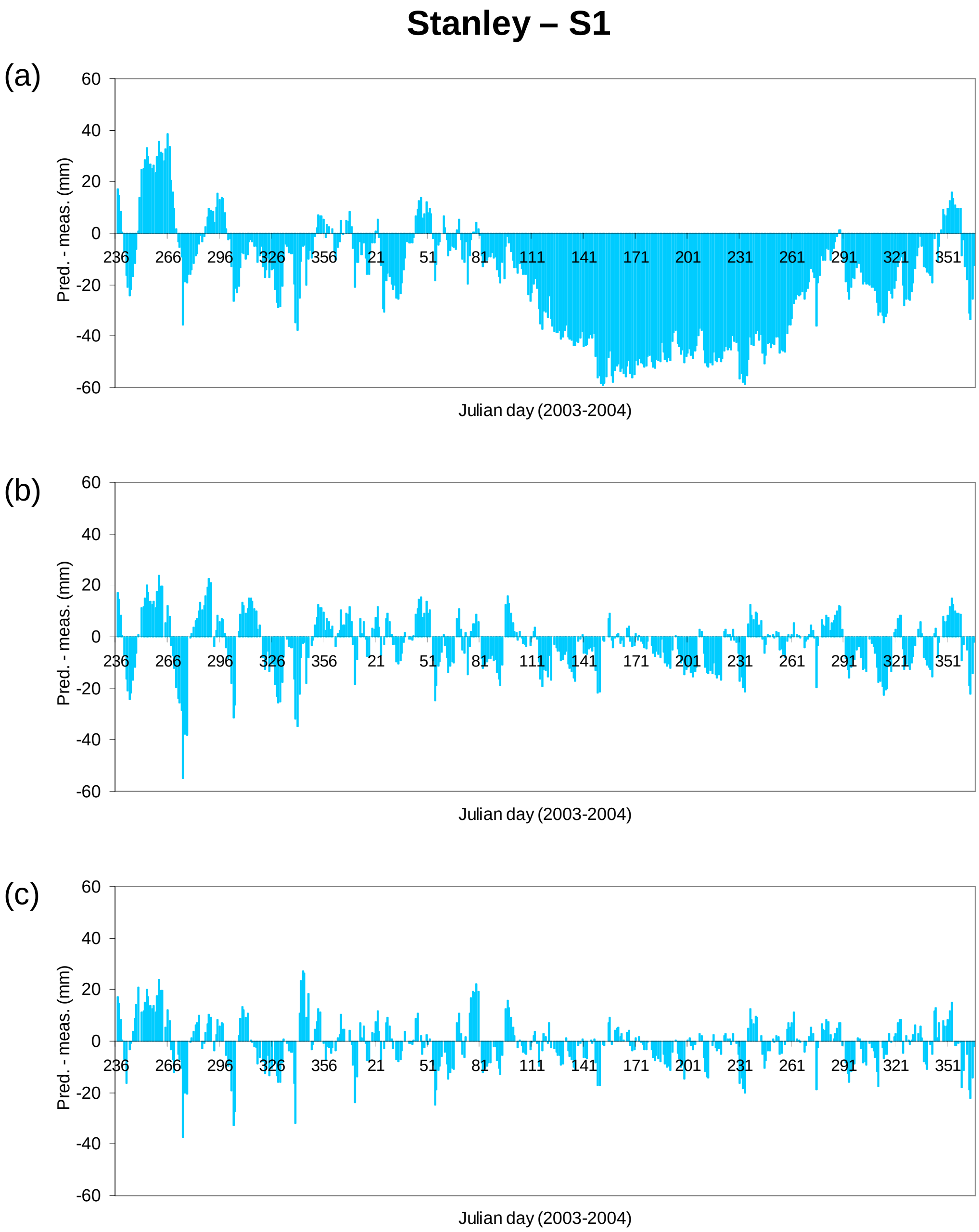

Figure 4.7: Distribution of the difference between predicted and measured soil moisture values for 0-90cm at S1: a) without assimilation of measured data, b) with assimilation of measured data at two-week intervals, and c) with assimilation of measured data at weekly intervals.

Table 4-1: Monthly sum of squared error (SSE) values between predicted and measured moisture values without assimilation and with assimilation measured soil moisture for 0-90 cm soil layer at S1.

Year	Month	Without assimilation	Assimilated at two-week intervals	Assimilated at weekly intervals
2003	Aug-24	590.4	590.4	11.7
	Sep	82.2	812.6	110.1
	Oct	466.0	700.5	754.8
	Nov	25.5	0.8	0.8
	Dec	26.4	113.5	113.5
2004	Jan	400.0	8.2	8.2
	Feb	5.2	10.2	16.3
	Mar	203.2	188.3	56.0
	Apr	1044.2	236.7	0.6
	May	3483.9	2.1	2.1
	Jun	2423.0	29.8	29.8
	Jul	2521.2	166.0	166.0
	Aug	2151.6	0.7	27.4
	Sep	1291.8	390.3	361.7
	Oct	396.5	189.4	95.9
	Nov	24.5	1.4	1.4
	Dec	267.4	38.3	38.3
	Total	15403.1	3479.4	1794.7
% reduction of SSE		-	77%	88%

Assimilation of measured moisture data into the bucket model also helps to remove the large prediction errors such as observed in 0-30 cm soil layer at S7. As seen in Figure 4.8 and in Table 4-2, the assimilation of measured moisture values helps to reduce the prediction errors by 85% and 93% for the two-week interval and one-week interval assimilation cases, respectively.

Similar to the two examples presented (i.e. S1 and S7), as expected, water balance model runs at all other sites show significant improvement in the predicted moisture contents when measured soil moisture data are assimilated into the model on a regular basis.

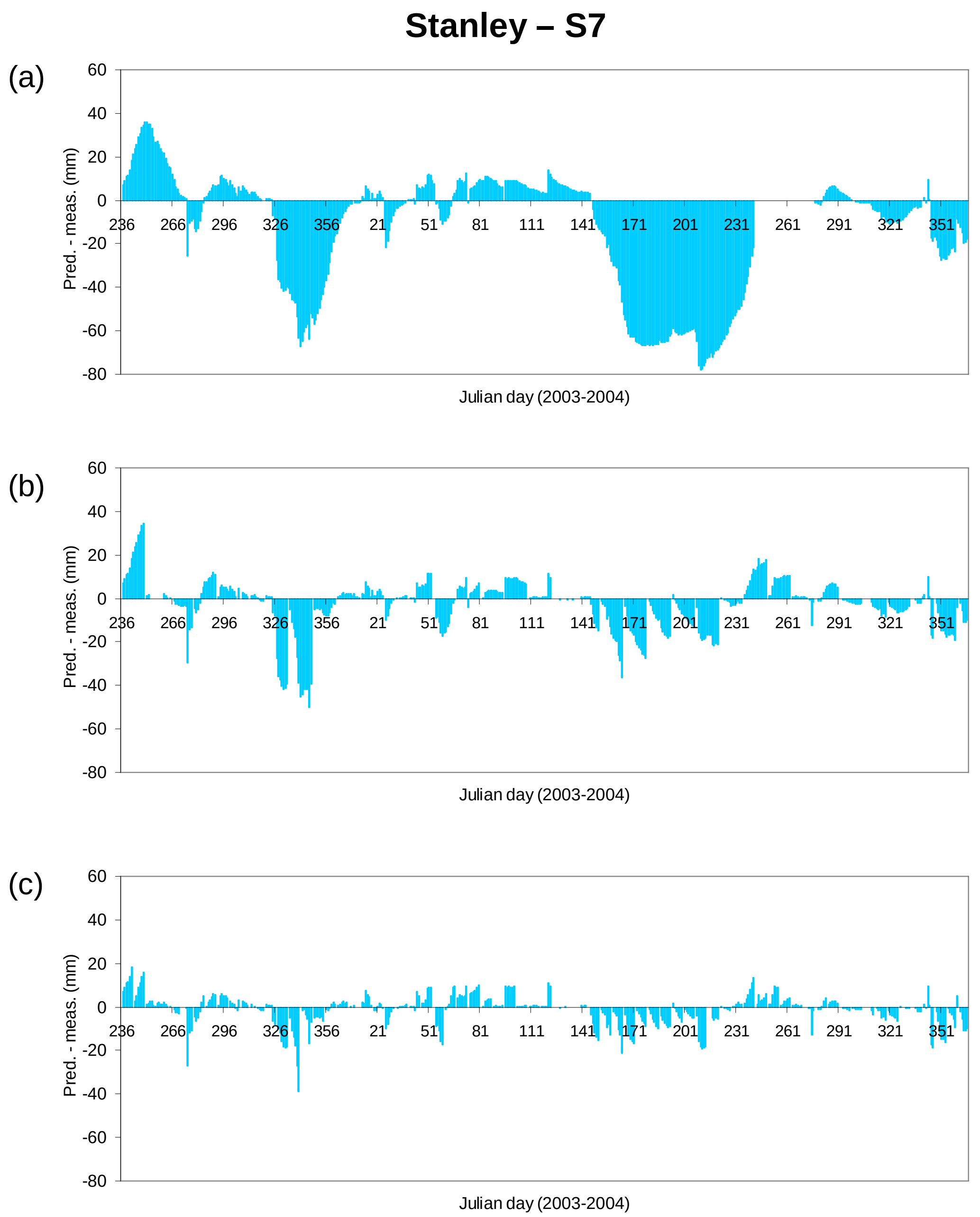

Figure 4.8: Distribution of difference between predicted and measured soil moisture values for 0-30 cm at S7: a) without assimilation of measured data, b) with assimilation of measured data at two-week intervals, and c) with assimilation of measured data at weekly intervals.

Table 4-2: Monthly sum of squared error (SSE) values between predicted and measured moisture values without assimilation and with assimilation of measured soil moisture for 0-30 cm soil layer at S7.

Year	Month	Without assimilation	Assimilated at two-week intervals	Assimilated at weekly intervals
2003	Aug-24	561.1	561.1	6.6
	Sep	0.6	12.6	0.7
	Oct	38.7	19.9	9.5
	Nov	1843.2	27.5	27.5
	Dec	35.3	7.9	7.9
2004	Jan	14.5	0.3	0.3
	Feb	95.1	232.7	1.0
	Mar	59.1	9.5	0.1
	Apr	163.8	107.2	102.9
	May	214.6	2.0	2.0
	Jun	4383.7	46.6	46.6
	Jul	5312.3	291.1	291.1
	Aug	201.4	337.5	30.5
	Sep	118.8	155.5	165.3
	Oct	1.1	5.2	1.7
	Nov	8.1	0.6	0.6
	Dec	476.5	222.3	222.3
	Total	13527.9	2039.5	916.6
% reduction of SSE		-	85%	93%

4.2.1.4 Discussion of water balance approach

Evaluation of site specific calibration parameters is important for soil moisture measurements with CS616 sensors. Simple bucket type water balance models provide convenient way of evaluating the calibration parameters of moisture sensors. The application of single layer bucket models for balancing the inputs and outputs of water in the Stanley catchment confirmed that the soil moisture data collected during the study period are realistic. The predicted soil moisture values were found to be comparable with the measured soil moisture contents. Hence, the calibration parameters are acceptable and the soil moisture data collected during the study period could be used for other applications with some confidence.

Simple bucket type water balance models can be used to predict soil moisture values for virtually any soil depth considered for the bucket. In the present study, this modelling technique has been employed for the prediction of soil moisture values over 0-30cm and over 0-90cm depths. The obtained results are encouraging but mask significant assumptions regarding the existence of run-off, run-on and deep-drainage. The results confirm that the use of a single moisture measurement at the beginning of modelling period is not sufficient for accurate predictions of subsequent moisture contents over longer periods. Note that the buckets used in these simulations do not consider any water inputs from neighbouring "buckets". Particularly, at the hillslope scale, sites in steep areas (e.g. S3 and S4) are likely to receive water from the upslope area. Because of this reason, moisture predictions will show underestimates if run-on exceeds run-off. One way of overcoming this error is the assimilation of measured moisture contents whilst ignoring the Q term.

This study confirms that assimilation of measured data can reduce the prediction errors in simple bucket type modelling. Attempt is made to evaluate the predicted moisture values based on regular two-week and one-week assimilation options. It is clear that assimilation of measured soil moisture data into the model is important for minimizing the propagation of modelling errors over longer time periods.

Ignoring rainfall distributions within the catchment can also introduce errors in the predicted moisture values. In this study, rainfall distribution within the Stanley hillslope catchment is assumed to be uniform. This is because for the small size of the catchment (170 ha) and because of similar rainfall amounts collected in the collecting rain gauges. These collecting rain gauges however, were located at S2 (weather station), S1, S3, S5 and S6 and none were sited close to the catchment boundary (i.e. S4 or S7). The very high moisture contents observed during day 141 to 260 in 2004 at S7 appear to be due to rainfall as it is unlikely that this site receives drainage water from nearby areas due to its higher absolute elevation and flat surrounding area (see Figure 4.4(f)). Therefore, even in a smaller hillslope catchment, rainfall anomalies can introduce serious errors in the model predictions. Accurate rainfall measurements are important in water balance modelling.

The quality of the soil moisture predictions from bucket type water balance modelling is clearly determined by the input data used. In this study, rainfall measurements were collected within the catchment using an automatic rain-gauge. All meteorological data required for the computation of ETo from Penman-Monteith method were measured in the climate station located at S2 (see Section 3.6.5). The bucket size (i.e. the storage capacity) at each location was determined from the actual soil moisture observations. Thus, the availability of all this data provides an ideal situation for the model application whilst ignoring lateral water movement.

4.2.1.5 Conclusions

Single layer bucket models provide convenient way of evaluating site specific calibration parameters of the CS616 soil moisture sensors. Application of these models in the Stanley catchment confirmed that the soil moisture data collected during the study period are realistic. The calibration parameters of the sensors are acceptable.

Simple one-dimensional water balance approaches such as the single layer bucket model have limited usefulness for hillslope-scale hydrological studies because they ignore the Q term. They provide *estimates* of soil moisture content over time by considering only rainfall inputs, evapotranspiration outputs and parameters such as soil water holding capacity. Such soil moisture contents estimates can be used in assessing the field measured soil moisture contents obtained from a range of techniques. However, they ignore position in the land-scape and the three components of the Q term in Eq. 4.2

Soil moisture *measurements* collected at irregular intervals may assist in generating soil moisture trajectories over extended periods. With measurements of rainfall and estimates of ET_a and soil water storage capacity, one can use a water accounting system based on a simple bucket type water balance model to generate soil moisture trends over longer time periods. This would provide a methodology for the scaling of soil moisture in the temporal domain. However, ET_a value remains a significant unknown.

4.3 TERRAIN BASED HYDROLOGICAL MODELLING CONCEPTS FOR REGIONALISATION OF POINT-SCALE OBSERVATIONS

Accurate patterns of root-zone soil moisture data are important in hillslope scale studies. However, such root-zone soil moisture patterns are usually not available at the required time-space scale because, except for selected small catchments, point-scale root-zone soil moisture data are usually only available for a few locations within a hillslope catchment. This lack of data prevents the generation of accurate root-zone moisture patterns in a hillslope catchment and important concepts such as the organization of soil moisture fields can not be studied properly. A possible alternative may be provided through generation of root-zone moisture patterns from a limited number of point scale measurements. In this regard, terrain-based modelling concepts appear to be useful.

A wide variety of hydrological models have been used for predicting soil moisture in recent decades, ranging from simple conceptual models to complex systems that require sophisticated numerical algorithms and powerful computers. Three different types can be identified: lumped models, semi-distributed models and distributed models. Distributed and semi-distributed models represent the spatial variability of soil moisture using a distribution function. Often, this distribution function can be derived from the catchment topography, as in the case of the TOPMODEL (Beven and Kirkby, 1979). Sometimes, a theoretical distribution function may be used, as in the case of lumped model such as the Variable Infiltration Capacity (VIC) model (Wood *et al.*, 1992). For soil moisture pattern studies, it is useful to consider distribution functions which are based on catchment topography because it is then possible to map simulated soil moisture back into the catchment to produce a predicted moisture pattern. Distributed models can incorporate the spatial distribution of various inputs and boundary conditions, such as topography, vegetation, land use, soil characteristics, rainfall, and evaporation, and produce spatially detailed outputs such as soil moisture fields. However, the application of distributed and semi-distributed models is often difficult. Owing to the mismatch between model complexity and the scale of data used to parameterize, initialize, and calibrate models, many problems can arise in the implementation. Hence, more simplified approaches are needed to develop which can help to map the soil moisture distributions in any catchment.

The following sections therefore investigate the development of a simplified approach for soil moisture distribution in a hillslope catchment.

4.3.1 DEVELOPMENT OF SOIL-ADJUSTED TOPOGRAPHIC WETNESS INDEX (STWI)

As discussed in Section 1.3, topography plays a dominant role in the spatial pattern of soil moisture contents. Topographic information derived from digital elevation models (DEMs) is widely used as a covariate for parameter distributions in hydrological catchment modelling. This is because topography has a major impact on the hydrological processes in a catchment. Also, the availability of digital DEM data facilitates such applications. For example, Beven and Kirkby (1979) introduced a terrain based moisture index, known as the topographic wetness index (TWI) in their TOPMODEL approach. The TWI in a given location is defined as:

$$TWI = \ln\left(\frac{\alpha}{\tan\beta}\right) \tag{4-5}$$

where α is the area draining past a particular point from upslope per unit contour (m) and tan β is the local slope of the ground surface. The TOPMODEL framework assumes:

- Quasi-steady state condition
- The local hydraulic gradient is equal to local slope of the ground surface
- Uniform recharge across the catchment
- Lateral transmissivity is laterally homogeneous over the catchment

The main advantage of the TWI is its ability to represent topographical heterogeneity in a simple way and it can therefore, be applied conveniently in distribution functions. Many applications of the TOPMODEL concept can be found in the TOPMODEL web site on one of the Lancaster University Server Sites at http://www.es.lancs.ac.uk/es/Freeware/ Freeware.html.

A number of studies have compared various terrain index patterns with soil moisture patterns based on the TOPMODEL approach (Rodhe and Seibert, 1999; Western *et al*., 1999; Sulebak *et al.*, 2000; Pellenq *et al*., 2003). As cited by Rodhe and Seibert, (1999) a weak correlation between distributed field measurements of soil moisture or ground-water levels and TWI has been reported by Burt and Butcher, 1985; Iorgulescu and Jordan, 1994; Moore and Thompson, 1996; and Seibert *et al*., 1997. One of the reasons for the relatively poor relationships with measured data is the inability of TWI to properly describe the actual soil saturation capacity. Pellenq *et al.* (2003) applied the TOPMODEL concepts for the disaggregation of soil moisture and reported that topography is not sufficient to explain the variability in soil moisture. They also found that the consideration of soil depth information improved the retrieval of local moisture patterns. This confirms that adding a soil specific parameter such as saturated conductivity or soil depth to the TWI can lead to improved model predictions. This information is often not available and it was the case with the current study as well. Hence, other soil related information may be considered.

Assuming (1) that topography is the dominant source of heterogeneity in the soil-water system of a hillslope catchment, and (2) that the amount of soil saturation is the dominant source of heterogeneity in soil water storage capacity, a relation can be established for a given location in a catchment to describe the moisture content. For a given location, soil water storage capacity (θ^*) can be computed as:

$$Soil\ \ water\ storage\ capacity\ = \theta^* = \frac{FC - PWP}{FC} \qquad \textbf{[-]} \qquad \textbf{(4-6)}$$

The product of *TWI* and θ* can a give soil-adjusted topographic wetness index (STWI):

$$STWI = TWI * \theta^* \qquad \textbf{[m}^2\textbf{/m/m/m]} \qquad \textbf{(4-7)}$$

STWI represents an intrinsic characteristic describing any given location in a catchment. The STWI of a given location varies with the water holding capacity of the soil in that location and the propensity of the geographic positioning of that location to receive water from the upslope contributing area. As described below the relationship between the temporarily variable soil saturation ratio on a given day and the location-specific STWI provides a methodology to derive hillslope scale soil moisture distributions from a limited number of measurements. Here, soil saturation ratio is defined as:

$$Soil\ Saturation\ Ratio_i = \frac{AWC_i - PWP}{FC} \quad \text{[-]} \qquad \textbf{(4-8)}$$

where AWC_i is the actual soil water content on the i^{th} day.

4.3.2 DEVELOPMENT OF DIGITAL ELEVATION MODEL FOR STANLEY CATCHMENT

The implementation of the STWI approach requires accurate TWI values from a high resolution DEM. The creation of an accurate DEM requires as a minimum, contour or spot height data. In the present study spot height data have been collected across the catchment as the suitable contour map for the catchment was not available. To collect spot heights, a differential geographic positioning system (GPS) manufactured by Trimble was employed as shown in Figure 4.9. About 16,000 spot heights were collected from the catchment during this topographic survey. These spot heights were then used with the ArcView Spatial Analyst (ESRI, 1996b) software to create a DEM with 5m grid spacing. The computation of TWI from the DEM was based on the Terrain Analysis Arc-script program module by Schmidt (2002). Figure 4.10 shows the computed topographic wetness indices for the catchment.

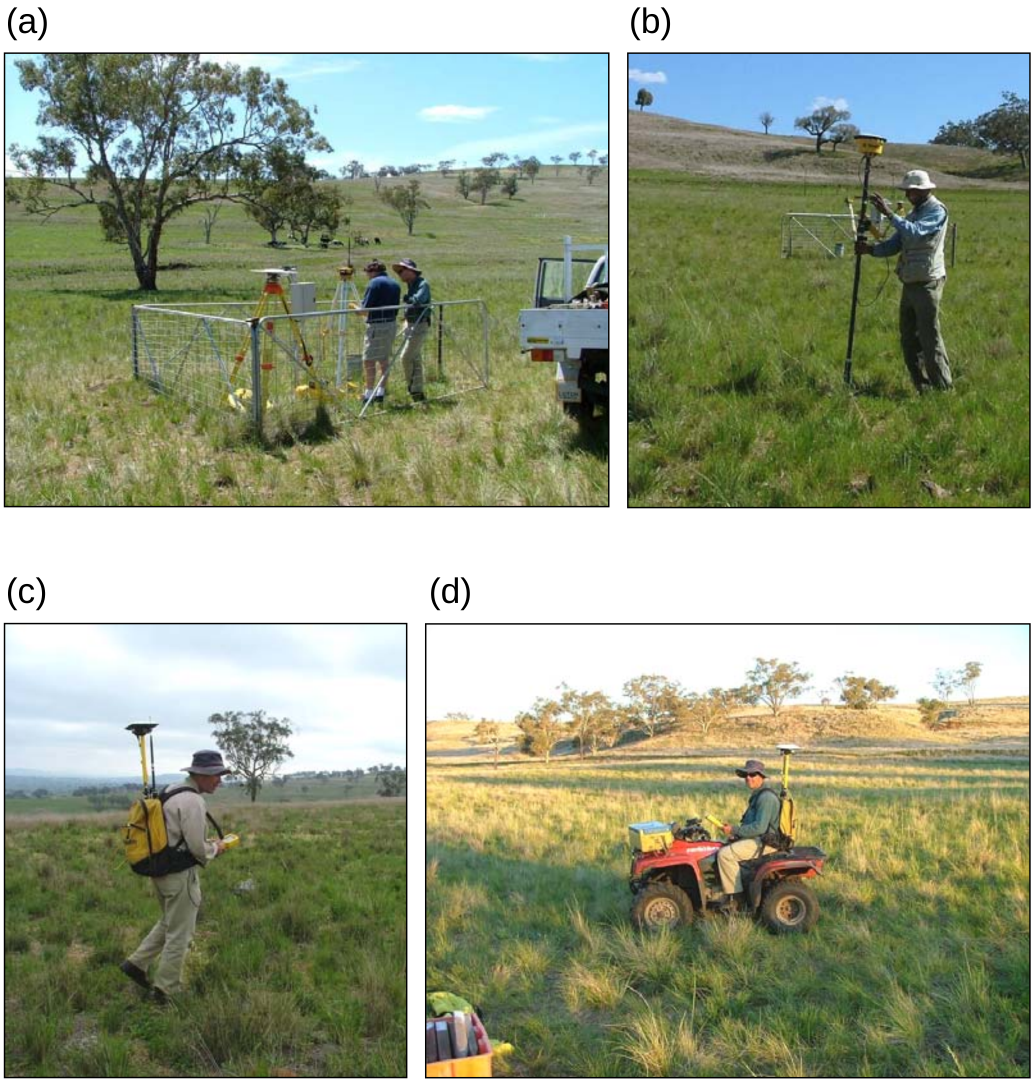

Figure 4.9: Differential GPS survey in the Stanley Catchment. (a) setting-up the Trimble Differential GPS base station at S5, (b) collecting elevation data with GPS receiver mounted on a rod, (c) backpack GPS receiver, and (d) use of all terrain vehicle for collecting elevation data.

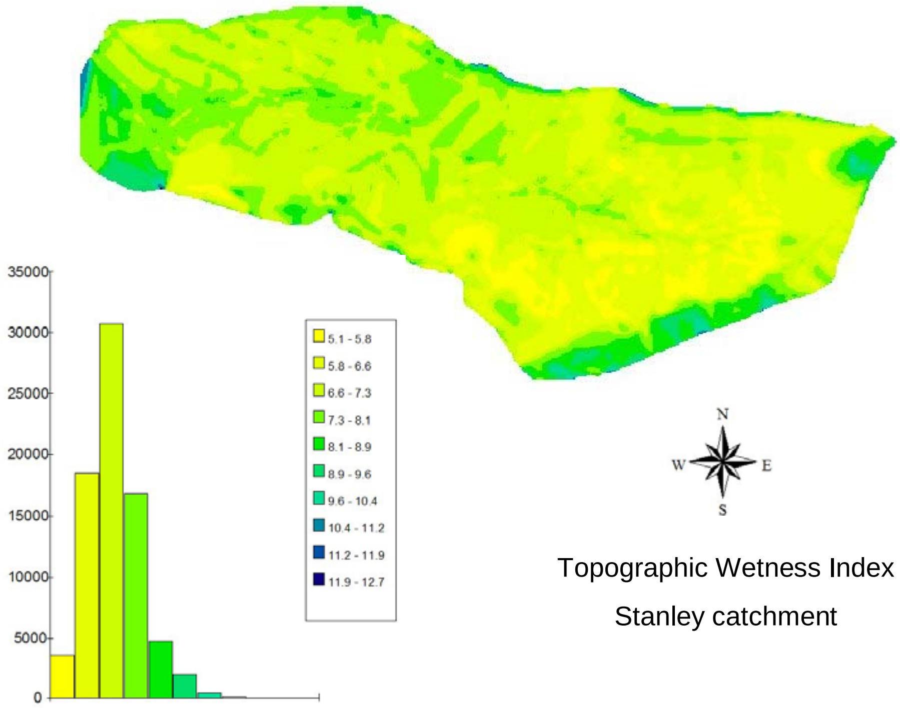

Figure 4.10: Computed topographic wetness index (TWI) for the Stanley hillslope catchment.

4.3.3 RELATION BETWEEN SOIL-ADJUSTED TOPOGRAPHIC WETNESS INDEX AND SATURATION RATIO

Accurate determination of maximum storage (saturation) capacity is important for the estimation of STWI values. Upper and lower soil water storage limits for different soil types may be obtained from published data sets. For the present study, these limits were estimated from the measured maximum and minimum soil moisture content data.

In general, a negative relationship exists between STWI and soil saturation ratio. For example, Figure 4.11 shows a negative linear relationship between STWI and saturation on day 136 in 2003. Considering the top 0-30 cm soil layer, the linear relationships between the degree of soil saturation and the STWI based on the six measuring sites have been studied for 2003-2004 and presented in Figure 4.12.

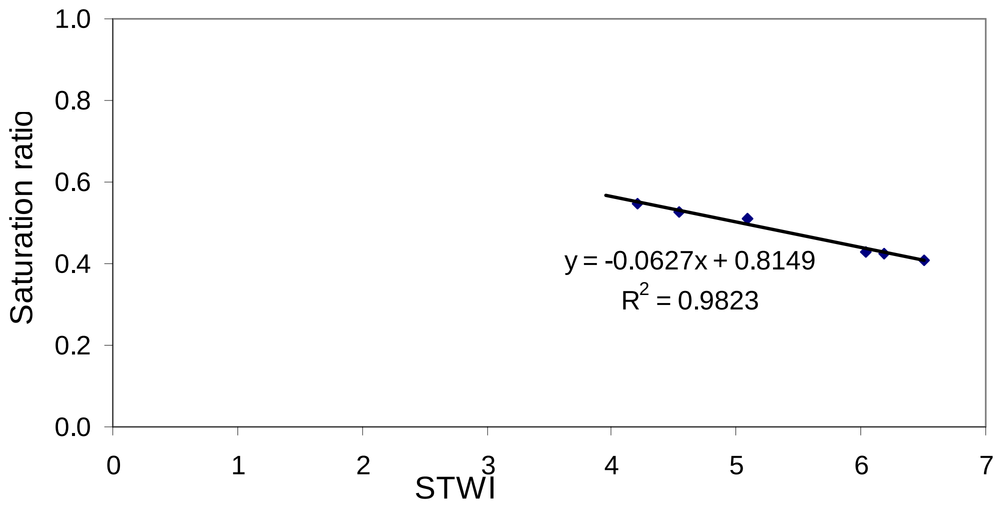

Figure 4.11: Relationship between STWI [m^2/m/m/m] and soil saturation ratio [-] on day 136 in 2003.

Part (a) of Figure 4.12 shows a time plot of R^2 values and slopes for the linear relationships between the soil saturation ratio and the STWI. As seen in the figure, in general, the Stanley catchment shows a negative correlation between saturation ratio and STWI. The R^2 values however vary with time. In order to interpret the variations in R^2 values, catchment-scale average saturation ratio and rainfall values are presented in part (b) of Figure 4.12. As can be seen in part (a) and part (b), higher R^2 values are present on days with moderate soil water contents. Rainy days or days with high saturation ratio are generally characterized by lower R^2 values. However, the period between day 155 and 245 in 2004 did not follow this general pattern. As discussed in Section 4.2.1.4, the lower R^2 values during this period may be due to greater temporal variation of rainfall.

Theoretically, the relationship between saturation ratio and STWI should vary with the available soil moisture levels. As reported by Grayson and Blöschl (2000), surface and subsurface lateral flows occur during wet periods, particularly in gullies, which can produce topographically organised wetness patterns. For this reason one can expect higher correlation between the saturation ratio and STWI during wet periods. During dry periods, in contrast, there is a minimum of lateral redistribution and fluxes are essentially in the vertical dimension. Therefore, soil moisture patterns during very dry periods are not necessarily related to catchment topography but to the soil moisture storage capacity. Similarly, immediately after rainfall events, root-zone moisture in a catchment may take higher values irrespective of the topographic position. This situation may lead to a lower correlation between saturation ratio and STWI.

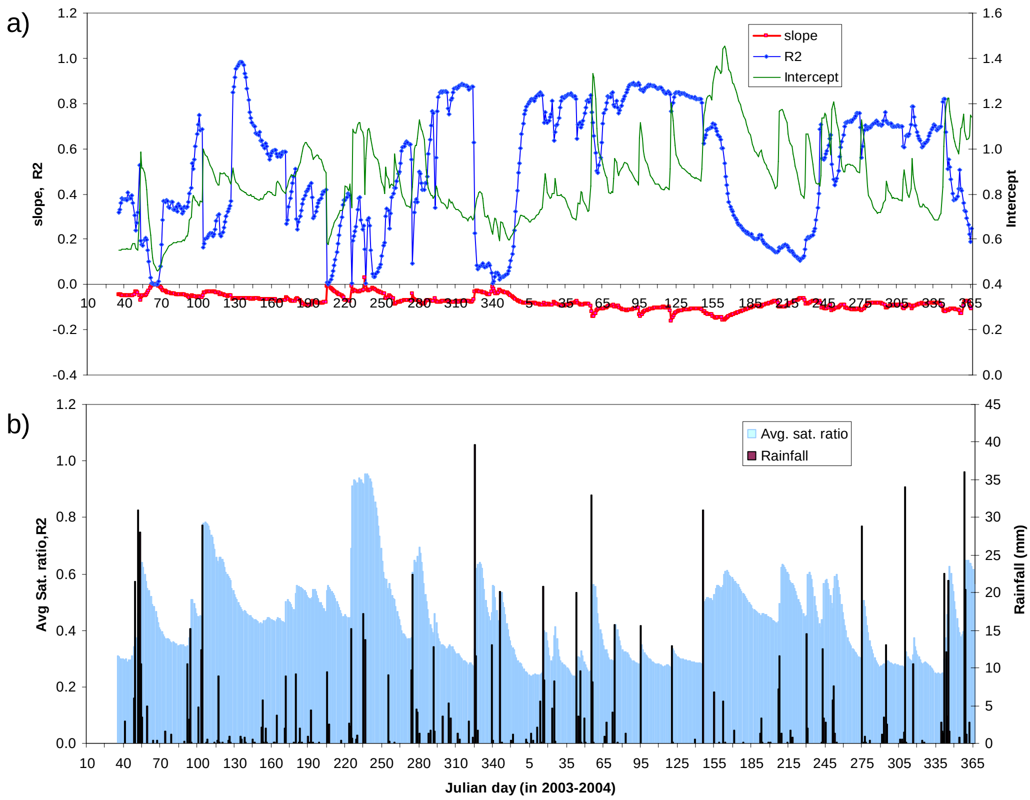

Figure 4.12: (a) Slope, intercept and R^2 values for the established linear relationships between STWI and saturation ratio during study period. (b) Average saturation ratio and rainfall pattern for the same period.

It appears that the relationship between soil saturation ratio and STWI is generally strong during periods with intermediate wetness and shows a poor relationship during prolonged wet periods or when two-day rainfall exceeds 30 mm. Therefore, linear regression between saturation ratio and STWI may provide a methodology to understand the distribution of moisture along a hillslope particularly when moisture conditions are between very wet conditions (close to field capacity) and very dry condition (close to wilting point).

4.4 APPLICATION OF SOIL-ADJUSTED TOPOGRAPHIC WETNESS INDEX FOR GENERATING HILLSLOPE MOISTURE PATTERNS

The STWI-based model developed in the previous section has been applied to generate hillslope-scale maps of 0-30 cm soil moisture content using the field measured point-scale moisture contents. The following sections describe the data used for the model.

4.4.1 DESCRIPTION OF CATCHMENT PARAMETERS USED

Apart from the TWI computed from a DEM (see Section 4.3.2), computation of STWI requires soil water storage capacity (see Eq. 4.5). Soil water storage capacity is a property which depends on the soil texture. Thus, it can be assumed that the hillslope scale soil water storage capacity pattern can be represented by the soil distribution map. Based on the property-scale soil landscape map prepared by the NSW Department of Sustainable Natural Resources, soil distribution within the hillslope is shown in Figure 4.13. The two soil types in the catchment are (i) clay to clay-loam soils and (ii) silty-loam soils.

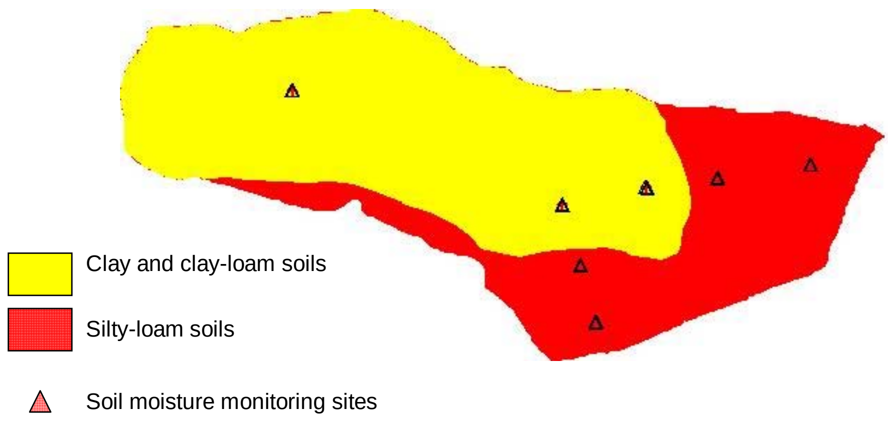

Figure 4.13: Soil distribution in the Stanley hillslope catchment. (Redrawn based on the Soil Landscapes Map (2003) by Resource Information Unit, NSW Department of Sustainable Natural Resources).

The next two soil-based parameters required for the model are the minimum and maximum soil moisture values over 0-30 cm depth for these two soil types. The two-year period of soil moisture measurements provides reasonably good estimates of these two extreme moisture values for the catchment. Table 4-3 shows the field-measured minimum and maximum soil moisture values for each soil type observed during the two-year study period. The computed relative soil water storage capacity (θ*) for each soil type is also shown in the table. As expected, clay and clay-loam soils have a higher θ* value (i.e. 0.83) than silty-loam soils (i.e. 0.74).

Table 4-3: Characteristics of the soil water storage capacities of the catchment soil types.

Soil type	Average min. SWC	Average max. SWC	θ*
Clay, clay loam and silty clay soils (S1, S2 and S5)	0.11	0.62	0.83
Silty loam soils (S3, S4 and S7)	0.14	0.55	0.74

4.4.2 SELECTION OF DATES

Selection of dates is important in any soil moisture related study, particularly for soil moisture scaling studies. The main objective of the present study is to generate soil moisture patterns over the entire hillslope catchment at the scale of the 5m DEM for all wetness conditions. In the absence of soil moisture maps for catchment to evaluate the predicted patterns, the approach taken here has been to generate soil moisture maps representing several dominant environmental episodes. Next these predictions are reviewed critically and interpreted qualitatively. Four case study periods were selected to represent different seasons with periods of different lengths. For each case study period, three days based on the first, last and the middle day of each period was considered as shown in Table 4-4. Thus, altogether 12 days were chosen for the model application. In fact, these dates were selected mainly to accommodate a range of soil wetness conditions based on field measured data as shown in Table 4-5.

Table 4-4: Case studies and selected dates.

Case study	Period (Julian day)	Season	Total number of days	Days selected		
1	107 - 167 (2003)	Autumn	61	107	136	167
2	236 - 273 (2003)	Winter	38	236	250	273
3	350 (2003) - 14 (2004)	Summer	30	350	364	14
4	215 - 272 (2004)	Winter	58	215	243	272

Table 4-5: Minimum, maximum and mean values of actual soil moisture content ($cm^3.cm^{-3}$) for the top 0-30 cm at the six monitoring sites in the catchment on the selected dates (shown by year-day number).

Case Study		Day-1	Day-2	Day-3
1	Day	2003-107	2003-136	2003-167
	Min. SWC	0.421	0.211	0.172
	Max. SWC	0.507	0.324	0.346
	Mean SWC	0.452	0.276	0.258
2	Day	2003-236	2003-250	2003-273
	Min. SWC	0.496	0.220	0.131
	Max. SWC	0.637	0.446	0.309
	Mean SWC	0.555	0.381	0.215
3	Day	2003-350	2003-364	2004-014
	Min. SWC	0.177	0.075	0.065
	Max. SWC	0.370	0.216	0.214
	Mean SWC	0.259	0.156	0.142
4	Day	2004-215	2004-243	2004-272
	Min. SWC	0.184	0.183	0.076
	Max. SWC	0.497	0.343	0.293
	Mean SWC	0.342	0.254	0.178

4.4.3 RESULTS

The regression models developed between STWI and measured actual soil saturation ratio for the selected dates are summarized in Table 4-6. It is evident that, in general, a negative relationship exists between the STWI and measured soil saturation ratio.

Table 4-6: Properties of the linear regression equations developed for the case study dates.

Day	Intercept	Slope	R^2	t-statistics Intercept	t-statistics Slope
2003-107	0.963523	-0.034000	0.0207	5.26	-1.02
2003-136	0.814864	-0.062741	0.9820	35.19	-14.90
2003-167	0.833746	-0.072500	0.5633	4.75	-2.27
2003-236	0.796076	0.028897	0.1569	4.32	0.86
2003-250	0.851111	-0.037870	0.1258	3.10	-0.76
2003-273	0.739780	-0.068890	0.6204	4.99	-2.56
2003-350	0.647394	-0.035220	0.0384	1.34	-0.40
2003-364	0.706732	-0.080220	0.6644	4.51	-2.81
2004-014	0.729509	-0.089070	0.8483	7.04	-4.73
2004-215	1.113931	-0.095090	0.1732	1.95	-0.92
2004-243	0.881117	-0.081840	0.7082	6.10	-3.12
2004-272	0.902670	-0.109920	0.7575	5.28	-3.53

The generated spatial patterns of the 0-30 cm soil water contents values (in $cm^3.cm^{-3}$) are presented in Figures 4.14 to 4.17 for different case studies. In general, it can be seen that more "organization" exists when (i) R^2 values are high and (ii) absolute slope values are greatest.

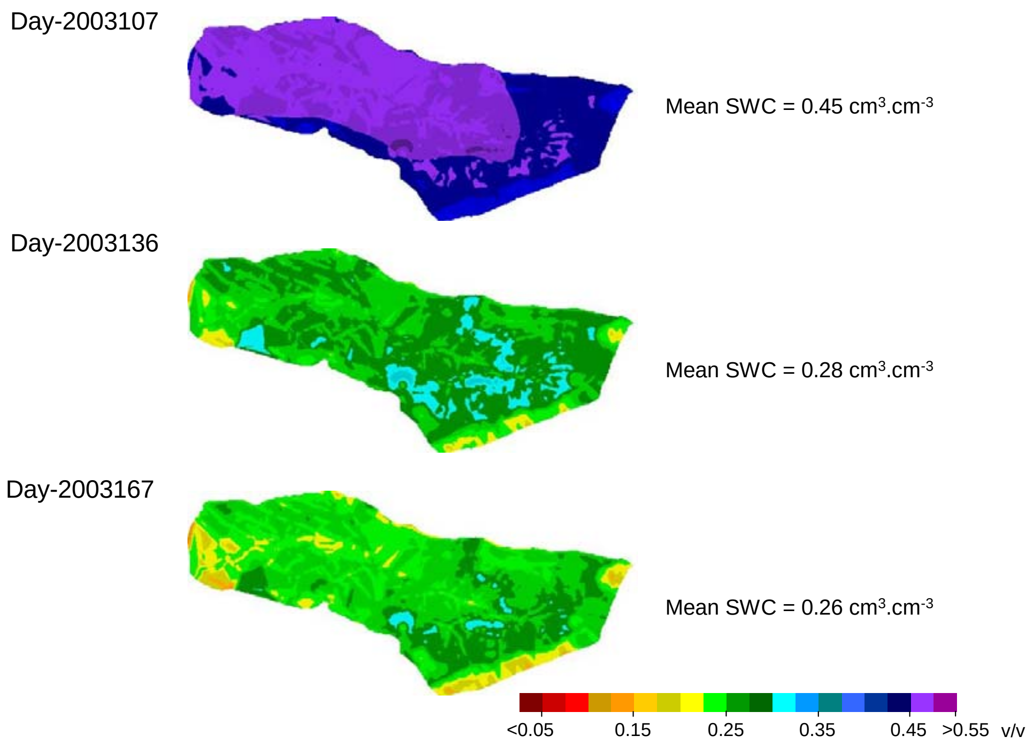

Figure 4.14: Predicted 0-30cm near-surface soil water patterns in the Stanley catchment for the three days (2003-107, 2003-136 and 2003-167) selected in case study-1.

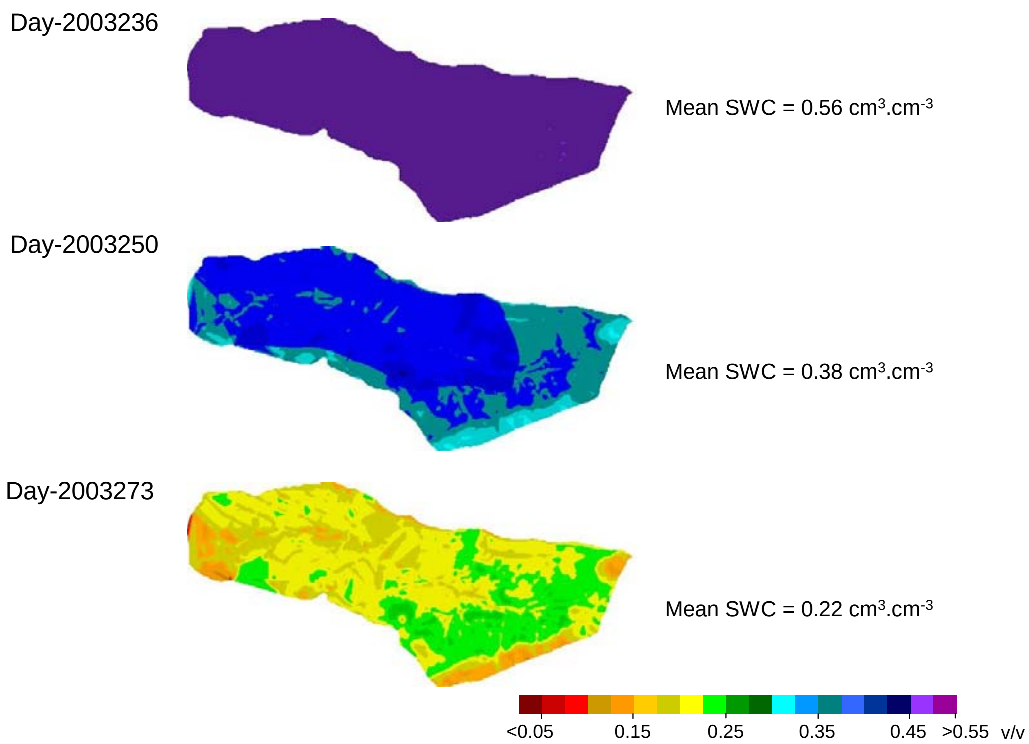

Figure 4.15: Predicted 0-30cm near-surface soil water patterns in the Stanley catchment for the three days (2003-236, 2003-250 and 2003-273) selected in case study-2.

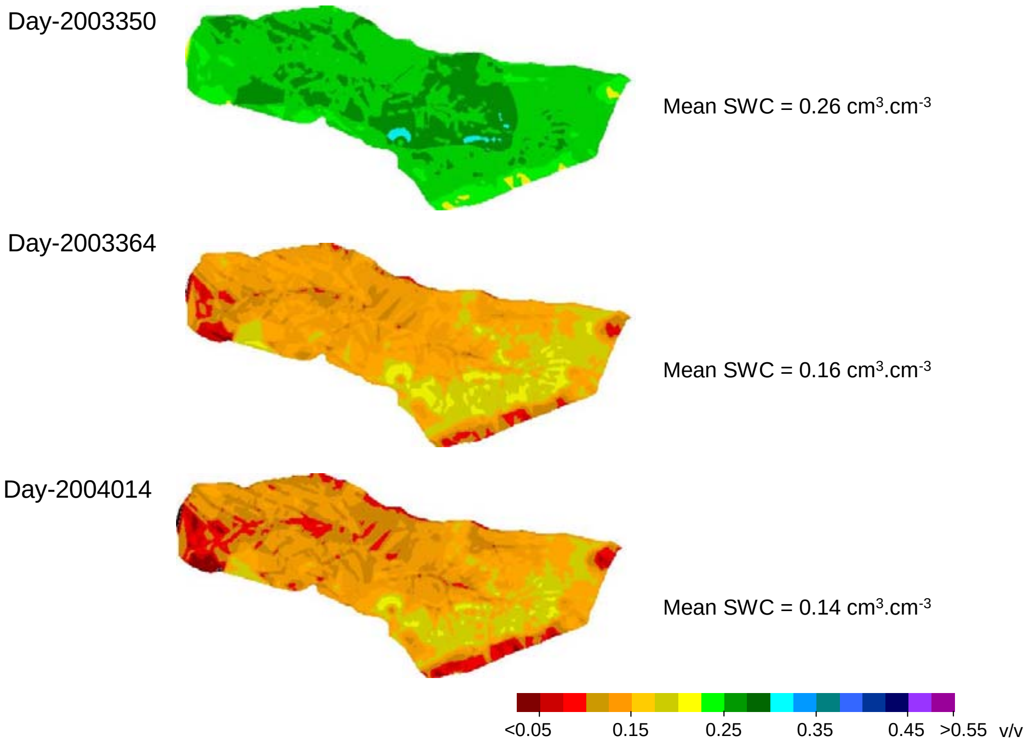

Figure 4.16: Predicted 0-30cm near-surface soil water patterns in the Stanley catchment for the three days (2003-350, 2003-364 and 2004-014) selected in case study-3.

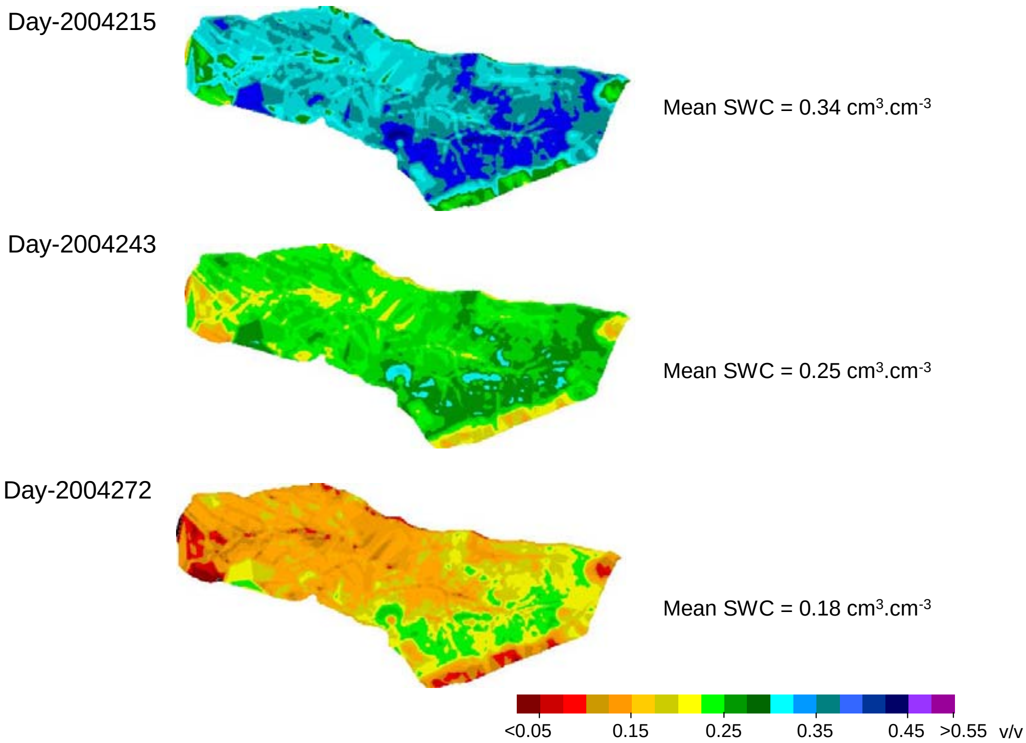

Figure 4.17: Predicted 0-30cm near-surface soil water patterns in the Stanley catchment for the three days (2004-215, 2004-243 and 2004-272) selected in case study-4.

4.4.4 DISCUSSION

In the absence of suitable field measurements for validation of the predictions, meaningful explanations of the spatial patterns of predicted soil water contents must consider environmental conditions and catchment properties. In this context, it is important to consider antecedent rainfall, catchment scale characteristics, and quantitative evaluation of predicted values.

4.4.4.1 Evaluation of predicted patterns based on response to antecedent rainfall

As noted in Figures 4.14 to 4.17, soil moisture patterns in the catchment for any case study day is related to environmental conditions and particularly to the recent rainfall. This is evident from the historical rainfall pattern as shown in Table 4-7. The predicted patterns of soil moisture appear to be closely related with the recent rainfall pattern. For example, on day 2003236 during winter, due to high rainfall of 31 mm during past three days, the predicted SWC pattern showed very wet conditions. In contrast, during the summer months, smaller rainfall amounts may not be sufficient to increase the soil wetness. As a result, the catchment may continue to exhibit dry condition. This was the case with day 2004014 when rainfall of 5.8 mm during the previous three days did not result in increasing the surface wetness. Therefore, predicted SWC values appear to reflect recent rainfall conditions.

Table 4-7: Rainfall history for the selected case study days.

		Rainfall (mm) during past -			
Case study	Day	3 days	7 days	14 days	30 days
1	2003-107	0.2	46.4	61.8	77.1
	2003-136	1.6	1.6	3.2	14.0
	2003-167	0.0	4.2	6.6	16.4
2	2003-236	31.0	32.1	53.4	56.4
	2003-250	0.0	0.0	0.0	53.4
	2003-273	0.0	0.0	0.2	9.5
3	2003-350	0.0	20.4	33.9	87.7
	2003-364	0.0	0.0	1.6	35.5
	2004-014	5.8	8.4	10.6	12.2
4	2004-215	0.2	1.6	20.4	25.8
	2004-243	12.8	12.8	29.4	32.2
	2004-272	0.0	0.0	0.0	33.8

4.4.4.2 Evaluation of spatial patterns based on the catchment-scale dominant physical controls

The spatial distribution of predicted soil moisture content must be discussed in relation to variations of soil properties, topography, and land use type. Soil physical properties and topography control spatial variations of soil moisture content. According to Chang and Islam (2003), for certain situations, topographic control over soil moisture will dictate the distribution of soil moisture while in other cases soil physical properties will be the main factor that controls variations of soil moisture. Thus, predicted patterns may reflect some relation to soil properties and/or topography.

Part of the spatial variations of soil moisture may be attributed to the soil type. The present hillslope catchment consists mainly of two soil types: clay to clay loam and silty loam soils. Based on field measurements it was found that the storage capacity of clay to clay loam soil (0.11 - 0.62 $cm^3.cm^{-3}$) is higher than that of silt loam soils (0.14 - 0.55 $cm^3.cm^{-3}$). In a situation where soil water content gets close to field capacity levels, it is the soil type which determines the spatial pattern of water content. For example, soil water contents during day 1 in case study-1 (Day-2003107 in Figure 4.14) and day 2 in case study-2 (Day 2003-250 in Figure 4.15) show situations where water contents are close to field capacity levels (0.46 and 0.38 $cm^3.cm^{-3}$, respectively). The predicted soil water patterns during these two cases demonstrate the influence of soil type on near-field capacity moisture conditions. Moreover, such variations may disappear with saturated conditions such as observed in Day-2003236 (see Figure 4.15). Thus, predicted 0-30cm moisture patterns reflect the soil water presents according to soil physical properties.

Spatial variations of soil moisture may also be attributed to the position in the landscape. Wet patches appear to occur in lower slope areas whereas dry patches are normally located on hill tops. As seen on Day-2003136 and Day-2003167 (see Figure 4.14), on Day-2003273 (see Figure 4.15) and on all three days in case study-4 (see Figure 4.17) it is apparent that wetter areas are present in the lower part of the hillslope. Because the lower parts of hillslope can behave as soil-water converging zones. For example, S3 is located in such an area and from the water balance study it was found that the site is continuously receiving some sub-surface water (see Figure 4.5 (c)). In contrast, a higher position leads to rapid down slope drainage during precipitation events. Consequently, soil moisture content is lower on hilltops than in valley bottoms. This situation can be observed in the predicted patterns; for example, on Day-2003250 and Day-2003273 (Figure 4.15) and for all case study days in Figure 4.17. Similarly, aspect influences solar irradiation and evaporation, therefore, a lower soil moisture content in 0-30 cm may in part be attributed to higher evapotranspiration on north- and west-facing slopes. This effect is apparent in the south-eastern parts of the SHC particularly on Day-2003364 and Day-2004014 (see Figure 4.16) and on Day-2004272 (see Figure 4.17) where dry patches are apparent. Topographically controlled soil moisture patterns (i.e. random or organized) have been reported by many previous studies (Moore *et al.*, 1988; Famiglietti *et al.*, 1998; Western *et al.*, 1999). Therefore, predicted soil water patterns appear to reflect topographic effects on soil moisture distribution in this hillslope catchment.

Land use also influences the spatial distribution of soil moisture. This hillslope catchment is used for grazing and the dominant vegetation includes annual and perennial pasture varieties, small shrubs and sparsely distributed eucalyptus trees.

Annuals and low shrubs have generally shallow root systems (typically < 50cm) and will therefore extract more soil water from the near-surface soil layer. Due to near-uniform vegetation patterns, such water extraction should lead to near-uniform moisture patterns particularly in flat areas with similar soil properties. Predicted soil water patterns on all case study days reflect this phenomenon and large continuous patches of similar water contents can be found in the flat part of the catchment. Thus, predicted soil water patterns appear to reflect the natural vegetation status of a hillslope catchment.

We may therefore conclude that the predicted soil water distributions appear to reflect variations in soil type, position in the landscape and vegetation type.

4.4.4.3 Quantitative evaluation of predicted patterns

To evaluate the robustness of the upscaling methodology, it is necessary to compare the results with relevant field observations. The only available field measurements are limited point-scale 0-30 cm soil moisture measurements at the permanent monitoring sites. However, it is also possible to generate some information from the predicted patterns and evaluate those with the other published results.

First, average measured moisture values (based on the 6 sites) and catchment-scale averages from the predicted moisture values are compared. Figure 4.18 shows the measured and predicted soil water contents during all case study days. It is clear that the predicted average SWC values are nearly identical to the measured average SWC values.

Statistical properties of the predicted 0-30cm soil water content have been calculated for all case study days and are presented in Table 4-8. It can be seen that the range and mean values of the predicted soil moisture values are comparable with measured values (see Table 4-5 and Table 4-8).

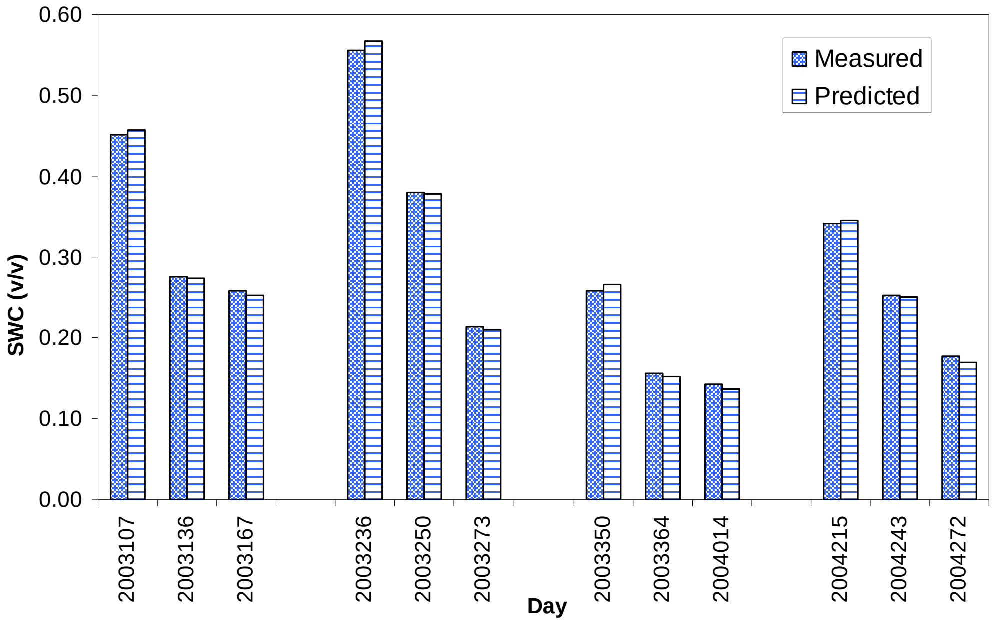

Figure 4.18: Comparison of measured (from 6 sites) and predicted (considering entire catchment) average 0-30 cm near-surface soil water contents ($cm^3.cm^{-3}$).

Table 4-8: Statistical properties of the predicted 0-30 cm soil water content values during case study days.

Case study		Day-1	Day-2	Day-3
1	Day	2003-107	2003-136	2003-167
	Min. SWC	0.382	0.161	0.120
	Max. SWC	0.507	0.339	0.324
	Mean SWC	0.458	0.275	0.253
	Standard deviation	0.037	0.052	0.060
2	Day	2003-236	2003-250	2003-273
	Minimum SWC	0.496	0.303	0.081
	Maximum SWC	0.652	0.427	0.276
	Mean SWC	0.567	0.379	0.210
	Standard deviation	0.046	0.037	0.057
3	Day	2003-350	2003-364	2004-014
	Minimum SWC	0.203	0.000	0.001
	Maximum SWC	0.308	0.225	0.217
	Mean SWC	0.267	0.153	0.137
	Standard deviation	0.031	0.065	0.063
4	Day	2004-215	2004-243	2004-272
	Minimum SWC	0.170	0.098	0.001
	Maximum SWC	0.438	0.329	0.270
	Mean SWC	0.345	0.251	0.170
	Standard deviation	0.078	0.067	0.078

The relationship between the variance of the predicted 0-30 cm soil water contents and mean soil moisture also provides some indication of the reliability of the predicted distribution patterns as shown in Figure 4.19. It can be seen in the figure that the variance of predicted soil moisture content decreases with increasing mean soil moisture content. Famiglietti *et al.* (1999) reported similar observations during their Southern Great Plains hydrology experiment. However, other studies have suggested that the variance of soil moisture increases with increasing mean soil moisture (Robinson and Dean, 1993; Famiglietti *et al.,* 1998). Charpentier and Groffman, (1992) observed no systematic relationships but their findings are based on large-area remotely sensed observations and therefore, may not readily be compared with the predicted soil water contents of 5m grid cells generated in the present study. Moreover, some of these studies were based on 0-5 cm near-surface soil moisture values (e.g. Famiglietti *et al.,* 1998). It is concluded that in the case of Stanley catchment, there is a negative correlation between the variance of predicted soil moisture in top 0-30 cm and mean values.

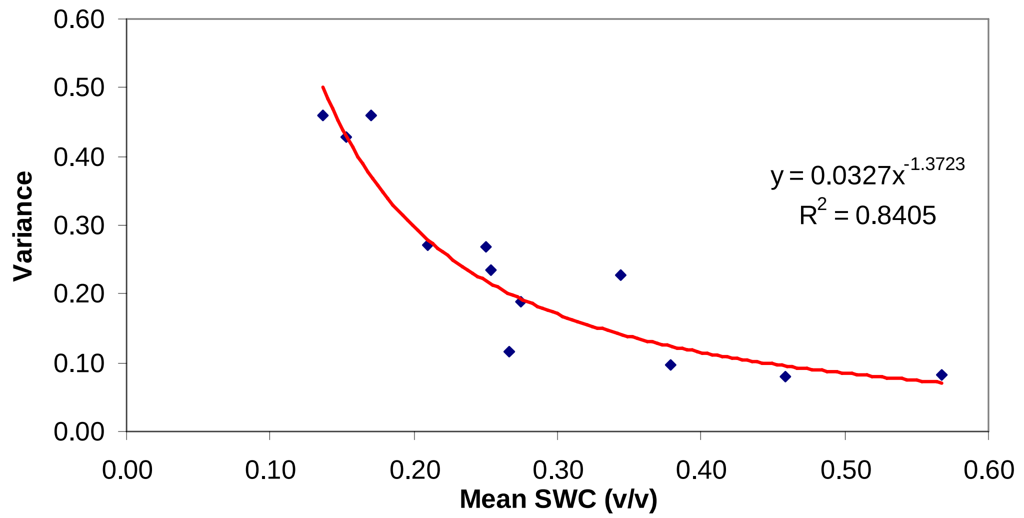

Figure 4.19: Relation between the variance (in $cm^3.cm^{-3}$) of predicted 0-30cm SWC and mean soil moisture.

The field observations discussed above show quantitative agreement of predicted soil moisture in the hillslope catchment with respect to the mean and variance of the predicted moisture values. It can therefore argue that the predicted soil water contents for the hillslope appear to be realistic.

4.4.4.4 Evaluation based on frequency distributions of predicted 0-30 cm soil moisture patterns

The statistical distribution of predicted moisture content values also provides some insight into whether the predicted moisture patterns are satisfactory. Because some researchers have reported that surface soil moisture content values are normally distributed (e.g. Francis *et al.*, 1986, Nyberg, 1996). Figures 4.20 and 4.21 show frequency distributions of the predicted soil water content values. As seen, during most days, the predicted SWC values are normally distributed. Under very wet conditions however, the SWC values produce a bimodal distribution (e.g. day 1 in the case study 1 and 2). Under saturated conditions, it is soil texture through θ^* that determines the SWC and the two dominant soil types in the catchment may well lead to a bimodal distribution under saturated conditions.

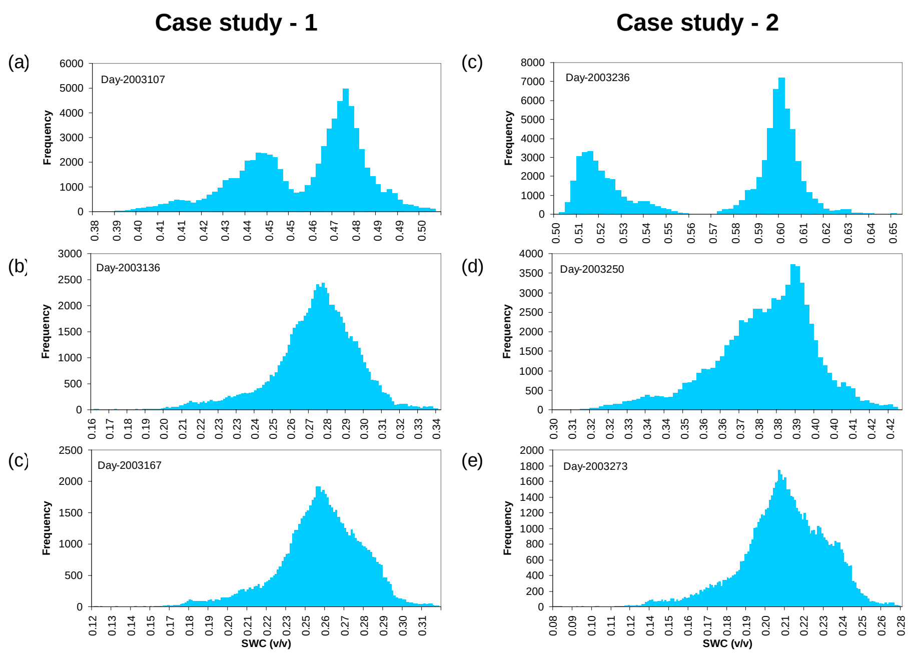

Figure 4.20: Frequency distributions of predicted soil water contents during case study-1 and case study-2. (Note the difference in horizontal scale)

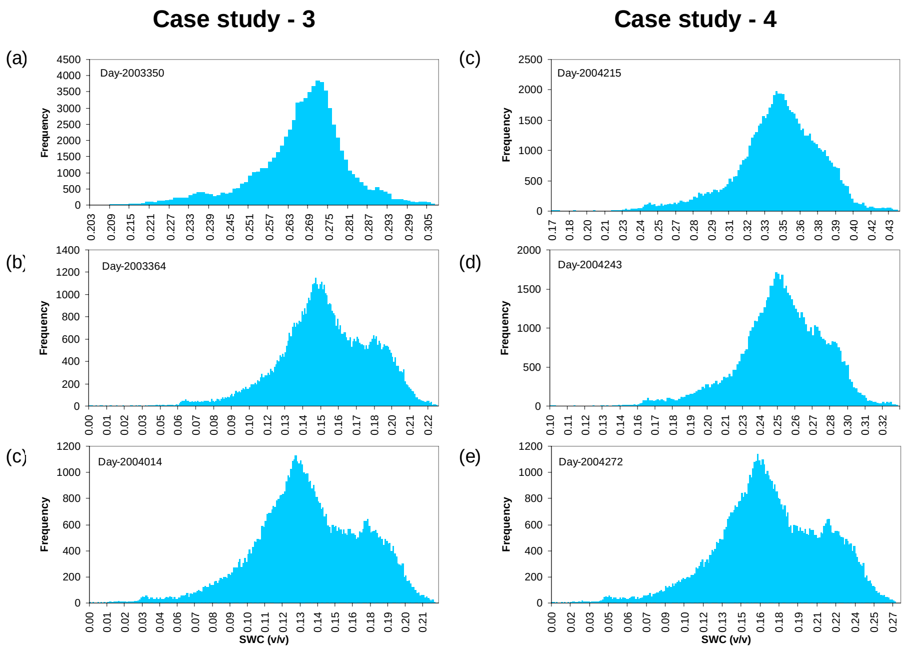

Figure 4.21: Frequency distributions of predicted soil water contents during case study-3 and case study-4. (Note the difference in horizontal scale)

4.4.4.5 Validation of predicted patterns

The outcome of the qualitative and quantitative validation of the SWC values predictions for the hillslope catchment as reported in the previous sections have been summarized in Table 4-9 and 4-10.

Table 4-9: A summary of key issues considered in evaluating the predicted 0-30 cm soil water contents during case study-1 and case study-2.

Evaluation parameter	Case study-1			Case study-2		
Day =>	107	136	167	236	250	273
Predicted wetness	Wet	Mod.	Mod.	Wet	Wet	Mod.
Rainfall						
Is predicted pattern representing antecedent rainfall?	Yes	Yes	Yes	Yes	Yes	Yes
Spatial organization						
Is there any pattern present?	Yes	Yes	Yes	No	Yes	Yes
Does this pattern appear to be related to topography?	No	Yes	Yes	No	Yes	Yes
Is this pattern related to soil type?	Yes	No	No	No	Yes	No
Are these predicted values normally distributed?	No	Yes	Yes	No	No	Yes/No
Hillslope scale SWC						
Does the predicted average match with the measured average?	Yes	Yes	Yes	Yes	Yes	Yes
Does the predicted range match with the measured range?	Yes	Yes	Yes	Yes	Yes	Yes

Table 4-10: A summary of key issues considered in evaluating the predicted 0-30 cm soil water contents during case study-3 and case study-4.

Evaluation parameter	**Case study-3**			**Case study-4**		
Day =>	350	364	014	215	243	272
Predicted wetness	Mod.	Dry	Dry	Wet	Mod.	Dry.
Rainfall						
Is predicted pattern representing antecedent rainfall?	Yes	Yes	Yes	Yes	Yes	Yes
Spatial organization						
Is there any pattern present?	Yes	Yes	Yes	Yes	Yes	Yes
Does this pattern appear to be related to topography?	Yes	Yes	Yes	Yes	Yes	Yes
Is this pattern related to soil type?	Yes	No	No	No	No	No
Are these predicted values normally distributed?	Yes	No	No	Yes	Yes	No
Hillslope scale SWC						
Does the predicted average match with the measured average?	Yes	Yes	Yes	Yes	Yes	Yes
Does the predicted range match with the measured range?	Yes	Yes	Yes	Yes	Yes	Yes

Several points may be drawn from this study:

(1) During very wet days as on day 2003 - 236 with average SWC of 0.567 $cm^3.cm^{-3}$ soil moisture values do not show any pattern with respect to soil type or topography.

(2) During wet days as on day 2003 - 107 with average SWC of 0.458 $cm^3.cm^{-3}$ the soil moisture distribution may show some pattern which is broadly based on

soil type. In this situation, the frequency distribution of soil moisture values may not show a normally distributed pattern.

(3) During some wet days (as on day 2003 - 250) with average SWC of 0.379 $cm^3.cm^{-3}$ soil moisture distribution may show a pattern which has some relationship with both soil type and the topography.

(4) For moderately wet conditions (i.e. average SWC between 0.25 - 0.35 $cm^3.cm^{-3}$ as on days 2004-243 or 2004-215) SWC values in the catchment may be distributed normally. Under these conditions, topography appears to play a dominant role.

(4) Under dry conditions (i.e. average SWC between 0.14 - 0.17 $cm^3.cm^{-3}$ as on days 2003-364 or 2004-014) the topography appears to play a dominant role but catchment scale SWC values may not be distributed normally.

The predicted soil moisture therefore exhibits organized characteristics under some, but not all circumstances. The degree of organization depends on the catchment's current wetness state. Similar observations have been reported by other researchers (Grayson *et al*., 1997; Western *et al*, 1999). It can therefore be concluded that the STWI-based approach offers a suitable tool for upscaling point-scale 0-30 cm measurement across a hillslope catchment such as the SHC.

4.4.5 CONCLUSIONS

A Soil-adjusted Topographic Wetness Index (STWI) has been developed for upscaling point-scale 0-30 cm soil moisture measurements to derive hillslope scale soil moisture distributions. The Soil-adjusted Topographic Wetness Index appears to be an important, physically-based characteristic of a given location in the catchment. This is perhaps the first attempt to combine the effect of topography and soil properties in deriving soil moisture patterns from point-scale field measurements.

The proposed approach assumes that the STWI at a given location varies with the capacity of the soil in that location to hold moisture and the propensity of the geographic position of that location to receive water from the upslope contributing area. By considering the top 0-30 cm soil layer and assuming a linear relationship between the amount of soil saturation and the STWI, this approach provides a methodology to understand the distribution of moisture along a hillslope particularly when the moisture condition is between field capacity and wilting point. The soil saturation ratio and STWI generally display a strong relationship during partially wet or partially dry periods but show a poor relationship during prolonged wet or prolonged dry periods. The relationship between the temporarily variable soil saturation ratio on a given day and a location-specific intrinsic property such as STWI provides a methodology for obtaining hillslope scale soil moisture distributions from a limited number of measurements.

The results shown here have focussed on the driest days, wettest days and days with intermediate moisture contents during the two-year study period. The present study has demonstrated that a limited number of point-scale 0-30 cm field measured soil moisture values can be used to generate high resolution (5m grid cells in this study) soil moisture patterns in a hillslope catchment. Such generated patterns, appear to reflect the natural soil moisture pattern in a hillslope catchment reasonably well. Further detailed studies will be required using more extensive data sets obtained with high-resolution ground based observations and/or airborne microwave measurements. The methodology will also need to be evaluated on a range of different catchments in other environments. Also, it will be useful to further investigate the TWI with recharge, saturated conductivity and soil depth information for such soil moisture scaling studies.

4.5 CHAPTER SUMMARY

The application of single layer bucket models for balancing the inputs and outputs of water at six locations within the Stanley hillslope catchment confirms that the ignoring of the Q term causes significant errors in soil moisture predictions. Therefore, inclusion of Q term is crucial in soil moisture prediction studies.

Soil moisture measurement collected at irregular intervals will minimize the difference between predictions and measurements and may be used to generate soil moisture trajectories over extended periods. Adopting simple bucket type water balance models, soil moisture patterns can be generated over longer time periods. Hence, simple water balance approaches are an option for interpolating soil moisture measurements in the temporal domain. Applications of single layer bucket models need to be done with some caution. Because of the lateral surface and subsurface flows which are dominant in the hillslope scale during certain periods, it is important to include such water inputs into the model. This observation provides the link with the second part of this chapter.

The application of single layer bucket models for balancing the inputs and outputs of water in the Stanley hillslope catchment confirmed that the soil moisture data collected during the study period are realistic. The predicted soil moisture values were found to be comparable with the measured soil moisture contents. Hence, soil moisture data collected during the study period could be used for other applications with some confidence.

A Soil-adjusted Topographic Wetness Index (STWI) has been developed and applied for upscaling point-scale 0-30 cm soil moisture measurements to derive hillslope scale soil moisture distribution patterns. The STWI is a physically-based intrinsic index which can be used to characterise the soil wetness in a given location based on the topographic position and soil properties.

Linear relationships have been established between the STWI and the soil saturation ratio derived from measured data and these have been then applied for a hillslope catchment to derive spatial patterns of soil moisture. This study demonstrates that a location-specific intrinsic property such as STWI provides a tool to derive hillslope scale soil moisture distributions from a limited number of measurements, especially for inter-mediate wetness conditions.

CHAPTER FIVE

5. ESTIMATION OF CATCHMENT AVERAGE SOIL WATER CONTENTS FROM POINT-SCALE ROOT-ZONE SOIL MOISTURE MEASUREMENTS

This chapter examines the prediction of catchment average soil water content (SWC) from the Catchment Average Soil Moisture Measurement (CASMM) sites. This approach is based on studying the temporal stability characteristics of soil moisture across a range of scales. This work aims to gain insight into the temporal behaviour of soil moisture at each site and to identify which stations are representative of the mean soil moisture values across the study area at a range of scales.

5.1 INTRODUCTION

Knowledge of soil moisture processes and their spatial distribution provides essential information for hydrologic and climatic models. Therefore, soil moisture observations at a range of scales may be valuable in assisting the improved formulation and parameterisation of soil moisture impacts on land surface processes such as runoff, vegetation growth and soil carbon dynamics. Furthermore, heterogeneity in soil moisture is undoubtedly a major factor for hydrological modelling. Point-scale soil moisture observations made at chosen locations therefore, may not necessarily describe the average soil moisture content at some larger spatial scale. As such, dependable methodologies are required to derive spatially averaged soil moisture estimates from point scale observations.

Upscaling (or aggregation) is a mathematical procedure whereby parameters are derived from data collected at smaller spatial scales. Different approaches have been applied to the problem of upscaling soil moisture content: these include simple spatial averaging, a variety of interpolation techniques, fractal geometry, and the use of proxy variables. Spatial averaging is the most basic and simple approach. The use of simple averages based on soil moisture measurements from few locations however does not always guarantee good results. On the other hand, a range of interpolation techniques may be applied to derive average moisture content or surface patterns from point scale measurements. For example, linear interpolation is an option to derive spatial patterns from point observations. This approach however, rarely provides dependable wetness patterns. Soil moisture is highly variable in space as well as in time. Furthermore, soil moisture fields are not completely random variables due to their association with known geographic locations. A better approach therefore would be the use of geo-statistical techniques such as inverse distance weighting (IDW) or kriging for soil moisture fields. Many researchers have studied the spatial distribution of soil moisture content, using geostatistical methods based on remotely sensed and field-measured data (Thattai and Islam, 2000; Glenn and Carr, 2003). Several studies have however reported little spatial correlation of SWC and geostatistical parameters (Mohanty *et al*., 2000). Furthermore, all of these statistical interpolation approaches hinge on the assumption of the variable under consideration being a Gaussian spatially correlated random variable. For soil moisture fields however, this is not necessarily a valid assumption (Western and Blöschl, 1998a). Statistical interpolation techniques therefore seem not to be the best way to follow in deriving spatial distributions of soil water contents over large catchments. Fractals are based upon the idea that a spatial pattern observed at one scale is repeated at other scales. Using this approach, several authors have derived scale-dependent expressions for SWC (Le Toan *et al*., 1998; Kim and Barros, 2002b). Soil moisture data collected during the present study are not ideal for geostatistical or fractal based applications. In the present study only twenty-six soil moisture monitoring sites have been monitored in a 6540 km^2 catchment. Alternative methods are therefore needed to derive catchment average (representative) moisture contents from a limited number of ground-measured point scale observations.

This chapter explores the temporal stability characteristics of soil moisture across a range of scales. This work analyses the temporal stability of soil moisture and identifies representative mean soil moisture measuring stations for each sub-catchment.

5.2 METHODOLOGY

When a catchment is regularly monitored for soil moisture content, locations can often be identified where the soil is consistently wetter or drier than the average across the surveyed area. The existence of such sites is important for soil management. Similarly, some locations can be identified where the soil moisture is close to the average across the entire catchment. Identification of these characteristic sites is potentially useful for field validation of area-average soil moisture measurements from passive microwave sensors. Furthermore, it is also important to identify sites for coarse scale characterization and hydrological model simulation, e.g., establishing field level or catchment-scale antecedent moisture conditions for runoff simulations. This phenomenon has been called the *time stability*, the *temporal stability*, or the *temporal persistence* in spatial patterns of soil water contents. Grayson and Western (1998) showed that this phenomenon can be applied for locating catchment average soil moisture monitoring (CASMM) sites. Analysis of temporal stability characteristics has been shown to be very useful in estimating catchment average soil moisture. As cited by Martinez-Fernandez and Ceballos (2005), Vachaud *et al.* (1985) introduced the concept of temporal stability as the time-invariant association between spatial locations and classical statistical parametric values of a given soil property. Temporal stability analyses of soil moisture therefore provide a method that would reduce the number of monitoring sites required for characterising the behaviour of the soil moisture content across a study domain. Indirectly, such analyses provide a meaningful way of applying point scale soil moisture measurements to explain catchment-scale average content, thus providing an up-scaling methodology.

To identify a CASMM site, it is first necessary to perform an analysis of temporal stability. As reported by many researchers (Vachaud *et al*., 1985; Grayson and Western, 1998; Gómez-Plaza *et al*., 2000; Mohanty and Skaggs, 2001; Martinez-Fernandez and Ceballos, 2003, 2005; Starr, 2005; Cosh *et al*., 2006; Starks *et al*., 2006) it may be inferred from analysing which sites are representative of wet conditions and which are representative of dry ones and which site represents the average moisture content of the whole catchment. Grayson and Western (1998) considered that representative stations are those sites where the mean relative difference (mrd) approached zero. The mean relative difference is defined as:

$$\bar{\delta}_{*,j} = \frac{1}{n}\sum_{i=1}^{n}\frac{S_{i,j} - \bar{S}_{i,*}}{\bar{S}_{i,*}} \qquad \textbf{(5-1)}$$

where,

$\bar{\delta}_{*,j}$ = mean relative difference at the j^{th} site

S_{ij} = i^{th} sample of n samples at the j^{th} site within the study region

$\bar{S}_{i,*}$ = computed average among all sites for a given date and time, i

Later, Van Pelt and Wierenga (2001) introduced the standard deviation of 5% as the criterion. Such a 5% standard deviation criterion may however not be valid for a large catchment as the study site of Van Pelt and Wierenga was very small (1 ha), with high temporal stability.

A CASMM site therefore, would be the one that is closest to the zero relative difference value and that, additionally, has a low standard deviation value. It is difficult to set general reference values, of both relative difference and standard deviation to choose the representative station in a given network of stations. The group of sites above the zero relative difference value would systematically overestimate the mean soil moisture value and those below zero would underestimate it. Grayson and Western (1998) noted that time-stable sites having a non-zero mean relative difference could be used to represent catchment average soil moisture content provided that the offsets between the mean value and the non- zero time-stable sites were known. Comegna and Basile (1994) have found that temporal stability analyses are not suitable for smaller catchments with homogeneous soils.

The objectives of this work are: (a) to demonstrate the temporal persistence in soil water contents measured at each site; (b) to upscale water contents from point measurements to the subcatchment and to catchment scale; (c) to identify representative locations for monitoring total soil water content; and (d) to estimate the length of time for soil moisture monitoring sufficient to characterize temporal persistence in water content.

5.3 RESULTS AND DISCUSSION

5.3.1 APPLICATION TO THE WHOLE GOULBURN RIVER CATCHMENT

Figure 5-1 shows the results of temporal stability of SWC for the whole Goulburn River catchment and the complete two-year study period. For easy understanding of the results, the data on relative differences in each case were ordered from smaller to greater, indicating the standard deviations by error bars above and below the points. With this type of approach, it is possible to identify the points that systematically overestimate or underestimate the mean soil moisture value. Figure 5-1 shows the results for the mean data on 0-30 cm soil moisture from the 25 stations for 2003, for 2004 and for the period 2003-2004. It can be seen that, there is symmetry with respect to the zero value of relative difference among sites. Approximately 12-13 sites are either above (i.e. wet sites) or below (i.e. dry sites) the mean value. It is also found that the temporal stability is lower (greater standard deviation) at the stations characterising the wet sectors.

a)
b)
c)
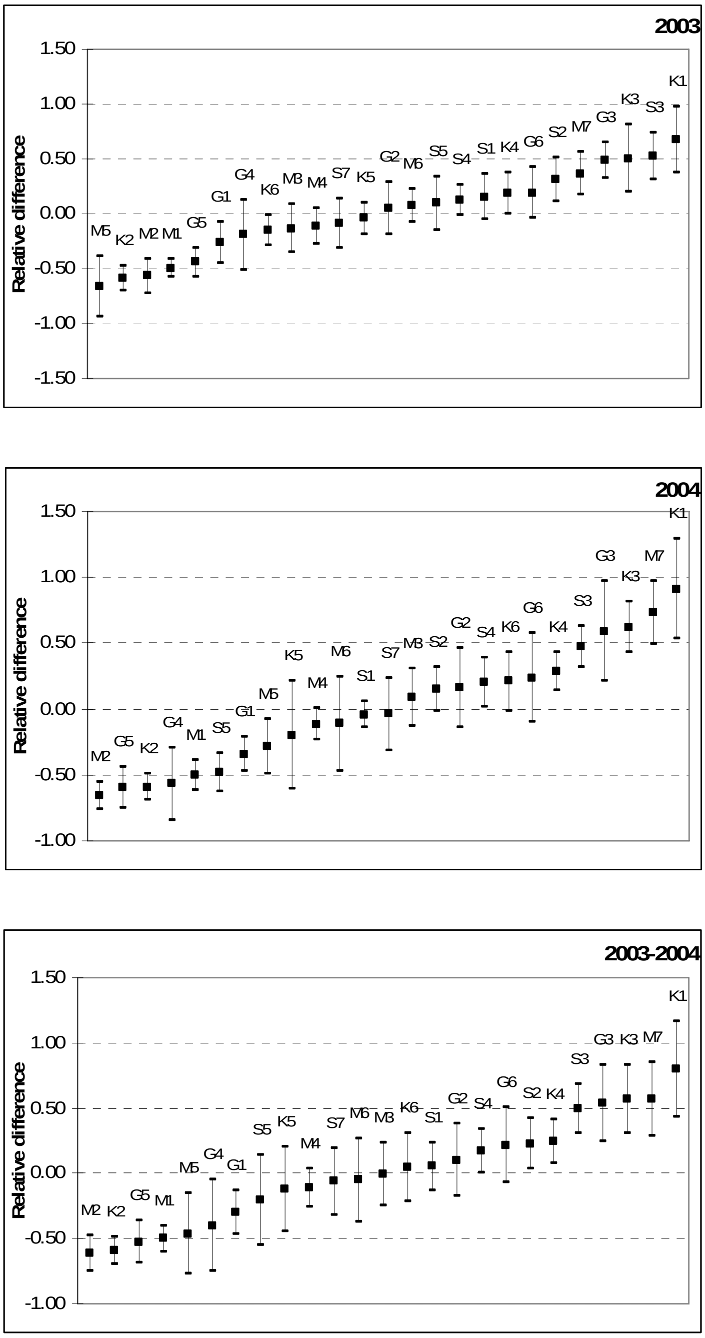

Figure 5-1: Plots of relative differences for 0-30cm SWC for whole study area for: a) 2003, b) 2004, and c) whole period 2003-2004. Vertical bars correspond to associated time standard deviation.

Following Grayson and Western (1998), CASMM sites were identified. At the Goulburn River catchment scale, the station fulfilling the two conditions of mean relative value close to zero and smallest standard deviation (SD = 0.097, in 2004 and SD = 0.186 in 2003-2004) is S1 (Figure 5-1a and Figure 5-1b). Likewise, M2, K2 and G5 are representative of dry conditions, and K1, K3 and M7 are representative of wet conditions. The wet sites K1, K3 and M7 however, show some degree of uncertainty because they are very unstable (as reflected in the high standard deviation). While the observed range of variations in the mean relative difference between nearly ±0.75 is high when compared with some published results (Grayson and Western, 1998; Van Pelt and Wierenga, 2001), it is closer or similar to Mediterranean conditions (Gómez-Plaza *et al.*, 2000) and arid conditions in Spain (Martinez-Fernandez and Ceballos, 2003). The higher variations may be due to the large size of the study region and hence its diversity from the point of view of soil types, landscape positions, land use types, and vegetation patterns.

The lower limit of (-0.50) is always maintained indicating the presence of a physical threshold with respect to water storage and pointing to the high temporal stability of the sites located in drier areas. The upper limit varies, sometimes surpassing 0.75 (K1) due to the strong seasonality of agricultural soils. As result of diverse cropping patterns and farm activities, agricultural soils behave differently compared to natural landscapes.

It is also possible to identify temporally stable sites whose characteristics represent dry and wet extremes for the catchment, considering only the minimum standard deviation criterion. At the Goulburn River Catchment scale, while S3 is the best candidate fulfilling this condition for a wet site (SD= 0.15, in 2004 and SD=0.18 in 2003-2004), M1 can be considered to represent a dry site (SD= 0.11, in 2004 and SD=0.10 in 2003-2004). It is important to note that the average moisture content of these two sites is approximately equal to the moisture content at S1. Temporally stable sites having very high and very low soil moisture content are therefore important to consider for catchment studies because they can provide an insight into the range of moisture content in the catchment. Additionally, these two sites can be used to estimate the catchment average moisture condition. Furthermore, as these sites are temporally stable, the offset between the higher and lower moisture contents is a constant irrespective of the day of year. For this reason, Starks *et al.* (2006) have considered two sites, one for representing dry site and other for wet conditions, for their temporal stability analysis.

Figure 5-1a and Figure 5-1b show the results for 2003 and 2004 respectively. In general, the sites maintain their position irrespective of the observed period. The groupings of sites characterizing dry and wet locations are nearly identical. Whereas only one site (M3) moved from the dry to the wet side, two sites (S5 and M6) moved from the wet to the dry side, during 2003 to 2004. Interestingly, all sites on the dry side consist of sandy type soils (with >70% sand fraction) as shown in the Table 3.7 in Chapter 3, reflecting the inability of the soils to retain water. This explains why the soil moisture content of these sites is never high and why their temporal stability is comparatively high. In contrast, apart from K1, wet-end sites consist of either clay or clay loam type soils and hence are capable of holding more water at various tensions. Accordingly, the soil moisture content of these sites is usually high and exhibits less temporal stability.

5.3.2 APPLICATION TO THE KRUI SUBCATCHMENT

Figure 5-2 shows the data on the relative differences for the Krui catchment for the period 2003(a), 2004(b) and 2003-2004(c). The data are ordered from lowest to highest as in whole Goulburn River catchment analysis.

At the Krui catchment scale, two stations can be identified which fulfil the two conditions of mean relative value close to zero and smallest standard deviation. The first is the K6 (mean of 0.0035 and SD of 0.178, in 2004 and mean of -0.099 and SD of 0.192 in 2003-2004) and the second site is the K4 (mean of 0.067 and SD of 0.102, in 2004 and mean of 0.065 and SD of 0.113 in 2003-2004). Here, two methods can be applied for the determination of catchment average moisture content. First, we consider both sites for catchment average moisture estimates. Considering the stability of sites, alternatively, K4 can be selected as the candidate for Krui catchment. The marked temporal instability of K6 may be attributed to its location, as this site is situated on a top of a hill and near a very steep cliff.

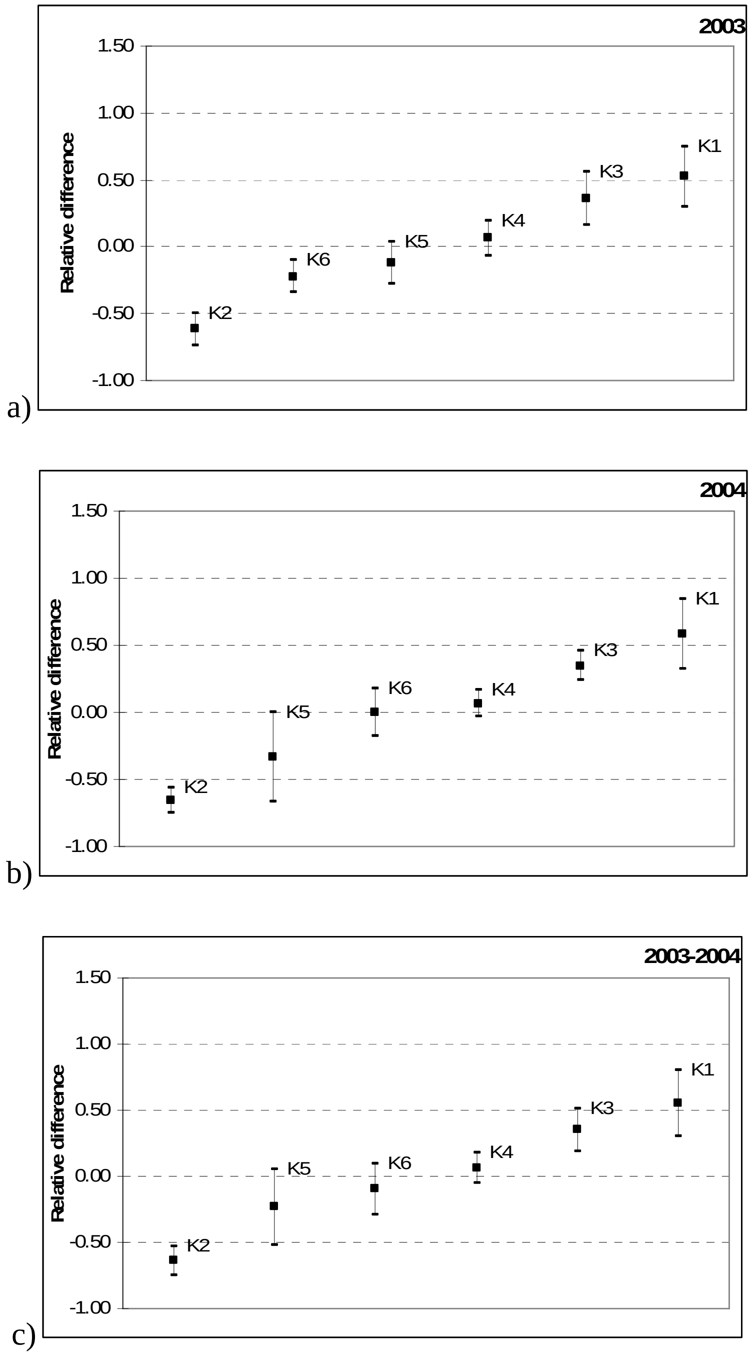

Figure 5-2: Plots of relative differences for 0-30cm SWC for Krui catchment for: a) 2003, b) 2004, and c) whole period 2003-2004. Vertical bars correspond to associated time standard deviation.

As far as the dry and wet ends are concerned, the driest site is K2 and K1 remains the wettest site. The observed range of variations in the mean relative difference was limited to between ±0.5 and this may be due to the smaller catchment size. Moreover, the groupings of sites characterizing dry and wet locations are nearly identical throughout the study period. All wet sites maintain their order during both 2003 and 2004. However, a slight change of order of dry sites was noted between K5 and K6 where K6 became a less dry site from 2003 to 2004.

5.3.3 APPLICATION TO THE MERRIWA SUBCATCHMENT

Figure 5-3 shows the data on the relative differences corresponding to Merriwa catchment for the period 2003(a), 2004(b) and 2003-2004(c). The data are ordered from lowest to highest as in previous analyses.

At the Merriwa catchment scale, two stations can be identified which fulfill the two conditions of mean relative value close to zero and smallest standard deviation. The first is the M4 (mean of 0.007 and SD of 0.113, in 2004 and mean of 0.085 and SD of 0.293 in 2003-2004) and the second site is the M6 (mean of 0.0004 and SD of 0.365, in 2004 and mean of 0.092 and SD of 0.342 in 2003-2004). As far as M4 is concerned, it can be considered to represent the entire Merriwa catchment due its lower standard deviations. Although M6 is better in giving a mean relative value close to zero (at least in 2004) due to consistent temporal instability, it is not an ideal site compared to M4. According to the owner of the property, M4 is located in a transition zone, where part of the property generally receives higher rainfall while the other part receives less rainfall. This partly explains the higher range of soil moisture variability at M6. The lack of a suitable site during 2003 must be emphasized. None of the sites was ideal as a CASMM site during 2003.

As far as the dry and wet ends are concerned, the driest sites are M2 and M1, both with predominantly sandy soils. The wettest site is M7, a clay loam site in a higher rainfall area. As for the Krui catchment, the observed range of variations in the mean relative difference was limited to between ±0.5 (except for M7) and this might be the result of the smaller catchment size. Furthermore, the groupings of sites characterizing dry and wet locations follow a nearly similar pattern throughout the study period as in the Krui catchment. Interestingly, both wet and dry sites change their order from 2003 to 2004. The most significant change occurred in M5, which moved from the driest position to close to zero level. M5 is on a clay type soil (69 % clay) and this might be due to the deep cracks observed around the soil moisture sensors during early 2003. These cracks caused poor contact between the sensor and soil and therefore the CS616 sensor reported under-estimated moisture contents. Later, with the healing of cracks around the sensor, which improved the contacts between sensor and soil, it commenced reporting the actual moisture contents. As a result, M5 shows that it recovered from dry state and slowly moved up towards to the wet side.

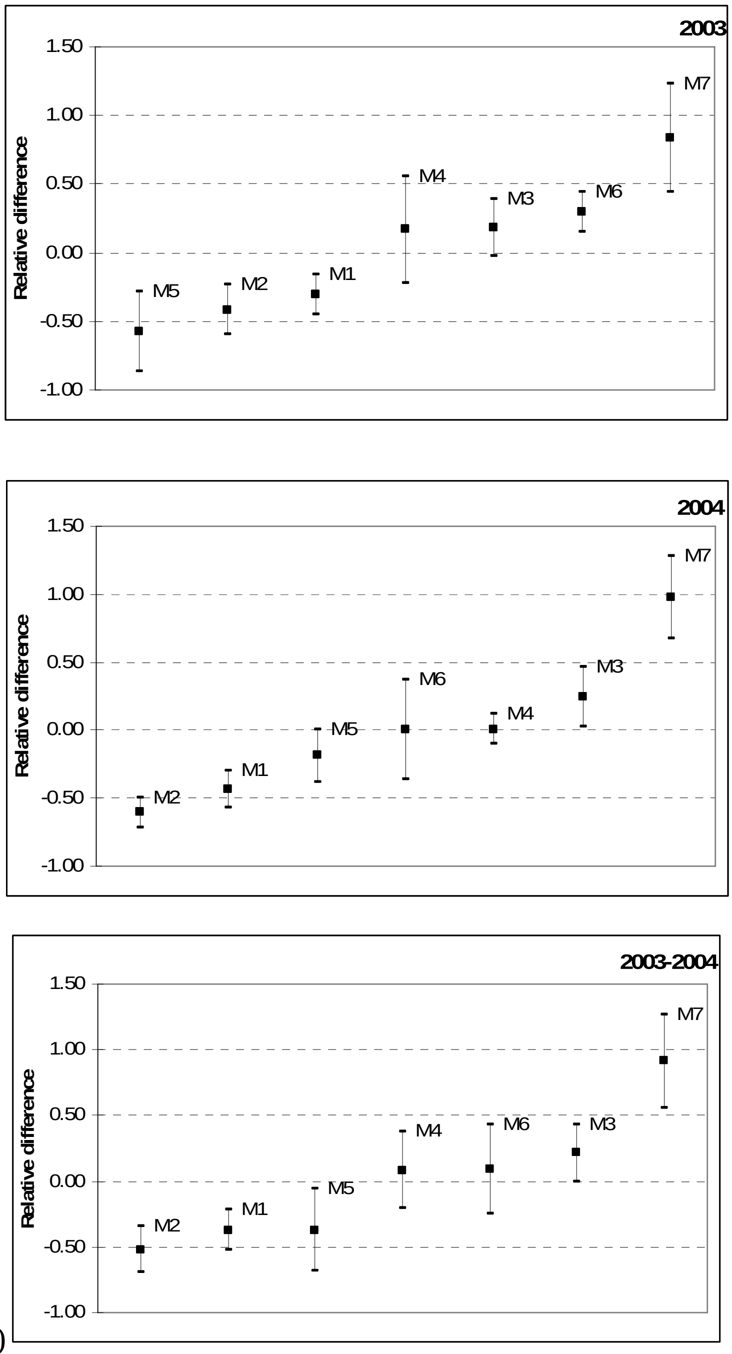

a) b) c)

Figure 5-3: Plots of relative differences for 0-30cm SWC for Merriwa catchment for: a) 2003, b) 2004, and c) whole period 2003-2004. Vertical bars correspond to associated time standard deviation.

5.3.4 APPLICATION TO THE SOUTHERN-GOULBURN RIVER SUBCATCHMENT

It is also of practical importance, to locate a CASMM site from a limited number of sites spread across a large catchment. The six sites spread across the Southern-Goulburn River catchment in a east-west direction provide an opportunity to study this. Figure 5-4 shows the data on the relative differences corresponding to Southern Goulburn sites for the period 2003(a), 2004(b) and 2003-2004(c). The data are ordered from lowest to highest as in previous analyses.

At the Southern-Goulburn River scale, with six sites, it is difficult to identify a suitable CASMM site. None of the sites fulfils the two conditions of mean relative value close to zero and smallest standard deviation. The most obvious approach is to monitor two sites; that is monitoring of both G5 (from the dry side) and G3 (from the wet side) and considering the average.

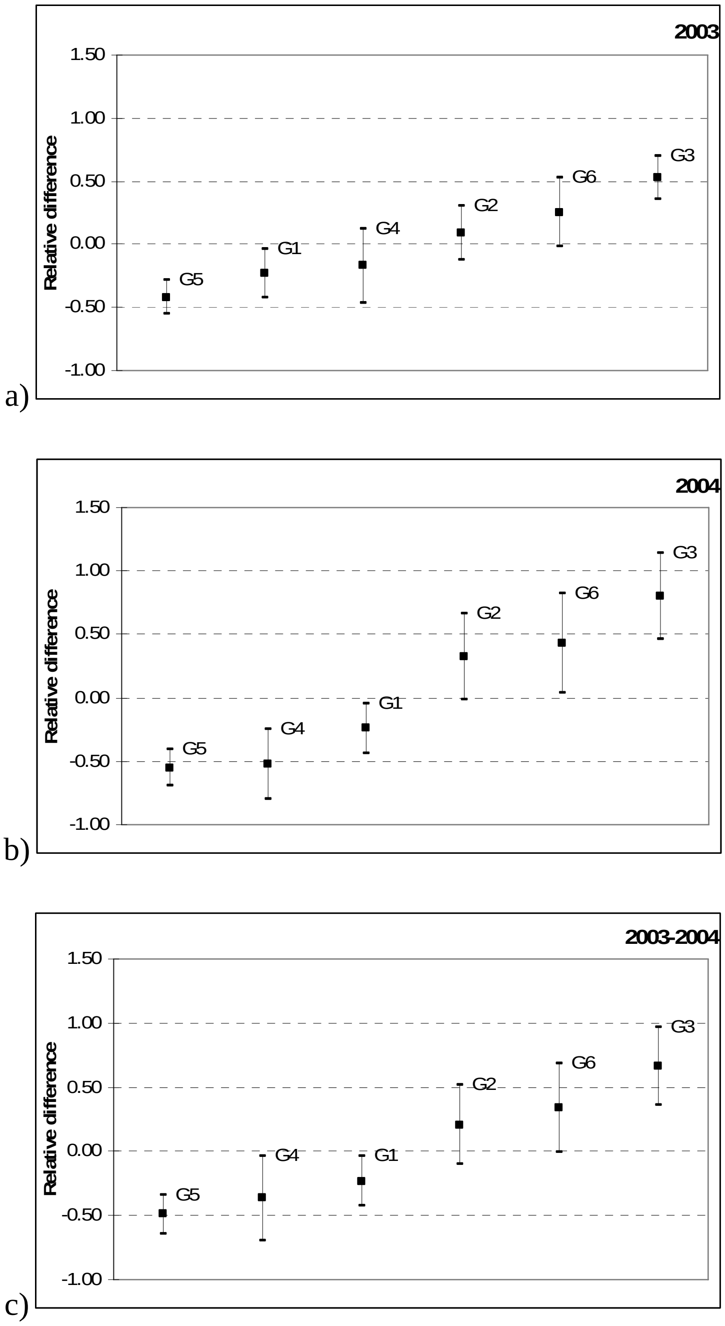

Figure 5-4: Plots of relative differences for 0-30cm SWC for Southern Goulburn catchment for: a) 2003, b) 2004, and c) whole period 2003-2004. Vertical bars correspond to associated time standard deviation.

5.3.5 APPLICATION TO THE STANLEY SUBCATCHMENT

Applications of temporal stability analyses for small catchments such as Stanley catchment are also important if a reasonable number of sampling sites is available. Seven sites have been monitored in Stanley since early 2003. One site (S6) however, showed intermittently unusually high readings and for this reason, S6 was not considered suitable for inclusion in the temporal stability analysis.

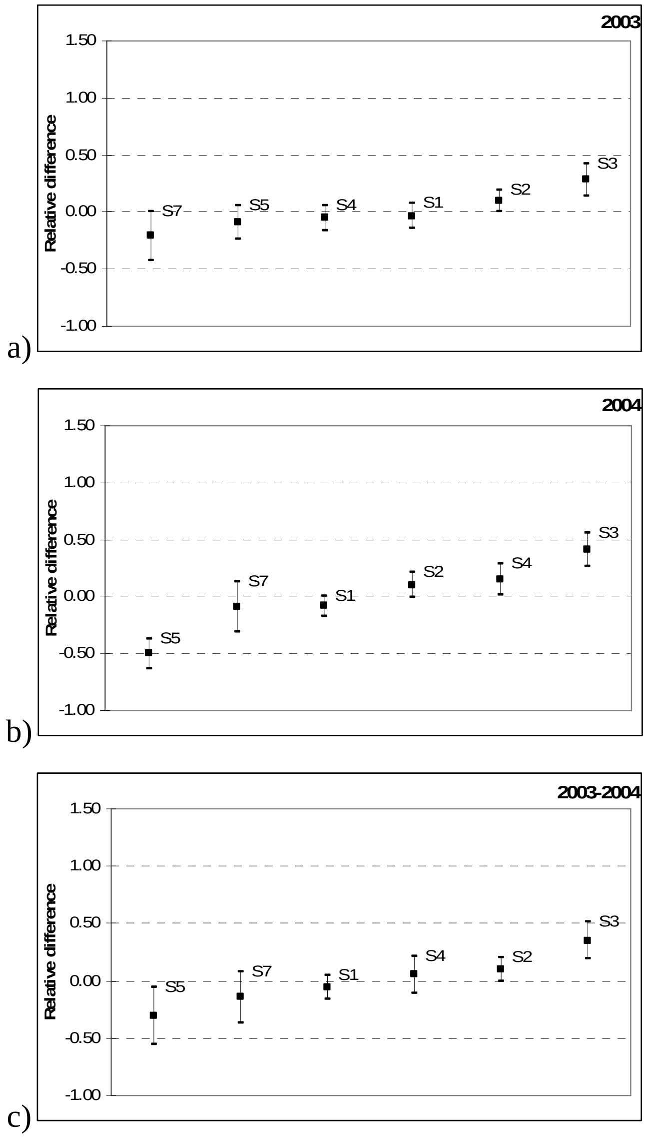

Figure 5-5: Plots of relative differences for 0-30cm SWC for Stanley subcatchment for: a) 2003, b) 2004, and c) whole period 2003-2004. Vertical bars correspond to associated time standard deviation.

Figure 5-5 shows the results for the mean data on soil moisture from the six sites for 2003, 2004 and for the period 2003-2004. As can be seen in the figure, there is symmetry with respect to the zero value of relative difference among sites. Generally, three sites are either above (i.e. wet sites) or below (i.e. dry sites) the mean value. Except for S7, it can be seen that the temporal stability is higher for all sites, i.e. a smaller standard deviation exists for all sites.

At the smaller 167 ha catchment scale, station S1 fulfils the two conditions of mean relative value close to zero and smallest standard deviation (mean of -0.08 and SD of 0.09, in 2004 and mean of -0.06 and SD of 0.102 in 2003-2004; see Figure 5-5b and Figure 5-5c). Surprisingly, at the Goulburn River catchment scale, S1 is also the most suitable CASMM site. This is an interesting finding and proves an important property of CASMM sites. With this study, it is evident that once identified properly, under normal circumstances, moisture measurements at CASMM sites may be used across a catchment at many scales.

It is also clear from Figure 5-5 that, S5 and S7 are representative of dry conditions, and S3 is representative of wet conditions. Whereas S1 is located in a valley bottom, S3 is located in a steep transition zone. Therefore, as seen in Figure 5-5, S1 shows very stable conditions compared to S3. The observed range of variations in the mean relative difference is between nearly ±0.35 and this is even narrower than that of the Krui and Merriwa catchments. The narrow range of variations may be due to the smaller study site which is less diverse from the point of view of soil types, land use types, and vegetation patterns.

5.3.6 MINIMUM SAMPLING TIME REQUIRED TO IDENTIFY A REPRESENTATIVE SITE

For practical applications, it is useful to know how much monitoring time is required to determine which site is representative of the mean soil moisture content of a given catchment. Often soil moisture monitoring programs are established with networks of sites that are quite dense initially. Maintaining a dense network of soil moisture sites however is very expensive and tedious. Hence, it would be worth considering the possibilities of reducing effort and cost by continuing monitoring at fewer sites.

In order to determine the minimum sampling period, it is necessary to study the evolution of the mean relative difference (mrd) and the standard deviation (SD) of the relative difference throughout the study period. Theoretically, after a minimum sampling period, both mrd and SD of the relative difference should not vary with time and remain at a constant level. It is easier to understand such results when results are plotted against time. In these plots, mrd stays closer and parallel to the time-axis after reaching a minimum sampling period, thus indicating no more significant changes with time. The SD of the relative difference however, may take a different trajectory and usually stabilizes at some distance away from the horizontal time-axis depending on the sample size and the range of moisture contents in the catchment. The SD appears to run near-parallel to the time-axis after reaching a minimum sampling period, similar to the mrd plot. A catchment shows a wide range of moisture contents at any given moment. Thus, the SD of the relative difference will rarely be close to zero but it may be stabilize with time. Figure 5-6 shows the results of the analysis for Stanley, Krui, Merriwa and whole Goulburn River catchments. As seen in Figure 5-6a, for the smaller catchment such as in Stanley, stabilization of both SD and mrd occurs at around 360 days or 12 months. In larger catchments such as Krui (Figure 5-6b) and Merriwa (Figure 5-6c) stabilization of both SD and mrd occurs at around 450 days or 15 months. A similar pattern is found for the entire Goulburn Catchment (Figure 5-6d). It can therefore be inferred that after reaching the stable point, the temporal behaviour of all stations remained stable. However, as seen in Figure 5-6a, significant changes of moisture contents at one site may introduce some uncertainty about the above conclusion particularly in a situation with smaller sample size. As shown in the figure, two SD values are plotted in the Stanley catchment to represent the situation with all six sites and the situation without S5. The significant change of soil moisture values at S5 from 2003 to 2004 (see Figure 5-5) causes instability of SD of the relative difference of mean moisture contents in two-year period and this is evident from the upward trend of SD plot when all six sites are considered. Without S5 however, SD plot gave the expected result. Thus, care has to be taken in interpreting results when smaller numbers of sites are considered.

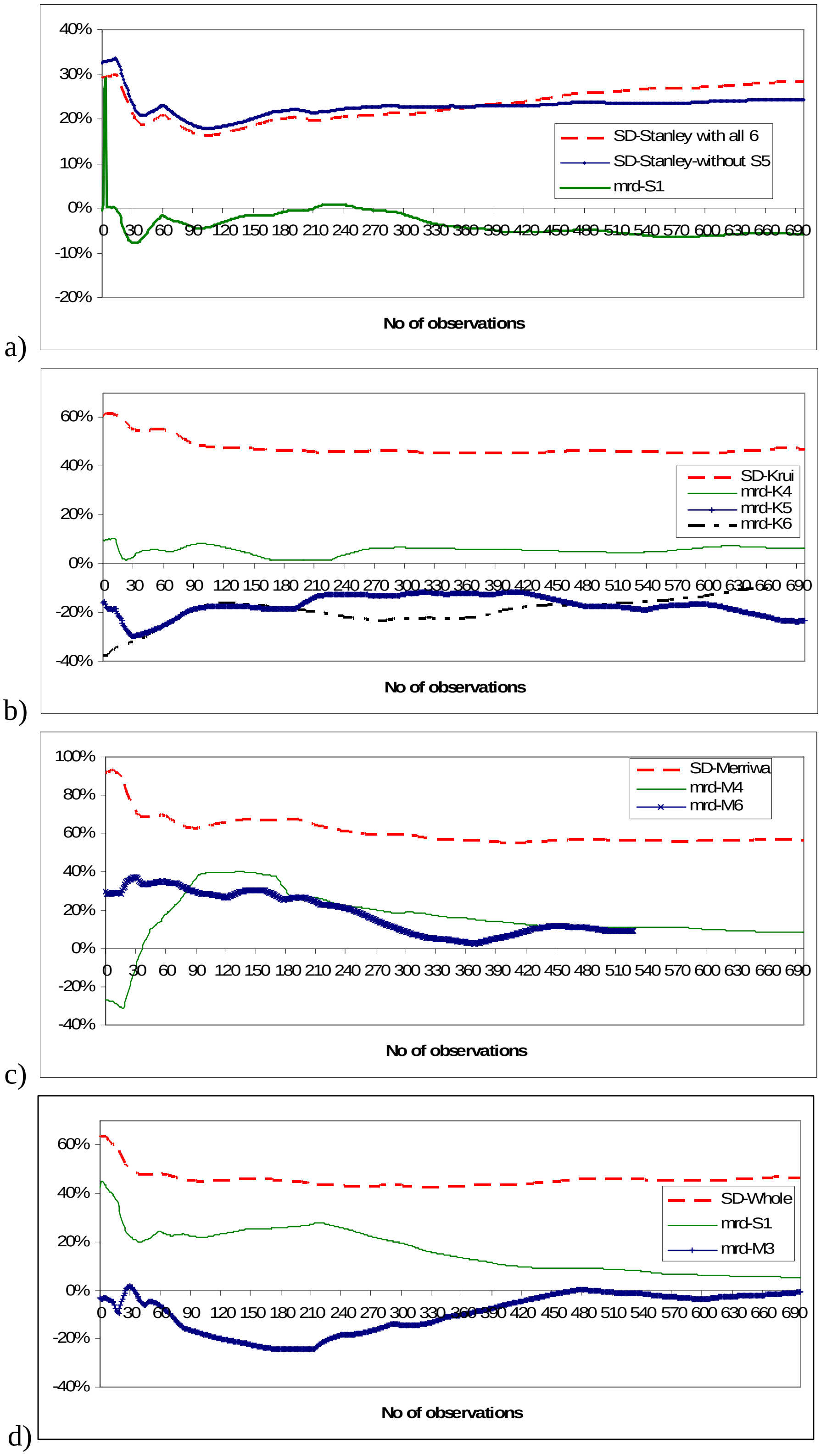

Figure 5-6: Mean relative difference (mrd) and the standard deviation (SD) of the relative difference calculated for all observations during 2003-2004: a) Stanley, b) Krui, c) Merriwa, and d) whole Goulburn catchment.

From this analysis, it can be concluded that the minimum time required for determining the CASMM site is approximately 12-15 months. This result agrees with a similar period observed by other researchers (Martinez-Fernandez and Ceballos, 2003). It is important to note that this minimum sampling period coincides with a complete seasonal cycle. According to Martinez-Fernandez and Ceballos (2003), at the beginning of the seasonal cycle, the representativeness of the site perseveres because the temporal pattern is repeated. This is clearly occurring as an annual cycle in a smaller catchment such as Stanley. However, rainfall variations and delays in the onset of seasons may modify the annual cycle. These effects are generally more prominent in large catchments due to wide range of variations and therefore a slightly longer period (of 15 months) is required. The minimum period of one year for determining the representative mean soil moisture site as proposed by Martinez-Fernandez and Ceballos (2003) is not valid for the Goulburn River catchment. This is because their work was carried out in smaller catchments (1285 km^2 and 0.62 km^2) and because the present study was conducted in elongated catchments with similar areas (e.g. Krui and Merriwa, approximately 631 km^2 and 871 km^2 respectively) and in a larger catchment (6800 km^2). Furthermore, as shown in Figures 3.15 and 3.16, there is also considerable spatial and temporal variation of rainfall across the region. Therefore, at least in subhumid catchments in Australia, a 15-month period will be needed in order to determine representative mean soil moisture sites.

5.4 CONCLUSIONS

This study describes the characterization of temporal stability of soil moisture for a network of measurement sites, adopting the methodology described by Vachaud *et al.* (1995). It is demonstrated that catchment average soil moisture monitoring (CASMM) sites may be identified at different levels of the catchment. It is suggested that the selection of catchment average soil moisture monitoring sites within each subcatchment simplifies the accurate representation of spatially averaged soil moisture contents for hydrological modelling.

This study shows that it is possible to select a station that is representative of the mean moisture content of the soil in a given catchment from a pre-established network of measuring stations. The study was carried out at three very different scales (1.67 km^2, about 1000-1500 km^2 and about 6540 km^2) with a similar methodology.

The results indicate that temporal stability persists across the entire study period (about 23 months). The stations preserve their characteristics regardless of the time, even under extreme conditions of soil moisture content. Moreover, the results show that temporal stability is more pronounced during dry periods. It is also found that a clear correlation exist between mean soil moisture contents and variance for the whole measurement range considered. In general, locations representative of dry conditions are more stable, and locations representative of wet conditions are less stable. The temporal stability is generally lower during the transition periods between dry and wet moisture conditions.

According to Starks *et al.* (2006) contributing factors that can affect temporal stability include soil texture, topographic features such as slope and aspect, vegetation, and precipitation pattern. Considering the effect of spatially variable precipitation on temporal stability, Starks *et al.* (2006) showed the difficulty of determining the actual effect of variations of precipitation. They argued that soil factors contributed more to temporal stability than did spatially variable precipitation. The present study has led to similar observations. While the ‘dry’ temporally stable sites are located in sand or loamy sand (e.g. M1, which drain more quickly than clay soils), the ‘wet’ temporally stable sites are found in clay type soil (e.g. S3, which holds water for a longer period). Hence, for future soil moisture studies, Starks *et al.* recommended characterization of soils in the catchment before selecting the soil moisture measurement sites.

Knowledge of this temporal pattern of soil moisture is important for the design and implementation of field sampling campaigns. It is evident that when the soil is dry, homogeneity is greater. During the transition periods however, soil moisture content varies across the catchment and increases the uncertainty of the temporal pattern. Therefore, when estimating soil moisture for large areas such as for modelling applications or validation of satellite-based moisture contents, it would be appropriate for sampling to be performed under circumstances that will guarantee the least variability.

The study shows that in order to be able to select a representative site, it would suffice to maintain the measuring station network over approximately 12-15 months. While for smaller catchments (< 200 ha) a period of 12 month is sufficient, for larger catchments (>1000 km^2) with distinct annual rainfall variations, at least 15 months are required. From that time onwards, monitoring (the mean) soil moisture content could be carried out at a single site or a small number of selected sites.

According to these results, two types of sampling procedures can be proposed for future soil water content monitoring programs in Australian catchments. First, in case of permanent monitoring programs, identification of time-stable locations that are representative of the soil moisture status of the catchment is important. This is useful in order to reduce the number of sampling sites maintained on a permanent basis. Second, in case of non-permanent monitoring programs emphasis should be given to the sampling frequency compared to the number of sampling sites. For this purpose, a two-step approach can be adopted to identify suitable locations and to increase the sampling frequency. The objective of the first step is to identify the time-stable locations that are representative of the soil moisture status of the catchment. Then, in a second step, the number of sampling points can be reduced and resources can be allocated to increase the sampling frequency. This approach helps to collect more representative soil moisture fields of higher temporal resolution for modelling applications.

It is equally important to consider temporally stable sites whose moisture contents are always under- or over-estimates of the catchment average moisture content. This is because, apart from providing mean moisture content of the catchment, such sites are useful in determining ranges of moisture content within the catchment.

In some situations, area average soil moisture is needed to validate the soil moisture products from remote sensing with large footprints such as from AMSR-E. In such instances, suitable dates can be selected based on the mean relative difference of soil moisture computed from all the monitoring sites within the chosen catchment or ideally from all monitoring sites within the selected pixel. This would assist in reducing the level of uncertainly in the measured soil moisture contents if the selected dates are of low mean relative difference.

Table of contents

List of Figures

List of Tables

No

CHAPTER SIX

6. DERIVING SPATIAL PATTERNS OF ROOT-ZONE SOIL MOISTURE FROM POINT-SCALE MEASUREMENTS

This chapter studies the prediction of SWC from remotely sensed land surface temperature and vegetation observations. This work aims to develop empirical relationships to predict soil water content from a limited number of point scale soil moisture measurements, remotely sensed information and soil physical characteristics. The published literature provides no clear guidance on deriving surface soil water distributions from combined use of *in-situ* 0-30 cm soil moisture measurements and remotely sensed information. The main objective of this chapter is to develop new methodologies to regionalize the *in-situ* point-scale soil moisture measurements based on remotely sensed land surface temperature and vegetation observations. Thus, the ultimate goal of this study is to infer the catchment scale soil moisture distribution pattern from a limited number of soil moisture measurements. The methodologies proposed here establish the foundation for using remotely sensed surface temperature and vegetation indices as surrogate variables to derive spatial patterns of soil moisture distributions.

6.1 INTRODUCTION

The magnitude of a state variable such as soil moisture content of the upper soil layers at a given location and at any given time is a reflection of the prevailing water and energy balances at the time of measurement (Gomez-Plaza *et al.,* 2000). Furthermore, any such soil moisture value is the result of recent hydrological processes that have occurred at that location. From a hydrological modelling perspective, the soil moisture status of a catchment is an important factor. In applications of traditional Hortonian infiltration models, it is often assumed that the moisture content is uniform across the catchment. Yet, it is generally accepted that the variability of soil moisture at point and field scales is considerable, even for near-uniform soil (Sivapalan and Wood, 1986; Famiglietti *et al*., 1998). Furthermore, even in small catchments soil moisture may exhibit considerable spatial heterogeneity (Sivapalan and Jeevaraj, 1992; Grayson *et al.*, 1997). Such spatial variability of the near-surface soil moisture content is mainly determined by variations in soil characteristics, topography, water routing processes and evapotranspiration (Merz and Plate, 1997). Thus, estimation of catchment scale soil moisture content from point scale observations will remain a difficult task.

Soil moisture content is traditionally measured with ground-based techniques. As discussed in Chapter 2 ground-based techniques often relate to a small land area. Furthermore, ground based measurement techniques are usually expensive and costs limit the number of measurement sites in the catchment. In addition, some unavoidable restrictions are present in selecting sites for measurements. For example, due to difficulties in accessing the sites, not every selected site will be included in a measurement program. The limited number of point scale measurements therefore may not always provide accurate information on the spatial pattern of the soil moisture distribution. On the other hand, currently available passive microwave techniques are also not very appropriate for study of the catchment scale moisture distribution due to their coarse resolution and to the relatively shallow layer of soil considered. Theoretical calculations have shown that the maximum depth measured with microwave technology is approximately one tenth of the wavelength of the microwave band used or 10-15 mm. *In-situ* point scale measurements are therefore needed to understand the soil moisture content at deeper layers as well as the spatial distribution of land surface soil moisture. The main problem addressed here is to up-scale limited point-scale measurements and to derive the surface wetness patterns.

It is obvious that a limited number of point scale measurements do not provide detailed information on the spatial pattern of the soil moisture distribution. Furthermore, soil moisture measurements from sparse networks do not contain sufficient information to study concepts such as preferred states in spatial soil moisture patterns. Remotely sensed observations, on the other hand, provide information on the spatial distribution of soil moisture. Thus, combined use of point-scale soil moisture measurements and remotely sensed observations may be useful in deriving catchment-scale surface wetness patterns.

In many catchment scale studies, it is common to measure soil moisture in a number of locations. To get the maximum benefit from a network of monitoring sites, it is required to infer a soil moisture distribution across the catchment from these point scale measurements. The derivation of a catchment scale soil moisture distribution from limited numbers of monitoring sites is a complex process. The most convenient approach is to select a variable as predictor which meets at least two basic requirements. First, the selected variable must have a strong relationship with soil water content. This ensures the development of suitable empirical equation. Second, the selected variable should be able to be measured accurately and conveniently. Often, remotely sensed data such as land surface temperature and vegetation indices meet this condition.

Vegetation health and land surface temperature are two key indicators of soil water near the land surface. Vegetation health may be conveniently expressed in terms of vegetation indices. The status of the surface vegetation is required for modeling vegetation productivity, land surface climates (Sellers *et al.*, 1997), and global carbon budgets and in agricultural resource management, whilst land surface temperature variations are required in study of the surface energy balance components. Both of these parameters are related to the soil moisture. In order to quantitatively and accurately characterize the regional dynamics of soil moisture, to differentiate short-term and long-term trends, as well as to distinguish regional from point-scale phenomena, these two parameters must be observed periodically and regionally with high accuracy. Satellite remote sensing is the most effective means of collecting such regional data on a regular basis. Remotely sensed land surface temperature (LST) data are now available on a daily basis. Computed vegetation indices (VIs) are also available for a range of spatial and temporal scales.

Many researchers (e.g. Price, 1980; Carlson *et al*., 1994, 1995; Moran *et al.*, 1996; Wang *et al*., 2001; Wan *et al*., 2004) have studied the relationship between soil moisture and remotely sensed LST and VI. The knowledge gathered so far however, is not adequate to use LST-VI relationships to predict soil water content in a given catchment with confidence, due to the complex nature of the behaviour of soil moisture and the range of dominant variations in climatic, geographical and geological conditions in different catchments. As reported by Capehart and Carlson (1997), soil moisture derived from land surface temperature cannot easily be used in calculating the column-average soil water content as required for hydrological modelling applications. For this reason, further studies are needed of the links between LST-VI relationships and field measured 0-30cm soil moisture contents. The objectives of such studies must be three-fold: First, it is necessary to explore the possibility of establishing dependable relationships between LST-VI and 0-30 cm (root-zone) soil moisture. Second, it is necessary to explore the use of such relationships to derive spatial moisture patterns using LST and VI as surrogate variables. Finally, the use of LST and VI relationships must be extended to use in the disaggregation of large area soil moisture measurements.

The present study explores new methods of deriving soil moisture distributions which are based on a limited number of *in-situ* soil moisture measurements and remote sensing observations, with the ultimate aim of utilising daily LST and 16-day vegetation index products from the MODIS sensors. First, various approaches are presented to predict soil moisture from combined use of *in-situ* measurements, LST and other information like air temperature and soil types. Next, this study focuses on predicting soil moisture based on a catchment average soil moisture measurement and remotely sensed wetness indices. Both approaches are developed as independent methods to upscale the measured soil moisture from a given network of monitoring sites and depend on the use of remotely sensed data from the MODIS sensor. This study therefore begins with an evaluation of MODIS products, mainly the LST and vegetation indices.

Additionally, the knowledge gained in this study also offers insight into the selection of an appropriate covariate for disaggregation of large area soil moisture measurements.

6.2 DATA SETS AND PRE-PROCESSING

The following data sets have been used in the analysis.

a. Daily measured 0-30 cm (root-zone) soil moisture from 25 sites (out of 26 sites) as described in Chapter 3.

b. Daily soil temperature measurements (at 15 cm from the surface) from the soil moisture monitoring sites.

c. Climatic variables observed in S2 and K6 climate stations.

d. Aqua-MODIS Vegetation Indices (VI) 16-day L3 Global products (i.e. MYD13A2): The data version used in this study was V003. The Goulburn catchment is within the tile number h30v12 and all images for 2003 and 2004 were downloaded from the EOS data gateway.

e. Aqua-MODIS Land Surface Temperature (LST) and Emissivity Daily L3 Global product (i.e. MYD11A1): MYD11A1 products provide per-pixel temperature and emissivity values. The data version used in this study was V003. Similar to the VI products, the tile number h30v12 contains the LST for entire Goulburn catchment. All available daily data for the year 2004 were downloaded from the EOS Centre. In case of 2003 daily LST data however, only selected images were downloaded at weekly intervals.

Data sets (a) to (c) have been taken directly from the field measurements. The 0-30 cm soil moisture is from the field calibrated CS 616 sensors as described in Chapter 3. Data sets (d) and (e) require pre-processing for two reasons: first, to reduce the file size and to extract data only from the area covered by the Goulburn river catchment and second, to re-project the map layers into a standard geographic latitude and longitude coordinate system to match with the other map layers of the area. A rectangular area spread between the upper left coordinate of 149.64°E, 31.75°S and the lower right coordinate of 150.71°E, 32.87°S has been used to extract the raster layers. This area gave 114 (lines) x 109 (columns) data points in a 0.0099 degree (about 1100 m) pixel. Both the data extraction and the re-projection have been carried out using MODIS Re-projection Tool (see the website at http://nsidc.org/PROJECTS/HDFEOS/MS2GT/ for more details). ERDAS Imagine spatial analysis software has been used in the next step of processing where the pixel level data were extracted from the locations of the ground-based soil moisture monitoring sites. For this purpose, a data extraction model was developed with the spatial modeller program of ERDAS Imagine.

Resolution of the MODIS-based LST and VI data used for the present study is 1.1x1.1 km^2. Despite the availability of high resolution (250x250 m^2) MODIS VI data, the MODIS LST data are not available in 250x250 m^2 resolution. In order to match with the resolution of the available LST data, both LST and VI data have been downloaded in 1.1x1.1 km^2 format.

The LST and VI data downloaded for the year 2004 were mainly used for the establishment of relationships with measured soil water content (SWC). It was also noted that due to cloud contamination not all downloaded LST images were suitable for the analysis. For example, as shown in Table 5-1 only 20 images had less than 5% of cloud cover. Images with over 5% of cloud cover were chosen visually and images were carefully selected based on the position of the clouds to ensure a minimum effect on the studied sub-catchments. Consequently, 124 LST images (out of 360) were considered suitable for the subsequent analysis. In case of 2003 data, MODIS LST images were selected on weekly basis and 58 images were downloaded as shown in Table 6-2. Due to cloud contamination however, only 28 images were found usable.

Table 6-1: Cloud cover percentages of the LST images selected from year 2004 for the analysis.

% Cloud cover	No of selected Images
0 - 5 %	20
5 - 10%	67
10 - 15%	25
15 - 20%	4
20 - 25%	2
Over 25%	6
Total no. of images	124

Table 6-2: Description of 2003 MODIS LST images downloaded. Images selected for the analyses are shown in bold characters.

Day	Clouds	LST (K)		Day	Clouds	LST (K)	
#	%	min	max	#	%	min	max
7	64%	286.5	332.0	**210**	**2%**	277.7	295.1
14	**31%**	287.6	331.8	**217**	**47%**	281.9	300.8
21	**26%**	295.8	339.8	224	59%	286.1	297.8
28	76%	297.6	318.9	**231**	**16%**	276.7	299.0
35	51%	281.7	325.0	238	80%	276.4	296.2
42	**15%**	291.9	326.5	**245**	**9%**	279.1	302.9
49	98%	293.7	301.9	**252**	**50%**	281.2	305.2
56	58%	290.4	307.3	259	98%	278.7	294.9
63	100%			266	100%		
70	77%	279.8	306.3	**273**	**48%**	274.4	302.9
77	**6%**	288.1	320.8	**280**	**52%**	281.1	297.4
84	**23%**	282.5	317.3	**287**	**47%**	280.6	303.1
91	**23%**	284.3	316.6	301	99%	287.2	296.5
98	51%	281.2	317.3	**308**	**0%**	287.8	317.7
105	**0%**	287.3	302.7	**309**	**13%**	291.9	325.0
112	**18%**	283.3	306.2	310	98%	289.4	301.2
119	58%	281.8	305.8	311	99%	293.0	304.9
126	76%	280.9	297.2	312	80%	288.2	303.7
133	**44%**	282.1	301.0	**313**	**10%**	282.9	323.5
140	53%	273.2	299.0	314	68%	287.2	318.4
147	89%	280.8	293.4	**315**	**34%**	280.9	319.8
154	77%	278.8	297.4	**322**	**6%**	287.8	320.4
161	70%	276.8	294.1	**329**	**43%**	280.9	312.8
168	**1%**	283.2	295.9	336	99%	289.2	306.0
175	98%	274.5	283.4	**343**	**8%**	287.7	324.6
182	91%	275.2	288.8	350	57%	288.6	318.6
189	100%			**357**	**1%**	296.2	329.8
196	**0%**	284.0	298.5	**364**	**7%**	295.7	330.7
203	90%	276.6	296.4				

6.2.1 DISTRIBUTION OF LAND SURFACE TEMPERATURES IN THE GOULBURN CATCHMENT

Surrogate variables that can be measured accurately on a routine basis could potentially provide a useful method for deriving spatial distributions of soil water contents over large catchments. Soil temperature is one promising variable due to a range of supporting factors. First, it shows very strong correlation with soil moisture content. For instance, when dry soil is exposed to solar radiation, soil temperature increases due to the absorption of radiation. The temperature of a wet soil does not increase as much with solar radiation, due to the higher specific heat of water. Therefore, in a given region and under the same atmospheric conditions, soil temperatures of wet areas are less than those of dry areas. Second, as discussed in section 2.3.3 current remote sensing techniques for LST measurements are well developed and reasonably accurate estimates may be obtained (e.g. 1^{o}K accuracy from MODIS LST products). Third, remotely sensed LST measurements may be computed for a range of spatial scales (e.g. 30m in Landsat TM, 90m in ASTER, 1km in MODIS and ATSR, 1.1km in NOAA AVHRR). Several current satellites also provide higher temporal resolution. For example, two MODIS sensors (in Aqua and Terra satellites) give four overpasses (two day-time and two nighttime) per day. Finally, a reliable daily LST product is freely available for the MODIS sensor. Therefore, it may be assumed that remotely sensed LST measurements provide the best readily available and spatially distributed surrogate variable for soil moisture interpolation.

6.2.1.1 Comparison of LST products from MODIS and NOAA sensors

LST can be computed from a variety of sensor data. Many LST retrieval algorithms have been developed for NOAA data and some of these methods have been extended to other sensors such as MODIS as discussed in Chapter 2. In order to assess the suitability of MODIS LST products, an analysis was performed with LST computed from NOAA-16 image with site-specific climatic data. Characteristics of the NOAA image and the climatic features at the time of image acquisition are shown in Table 6-3 and the estimated LST based on the Split Window Technique (SWT) as discussed in Section 2.3.3.2 using Eq. 2-10 over the catchment is shown in Figure 6.1(a). The emissivity values which are required to compute the SWT coefficients were derived from the 'vegetation cover' approach as described by Valor and Caselles (1996).

Table 6-3: Characteristics of the NOAA Image and associated climatic features (at S2) at the time of image acquisition.

Satellite name	NOAA-16
Orbit number	18605
Acquisition start	02 May 2004 at 14:44:15 EST
Acquisition end	02 May 2004 at 14:58:18 EST
Overpass direction	Ascending
Sun zenith angle	57.79^{o}
Air Temperature	$15.52^{o}C$
Soil Temperature @ 2.5 cm depth	$15.51^{o}C$
In/out Short-wave radiation	450.1/84.5 Wm^{-2}
In/out Long-wave radiation	143.1/16.6 Wm^{-2}
Relative humidity	33%
Atmospheric pressure	97.4 kPa
Soil heat flux	13.8 Wm^{-2}

Figure 6.1(b) also shows the MODIS daytime LST estimates (acquired about 14:30 hrs on 2 May 2004), but due to presence of clouds, a number of missing pixels are apparent. Despite the fact of different image capturing times, it appears that the two images show many similar patterns. It can be argued that LST computed from two separate radiometers can provide similar results. For this study, as the MODIS LST products are readily available, all other analyses were continued with MODIS LST products.

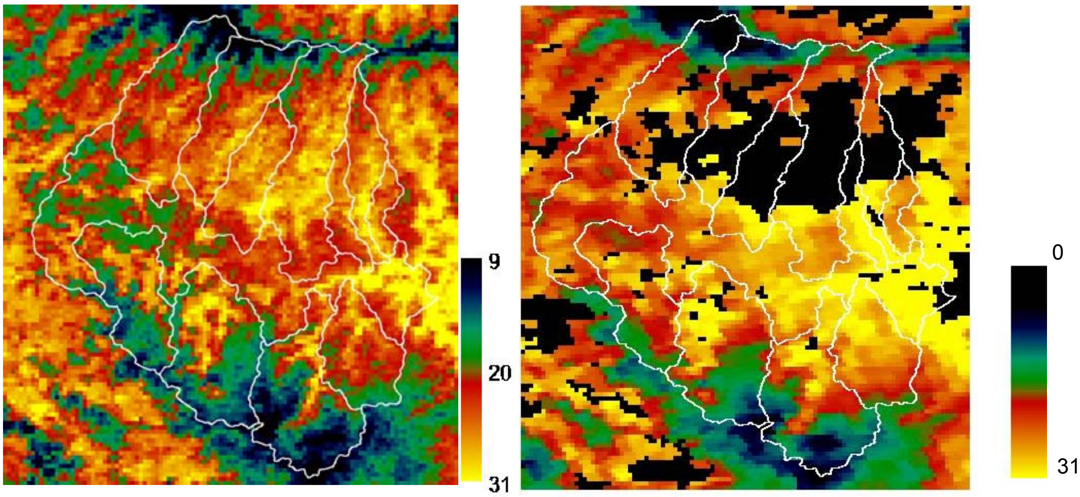

(a) (b)

Figure 6.1: (a) Daytime land surface temperatures (in oC) for Goulburn River Catchment computed from NOAA image captured on 2 May, 2004 at 14:50 and (b) MODIS daytime LST product on the same day at 14:30. (Note: missing data pixels in part (b) are shown as black).

6.2.2 QUALITY OF MODIS LST DATASETS

Figure 6.2 shows MODIS LST estimates (in K) for the Goulburn River Catchment during 2004 for a) a cloud free winter day (day 123), b) a clear summer day (day 320), and c) the difference between the both days. Figure 6.2 shows cooler land surface temperatures in dense vegetation areas particularly in the southern half of the catchment and along the northern boundary. The hot spots in the northern half of the catchment are either agricultural areas or sparsely vegetated zones. The cool spots are related to wet soil conditions.

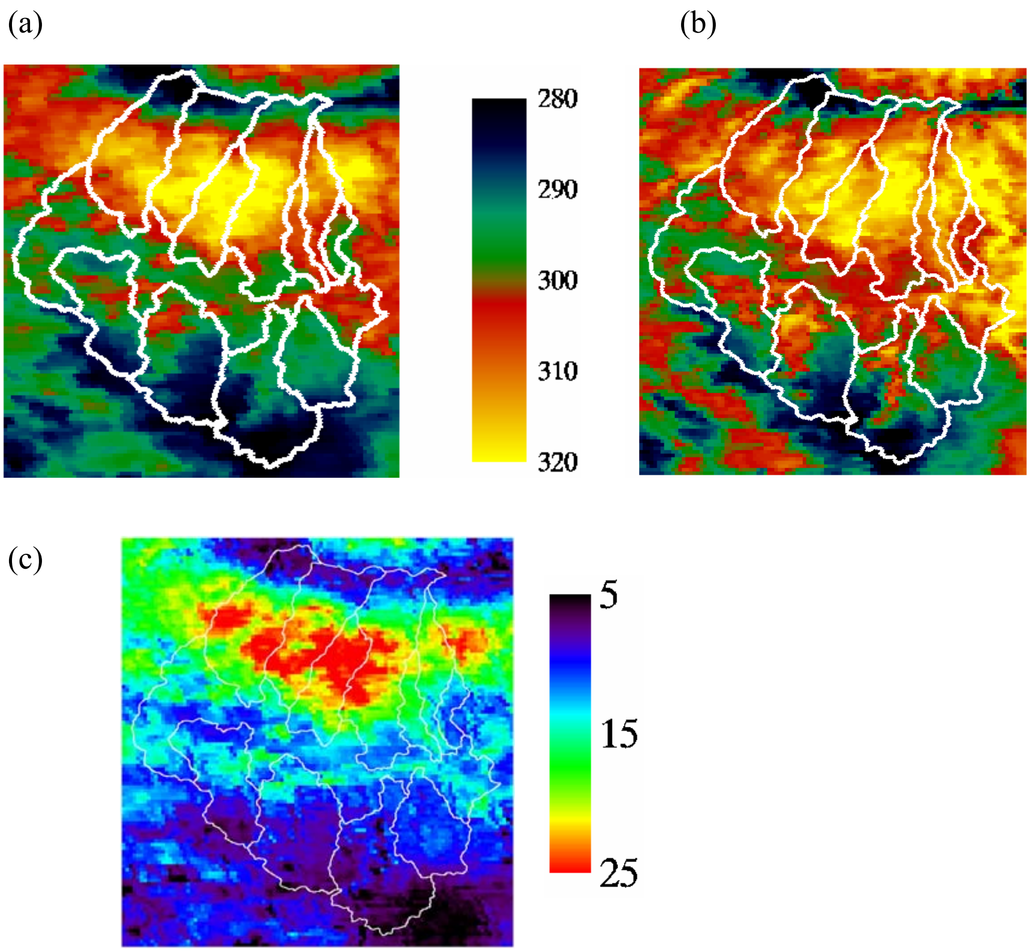

Figure 6.2: Daytime MODIS LST estimates (in K) for Goulburn catchment during 2004: a) a cloud free winter day (day 183), b) a clear summer day (day 320), and c) the difference between summer (day 320) and winter (day 183) temperatures.

The greater difference between summer and winter LST estimates provides an indication of bare soil or sparse vegetation conditions. As seen in Figure 6.2c the upper half of the catchment shows temperature difference of over 20 K between the two seasons. This is due to comparatively sparse vegetation in the area as observed during field visits. Therefore, these observations indicate in a qualitative way that MODIS LST data provide realistic estimates of land surface temperatures.

In order to obtain a better insight into the suitability of MODIS LST data over the Goulburn catchment, a comparison has been made with ground-based measured near-surface soil temperature data as shown in Figure 6.3. It is evident that MODIS LST measurements are comparable with ground-based measured soil temperature measurements. As seen in Figure 6.3a, daytime (between 1.30 – 3.00

pm in Aqua MODIS) LST measurements show slightly higher values than the actual soil temperature measured at 15 cm below the surface. Under normal climatic conditions, daytime heat fluxes are in the downward direction and therefore, land surface temperatures are generally higher than the subsurface temperature. During the night however, the soil heat flux direction changes in the absence of solar radiation. This situation is characterised by lower surface temperature and higher subsurface temperature as shown in Figure 6.3b. The slope of this regression coefficients between MODIS LST and field measured soil temperatures are 0.567 and 0.884 for daytime and nighttime respectively. In addition, as discussed in section 2.3.3.2, more stable nighttime conditions improved the performance of the LST retrieval algorithm as evidenced by the higher R^2 value for the nighttime observations (0.81) against the daytime observations (0.77). Furthermore, as seen in Figure 6.3c the temporal patterns of MODIS LSTs are comparable with the temporal patterns of measured soil temperature. When considering the scales of measurement of the MODIS LST at 1 km^2 and the soil temperatures at point scale and the obtained regression coefficients, it can be argued that remotely sensed LST observations such as from the MODIS sensor are useful substitutes for the *in-situ* soil temperature measurements.

a)

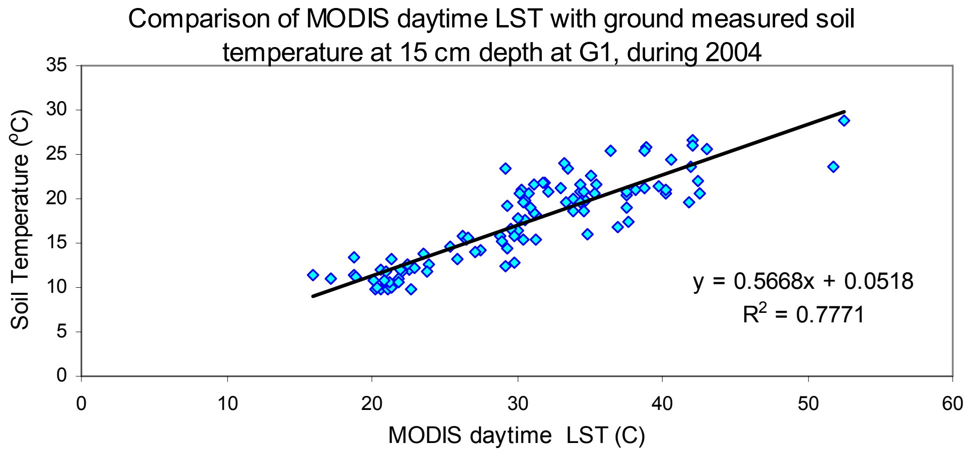

b)

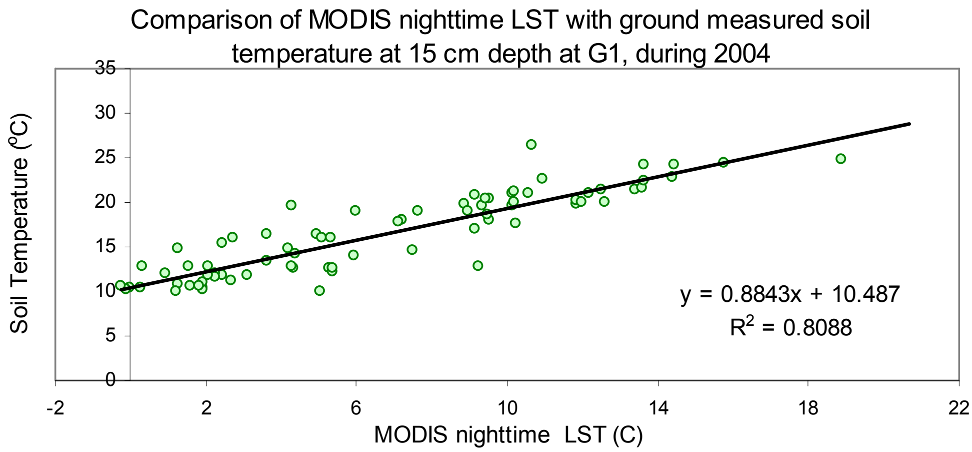

c)

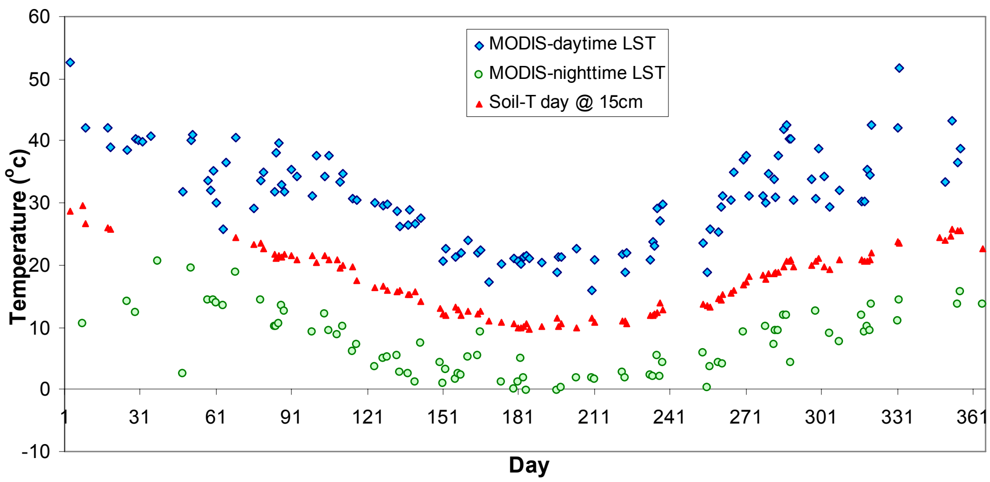

Figure 6.3: Comparison of MODIS LST (X-axis) and ground measured soil temperature at 15 cm depth (Y-axis): a) daytime MODIS observations and daily maximum soil temperature; b) night-time MODIS observations and daily minimum soil temperature; c) temporal patterns of MODIS daytime and nighttime LST and daily maximum soil temperature at G1 during 2004.

6.2.3 DISTRIBUTION OF VEGETATION INDICES IN THE GOULBURN CATCHMENT

The temporal changes of vegetation indices may reveal insight into vegetation health and water availability during the period concerned. NDVI is the most popular vegetation index but it does not consider the canopy background effect. Consideration of the canopy background correction in the computation of vegetation index is relevant to the Goulburn River catchment due to its sparse vegetation nature. Because the northern half of the catchment consists of darker, basalt derived soils in contrast to the southern half which is dominant with light-coloured sandstone-derived soils, this suggests the need of removing the soil background effect from the vegetation indices. Both NDVI and EVI are therefore considered.

The temporal dynamics of MODIS derived NDVI and EVI at four selected locations in the Goulburn catchment over the two-year study period are shown in Figure 6.4 and summarized in Table 6-4. It is clear from the data that the NDVI values are consistently higher than the EVI values. This is due to the effect of background soil in sparse vegetation conditions. While the temporal changes of vegetation indices at G5 are at a minimum due to low water availability of sandy loam soil (Figure 6.4a), M7 exhibits 52% change of EVI and 42% change of NDVI over the same period (Figure 6.4d). This is due to wetter conditions at M7 and the greater water holding capacity of the clay loam soils. The progress of cropping patterns is obvious from the temporal pattern of the vegetation indices shown in Figure 6.4b and Figure 6.4c. The response is due to different crop types and management practices such as grazing. Figure 6.4 also helps to understand the evolution of seasonal patterns of vegetation. The seasonal rainfall pattern during 2003 was not normal due to the long drought in the 2002-2003 period. This is reflected by the sharp increase in vegetation indices during the early part of 2003 and sharp decrease in vegetation indices towards the latter part as in G3 or as a plateau seen in M7 (Figure 6.4d). In 2004, a bimodal distribution of vegetation index values in response to the seasons is evident at many sites such as G3, K1 and M7. Peak vegetation periods in 2004 occur in early to mid autumn and in mid spring.

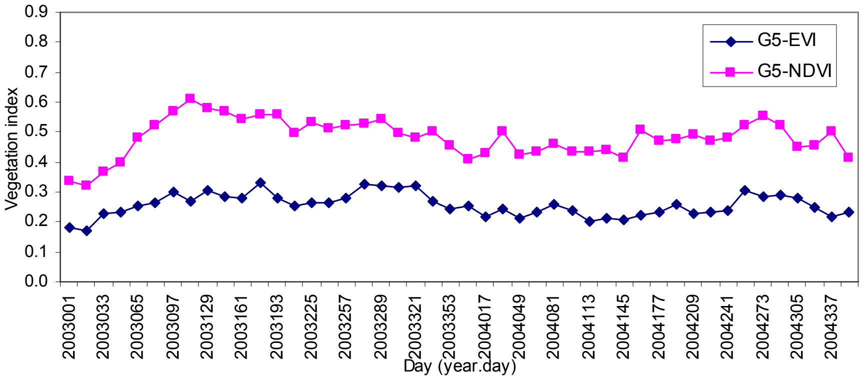

a)

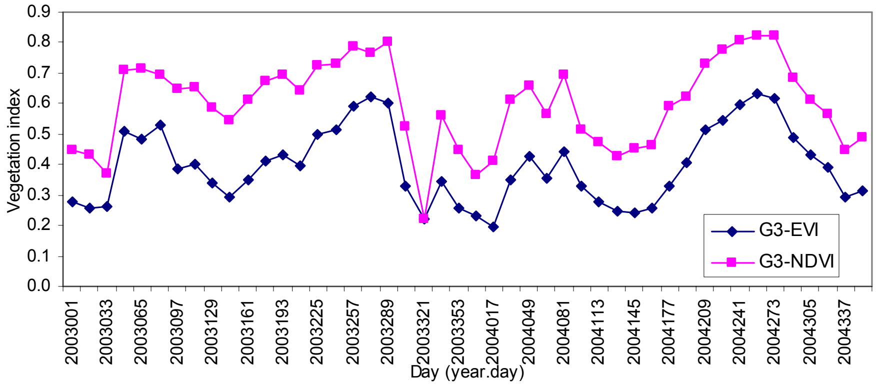

b)

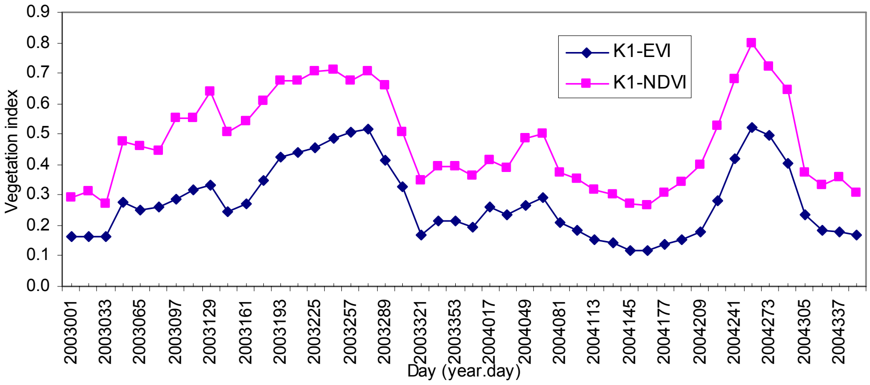

c)

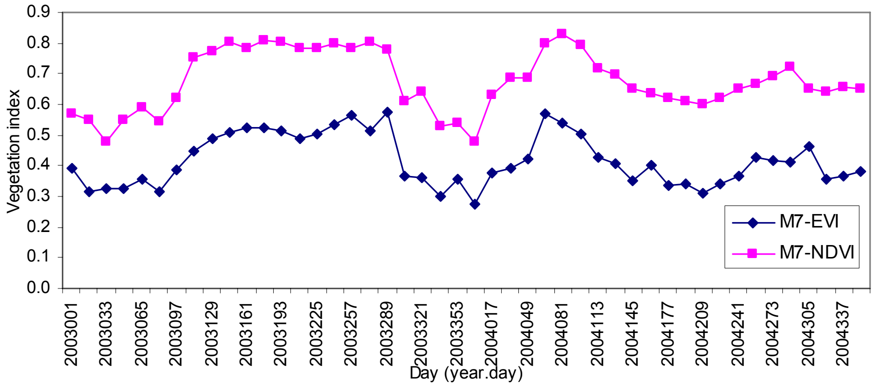

d)

Figure 6.4: Vegetation index values over two-year period at four selected locations in the Goulburn river catchment. a) G5 – native grass in sandy soil, b) G3- crops in black cracking clay soil, c) K1- crops in red clay soil, and d) M7- native pasture in black clay loam soil.

Table 6-4: Temporal variations of vegetation indices during 2003-2004 at four selected locations in the Goulburn River Catchment.

Site	Site Properties	EVI Min	EVI Max	EVI Avg.	NDVI Min	NDVI Max	NDVI Avg.
G5	Native grass, sandy loam soil	0.172	0.331	0.256	0.321	0.611	0.482
G3	Cropping area, black clay soil	0.193	0.633	0.396	0.222	0.825	0.600
K1	Cropping area, red silt loam soil	0.115	0.522	0.278	0.265	0.799	0.477
M7	Native grass, black clay loam soil	0.273	0.574	0.416	0.479	0.831	0.675

The spatial patterns of the vegetation indices (VI) help to understand the relative distributions of healthy vegetation and possible water stressed areas. Figure 6.5 shows the spatial and temporal evolution of NDVI distributions across the Goulburn catchment during 2004. It can be seen, that there is a level of consistency in spatial structure evident throughout the region. Particularly along the northern border and in the southern part of the catchment healthy vegetation is present throughout the year. This may be due to adequate soil moisture in these regions. The vegetation in the northern half of the catchment shows a greater seasonal behaviour. In general, it is not dense and reaches its maximum values around days 45-81 (i.e. mid-February to mid-March). The maximum NDVI values thus indicate favourable conditions for plant growth such as adequate soil moisture. This is obvious when comparing these values with the monthly rainfall distribution pattern (see Figure 3.16 in Chapter 3)

The spatial distribution and temporal behaviour of EVI across the Goulburn catchment during 2004 is shown in Figure 6.6. The EVI distribution (Figure 6.6) across the catchment shows considerable similarity to that of NDVI distribution (Figure 6.5). However, when compared, the magnitude of EVI values is less than the NDVI values. Elimination of the background soil signature from the EVI computation procedure results in low EVI values. Despite the fact that EVI is a better indicator than the NDVI, it is important to also consider the NDVI due to its wider use. In addition, the considerable differences between NDVI and EVI provide valuable information on the nature of land surface temperature signatures derived from remote sensing. Very low values of EVI, especially for the northern half of the catchment, suggest that bare soils are dominant in LST signatures. This is advantageous as the LST can be correlated with soil moisture and LST distributions may be used to establish soil moisture scaling relationships in the study catchment. For this reason, the northern half of the catchment appears suitable for studying the downscaling of large area soil moisture estimates with LST based approaches.

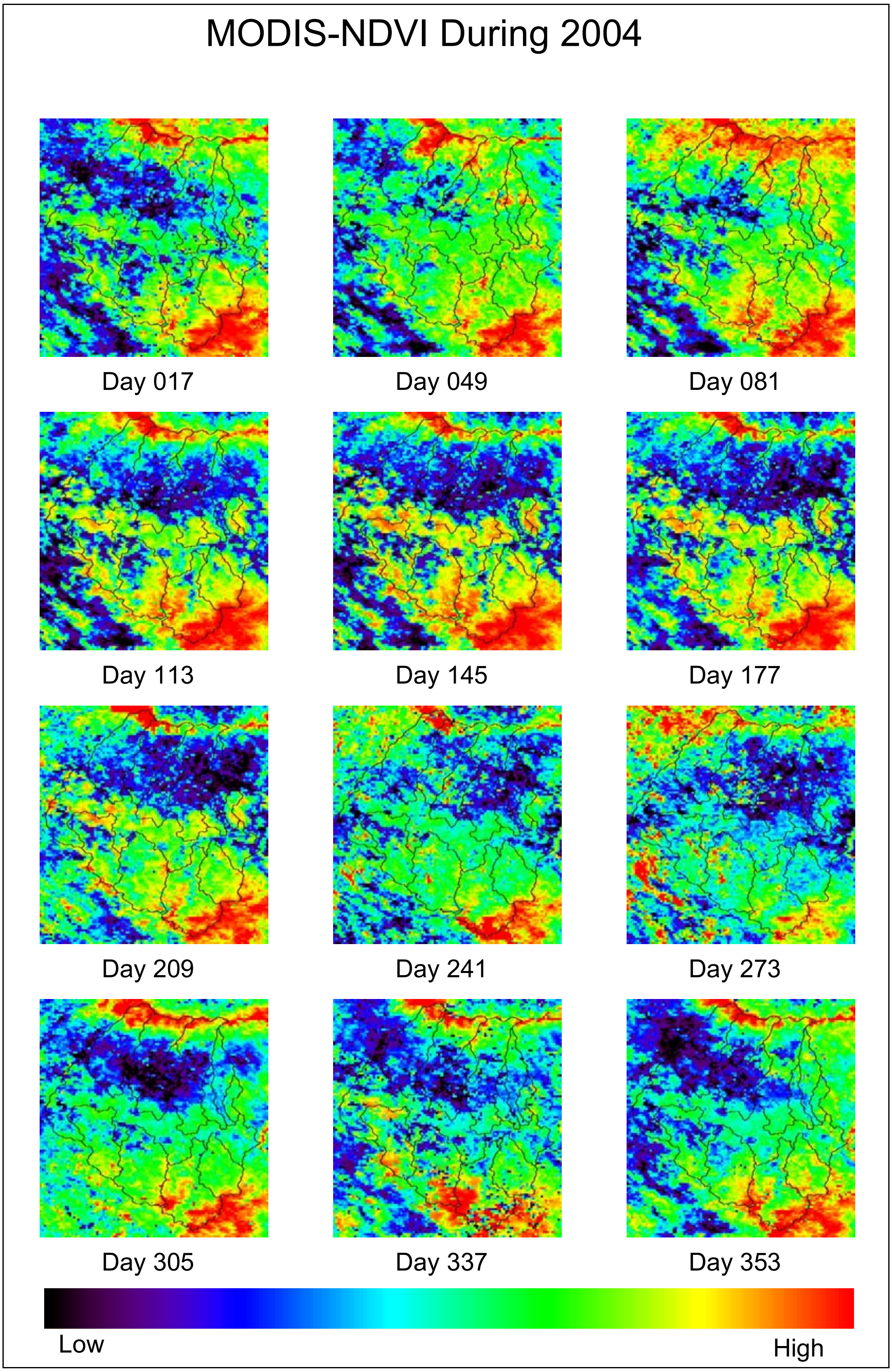

Figure 6.5: Spatial distribution and temporal behaviour of NDVI as computed from MODIS images for the Goulburn river catchment during 2004.

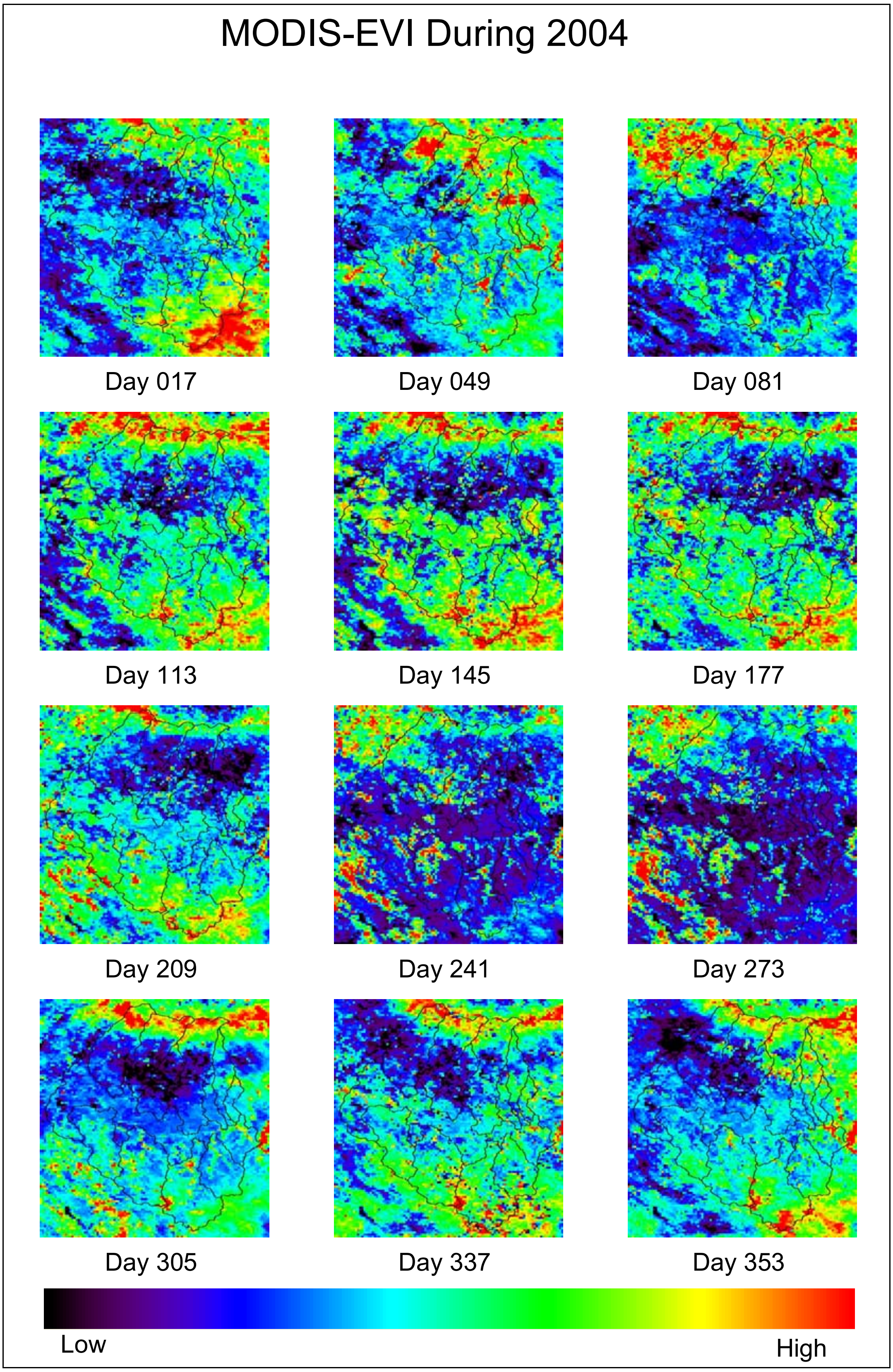

Figure 6.6: Spatial distribution and temporal behaviour of EVI computed from MODIS images at Goulburn catchment during 2004.

6.2.3.1 Vegetation indices and soil water contents

Vegetation indices can be used as a surrogate variable for deriving spatial soil moisture distributions because vegetation health is a good indicator of soil moisture status. In general, higher vegetation index (VI) values are associated with favourable growing conditions that usually result from unrestricted supply of soil water for plant growth. In contrast, a low VI value during the growing season indicates soil water restrictions for healthy plant growth. Thus, VI provides some information on the SWC. The information derived from VI however, is not sufficient to adequately predict the SWC. For example, when the measured SWCs are plotted against the Enhanced Vegetation Index (EVI), positive trends can be seen only in some catchments (see Figure 6.7 and Table 6-5). The use of VI as the only variable for predicting SWC is therefore inappropriate.

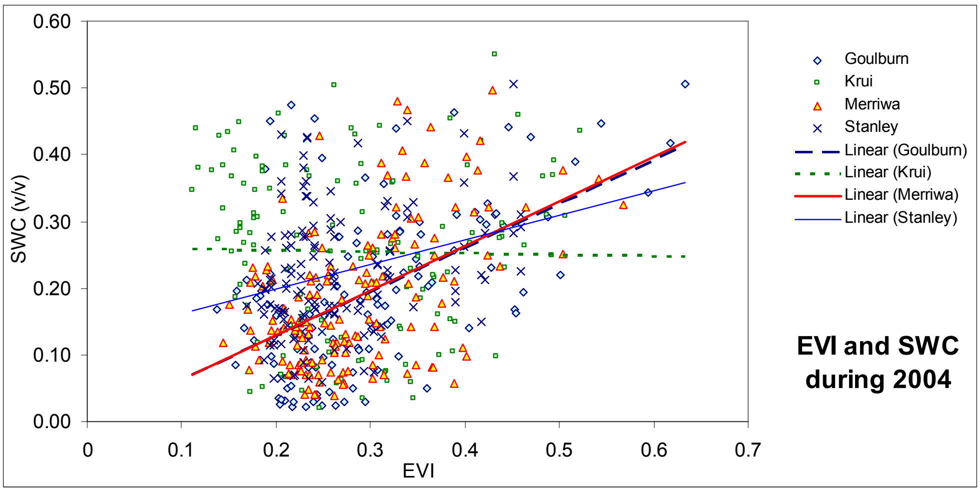

Figure 6.7: Relationships between fortnightly EVI and fortnightly-averaged 0-30 cm SWCs (cm^3cm^{-3}) during 2004 in study catchments.

Table 6-5: Results of the simple linear correlation analyses between fortnightly-EVI in 2004 and average SWC during the same period in different sub catchments.

Catchment	*n*	Intercept	Regression coefficient	correlation coefficient (r^a)
S. Goulburn	121	0.21	0.4466	0.542^{**}
Krui	132	0.28	-0.0144	-0.017^{ns}
Merriwa	154	0.22	0.3697	0.496^{**}
Stanley	132	0.22	0.2163	0.538^{**}
Goulburn	539	0.23	0.2208	0.282^{**}

n = sample size, $r^a = {}^{**}$ significant at 1% level, $r^a = {}^{*}$ significant at 5% level, and $r^a = {}^{ns}$ non significant

Any weak linear relationship between SWC and vegetation index has limited practical value due to the complex nature of the relationship between the vegetation status and the soil water content. Physiological changes in the vegetation due to seasonal effects can have a significant impact on the VI. A range of vegetation types within a 1-km pixel and their variable responses due to soil water availability make it difficult to interpret changes in the vegetation index as caused by changes in SWC at the scale of most satellite footprints. For this reason, vegetation indices can provide qualitative information rather than result in a quantitative measure of soil water content.

The combined use of LST and vegetation indices is expected to perform better in establishing relationships with SWC. Section 2.3.5 has summarized the application of LST and vegetation indices for deriving wetness indices. It is expected that wetness indices derived in part from satellite-based vegetation indices are capable of providing a better quantitative measure than vegetation indices alone. They are thus potentially suitable for a range of practical applications including soil moisture scaling studies as discussed in Section 2.3.5. The present study, therefore will consider the use of wetness indices for predicting soil water contents.

6.3 DERIVING SOIL WATER DISTRIBUTIONS FROM LST, AIR TEMPERATURE AND SOIL CHARACTERISTICS

Scaling relationships provide a means to relate soil water content of different soil types or spatial locations using simple conversion factors called scaling factors. It is a useful technique for describing the spatial variability of soil water content. According to Williams and Ahuja (2003), there are two basic ways to derive scaling factors: dimensional analysis and empirical methods. Dimensional analysis is based on the existence of physical similarity in the system. The empirical methods are based on regression analysis. Miller and Miller (1956), as cited by Williams and Ahuja (2003) were the first to present physically based scaling factors for soil hydraulic properties that were based on the assumption of a geometric similarity existing among different soil types. The empirical methods are quite popular among researchers and many studies have been found relating soil water content to topographic parameters (Sulebak *et al*. 2000, Svetlitchnyi *et al*., 2003), wetness indices and remotely measured land surface parameters (Jackson *et al*., 1981a; Moran *et al*., 1996; McVicar and Jupp, 2002; Scott *et al*., 2003). This study focuses on regression based empirical scaling models to scale the field measured surface (0-30 cm) soil water content across a catchment using remotely sensed LST and vegetation data, and other information such as air temperature and soil type.

6.3.1 ENERGY BALANCE CONSIDERATIONS FOR SOIL MOISTURE PREDICTIONS

The exchange processes occurring at the land surface are very important for the redistribution of moisture and heat in soil and atmosphere. The land surface connects the moisture and heat balances of the soil and atmosphere. The energy balance for land surface can be written as:

$$R_n = G + H + \lambda E \qquad \textbf{(6-1)}$$

where R_n is the net radiation (Wm^{-2}), G is the soil heat flux at the land surface (Wm^{-2}), H is the sensible heat flux (Wm^{-2}) from the land surface to the air, and λE is the latent heat flux to the air (Wm^{-2}).

The soil wetness conditions are to a great extent controlled by hydrological processes such as rainfall, evaporation, transpiration, infiltration, capillary rise, percolation and drainage. The land surface hydrology affects the near-surface moisture conditions and therefore controls the partitioning between G, H and λE. It is generally assumed that under conditions of complete canopy closure, approximately 10 percent of net radiation is transferred to the soil or (R_n - G) = 0.9Rn. Soil wetness is therefore manifested in the surface energy balance by the relative magnitudes of H and λE. Furthermore, the sum of H and λE will depend on R_n. Thus, if a soil is dry, H will be large and λE will be small, and the contrary holds true for wet soils. With this assumption, it can be argued that the estimation of H and λE (i.e. the Bowen ratio approach) should provide a method of estimating near-surface moisture conditions.

Both H and λE depend on land surface temperature. For example, H can be expressed as (Jackson *et al.* 1981a):

$$H = \rho c_p (T_s - T_a) / r_a \qquad \textbf{(6-2)}$$

where ρ is the density of air (kg m^{-3}), c_p the heat capacity of air (J kg^{-1} ^{o}C^{-1}), T_s the canopy temperature or land surface temperature (^{o}C), T_a the air temperature (^{o}C), and r_a the aerodynamic resistance (s m^{-1}). As ρ, c_p and (to a lesser extent) r_a are approximately constants, it is apparent that the value of H is determined by the difference between the land surface temperature and the air temperature (for average wind speed conditions).

Moreover, the latent heat flux, λE is the product of the evaporative flux, E (kg s^{-1} m^{-2}), and the latent heat of evaporation, λ (2.44 x 10^{6} J kg^{-1} at 25^{o}C). The value of λ is also temperature dependent (Evett, 2002):

$$\lambda = 2.501 - 2.370 \times 10^{-3} T \qquad (r^2 = 0.99995) \qquad \textbf{(6-3)}$$

where T is in ^{o}C. Because of the strong connection between the soil moisture and temperature, measurement of land surface temperature gives an indirect way of estimating soil wetness status. Many researchers have therefore attempted to use the land surface temperature for soil moisture estimation (Jackson *et al.* 1981a; Choudhury and Golus, 1988; Smith and Choudhury, 1991; Carlson *et al*., 1994, 1995; Moran *et al*., 1996; Bastiaanssen *et al*., 1997; Gillies *et al*., 1997; Goetz, 1997; McVicar and Jupp, 2000; Wang *et al.,* 2001; Goward *et al*., 2002; Li and Islam, 2002; Sandholt *et al*., 2002; Luquet *et al*., 2004; Wan *et al*., 2004). In some of these studies, spatial variability of surface soil moisture is implied by the large range in surface radiant temperature present in the satellite imagery.

Jackson *et al.* (1977) as quoted by McVicar and Jupp (2000) developed an empirical model to estimate daily actual evapotranspiration (ET_{a_DAY}) by:

$$ET_{a\_DAY} - Rn_{DAY} = A - B(T_s - T_a) \qquad \textbf{(6-4)}$$

where Rn_{DAY} is daily net radiation (W m^{-2}), T_s is surface temperature (K), T_a is air temperature (K) and A and B are empirical coefficients which are consistent over areas with similar land cover structures.

Later, Jackson *et al.* (1981a) combined the Penman – Monteith equation with a one-dimensional energy balance equation to derive an expression for land surface-air temperature.

$$(T_s - T_a) = \left[r_a (Rn - G)/C_v\right]\left[\gamma\left(1+\frac{r_c}{r_a}\right)\Big/\left\{\Delta+\gamma\left(1+\frac{r_c}{r_a}\right)\right\}\right] - \left[VPD\Big/\left\{\Delta+\gamma\left(1+\frac{r_c}{r_a}\right)\right\}\right] \tag{6-5}$$

where C_v the volumetric heat capacity of air (J $^oC^{-1}$ m^{-3}), r_c the canopy resistance (s m^{-1}) to vapour transport, γ the psychrometric constant (Pa $^oC^{-1}$), and Δ is the slope of the saturated vapour pressure-temperature relation (Pa $^oC^{-1}$). The above relationship has been used to develop indices such as Crop Water Stress Index (CSWI, Jackson *et al.,* 1981a) and Water Deficit Index (Moran *et al.*, 1996; more discussion is given in Section 2.3.5.1) to characterize the land surface wetness conditions using the difference between remotely-sensed measurements of land surface temperatures and air temperatures (T_s-T_a).

The T_s–T_a method can be regarded as yielding a specific time-of-day measure of the land surface wetness condition. It is a good indicator characterizing the land surface moisture status during warmer months (e.g. in summer). In theory, higher T_s –T_a values are associated over dry surfaces and lower values indicate wet conditions. The estimated T_s–T_a values over an area therefore should provide a useful covariate for approximately describing field spatial variability of soil moisture conditions. The main strength of the T_s –T_a approach is its strong physical nature. However, it is difficult to compare T_s –T_a measurements with soil water contents over longer time scales.

Apart from a one-time LST measurement, consideration of two LST measurements such as one during daytime and the other during nighttime can also provide some indication of soil moisture status. Diurnal cycles in the surface temperature are strongly dependent on the thermal and physical properties of the top several centimetres of the soil. Many factors including albedo, dust opacity, and atmospheric pressure have an effect on surface temperature but thermal inertia is a key property in controlling these diurnal temperature oscillations. Thermal inertia (I) is defined as a combination of thermal diffusivity (k), density (ρ), and specific heat capacity (c):

$$I \equiv \sqrt{kpc} \qquad \textbf{(6-6)}$$

Thermal diffusivity governs the rate of temperature change within a material; it is a measure of a substance's ability to transfer heat in and out of that portion that received solar heating during the day and cools at night. For a substance like soil, k is strongly dependent on the soil water content.

Thermal inertia represents the ability of the subsurface to conduct and store heat energy away from the surface during the day and to return that heat energy to the surface through the night. In addition, it is a measure of the heat transfer rate across a boundary between two materials. e.g., air/soil. Because materials with high thermal inertia possess a strong inertial resistance to temperature fluctuations at a surface boundary, they show less temperature variation per heating/cooling cycle than those with lower thermal inertia. For soils, higher SWC means stronger inertial resistance to temperature fluctuations due to high specific heat of water. Therefore, the drier the soil, the greater the amplitudes of the diurnal temperature variations.

6.3.2 LST BASED MODELS FOR SOIL MOISTURE PREDICTION

6.3.2.1 Preliminary study

Based on the theory described in Section 6.3.1 and the availability of required datasets, it is possible to identify at least 5 LST based empirical models to predict soil water content (henceforth known as SWC-based models):

a) Daytime LST (T_s)

b) Daytime LST - T_{air} (T_s–T_a)

c) Nighttime LST ($T_{s\text{-night}}$)

d) Nighttime LST - T_{air} ($T_{s\text{-night}}$–T_a)

e) Daytime – Nighttime LST (Δ-LST)

In order to evaluate these models, it was decided to use 20 of the sites for developing the models and the other 5 sites for testing the predicted water contents. Accordingly, the 5 validation sites were selected randomly from the catchment. First, four sites were selected randomly in a way to represent one from each subcatchment. Then, the fifth site was selected considering all remaining sites. Adopting this technique, sites G1, K2, M5 and S2 were chosen in the first round and the G3 was selected in the second round. These five sites were used to evaluate the soil moisture predictions from the empirical equations which were developed with the other 20 sites. Twelve days were selected approximately on 30 days interval throughout 2004 for developing the empirical models. All empirical models were based on linear regression techniques.

6.3.2.2 Results and discussion - preliminary study

The five models developed for the selected 12 days are summarized in Table 6-6. It is evident that, in general both during daytime and nighttime, a negative relationship exists between LST and SWC. The diurnal temperature variation (ΔLST) also shows a negative correlation with SWC. The higher R^2 values (in 5 days out of 12 days) with Daytime LST based models indicate that Daytime LST works somewhat better in these models than does nighttime LST or ΔLST. Furthermore, T_s–T_a appears to produce better regression models than considering daytime LST only. This observation confirms findings by other researchers (e.g. Jackson *et al.,* 1981a; Moran *et al.*, 1996). The poor performance of the nighttime LST models may partly due to the redistribution of soil water during nighttime. The use of diurnal temperature ranges (ΔLST) appears better than using nighttime LST. However, except for T_s–T_a, none of these methods is convincing and they are not suitable for predicting catchments scale soil moisture patterns.

Table 6-6: Results of the linear regression analyses between LST (X-axis °C: Daytime LST, Daytime LST-T_{air}, Nighttime LST, Nighttime LST-T_{air} and Δ-LST) and measured soil water contents (Y-axis) during 2004 (*n* = number of data points).

DOY	*n*	slope	Intercept	R^2	*n*	slope	Intercept	R^2
		Daytime LST				Daytime LST - T_{air}		
38	14	-0.010	0.614	0.374	14	-0.011	0.282	0.433
58	20	0.000	0.303	0.000	20	0.000	0.310	0.000
86	18	-0.008	0.496	0.082	18	-0.008	0.234	0.059
87	20	-0.010	0.487	0.106	20	-0.011	0.234	0.096
115	20	-0.015	0.600	0.085	20	-0.023	0.390	0.110
151	20	-0.012	0.503	0.026	20	-0.019	0.364	0.051
210	20	-0.024	0.683	0.124	20	-0.030	0.394	0.154
224	20	-0.012	0.535	0.051	20	-0.013	0.376	0.049
262	20	-0.023	0.912	0.166	20	-0.024	0.436	0.161
297	18	-0.009	0.491	0.176	18	-0.010	0.237	0.172
317	19	-0.014	0.667	0.178	19	-0.017	0.353	0.287
321	20	-0.005	0.419	0.087	20	-0.005	0.269	0.076
		Nighttime LST				Nighttime LST - T_{air}		
38	9	-0.005	0.272	0.020	9	-0.005	0.153	0.020
58	20	-0.084	1.339	0.349	20	-0.033	0.256	0.133
86	20	0.009	0.085	0.012	20	-0.015	0.143	0.044
87	18	-0.038	0.633	0.112	18	-0.038	0.074	0.112
115	20	-0.015	0.251	0.015	20	-0.017	0.091	0.019
151	20	-0.023	0.279	0.048	20	-0.022	0.160	0.033
210	20	-0.055	0.401	0.073	20	-0.046	0.193	0.061
224	0	-	-	-	0	-	-	-
262	19	-0.033	0.402	0.134	19	-0.027	0.162	0.145
297	16	0.016	0.007	0.046	16	0.002	0.193	0.001
317	20	0.007	0.124	0.008	20	-0.013	0.160	0.017
321	20	-0.027	0.505	0.057	20	-0.026	0.121	0.050
		Δ-LST						
38	9	-0.006	0.354	0.207				
58	20	0.006	0.186	0.024				
86	18	-0.005	0.324	0.054				
87	18	0.007	0.027	0.034				
115	20	-0.010	0.400	0.045				
151	20	0.000	0.284	0.000				
210	20	-0.021	0.619	0.078				
224	0	-	-	-				
262	19	-0.005	0.391	0.016				
297	16	-0.007	0.340	0.106				
317	19	-0.011	0.442	0.175				
321	20	-0.005	0.333	0.067				

In addition, longer time periods were also considered in developing regression models to predict SWC from MODIS LST measurements. These analyses were performed only using daytime LST, nighttime LST and ΔLST on a weekly, monthly and seasonal basis. Models were developed for the all subcatchments as well as for the entire Goulburn River catchment. The regression models obtained with these longer time periods were not realistic, suggesting that LST based models are not suitable for longer time periods because changes in weather conditions during longer periods can confound any unique relationship between LST and SWC.

The relationships between any of the five LST-derived covariates and SWC clearly depend on atmospheric conditions and will vary with seasons. For example, as shown in Figure 6.8, $T_s - T_a$ shows wider range of values during summer than during winter for nearly the same range of soil water content throughout 2004. Furthermore, the computed $T_s - T_a$ values during summer days tend to be larger than the values computed for winter days. This suggests that it is often possible to have large variations of $T_s - T_a$ values for the same soil water content. Thus, improved relationships are needed for deriving soil wetness patterns form land surface temperature measurements.

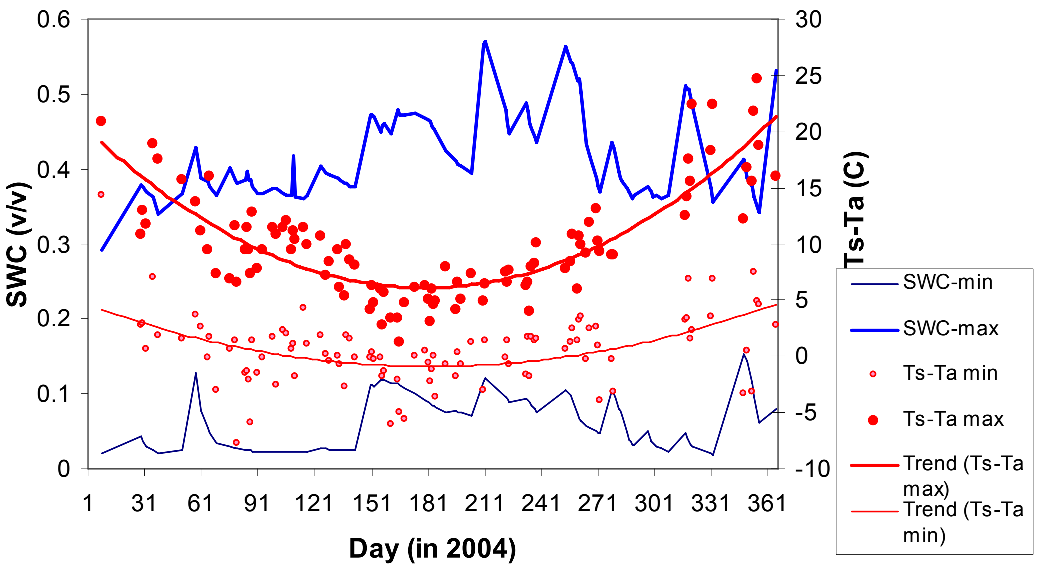

Figure 6.8: Temporal patterns of soil water contents (0-30cm) and T_s-T_a during 2004.

Land surface temperatures will also depend on other factors such as ground cover and soil types. Satellite-based LST measurement gives a mixed signature and reflects the combined temperature of soil and vegetation in sparsely vegetated areas. The contribution of vegetation may therefore be significant for any satellite-based LST-SWC schemes as discussed in Section 2.3.5. Similarly, soil types may also affect LST due to their physical properties such as colour and water holding capacity. As shown in Figure 6.9 the observed ranges of SWC vary with soil type. Therefore, the effect of soil type on LST based SWC prediction models may need to be considered. One way of introducing the soil factors into the LST based SWC prediction models is to use normalized SWC values in their development. Section 6.3.3 therefore investigates the use of normalized forms of LST and SWC into the soil water prediction models. Later, in Section 6.4, these analyses are extended to the combined use of LST and vegetation information.

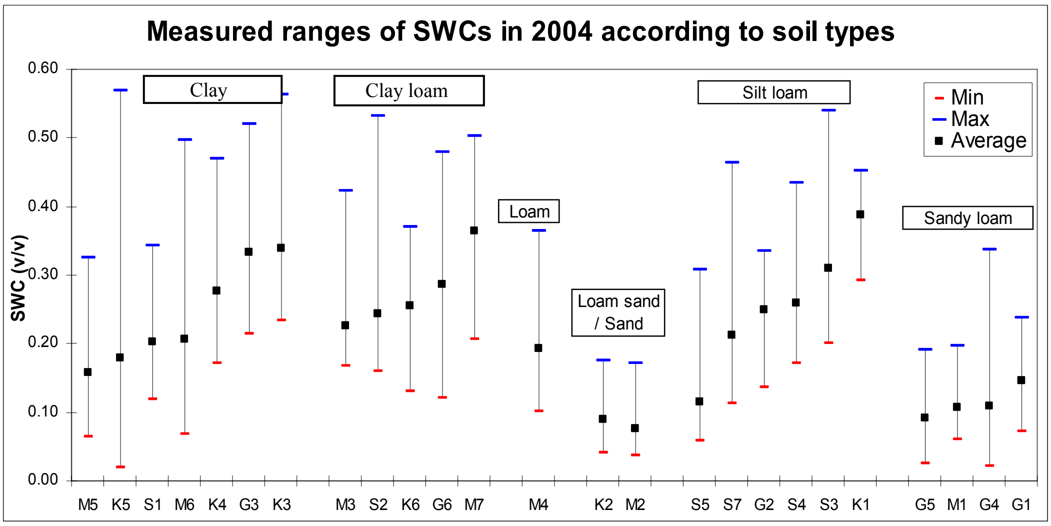

Figure 6.9: Observed ranges of SWC in various soil types during 2004.

6.3.3 REGIONALLY NORMALISED TEMPERATURE INDEX (RNTI)

Spatially dense MODIS LST data over a large catchment (>5000 km^2) provide a range of LST measurements which represent many possible soil water conditions within the area. Thus, it can be argued that space-borne LST data alone will be sufficient for developing a simple index to describe the surface wetness or dryness conditions in a region. This has led to the development of a Regionally Normalised Temperature Index (RNTI) which for a given pixel is defined as:

$$RNTI = \frac{LST_i - LST_{\min}}{LST_{\max} - LST_{\min}} \quad \textbf{(6-7)}$$

where the two bounding temperatures, LST_{min} and LST_{max}, are derived from the LST measurements over the entire region and LST_i is the measured temperature in a given pixel. The RNTI can be regarded as a special version of the $T_s - T_a$ approach and can be applied without using the measured air temperature. For example, as seen in Figure 6.10, RNTI holds strong linear relationship with $T_s - T_a$. Interestingly, the range of variations of RNTI throughout the year seems more or less the same, irrespective of the season. Generally, RNTI varies from 0.4 to 0.9 during all 12 selected days which were chosen with approximately 30-day intervals. The range of $T_s - T_a$ variations on the other hand, is not consistent and is usually narrower during winter (e.g. day-165, day-197) and wider during summer (e.g. day-035, day-353). It is clear that RNTI appears more stable to seasonal variations than does $T_s - T_a$.

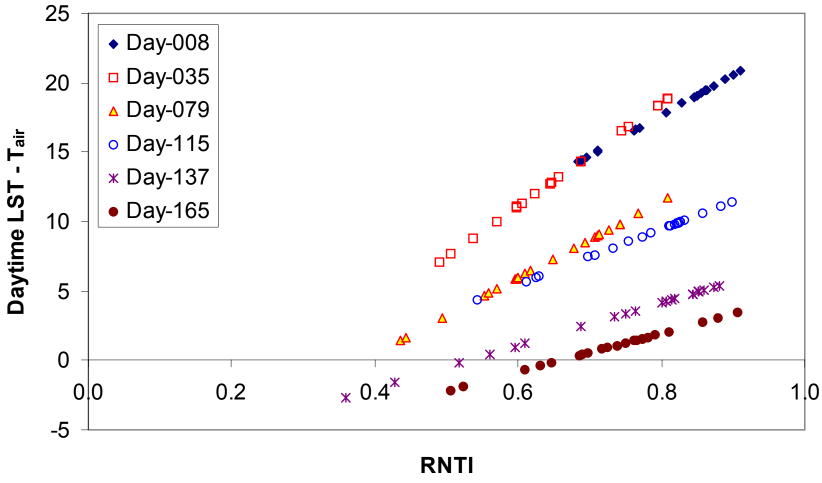

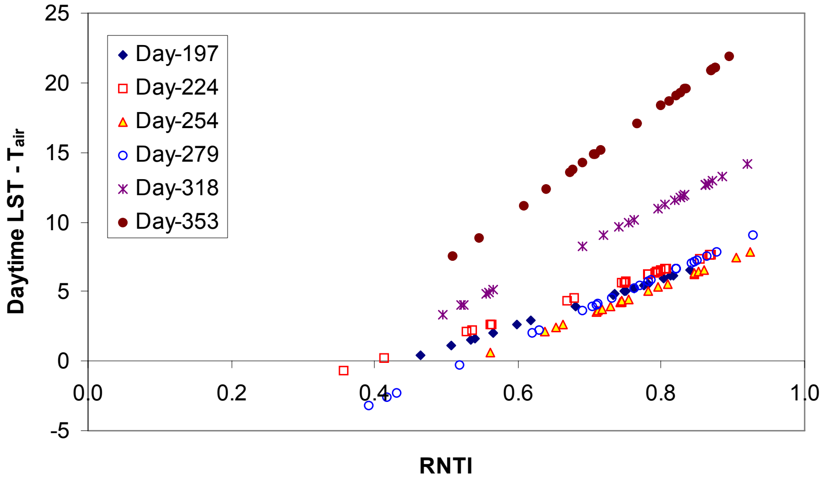

Figure 6.10: Relationships between RNTI and Daytime LST – T_{air} (T_s-T_a) during 2004.

RNTI has some advantages compared to T_s–T_a. Due to the linear relationships between T_s–T_a and RNTI, it can be argued from Eq. 6.7 that RNTI also provides information on soil water status with a strong physical basis. As reported by Jackson *et al.*, (1981a, 1986, 1988), T_s–T_a can be explained by the components used in the surface energy balance and due to the linear relationship between T_s–T_a and RNTI, the RNTI can also be described with the same energy balance components. The main advantage of the RNTI is that its values are consistent throughout a year. In case of T_s–T_a, it is not possible to obtain such consistent values. Furthermore, the computation of RNTI does not require air temperature measurements within a catchment and can be computed from the satellite observations alone.

6.3.3.1 Empirical models between soil water content and RNTI

The physical basis of RNTI and its convenient computation are attractive for soil moisture scaling studies and for predicting soil moisture distributions over catchments. Note that the correlation between soil moisture content and RNTI should be negative because soil water content also gives a negative correlation with T_s–T_a.

For example, Figure 6.11 shows a typical soil moisture pattern and computed RNTI during 2004 at site G6. This figure is based on 121 RNTI observations made during 2004 and it confirms that increases of RNTI due to decreases of SWC are consistent throughout the year. Figure 6.11 also provides insight into the range of RNTI variations and the range of SWC throughout a typical year. At G6, while SWC varies from 0.48 to 0.11 cm^3cm^{-3} the RNTI varies from 0.34 to 1.

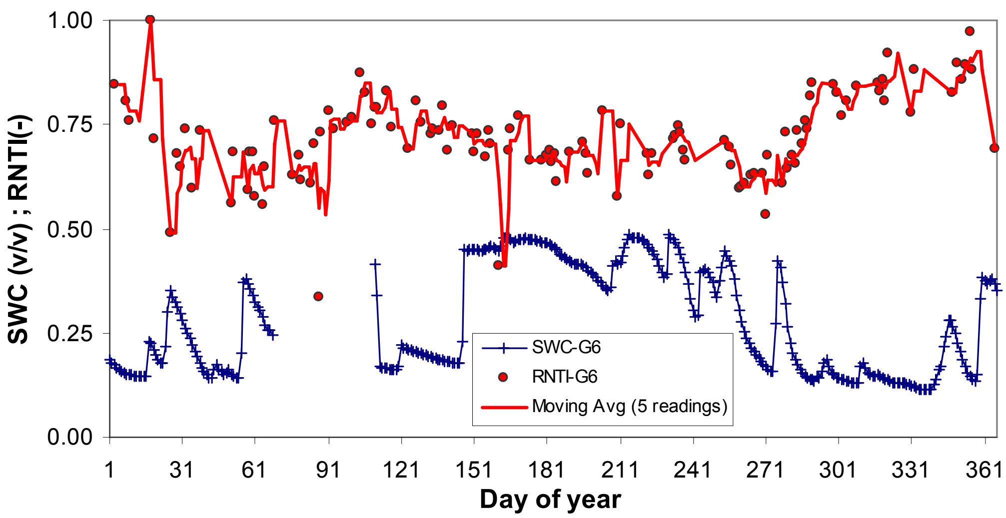

Figure 6.11: Temporal patterns of RNTI and measured SWC at site G6 during 2004.

The computed RNTI values were used to develop linear regression models to predict SWC for the same dates as used for Table 6-6 (henceforth known as RNTI-SWC). The summary results are presented in Table 6-7. As expected, despite relatively low R^2 values, a strong negative relationship was found between RNTI and SWC except for day-58 (Note that the other regression models developed with daytime LST also showed a poor relationship for this particular day). Examination of the RNTI-SWC relationships indicates that stronger slopes can be obtained with similar R^2 values than with $T_s – T_a$.

Table 6-7: Results of the linear regression analyses between RNTI (X-axis) and measured soil water contents (Y-axis) during 2004 (*n* = number of data points).

DOY	*n*	slope	Intercept	R^2	*t* statistics slope	*t* statistics - intercept
38	13	-0.313	0.384	0.374	-2.56	4.22
58	19	0.006	0.308	0.000	0.03	1.96
86	18	-0.245	0.330	0.082	-1.20	2.84
87	20	-0.242	0.319	0.106	-1.42	3.19
115	20	-0.298	0.410	0.085	0.11	0.75
151	20	-0.169	0.402	0.026	0.25	1.32
210	20	-0.333	0.572	0.124	-1.59	4.11
224	20	-0.193	0.444	0.051	-0.98	3.18
262	20	-0.412	0.541	0.166	-1.89	3.63
297	18	-0.225	0.360	0.176	-1.85	3.91
317	19	-0.295	0.416	0.178	-1.27	2.94
321	20	-0.194	0.329	0.087	-0.95	2.42

The regression models of Table 6-7 were also used to compute the SWC at the 5 test sites using the RNTI values. These computed SWCs were then compared with measured SWC as shown in Figure 6.12. It is evident that, RNTI based models show better results than $T_s – T_a$. However, careful analysis of Figure 6.12 reveals, that the predicted water contents are biased, particularly for soil types. For example, sites G3 and S2 show predicted water contents that are less than the measured values. In contrast, at two other sites, K2 and M5 water contents are slightly over-estimated. Surprisingly, under-estimated SWC values were found in clay type soils with naturally wet sites (see sites G3 and S2 in Figure 6.9), and over-estimated SWC values were found in loam sandy/clay type soils in naturally dry sites (see sites K2 and M5 in Figure 6.9). This indicates that the soil's capacity to hold water may be an important component in SWC prediction models. Satellite based LST measurement provides a mixed signature of SWC. Apart from the information of SWC in the near-surface soil layer, it also provides indirect information on water availability in the root zone by measuring plant surface temperatures. The separation of these two quantities is not yet possible with current knowledge. Regression models relating 0-30cm SWC to LST will therefore provide imperfect results. One way of overcoming this difficulty is to use normalized water contents in the regression equations.

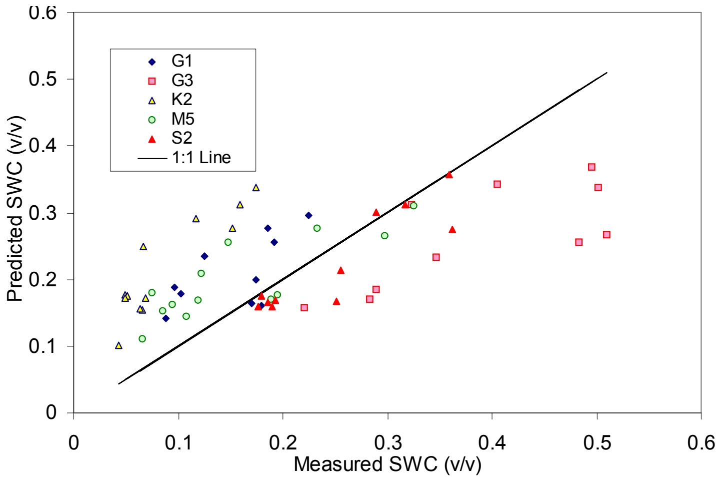

Std error of predictions

G1 - 0.055
G3 - 0.043
K2 - 0.017
M5 - 0.028
S2 - 0.045

Figure 6.12: Measured 0-30 cm SWC plotted against computed SWC based on RNTI based models at validation sites.

6.3.4 NORMALIZED WATER DEFICIT INDEX (NWDI)

Volumetric soil water content (θ) can be expressed in normalized form (θ^*) in terms of the soil water content at saturation, θ_{max}, and a residual soil water content, θ_{min} as

$$\theta^* = \frac{\theta - \theta_{\min}}{\theta_{\max} - \theta_{\min}} \qquad \textbf{(6-8)}$$

where the θ_{min} is often taken to be zero (Capehart and Carlson, 1997). Thus equation 6-8 becomes:

$$\theta^* = \frac{\theta}{\theta_{\max}} \qquad \textbf{(6-9)}$$

Note that the water availability index θ^* can also be related to evaporative fraction, Λ (Scott *et al*., 2003). According to Ahmad and Bastiaanssen (2003), the value of Λ under non-advective conditions ranges usually between 0 and 1, where maximum evapotranspiration is represented by zero. The value of θ^* varies between 0 (oven dry) to 1 (complete saturation) and is a standard measure that can be applied to a wide range of soils (Scott *et al*., 2003).

Describing soil water deficit as the difference between actual and saturation values (i.e. θ_{max}-θ), equation (6-9) can be rearranged to give a Normalized Water Deficit Index (NWDI) for a given location.

$$NWDI_j = \frac{\theta_{\max_i} - \theta_i^j}{\theta_{\max_i}} \qquad \textbf{(6-10)}$$

where θ_{max_i} is the maximum soil water content observed at site i and θ^j_i is the observed soil water content for site i on j^{th} day. In the above equation, dividing θ_{max}-θ by θ_{max} gives a normalized form which helps to eliminate variations of SWC due to properties associated with soil type. As discussed in Section 5.3, some sites in the study catchment always show wetter conditions (e.g. in clay soils) than other sites such as those in sandy soils. Furthermore, as seen in Table 6-8, the field measured range of maximum SWC varies from 0.24 – 0.64 cm^3cm^{-3}. Hence, the highest maximum SWC value is almost three times the lowest maximum SWC value. These SWC anomalies therefore need to be removed from the prediction models. Such anomalies due to soil physical properties can be eliminated using equation 6-10. The equation 6-10 can be applied to a wide range of soils. It should be noted that equation 6-9 describes the moisture deficit of the entire measurement depth considered (i.e. 0-30 cm in this study).

Table 6-8: Maximum soil water content observed for each site during 2003-2004.

Site	Max SWC ($cm^3.cm^{-3}$)	Site	Max SWC ($cm^3.cm^{-3}$)
G1	0.49	M1	0.25
G2	0.36	M2	0.33
G3	0.53	M3	0.47
G4	0.56	M4	0.48
G5	0.31	M5	0.44
G6	0.49	M6	0.50
K1	0.49	M7	0.51
K2	0.24	S1	0.63
K3	0.59	S2	0.59
K4	0.47	S3	0.62
K5	0.57	S4	0.53
K6	0.38	S5	0.64
		S7	0.50

6.3.4.1 Empirical models between NWDI and RNTI

Figure 6.13 shows a typical NWDI pattern and computed RNTI during 2004 at G6. This figure is based on 325 NWDI observations made during 2004 and it confirms that increases of RNTI due to increases of NWDI are consistent throughout the whole period. Figure 6.13 also provides insight into the range of NWDI variations throughout a typical year. At G6, NWDI varies from 0.02 to 0.77 and RNTI varies from 0.34 to 1. Thus, the change of NWDI due to a unit change of RNTI gives higher value than the change in SWC due to a unit change of RNTI. This is advantageous for deriving surface wetness patterns from LST measurements, as differences between the RNTI in neighbouring pixels may take smaller values.

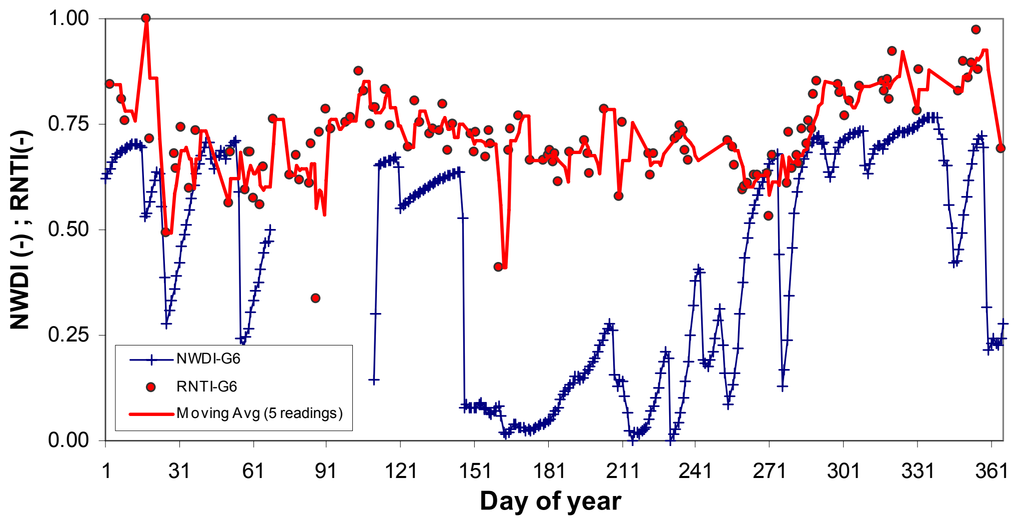

Figure 6.13: Temporal patterns of RNTI and NWDI at G6 during 2004.

Next NWDI and LST relationships were obtained for the dates also used in Table 6-6 and Table 6-7. The computed NWDI values replaced the SWCs and a new set of regression equations (henceforth known as NWDI based models) were developed with all LST based data types used in the previous sections. The summary results are presented in Table 6-9.

It is evident that the introduction of the NWDI leads to significant improvement in models particularly those developed with daytime LST measurements. Importantly, it is also evident that these improvements are consistent throughout all the dates considered. For example on day 321, the Daytime model developed with NWDI (slope = 0.022, R^2 = 0.303) showed approximately four-times improvement in the regression coefficient and R^2 values than the model developed with SWCs (regression coefficient = -0.005, R^2 = 0.087). A similar improvement can be seen with the Daytime LST–T_{air} on the same day. Thus it may be concluded that the introduction of NWDI can potentially better explain the variations of daytime LST measurements in LST-based regression models for soil water prediction. Thus, introduction of a soil related parameter such as saturated water content will improve the model predictions.

Table 6-9: Results of the linear regression analyses between LST (°C in X-axis; Daytime LST, Daytime LST-Tair, Nighttime LST, Nighttime LST-Tair, Δ-LST, and RNTI) and the Normalized Water Deficit Index (NWDI, in Y-axis) during 2004 (*n* = number of data points).

DOY	*n*	slope	Intercept	R^2	*n*	slope	Intercept	R^2
	Daytime LST				Daytime LST - T_{air}			
38	14	0.020	-0.285	0.393	14	0.021	0.430	0.401
58	20	0.016	-0.180	0.045	20	0.011	0.257	0.016
86	18	0.021	-0.148	0.113	18	0.016	0.514	0.056
87	20	0.029	-0.282	0.214	20	0.031	0.473	0.173
115	20	0.048	-0.732	0.224	20	0.063	0.045	0.211
151	20	0.048	-0.462	0.136	20	0.064	0.145	0.184
210	20	0.045	-0.336	0.152	20	0.047	0.214	0.132
224	20	0.036	-0.325	0.131	20	0.032	0.193	0.083
262	20	0.070	-1.549	0.393	20	0.070	-0.050	0.338
297	18	0.027	-0.277	0.298	18	0.029	0.464	0.274
317	19	0.052	-1.155	0.488	19	0.052	0.119	0.394
321	20	0.022	-0.339	0.303	20	0.022	0.258	0.270
	Nighttime LST				Nighttime LST - T_{air}			
38	9	-0.002	0.680	0.001	9	-0.002	0.621	0.001
58	20	0.066	-0.446	0.071	20	0.061	0.463	0.153
86	20	-0.043	1.104	0.066	20	0.044	0.739	0.093
87	18	0.003	0.631	0.000	18	0.003	0.671	0.000
115	20	-0.023	0.746	0.009	20	-0.015	0.559	0.004
151	20	-0.030	0.413	0.026	20	-0.039	0.197	0.036
210	20	0.052	0.233	0.024	20	0.018	0.342	0.004
224	0	-	-	-	0	-	-	-
262	19	0.028	0.351	0.026	19	0.053	0.663	0.156
297	16	-0.058	1.265	0.110	16	-0.011	0.567	0.004
317	20	-0.033	0.938	0.035	20	0.038	0.699	0.033
321	20	0.021	0.363	0.008	20	0.013	0.646	0.003
	Δ-LST				RNTI			
38	9	0.013	0.253	0.234	14	0.661	0.199	0.393
58	20	0.007	0.199	0.013	20	0.381	0.124	0.045
86	18	0.016	0.217	0.104	18	0.604	0.262	0.113
87	18	-0.002	0.701	0.001	20	0.712	0.215	0.214
115	20	0.040	-0.315	0.203	20	0.958	-0.119	0.224
151	20	0.025	-0.042	0.093	20	0.673	-0.060	0.136
210	20	0.045	-0.299	0.132	20	0.620	-0.130	0.152
224	0	-	-	-	20	0.580	-0.051	0.131
262	19	0.030	-0.272	0.140	20	1.272	-0.405	0.393
297	16	0.028	-0.002	0.306	18	0.655	0.102	0.298
317	19	0.041	-0.303	0.456	19	1.088	-0.233	0.488
321	20	0.022	-0.070	0.294	20	0.773	0.022	0.303

Neither regression coefficient nor R^2 have increased with the nighttime LST values. This was found for all dates considered. Nighttime LST measurements are therefore not appropriate for considering soil moisture predictions. The combined use of nighttime and daytime LST in ΔLST however, appears to perform better with NWDI than using nighttime LST alone. Thus, ΔLST gives also better results with NWDI than with SWC. The relationships obtained from ΔLST and NWDI are slightly poorer than the RNTI-based or Daytime LST-based models. Hence, similar to nighttime LST based models, the ΔLST based models should not be considered for further analysis. Because soil moisture can re-distribute during nighttime, the use of both nighttime and daytime information may potentially dampen the range of soil moisture values in the catchment. This effect might be more significant in wet to partially wet catchments than in very dry catchments.

The best relationships however, were found between RNTI and NWDI for all days considered. Comparison of the RNTI-NWDI relationships with the other models reveals that stronger regression coefficients can be obtained with the RNTI-NWDI models while maintaining high R^2 values. Using these RNTI-NWDI models to predict catchment scale SWC distribution, more detailed spatial patterns can be obtained. It is also important to note that the both predictors and predicted variables used in the RNTI-NWDI models are dimensionless variables. This is advantageous because such models may potentially be applied across a wide range of scales. Hence, for soil moisture scaling studies, models such as the RNTI-NWDI methods are potentially useful.

The regression models developed with RNTI were also used to compute SWC values for the 5 validation sites. When applying these models, NWDI values were computed and these indices were then converted into SWC using Eq. 6.10 and the θ_{max} from Table 6-8. These computed SWCs were then compared with measured SWC as shown in Figure 6.14. It is evident that, the RNTI-NWDI models can be applied to predict SWC with a higher degree of confidence than any other models presented previously. Underestimation associated with wet areas (e.g. clayey soils at G3 and S2) and overestimation associated with dry areas (e.g. sandy soils at K2 and M5) in Figure 6.12 has been reduced with the RNTI-NWDI model. Except for four computed SWCs of G3, all the other computed SWCs in test sites are closer to the measured values. These findings indicate that the 'soil effect' has been removed from the regression models by considering a dryness index approach.

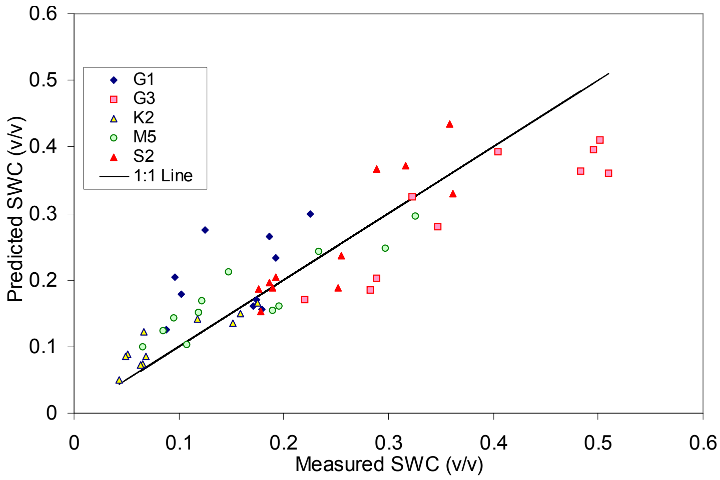

Figure 6.14: Measured 0-30 cm SWC Vs computed SWC based on RNTI-NWDI models in testing sites.

Finally, it is important to note that these RNTI-NWDI models were developed with point scale, *in-situ* soil moisture measurements representing 0-30 cm depth and remotely sensed LST measurements with 1.1 km^2 pixels. Considering the vast scale difference between these two variables, the SWC values predicted from the RNTI-NWDI models are very encouraging. Hence, this implies that deriving catchment scale soil moisture pattern from a limited number of *in-situ* soil moisture data is feasible with RNTI-NWDI models.

6.3.5 APPLICATION OF LST-BASED MODELS FOR SOIL MOISTURE PREDICTIONS

The LST based models discussed in the previous sections provide insight into the appropriateness of satellite-based LST measurements for catchment scale SWC predictions. To better assess model performance, error analyses were carried out. Complete results for all five evaluation sites are given in Annex-IV, whilst results for site K2 are given in Figure 6.15 as an example. For these error analyses, all LST based models discussed in the previous sections have been considered including the use of SWC (see Figure 6.15(a)) and NWDI (see Figure 6.15 (b)) in these models. Similar results have been obtained for the other four test sites used in the study. From the error analyses, it is concluded that:

a) Use of non-normalized 0-30 cm SWC values (i.e. SWC-based models) introduces serious errors in the predictions.

b) Use of NWDI in all models significantly improves the model performance.

c) Reasonably good SWC predictions may be obtained when a scaled variable is used for the independent variable (i.e. RNTI) and a normalized SWC is used for the dependent variable.

The RNTI-NWDI model uses normalized variables for the independent variable as well as for the predicted variable. The use of scaled variables helps to remove some potential scale problems associated with the prediction of SWCs from similar type of models. Furthermore, the use of RNTI assures a wide range of RNTI values across the catchment on a given day. Because of its strong physical basis, these RNTI values are useful in describing the surface wetness pattern in the catchment. Similarly, the use of NWDI helps to remove the 'soil effect' to a considerable extent. The use of indices for both the predictors and predicted variable in regression models therefore provides a useful approach to deriving soil water contents from the combined use of *in-situ* SWC data at a limited number of sites and remotely measured LST.

These results indicate that RNTI-NWDI type models based on a limited number of *in-situ* soil moisture data and remotely sensed LST data can be used for deriving the catchment scale moisture patterns. Knowledge of catchment-scale spatial patterns of θ_{max} is however required for deriving accurate moisture distributions.

For soil moisture prediction studies, one way of investigating the sources of errors in the predictions is to examine the temporal behaviour of model errors. As noted earlier, LST based models may be sensitive to seasonal weather patterns. As seen in Figure 6.15 model prediction errors show some degree of sensitivity to time of year. In general, while a higher error range is associated with autumn (day 115) and spring (e.g. days 224, 262), prediction errors for winter (day 210) and summer (e.g. day 58, 321) seasons occur within a lower range. In autumn and spring seasons, ambient temperatures are gradually decreasing or increasing, respectively and this may be the reason for higher error levels. In contrast, during winter and summer, more stable temperatures are maintained throughout the season and better predictions of SWC based on LST may be obtained.

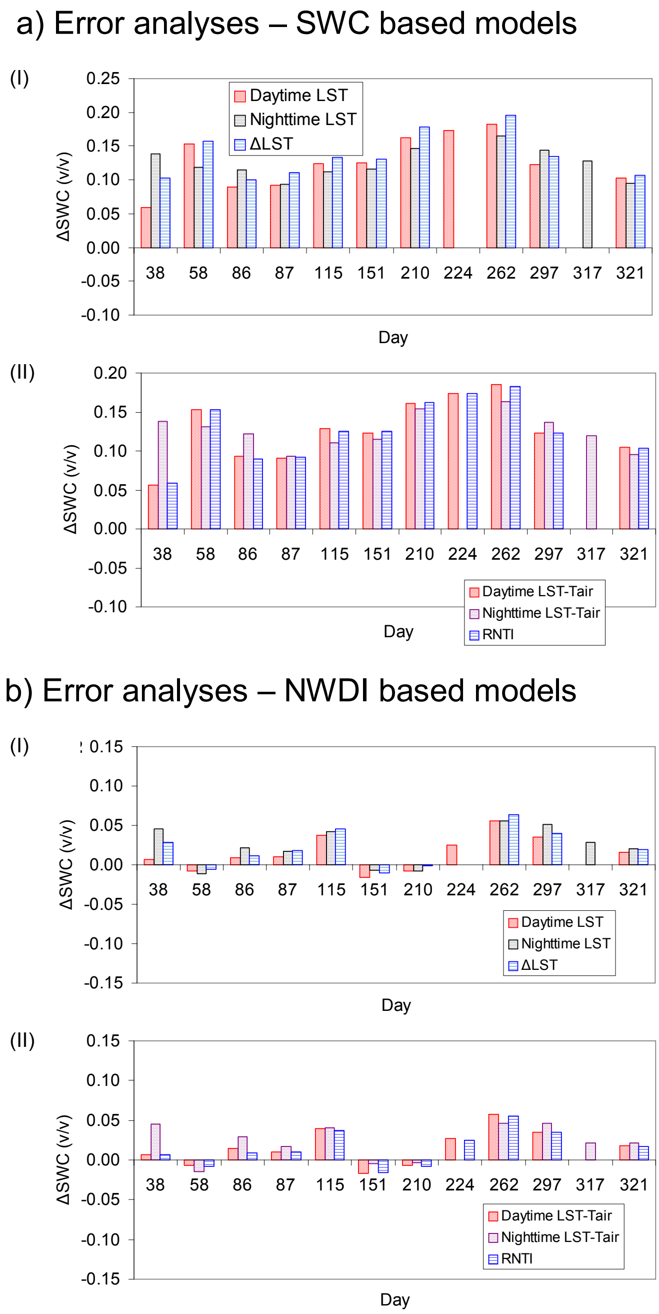

Figure 6.15: Frequency distribution of errors in the soil moisture predictions at K2 for 2004 with the various LST based models: a) using SWC, b) using NWDI.

6.4 DERIVING SOIL WATER DISTRIBUTIONS FROM LST AND VEGETATION INDICES

Previous section has confirmed that use of LST data alone may lead to inaccurate predictions of soil moisture contents. Consideration of vegetation is one of including the root-zone moisture contents into the prediction models. Recent analyses of multispectral (thermal and visible bands) measurements made from aircraft and satellite platforms (Moran *et al*., 1994; Carlson *et al*., 1995; Moran *et al*., 1996; Bastiaanssen *et al*., 1997; Gillies *et al*., 1997; McVicar and Jupp, 2000; Wang *et al.,* 2001; Goward *et al*., 2002; Wan *et al*., 2004) show considerable variation in both surface radiant temperature and vegetation cover, which in combination can be used to predict surface wetness conditions. Yet, owing to the underlying concepts of remote sensing and modelling techniques, soil moisture content derived from surface radiant temperature is very different from field measured or modelled water contents (Capehart and Carlson, 1997). The focus of this section is to compare ground based soil moisture measurements and remotely sensed wetness indices. Examination of the spatial and temporal characteristics of measured and computed wetness indices may offer insight into the suitability of a wetness index for: a) the disaggregation of large area measurements and, b) the selection of an appropriate covariate for the interpolation of point scale measurements.

The actual selection of a wetness index requires some discussion. As described in section 2.3.5, wetness indices may be computed from LST information or combined use of LST and VI with a varying degree of complexity. Whereas some indices such as water deficit index (WDI, Moran *et al.,* 1996) require additional ground based measurements to compute the wetness characteristics, other indices such as vegetation temperature condition index (VTCI, Wang *et al.,* 2001) or vegetation temperature dryness index (VTDI, Sandholt *et al*., 2002) may be computed entirely from satellite-based observations. Because of the simplicity of the computational procedure and its strong physical background, the VTCI has been selected for further study. VTCI is defined as:

$$VTCI_i = \left(\frac{LST_{\max} - LST}{LST_{\max} - LST_{\min}} \right)_{NDVI^i} \qquad \textbf{(6-11)}$$

Computation of VTCI is shown in Figure 6.16 indicating that $(LST_{max})_{NDVIi} - (LST)_{NDVIi} = \boldsymbol{A}$, and $(LST_{max})_{NDVIi} - (LST_{min})_{NDVIi} = \boldsymbol{B}$. The $(LST_{max})_{NDVIi}$ and $(LST_{min})_{NDVIi}$ are the maximum and minimum LSTs of pixels which have the same $NDVI^i$ values. $(LST)_{NDVIi}$ denotes LST of a chosen pixel whose NDVI value is $NDVI^i$. Greater VTCI values indicate wet conditions and smaller values indicate dry conditions.

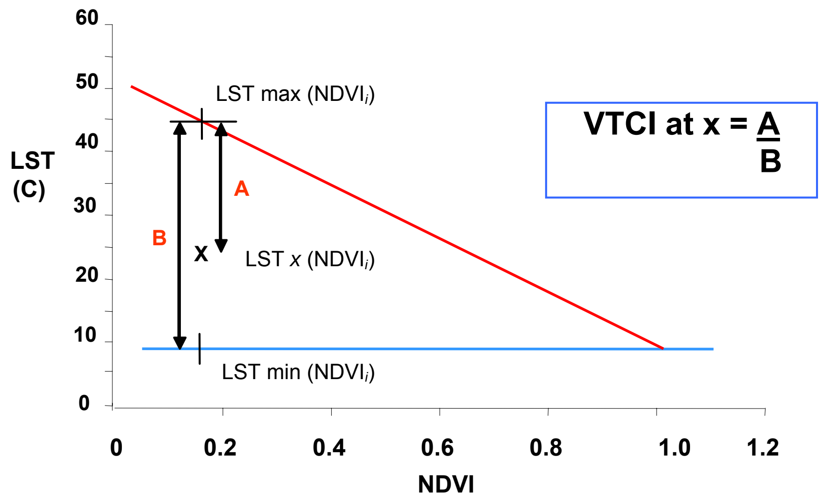

Figure 6.16: Schematic representation of the computation of Vegetation Temperature Condition Index (VTCI).

6.4.1 FIELD OBSERVATIONS OF VTCI CHARACTERISTICS

It is important to understand the behaviour of VTCI characteristics during a year before applying it in soil moisture scaling studies. It is equally important to understand how to interpret the VTCI scatter plots properly. Thus, VTCI characteristics across Goulburn River catchment were studied based on 124 MODIS LST images and 23 images of 16-day MODIS vegetation products for 2004 as shown in Table 6-10. MODIS LST images downloaded at weekly intervals for 2003 were not used for the detailed study as 28 images out of 58 images were contaminated with clouds. All 2003 images were therefore used to evaluate the derived moisture contents. All image analyses were done using ENVI image processing software. Statistical representations called scatter plots were drawn with LST as a function of VI for each selected LST image as shown in Figure 6.17 (All scatter plots are given in the Annex-V).

Table 6-10: Combinations of NDVI images and LST images used for VTCI analyses.

NDVI day	LST image days (2004)	NDVI day	LST image days (2004)
17	3, 8, 9	209	196, 197, 198, 204
33	18, 19, 26, 29, 30, 32	225	210, 211, 222, 223, 224
49	35, 38, 48	241	233, 234, 235, 236, 237, 238
65	51, 52, 58, 59, 60, 61, 64, 65	257	254, 256, 257
81	69, 76, 79, 80	273	260, 261, 262, 265, 266, 270, 271, 272
97	84, 85, 86, 87, 88, 91, 93	289	278, 279, 280, 282, 283, 284, 286, 287, 288, 289
113	99, 101, 104, 106, 109, 110, 111	305	290, 297, 299, 300, 302, 304
129	115, 117, 124, 127, 129	321	308, 317, 318, 319, 320, 321
145	133, 134, 137, 138, 140	337	331, 332
161	150, 151, 152, 156, 157, 158, 161	353	348, 350, 352, 353
177	165, 166, 169, 174	1 (2005)	355, 356, 365
193	179, 181, 182, 183, 184, 185, 190		

The scatter plot in Figure 6.17 shows the full range of soil water content and vegetation fraction in the particular image. Pixels sampled over dense vegetation appear in the bottom right part of the cluster, where temperature is typically close to a mean air temperature (Gillies *et al*., 1997). It indicates that spatial variations in the LST (and therefore the surface energy fluxes) are determined by the distribution of surface soil water content, whose signal is modulated by the vegetation cover. This conclusion was also reached by Friedl and Davis (1994) and Capehart and Carlson (1997).

Examination of a series of scatter plots between LST and VI shows that the land surface when exposed to sunlight dries out very unevenly in space and time, with some pixels experiencing rapid drying and others drying out slowly. The uneven drying results in points first becoming quickly dispersed over the entire triangle. Then over time, the population of pixels shifts towards the upper edge with its higher temperatures and lower moisture availability. This upper boundary is therefore known as the 'warm edge' and it constitutes a physical lower limit to the surface water content (Gillies and Carlson, 1995). The shifting of the pixel population continues until the next precipitation event, after which the pixel distribution shifts back towards the lower boundary (i.e. cold edge or base of the triangle). According to Gillies *et al.*, (1997), pixels undergo large seasonal cyclic variations within the triangle as the surface greens up (e.g. during spring) and then dries out during summer. The relative position of a given pixel within the triangle with respect to the warm edge and cold edge may provide an indication of wetness condition. The warm edge can sometimes be easily recognized by the sharp boundary in the data points on the upper side of the triangle. The cold edge is usually less well defined than the warm edge. The VTCI approach computes the relative position of a given pixel within the triangle.

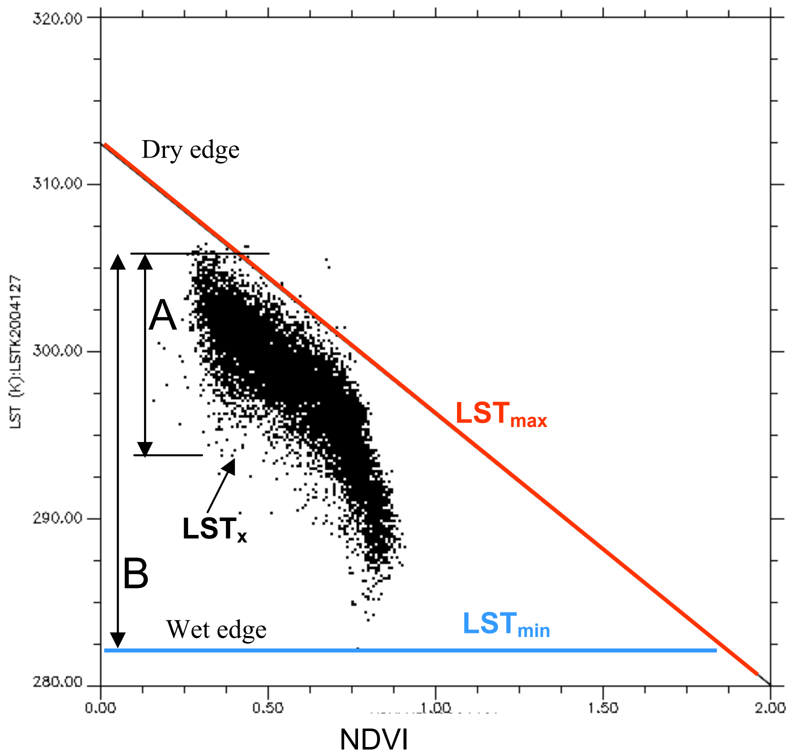

Figure 6.17: A scatter plot of MODIS LST on day 127 and NDVI on day 129 for 2004. LST_{min} is the wet edge and LST_{max} is the dry edge used for the computation of VTCI. VTCI at LST_x is computed as A/B.

The computation of VTCI needs determination of the 'warm or dry edge' (LST_{max}) and the 'cold or wet edge' (LST_{min}). LST_{max} is defined as:

$$\mathbf{LST_{max} = Co + C1 \times NDVI} \qquad \textbf{(6-12)}$$

where Co is the intercept and C1 is the slope.

The determination of the cold edge involves identifying the minimum observed LST over the area and drawing a line through the minimum LST parallel to the x-axis, whereas the determination of the warm edge is more challenging. The dry edge parameters may be determined by first, extracting the maximum temperatures observed for small intervals of VI in the VI-LST space and then, determining the parameters of the sloping side of the upper edge by adopting linear regression techniques. However, in practice this is not efficient due to the concave shape of the triangles or the oval shape of scatter plots particularly during late summer and autumn seasons. Changes of vegetation densities due to the complete drying out in summer and the shedding of leaves in autumn cause gaps in the basic triangular shape of the VI- LST space. The presence of clouds in the selected LST images also contributes to an incomplete triangular shape. The triangular shape is clearly visible during the spring season because of the wide range of NDVI coverage together with a range of soil moisture contents across the catchment. The Goulburn River Catchment is located in a dry region and therefore, scatter plots between LST and VI often display a band-like distribution as seen in Figure 6.17 rather than a triangular shape. For this reason, it may be possible to derive the sloping side of the upper edge adopting linear regression techniques. However, in this study dry edges were determined manually.

For convenience of plotting, it was found that the selection of appropriate scales for the axes is important. Accordingly, the Y-axis scale was set such that the minimum observed LST is close to the lowest point in the Y-axis and the maximum LST of approximately 30-50^{o} higher than the lowest LST. In addition, a maximum VI of about 1.5 to 2.0 was used as the upper limit of the X-axis as shown in Figure 6.17. The main reason for selecting a higher VI value was to accommodate the extended dry edge meeting the X-axis. This was to ensure easy plotting and computation of the slope of the dry edge. Adopting this technique, usually a common dry edge was obtained for near-by dates. It is not uncommon to combine several images and superimposed them with respect to a common warm edge to identify the triangular shape (Capehart and Carlson, 1997). The technique used to identify the dry edge therefore provides the best estimate of the upper boundary.

Following the above methodology, dry edges of the NDVI-LST scatter plots (i.e. LST_{max}) have been defined and the temporal evolution of the properties of these dry edges is presented in Figure 6.18. The observed minimum LST values (i.e. the wet edges) are also shown in the same figure. No publications have been identified which report on studies of temporal characteristics of the NDVI-LST scatter plots. Figure 6.18 therefore characterises the temporal behaviour of VTCI and it can be concluded that: a) the constant (q) of the *linear relationship* follows the same pattern as the minimum temperature, (approximately, constant q = 20°C + minimum LST), b) the lowest q values occur during winter, and the highest q values occur during summer, and c) the slope of the dry edge varies but is always negative.

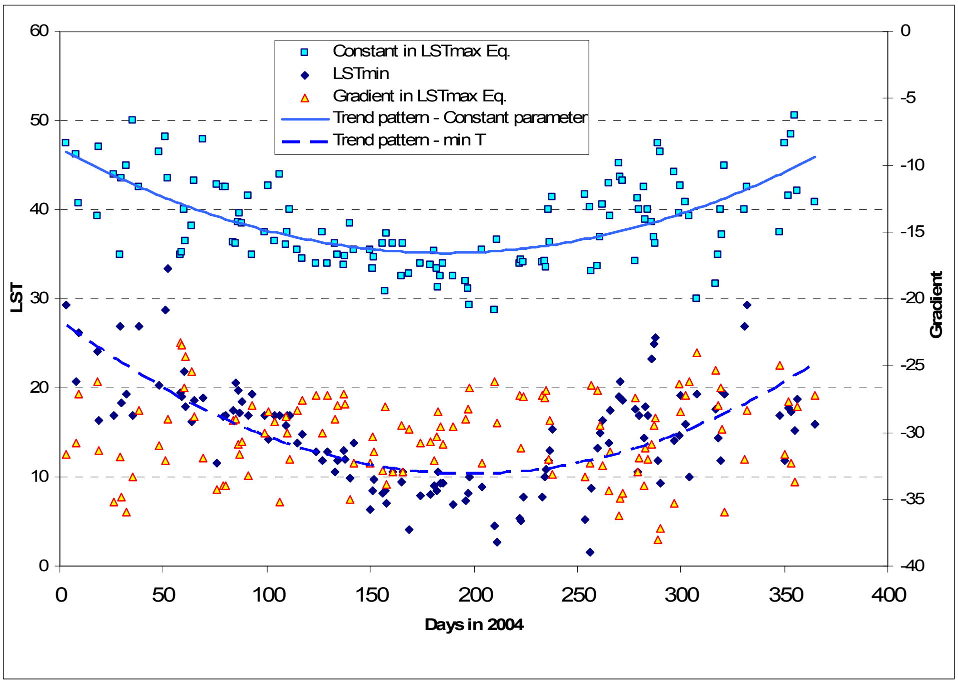

Figure 6.18: Properties of the parameters defining the dry edge modeled as a linear fit to data as LSTmax = a + b NDVI, where a = constant and b = gradient. Temporal pattern of the constant parameter and the minimum temperature during 2004 are also shown in the graph.

It is also important to decide which vegetation index (such as NDVI or EVI) should be used to compute the VTCI. Theoretically, any vegetation index may be used in the computation. In the current study both NDVI and EVI based VTCI values have been computed. Figure 6.19 shows the comparison of approximately 2500 VTCI-EVI and VTCI-NDVI values for 2004. It can be concluded from the figure that EVI and NDVI give similar results.

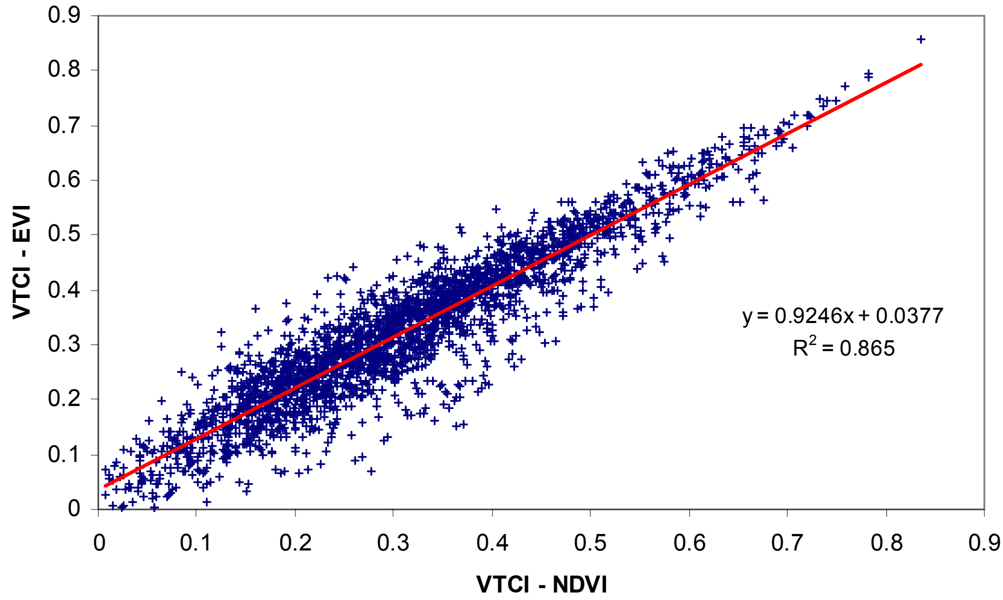

Figure 6.19: Relationship between NDVI-based VTCI and EVI-based VTCI during 2004.

6.4.2 A COMPARATIVE STUDY OF REMOTELY SENSED WETNESS INDICES AND FIELD MEASURED SOIL MOISTURE

The satellite-based wetness indices require field validation. Previous studies with the VTCI have justified their results using information on drought occurrences (Wang *et al.*, 2001) and by analysing historical rainfall patterns (Wan *et al.*, 2004). No published reports have been found reporting on a comparison of VTCI values and field based soil moisture content values on a regional scale. This has been attempted in the current study. Linear regression analyses were conducted for all soil moisture monitoring sites between the computed VTCI for all selected days and the associated soil moisture contents. Furthermore, both NDVI and EVI have been used when computing VTCI to obtain better insight into the selection of a vegetation index for the computation process. In the current study, VTCI computed with NDVI is termed VTCI-NDVI and similarly, VTCI computed with EVI is termed VTCI-EVI. Table 6-11 summarises the results of the linear regression analyses between (a) VTCI-NDVI and field measured SWC, and (b) between VTCI-EVI and SWC for all monitoring sites.

As seen in Table 6-11 (a), in general, VTCI-NDVI shows a positive relationship with measured SWC. 17 sites out of 22 sites showed a regression coefficient (i.e. slopes) greater than 0.10 and at least on 10 occasions the computed regression coefficients were more than 0.25. This gives an indication of the strength of VTCI-NDVI as a moisture indicator. However, five sites showed weaker relationship with regression coefficients of below 0.10. Particularly, at G2, a negative coefficient of -0.08 was reported. This may be attributed to the wrong NDVI signature at this site due to large farm buildings on this property (Note: G2 is located within a commercial horse-breeding centre). When subcatchment scale results are considered, all catchments showed strong positive regression coefficients varying from over 0.36 (Merriwa and Stanley Catchments) to 0.11 (in Krui). Finally, at the whole Goulburn Catchment scale, a positive regression coefficient of 0.26 is observed between VTCI-NDVI and SWC.

Linear regression analyses between computed VTCI-EVI and measured SWC also provide similar results (see Table 6-11 b). Regression coefficients obtained with EVI however, showed more positive coefficients, i.e. apart from G2 all sites showed a regression coefficient of over 0.10. Many sites showed a regression coefficient of more than 0.25 and at some sites, the coefficients were more than 0.50 (G6, M6 and S7). The only site reported with a low coefficient was G2 as previously mentioned. Interestingly, some sites showed regression coefficients which are lower than the VTCI-NDVI. For example, sites such as in M3, M4 and M5 show a decrease in the regression coefficient. When subcatchment scale results are considered, all catchments showed slightly better positive regression coefficients than those obtained from VTCI-NDVI. At the Goulburn Catchment scale, a similar positive regression coefficient of 0.28 was found for VTCI-EVI and SWC.

As can be seen from the table, R^2 values obtained in the linear regressions for both VTCI-NDVI and VTCI-EVI were not very high. This may be attributed to the differences in scales between the observed SWCs and the computed values of VTCI. The positive correlation between SWC and VTCI is a more important observation rather than the R^2 value. Thus, the main purpose of the Table 6-11 is only to determine the nature of the relationship between SWC and VTCI. It is important to note that these regressions are not used to predict SWCs in the catchment as was done with LST-based models.

Another important outcome of this analysis is the behaviour of site S1 and the whole Goulburn catchment. As seen from the Table 6-11, the regression equations developed for the site S1 and for the Goulburn catchment show similarity. S1 was found to be the representative CASMM site for the entire Goulburn Catchment (see Section 5.2.1) and the present finding suggests that the identification of CASMM site from point-scale data has some validity and may have practical meaning, even at the pixel-level.

Table 6-11 : (a) Properties of the linear relationships between VTCI-NDVI and field measured SWC for all soil moisture monitoring sites. (2004 data)

	VTCI based on NDVI			95% Confidence Interval	
Site	Coefficient	Constant	R^2	Coefficient	Constant
G1	0.0382	0.1292	0.0054	-0.072-0.148	0.098-0.161
G2	-0.0767	0.2851	0.0154	-0.204-0.050	0.234-0.337
G3	0.3302	0.2011	0.2267	0.195-0.465	0.146-0.256
G4	0.3284	0.0007	0.1489	0.173-0.484	-0.058-0.059
G5	0.2291	0.0141	0.2161	0.145-0.313	-0.017-0.045
G6	0.4392	0.1670	0.2103	0.269-0.610	0.115-0.219
K1	0.0649	0.3703	0.0456	0.008-0.122	0.352-0.388
K2	0.0653	0.0724	0.0284	-0.006-0.136	0.052-0.093
K3	0.2427	0.2719	0.0841	0.097-0.389	0.229-0.315
K4	0.3308	0.1879	0.1365	0.178-0.484	0.144-0.232
K5	0.1384	0.1207	0.0141	-0.070-0.347	0.033-0.209
K6	0.1196	0.1898	0.0522	0.024-0.215	0.137-0.243
M1	0.1264	0.0672	0.0980	0.057-0.196	0.045-0.090
M2	0.0961	0.0542	0.0536	0.019-0.173	0.035-0.073
M3	0.1843	0.1885	0.1088	0.092-0.300	0.165-0.209
M4	0.3049	0.1400	0.1790	0.188-0.430	0.116-0.164
M5	0.3456	0.1034	0.3038	0.250-0.441	0.086-0.121
M6	0.4372	0.0776	0.1364	0.237-0.638	0.016-0.139
M7	0.1867	0.2598	0.0845	0.070-0.303	0.195-0.324
S1	0.2592	0.1428	0.1963	0.166-0.368	0.115-0.167
S2	0.3002	0.1656	0.2210	0.188-0.412	0.132-0.199
S7	0.4868	0.1042	0.1963	0.297-0.695	0.050-0.156
Sub catchments					
S. Goulburn	0.2461	0.1148	0.0575	0.159-0.323	0.088-0.147
Krui	0.1073	0.2072	0.0166	0.074-0.138	0.185-0.234
Merriwa	0.3840	0.0840	0.2970	0.349-0.430	0.070-0.096
Stanley	0.3610	0.1274	0.2081	0.285-0.445	0.111-0.155
Whole catchment	0.2575	0.1346	0.0953	0.219-0.282	0.127-0.148

Table 6-11: (b) Properties of the linear relationships between VTCI-EVI and SWC for all soil moisture monitoring sites. (2004 data).

	VTCI based on EVI			95% Confidence Interval	
Site	Coefficient	Constant	R^2	Coefficient	Constant
G1	0.1940	0.0866	0.1192	0.088-0.302	0.053-0.116
G2	0.0510	0.2356	0.0059	-0.084-0.186	0.180-0.291
G3	0.3474	0.1890	0.2705	0.221-0.473	0.136-0.242
G4	0.3754	0.0173	0.1866	0.231-0.533	-0.079-0.036
G5	0.2605	-0.0034	0.3199	0.188-0.333	-0.033-0.026
G6	0.5110	0.1387	0.2899	0.351-0.671	0.087-0.190
K1	0.1099	0.3552	0.1411	0.058-0.162	0.338-0.372
K2	0.1074	0.0596	0.0774	0.039-0.176	0.039-0.080
K3	0.3321	0.2434	0.1661	0.196-0.468	0.202-0.285
K4	0.4693	0.1431	0.2708	0.330-0.606	0.100-0.184
K5	0.2386	0.0758	0.0445	0.039-0.439	-0.012-0.163
K6	0.1598	0.1659	0.0866	0.063-0.257	0.111-0.221
M1	0.1511	0.0558	0.1505	0.086-0.217	0.033-0.078
M2	0.1335	0.0416	0.1287	0.067-0.200	0.023-0.060
M3	0.1834	0.1825	0.1324	0.098-0.284	0.158-0.204
M4	0.2981	0.1320	0.2087	0.189-0.407	0.107-0.157
M5	0.2988	0.1051	0.2870	0.213-0.385	0.088-0.123
M6	0.5106	0.0447	0.1930	0.320-0.701	-0.018-0.107
M7	0.1922	0.2599	0.1033	0.085-0.300	0.202-0.318
S1	0.2904	0.1369	0.3405	0.214-0.370	0.117-0.157
S2	0.3480	0.1483	0.3180	0.247-0.449	0.117-0.179
S7	0.5654	0.0800	0.3072	0.386-0.726	0.039-0.132
Sub catchments					
S. Goulburn	0.3027	0.0919	0.0879	0.217-0.377	0.064-0.124
Krui	0.1546	0.1909	0.0368	0.134-0.186	0.168-0.228
Merriwa	0.3902	0.0743	0.2836	0.354-0.440	0.059-0.087
Stanley	0.4071	0.1135	0.3173	0.338-0.472	0.103-0.140
Whole catchment	0.2797	0.1237	0.1109	0.240-0.303	0.116-0.138

Analysis of the temporal behaviour of VTCI and its response to the different soil moisture regimes requires careful analysis of computed VTCI and measured SWCs. Figure 6.20 compares computed VTCI and measured SWC at G4 during 2004. As seen in the figure, the observed overall tendency for the VTCI was to be high immediately after rainy days, to be low before rainy days, and to take intermediate values during longer dry periods (e.g. day 61 – 151 in Figure 6.20). Furthermore, as seen in Figure 6.20 because of the considerable scatter, the point-scale observations of surface soil moisture contents are not well defined with VTCI probably due to the differences of scale between the data sources.

Therefore, it may require other approaches such as use of cumulative data for analysis. Cumulative plots help understanding long-term trend patterns. These plots illustrate that a certain change in SWC will yield the same pattern of change in VTCI irrespective of the actual SWC value. Surprisingly, when cumulative values are analysed, as shown in the Figure 6.21, a positive relationship can be seen between cumulative VTCI and cumulative SWC. Furthermore, such cumulative plots may be useful to identify wet sites (e.g. K3) and dry sites (e.g. G4) and compare them with the CASMM site (S1). It therefore appears that cumulative VTCI values provide better indication of soil moisture status than the individual VTCI values.

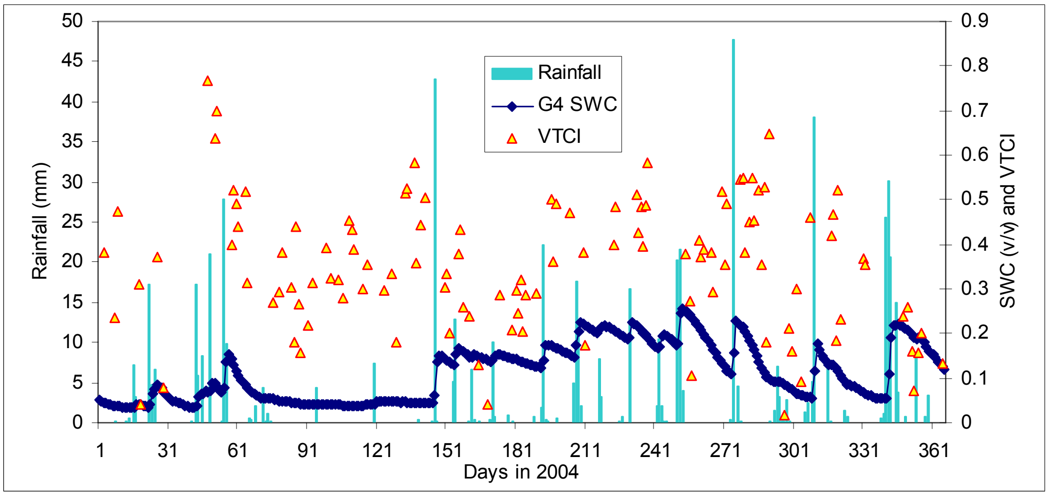

Figure 6.20: Temporal pattern of rainfall, soil moisture and computed VTCI at G4 during 2004.

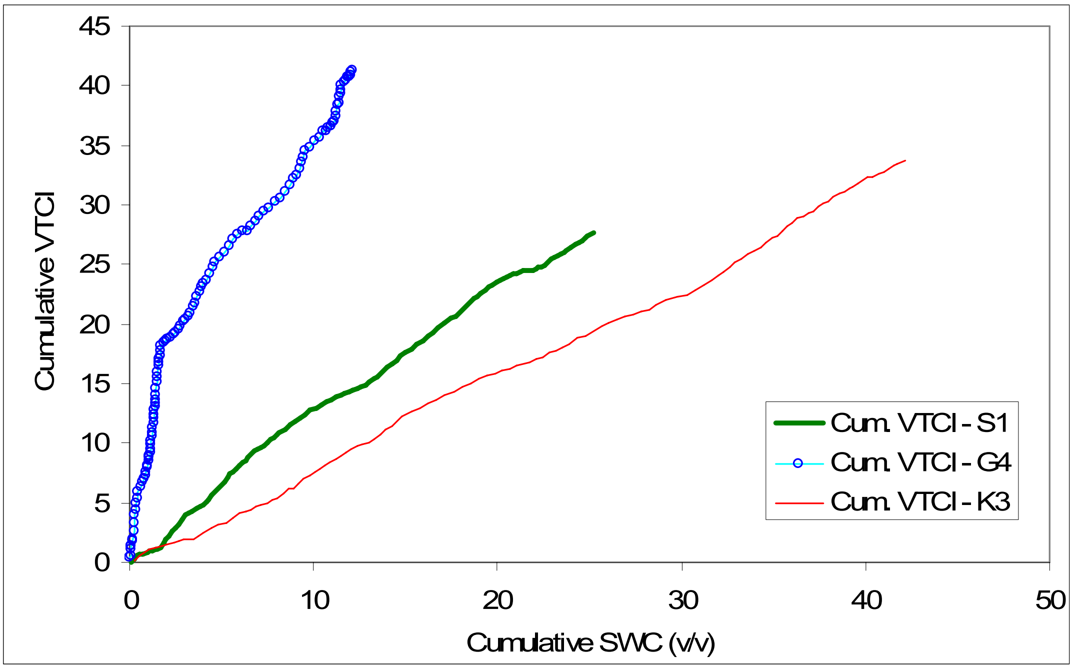

Figure 6.21: Cumulative soil water contents and cumulative VTCI at S1, G4 and K3 during 2004.

Further analysis considering all 22 soil moisture monitoring sites together with spatial and temporal distributions of computed VTCI values may also help understanding the strengths of a wetness index. Figure 6.22 shows the results of measured SWC (Figure 6.22 (a)) and computed VTCI-NDVI (b) and VTCI-EVI (c) for the whole Goulburn River catchment based on 22 locations during 2004. Considerable scatter can be seen in VTCI values when all 124 days at each station are considered. For easy understanding of the results and to show the magnitude of spatial variations, mean values ±1SD are given for each day. As can be seen there is similarity with respect to the evolution of VTCI-NDVI (Figure 6.22b) and VTCI-EVI (Figure 6.22c). A similar degree of correspondence can be also observed with respect to the higher and lower values of SWCs (Figure 6.22a) and VTCI (Figure 6.22b and c). Therefore, temporal patterns of VTCI can explain the temporal pattern of soil water contents. Furthermore, Figure 6.22 is useful in explaining the range of variability of a wetness index. The range of variability of measured SWCs and computed VTCI throughout the study period is similar.

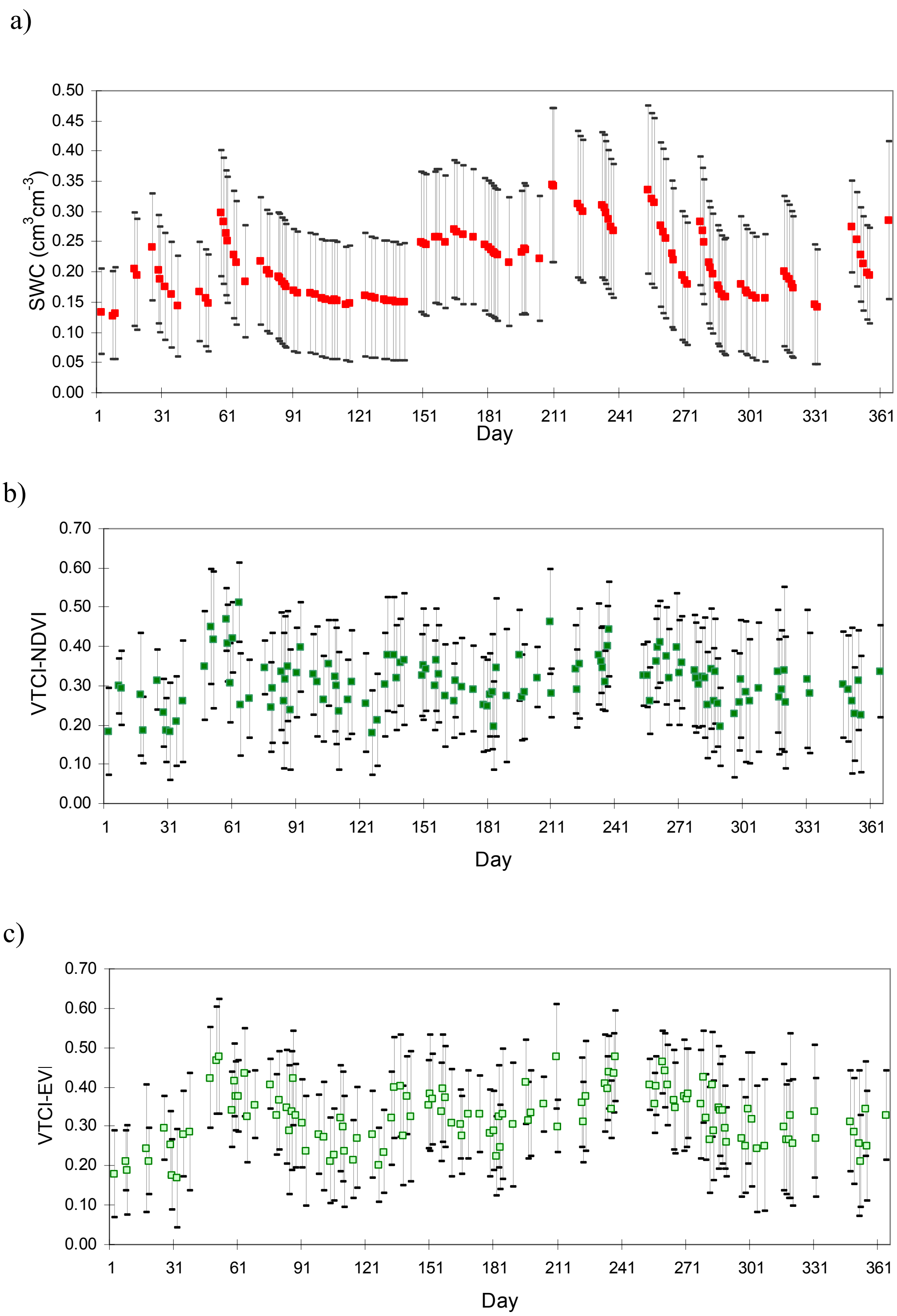

Figure 6.22: Temporal behaviour and range of variability of: a) field measured SWC, b) NDVI-based VTCI, and c) EVI-based VTCI for selected 22 locations in the Goulburn River catchment during 2004 (error bars to show ±1 standard deviation).

The relationship between the means of measured SWC and means of computed VTCI also shows a positive trend. As shown in Figure 6.23, despite the scatter of data points, both VTCI-EVI and VTCI-NDVI show a positive relationship with measured SWC. Furthermore, it can be seen that the VTCI-EVI explains the SWC better than the VTCI-NDVI. Wetness indices such as VTCI-EVI and VTCI-NDVI therefore provide wetness characteristics of selected locations or provide information on the variability of the wetness in a given catchment. From these results, it appears that the VTCI is providing meaningful information on surface wetness conditions in a given catchment.

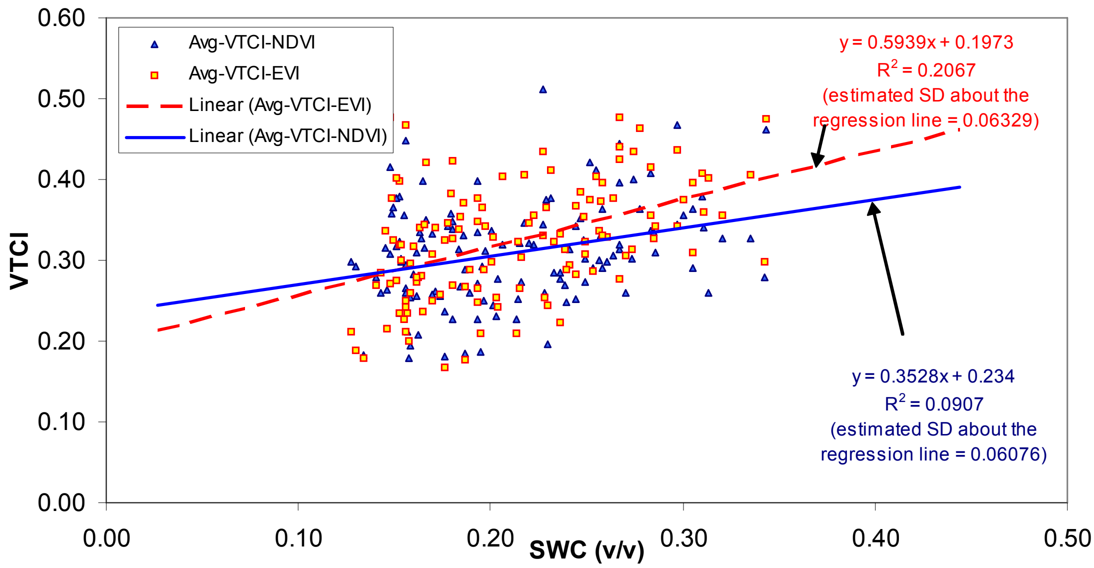

Figure 6.23: Relationship between the means of measured SWC and means of computed VTCI based on 22 sites.

Wetness indices however provide a *relative* value of moisture conditions and this information needs to be converted into actual water contents. One way of converting the wetness index value into actual soil moisture content is the use of field measured soil moisture data. It is possible to convert for an individual day VTCI values into actual SWC values if soil water content is known for at least at one location with some degree of confidence. The ratio of actual moisture content over the computed VTCI at any known location *on a given day* should provide a conversion factor to derive SWCs from VTCI. The field-monitoring network of the present study provides 22 pixels to be used for this purpose. The most appropriate choice however, is to consider the use of soil moisture contents measured at a CASMM site. S1 is the CASMM site for the whole Goulburn River catchment (see Section 5.3.1) and for the Stanley subcatchment (see Section

5.3.5). In this study therefore, measured soil water contents and computed VTCI at S1 have been used to derive the conversion factors.

One of the major limitations to the ability of land surface schemes to estimate runoff is uncertainty in the parameterisation of soil moisture contents over a range of modelling scales. One way of dealing with this situation would be to use a wetness indicator for soil moisture scaling studies. Indices such as VTCI can be used to compute the wetness at a range of satellite or airborne footprints scales. These indices can then be used to derive catchment-scale average soil moisture contents. Based on the results presented in the Figure 6.22 and Figure 6.23, it can be argued that VTCI is capable of describing the variability of surface wetness conditions within a large area such as the Goulburn River catchment and may be considered as a surrogate variable for soil moisture scaling applications. Furthermore, considering the above results, it can be seen that both VTCI-NDVI and VTCI-EVI provide similar results but that VTCI-EVI performs slightly better.

6.4.3 APPLICATIONS OF VTCI-BASED MODELS FOR CATCHMENT SCALE SOIL MOISTURE RETRIEVAL

It is useful to evaluate the conclusions derived from VTCI-based relationships that have been developed with 2004 data, with similar data from another year. Thus, MODIS LST and vegetation data acquired for year 2003 and the measured soil moisture for the same period have been used to evaluate the strengths of VTCI as a soil moisture predictor. As shown in Table 6-2 not all MODIS LST images (58) downloaded on weekly basis were suitable for the VTCI computation due to higher percentage of clouds. Only 28 LST images could be considered. Following the methodology developed with 2004 data, wet edges and dry edges of the VI-LST scatter plots were defined. Derived wet edges and the properties of the linear equations describing the dry edges are presented in Table 6-12. Based on the dry edge and wet edge, for all selected days, VTCI values were computed for all the pixels which contain monitoring sites. The computed VTCI values were then converted into ‘predicted SWCs’ using the measured SWC at the CASMM (S1) site.

Figure 6.24 shows the scatter diagrams of measured (in X-axis) and predicted (in Y-axis) SWC based on NDVI and EVI VTCI models respectively. This figure is based on the data from all cloud-free pixels over the monitoring sites from 2003 data set (i.e. from 28 days). The results show a positive regression coefficient of 0.52 with NDVI and 0.45 with EVI between measured and predicted SWC. Considering the longer time scale used in the analyses (i.e. the whole 2003 data set), it can be concluded that the results are encouraging. It is also evident that the predicted SWC values provide a wider range of values. However, due to limited number of data points used, there is considerable scatter in the data.

Table 6-12: Minimum LST and the properties of the linear equations used to estimate the maximum LST at each vegetation index level during 2003.

		Linear equation parameters used to derive LST_{max}			
Day #	LST_{min}	NDVI		EVI	
	(^oC)	Constant	Gradient	Constant	Gradient
14	14.4	71.8	-40.00	71.8	-54.55
21	22.7	78.1	-37.50	74.3	-40.08
42	18.8	76.8	-40.00	69.3	-40.08
77	14.9	61.8	-30.00	61.8	-39.22
84	9.3	63.1	-28.13	59.3	-34.31
91	11.1	63.1	-28.13	59.3	-34.31
105	14.1	41.8	-17.50	41.8	-22.88
112	10.2	44.3	-18.75	41.8	-22.88
133	9.0	36.8	-15.00	36.8	-19.61
168	10.0	31.8	-12.50	31.8	-16.34
196	10.9	34.3	-13.75	34.3	-17.97
210	4.6	34.3	-16.25	34.3	-21.24
217	8.8	39.3	-16.25	39.3	-21.24
231	3.6	39.3	-18.75	39.3	-24.51
245	6.0	46.8	-22.50	46.8	-29.41
252	8.1	46.8	-20.00	46.8	-26.14
273	1.3	51.8	-27.50	51.8	-35.95
280	7.9	36.8	-15.00	36.8	-19.61
287	7.4	41.8	-17.50	41.8	-22.88
308	14.6	51.8	-20.00	51.8	-26.14
309	18.7	56.8	-20.00	56.8	-26.14
313	9.8	61.8	-27.50	61.8	-35.95
315	7.7	61.8	-27.50	61.8	-35.95
322	14.6	61.8	-25.00	61.8	-32.68
329	7.8	51.8	-22.50	51.8	-29.41
343	14.6	66.8	-27.50	61.8	-32.68
357	23.0	64.3	-21.25	61.8	-26.14
364	22.6	64.3	-21.25	61.8	-26.14

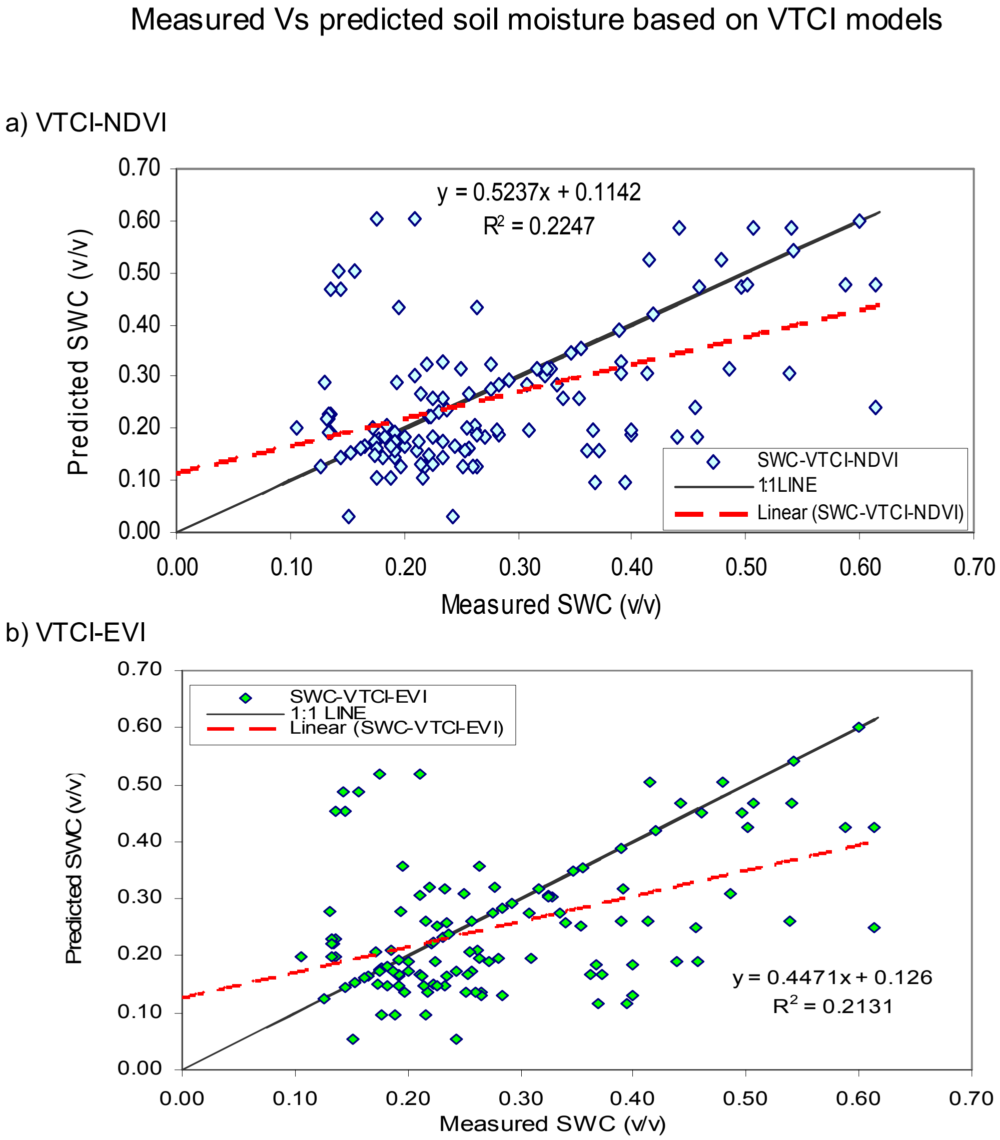

Figure 6.24: Measured SWC Vs computed SWC in 2003 based on VTCI model developed for the entire Goulburn River catchment computed with: a) NDVI and b) EVI. (Measured SWC on X-axis and computed SWC on Y-axis).

To better understand the VTCI model performances, error analyses were done and the frequency distribution of errors in predicting SWCs are shown in Figure 6.25 for NDVI-based and EVI-based VTCI models. From the error analyses, we can conclude that:

1. Both VTCI models have some potential in predicting the measured SWC.

2. Reasonably good SWC predictions may be obtained when a higher error level (e.g. ±0.05 cm^3cm^{-3}) is allowed.

3. Errors of SWC predictions using VTCI-NDVI and VTCI-EVI show near-normal distribution.

As with the LST based models, VTCI-SWC models may also sensitive to seasonal weather patterns. Figure 6.26 shows the temporal response and the magnitude of model errors for NDVI-based and EVI-based VTCI respectively. It is evident that model prediction errors show some degree of sensitivity to date (as indicated by day number), as was the case for LST based models.

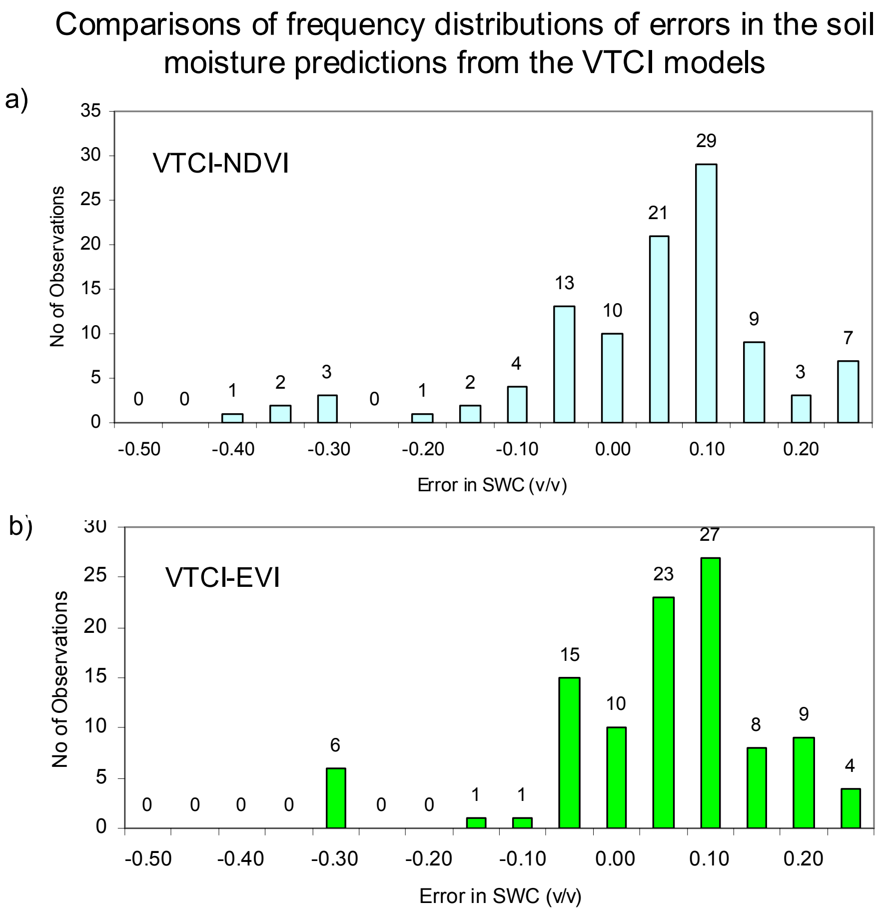

Figure 6.25: Frequency distribution of errors in the soil moisture predictions for 2003 from VTCI-SWC models based on: a) NDVI and b) EVI.

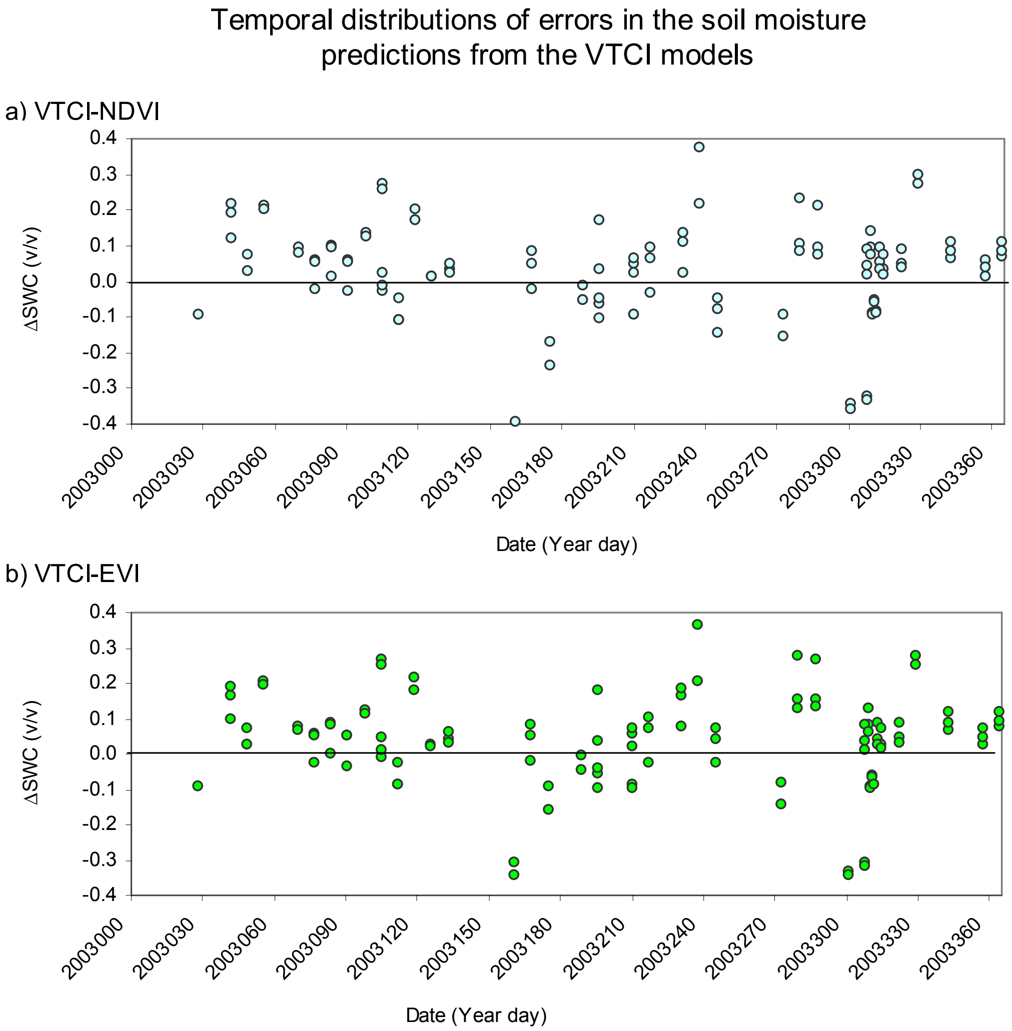

Figure 6.26: Temporal distribution of errors in the soil moisture predictions for 2003 from VTCI-SWC models based on: a) NDVI and b) EVI.

6.5 EVALUATION OF DERIVED SOIL MOISTURE PATTERNS

Upscaling of point-scale *in-situ* soil moisture measurements has been investigated with the thirteen approaches developed in preceding sections. Eight approaches use only remotely sensed LST observations (Daytime LST, Nighttime LST, ΔLST and RNTI; each with SWC and NDWI), four approaches use remotely sensed LST observations and measured air temperature (Daytime LST and Nighttime LST with SWC and NDWI), and the last approach is based on the combined use of LST and VI. In the previous sections, all these models have been evaluated with the data from point scale measured values and it was found that these models predict SWCs with various degrees of accuracy. It is often more useful, especially when dealing with soil moisture, to study the soil moisture patterns across a catchment than considering selected locations. Predicted soil moisture patterns may be used for interpreting the organization of soil moisture fields within a catchment in response to various climatic events. To better understand the performance, all these upscaling models have been used to generate surface moisture patterns.

In order to improve the quality of regression equations used in LST based models (both SWC-based and NWDI-based models) new regression equations have been developed considering all 25 sites by also including the five sites hitherto used as test sites (see Annex-VI for details). A significant improvement of R^2 values has been noted in all equations suggesting that higher number of *in-situ* measurements is potentially useful in establishing reliable regression equations. These new equations were used to predict the SWC for the selected dates.

Three dates have been selected in 2004 for which spatial patters of SWC have been generated. The dates were selected based on their hydrological importance and to capture a range of SWCs as shown in Table 6-13 and also in Figure 6.27. The first selected date was day 58 (27 February). This chosen time was a few days after an unevenly distributed rain event, which brought rain mainly to the northern and southern parts of the catchment (Figure 6.27).

The spatial pattern of SWC after a long dry period is of interest in a sub-humid catchment. The second date (day number 115, 24 April) was representative of long dry spell conditions as no rain during the previous 7 days and only 3 mm of average rainfall fell during the previous 30 days period.

The third day was selected to represent an intermediate situation without rain in the previous week but with reasonable rain during the previous month. Day 262 (18 September), had no rain during the previous 7 days but 52 mm rainfall in the previous 30 day period. During this month, rain mainly occurred in the south western part of the catchment (Figure 6.27).

It can be noted that these three dates also represent three seasons; viz. end of summer (day 58), mid-autumn (day 115) and early spring (day 262) respectively. The comparison of soil water contents maps generated for these three days with the monthly rainfall patterns may therefore assist in appraising the upscaling methods developed in the current study.

Table 6-13: Selected dates in 2004 for catchment-scale soil water distribution maps, associated rainfall during past 7 days and past 30 days period, and reasons for the selection.

Selected day	Average rainfall (mm) during previous 7 / 30 days	Comments on selected dates
58 (27 Feb)	72 / 109	After an unevenly distributed rain event; at the end of summer
115 (24 Apr)	0 / 3	After dry period; during mid- autumn
262 (18 Sep)	0 / 52	Situation towards the end of a recharge period; during early spring

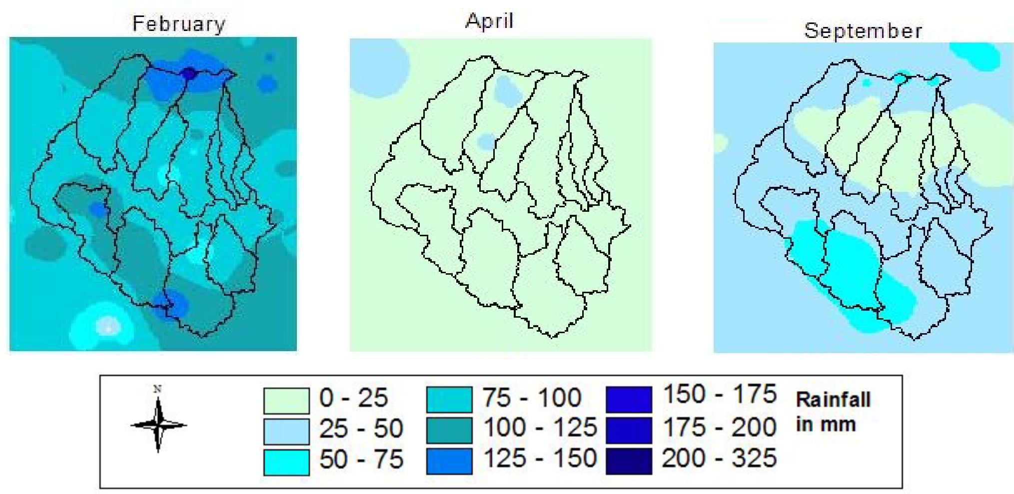

Figure 6.27: Rainfall distribution in the study catchment during February, April and September 2004 (see Section 3.6 and Figure 3.16 for more details).

Figure 6.28 summarises the results of the application of all the models to the Goulburn River catchment on day 58. Similarly, Figure 6.29 and Figure 6.30 summarize the predicted soil water distributions on day 115 and day 262 respectively. These results are based on 0-30cm (root-zone) SWCs. During the process of converting the computed NWDI into SWC values, published values for maximum soil water content of six major soil types were used. The major soils in the Goulburn River catchment are clay, clay loam, loam, sand, sandy clay and sandy loam soils and the saturation water content of these soils are 0.385, 0.389, 0.436, 0.417, 0.321, and 0.412 cm^3cm^{-3} respectively. The conversion of VTCI into

SWC also requires reference soil water content values. In this study, measured soil water content from the catchment scale CASMM site (e.g. S2) has been used to convert VTCI into SWC values. LST based models however, do not require any measured SWC from a CASMM site.

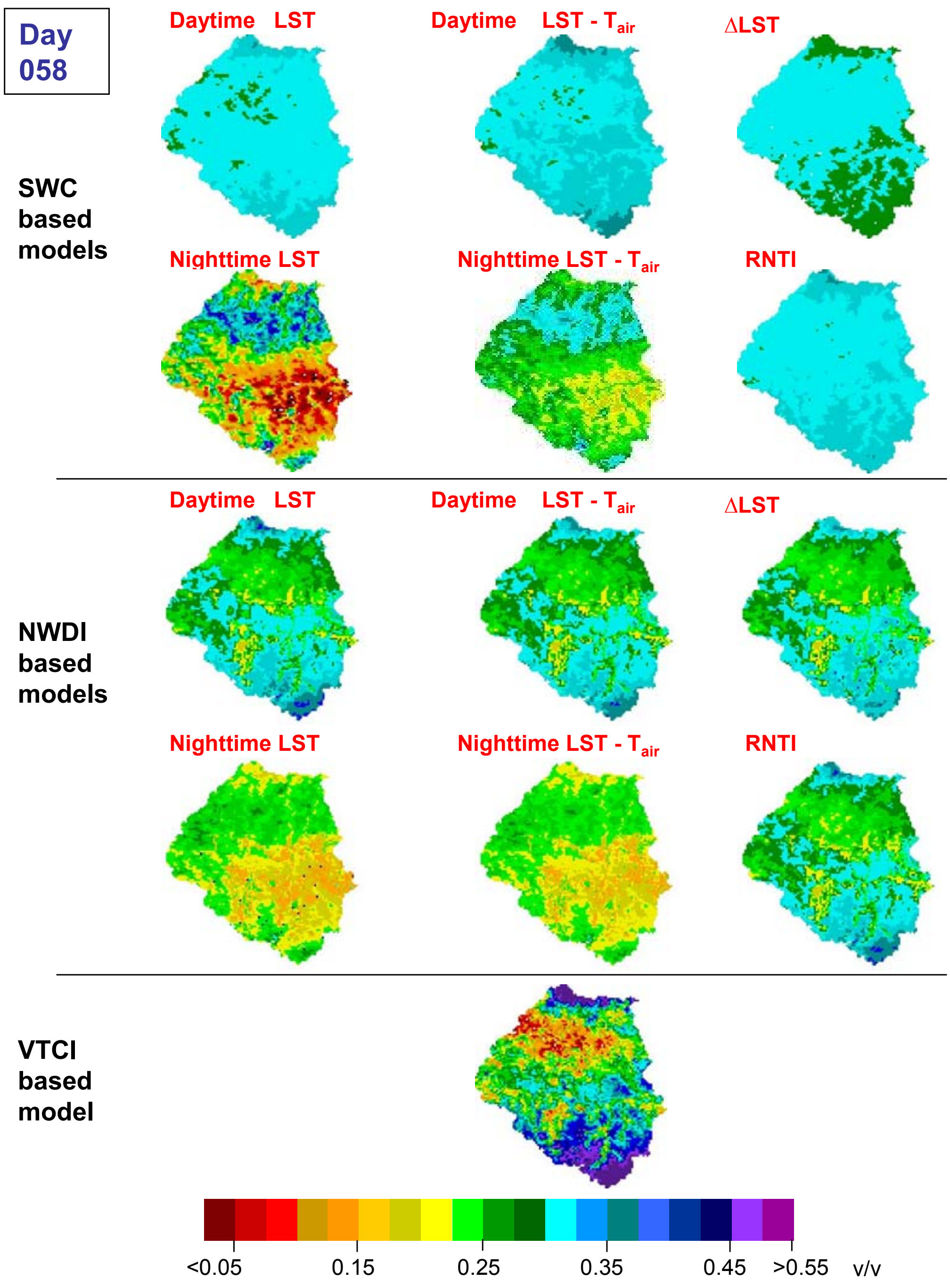

Figure 6.28: Spatial patterns of soil water contents (0-30cm) within the Goulburn River catchment derived from the various models for days 58 in 2004.

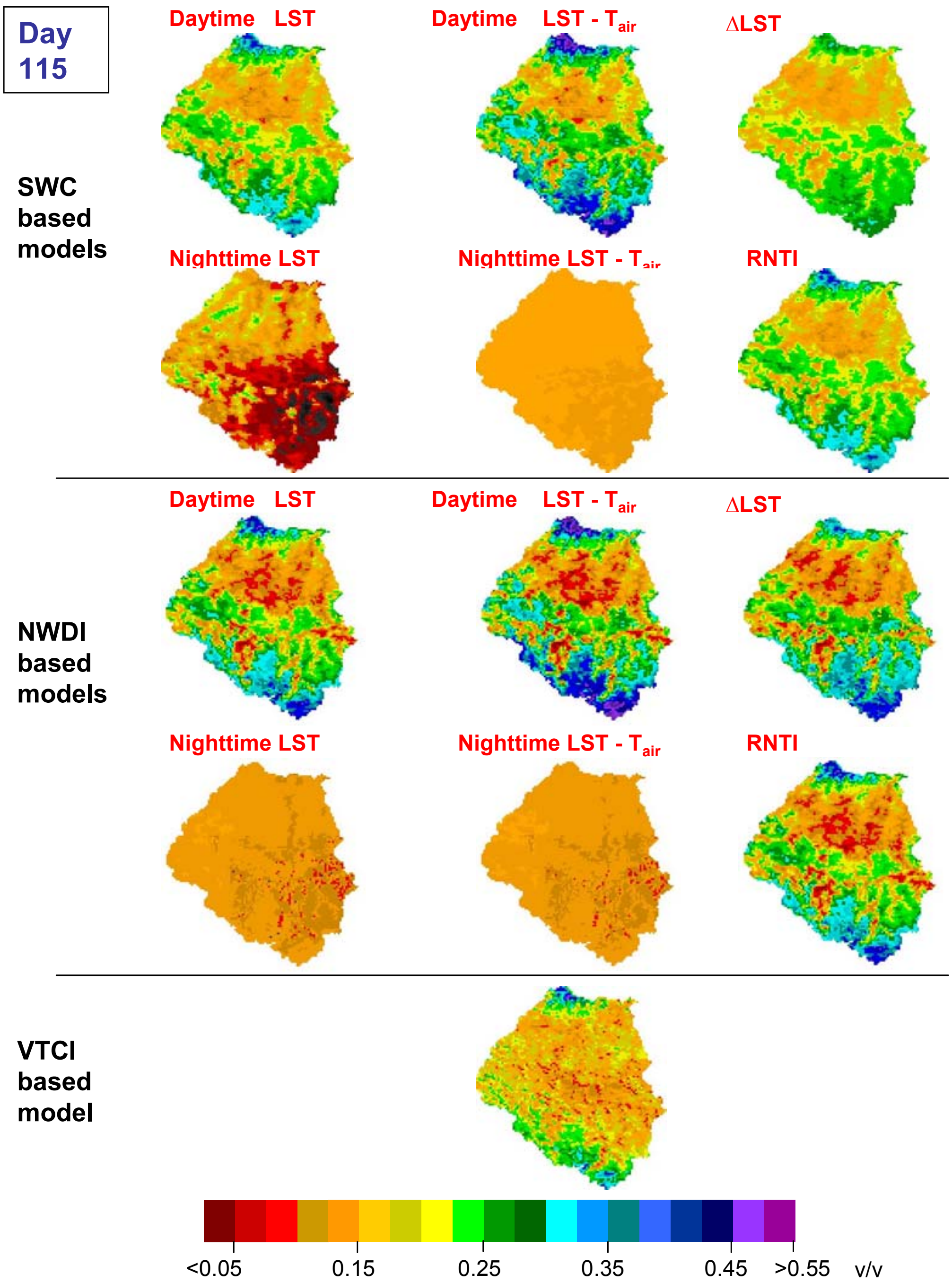

Figure 6.29: Spatial patterns of soil water contents (0-30cm) within the Goulburn River catchment derived from the various models for days 115 in 2004.

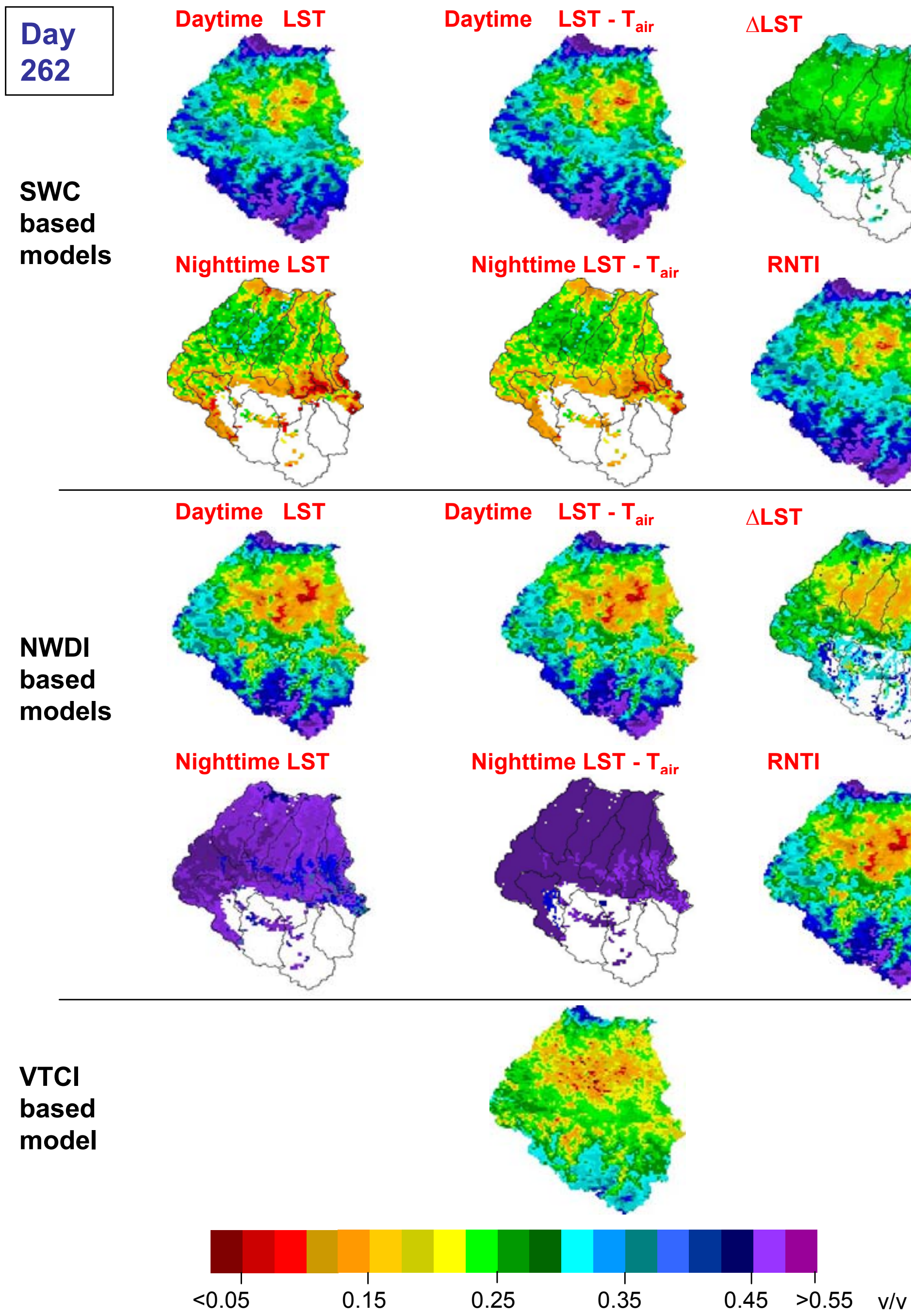

Figure 6.30: Spatial patterns of soil water contents (0-30cm) within the Goulburn River catchment derived from the various models for days 262 in 2004.

In order to gain better insight at the subcatchment scale soil water distributions, VTCI based SWC maps are also given for the Krui and Merriwa subcatchments (Figure 6.31). During the process of converting the computed VTCI into SWC values, measured SWCs of K4 and M4 have been used for the Krui and Merriwa catchments respectively, because these sites have been identified as the CASMM sites in the Krui (K4) and Merriwa (M4) subcatchments.

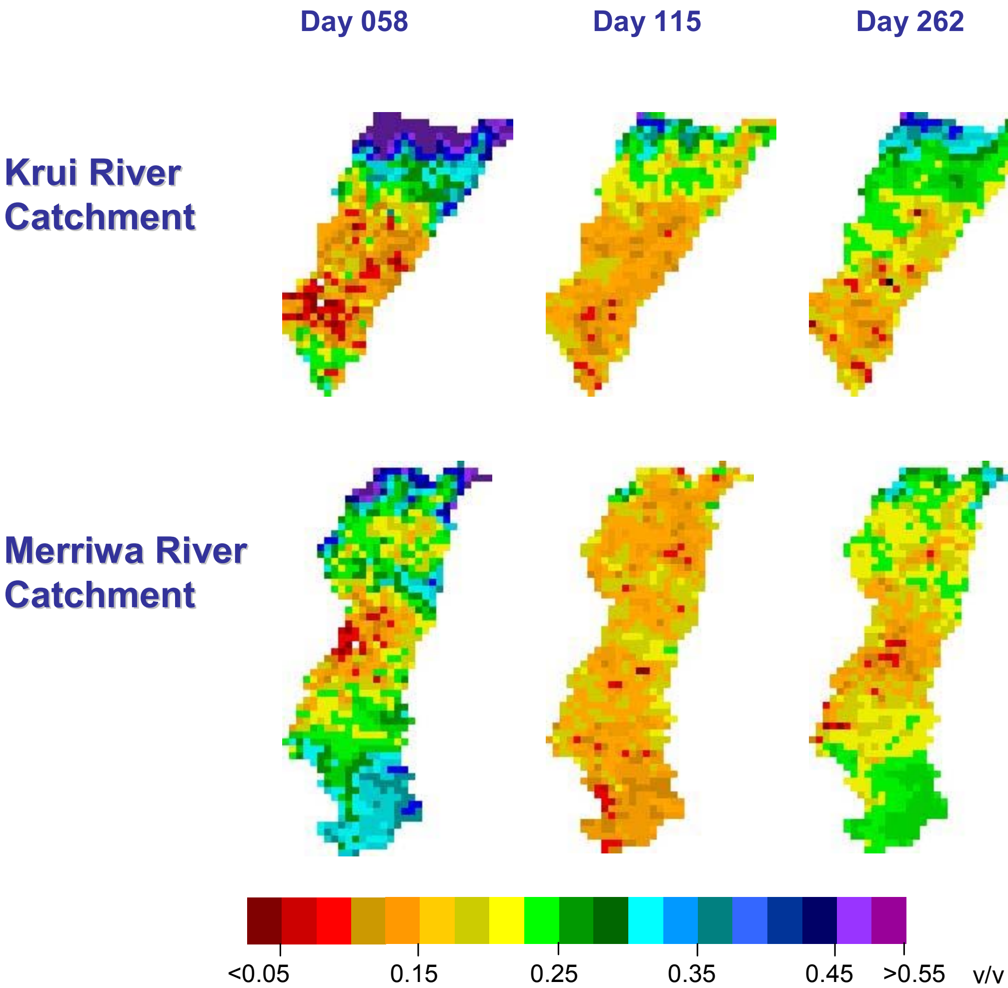

Figure 6.31: Spatial patterns of soil water contents (0-30cm) within the Krui and Merriwa River catchments derived from the VTCI models for days 58, 115 and 262 in 2004.

At first glance, it is clear that all these models are capable of providing some information on SWC variation across the catchments. More careful investigation reveals that the level of detail in the spatial patterns increases in the following sequence: 1) SWC-based models 2) NWDI-based models, and 3) VTCI. This trend is consistent for all three days selected. Thus, it confirms that the consideration of soil and vegetation information is vital for detailed predictions from LST based models.

It appears from Figure 6.28-6.31 that the surface water content patterns across a catchment can be generated from a combined use of a limited number of ground-based soil moisture measurements and remotely observed LST and VI. Unfortunately, no field measured SWC values at the pixel scale of 1.1 km^2 are available for critical comparison with the predicted values. The results obtained with these models however can be explained with three approaches: comparison with the environmental observations (i.e. observed rainfall), with the range and average of predicted values, and with the details in the derived patterns.

First, the derived SWC maps may be compared with the rainfall distribution maps. SWC patterns on day 58 can be compared with the rainfall distributions during February 2004 (see Figure 6.27). During this month, more rain occurred across the northern and the southern parts of the catchment and this is clearly reflected in the wetter areas in the VTCI-based map on day 58. All LST (only) based models are poor in describing the driest and wettest parts of the catchment, particularly on day 58 and the patterns cannot be compared with the distribution of rainfall. In case of NWDI and daytime LST based models however, these wet areas are visible but not as prominent as with the VTCI.

Similarly, due to absence of a major rain event during April, the VTCI-based SWC pattern map on day 115 shows a drier catchment than those obtained with the daytime LST based models. The SWC map derived with the VTCI model on day 262 shows a pattern similar to the rainfall distribution in September (see the September map in Figure 6.27). The rainfall map shows that the northern half of the Goulburn catchment received less rain than the other parts. As seen in the VTCI map on day 262, the derived SWC clearly indicates this difference. In case of NWDI (or SWC) and daytime LST based models however, soil moisture variations due to this rainfall pattern is unclear.

The LST models used in this study do not consider the effect of vegetation on soil moisture predictions. This implies that LST alone is not sufficient for predicting soil moisture and that vegetation information must be considered. Furthermore, including vegetation information gives more information on the moisture status in the soil profile than at the surface layer alone. Soil moisture prediction models are more useful if the models are capable of considering deeper layers than the surface layer. The VTCI model considers both LST and vegetation for predicting the root-zone soil moisture content and a wide range of moisture patterns could therefore be obtained.

Second, the actual SWCs predicted at the Goulburn River catchment scale also help to evaluate the performance of the thirteen models developed in the current study. Table 6-14 summarises for each of the three days the results of computed average SWCs for the Goulburn River catchment based on these models. As a reference, the average SWC based on the field measurements at the 25 sites and the SWC at the CASMM site (S1 in case of Goulburn River Catchment) are also given in the table. It is shown that, the average SWCs derived with the VTCI-based method and calculated from the field measured SWC are comparable. The catchment-scale SWC values derived from the VTCI method are similar to the measured water content at CASMM site S1. Furthermore, during some occasions such as on day 58, a similar standard deviation may obtained for the measured (0.102) and predicted (0.114) SWCs. It is also found that approximately, over 86 % of the computed SWC values from VTCI method were within 0.18 cm^3cm^{-3} (SWC observed at the temporally stable driest site, M1) and 0.41 cm^3cm^{-3} (SWC observed at the temporally stable wettest site, S3) on day 262. The other methods however, produce either low (day 58 and 262) or higher (day 115) water contents. According to this study, the VTCI approach is capable of predicting the catchment average soil water content within ±0.03 cm^3 cm^{-3} accuracy.

Table 6-14: Comparison of statistics among predicted soil water contents from the all models and the field measured soil water contents.

Day	Model type		Avg.	Min.	Max.	SD.
58	LST and SWC	Daytime LST	0.315	0.284	0.352	0.010
		Daytime LST-Ta	0.325	0.285	0.374	0.013
		Nighttime LST	0.217	0.003	0.569	0.097
		Nighttime LST-Ta	0.265	0.168	0.403	0.038
		Δ LST	0.304	0.279	0.328	0.008
		RNTI	0.321	0.293	0.355	0.009
	LST and NWDI	Daytime LST	0.289	0.180	0.395	0.039
		Daytime LST-Ta	0.285	0.183	0.382	0.036
		Nighttime LST	0.221	0.129	0.417	0.034
		Nighttime LST-Ta	0.222	0.138	0.308	0.029
		Δ LST	0.287	0.186	0.425	0.037
		RNTI	0.284	0.175	0.391	0.039
	VTCI and SWC	VTCI	**0.289**	0.002	0.759	0.114
	Measured SWC	**All sites**	**0.306**	**0.127**	**0.429**	**0.102**
		CASMM site (S1)	**0.216**			
115	LST and SWC	Daytime LST	0.216	0.089	0.414	0.058
		Daytime LST-Ta	0.250	0.070	0.528	0.082
		Nighttime LST	0.117	0.000	0.276	0.059
		Nighttime LST-Ta	0.153	0.143	0.164	0.004
		Δ LST	0.209	0.112	0.317	0.042
		RNTI	0.221	0.096	0.416	0.057
	LST and NWDI	Daytime LST	0.210	0.033	0.473	0.082
		Daytime LST-Ta	0.230	0.013	0.568	0.104
		Nighttime LST	0.129	0.092	0.158	0.011
		Nighttime LST-Ta	0.131	0.093	0.160	0.012
		Δ LST	0.219	0.029	0.560	0.087
		RNTI	0.205	0.030	0.471	0.083
	VTCI and SWC	VTCI	**0.181**	0.020	0.469	0.052
	Measured SWC	**All sites**	**0.149**	**0.022**	**0.361**	**0.092**
		CASMM site (S1)	**0.163**			

Table 6.14 continued.

Day	Model type		Avg.	Min.	Max.	SD.
262	LST and SWC	Daytime LST	0.332	0.088	0.606	0.084
		Daytime LST-Ta	0.333	0.073	0.625	0.090
		Nighttime LST	0.206	0.009	0.375	0.063
		Nighttime LST-Ta	0.206	0.038	0.345	0.051
		Δ LST	0.272	0.210	0.360	0.027
		RNTI	0.326	0.080	0.602	0.085
	LST and NWDI	Daytime LST	0.284	0.030	0.553	0.096
		Daytime LST-Ta	0.290	0.035	0.559	0.096
		Nighttime LST	0.479	0.339	0.573	0.039
		Nighttime LST-Ta	0.579	0.412	0.648	0.048
		Δ LST	0.256	0.125	0.436	0.066
		RNTI	0.285	0.030	0.552	0.096
	VTCI and SWC	VTCI	**0.277**	0.010	0.518	0.067
	Measured SWC	**All sites**	**0.255**	**0.063**	**0.501**	**0.126**
		CASMM site (S1)	**0.235**			

Finally, the spatial variability of the predicted SWC values also helps is assessing the validity of these models. Western *et al*. (1998b) documented a seasonal evolution of soil water patterns that was related to lateral redistribution of soil moisture during wet seasons. Lateral redistribution tends to increase spatial variability. Wet periods with runoff events are therefore expected to show higher spatial variability of SWC than dry periods (Famiglietti *et al*., 1998; Western *et al*., 1998b). The soil moisture patterns derived from this study imply that a wide range of surface soil moisture variability may be obtained for 0-30cm depths across a catchment particularly for day 58 or 262. The broadest range of SWC patterns are derived from the daytime LST based models and from the VTCI model, whereas the smallest range of SWC patterns was obtained from the nighttime LST based models. The daytime LST is also an important component in VTCI approach. It appears that the daytime LST is the most important variable which helps distributing soil water contents across a catchment.

The spatial patterns derived from the daytime LST, daytime LST – T_{air}, ΔLST and RNTI in NWDI-based models are also capable of giving some information more than with SWC-based models on the soil water distribution across the catchment. Details obtained with these models are encouraging, particularly with the daytime LST – T_{air} or with the RNTI. It can be therefore assume that the use of LST – T_{air} or RNTI with NWDI can provide a reasonable basis to derive catchment scale soil moisture patterns.

On the larger scale of the 1.1 km^2 pixels in the current study, the redistribution of soil moisture during wet events and the associated higher variability across a range of catchments can be best described with the SWC maps for day 58 derived with the VTCI method for Goulburn (Figure 6.28), Krui and Merriwa (Figure 6.31) river catchments. Kachanoski and De Jong (1998) have also reported greater spatial variability in recharge periods than in drying periods. Comparison of the VTCI based SWC maps obtained for days 58 or 262 with day 115 demonstrate this. The three SWC maps derived with the VTCI method provide representations of SWC across the study catchment. Hence, the prediction of catchment scale soil water patterns with the VTCI based models appears realistic.

In contrast, the surface water content values derived from the nighttime LST model show less detail compared to other models. For example, on day 58 the Goulburn catchment shows near uniform SWC patterns which are poorly related to the observed rainfall pattern. Often the range of values predicted with nighttime LST model is limited. As a result, some wet areas are appearing as dry areas and likewise, drier areas are appearing as wetter areas. Due to the narrow range of predicted SWCs, it can be seen that the details obtained from the nighttime LST model are limited. Thus, it appears that predicted soil moisture patterns from nighttime LST models are not realistic. The use of nighttime LST in combination with daytime LST (as in ΔLST models) however, shows mixed results particularly in day 58 and 262 (both are wet days).

Because many hydrological, biological, ecological and atmospheric processes are nonlinearly related to the surface soil moisture, knowledge of statistical distribution of soil moisture within a catchment would greatly increase the utility of up-scaled soil moisture products. Many authors have reported that surface soil moisture content values distribute normally within their study areas (Francis *et al*., 1986; Nyberg 1996). Figure 6.32 summarises the results of frequency distribution analyses of derived SWCs from the five selected models (four models with the

NWDI approach, i.e. Daytime LST, Daytime LST-T_{air}, Δ-LST, and RNTI, and the fifth model with the VTCI approach). It is clear from the figure that the VTCI-based model is the only model producing SWCs, which are distributed normally on all three days. Other models occasionally produce SWCs which are normally distributed (as in day 58 and 262 with RNTI) but may also can produce bi-modal distributions (e.g. in day 115, daytime LST, daytime LST-T_{air}, or ΔLST models). The distribution pattern of computed SWCs also confirms the VTCI model as a potentially useful upscaling method for soil moisture measurements.

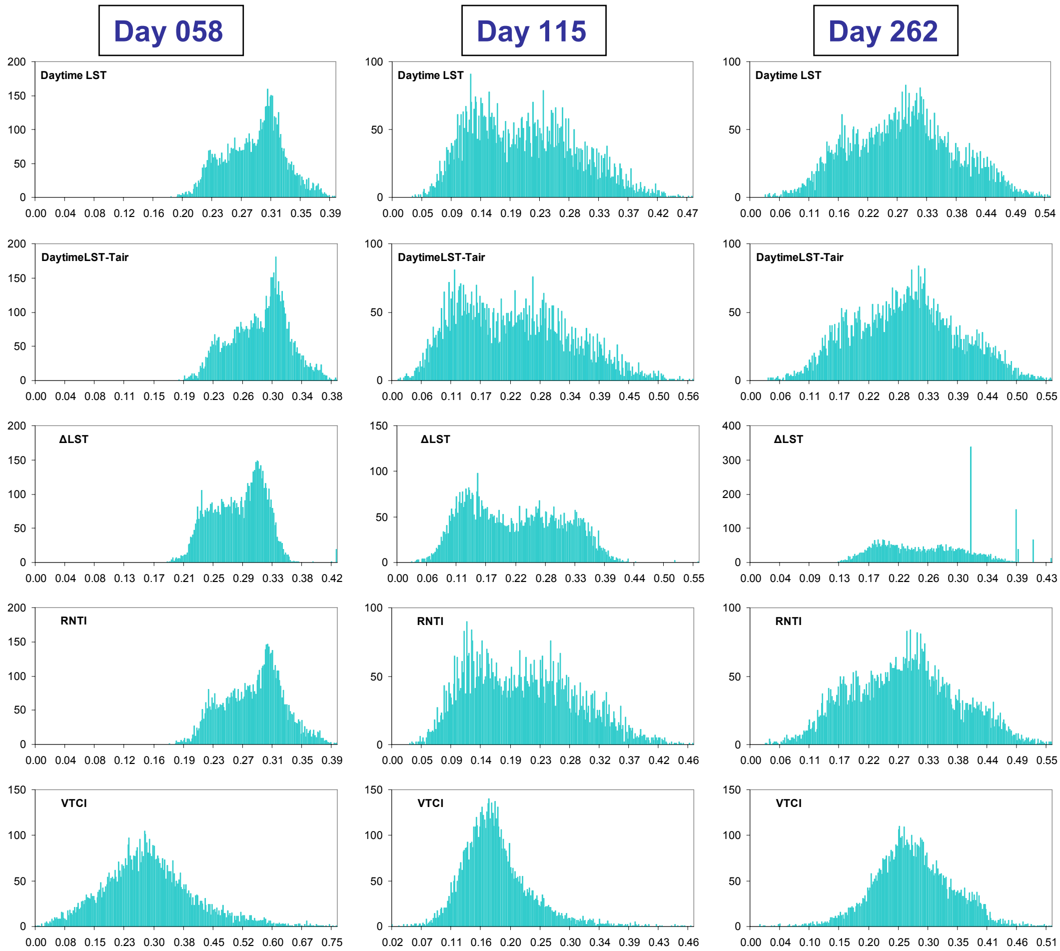

Figure 6.32: Summary of frequency distributions of soil moisture contents within the Goulburn River catchment obtained from the application of NWDI and daytime LST based models (i.e. Daytime LST, Daytime LST-T_{air}, Δ-LST, and RNTI) and the VTCI model for three dates selected (note: computed SWC (cm^3cm^{-3}) in X-axis and number of pixels in Y-axis).

Several aspects are clear from this study: (1) models based on linear correlation between SWC and measured daytime or nighttime LST are not able to reproduce the wide range of soil water contents usually present in a catchment; (2) models based on linear correlation between NWDI and daytime based LST are suitable for deriving catchment scale SWC patterns; (3) the nighttime LST is unsuitable for predicting soil water content; (4) the VTCI approach gives a range of SWC values which is closer to the range of measured values; and (5) models based on the NWDI and measured daytime LST must be further developed on a daily basis.

The methods presented in this study attempted to derive spatial patterns of root-zone soil moisture content from the combined used of ground-based soil moisture measurements and remotely sensed LST and VI. Table 6-15 summarises the salient features, advantages, disadvantages and practical significance of the LST-based and VTCI-based models studied in this chapter. According to this study, the most plausible method to derive spatial patterns of soil water distribution is the VTCI-based approach which uses field measured soil moisture at a CASMM site.

Table 6-15: Comparison of the use of LST-based models and VTCI-based models for soil water content predictions.

	LST-SWC models	LST-NWDI models	LST + VI model (e.g. VTCI)
Key features	• Predictions are based on empirical equations • Considers current LST • Predictions may require air temperatures (in case of T_s-T_a models)	• Predictions are based on empirical equations • Considers current LST • Require θ_{max} for each soil type	• Predictions are not based on empirical equations • Considers current LST and vegetation status • Predictions require SWC from a CASMM site.
Advantages	• Easy to establish	• Easy to establish • Detailed patterns can be obtained • Predictions reflect SWC from deeper layer • Less seasonal effect	• Detailed patterns reflect near-true SWC situation • Predictions reflect SWC at deeper layers • No seasonal effect
Dis-advantages	• Models may not provide details • Predictions consider only LST • Predictions reflect SWC at surface layer than the deeper layers • Seasonal effects may hinder predictions	• Require accurate soil map of the catchment	• Required to compute the VTCI index for every application • Required to consider larger catchment for accurate determination of boundary conditions
Practical significance	• Application of a simple regression equation with measured LST provides a surface SWC distribution	• Good SWC pattern across any catchment is possible with daytime LST	• Realistic SWC pattern across any catchment is possible

6.6 IMPLICATIONS FOR FUTURE WORK

In drier sub-humid environments, subsurface water redistribution is restricted to a limited number of short periods during a year. Most of the time, moisture transport is dominated by vertical fluxes, often with no connection between adjacent areas. Soil moisture may also controlled by factors such as vegetation, local topography and aspect of the hillslope. As a result, in sub-humid areas, the temporal and spatial patterns of soil moisture are difficult to predict. Furthermore, sub-humid environments are subject to dramatic and sudden changes in soil moisture contents. The soil moisture content in such areas plays a fundamental role in the hydrological response, and prediction of catchment-scale moisture content from point-scale measurements is therefore an important issue. These catchment-scale predictions can be based on spatial wetness patterns derived from satellite observations.

Knowledge of the variation in spatial distribution of soil moisture rather than just average soil moisture content over a catchment may lead to understanding significant differences in the hydrological responses of the catchment. The present study has developed a number of models that enable the generation of soil moisture patterns based on the field measured soil moisture and MODIS derived land surface temperature (LST) and vegetation index (VI). The first set of methods is based on a relationship between various forms of LST (e.g. daytime, nighttime, Δ LST, daytime LST-T_a, nighttime LST-T_a and RNTI – i.e. 6 types) and field measured soil moisture measurements. The second set of methods use relationships between various forms of LST (as mentioned previously) and a normalized soil moisture index (NWDI). Finally, based on the triangular-shape scatter diagrams between MODIS derived LST and VI (such as NDVI or EVI) over a catchment, an index has been derived to characterise the surface wetness conditions (VTCI). This index has been used with measured soil moisture values obtained at a catchment average soil moisture monitoring (CASMM) site to generate soil moisture patterns across a catchment. Among the fourteen methods studied, the most detailed SWC patterns were obtained from the VTCI and RNTI-NWDI approaches.

It appears that a combination of LST and VI is necessary for obtaining a more complete picture of the soil water distribution than any of the other methods studied in the current thesis. It would therefore be appropriate to re-examine field-measured data from existing soil moisture networks across many regions and investigate the use of the vegetation-temperature condition index described in this thesis.

Furthermore, the methodology developed in this chapter may assist in the development of downscaling strategies for large-area measurement of soil moisture from AMSR-E because the broad range of variation of wetness characteristics obtained with the VTCI and RNTI-NWDI methods provide an useful covariant. This will be explored further in Chapter 8.

The current study found that it is possible to derive catchment scale SWC distribution maps from a sparse network of soil moisture monitoring sites. Such maps are not only useful for scaling studies and hydrological model applications but also for practical applications such as for achieving optimum usage of limited water resources.

6.7 CONCLUSIONS

This study has illustrated that in sub-humid regions of Australia (and similar climates elsewhere), soil moisture spatial patterns can be predicted for a given day with the combined use of ground-based measurements and remotely sensed land surface temperature and vegetation indices.

This study considered only 1.1x1.1 km^2 pixel size for deriving soil moisture patterns. It would be appropriate to continue the study with 250mx250m^2 pixels as the high resolution data are available from the MODIS sensor.

Future soil moisture scaling studies should consider the use of satellite derived wetness indices. It will also be useful to further investigate the implication of soil physical information for soil moisture scaling studies.

Table of contents

List of Figures

List of Tables

CHAPTER SEVEN

7 Near-surface soil moisture estimations with active and passive microwave sensors: Theoretical basis and field validation of AMSR-E

This chapter is concerned with near-surface soil moisture estimation with active and passive microwave sensors. The chapter presents first, a review of the radiative transfer theory and an overview of satellite based microwave radiometers. Next, this chapter describes soil moisture validation studies for the passive microwave AMSR-E system soil moisture system based on three intensive field campaigns. While the comparisons between the AMSR-E products and field measurements are not straightforward as the 75km x 43km of Instantaneous Field Of View (IFOV) by the 6.925 GHz channel of AMSR-E and the 25 km resolution of the soil moisture product significantly exceed the typical plot size used in field sampling, the results presented here give an *indication* of future research directions such as use of airborne sensors for validation purposes. Examination of temporal trends of AMSR-E derived near-surface moisture and ground-based moisture measurements throughout the study period will provide much greater range of environmental conditions to improve the present soil moisture computation methodology. While the analysis presented is restricted to 1-2 AMSR-E pixels, the approach presented here establishes the foundations for future studies.

7.1 INTRODUCTION

The moisture status of the soil is a directly observable hydrologic variable and remote sensing techniques may be employed in its measurement. Techniques have been developed using the visible, infra-red and microwave windows of the electromagnetic spectrum. Measurements in the microwave region can provide all-weather quantitative estimates of near-surface soil moisture under low-to-moderate vegetation cover because the measured soil reflectivity is strongly influenced by the soil moisture content. Furthermore, microwave frequencies respond to the variations in moisture content due to the polar nature of the water molecule. Indeed, the microwave region permits truly quantitative estimates of soil moisture using physically based, radiative transfer models. Furthermore, microwave technology is the only remote sensing method that measures a direct response to the absolute amount of water in the soil.

Microwave remote sensing is based on the differences in electromagnetic and dielectric properties between dry and wet soils. The water content of a soil strongly influences its dielectric properties, the propagation of electromagnetic radiation through it and the emission of thermal microwave radiation from the soil surface. The dielectric constant is a measure of the propagation characteristics of an electromagnetic wave in the medium (Tansey *et al.,* 1999). Because of the large difference between the dielectric constant of water (about 80 at frequencies <5 GHz) and that of dry soil (about 3.5), the emissivity of soil varies over a wide range: from approximately 0.6 (for saturated soils) to greater than 0.9 for dry soils. For a typical Earth surface temperature of 300 K this variation of emissivity corresponds to a soil brightness temperature variation of 90 K (Njoku and Entekhabi, 1995). Because this variation in the brightness signal is significantly larger than the noise sensitivity threshold of a microwave radiometer (approximately less than 1K), microwave techniques hold great promise for soil moisture estimation.

Over the last two decades considerable efforts have been devoted to develop and improve active and passive microwave techniques as well as interpretation tools (Ulaby *et al.,* 1981; Jackson and Schmugge 1989, 1995; Engman and Chauhan, 1995; Njoku and Entekhabi, 1995; Sano *et al.,* 1998; Schmugge, 1998; Wigneron *et al.*, 1998, 2003; Biftu and Gan, 1999; Owe *et al.,* 2001; Laymon *et al.,* 1997). Microwave remote sensing uses the microwave region of the electromagnetic spectrum which consists of wavelengths between 1 mm and 100 cm. This region is subdivided into bands as shown in Table 7-1 which are often referred to by alphabetic characters. For remote sensing applications however, only wavelengths greater than about 5 cm are useful, because the higher the wavelength, the smaller the effects of atmosphere and vegetation. In addition, longer wavelengths can penetrate deeper into the surface soil layer and are therefore, more sensitive to soil moisture (Njoku and Entekhabi, 1995; Jackson *et al.,* 1996). In general, microwave sensors have their maximum sensitivity at lower frequencies (i.e. in the L-band and C-band).

Table 7-1: Microwave band names, wavelengths and frequencies (Ulaby et al., 1981).

Band Name	***Wavelength (cm)***	***Frequency (GHz)***
Ka	0.75 – 1.10	40.0 – 26.5
K	1.10 – 1.67	26.5 – 18.0
Ku	1.67 – 2.40	18.0 – 12.5
X	2.40 – 3.75	12.5 – 8.0
C	3.75 – 7.50	8.0 – 4.0
S	7.50 – 15.0	4.0 – 2.0
L	15.0 – 30.0	2.0 – 1.0
P	30.0 – 100.0	1.0 – 0.3

Microwave techniques for measuring soil moisture include both passive and active microwave approaches. The main difference between active and passive microwave remote sensing is the source of the energy. In active microwave systems, otherwise known as radar systems, the electromagnetic signal produced by a power source on a remote sensing platform is propagated through space to the target on the land surface, from where it is reflected back to space. The sensor, which is also mounted on the same platform, receives the reflected signal or backscatter. Therefore, active systems depend on their own energy sources and are capable of controlling the emitted radiation and hence have indirect control of backscattered radiation.

In contrast, passive microwave remote sensing does not depend on its own energy source and depends entirely on the naturally emitted radiation from the earth surface. Since all matter at temperatures above absolute zero emits electromagnetic radiation due to the motion of the charged particles of its atoms, so does the earth surface. Passive microwave remote sensing measures this naturally emitted radiation. Since the naturally emitted radiation signal is very weak, very sensitive radiometers need to be used and often reasonable signal strength is obtainable only from a substantially large ground area. Therefore, passive systems can provide spatial resolutions on the order of tens of kilometres; about 10-20 km in the L-band (1.4 GHz) or about 50 km in the C-band (6.9 GHz). In comparison with radars, passive systems have a greater sensitivity to soil moisture and are less sensitive to surface geometry. Therefore, simplified algorithms can be used to account for soil surface roughness and vegetation structure.

Passive microwave radiometers have been flown on a number of satellites, mainly the Electronically Scanning Microwave Radiometer (Nimbus 5, in the 1970s), the Scanning Multi-channel Microwave Radiometer (Nimbus 7), the Special Sensor Microwave Imagery (in Defence Meteorological Satellite Program), and more recently the Advanced Microwave Scanning Radiometer for EOS (AMSR-E, in Aqua satellite since 2002).

7.2 ACTIVE MICROWAVE REMOTE SENSING

Active microwave sensors measure the phase and amplitude of backscatter and enable a received/transmitted power ratio or backscatter coefficient (also know as the radar cross-section σ^o, measured in dB) to be calculated. Different surfaces have specific σ^o at different wavelengths. These differences are due to the interactions of radiation with scatterers of varying size. The amount of moisture in the near-surface layer however, also influences backscatter by affecting the amplitude of the backscatter coefficient. The σ^o is related directly to soil moisture and is written in functional form as;

$$\sigma^o = f(R, \alpha, \theta_v) \tag{7-1}$$

where R is a surface roughness term, α is a soil moisture sensitivity term, and θ_v is the volumetric soil water content. Besides the fact that R and α are known to vary with wavelength, polarization, and incident angle, no satisfactory theoretical model is currently available for estimating these terms independently (Engman and Chauhan, 1995). Therefore, the relationship between measured backscatter and soil moisture requires an empirical relationship with field data, even for bare soil. Many empirical and semi-empirical models have been proposed to relate the σ^o to surface moisture (Biftu and Gan, 1999; Quesney *et al.,* 2000; Srivastava *et al.,* 2003). For example, the most widely used semi-empirical linear model relates surface moisture and radar signal as:

$$\sigma^o = \alpha\theta_v + \beta \quad \textbf{(7-2)}$$

where θ_v is the volumetric soil water content, and α and β are constants. This linear model has been validated using data obtained over many agricultural watersheds (Quesney *et al.,* 2000). Due to its empirical nature, the slope α of this model is not constant from one watershed to the next, and must be calibrated each time. In addition, the roughness effects are neglected in this linear model, thus preventing its application to large areas.

In active microwave remote sensing, the depth to which soil moisture can be detected depends on the wavelength of the radar system. Active systems also offer possibilities of high spatial resolution (10 m for Synthetic Aperture Radar (SAR) systems in ERS and Radarsat satellites). Their measurements however, are very sensitive to geometric features of the surface such as soil roughness, vegetation structure, row effects due to crop rows or tillage, look angle etc.

Satellite based scatterometers are active microwave sensors or radars designed to measure wind speed and direction over the oceans. For example, ERS scatterometers in European Remote Sensing Satellite ERS-1 and ERS-2, Japanese Earth Resources Satellite (JERS-1), and the Canadian RADARSAT are operating at present. While ERS and RADARSAT are radars operated in C-band, JERS-1 is operated in L-band. The SAR systems offer an opportunity to measure soil moisture routinely and many such attempts are described in the literature (Ragab, 1995; Tansey *et al.,* 1999; Srivastava *et al.,* 2003). Although it is believed that an L-band system would be optimum for soil moisture, the preliminary results from the ERS-1 with C-band demonstrate its capability for soil moisture measurement. Tansey *et al.* (1999) have observed that use of SAR data to determine soil moisture in a desert environment is deemed realistic. However, Merot *et al.*

(1994) has shown that radar data become ambiguous when free water pools are present within the observed ground area.

Present techniques developed for soil moisture retrieval from active microwave are well suited for the small scale (≈ 10 ha). Interpretations of radar signals face problems at larger scales because of the insufficient information about the influence of the topography and vegetation on the return signal. As a result, the research emphasis in soil moisture retrieval from microwave signals has changed from active to passive.

7.3 PASSIVE MICROWAVE REMOTE SENSING FOR NEAR-SURFACE MOISTURE ESTIMATION

Passive microwave theory has been extensively described by a number of authors (Njoku and Kong, 1977; Ulaby *et al.,* 1981, 1986; Van de Griend and Owe, 1994b; Engman and Chauhan, 1995; Njoku and Entekhabi, 1995; Wigneron *et al.*, 2003). Furthermore, many studies have successfully demonstrated that passive microwave remote sensing has great potential for monitoring soil moisture at larger scales (Jackson and O'Neill, 1990; Owe *et al.,* 2001; Van de Griend and Owe, 1994a; Njoku, 1999). This section gives a brief overview of the theory relevant to the present study.

Remote sensing approaches using the passive microwave region are based on the measurement of the natural thermal emission of the land surface at microwave lengths using very sensitive radiometers. This natural thermal emission largely depends on the physical temperature and the emissivity of the radiating body. The emitted radiation in the microwave region (λ = 1-1000 mm) is extremely low as compared with long-wave infrared radiation (λ = 1-100 μm).

Thermal radiation emitted from the Earth's surface can be described by Plank's blackbody radiation theory. At microwave wavelengths ($\lambda > 0.3$ *cm*), and for the typical Earth surface temperatures (≈ 300 K), the Rayleigh-Jeans approximation (when f < 117 GHz) to Plank's law holds, and the specific intensity of blackbody radiation (B_l) at temperature T can be written as (Ulaby *et al.*, 1981);

$$B_I = \frac{kT}{\lambda^2} \qquad \textbf{(7-3)}$$

where λ is wavelength (m), k is Boltzmann's constant, and B_I has units of Wm^{-2} Hz^{-1} $steradian^{-1}$.

The relationship of the brightness temperature of a thermally radiating body to its true temperature is given by;

$$T_{b(p)} \approx e_{s(p)}T \qquad \textbf{(7-4)}$$

where p refers to either horizontal or vertical polarization, T_b is the observed microwave brightness temperature, T is the physical (thermodynamic) temperature of the emitting layer, and e_s is the smooth-surface emissivity (For a blackbody e_s = 1).

According to Kirchhoff's reciprocity theorem, the emissivity e_s relates to the reflectivity Γ of the surface as:

$$e_s = 1 - \Gamma \qquad \textbf{(7-5)}$$

If the assumption is made that the dielectric constant in the soil has smooth boundary and that the temperature and surface moisture distributions are uniform, the reflectivity, Γ, at vertical and horizontal polarization may be derived from the Fresnel equation:

$$\Gamma_h = \left| \frac{\cos\theta - \sqrt{\varepsilon - \sin^2\theta}}{\cos\theta + \sqrt{\varepsilon - \sin^2\theta}} \right|^2 \qquad \textbf{(7-6)}$$

and

$$\Gamma_v = \left| \frac{\varepsilon\cos\theta - \sqrt{\varepsilon - \sin^2\theta}}{\varepsilon\cos\theta + \sqrt{\varepsilon - \sin^2\theta}} \right|^2 \qquad \textbf{(7-7)}$$

where ε is the complex dielectric constant (relative permittivity) of the soil-water medium, θ is the incidence angle of the sensor (measured from the surface normal) and v and h refer to the polarization of the emitted radiation. The reflectivities, and therefore the emissivities and brightness temperatures, thus depend on the dielectric constant, the incidence angle, and the polarization of the radiation. While the absolute magnitude of the soil emissivity is somewhat lower at horizontal polarization, the sensitivity to changes in surface moisture is significantly greater than at vertical polarization for both clay and sandy soils

(Figure 7-1). The variable sensitivity of horizontal and vertical polarization gives an opportunity to relate this difference to the soil moisture content. The polarization difference (PD; Jackson, 1997) and polarization ratio (Njoku, 1999) are also a function of the moisture content of the soil and increase with soil moisture. One advantage of PD and polarization ratio is that both are less sensitive to temperature than the individual vertical or horizontal signals.

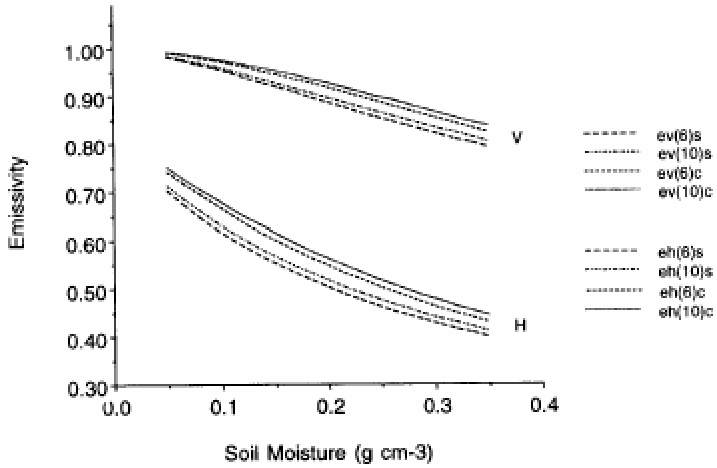

Figure 7-1: Emissivity dependency on soil moisture for a smooth soil at 6 and 10 GHz, Vertical (V) and Horizontal (H) polarization, and for sand (s) and clay (c) soils (From Njoku, 1999).

7.3.1 MICROWAVE DIELECTRIC PROPERTIES OF SOIL

The dielectric properties are measured by the dielectric constant (ε), which is a complex number representing the response of a material to an applied electromagnetic wave (Schmugge, 1998; Tansey *et al.,* 1999). It consists of both real (ε') and imaginary (ε") parts by the relationship $\varepsilon = \varepsilon' + i\,\varepsilon''$, and is usually measured relative to that of free space in the material (i.e. complex relative dielectric constant, $\varepsilon_r = \varepsilon / \varepsilon_o$ where $\varepsilon_o = 8.85 \times 10^{-12}$ farad m^{-1}). While the real component determines the propagation characteristics of the electromagnetic wave in the material such as its velocity, the complex component determines the energy losses or absorption as the electromagnetic wave travels through the material (Engman and Chauhan, 1995; Zegelin, 1996). This energy loss is due to vibration and/or rotation of the water molecules (Wütherich, 1997) and is often referred to as the dielectric loss factor (Zegelin, 1996).

The real part of the relative dielectric constant (ε_r') of dry soil particles varies from a value of 2 to 5 independent of frequency (Dobson and Ulaby, 1986) and the imaginary part ($\varepsilon r''$) is typically less than 0.05 for dry soils (Ulaby *et al.,* 1996). In contrast, the free water dielectric constant (at 1 GHz, at room temperature) is approximately 80 for the real component and 4 for the imaginary component (Ulaby *et al.,* 1996). The large difference between the dielectric constant of water and the soil solids makes it suitable for the measurement of soil water content.

A number of relationships have been proposed to relate soil moisture content with the soil dielectric constant. Topp *et al.* (1980) showed that the volumetric soil moisture content can be derived from the real part of the dielectric constant by means of multiple regression approach. The main advantages of their approach include that it does not require the determination of any soil parameters nor does it require information on the observation frequency or soil temperature. Furthermore, Topp *et al.* (1980) found that for frequencies between 1 MHz and 1 GHz the real part of the dielectric constant was almost independent of soil density, soil texture, soil salinity and soil temperature between 10^oC and 36^oC. Nevertheless, the validity of this empirical relationship has not been demonstrated for all possible soil moisture contents and porosities (Roth *et al.*, 1990).

Figure 7-2 shows the relationship between dielectric constant and volumetric soil moisture content for a variety of soil types at a frequency of 1.4 GHz and a soil temperature of 23^oC. The dependence on soil type (or 'texture') is due to the different percentages of water bound to the particle surfaces in the various soils (Njoku and Entekhabi, 1996). Bound water molecules do not freely rotate at microwave frequencies, and hence cause a smaller dielectric effect than the free water in the pore spaces. This is most evident in clay soils, which have greater particle surface areas per unit mass and more affinity for binding water molecules. *A priori* knowledge of the soil textural composition is therefore important to interpret the dielectric constant of a soil.

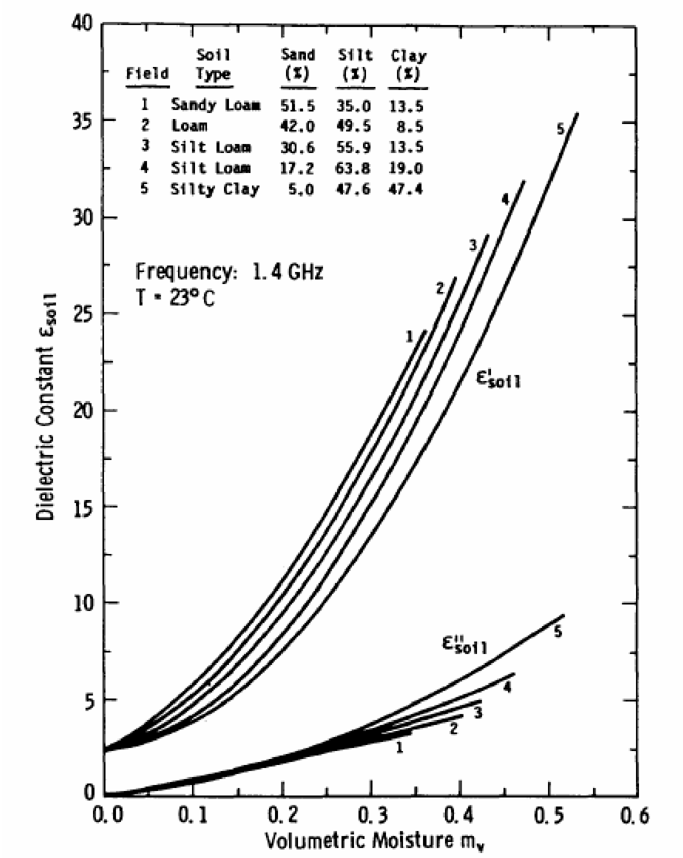

Figure 7-2: Dielectric constant as a function of volumetric soil moisture for five soil types at 1.4 GHz. Smooth curves were drawn through measured data points (From Ulaby et al., 1986, 1996).

To overcome the dependence on the relationship between soil type and dielectric constant Wang and Schmugge (1980) presented two relationships for dielectric constant, depending on whether the soil moisture content is above or below a transition soil moisture content. An empirical relationship between the transition soil moisture content and the wilting point moisture content, given as a function of the sand and clay content, was also introduced. Finally, in order to describe the observed dielectric constant of soil-water mixtures at frequencies between 1.4 and 5 GHz, a simple empirical model was proposed. In this model, the dielectric constant of a soil-water mixture is computed from the known dielectric constants of air, ice, dry soil and water, and the volume fraction of each constituent in the mixture.

The effect of frequency on the soil dielectric constant is also important. At frequencies below approximately 5 GHz there is little variability in the real part of the dielectric constant and therefore, frequency dependence of the soil emissivity in this range is very limited. The imaginary part of the dielectric constant, however, exhibits considerable frequency dependence in this range. This leads to frequency-dependent attenuation of radiation through the medium. This can be explained by a parameter known as the 'penetration depth' which is discussed in Section 7.3.2.

For frequencies between 1.4 and 18 GHz, Hallikainen *et al.* (1985) have presented empirical relationships with separate polynomial expressions for both the real and imaginary parts of the dielectric constant. These polynomial expressions relate the real and imaginary parts of the complex dielectric constant to the volumetric soil moisture content and the percentages of sand and clay. The coefficients of these expressions depend on the observation frequency.

Dobson *et al.* (1985) have presented two dielectric mixing models, viz. a theoretical and a semi-empirical model. The theoretical dielectric mixing model deals with both the bound water volume fraction and the free water volume fraction in the soil-water mixture, in accordance with the pore-size distribution. The semi-empirical dielectric mixing model relates the dielectric constant as a function of soil temperature, soil moisture content, soil texture, and observation frequency, for both the real and imaginary parts. This model is valid for frequencies between 1.4 and 18 GHz. Dobson *et al.* (1985) have shown that their semi-empirical mixing model is capable of matching measured data at frequencies above 4 GHz. Apparently, this frequency range is an advantage for applications in saline soils because at frequencies higher than 4 GHz, the effects of soil salinity may be ignored (Ulaby *et al.,* 1986). However, at frequencies less than 4 GHz, the mixing model does not fully account for the dielectric properties of bound water at low soil moisture contents.

In further work on the semi-empirical dielectric mixing model of Dobson *et al.* (1985), Peplinski *et al.* (1995) have extended the model to frequencies between 0.3 and 18 GHz. In this new model, an adjustment has been introduced to correct the expression of Dobson *et al.* (1985) for the real part of the relative dielectric constant, at frequencies between 0.3 and 1.3 GHz. Similarly, for the imaginary part of the relative dielectric constant, a new equation was introduced for frequencies between 0.3 and 1.3 GHz. At present, the most widely used soil-water-air dielectric mixing model is the model of Peplinski *et al.* (1995). It provides the best compromise between the complexity of the theoretical model and the simplicity of the empirical models (Walker, 1999). This mixing model has the widest validity range in terms of observation frequency. In addition, it accounts for the most important factors, including observation frequency, soil texture and soil temperature.

7.3.2 PENETRATION DEPTH

The penetration depth is defined as the distance in the medium over which the intensity of the propagating radiation decreases by about 63% due to attenuation by an exponential factor. The wavelength is an important parameter in determining the penetration depth. Figure 7-3 shows the dependence of penetration depth on wavelength and moisture content for a sandy soil. Accordingly, at 1.5 GHz the penetration depth varies from approximately 10 cm to 1 m for soil conditions ranging from saturated to dry. However, at 30 GHz the penetration depth is shallower for similar conditions and varies from less than 1 mm to a little over 1 cm. The penetration depth is important because it gives an indication of the thickness of the surface layer within which variations in moisture and temperature can significantly affect the emitted radiation. Figure 7-3 confirms that longer wavelengths with greater penetration depths sense moisture and temperature changes deeper in the soil than shorter wavelengths. Therefore, by increasing the wavelength it may be possible to sense a thicker layer of soil. However, due to radio frequency interference at wavelengths beyond the L-Band, an upper limit on the wavelength exists for practical applications (Jackson, 1993). It is also important to note that the penetration depth is dependent on the soil moisture content. Figure 7-3 shows that as the soil moisture content increases, the penetration depth decreases (Njoku and Kong, 1977; Engman and Chauhan, 1995).

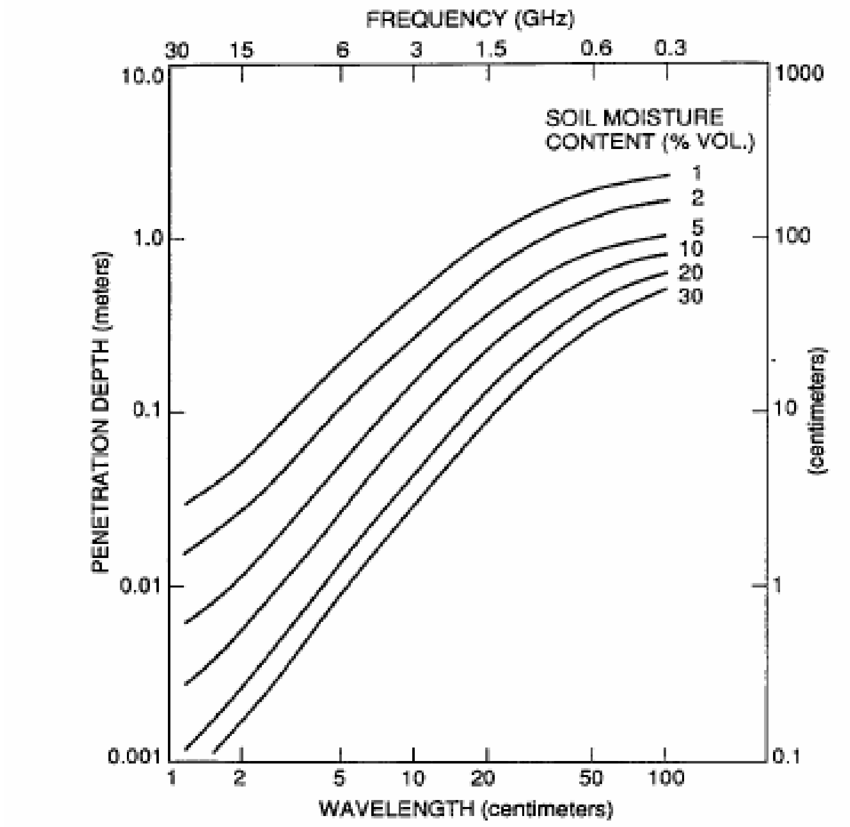

Figure 7-3: Soil penetration depth of microwave as a function of frequency and moisture content (from Njoku and Entekhabi, 1996).Soil penetration depth of microwave as a function of frequency and moisture content (from Njoku and Entekhabi, 1996).

The viewing angle of the sensor is also important in estimating the dielectric properties of the soil. Figure 7-4 shows the computed dependence of emissivity on soil moisture content and viewing angle for a sandy soil. These graphs assist in the selection of the optimum viewing angle as well as into the development of new inversion models.

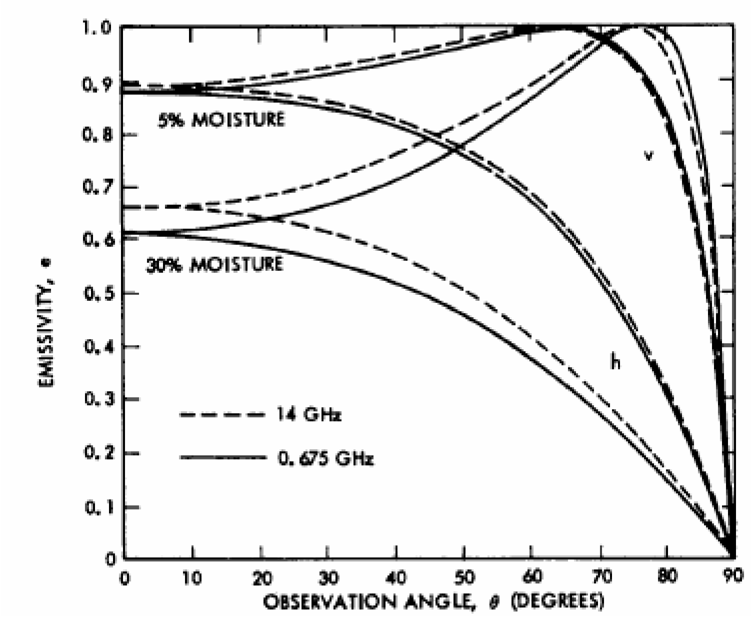

Figure 7-4: Computed emissivity as a function of viewing angle for a sandy soil with moisture contents of 5% and 30%. The curves are for frequencies of 0.675 GHz and 14 GHz, and indicate the different behavior of the vertical (v) and horizontal (h) polarizations (from Njoku and Entekhabi, 1996).

7.3.3 ROUGHNESS EFFECTS

Surface roughness characteristics have generally been described in terms of the root mean square of surface height, roughness correlation length and a correlation function. For example, Choudhury *et al*. (1979) have proposed an empirical roughness model described as:

$$e_{r(l)} = 1 - R_{(l)} \exp(-h \cos^2 u) \qquad \textbf{(7-8)}$$

where $e_{r(l)}$ is the rough surface emissivity, h is an empirical roughness parameter (related to the root mean square (rms) height variation of the surface and the correlation length), and u is the incidence angle of the observation. Typical values for h have been suggested, ranging from 0 for a smooth surface, 0.3 for a disked field, to 0.4 for a rough ploughed field. A more complex formulation, which also includes a polarization mixing parameter, has subsequently been proposed by Wang and Choudhury (1981). However, little work has since been conducted to quantify the relative magnitudes of either the roughness parameter or the polarization mixing parameter.

Surface roughness reduces the sensitivity of emissivity to soil moisture variations. This is due to an increase in the apparent emissivity of natural land surfaces, which is caused by increased scattering from rough surfaces due to the increase in surface area of the emitting surfaces (Schmugge, 1998). Therefore, roughness of the soil surface reduces the range in measurable emissivity from dry to wet soil conditions (Wang, 1983; Van de Griend and Engman, 1985).

In addition, the path through the atmosphere between the surface and the sensor depends on the slope and the elevation of the emitting surface and this effect is significant at frequencies >10 GHz . This is due to the fact that these frequencies are affected by atmospheric attenuation (Mätzler and Standley, 2000). Therefore, corrections for roughness are necessary to obtain accurate soil moisture estimates. Some studies have shown that an accurate knowledge about the correlation length is important at lower incident angles, while the rms surface roughness has to be accurately known at higher incident angles (Su and Troch, 1996). Njoku and Entekhabi (1996) suggest that within certain broad classes of surface types, the natural variability of roughness can be small enough to be corrected using simple estimates of the roughness parameters.

It is also assumed that the effect of surface roughness is minimal in most locations at satellite scales, except in mountainous terrain or areas with extreme relief. Van de Griend and Owe (1994b) have observed in a field study that a surface roughness of 0 value gave the lowest rms errors in satellite-derived soil moisture.

7.3.4 INFLUENCE OF VEGETATION

Vegetation may absorb or scatter the radiation emanating from the soil, but it also emits its own radiation. Therefore in areas of sufficiently dense canopy, the emitted soil radiation will become masked, and the observed emissivity will be due largely to the vegetation. The magnitude of the absorption by the canopy depends upon the wavelength and the vegetation water content. At low frequencies the effects of scattering at the air-vegetation interface and within the volume of the vegetation are small and are often neglected.

The most frequently used wavelengths for soil moisture sensing are in the L-Band ($\lambda \approx 21$ cm) and C-Band ($\lambda \approx 5$ cm), but only L-band sensors are able to penetrate vegetation of any significant density. While observations at all frequencies are subject to scattering and absorption and require some correction if the data are to be used for soil moisture retrieval, shorter wave bands are especially susceptible to vegetation influences.

A range of canopy models have been developed to account for the effects of vegetation (Kirdiashev *et al.,* 1979; Mo *et al.,* 1982; Ulaby *et al.,* 1986). The outgoing radiation from the land surface as observed from above the canopy may be expressed in terms of the brightness temperature, T_b, and is given as a simple radiative transfer equation (Mo *et al.,* 1982);

$$T_{b(l)} = T_s e_{r(l)} \Gamma_{(l)} + (1-\omega_{(l)}) T_c (1-\Gamma_{(l)}) + (1-e_{r(l)})(1-\omega_l) T_c (1-\Gamma_{(l)}) \Gamma_{(l)} \qquad \textbf{(7-9)}$$

where T_s is the soil temperature, T_c is the canopy temperature, ω is the single scattering albedo, Γ the transmissivity of the canopy and subscript l denotes vertical or horizontal polarization.

The first term of the equation 7.9 defines the radiation from the soil as attenuated by the overlying vegetation. The second term describes the upward radiation directly from the vegetation and the third term defines the downward radiation from the vegetation, reflected upward by the soil and again attenuated by the canopy. These three terms are shown in Figure 7-5. The derivation of equation 7.9 assumes a specular soil surface with no reflection at the air-vegetation boundary. This expression has been found to be a good approximation up to ~10 GHz for a vegetation layer overlying a rough soil surface and has been used in theoretical and experimental studies (Wang and Choudhury, 1995; Njoku and Li, 1999; Njoku *et al.*, 2003).

The transmissivity (Γ) is defined in terms of the optical depth or vegetation opacity (τ) and incidence angle (u) as shown in equation 7.10.

$$\Gamma_{(l)} = \exp \frac{-\tau_{(l)}}{\cos u} \qquad \textbf{(7-10)}$$

The magnitude of the vegetation opacity depends on vegetation structure, water content of the vegetation, and the wave frequency. For frequencies less than 10

GHz, vegetation opacity has been shown to be a linear function of vegetation water content. Typical values of τ for agricultural crops are generally given are less than one (Mo *et al.,* 1982; Jackson and O'Neill, 1990). Several works found that τ could be linearly related to the total vegetation water content W_c (kg/m^2) using the so-called b parameter (Wigneron *et al.,* 1998; Jackson et al., 1999):

$$\tau = bW_c / \cos\theta \qquad \textbf{(7-11)}$$

where, cos θ accounts for the slant path through the vegetation. The *b* parameter depends on canopy structure and microwave frequency and may be calibrated for each crop type or for broad categories of vegetation. The value of *b* also depends on the gravimetric water content of the vegetation. Temperature also affects the *b* parameter, especially in the C-Band. Also, it has been found that *b* strongly depends on polarization and incidence angle, particularly for vegetation canopies with dominant vertical structure found in stem dominated canopies such as those of cereal crops (Wigneron *et al.,* 1996).

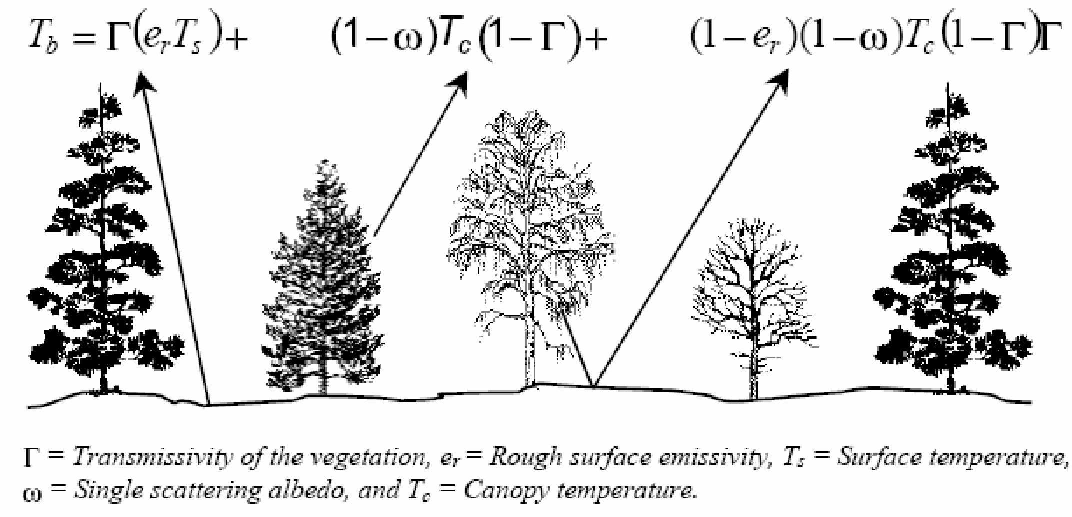

Figure 7-5: Schematic representation of the partitioning of microwave radiation from a vegetated land surface in terms of the brightness temperature (From Van de Griend and Owe, 1993).

Theoretical calculations by Ulaby *et al.* (1986) have shown that the sensitivity of above-canopy brightness temperature measurements to variations in soil emissivity decreases with increasing optical depth or canopy thickness. This is due to the attenuation of soil emission by the canopy: the emission from the vegetation canopy tends to saturate the signal with increasing optical depth. This subsequently results in a decrease of the sensor sensitivity to variation in soil moisture variations below the canopy.

A transmissivity of 1 corresponds to an optical depth of 0 and indicates bare soil. Conversely, a transmissivity of 0 indicates a thick canopy, without any penetration of the upwelling soil emission.

7.4 SOIL MOISTURE RETRIEVAL MODELS

Microwave remote sensing techniques for soil moisture measurement are based on inversion of radiative transfer models that link geophysical surface variables to the observed brightness temperature, T_b. As discussed previously, the primary geophysical variables influencing the brightness temperature are the volumetric soil moisture θ_v, the vegetation water content W_c, and the surface temperature T_s. Other factors such as surface roughness, vegetation type, and soil texture are also important but to a lesser degree. Thus, retrieval of soil moisture must include corrections for vegetation and surface temperature effects, uncertainties in other variables contribute to the geophysical error. In practice, the following steps are involved in extracting soil moisture information;

1. Calibrating the output (brightness temperature) of the sensor
2. Correction for atmospheric moisture (particularly for situations with heavy cloud cover and rain)
3. Categorization of the ground elements (land/water, forest/dense vegetation, snow/ice, vegetation types, bare soil etc.)
4. Computation of the surface emissivity (computed by dividing the brightness temperature by the physical temperature of the target, as in equation 7.4)
5. Removing the effect of vegetation or land cover (see equation 7.9 – 7.11)
6. Accounting for the effect of soil surface roughness characteristics (e.g. as in equation 7.8)

7. Relating the emissivity measurement to soil dielectric properties (by inverting the Fresnel equation to determine an effective dielectric constant for the surface layer, see equations 7.6 - 7.7)

8. Relating the dielectric properties to soil moisture (using dielectric mixing model relationships and soil texture properties)

A number of algorithms of varying complexity have been developed in recent years to retrieve soil moisture from brightness temperature measurements at microwave frequencies (Jackson, 1993; Wigneron *et al*., 1993; Njoku, 1999; Njoku and Li, 1999; Owe *et al*., 2001; De Jeu, 2003; Pardé *et al*., 2003, Wen *et al*., 2003; Drusch *et al*., 2004; Gao *et al*., 2004). The computational processes of the algorithms of Jackson (1993), Owe *et al*. (2001), and Wen *et al.* (2003) are shown in Figure 7-6. The main features are:

- The Jackson (1993) algorithm solves the inverted version of equation 7.9 and uses additional vegetation information to estimate τ. Temperatures of surface and canopy are assumed equal and derived empirically from a high frequency channel such as from the 37 GHz channel of AMSR-E (de Jeu, 2003).

- The Owe *et al*. (2001) algorithm solves equation 7.9 iteratively using dual-polarized microwave brightness temperature observations for vegetation optical depth and surface emissivity simultaneously. De Jeu (2003) also proposed an algorithm that is quite similar to the Owe *et al*. approach. Temperatures are derived empirically from a high frequency channel as in the Jackson algorithm. The radiative transfer approach does not use ground observations of soil moisture, canopy biophysical data, or other geophysical data as calibration parameters. This model may be applied at any frequency.

- The Wen *et al.* (2003) algorithm also solves equation 7.9 iteratively. The solved quantities in this case, are surface temperature and surface emissivity.

Most methods proposed for soil moisture measurement based on microwave remote sensing have attempted to relate remotely sensed estimates of soil moisture to observed ground data, and then solve for the optical depth as a residual. These approaches however are not ideal because of poor ground-based data sets. Also, some of these approaches are inadequate because they are not physically based and hence do not adequately account for many of the properties that affect the microwave emission process (Owe *et al*., 2001) Furthermore, it is very difficult to obtain accurate spatially representative estimates of surface soil moisture and vegetation biophysical properties at satellite scales. In order to overcome this, Owe *et al*. (2002) introduced a methodology, which solves simultaneously for surface moisture and vegetation optical depth, without the use of observations of surface moisture or biophysical parameters. Their technique only uses the horizontal and vertical polarization brightness temperatures at one frequency and a surface temperature algorithm based on the vertical polarized 37 GHz signal.

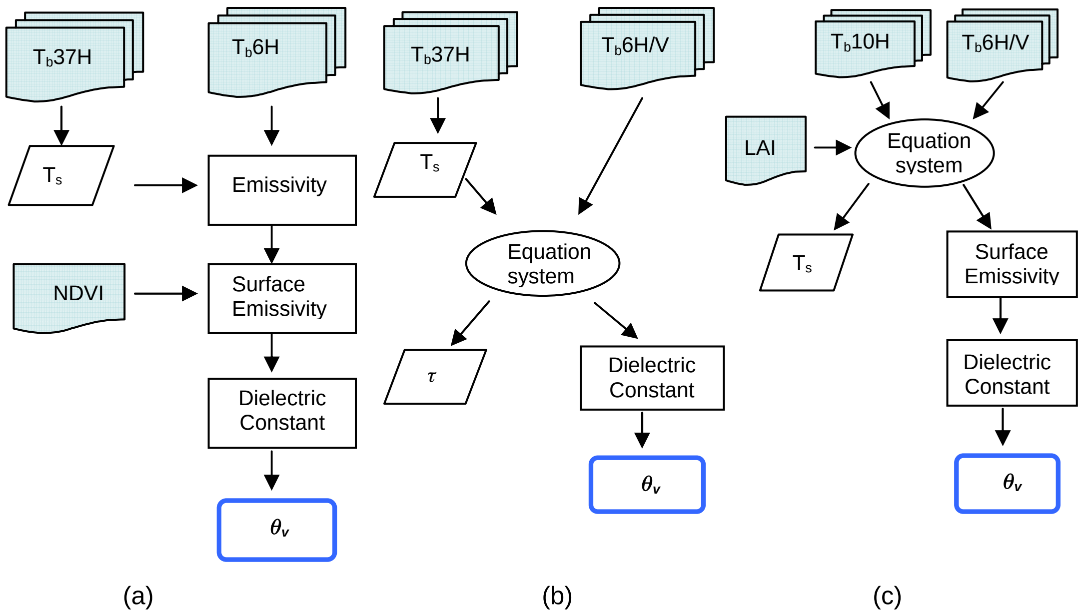

Figure 7-6: Schematic representation of computational process of soil moisture retrieval algorithms: (a) Jackson, (b) Owe *et al*., and (c) Wen *et al*. (based on Hurkman *et al*., 2004).

Despite all these attempts, the application of radiative transfer theory for soil moisture retrieval is not entirely straightforward for various reasons. Indeed, most of the radiative transfer mechanisms are known but the inverse problem of separating brightness temperature observed at satellite altitudes into its component parts is still a complex issue (Owe *et al*., 2001). A number of obstacles have contributed to this and some of these as reported by Owe *et al*. (2001) are:

- a large number of factors affect the emission process (e.g. soil physical properties, vegetation properties, atmospheric variables)
- nonlinearity of the emission process
- heterogeneity of the land surface
- inherent spatial variability of soil physical properties at satellite scales
- lack of suitable validation data sets at satellite scales

7.5 THE AMSR-E SOIL MOISTURE PRODUCT

Although numerous radiometers and scatterometers based on active and passive microwave radiation are in existence and have been used for measurement of near surface soil moisture, it is the Advanced Microwave Scanning Radiometer for EOS (AMSR-E) which has opened up a new era in satellite based soil moisture measurements. AMSR-E provides improved spatial resolutions over the earlier satellite based passive-microwave instruments, and its 6.9 GHz and 10.7 GHz channels allow soil moisture measurements that are not obtainable with previous radiometers such as SSM/I. AMSR-E C-band (6.9 GHz) and X-band (10.7 GHz) channels are strongly related to land surface soil moisture and are used to generate global land data products. Soil moisture is the principal retrievable Aqua AMSR-E land surface parameter. Surface temperature and vegetation water content are also retrieved by the algorithm.

Processing of AMSR-E data is a complex process and various research centers are involved in processing the data to different levels. During the data processing cycle, AMSR-E raw data received in the United States through the EOS Data and Operation System (EDOS), are transmitted to the NASDA Earth Observation Centre in Japan for engineering processing to Level 1A and, are then routed to AMSR-E Science Information Processing System (SIPS) in the US. At the SIPS, the data are converted into geophysical data products that are sent to the National Snow and Ice Data Centre (NSIDC) Distributed Active Archive Centre (DAAC) for retrieval and distribution. In level 2A processing, the data are quality checked, co-registered, resolution matched and finally, output as half-orbit data file granules. The Level 2A data contain as a subset the original Level 1A data (Njoku *et al.*, 2003).

Soil moisture retrieval from AMSR-E data is taking place at the Global Hydrology and Climate Centre (GHCC), a facility under SIPS. The processing generates Level 2B and Level 3 soil moisture and ancillary data products as shown in Figure 7-7 (a). The soil moisture retrieval algorithm of AMSR-E is discussed in section 7.5.1. Level 2B soil moisture data consists of half-orbit data granules. Level 3 product is derived by compositing the Level 2 parameters daily into global maps in Hierarchical Data Format (HDF), separating ascending and descending passes so that diurnal effects can be evaluated. Figure 7-7 (b) shows the detailed Level 2B processing flow. Soil moisture is not retrievable when significant fractions of snow cover, frozen ground, dense vegetation, precipitation, open water, or mountainous terrain occur within the sensor footprint (as determined by a classification algorithm and ancillary information). The algorithm products cover global land surfaces, excluding snow covered and densely vegetated areas. Input 6.9 GHz data, corresponding to a 56 km mean spatial resolution, are re-sampled to a global cylindrical 25 km Equal-Area Scalable Earth Grid (EASE-Grid) cell spacing.

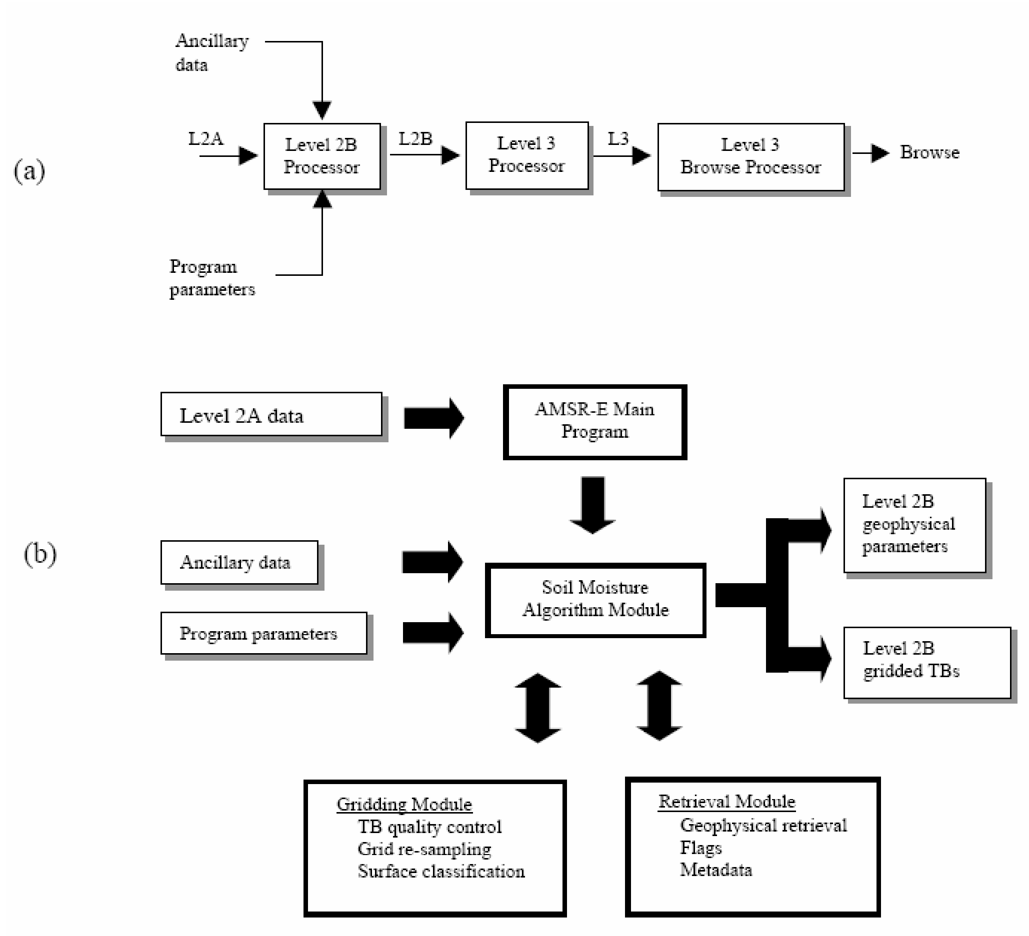

Figure 7-7: Schematic representation of AMSR-E soil moisture algorithm processing flow. (a) Overview, (b) Level 2B processing detail. (From Njoku *et al.*, 2003).

AMSR-E provides a range of land products and Table 7-2 gives a listing of all the products. The derived AMSR-E products include measurements of rainfall, snow, sea ice and many other land and ocean geophysical variables. Similar to soil moisture, all these products are provided as HDF raster data files and projected in 25 km EASE grid format. All AMSR-E products including daily Level-3 soil moisture data are now available from a few days after launch onwards from the NSIDC website at http://nsidc.org/data/amsre.

Table 7-2: AMSR-E land products (Njoku, 1999)

Product Level	Parameter	Estimated accuracy	Spatial Resolution	Grid Spacing	Temporal Resolution
2	Soil Moisture	0.06 g cm^{-3}	56 km	25 km	Half-orbit
2	Vegetation Water Content	0.15 kg m^{-2}	56 km	25 km	Half-orbit
2	Surface Temperature	2.5 C	56 km	25 km	Half-orbit
3	Soil Moisture	0.06 g cm^{-3}	56 km	25 km	daily*
3	Vegetation Water Content	0.15 kg m^{-2}	56 km	25 km	daily*
3	Surface Temperature	2.5 C	56 km	25 km	daily*
3	Brightness Temperatures	0.3 – 0.6 K	12,56 km	25 km	daily*

(* - Ascending and descending separate)

AMSR-E holds great promise for estimating soil water content in the top 1cm layer of soil with an accuracy of 0.06 g cm^{-3} for relatively low vegetation cover (biomass less than 1.5 kg m^{-2}) (Njoku and Li, 1999; Schmugge *et al.,* 2002). The C-band of the AMSR-E (6.9 GHz) has a better sensitivity than the 19.4GHz channel of the SSM/I to retrieve soil moisture. Limiting features of the AMSR-E measurements are its coarse footprint resolution (~40-60 km), low sensitivity to soil moisture under moderate to high vegetation water content, and shallow sensing depth (~1 cm in soil). However, the AMSR-E observations provide routinely produced and scientifically validated space-borne soil moisture measurements and hitherto unavailable information on global surface moisture variability.

The initial AMSR-E data has been found to contain significant radio frequency interference (Li *et al.*, 2004) and large calibration bias errors. In order to modify the algorithm for instrument errors and to verify the algorithm performance, continuing algorithm improvement and product validation activity on a global basis is important.

7.5.1 AMSR-E SOIL MOISTURE RETRIEVAL METHODOLOGY

Various retrieval approaches have been proposed for AMSR-E soil moisture computations. According to Njoku *et al*. (2003) these proposed retrieval techniques differ mainly in their approaches to the vegetation and surface temperature corrections. In general, four types of correction approaches were identified by Njoku *et al*. (2003).

1. Use of external ancillary data for sequential corrections
2. Iterative parameter fitting to a multi-channel brightness temperature model
3. Adoption of brightness temperature indices and regression techniques
4. Combination of the above methods

After assessing these approaches, the AMSR-E science committee selected an iterative multi-channel retrieval algorithm for soil moisture computation. The algorithm and its implementation are described in Njoku (1999), Njoku and Li (1999) and Njoku *et al*. (2003) and the reader is referred to these papers for more details. The AMSR-E approach for retrieving soil moisture is based on inversion of the microwave radiative transfer model. The procedure is similar to the retrieval techniques presented in section 7.4. The primary rationale for the selection of Njoku and Li methodology was to minimize the dependence on external ancillary data in the operational algorithm. The salient features of the current soil moisture retrieval model include;

- The algorithm is based on change-detection approach using the polarization ratio (ζ) which is defined as,

$$\zeta = \frac{T_{Bv} - T_{Bh}}{T_{Bv} + T_{Bh}} \qquad \textbf{(7-12)}$$

- The brightness temperature polarization ratios effectively normalize the surface temperature, leaving a quantity that is dependent primarily on soil moisture and vegetation. Use of both vertical and horizontal channels therefore forms a basis for a multi-channel approach.

- A combined vegetation-roughness estimate (g) is assumed. Vegetation and roughness have similar effects on polarization ratio (ζ) and hence are lumped together as a single parameter. This is used as a correction for the soil moisture retrieval.

$$g = \beta_o + \beta_1 In(\zeta_{10.7}) + \beta_2 In(\zeta_{18.7}) \quad \textbf{(7-13)}$$

$$\theta_v = \theta_v^* + \alpha_o g + \alpha_1(\zeta_{10.7} - \zeta_{10.7}^*)\exp(\alpha_2 g) \quad \textbf{(7-14)}$$

Where α and β coefficients are calibrated empirically using AMSR-E data over a range of vegetation, roughness, and soil moisture conditions (desert to forest transects, dry to flood temporal variations etc). The quantities θ^* and ζ^* are baseline values of θ and ζ. They are obtained from monthly minimum θ and ζ over an annual cycle for bare and dry soils respectively.

- The ancillary data used in the processing include:
    1. percentage open water within a grid cell
    2. topography mode and range within a grid cell
    3. maximum snow cover and ice extent
    4. soil texture (from global databases)

- The values of geophysical parameters $\chi = \{ \theta_v, W_c,$ and $T_s \}$ are adjusted iteratively to minimize the weighted sum of the squared differences between observed and computed brightness temperatures.

- Areas of dense vegetation, permanent ice, and snow are masked out. Mountains, frozen grounds, and precipitation are not currently masked. Hence, data obtained over these areas need careful assessment.

7.5.2 PROPERTIES OF AMSR-E DATA

AMSR-E data are available as hierarchical data format (HDF) files. Brightness temperatures and computed parameters for both ascending and descending paths during a day are therefore available in the same file. Geographic referencing of AMSR-E data follows the EASE-Grid system developed by the National Snow and Ice Data Centre (NSIDC). AMSR-E uses the global, cylindrical, equal-area projection, with a nominal grid spacing of approximately 25 x 25 km (true at 30°N&S). The size of the grid is 1383 columns x 586 rows. A description of the EASE-Grid can be found at the NSIDC website at http://nsidc.org/data/ease/. The advantage of an equal-area grid is that the re-sampling statistics at each grid point are characteristic of the same number of input data points.

This thesis uses the Version 1 (i.e. B01) gridded Level-3 land surface product (AE_Land3) downloaded from NSIDC website. Soil moisture data of daily ascending and descending paths from 1 January 2003 to 31 December 2004 were used in the current study. Thus, raster data from over 700 HDF files were used.

7.6 AMSR-E SOIL MOISTURE VALIDATION STUDIES

AMSR-E provides an opportunity to determine global soil moisture patterns at scales suitable for inclusion in land surface models. The AMSR-E soil moisture retrieval algorithm is based on many assumptions and theoretical equations and therefore, the resulting soil moisture estimates are not necessarily representative of the actual soil moisture status in various agro-ecological conditions. Hence, the first steps towards the use of AMSR-E soil moisture products for modelling studies are algorithm assessment and inter-comparison with field measured near-surface moisture contents. This is however, not an easy task due to the large footprint size of the AMSR-E pixels and the technical difficulty of obtaining near-surface soil moisture measurements (over the first 1cm of soil) in sufficient numbers to describe the large footprint. Traditional validation techniques based on the collection of a large number of samples across the footprint can rarely be implemented at very large scales and over extended periods. In addition, most existing soil moisture monitoring networks are also not ideal for the validation of such near-surface measurements due to a mismatch of sensing depths and poor spatial coverage. Because of these reasons, short-term intensive field campaigns across the globe are necessary to investigate the performance of the soil moisture retrieval algorithm in various agro-climatic regions. Furthermore, new permanent monitoring networks for near-surface soil moisture measurements need to be established particularly in areas which are suitable for passive microwave observations. This would facilitate the evaluation of the temporal behaviour of AMSR-E soil moisture measurements. It would also beneficial to develop new analytical techniques so that the soil moisture information from existing monitoring networks may be used for AMSR-E validation. Hence, AMSR-E validation attempts should be multidimensional in nature and various approaches must be implemented in order to improve the current retrieval algorithm.

The primary objective of AMSR-E soil moisture validation activities is to characterize the radiometer signal and *in-situ* data errors to infer the soil moisture retrieval accuracy. According to Njoku *et al*. (2003) the scope of validation program includes:

1) Brightness temperature calibration checks throughout the Aqua mission.

2) Comparison between AMSR-E retrievals and data from long-term measurement networks over seasonal and annual cycles.

3) Short-term intensive field campaigns to measure soil moisture and other surface and atmospheric variables at the AMSR-E footprint scale.

4) Inter-comparisons with other satellite data

5) Hydrological modelling and data assimilation activities. This will be used to generate spatial soil moisture fields that bridge the gap between the field experiment scale and the regional and continental scale.

A number of AMSR-E soil moisture validation programs such as SMEX02, SMEX03, and SMEX04-NAME have been conducted since the launch of the Aqua satellite (Njoku *et al.,* 2003; see information online at http://nsidc.org/data/amsr_validation). Two field campaigns were also conducted in the central Australian desert (Walker *et al.,* 2003). Four watersheds are being monitored within US (Oklahoma, Georgia, Arizona, and Idaho) for comparison with long-term *in-situ* soil moisture measurements (Njoku *et al.,* 2003). Other validation sites include the Tibetan Plateau, Mongolia (Kaihotsu *et al*., 2002; Koike *et al*., 2003), and African deserts and areas in the Sahel (Njoku, 1999). These validation efforts are developed around *in-situ* validation data, primarily through long-term point measurements and a limited number of field campaigns using airborne radiometers and ground observation data. Wood (2004) attempted to validate AMSR-E data based on the SMEX02 data set and reported that studies are being conducted through a combination of process-based hydrological modelling and the simulation of the AMSR-E measurements. Using the SMEX02 data set, McCabe *et al.* (2005a and 2005b) also reported a consistent level of agreement of measured moisture contents within a AMSR-E footprint. Furthermore, data assimilation studies have also been conducted (Reichle *et al.*, 2001b; Walker and Houser, 2001) for global validation of AMSR-E products. Recently, Jackson *et al*. (2006) have also reported on a AMSR-E validation study. The goal of the Land Data Assimilation System (LDAS) project is to develop a near real-time operational land data assimilation system to monitor spatial-temporal AMSR-E soil moisture and snow observation.

The results of some of these validation attempts have been published (e.g. Walker *et al.,* 2003; McCabe *et al.,* 2005) and some are only available in unpublished form (e.g. Koike *et al*., 2003). One of the objectives of SMEX02 program conducted in Iowa, USA in June-July 2002 was to validate brightness temperatures and soil moisture products from AMSR-E. During this study an aircraft-based NOAA Polarimetric Scanning Radiometer (PSR) was used. The PSR has four C and four X sub-band channels and measured brightness temperatures from this instrument were compared with the AMSR-E brightness measurements. Good agreement between PSR C-band measured brightness temperature and AMSR-E X-band (10.7 GHz) was reported by Jackson *et al*. (2003), Wood (2004) and McCabe *et al.* (2005). They also reported AMSR-E has reasonable variability after rain events. Another validation study conducted during 1 July-20 September 2002 in Mongolia also reported a good agreement between ground-observed data and AMSR-E estimation (Kaihotsu *et al.*, 2004). Since large-scale soil moisture measuring techniques are still relatively new, satellite predictions of near-surface soil moisture need to be validated across a range of land surface and climatic conditions. More validation trials are needed in order to improve the accuracy of soil moisture retrieval methodology. In the Australian context, the accuracy of AMSR-E soil moisture measurements needs to be evaluated for a range of important land systems including sub-humid and semi-arid grasslands. The SASMAS study region provides suitable field conditions for such validation studies. As described in Chapter 3 vegetation characteristics and landscape properties within the SASMAS study region provide suitable conditions for passive microwave remote sensing studies. Two types of validation studies were conducted. The first type of validation study is based on three short-term intensive field campaigns and is discussed in sections 7.6.1 and 7.6.2. The second validation approach is based on a temporal analysis of soil moisture data from the permanent monitoring sites and is discussed in section 7.7.

7.6.1 FIELD VALIDATION CAMPAIGNS

For the field validation of AMSR-E footprints, a sampling area of 40 km x 50 km was selected in the SASMAS study region (see Figure 7-9) so that the large area was within the actual field of view of the sensor, with at least a full 25km × 25km soil moisture footprint situated within the sampling area. Due to the large footprint size, available resources, travel times and access issues, complete coverage was not possible within a single day. Therefore, the validation area was divided into four quarters and one quarter assigned to each of four teams of two observers. Each quarter was further subdivided into nine cells of approximately 7km x 8km, three of which were sampled per day over the three-day campaign period. Three-day field campaigns were justified on the basis that soil moisture content was not expected to vary greatly during the course of a few days as the surface soils are generally dry in sub-humid climate.

The number of overpasses per day was the main criterion in selecting the campaign dates. Overpass predictions based on the Overpass predictor at http://eobglossary.gsfc.nasa.gov/ MissionControl/overpass.html and the WXtrack-orbit predictor (Taylor, 2003) were used as a guide to plan the campaign days (see

Figure 7-8 and Table 7-3). Campaigns were undertaken on 7-9 November 2003, 1-3 May 2004 and 7-9 July 2004. These three campaigns captured seasonal variations in soil moisture and vegetation conditions, and coincided with AMSR-E overpasses so that there was at least 1 overpass each day with preferably 2 overpasses (am and pm) on the central day.

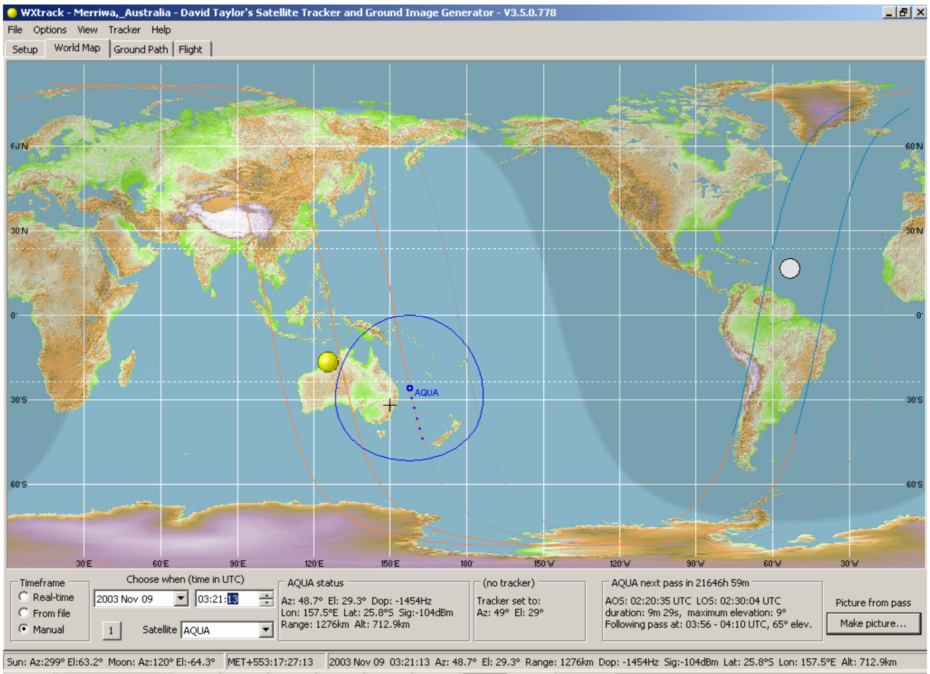

Figure 7-8: Overpass prediction screen of WXtrack orbit predictor for 9 November 2003. Blue circle shows the area visible from the Aqua satellite at the overpass time.

Table 7-3: Summary of Aqua overpasses during November 2003, May 2004 and July 2004 for the Goulburn river subcatchment. Dates selected for ground sampling have been highlighted (Based on the overpass predictor at http://earthobservatory.nasa.gov/Mission Control /overpass.html and the WXtrack orbit predictor).

Date	Time of peak elevation (GMT + 10.00)	Peak spacecraft elevation above horizon (degrees)	Day/Night	Orbit Number
06/11/2003	14:20:35	n.a.	Day	n.a.
07/11/2003	26:06:45	n.a.	Night	n.a.
08/11/2003	14:35:04 25:15:04	n.a.	Day Night	n.a.
09/11/2003	15:21:13 24:20:04	n.a.	Day Night	n.a.
10/11/2003	14:03:04	n.a.	Night	n.a.
27/04/2004	25:31:28	52.7	Night	10545
28/04/2004	13:36:04	59.0	Day	10553
29/04/2004	14:18:59	44.7	Day	10568
	25:19:48	72.4	Night	10574
30/04/2004	13:24:24	43.1	Day	10582
01/05/2004	14:07:27	60.8	Day	10597
	25:08:08	83.9	Night	10603
02/05/2004				
03/05/2004	13:55:47	82.6	Day	10626
	24:56:36	61.9	Night	10632
04/05/2004	25:39:31	42.4	Night	10647
04/07/2004	25:25:32	61.8	Night	11536
05/07/2004	13:30:08	50.4	Day	11543
06/07/2004	14:13:03	52.2	Day	11558
	25:13:52	84.1	Night	11565
07/07/2004				
08/07/2004	14:01:23	71.3	Day	11587
	25:02:12	72.1	Night	11594
09/07/2004				
10/07/2004	13:49:43	84.9	Day	11616
	24:50:32	52.7	Night	11623

Note: - Time >24 hrs indicates Date = Date + 1
- Peak spacecraft elevation and orbit number data are not available for Campaign-1 dates

The first validation campaign aimed at collecting soil moisture measurements at 325 pre-identified sites across the validation area. From each cell (7km x 8km area) about 9 measurements with a 3 x 3 grid pattern and a distance of about 2km to 2.5km between adjacent sites were identified as potential sampling sites. At the time of planning, when locating sampling sites on the 1:250,000 scale standard topographic maps, preference was given to locations closer to the roads or any marked access routes rather than follow a strict grid pattern. While this sampling method may have resulted in some bias in the final result, it was the best possible practical way of visiting and collecting soil samples from an area where most of the land is privately owned. In addition, access time to visit a site far away from roads was another concern in view of the limited human resources for field sampling. During the campaign each team was provided with a map showing all selected sites, a complete list of latitude and longitude coordinates of all the sites, and a hand-held GPS unit. Each team was expected to visit as many sites as possible within a day covering all three cell areas. To minimize the time required searching exact locations, teams were asked to use the predefined sites as a guide only. Also, the teams were allowed to move sampling sites if they experienced any access problem. When doing so however, they were advised to maintain a uniform distribution of sampling sites across a cell. At the end of the first campaign, it was found that a team of two can visit three different areas within a 20km x 25km area and collect approximately 20 samples per day. Hence the maximum number of sites that could be visited within a three-day period was about 225 sites. Building on the experience gained during the Campaign 1, subsequent campaigns aimed at collecting approximately 200 sites, considering the shorter day lengths as these campaigns were conducted in late autumn and in mid winter. During Campaigns 2 and 3, samples were collected where possible from the same sites visited during the first campaign.

It was expected that over 200 point measurements and their coverage should provide an adequate basis for the validation of the satellite soil moisture product and for the development of a procedure for downscaling average moisture measurements for large areas (see Chapter 7 for details). Five 0-1 cm soil moisture samples were obtained at each site with a steel sampling ring of 82 mm diameter and 10 mm in height. The five samples were combined and used to obtain volumetric soil moisture contents. In addition, five soil moisture observations were also made at each site with a Theta® probe which yielded volumetric soil moisture content values integrated over a 0-6 cm layer. Apart from soil moisture, other parameters including soil and air temperatures, soil type, and surface conditions were also recorded, and vegetation samples were collected for determining vegetation water content and dry biomass.

In addition, climatic data such as rainfall, solar radiation, and continuous observations of air and near-surface soil temperature were obtained from weather stations and permanent soil moisture monitoring sites within the validation area.

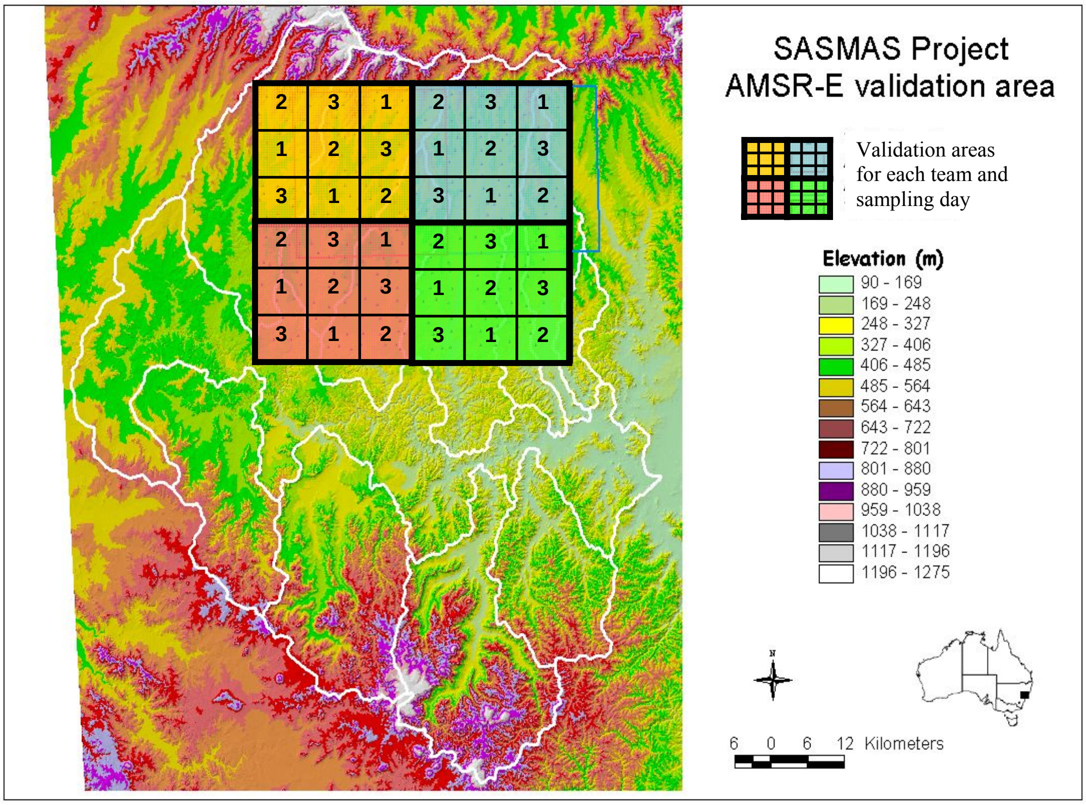

Figure 7-9: Validation footprint, area assigned to each group and daily sampling patterns within the Goulburn River catchment, Australia. Background image shows subcatchment boundaries and elevation (in meters above mean sea level).

At the time of field campaigns, AMSR-E soil moisture retrieval was carried out with a different algorithm. Later, as described in section 7.5.1 a new algorithm was introduced and all historical data were reprocessed. This study uses soil moisture products from the new algorithm (Manaka, 2005) and all AMSR-E data were downloaded on March 2005 from NSIDC.

The area selected for the validation was entirely within complete AMSR-E EASE-grid cells. Two pixels were found to be useful in validation analysis. The pixel at EASE-grid column number 1269 and row number 449 (c1269, r449) was entirely within the validation area and approximately more than 80 percent of the area of a second pixel at c1270, r449 was also within the selected study area. These pixels were named Pixels A and B and their locations are shown in the Figure 7-10. AMSR-E measured soil moisture values for Pixel-A and B during three campaign days for each path are shown in Table 7-4. As seen in the table, AMSR-E measured soil moisture values appear stable during campaign days.

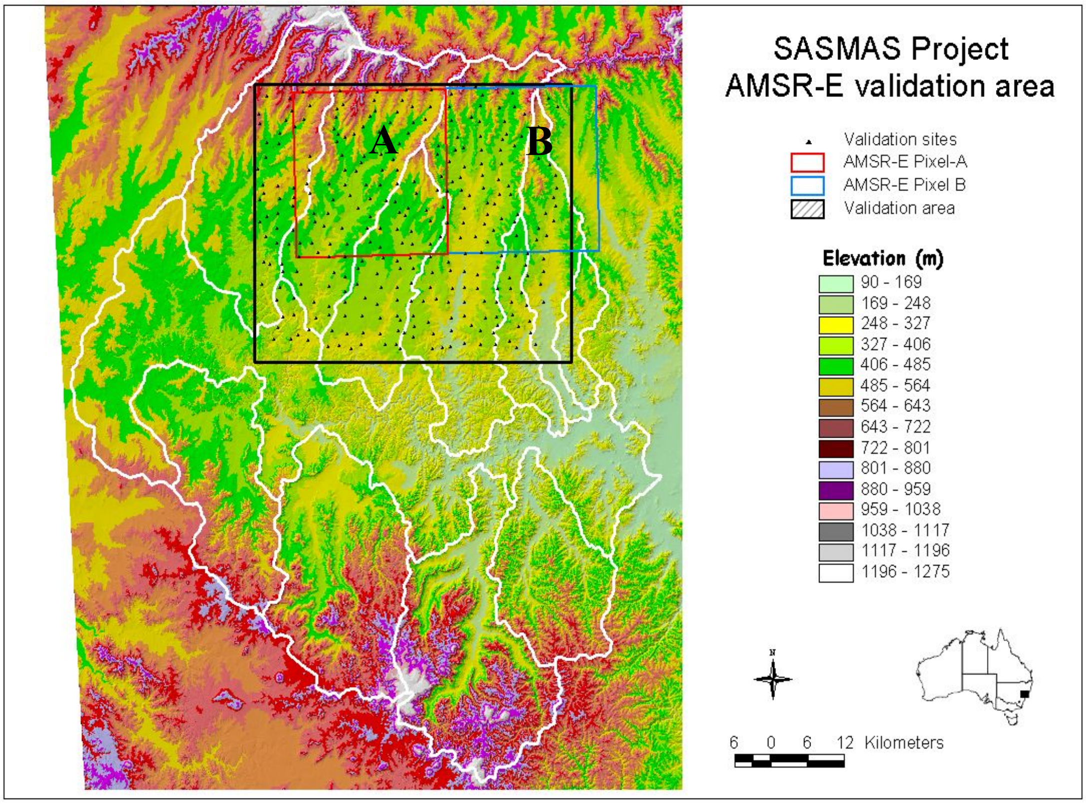

Figure 7-10: Field sampling sites, and locations of AMSR-E pixels A & B within the Goulburn River Catchment.

Table 7-4: AMSR-E soil moisture (cm^3 cm^{-3}) at Pixels A and B during three campaigns

Campaign	Day	Pixel-A Ascending path	Pixel-A Descending path	Pixel-A Avg.	Pixel-B Ascending path	Pixel-B Descending path	Pixel-B Avg.
1	1	0.083	0.082	0.083	0.085	0.083	0.084
	2	n.a.	0.076	0.076	n.a.	0.080	0.080
	3	0.077	n.a.	0.077	0.082	n.a.	0.082
	Avg.			0.079			0.083
2	1	0.129	0.113	0.121	0.135	0.113	0.124
	2	n.a.	0.106	0.106	n.a.	0.114	0.114
	3	0.118	n.a.	0.118	0.126	n.a.	0.126
	Avg.			0.115			0.122
3	1	0.115	0.110	0.113	0.111	0.108	0.110
	2	0.111	n.a.	0.111	0.113	n.a.	0.113
	3	0.115	0.105	0.110	0.111	0.099	0.105
	Avg.			0.111			0.109

7.6.2 SPATIAL DISTRIBUTION OF NEAR-SURFACE SOIL MOISTURE OVER VALIDATION FOOTPRINT

7.6.2.1 Areal distribution of ground-based soil moisture observations

Soil moisture samples were taken during the three campaigns at between 180 – 225 sites. Summary statistics of the measured soil moisture levels for the 0-1 cm and 0-6 cm soil layers are given in Table 7-5 and in Figure 7-11 - Figure 7-13. During Campaign 1 the measured volumetric soil moisture in the 0-6 cm layer (14.1 %) was higher than for the 0-1 cm soil layer (10.9 %). A similar pattern was found in Campaign 3 where the 0-1 cm top layer had 12.2 % and 0-6 layer had 17.2% moisture. However, during the second campaign, the measured soil moisture of 18.9% in 0-1 cm was slightly higher than the moisture content of 16.7% in the 0-6 cm soil layer. Figure 7-14 shows maps of volumetric soil moisture content for the top 1 cm and 6 cm layers for each of the three campaigns. The mapping grid cells used in these maps are 1.21 km^2 in area and have been chosen to enable comparisons with derived moisture distribution patterns obtained from MODIS data. Reasonably coherent soil moisture patterns emerge, with agreement between the maps for the 0-1 cm and 0-6 cm observation depths. It can also be seen that for all three campaigns the southern half of the study area appears to be slightly drier than the northern half. This is partly due to differences between the clayey soils in the north and the sandy soils in the south. However, better understanding of the surface wetness patterns also requires comparing the results with antecedent rainfall, prevailing climatic conditions and land surface conditions. This will be addressed in subsequent sections.

Table 7-5: Summary statistics of the measured soil moisture contents (in $cm^3\ cm^{-3}$) for 0-1 cm and 0-6 cm soil layers during three field campaigns.

Campaign	Soil depth (cm)	Number of samples	Moisture content ($cm^3\ cm^{-3}$)			
			Mean	Std dev.	Min.	Max.
1	0-1	201	0.109	0.050	0.014	0.301
(7-9 Nov 2003)	0-6	225	0.141	0.051	0.015	0.286
2	0-1	208	0.189	0.077	0.017	0.443
(1-3 May 2004)	0-6	211	0.167	0.077	0.010	0.380
3	0-1	181	0.122	0.048	0.014	0.320
(7-9 Jul 2004)	0-6	179	0.172	0.073	0.014	0.373

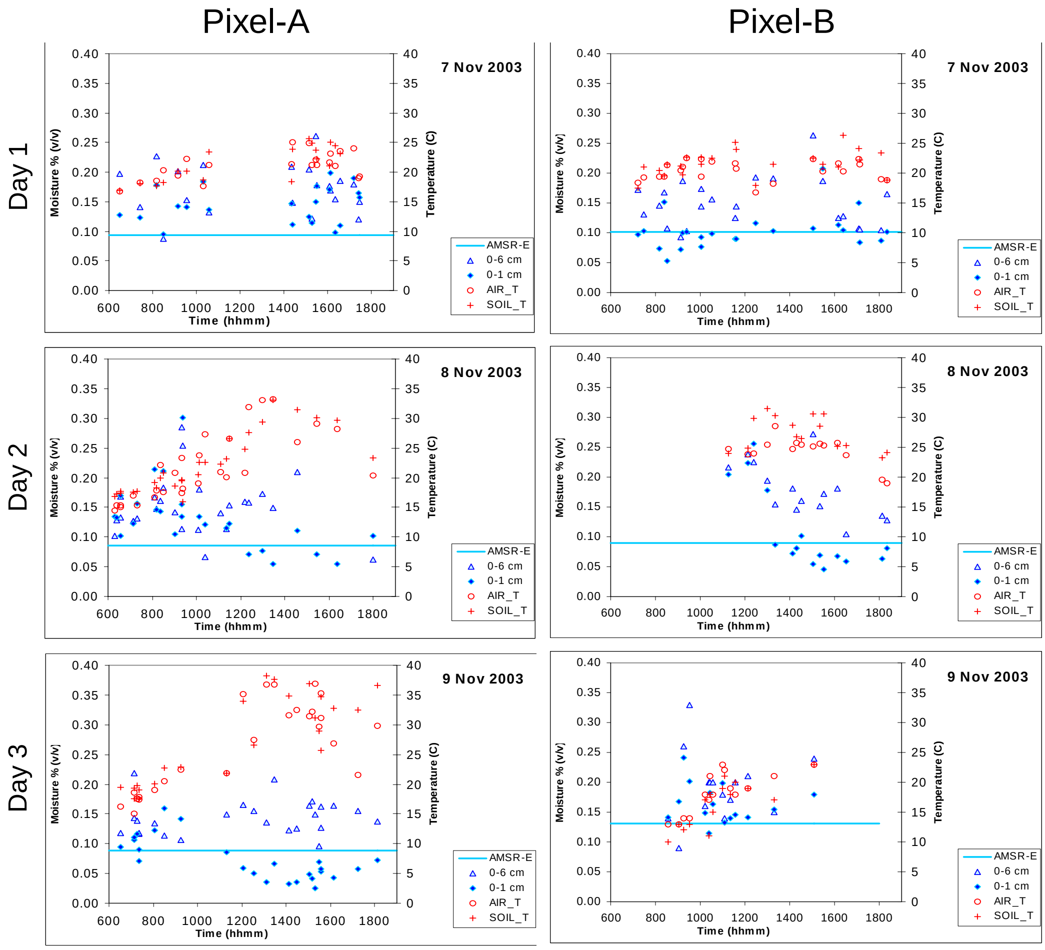

Figure 7-11: Time plots of measured soil water contents (0-1 and 0-6 cm; blue symbols), air and soil temperatures (red symbols), and average AMSR-E soil moisture estimates (shown as a blue continuous line) computed for the two AMSR-E pixels during Campaign-1.

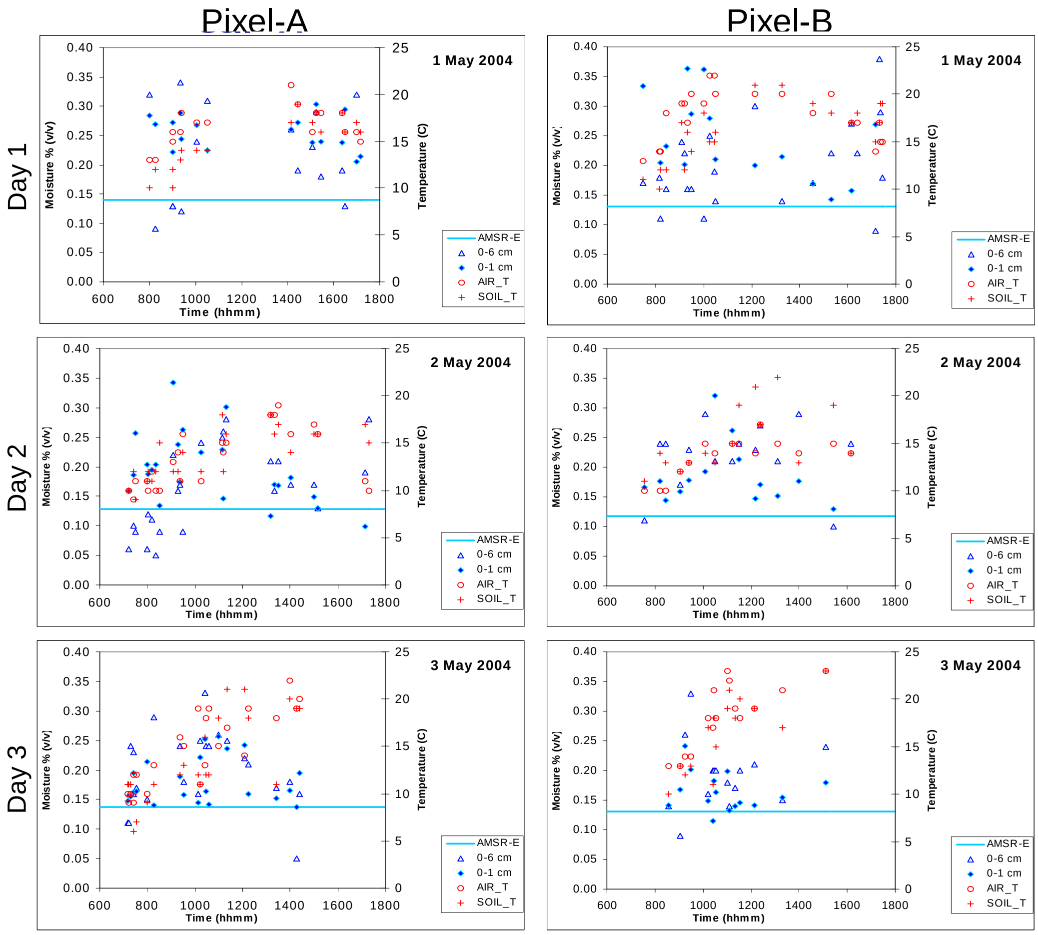

Figure 7-12: Time plots of measured soil water contents (0-1 and 0-6 cm), air and soil temperatures, and average AMSR-E soil moisture estimate (shown as a continuous line) computed from two AMSR-E pixels during Campaign-2.

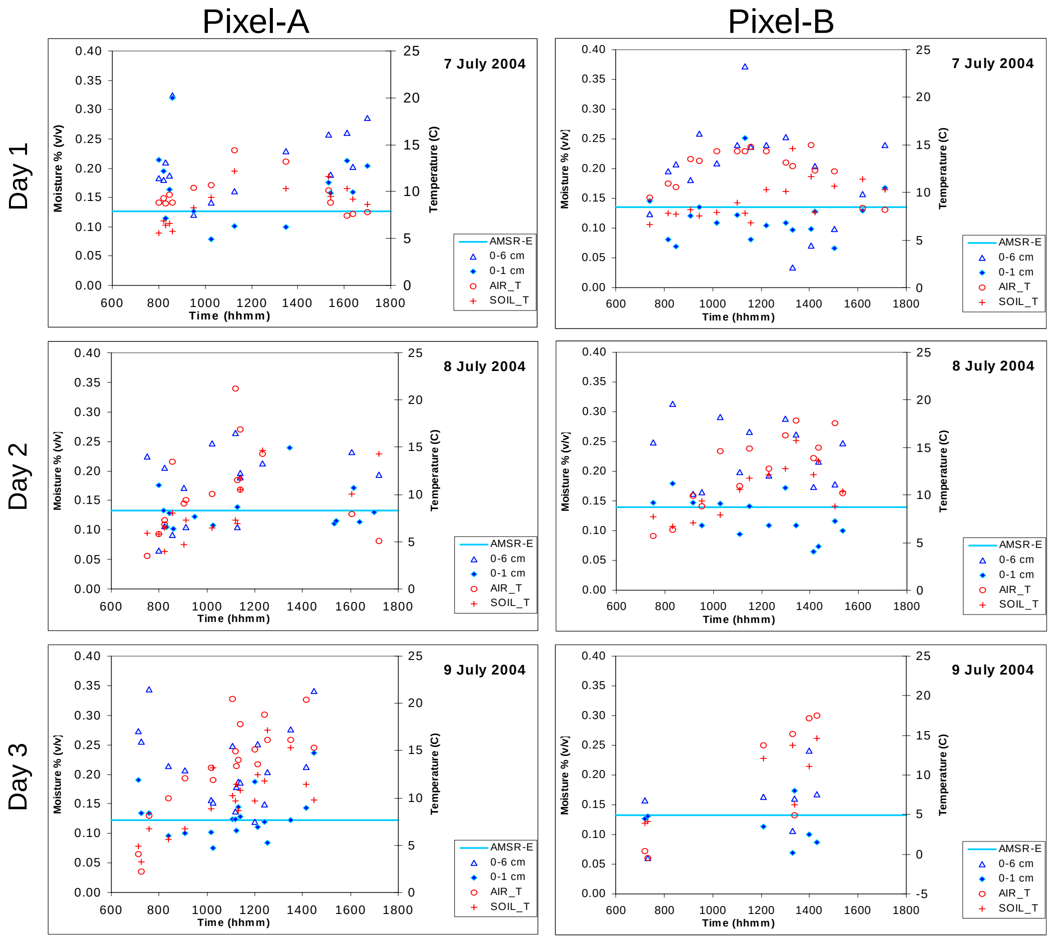

Figure 7-13: Time plots of measured soil water contents (0-1 and 0-6 cm), air and soil temperatures, and average AMSR-E soil moisture estimate (shown as a continuous line) computed from two AMSR-E pixels during Campaign-3.

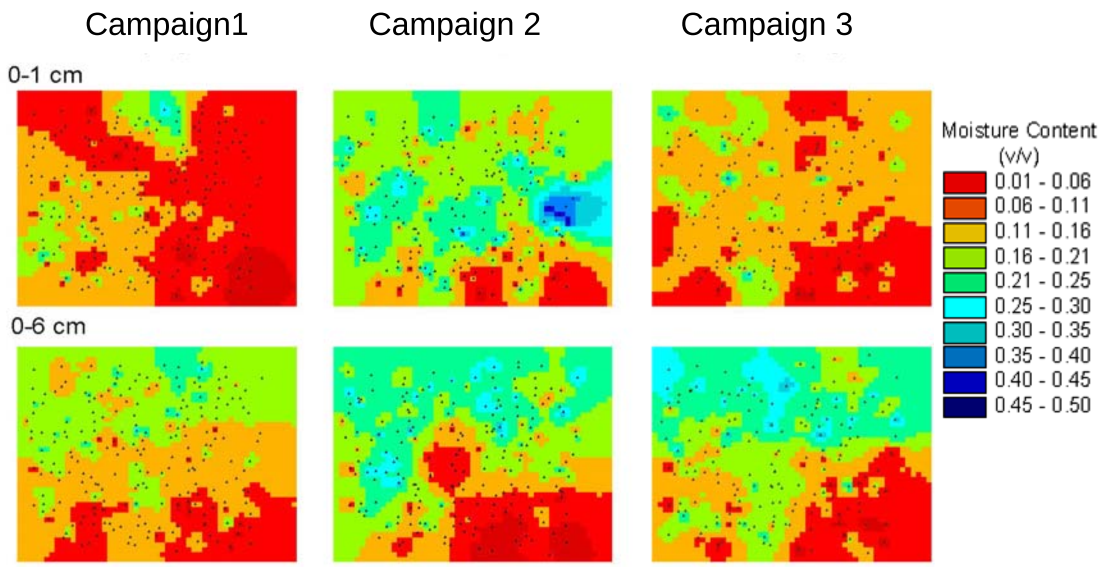

Figure 7-14: Top 0-1 cm and 0-6 cm volumetric soil water content (cm^3 cm^{-3}) distribution within the validation area for Campaigns 1, 2 and 3 (mapping grid cells are 1.21 km^2 in area and sampling locations are indicated as small dots).

As seen in Figure 7-14 the spatial patterns of measured soil water contents in the 0-1 cm and 0-6 cm layers confirm that during Campaign 1 and Campaign 3, the top 0-1 cm layer contains less moisture than 0-6 cm layer. During Campaign 2 however, the top 0-1cm layer appears to be wetter than the 0-6 cm layer.

Comparisons of point-scale measurements of the 0-1 cm and 0-6 cm layers during the field campaigns are important for determining the consistency of field measured data. Figure 7-15 compares the soil moisture measurements of the 0-6 cm and 0-1 cm depths. As can be seen, there is a positive correlation between 0-6 cm and 0-1 cm soil moisture measurements.

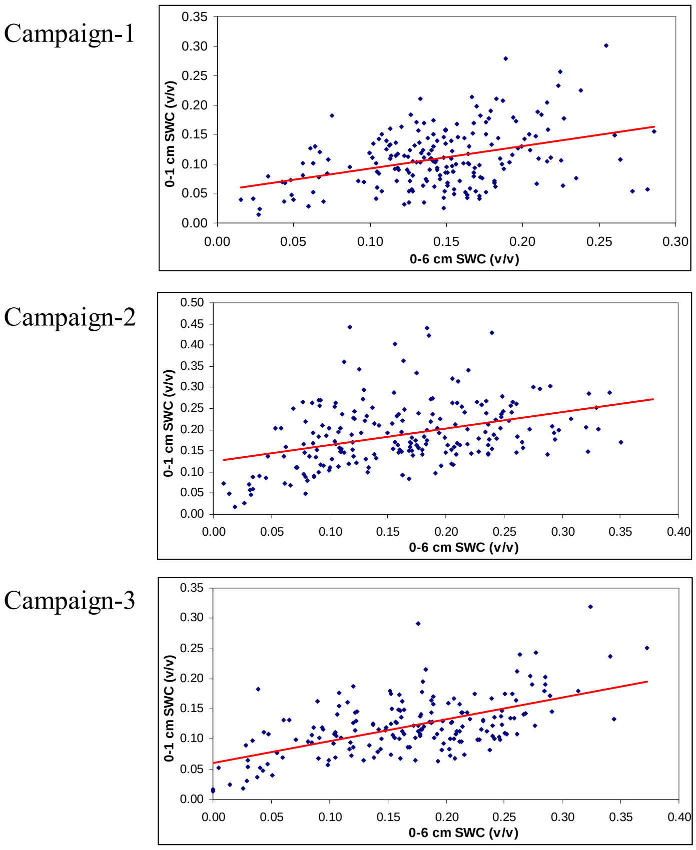

Figure 7-15: Comparison of measured soil moisture contents (cm^3 cm^{-3}) in the 0-6 cm and 0-1 cm layers (line indicates the linear fit between 0-6cm and 0-1cm data).

One of the major difficulties faced during the field campaigns was the collection of accurate soil samples from the top 0-1 cm layer for subsequent laboratory determination of soil moisture content. This was especially the case in dry basalt-derived soil. Also, the use of the Theta probe for soil moisture measurements in dry basalt-derived soils was besets with problems as because the soil was at times too hard to insert the probe, and numerous cracks in the soil frequently prevented close contact with the Theta probe.

7.6.2.2 Effect of climatic parameters on ground based observations

(i) *Antecedent rainfall*

The surface soil moisture distribution patterns shown above may be compared with the antecedent rainfall pattern. As shown in the Table 7-6 (a), rain during Campaign 1 was responsible for the wet conditions in the 0-1cm surface layer.

This rain mainly occurred in the northern part of the validation footprint and it explains the wet portions in the northern area. The highest weekly average rainfall of 14.2 mm was reported just before Campaign 2 which occurred in late autumn (Table 7-6 (b)). As a result, both the 0-1 cm and 0-6 cm soil layers showed relatively wet conditions, as shown in Figure 7-14 and Table 7-6(b). On the other hand, as shown in Table 7-6(c), despite the low rainfall before Campaign 3 (total rainfall was 0 mm and 21 mm in the previous 7 days and 30 days respectively) moderately wet conditions were found in the 0-6 cm soil layer during this mid-winter campaign. This could be due to the lower evaporative demand prevailing in the winter season. In general, there is an evidence of a decreasing rainfall gradient from North to South (e.g. from K6 to K4 to S2 and from M7 to M4) in all three campaigns (The reader may refer Figures 3.15, 3.16 and 3.17 in Chapter 3 for monthly/annual spatial rainfall distribution patterns in the Goulburn catchment). Also, during Campaign 2, an increase in rainfall from East (M4) to West (K4) is evident (see Table 7-6(b)). The results indicate that antecedent rainfall appears to be a important parameter in explaining the differences in surface wetness conditions.

Table 7-6(a): Total rainfall measured at K6 and S2 during the three-day Campaign 1 (days 311, 312 and 313) and over 7 days and 30 days before Campaign 1. (Refer Chapter 3 for location details of these sites).

Campaign #	Rainy days (day of the year)	Measured rainfall (mm) K6	S2	Average (mm)
1	275	23.0	22.4	22.7
	276	0.2	0.0	0.1
	278	0.0	4.6	2.3
	279	3.8	4.2	4.0
	280	0.2	1.4	0.8
	288	0.4	1.4	0.9
	289	0.0	1.8	0.9
	291	0.2	0.0	0.1
	292	16.2	12.8	14.5
	293	3.0	1.6	2.3
	298	0.2	0.0	0.1
	299	4.4	3.6	4.0
	304	14.2	5.4	9.8
	306	1.4	3.4	2.4
Day 1	311	3.8	1.4	2.6
Day 2	312	0.0	0.0	0.0
Day 3	313	0.2	0.6	0.4
Cumulative rainfall				
-previous 7 days		15.6	8.8	12.2
-previous 30 days		71.2	64.6	67.9
Rain during the campaign		4.0	2.0	3.0

Table 7-6(b): Total rainfall measured at K6, S2, K4, M7 and M4 during the three-day Campaign 2 and over 7 days and 30 days before Campaign 2 (days 122, 123 and 124). (Refer Chapter 3 for location details of these sites)

Campaign #	Rainy days (day of the year)	Measured rainfall (mm) K6	S2	K4	M7	M4	Average (mm)
2	95	6.2	15.6	6.6	0.0	0.0	5.7
	96	0.2	0.0	0.0	0.0	0.0	0.0
	100	0.0	0.0	0.0	0.2	0.0	0.0
	113	0.0	0.0	0.0	0.2	0.0	0.0
	120	20.0	13.0	15.2	11.4	10.6	14.0
	121	0.0	0.0	0.2	0.2	0.6	0.2
Day 1	122	0.8	0.0	0.0	0.2	0.0	0.2
Day 2	123	0.2	0.0	0.0	0.0	0.0	0.0
Day 3	124	0.0	0.0	0.0	0.0	0.0	0.0
Cumulative rainfall							
-previous 7 days		20.0	13.0	15.4	11.6	11.2	14.2
-previous 30 days		26.4	28.6	22.0	12.0	11.2	20.0
Rain during the campaign		1.0	0.0	0.0	0.2	0.0	0.2

Table 7-6(c): Total rainfall measured at K6, S2, K4, M7 and M4 during the three-day Campaign 3 and over 7 days and 30 days before Campaign 3 (days 189, 190 and 191). (Refer Chapter 3 for location details of these sites)

Campaign #	Rainy days (day of the year)	Measured rainfall (mm) K6	S2	K4	M7	M4	Average (mm)
3	155	9.8	6.8	7.2	8.0	7.6	7.9
	158	0.0	0.0	0.2	0.2	0.0	0.1
	162	11.8	5.6	6.4	14.2	4.2	8.4
	164	0.2	0.2	0.2	0.0	0.0	0.1
	165	0.0	0.0	0.0	0.0	0.2	0.0
	166	0.2	0.0	0.0	0.0	0.0	0.0
	167	0.8	0.0	0.0	0.0	0.0	0.2
	169	0.0	0.0	0.0	0.2	0.0	0.0
	171	8.4	1.8	3.6	4.6	1.6	4.0
	172	0.6	0.0	0.0	0.0	0.0	0.1
	178	0.2	0.2	0.2	0.0	0.0	0.1
Day 1	189	0.6	0.0	0.0	0.0	0.0	0.1
Day 2	190	0.0	0.0	0.0	0.0	0.0	0.0
Day 3	191	0.0	0.0	0.0	0.0	0.0	0.0
Cumulative rainfall							
-previous 7 days		0.0	0.0	0.0	0.0	0.0	0.0
-previous 30 days		32.0	14.6	17.8	27.2	13.6	21.0
Rain during the campaign		0.6	0.0	0.0	0.0	0.0	0.1

(ii) *Solar radiation and surface temperature during the sampling period*

Apart from antecedent rainfall patterns, other climatic parameters such as total incoming solar radiation, soil surface temperature and air temperature may also assists in explaining some of the temporal variations in the surface wetness pattern. These climatic parameters were obtained at climate station (S2) located within the validation footprint (see Section 3.4.5 and Table 3.5 for details of the S2 climate station). As shown in Figure 7-16a, during Campaign 1, the weather was drier than in other two campaigns and this was characterized by the higher solar radiation value of about 1000 Wm^{-2} and near-surface (at 7.5 cm) soil temperature between 18-26 ^oC. During Campaigns 2 and 3, the incoming radiation level was lower (less than 800 Wm^{-2} and 600 Wm^{-2}, respectively) and as a result, soil temperatures were also a lower (<16 ^oC and 10 ^oC, respectively).

The range of soil temperature variations during Campaign 1 was higher than during the other two campaigns. Soil temperature during the first day of Campaign 1 varied from 18.6-20.3 ^oC. During the second day, soil temperature ranged from 18.0-22.2 ^oC and by the third day, the range was between 18.6-25.3

^{o}C, a very high value compared to the first two days (see Figure 7-16a). The increase of soil temperature over the three-day period may be attributed to two main causes. First, the significant increase of solar radiation levels from day-1 to day-3 causing soil temperature to increase. Second, soil temperature may increase due to soil drying. As in Table 7-5 and in Figure 7-14 the measured near-surface soil moisture during Campaign 1 showed dry conditions. Soil temperature variation during Campaign 2 and 3 however, occurred within a narrower range and this may be due to factors such as shorter day length, lower solar radiation levels and higher soil moisture contents.

Comparison of the level of incoming radiation levels and the surface temperatures shows that the climatic conditions during Campaign 1 do not provide ideal conditions for collecting near surface soil moisture readings over an extended period to validate AMSR-E moisture data. On the other hand, Campaign 2 and 3 were associated with climatic conditions which appear suitable for such a purpose.

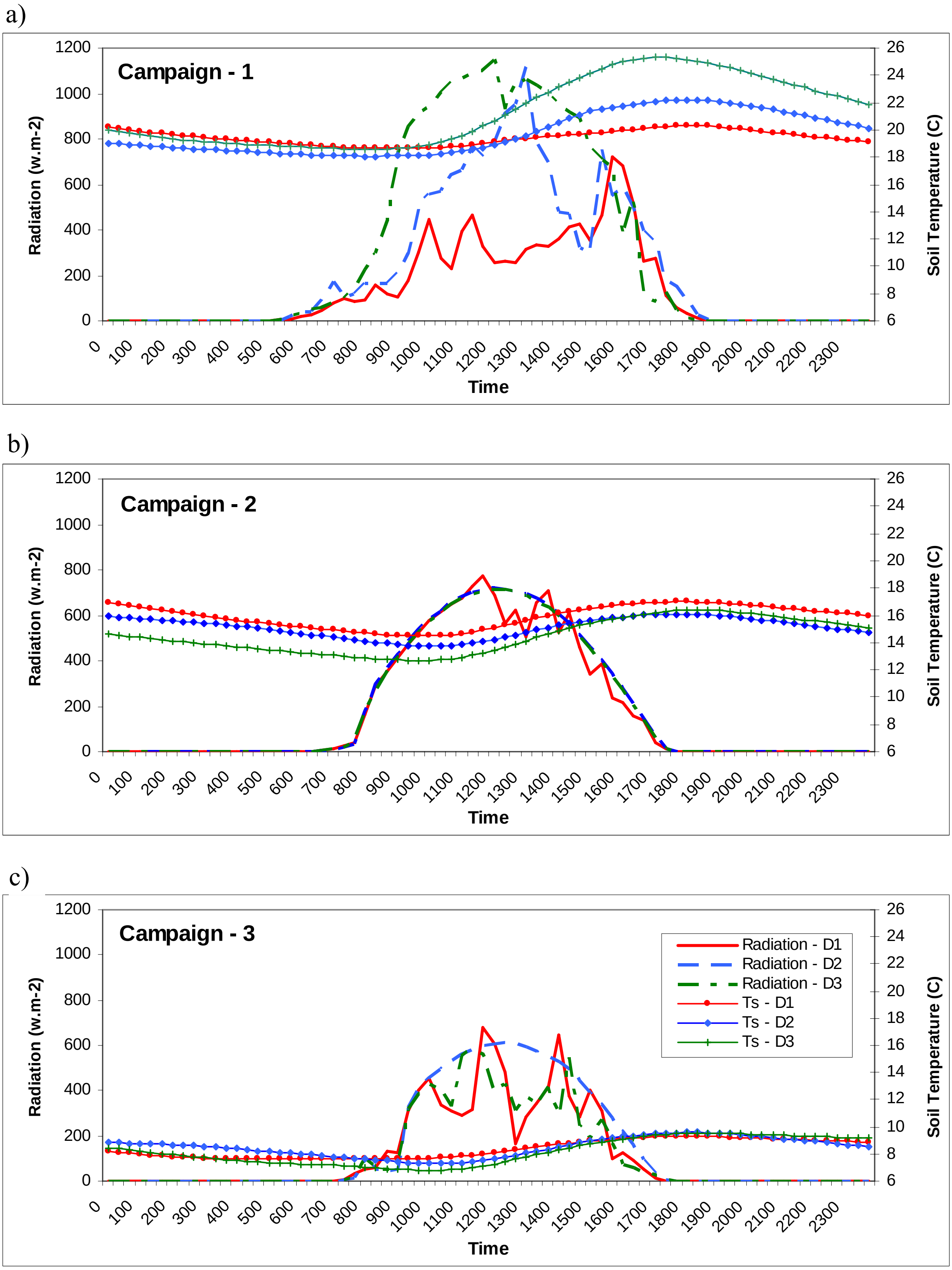

Figure 7-16: Incoming solar radiation and near-surface soil temperature (at 7.5 cm below the surface) as measured at climate station S2 during the three days of (a) Campaign 1, (b) Campaign 2, and (c) Campaign 3. (D1= day 1, D2 = day 2 and D3 = day 3).

Additionally, Figure 7-16 assists in selecting suitable remote sensing imagery for further analysis. The pattern of incoming solar radiation during a day is useful in determining the presence of clouds during the day. Clouds prevent the use of the image in estimating important parameters like land surface temperature and for evaluating land surface wetness conditions. The third day of Campaign 1, the second and third days during the Campaign 2, and the second day of Campaign 3 (Figure 7-16b) appear ideal for evaluating land surface wetness conditions based on remotely sensed observations.

(iii) *Effect of relative humidity during the sampling period*

Evaporation will reduce the moisture content of the 0-1 cm near-surface soil layer can change during a day. Evaporation depends on the dryness of the atmosphere. High relative humidity in the air will therefore help to minimize drying and the subsequent decrease in the soil moisture content of the near-surface layer, which is important when collecting soil moisture data over extended periods such as over 1-3 days.

Figure 7-17 shows relative humidity at climate station S2 during all three validation campaigns. As seen from the figure a lower humidity conditions (for example, less than 50%) were observed during day 3 of Campaign-1(Figure 7-17a), during whole Campaign-2 (Figure 7-17b) and during day 2 of Campaign-3 (Figure 7-17c). Therefore, soil moisture measurements made in the 0-1 cm near surface layer during these days may less accurately reflect the true soil moisture conditions at the time of the AMSR-E overpass. The actual effect of relative humidity values on near-surface soil moisture measurements during the campaigns is difficult to explain due to the complex nature of the soil evaporation process.

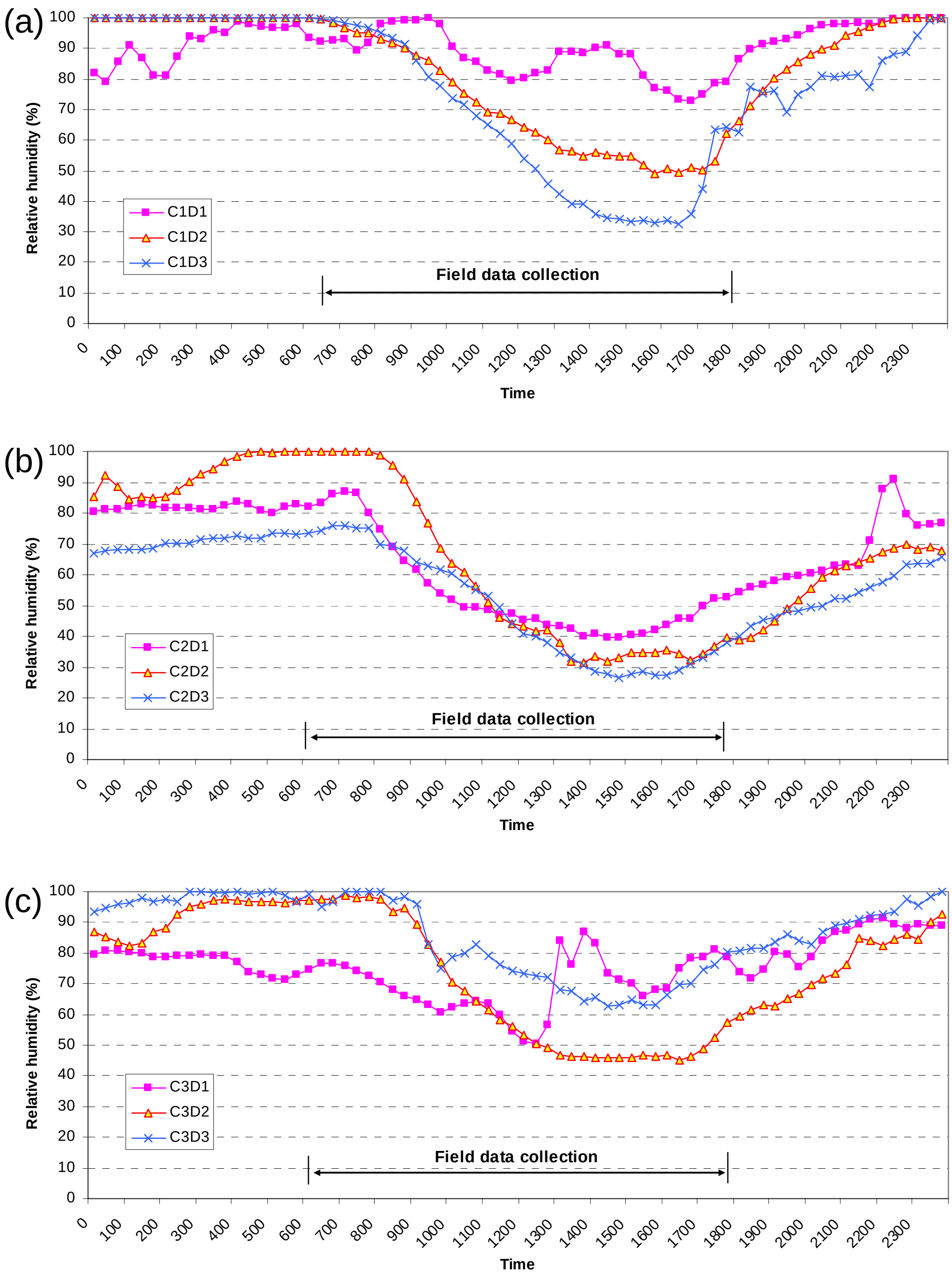

Figure 7-17: Relative humidity as measured at climate station S2 during (a) Campaign 1, (b) Campaign 2, and (c) Campaign 3. (D1= day 1, D2 = day 2 and D3 = day 3)

(iv) *Within-day soil moisture variations*

Ground based observations of the moisture content of the surface layer obtained up to three days in each campaign are compared with virtually instantaneous satellite based observations. It is therefore important to assess to what extent the moisture content has changed during each individual day. For this purpose, each team was encouraged to take its last soil moisture measurement for each day at the site of its first soil moisture observations of the day. Although, due to time limitations, not all the teams were able to collect repeat samples at the end of every day. A summary of these repeat measurements is shown in the Table 7-7 which shows that average diurnal changes in the 0-1 cm and 0-6 cm near-surface soil moisture content observations were relatively small and less than approximately 4%. The day-to-day differences were also found to be small.

The highest range of (3.3 % v/v in 0-1 cm and 4.1 % v/v in 0-6 cm) variations in soil moisture observations was found during Campaign 2 and this may be due to the favourable drying conditions such as cloud free sky (Figure 7-16b) and lower relative humidity (Figure 7-17b) prevailing during campaign 2, and a longer time period of 8 hours between the first and the last observation (see Table 7-7). Considering an expected accuracy of 0.06 v/v in AMSR-E soil moisture data (Njoku and Li, 1999), this observed range of diurnal variations during the campaign periods does not appear to have serious effect on the final results. Furthermore, consideration of average AMSR-E soil moisture computed from ascending and descending paths helps overcoming the effect of surface drying up to some extent. Therefore, the use of individual soil moisture measurements collected at some time during the three-day campaign for the computation of average near-surface soil moisture measurements appears to be acceptable. Since no significant rainfall occurred during any of the campaigns, it was possible to use all the data collected during each campaigns.

Table 7-7: Difference of the air and soil temperatures and 0-6 cm and 0-1 cm soil moisture levels between the first and the last observation of the same site during the campaign.

Campaign	No of sites	Average time between first and last observations (hour : minutes)	Average differences between first and last observations			
			Temperature (^oC)		Moisture (v/v)	
			Air	Soil	0-6 cm	0-1 cm
1	7	10:36	5.4	8.1	-0.4	-2.5
2	9	8:09	8.2	8.2	-4.1	-3.3
3	6	7:17	9.3	6.1	1.7	-1.6

7.6.2.3 Estimation of minimum sample size

An important task in the validation was to determine the minimum number of sampling sites reasonably required to obtain a representative areal average soil moisture value for such a large area. Figure 7-18 and Figure 7-19 show the effect of the number of *randomly selected* sampling sites on the area average soil moisture content over a 40 x 50 km area for the 0-1 and 0-6 cm depths, respectively. Graphs show the individual points as compared with the averages based on all available sites shown by horizontal lines (i.e. 230 sites during Campaign 1, 216 sites during Campaign 2 and 181 sites during Campaign 3). It is shown that for the 0-1cm observations the regional average *stabilizes* at about 100 sites, whilst for the 0-6 cm observations at least 150 sites are required. The stabilization of the computed average from *n* number of data points is illustrated by the convergence between data points and the average value which is represented as a horizontal line.

When field samples were collected after a long dry spell (as in Campaign 3) convergence of the graph occurs with a smaller number of sampling sites. This is due to the antecedent drying of the surface and the appearance of more uniform type moisture distribution across the catchment. A similar situation occurs immediately after reasonable precipitation (as in Campaign 2). However, different drying rates after a rain event in different parts of the catchment may also lead to the emergence of a preferred spatial pattern of moisture contents across the catchment. In such situations, convergence of the graph requires a greater number of samples. Therefore, the number of samples needed for the validation of large footprints will depend on recent rainfall and its distribution pattern. In general, if the sampling takes place after a long dry period or after a uniformly distributed rainfall, a smaller number of sampling sites (about 80-100) may be adequate. For all other situations, at least 100 samples are recommended.

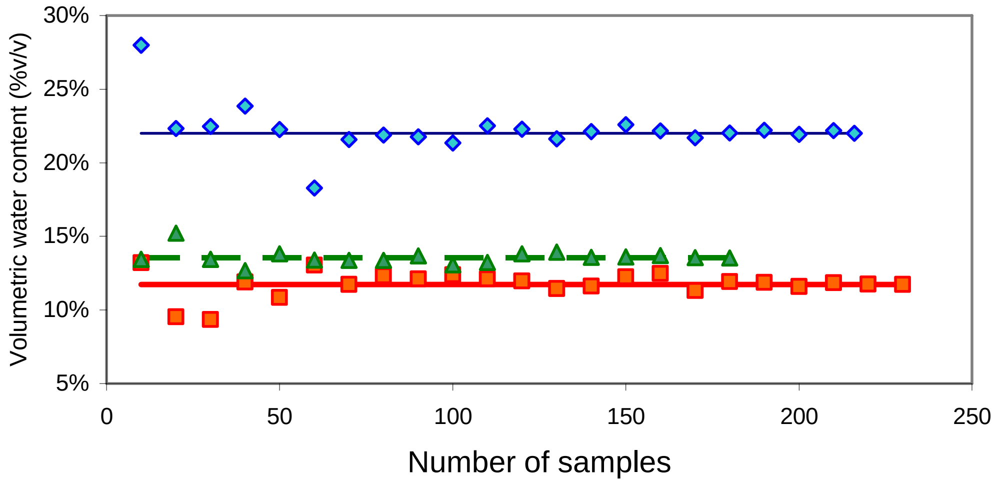

Figure 7-18 Spatial variation in field-measured soil moisture for top 1 cm soil layer during the three campaigns (see Figure 7.19 for the legend).

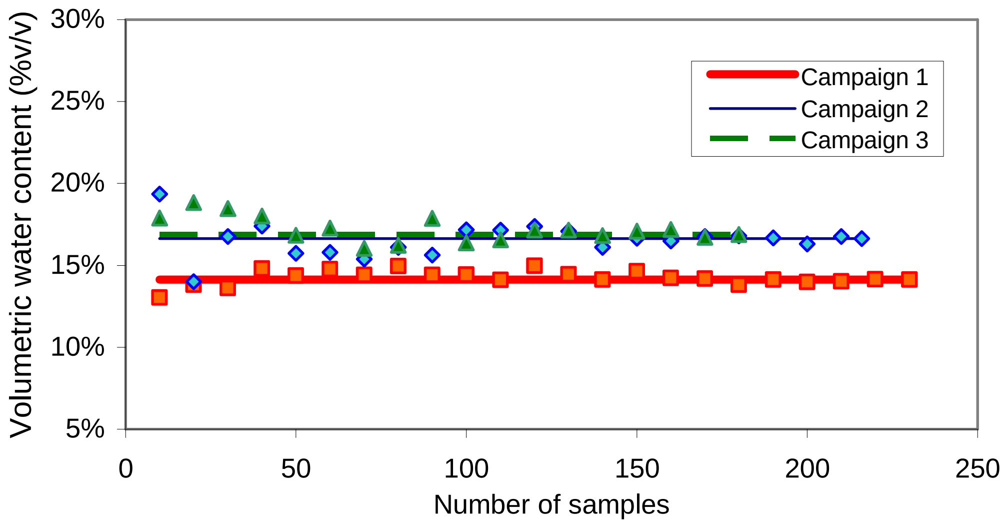

Figure 7-19: Spatial variation in field-measured soil moisture for top 6 cm soil layer during the three campaigns.

7.6.2.4 Vegetation characteristics within the footprint

Vegetation absorbs, emits, and scatters microwave radiation (Njoku and Entekhabi, 1996). Therefore, the study of vegetation characteristics is a very important component in any research employing microwave-based soil moisture measurements. Accordingly, in addition to the soil samples, a total of 192, 56 and 97 vegetation samples were collected from 50 cm x 50 cm quadrants during Campaigns 1, 2 and 3, respectively. Vegetation samples from trees were collected in a form of a cube representing approximately 0.125 m^3. The number of samples collected from each vegetation type varied from campaign to campaign and details are given in Table 7-8**.** In general, the dominant vegetation type in the validation area consists of grasses and herbs and the majority of the samples therefore represented grass type vegetation. The observed vegetation water content during Campaign 1 was about 60% which may due to the previous 30 day rainfall of 68 mm. (see Table 7-8). Vegetation water content during second and third campaigns was 46% and 34% respectively. Because nearly half the number of vegetation samples were collected from trees during the second campaign, it is difficult to compare the results with other data. The observed average dry biomass values during all three campaigns were less than the critical threshold level of 1.5 kg m^{-2} for near-surface soil moisture measurements with AMSR-E. Therefore, the chosen validation area meets the basic requirements. Also, based on equation 7.11, the computed optical depth or opacity (τ) of vegetation in the study area ranged from 0.0318 to 0.0593 (assuming b = 0.12, as suggested by Jackson *et al.* (1999) and considering grass as the dominant crop type). Theoretically, for small values of τ (associated with low vegetation density) the observed brightness temperature measured from microwave radiometers is close to the soil brightness temperature. This allows for accurate estimation of near-surface moisture conditions (Jackson *et al.*, 1982; Njoku *et al.*, 2003).

Table 7-8: Measured vegetation water content (kg kg^{-1}), biomass density (kg m^{-2}) and vegetation opacity (τ) during field campaigns.

	Campaign 1	Campaign 2	Campaign 3
Total no. of samples	189	57	97
grass/herbs samples	174	35	88
tree samples	3	18	8
shrub samples	0	2	0
crop samples	12	2	1
Veg. water content (%, kg kg^{-1})			
Average	60.55	45.92	33.66
Standard deviation	12.08	13.44	12.86
Dry biomass (kg m^{-2})			
Average	0.2912	0.3763	0.4950
Standard deviation	0.2447	0.1764	0.3340
Vegetation opacity (τ)			
Average	0.0593	0.0434	0.0318
Standard deviation	0.0566	0.0362	0.0282

7.6.2.5 Comparison of AMSR-E and measured ground-based data

Results from the three validation campaigns are shown in Table 7-9 and Table 7-10 where AMSR-E near-surface soil moisture values are compared with footprint averages of the volumetric soil moisture content in the top 1 cm and top 6 cm. Two AMSR-E pixels (A and B) were used for the comparison. As shown in Figure 7-10, pixel A is completely within the validation area. Even though only about 80 percent of pixel B falls within the validation area, both pixels A and B were used for the analysis. Note therefore, that for each campaign the total number of 0-1 cm samples used for comparison with pixel A and pixel B values does add up to a number less than the total number of 0-1 cm samples obtained. The difference refers to observation sites outside pixel A and pixel B.

Table 7-9 and Table 7-10 indicate that AMSR-E provide reasonable estimates of near-surface soil moisture content when compared with the averages of the point observations comprised within each pixel. AMSR-E measurements and field measured soil moisture values appear comparable (see Figure 7-20 and Figure

7-21). A positive correlation is present between AMSR-E soil moisture and both 0-1 cm and 0-6 cm field measured values. However, AMSR-E moisture measurements did not exceed 13% even at the higher measured soil moisture content of over 25%. Furthermore, both AMSR-E pixels A and B show significant under-estimates for 0-6 cm moisture contents. However, Figure 7-21, shows that Wood (2003) has observed much better relationship between 0-6 cm measured soil moisture and AMSR-E near-surface moisture estimates.

Table 7-9: Comparison of AMSR-E near-surface soil water content and field measured moisture contents in 0-1 cm and 0-6 cm layers and vegetation dry biomass, water content and opacity (τ) of pixel A. (*n* = number of AMSR-E images (cf. Table 7-4) or number of ground-based observations).

Campaign # (dates)	Soil moisture content (% v/v) AMSR-E	0-1 cm	0-6 cm	Vegetation biomass (kg ha^{-1})	water content (%)	opacity (τ)
1 (7-9 Nov 2003)	8.0 *(n=4)*	11.45 *(n=71)*	15.43 *(n=72)*	2718 *(n=68)*	61.48 *(n=68)*	0.060 *(n=68)*
2 (1-3 May 2004)	11.7 *(n=4)*	20.53 *(n=63)*	18.95 *(n=63)*	4200 *(n=16)*	45.63 *(n=16)*	0.045 *(n=16)*
3 (7-9 Jul 2004)	11.1 *(n=5)*	13.94 *(n=49)*	19.86 *(n=49)*	5517 *(n=30)*	28.49 *(n=30)*	0.030 *(n=30)*

Table 7-10: Comparison of AMSR-E near-surface soil water content and field measured moisture contents in 0-1 cm and 0-6 cm layers and vegetation dry biomass, water content and opacity (τ) of pixel B. (*n* = number of AMSR-E images or number of ground-based observations).

Campaign # (dates)	Soil surface water (% v/v) AMSR-E	0-1 cm	0-6 cm	Vegetation biomass (kg ha^{-1})	water content (%)	opacity (τ)
1 (7-9 Nov 2003)	8.3 (*n=4*)	9.53 (*n=52*)	15.98 (*n=55*)	2916 (*n=51*)	58.27 (*n=51*)	0.052 (*n=51*)
2 (1-3 May 2004)	12.2 (*n=4*)	21.19 (*n=47*)	20.19 (*n=52*)	3397 (*n=17*)	46.81 (*n=17*)	0.048 (*n=17*)
3 (7-9 Jul 2004)	10.8 (*n=5*)	11.94 (*n=38*)	19.94 (*n=38*)	6354 (*n=25*)	36.83 (*n=25*)	0.045 (*n=25*)

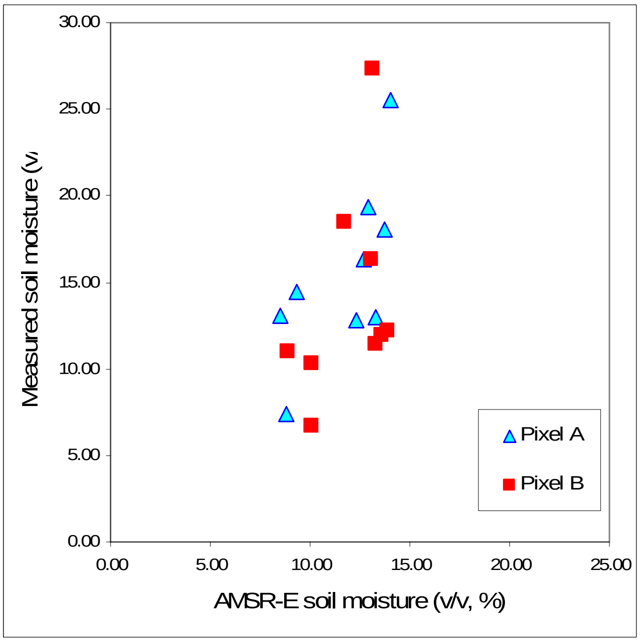

Figure 7-20: Relationship between averages of field-measured soil moisture (0-1 cm) and the AMSR-E soil moisture in pixels A and B during Campaign 1, 2 and 3.

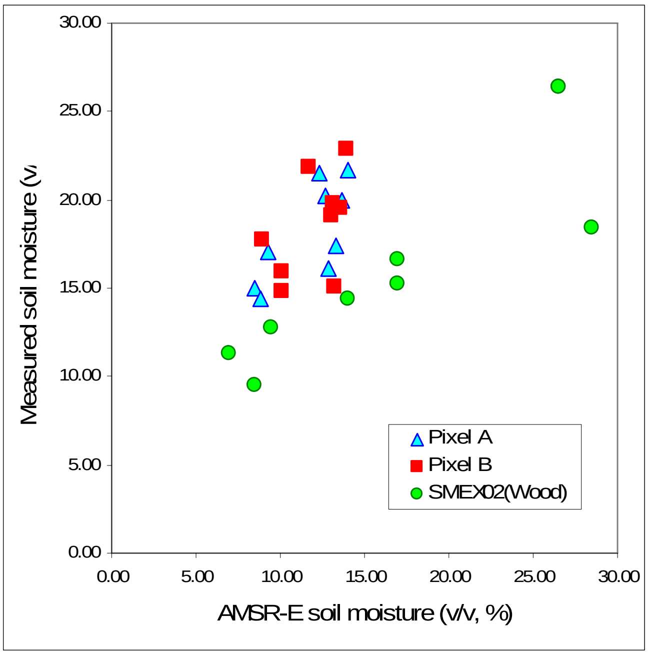

Figure 7-21: Relationship between AMSR-E soil moisture and field-measured 0-6 cm soil moisture during Campaign 1, 2 and 3. Figure also includes 0-6cm soil moisture and AMSR-E data from Wood (2003).

The differences between AMSR-E near-surface measurements and the observed 0-1 and 0-6 cm soil moisture in both Figure 7-20 and Figure 7-21 may be attributed to three main factors. First, the field measured data do not provide perfect estimates of *instantaneous* surface moisture contents measured by the AMSR-E in terms of the spatial extent and the depth. For example, a limited number of 0-1cm depth (collected using 82mm diameter rings) and 0-6 cm depth soil moisture measurements (measured with Theta probes where each reading represents a volume of about 50mm diameter and 60 mm depth) collected over a period of up to 1-3 days provides an indicative measure rather than an absolute measurement of soil moisture content. Often the 0-1 cm layer responds quickly to changes in atmospheric conditions and hence may dry or wet much more quickly than the 0-6 cm layer. Second, recent rainfall patterns can have a great impact on the data. This is probably more so for 0-6 cm than 0-1cm because the deeper layer can store more water and therefore its soil water content will reflect past rainfall better than the 0-1 cm layer. Finally, the effect of vegetation is not uniform across AMSR-E pixels. Both the amount of biomass and vegetation water content may vary temporally and spatially. Vegetation can extract soil moisture and cause variations in soil moisture patterns. Therefore, a perfect match between AMSR-E area values of near-surface soil moisture content and averages of ground-based point scale measurements over 0-1 and 0-6 cm may not always be attainable.

The field-measured average soil moisture content over an large area as computed in this study relies on relatively dense *in-situ* near-surface moisture data collected over 3-day periods. Despite this assumption, reasonably good correlations have obtained between the microwave observations and the field-measured soil moisture.

7.7 ANALYSIS OF TEMPORAL PATTERNS OF AMSR-E MEASUREMENTS

Analyses of the temporal evolution of AMSR-E measurements are important for at least two reasons. First, such analyses are expected to produce insight into the usefulness of AMSR-E soil moisture products for modelling applications. Temporal patterns of AMSR-E should generate useful information on sensor responses to natural events like precipitation and drying. Second, these analyses may help to establish relationships with ground-based soil moisture measurements collected from *permanent* sites. Often, 0-1cm (or 0-6cm) soil moisture is not measured in permanent measurement networks and it is common to measure 0-30 cm soil moisture as in the present study. In the present study temporal patterns of AMSR-E are compared with the SASMAS *in-situ* point scale measurements which have a much longer vertical length scale (i.e. 0-30 cm). However, one of the important factors to be considered when comparing AMSR-E soil moisture products with 0-30 cm *in-situ* observational data is the decrease in natural variability of the surface characteristics with increasing depth. The actual temporal range of average soil moisture over the 25 km scale EASE-grid footprint is expected to be less than that of the point scale *in-situ* measurements. According to Njoku *et al*. (2003) this is due to the spatial smoothing and less frequent temporal sampling (maximum of 2 samples per day) of the AMSR-E measurements. Anomalies due to the vertical scale sampling differences between AMSR-E (0-1 cm) and *in-situ* measurements (0-6 or 0-30 cm) also will contribute to this.

7.7.1 STUDY SITE AND DATA USED

The selection of AMSR-E pixels for the temporal pattern study was based on; a) their position within the SASMAS study region, b) the number and distribution of permanent soil moisture sites within the pixel, and c) the availability of climate data. A total of 11 different AMSR-E pixels were available at any one time within the SASMAS study region as shown in Table 7-11 for temporal analysis and comparison with *in-situ* data. After considering factors such as availability of climate stations, the number of soil moisture monitoring sites, and the preference for less dense vegetation within the pixel, the EASE-grid cell reference of column 1269 and row 449 (c1269, r449) was selected for the temporal analysis. Note that the same pixel (Pixel A) was used for the validation study described above so that the present comparison over time will help to better understand the spatial variations of soil moisture across the pixel.

Table 7-11: AMSR-E data pixels and permanent soil moisture sites within the pixels and suitability of pixels for further analysis.

EASE-grid reference (Column, Row)	SASMAS sites within pixel	Remarks
1267,450	G5	
1268,449	G6	
1268,451	G4	Dense vegetation, mountainous
1269,448	K6	Dense vegetation, mountainous, climate station
1269,449	S1-S7, K3, K4, K5	Climate station, less vegetation, more soil moisture monitoring sites
1269,450	K1, K2, M1	
1269,451	G3	Dense vegetation, mountainous
1270,448	M7	Dense vegetation, mountainous
1270,449	M3, M4, M5, M6	
1270,450	M2	
1270,451	G1, G2	Dense vegetation, mountainous

7.7.2 TEMPORAL PATTERNS OF THE 6.9 GHZ CHANNEL

The C-band channel of AMSR-E provides the main data input to the soil moisture retrieval algorithm. Hence, the temporal behaviour of the data in this channel must be first analysed. Figure 7-22 shows the scatter plots of brightness temperatures measured with the 6.9 GHz channel during 2003 and 2004. Both vertical and horizontal brightness temperatures measured during the ascending (day-time) path (Figure 7-22a) and descending (night-time) path (Figure 7-22b) are shown. 5-day moving window averaging was applied to smooth the data and this is shown as continuous lines. The significance of this figure is two-fold. First, confirms that vertically polarized signals are greater than the horizontally polarized signals as shown in Figure 7-1. The higher signal strength of the vertically polarized signal is evident throughout the study period. Second, both vertical and horizontal signals vary with time: about 260 – 305 K for day-time observations and about 260-290 K for night-time observations. Hence variations up to about 30K of brightness temperatures occurs under natural conditions. This gives an idea of the sensitivity of AMSR-E's 6.9 GHz channels under natural conditions. Daytime measurements are consistently higher than the night-time observations. Because it is a cloud-contaminated signal, raw brightness temperature values are not a good indicator for soil moisture and normalized forms, such as the brightness temperature polarization ratio given in the equation 7.12 are preferable.

(a) Day time (b) Night time

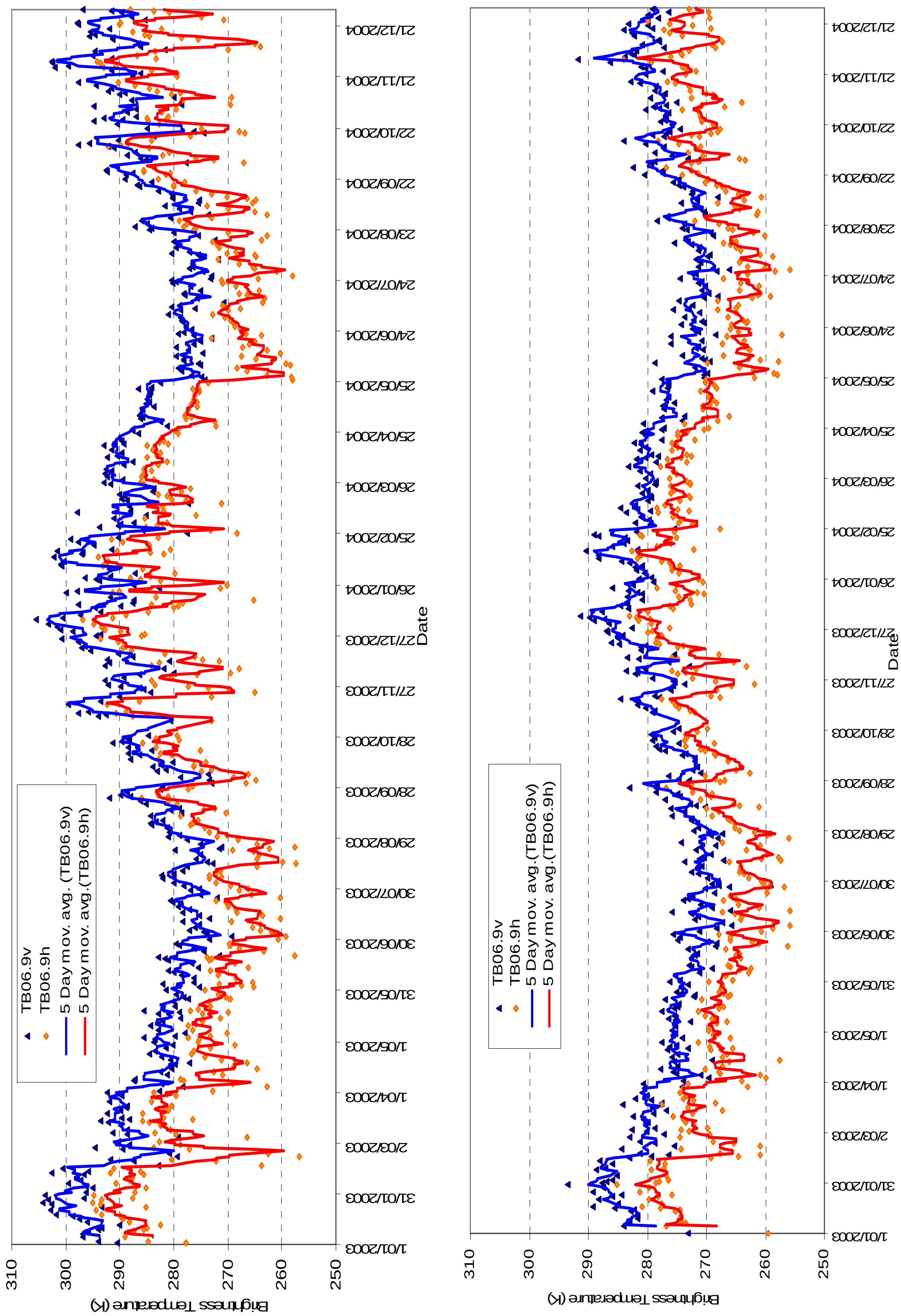

Figure 7-22: AMSR-E measured dual polarized brightness temperatures of the 6.9 GHz channel during 2003-2004. (a) Daytime and (b) Night-time observations. (Note: Y axis units are brightness temperature in K).

As noted in Section 7.5.1, brightness temperature polarization ratios (ζ) are used in soil moisture inversion algorithm when polarized off-nadir measurements are available. This is because at large incidence angles (above 35^o-40^o) there is a large difference between the vertically and horizontally polarized brightness temperatures, particularly for bare soils. Polarization ratios help to effectively normalize the surface temperatures and therefore, the signal is more representative of the actual soil moisture and vegetation moisture conditions. The off-nadir AMSR-E observations at constant incidence angle (54.8^o) are suitable for study of the temporal evolution of the ζ under natural conditions and may be compared with rainfall observations and ground-based soil moisture measurements. Figure 7-23 shows the scatter plots of ζ for daytime and night-time observations as well as rainfall observations throughout 2003 and 2004 The data has been smoothed with 5-day moving window averaging and is shown as a continuous line. Most of the peak values coincide with rainfall events, which confirm the sensitivity of ζ to precipitation. However, the magnitudes of these peaks can not be compared directly with the amount of rainfall due to differences in the measurements (point scale rainfall vs. 25km x 25km AMSR-E observations) and due to rainfall variations across the pixel. It is also evident from Figure 7-23 that daytime ζ values are generally higher than the night-time ζ values. However, day and night values are occasionally nearly equal which at times happens during or shortly after precipitation events. Figure 7-23 indicates that soil moisture temporal variability is a dominant signal and that AMSR-E data may reflect the temporal soil moisture changes reasonably well in areas such as the Goulburn River catchment.

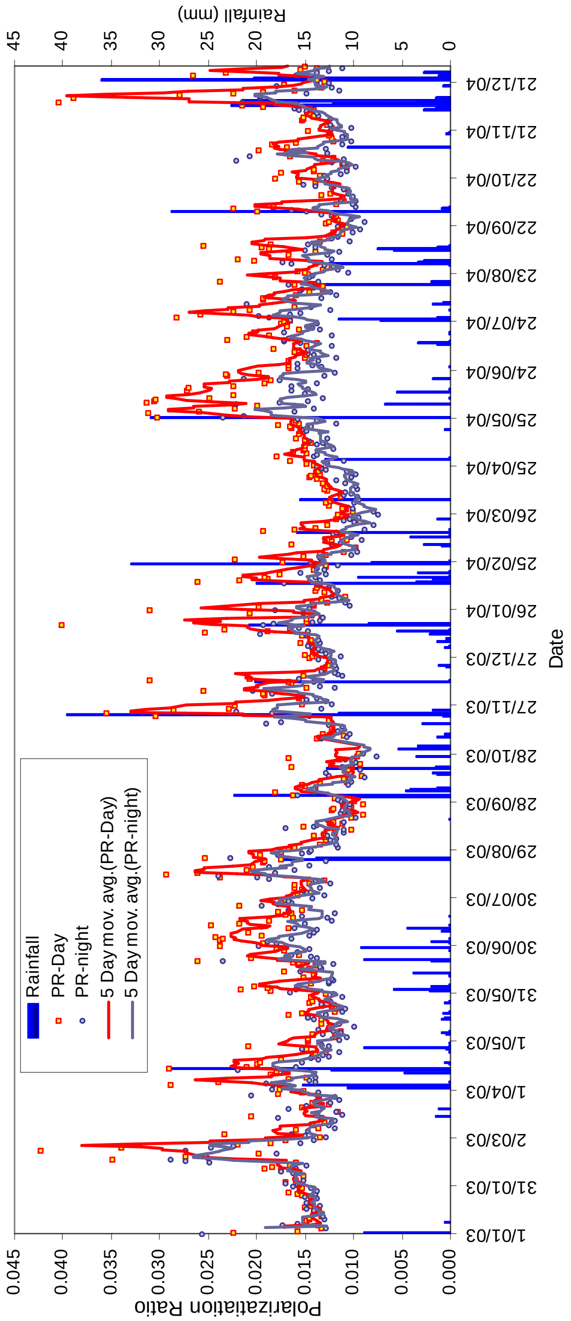

Figure 7-23: Computed polarization ratios (ζ) of the 6.9 GHz channel for daytime and night-time observations and measured rainfall during 2003-2004. (Note: some missing rainfall data during March 2003).

Another observation from Figure 7-23 concerns the pattern of day and night ζ values. It is evident that the fluctuations of daytime ζ values are more frequent than those of the night-time values. This may due to more stable environmental conditions during night time. On the other hand, at night, the soil moisture and temperature profiles are more uniform than at mid-day, and the soil-vegetation temperature differences are smaller. Thus night-time AMSR-E soil moisture retrievals are expected to have less errors and be more representative of the deeper-layer soil moisture than the daytime observations.

Figure 7-24 displays the temporal variation of computed AMSR-E soil moisture estimates and field measured rainfall during 2003-2004. The AMSR-E measured near-surface soil moisture values vary from 0.10 – 0.18 g cm^{-3}. As can be seen, there is some coincidence between peaks in the soil moisture values and precipitation events. For instance, this pattern is very obvious particularly after 30 May 2004. This gives an indication of the sensitivity of the retrieval algorithm.

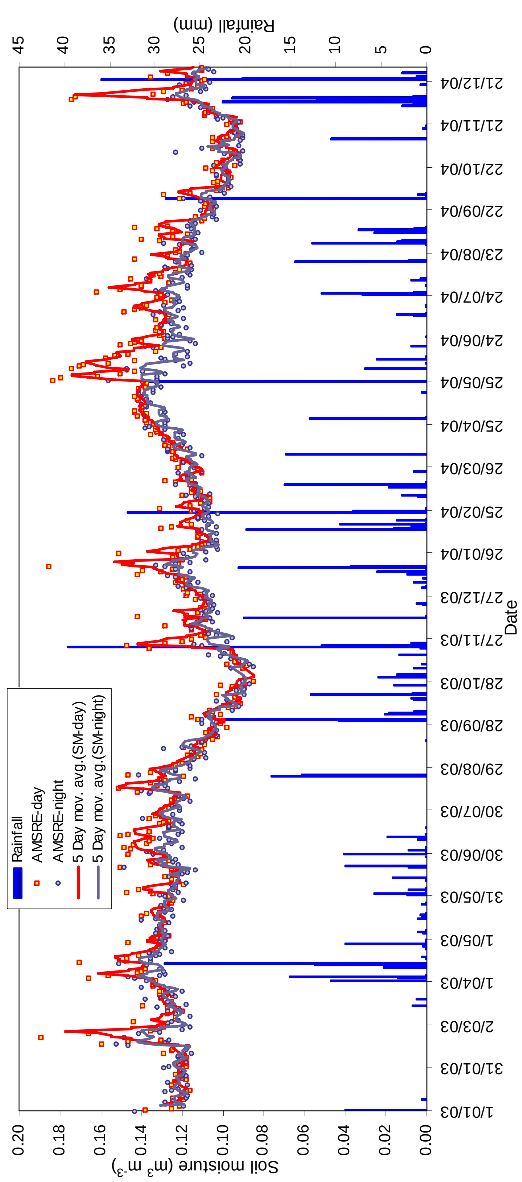

Figure 7-24: AMSR-E derived near-surface soil moisture estimates for daytime and night-time overpasses during 2003-2004. Precipitation measured within the pixel is also given for easy comparison. (Note: some missing rainfall data during March 2003).

To better understand the temporal pattern of the near-surface moisture, it is necessary to compare AMSR-E soil moisture with ground-based soil moisture content observations. As an example Figure 7-25 compares near-surface AMSR-E measurements with average 0-30 cm soil moisture measurements made at station S2 between 1 January 2003 and 31 December 2004. In general, the magnitudes of these two quantities are not same and AMSR-E moisture values are always less than the 0-30 cm moisture contents.

Interestingly, where as some of the soil moisture increases observed for the 0-30cm layer are also clearly present in the AMSR-E near-surface observations other soil moisture increases are not evident in the AMSR-E data. This is clearly visible around 29 August 2003. This may due to 1) a mismatch of scales (0-30 cm and 0-1 cm), 2) rainfall variations within the pixel, and 3) variations in vegetation patterns. Apart from the period during August to November 2003, significant correlation is observed between the near-surface measurements and average soil moisture data in the timing and magnitude of the soil wetting events and in the dry-down periods. The distribution of soil moisture within a AMSR-E pixel (for e.g. at c1269, r449) may, as expected, vary considerably. This is clear from Figure 7-26 which shows the moisture measurements from nine sites across the pixel. Therefore, instead of comparing soil moisture from one specific monitoring site, it would be better to use a representative site for further analysis. In this context, one possibility is to consider the temporal stability characteristics (see Chapter 5) of the permanent SASMAS monitoring sites within AMSR-E pixels. Comparison of AMSR-E soil moisture and field-measured averaged soil moisture will be discuss in the next section.

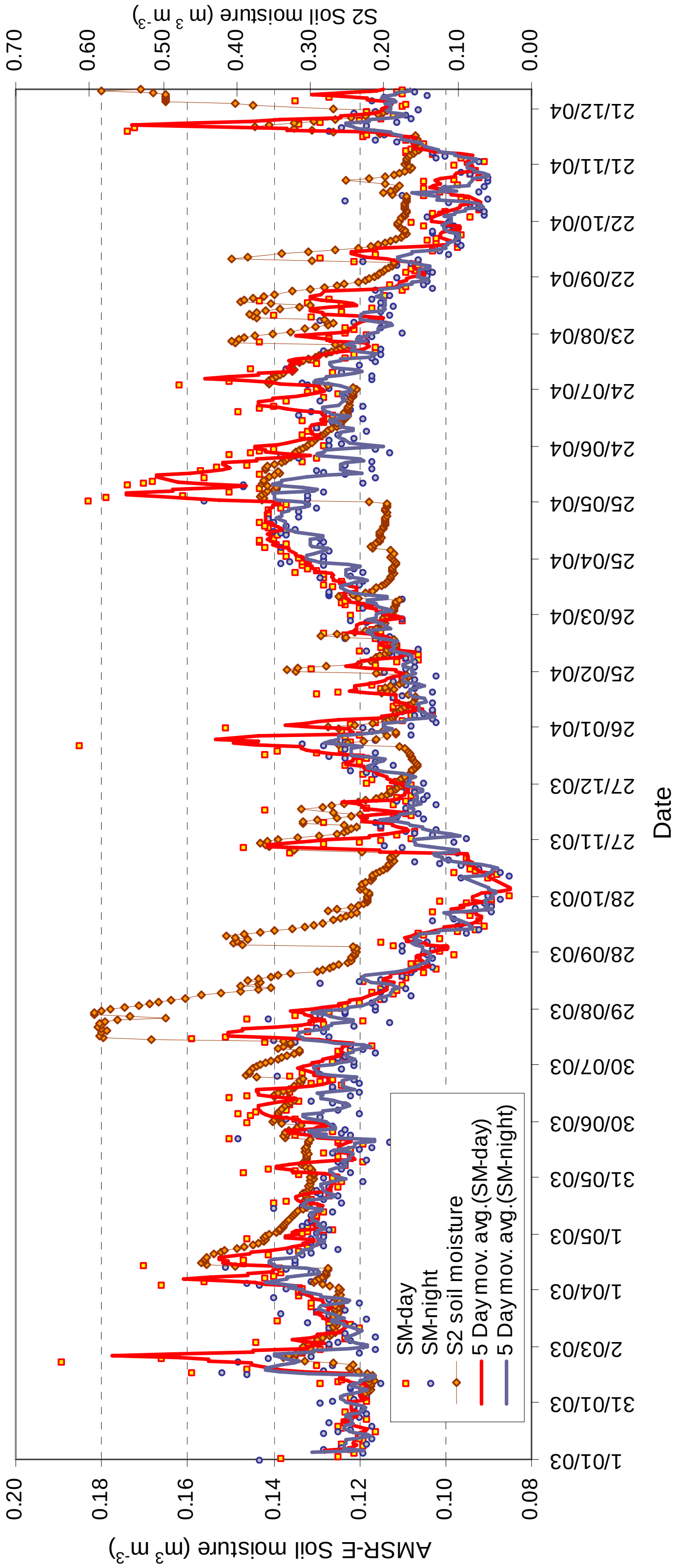

Figure 7-25: AMSR-E near-surface soil moisture estimates for daytime and night-time overpasses together with daily averaged 0-30 cm soil moisture at S2 during 2003-2004. (Note: scale differences in y-axes).

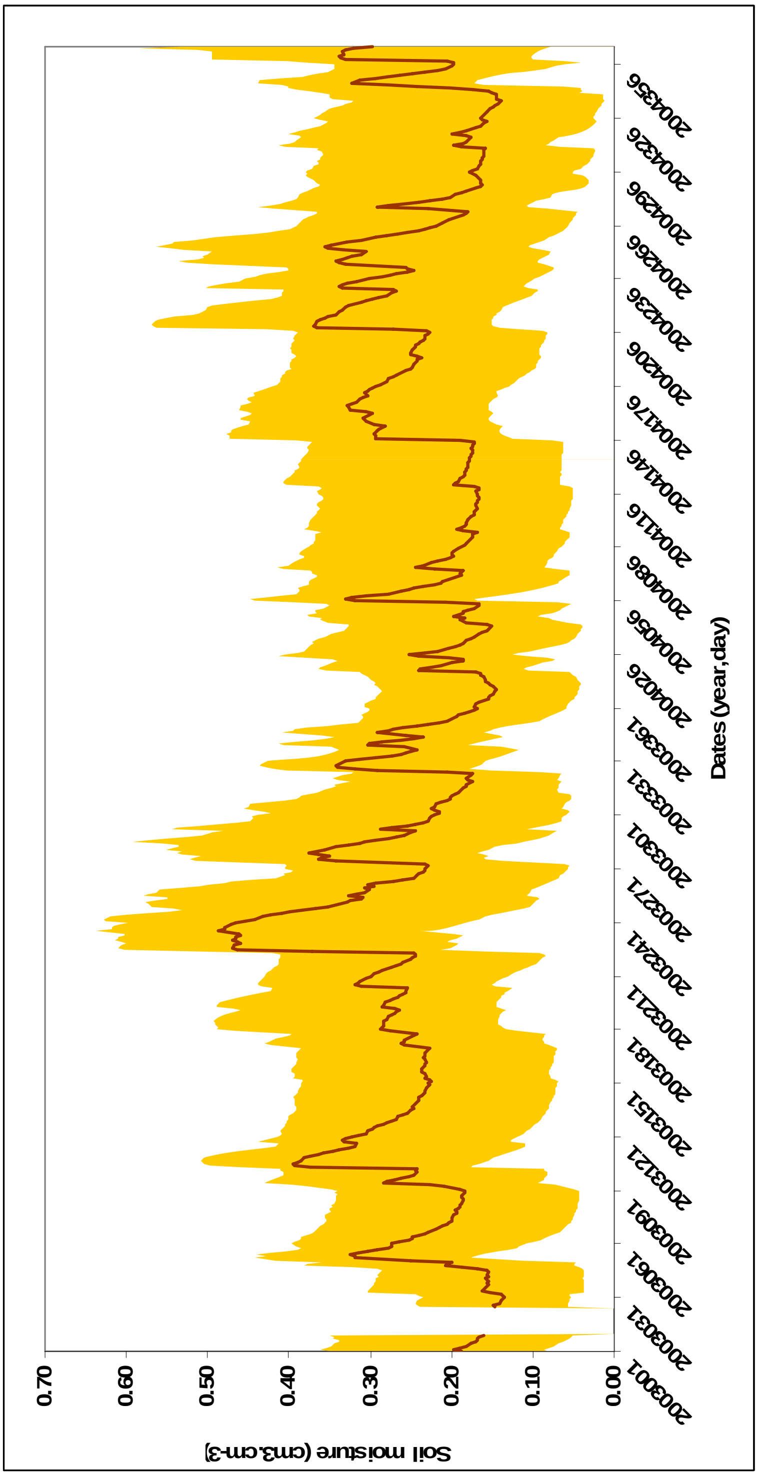

Figure 7-26: Temporal and spatial variations of 0-30 cm soil moisture ($cm^3.cm^{-3}$) measured during 2003-2004. The figure is based on 9 sites within AMSR-E pixel c1269, r449 and the line graph shows the average moisture content (Note: some missing data during January 2003).

7.7.3 TEMPORAL STABILITY ANALYSIS FOR IDENTIFICATION OF REPRESENTATIVE MONITORING SITES WITHIN AMSR-E PIXELS

The concept of temporal stability characteristics of measured soil moisture values as described in Chapter 5 may be used to determine which site best represents the average soil moisture condition for a given AMSR-E pixel. In the present study, two years of ground-based soil moisture observations have been used to select a representative station. Table 7-12 shows the data on the relative differences corresponding to soil moisture monitoring sites within selected AMSR-E pixels for the period between 1 January 2003 and 31 December 2004. The table shows that monitoring sites S4, M4 and M1 are the representative sites for pixels A, B and C (new pixel, see Table 7-12 for details) respectively. Site S4 seems a reasonable choice as it has been selected from 9 sampling sites. The other sites, M4 and M1, however, may not the best locations as their selection was only based on three sampling sites.

Table 7-12: Results of pixel average soil moisture measurement sites within AMSR-E pixels.

AMSR-E Pixel	Total no. of Days	Data Availability (# days)	Site Code	Pixel avg. water content ($cm^3.cm^{-3}$)	Mean relative difference (-)
A (c1269, r449) (estimated for days with >3 data sets)	712	707	K3	0.261	0.362
		651	K4		0.093
		707	K5		-0.245
		698	S1		-0.090
		697	S2		0.063
		698	S3		0.301
		698	**S4**		**0.016**
		697	S5		-0.324
		698	S7		-0.172
B (c1270, r449) (estimated for days with >2 data sets)	731	513	**M4**	0.170	**0.074**
		513	M5		-0.186
		513	M6		0.112
C (c1269, r450) (estimated for days with >2 data sets)	731	708	K1	0.192	0.961
		708	K2		-0.527
		708	**M1**		**-0.434**

Note: Values in bold characters best estimate the pixel average soil water content.

Figure 7-27 shows a graphical representation of relative differences at the monitoring sites within the three AMSR-E pixels. The data are ordered from lowest to highest and the standard deviation is represented by error bars above and below the points indicating the relative difference. All sites above the zero relative difference values would systematically overestimate the mean soil moisture value across the pixels. Similarly, those below zero would underestimate the mean moisture levels. It is clear from Figure 7-27 that representative sites only exist in pixels A and B. As far as the nine SASMAS sites within pixel A are concerned, it may be seen that the temporal stability is higher at Stanley sites (S1, S4 and S2) as indicated by lower standard deviation. All sites characterising the wet or dry sectors however show lower temporal stability (greater standard deviation). For pixel C, the available SASMAS sites are quite different from the mean soil moisture behaviour at the AMSR-E pixel scale.

The sites with soil moisture values that are most representative for mean soil moisture at the AMSR-E pixel scale would be the one that is closest to the zero relative difference value with the lowest standard deviation. For the three AMSR-E pixels studied, the site meeting these requirements is S4 (Figure 7-27A). S4 is within the Stanley micro-catchment and it is located on a plateau in an elevated landscape. To confirm the suitability of S4 as representative for AMSR-E pixel A at c1269, r449, a comparison has been made between the mean of the measurements at the remaining 8 sites and those at S4. Figure 7-28 shows a reasonable fit between the measured and estimated values with a high coefficient of determination ($R^2 = 0.71$).

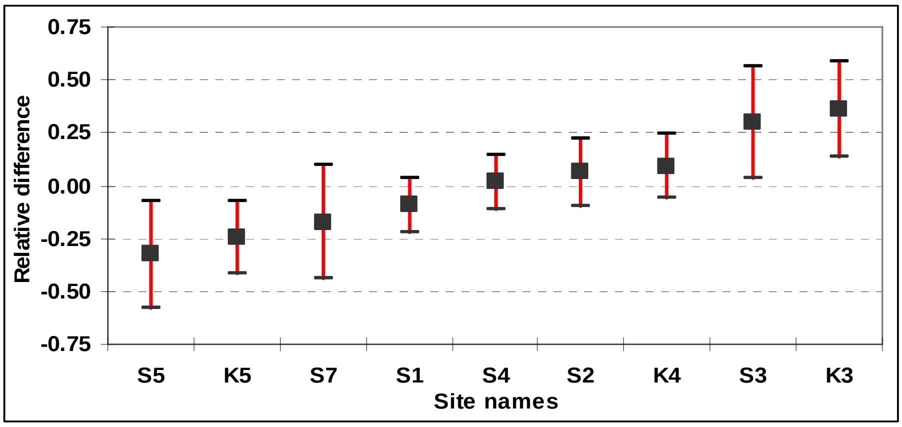

A)

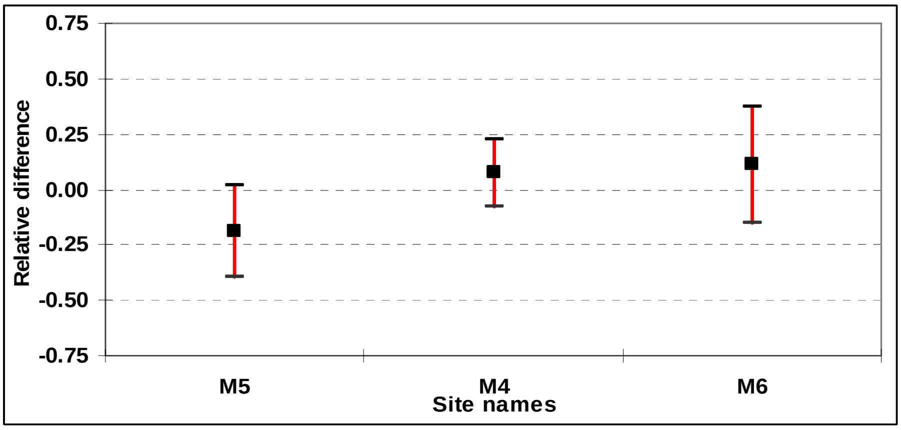

B)

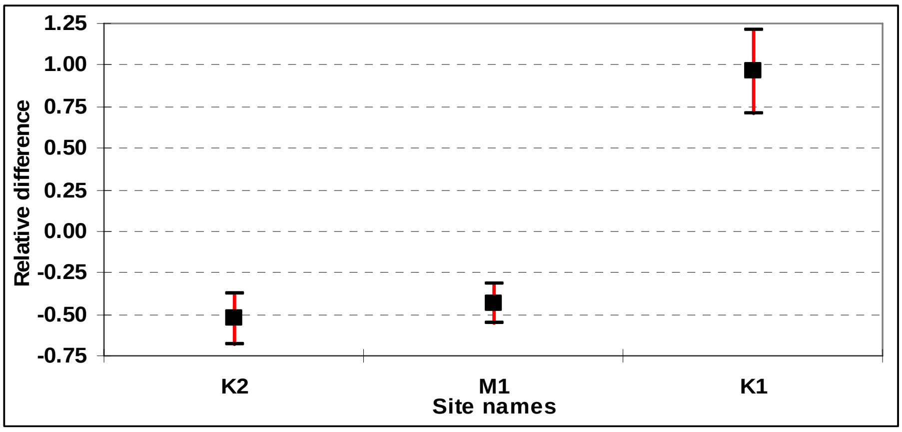

C)

Figure 7-27: Plots of relative differences for ground-based soil moisture monitoring sites within AMSR-E pixels A) c1269, r449; B) c1270, r449; and C) c1269, r450. These plots are based on the whole study period (1 January 2003 – 31 December 2004). Vertical bars correspond to associated standard deviations.

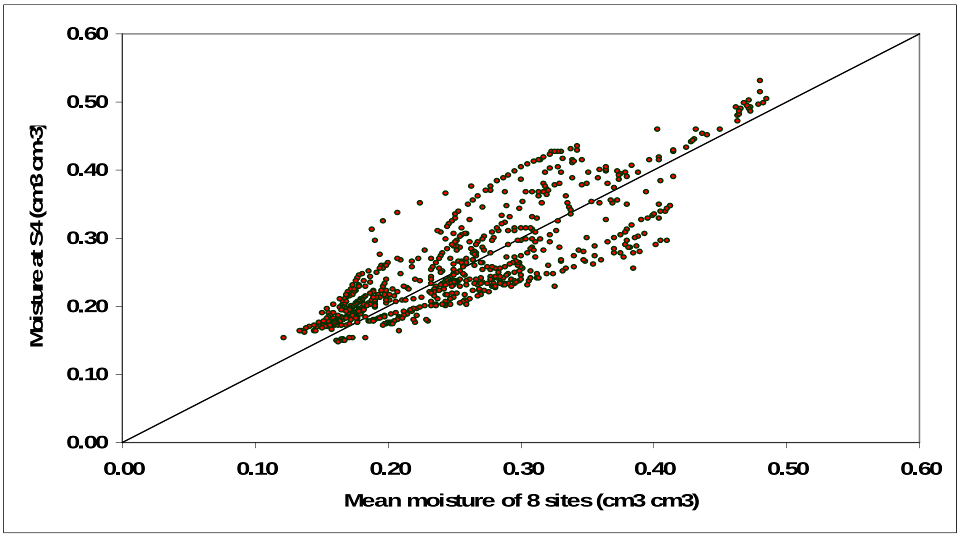

Figure 7-28: Measured soil moisture data of the representative mean soil moisture at AMSR-E pixel A (S4) and the mean soil moisture of the remaining 8 sites comparison during 2003-2004.

A comparison of AMSR-E near-surface soil moisture observations and soil moisture measurements at S4 during 2003 and 2004 is shown in Figure 7-29 and Figure 7-30 respectively. As noted previously, some of the soil moisture increases observed at S4 (at the 0-30cm scale) are clearly present in the AMSR-E near-surface observations but not all ground measured soil moisture changes are evident in the AMSR-E data. It is also important to note that due to the differences between AMSR-E soil moisture measurement depth (~1 cm) and the field measurement depth (0-30 cm), it is not possible to have a perfect match. Nevertheless, this analysis indicates that AMSR-E soil moisture estimates are capable of mimicking land surface soil moisture patterns reasonably well.

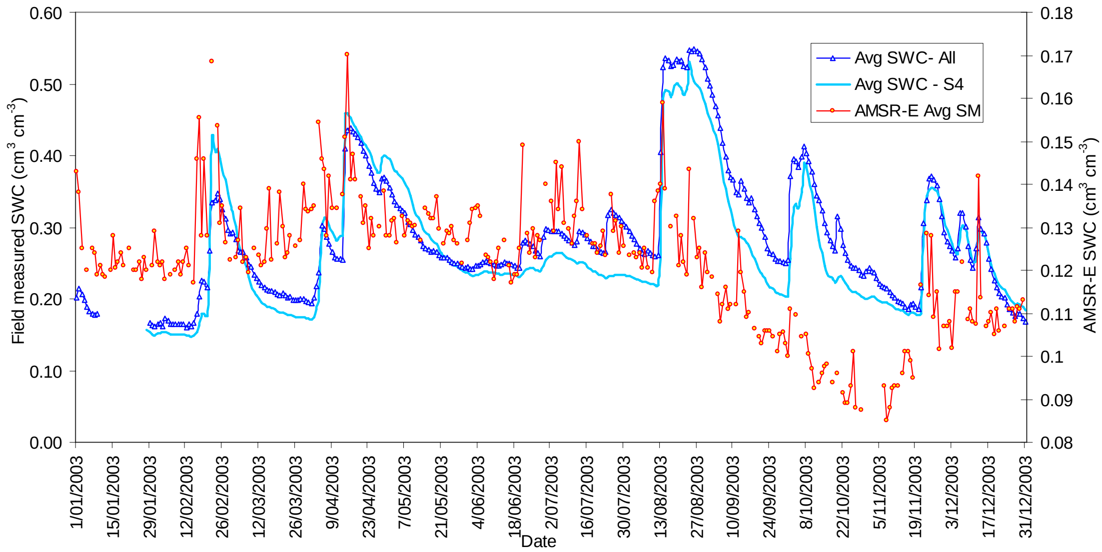

Figure 7-29: Comparison of average AMSR-E soil moisture measurements and field measured average soil water content for 0-30 cm based on (1) all monitoring sites and (2) representative site (S4) within the pixel during 2003. (Note: scale differences in y-axis).

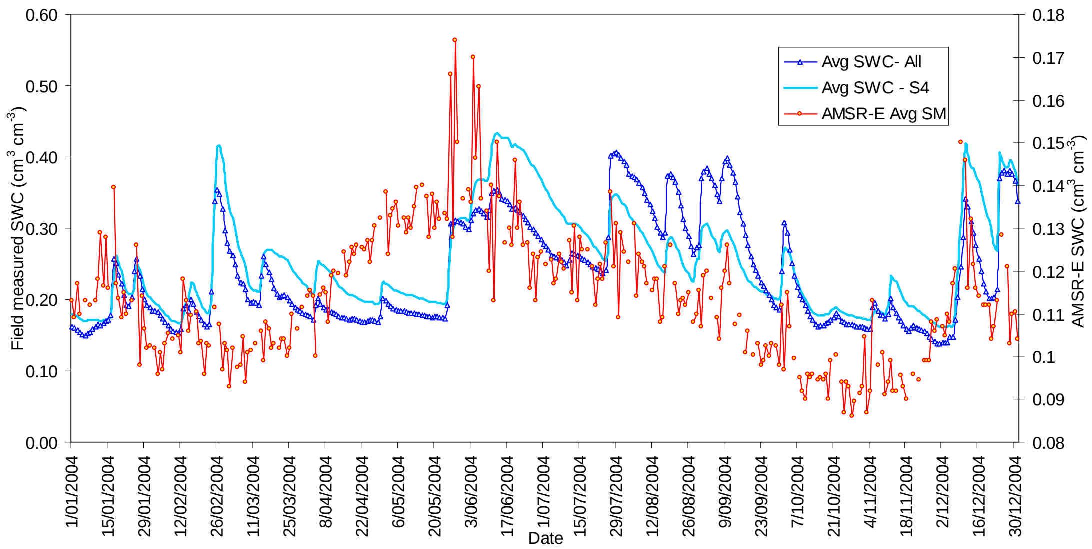

Figure 7-30: Comparison of average AMSR-E soil moisture measurements and field measured average soil water content for 0-30 cm based on (1) all monitoring sites and (2) representative site (S4) within the pixel during 2004. (Note: scale differences in y-axis).

7.7.4 TEMPORAL PATTERNS OF THE VEGETATION CHARACTERISTICS

Temporal patterns of the vegetation characteristics may also help understanding of near-surface soil moisture measurement. Microwave soil moisture inversion models use such information to derive model parameters. Figure 7-31 shows the temporal distribution of MODIS derived average NDVI values for the AMSR-E pixel at the r1269, c449 EASE-grid location. This figure helps in identifying the behaviour of vegetation within the selected AMSR-E pixel. Accordingly, the winter months and the summer months are characterized by less vegetation and smaller spatial variation (e.g. particularly, during May - August and November – December, 2004 in Figure 7-31). This more-uniform but less dense vegetation pattern creates ideal conditions for testing the soil moisture retrieval algorithm. The good performance of the retrieval algorithm is shown by the coincidence of the pronounced peaks associated with rainfall events and soil moisture estimation in the middle and towards the end of 2004 (see Figure 7-24).

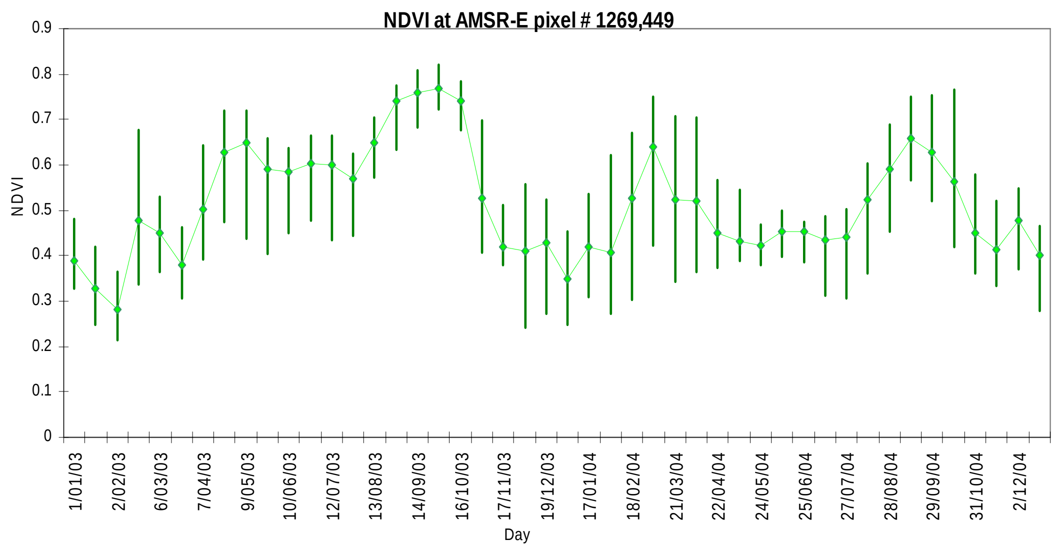

Figure 7-31: Temporal evolution of NDVI variations (as observed at 6 MODIS pixels) within the AMSR-E pixel.

7.7.5 COMPARISON OF SOIL MOISTURE MEASURED OVER 0-30 CM AND OVER 0-1 CM

Comparisons of 0-30 cm soil moisture measurements at S4 and the day-time and night-time AMSR-E near-surface moisture values during 2004 are given in Figure 7-32. It is shown that daytime AMSR-E values (R^2=0.24) are two times better correlated with *in-situ* measurements than night time values (R^2=0.10). The lower correlation for night time values may be due to the variations caused by redistribution of soil moisture at night in the absence of evaporation. It is also possible that dew formation causes rewetting of the surface layer, particularly at night time. Therefore, even when the 0-30 cm layer is generally dry, its thin surface layer may contain a slightly higher moisture level. This may partly explain the low correlation between night-time near-surface soil moisture measurements and the moisture contents of the 0-30cm deep layer. Nevertheless, poor correlations were observed between average 0-30 cm measurements and AMSR-E near-surface values for the whole period from 2003-2004 as shown by correlation coefficients for day-time (R^2=0.15) and night-time (R^2=0.07). This analysis however, confirms that 0-30 cm soil moisture measurements at S4 show a positive relationship with the AMSR-E data. The results indicate that it is possible to establish a site-specific empirical relationship to obtain an area-averaged near-surface moisture content from 0-30 cm measurements. For example, the daytime 0-1 cm near-surface soil moisture for the AMSR-E pixel-A may be derived from 0-30 cm measurements at S4 with the following linear relationship (R^2 = 0.24, *t* statistics of the intercept = 23.31, *t* statistics of the slope = 8.35 and *n* = 223).

$$\theta_{0-1} = 0.0919 + 0.01243 * \theta_{S4_{0-30}} \qquad \textbf{(7-15)}$$

Figure 7-33 compares the AMSR-E soil moisture with 0-1cm moisture estimates based on equation 7.15. It is evident that there is some similarity in temporal evolution between the predicted and measured moisture contents. By measuring the soil moisture at representative sites it may therefore be possible to derive near-surface soil moisture estimates over large areas.

(a)

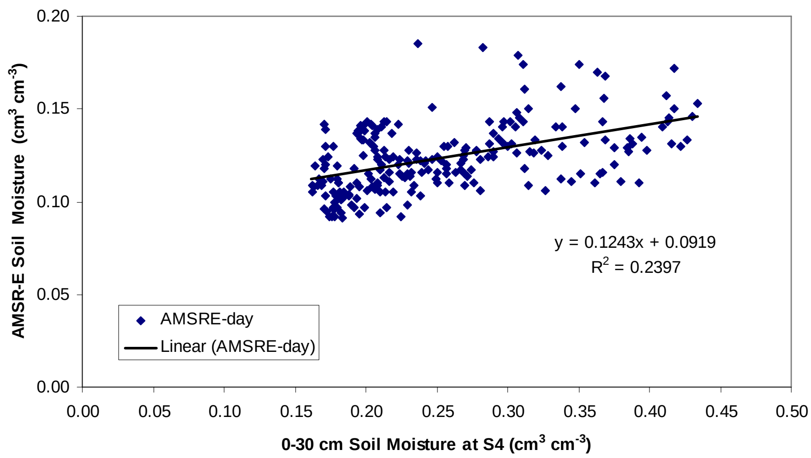

(b)

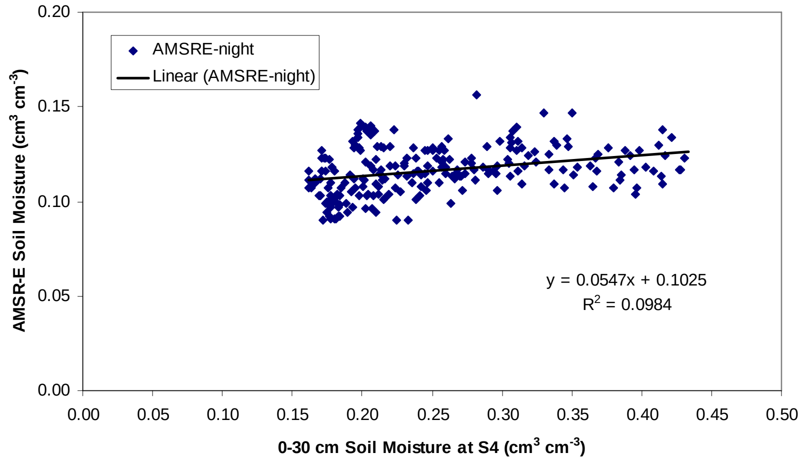

Figure 7-32: Correlation between 0-30 cm *in-situ* soil moisture measurements at S4 and 0-1 cm AMSR-E soil moisture observations during (a) day time, and (b) night-time in 2004.

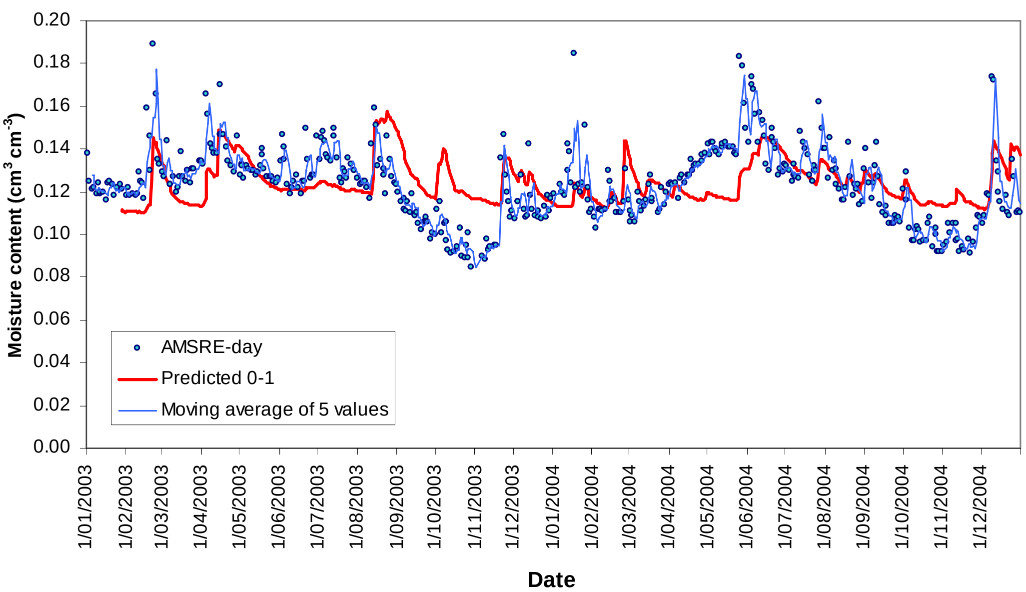

Figure 7-33: Comparison of AMSR-E day-time measured 0-1 cm near-surface soil moisture and estimated 0-1cm soil moisture content derived from the measured 0-30cm value at a representative site (S4) during 2003-2004.

7.7.6 COMPARISON OF VEGETATION MOISTURE CONTENTS AND FIELD MEASURED SOIL MOISTURE

In addition to near-surface soil moisture measurements AMSR-E also provides estimates of vegetation water content. For instance, Figure 7-34 shows the vegetation water contents measured over a two years. Field-measured averaged soil moisture contents (0-30 cm) are also shown in the figure. As can be seen, night-time vegetation water contents are always higher than the daytime water contents. This is likely to be due to the temporal wilting conditions of the leaves which are frequently present during mid-day and early afternoon. During night-time, with low transpiration rates, cells return to normal conditions, hence leaves contain more water. Passive microwave sensors are sensitive to day and night vegetation water content variations between day and night. Furthermore, as can be seen in the Figure 7-34 and Figure 7-35, these vegetation water content variations are in step with *in-situ* soil moisture measurements. For example, daytime vegetation water contents show a positive correlation with field measured soil moisture contents. These results provide a measure of confidence in the vegetation water content values measured by AMSR-E. However, this information must be used with some caution because it gives the vegetation water content over a 25 km pixel for the entire height of the vegetation cover. Hence it is easier to interpret the AMSR-E vegetation water contents for uniform vegetation condition. Applications to patchy and mixed types of vegetation however, are complex and need careful study of vegetation patterns across the pixel.

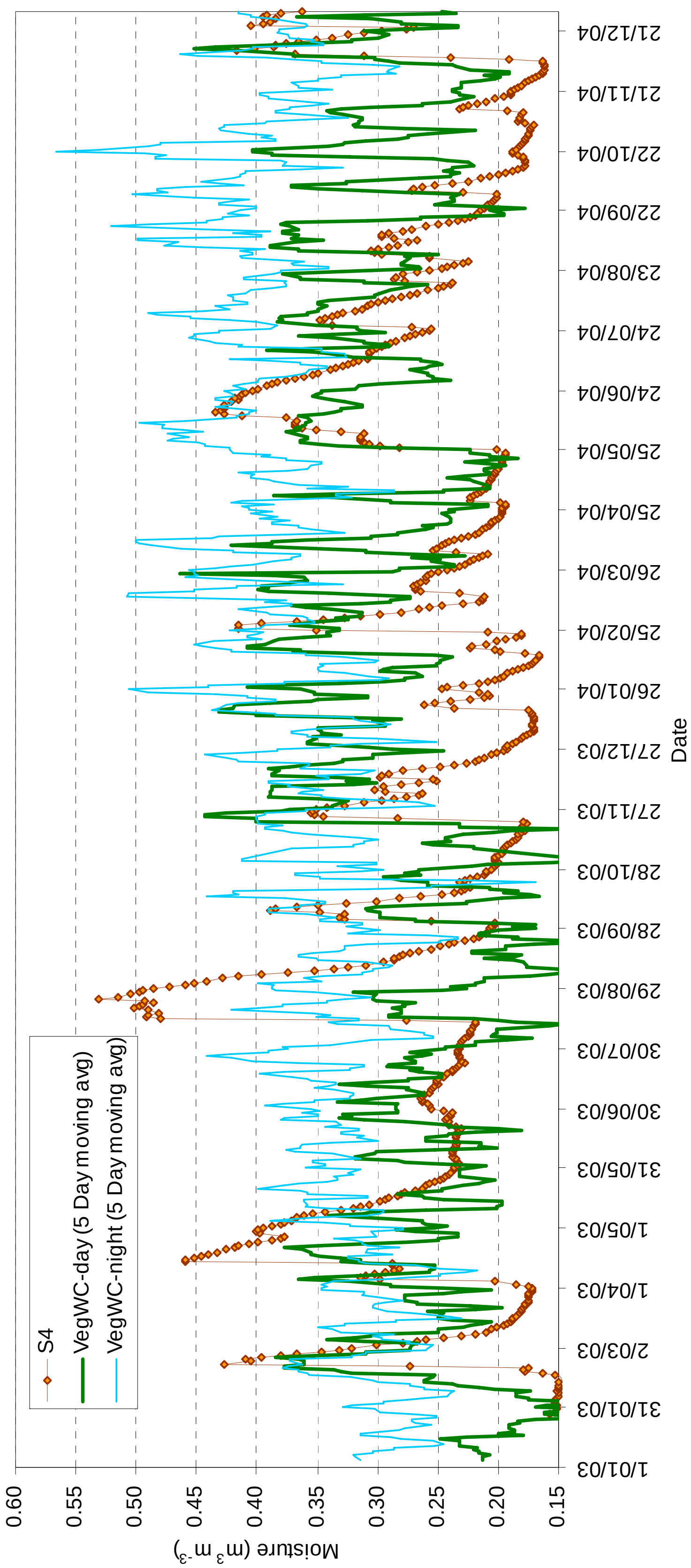

Figure 7-34: AMSR-E daytime and nighttime estimates of vegetation water contents and field measured soil moisture at S4 during 2003-2004. (Note: Y axis is for both soil moisture (cm^3 cm^{-3}) and vegetation water content (kg m^{-2}).

(a)

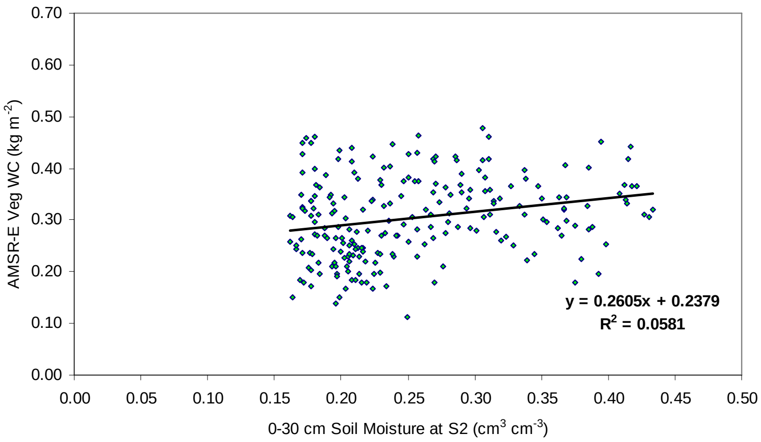

(b)

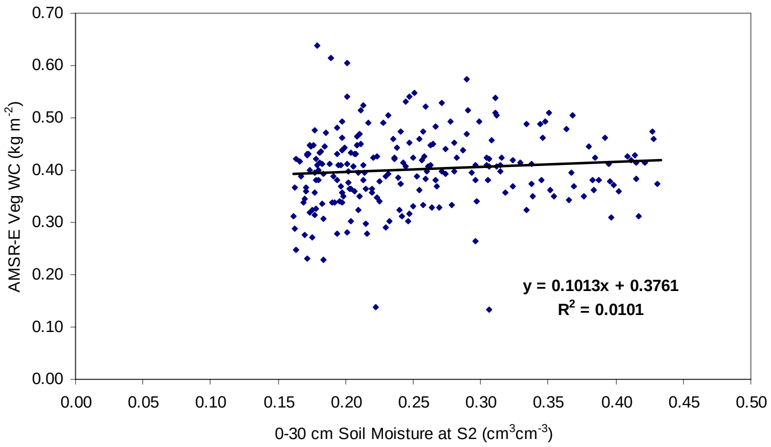

Figure 7-35: Correlation between 0-30 cm *in-situ* soil moisture at S4 during 2004 and AMSR-E vegetation moisture content based on (a) day-time, and (b) night-time observations.

7.8 CONCLUDING REMARKS

This chapter has reviewed the application of microwave remote sensing techniques for soil moisture measurements and the field validation of passive microwave soil moisture measurements based on intensive field campaigns and the use of temporal patterns in long-term soil moisture measurements at individual sites.

The results indicate that satellite based near-surface soil moisture measurements are feasible and that more reliable measurements may be obtained with more accurate site specific variables such as (pixel based) vegetation and soil parameters.

Passive microwave remote sensing for monitoring soil moisture offers new opportunities. First, it enables remote regions with limited field measurements to be regularly monitored. Second, it overcomes the difficulty of obtaining accurate estimates of large-area soil moisture measurements using point-scale ground-based techniques because of costs and the likelihood of instrument failures. Area-average soil moisture measurements are important for scaling studies. This simplifies the data scaling requirement of hydrological model applications and also assists in validating soil moisture up-scaling relationships. Validation of near-surface measurements is of primary importance to pave the way for better model predictions.

While the comparisons between the AMSR-E products and field measurements are not straightforward because the 75km x 43 km IFOV of the 6.9 GHz channel and the 25 km resolution of the soil moisture product significantly exceed the typical plot size used in field sampling. The results presented here suggest that future validation studies should consider the use of airborne sensors. Accurate validation is difficult to achieve because the footprint size of the AMSR-E observations is about 56 km (i.e. IFOV of 75km x 43 km area), and the available soil moisture data are resampled to 25km from the observation, .

Ideally, in validation studies, it is important to consider large areas with different wetness conditions within one day or several days which are associated with different wetness conditions. The resources available for the study did not support study over a large catchment. Despite this limitation, study described in the thesis attempted to capture a number of days with different moisture contents. Unfortunately, prolonged drought conditions throughout the study period did not support capturing a wider range of moisture contents.

The results presented here are encouraging for future development of passive microwave technology for global soil moisture observations. It is evident from the results that AMSR-E soil moisture estimates are reasonably accurate and consistent for low vegetation conditions (at vegetation opacity (τ) < 0.06). It should be noted that on theoretical grounds the 6.9 Hz channel of AMSR-E is expected to yield integrated soil moisture values for the top 0-1 cm. The observed difference between AMSR-E estimates and field measured values may be due to a vegetation effect. Therefore, further study is needed to compensate for the vegetation effect in the soil moisture determination algorithm.

Any indirect soil moisture measurement approach requires field validation of the result. However, field validation of a large-area soil moisture measurement (>1km) is very complicated and represents a cumbersome task. The main difficulty is how to relate a single observation value with a number of point scale measurements. The easiest approach is to collect a large number of point scale observations and to use arithmetic averages. When human resources are used for such point observations, there is a limit on the coverage and the number of samples. Therefore, sampling campaigns have to be conducted with certain assumptions such as the assumption of nearly-constant near-surface moisture over extended periods (e.g. up to 1-3 days). The results of the 3-day field experiments described here indicate that the use of a three-day period for the collection of near-surface soil moisture measurements to evaluate the average near-surface moisture measurements of AMSR-E did not appear to affect the final results. However, in situations where the surface is relatively wet and rapid drying can occur, it is advisable to consider shorter-duration field campaigns. In addition, the accessibility to sites within the footprint may present another major problem, because lack of access may prevent field observations from being carried out in a uniform manner across the area.

In order to allocate available resources more efficiently during field surveys, future validation campaigns should be planned to cover only the AMSR-E pixels. This is possible as AMSR-E soil moisture products are always coupled with fixed geographical locations based on the 25 km scale EASE grid representation. This allows for a large number of readings to be collected across a pixel within a shorter period.

It is also possible to use the soil moisture data from an existing ground-based monitoring network to validate the AMSR-E measurements. Continuous observations of soil moisture measurements from permanent networks provide information on temporal behaviour of soil moisture. In this context, analysis of temporal stability characteristics of ground-based monitoring stations are promising. Such an analysis also helps to reduce the number of measuring points required for characterising soil moisture trends for a given AMSR-E pixel. In the light of the above, the installation and maintenance of permanent networks of soil moisture measurement sites will be highly desirable when validating the soil moisture retrieval algorithm of microwave sensors.

While validation attempts based on point scale observations are obviously useful, a better approach is to collect spatially averaged data with an airborne radiometer. This may help in computing more representative average soil moisture values across large areas. It also results in faster data collection within a shorter window period to match with the Aqua overpasses and makes longer campaigns such as 3 days taken in the present study unnecessary. This approach also makes it unnecessary to assume constant soil moisture conditions over a three-day period. Above all, airborne data can be collected at a several altitudes and hence for a range of spatial scales provide the best data source for soil moisture scaling studies.

Spatial resolutions of soil moisture from passive microwave radiometers are very coarse and usually in the order of tens of km in pixel size. Future microwave soil moisture remote sensing missions should attempt to improve the spatial resolution to around 10 km.

Finally, appropriate technique must be developed for *in-situ* validation of microwave measurements and various field campaigns are therefore necessary for a range of ecological and climatic regions to build up a knowledge-base. Until they are fully validated, soil moisture data derived from satellite remote sensing will be used more in qualitative studies rather than for quantitative applications.

CHAPTER EIGHT

8. SPATIAL DISAGGREGATION OF LARGE-AREA NEAR-SURFACE SOIL MOISTURE MEASUREMENTS

The main limitation of near-surface soil moisture observations obtained with space-borne passive microwave sensors such as from AMSR-E is their inadequate resolution for many applications. The development of a range of disaggregation techniques is therefore important to overcome such limitations due to the inadequate spatial resolution. Disaggregation of large-area soil moisture fields is not straightforward and extracting the hidden soil moisture distribution pattern behind a single number is an elusive challenge. This chapter presents a methodology to disaggregate near-surface soil moisture estimates from AMSR-E. The chapter explores use of land surface temperatures and vegetation indices derived from higher resolution sensors to describe the variations of moisture within the large footprint of passive microwave soil moisture products. This methodology has been developed as an outcome of Chapter 6 where soil moisture scaling has been studied based on spatial and temporal data. The new methodology provides estimates of the change in soil moisture at the spatial resolution of approximately 1.1 km^2. It is expected that the methods used in this study can contribute to a range of catchment scale soil moisture studies when acquiring alternative soil moisture data is costly and time consuming.

8.1 INTRODUCTION

The distribution of soil properties can differ widely across a given catchment. This variation, in turn, causes large differences in the way dissimilar soil types store and transmit water. Improved information on distribution of soil water content across a catchment is needed for modeling surface and subsurface phenomena. Hydrological prediction at the meso- and local-scales is dependent upon the ability to characterize the spatial variability of soil moisture content. The lack of soil moisture data at the required spatial resolution is the greatest hindrance to the successful application of local and regional scale hydrological models.

Soil moisture measurements of AMSR-E hold great promise for monitoring soil water content across the globe owing to its strong physical basis. Because of the large field of view of the C band radiometer (nearly 76 x 44 km) due to the relatively poor passive microwave emission, the AMSR-E soil moisture product of 25km resolution is not the optimal tool for mapping soil water content, although it is the best currently available method for such a purpose. This type of large-area averaged soil moisture estimates may be used in catchment scale lumped models or models run at a coarse resolution, but will not be suitable for distributed or semi-distributed models when soil moisture estimates are desired at much finer scales, for example at 1 km^2. Current and future L-band and C-band satellite radiometers also have the problem of coarse spatial resolution, which has to be addressed before important applications, such as incorporation of remotely sensed soil moisture estimates in precision agricultural applications (Voltz, 1997).

Because of the spatial nonlinearities of land processes, the use of mean quantities causes considerable inaccuracies in the land surface scheme calculations with large-area average soil moisture fields. Hence, it is necessary to describe the soil moisture fields over catchments in statistical or disaggregated terms.

Ideally, the main objective of a disaggregation scheme is to produce ‘true’ sub-pixel patterns of soil moisture from lower-resolution remotely sensed observations. According to Tsegaye *et al*. (2003) it is difficult to develop and validate such a disaggregation scheme because the actual sub-pixel soil moisture pattern within a satellite footprint is rarely, if ever, known within acceptable error bounds. Thus, Tsegaye *et al*. (2003) argue that adequate data for developing statistical models do not exist and may never exist for areas larger than field scale.

As discussed in Chapters 2 and 6, neither sub-grid scale surface moisture data nor acceptable downscaling methods exist for AMSR-E data. An appropriate downscaling approach is necessary to avoid the propagation of errors from the observation scale to the modelling scale. This may be possible with the combined use of higher-resolution air-borne sensors or radar information from other microwave radiometers (Narayan and Lakshmi, 2005) or thermal imagers. Airborne imagery however, is not readily available and if available, it may incur high data acquisition costs. The most practical approach is therefore to use the information from satellite based remote sensing sensors such as MODIS and NOAA –AVHRR (Hemakumara, *et al*., 2004). This thesis studies downscaling approaches for the AMSR-E soil moisture product based on other higher-resolution radiometers in space. This chapter first discusses selected existing disaggregation techniques as described in the literature and then proposes two new methods to disaggregate AMSR-E soil moisture. Disaggregated soil moisture values are then compared with field measured values.

(In this chapter, the term low-resolution, and 25-km resolution are used interchangeably. Similarly, the term high-resolution and 1.1-km resolution are also used interchangeably.)

8.2 DISAGGREGATION TECHNIQUES

Kim and Barros (2002a) concluded that soil moisture fields exhibit multiscaling and multifractal behaviour. They further reported that such multiscaling and multifractal behaviour varies with the scales of observations and hydrometeorological forcing. Thus, use of simple scaling approaches to derive high-resolution soil moisture distributions from AMSR-E data may not always provide accurate spatial patterns. Perhaps, by using the scaling characteristics of suitable proxy variables such as the soil texture or vegetation water content it may be possible to explain patterns in soil moisture content.

Disaggregation of large-area soil moisture fields requires appropriate disaggregation schemes with a strong physical basis. Soil moisture disaggregation reveals the hidden moisture pattern built into the large-area observations. Aggregation, on the other hand, is the process of deriving a spatial average from a large number of small-scale observations. In general, spatial aggregation methods are less complicated than the disaggregation methods. However, disaggregation is not so simple and extracting the hidden soil moisture values from a single number is an elusive challenge.

A range of methods can employed to downscale large-area measurements to finer scale representations. In a broad sense, there are three categories of methods: a) statistical approaches, b) data assimilation approaches, and c) methods using information from higher-resolution sensors. All these approaches help in disaggregating large-area soil moisture fields into finer-scale fields with some degree of confidence. Below the concepts behind these disaggregation approaches are briefly discussed.

8.2.1 STATISTICAL APPROACHES

Statistical disaggregation techniques have been applied to soil moisture as well as to many other different geographical phenomena like haze assessment (Abuzar & Al-Ghunaim, 1997). However, typical interpolation techniques such as linear averaging, kriging, polynomial and fractal interpolation may not necessarily produce actual patterns of soil moisture distributions at a finer scale from the coarse-scale observations. This is because soil moisture patterns at any scale have a physical meaning and soil moisture is therefore not distributed purely on a random basis. Many statistical approaches are based on the assumption of random data distribution (some exceptions found, e.g. co-kriging). Thus, transferring soil moisture information across scales purely in statistical terms may introduce errors in the predictions.

There are few examples of successful application of statistical approaches to preserve the spatial variability of original data in transferring soil moisture across scales. This is mainly due to the fact that large-scale soil moisture measurements are relatively new. One promising method has been proposed by Kim and Barros (2002a) who showed the use of fractal interpolation method for disaggregating large-area soil moisture measurements. Their disaggregation method is based on a mathematical technique called 'contraction mapping' and uses ancillary data such as soil texture and vegetation water content. Application of their model to downscale 10 km soil moisture observations to a 1 km resolution was successful. However, their method is complex and it requires additional information such as soil texture and vegetation water content which is not always available.

Tsegaye *et al.* (2003) have proposed a disaggregation scheme called DisaggNet based on an artificial neural network approach for downscaling large-area soil moisture measurements from microwave sensors. Their approach consists of training (or calibrating) a neural network using surface hydrology-radiative transfer model output, and then testing its performance using actual remotely-sensed data. The main strength of their approach is the ability to simulate the fine-scale soil moisture in a catchment over extended periods. They assume that the surface hydrology-radiative transfer model used in the scheme accurately simulates the spatial patterns of soil moisture and brightness temperature within an actual satellite footprint. They assumed a linear relationship between microwave emissivity and soil moisture although this relationship is not perfectly linear (see Figure 7.1). Their approach requires calibration of the disaggregation scheme in a selected geographic domain so that the results are not readily transferable to other geographic regions. DisaggNet also assumes a linear relationship between rainfall and soil moisture which is not appropriate for many hydrophobic soils (i.e. soils which are difficult to wet because they repel water) found in Australian catchments.

It is also possible to design statistical disaggregation schemes based on fuzzy set algorithms. The discretisation of objects in spatial analyses through data models cannot be done with absolute precision and accuracy (Molenaar, 1998). Thus, the use of fuzzy set operators for spatial analyses of soil moisture may be advantageous. Fuzzy logic is appropriate for spatial analysis when the data used is highly subjective. In case of AMSR-E soil moisture, one can argue that microwave penetration depth is uniform across a pixel although, as discussed in Chapter 7, it is difficult to assume a uniform microwave penetration depth due to variable vegetation densities across a large footprint. The disaggregated soil moisture from microwave measurements therefore has some degree of uncertainty. For this reason, use of fuzzy set algorithms for disaggregation of AMSR-E soil moisture may be appropriate.

8.2.2 MODEL BASED APPROACHES – DATA ASSIMILATION TECHNIQUES

Data assimilation techniques using physically-based models provide an opportunity to downscale microwave-based large-area soil moisture observations. Based on a synthetic experiment, Reichle *et al.* (2001a) demonstrated that soil moisture can be estimated satisfactorily at scales finer than the original resolution of the brightness images. Their approach however requires micrometeorological, soil texture and land cover inputs at the finer scale, which are often not readily available. In addition, their approach focuses more on the downscaling of radio brightness measurements than of soil moisture products and is therefore not readily applicable for downscaling of soil moisture fields.

8.2.3 USE OF HIGH RESOLUTION IMAGES

Disaggregation schemes using higher-resolution radar observations may provide the means for interpreting large-area soil moisture observations at much finer scale. Narayan and Lakshmi (2005) presented an approach for disaggregation of coarser resolution radiometer estimates of soil moisture using higher-resolution radar backscatter and vegetation water content measurements. Their algorithm provides estimates of the change in soil moisture at the spatial resolution of the radar (observations obtained at the same temporal resolution as that of the coarse resolution data). They assume that the spatial variability of bare soil properties (texture, roughness) that influence radar sensitivity to soil moisture is not significant and hence the variability of the radar signal within the radiometer footprint is due to soil moisture and canopy vegetation water content variability only. This assumption helps to reduce the variables in the retrieval algorithm. The authors argue that if the lower resolution soil moisture estimates of the region for a particular time is known, assuming that the spatial variability in soil moisture for that time is very low (conditions are very dry or very wet), then the lower resolution estimate can be simply re-sampled to a higher resolution. The higher-resolution change in soil moisture derived from the radar image is then added to the high-resolution soil moisture image obtained from resampling to produce higher-resolution soil moisture images. This approach appears attractive, but requires appropriate radar images.

8.2.4 USING SURFACE WETNESS INDICES

Chauhan *et al.* (2003) proposed a process for obtaining high-resolution soil moisture data using a synergistic analysis of microwave-optical/IR data. Their algorithm combines the traditional accuracy of microwave sensors for soil moisture sensing with the capability of optical/IR sensors to determine soil moisture estimates at high resolution. This approach computes the soil wetness conditions using the NDVI-LST space proposed by Carlson *et al.* (1994) as discussed in Section 2.3.5. In addition to the land surface temperature and NDVI, they considered surface albedo in an attempt to strengthen the relationship between the soil moisture and measurable land parameters. The estimation of soil moisture at 1-km resolution was done using a system of linear equations between SSM/I-derived soil moisture and aggregated land surface parameters such as NDVI, albedo, and LST. The authors used this approach to disaggregate SSM/I data (frequency ~19.4 GHz, 25-km spatial resolution) with data from AVHRR (1.1 km spatial resolution). Their approach was found to be promising because it provides a useful methodology for using wetness indices for disaggregation of soil moisture measurements.

8.2.5 PROPOSED DISAGGREGATION STUDY

Most current schemes for disaggregation of large-area soil moisture fields are not adequate or applicable. Some available techniques are too complex for wider applications. Several authors (e.g. Kim and Barros, 2002b; Chauhan *et al.,* 2003; Tsegaye *et al.,* 2003; Narayan and Lakshmi, 2005) have discussed disaggregation of near-surface microwave based soil moisture measurements, but only few studies considered use of *in-situ* measurements for justifying their approaches. This study therefore investigates practical methods to disaggregate near-surface low-resolution soil water contents from microwave sensors and evaluate the methodology using field measured soil moisture data. It is also clear that any soil moisture disaggregation method should have a sound physical basis, be simple, and cost-effective and should be able to be applied over a range of geographical regions.

The primary objective of the present disaggregation study is to use information derived from high-resolution sensors to disaggregate passive microwave AMSR-E near-surface soil water contents. Because of the paucity of fine-scale microwave observations, the most viable approach is to use the fine-scale observations of visible and NIR bands from other radiometers such as MODIS and NOAA. Designing a disaggregation scheme based on non-microwave radiometers requires answers to the following questions:

- Is LST and VI information obtained with high resolution sensors suitable and can it be used for predictions?
- Is the method efficient for the time series of AMSR-E images?
- What is the regional applicability of the method?

To generate high spatial resolution soil moisture data from microwave measurements, a technique based on optical/IR remote sensing approaches will be used. As discussed in Chapter 6, information derived from visible and NIR bands provides a good physical basis for explaining land surface wetness characteristics. Particularly, the land surface temperature index such as the RNTI and the wetness index such as the VTCI are suitable variables for describing the subpixel moisture variations. The study of regionalization of point-scale soil moisture measurements (discussed in Chapter 6), has indicated that indices such as RNTI and VTCI are potentially useful for mapping soil wetness patterns across a catchment. In this chapter, two methods for disaggregating AMSR-E soil moisture are discussed which are based on RNTI and VTCI indices. The two approaches are evaluated with the point-scale soil moisture measurements collected during three-day AMSR-E validation campaigns (see Section 7.6).

8.3 METHODOLOGY

Satellite data from AMSR-E and Aqua-MODIS over the Goulburn River catchment were acquired for the three field campaign periods described in Chapter

7. Descriptions of AMSR-E and MODIS are given in Section 2.3.2.2.1 and in Section 2.3.2.1.2 respectively. The properties of MODIS land surface temperature data used in the present study are shown in Table 8-1. As seen in the table, only four MODIS data sets are suitable for the study: namely Campaign 1 Day 3, Campaign 2 Days 1 and 3, and Campaign 3 Day 2. Despite the fact that only Day 3 of Campaign 2 is suitable for the study, MODIS data on Day 1 (over 20% of clouds) are also considered due to small number of days available. In the case of AMSR-E data, daily average soil moisture contents (estimated from ascending and descending paths) were used. For some days only one data set (from either the ascending or the descending paths) was available and for those days it was assumed that the available data represent the average soil moisture contents for the day.

The ground-based soil moisture data used in this study were the volumetric soil moisture measurements at 180-225 locations in each field campaign obtained with a theta probe (0-6 cm soil moisture) and obtained with gravimetric method (0-1 cm soil moisture) during all three field campaigns as discussed in sections 7.6.1 and 7.6.2. During the three-day campaigns, field sampling was done in a diagonal pattern (see Figure 7.9) within the validation footprint of approximately 50 km × 40 km area. This enabled collection of point-scale *in-situ* soil moisture values from 12 different areas (3 areas per team x 4 teams) across AMSR-E pixels for each day in the field campaign. Additionally, efforts were made to collect soil moisture samples in the same general vicinity during all three campaigns.

Table 8-1: Properties of the LST data sets used in the downscaling study.

Campaign	Property	Day-1	Day-2	Day-3
1	Sensor type	MODIS/Aqua	MODIS/Aqua	MODIS/Aqua
	Daytime image	not suitable	not suitable	suitable
	Overpass time	-	-	13:36
	% clouds in the image			10.5%
	Min/Max LST (K)			282.9/323.5
	Air temp. (^{o}C)*			26.61
2	Sensor type	MODIS/Aqua	MODIS/Aqua	MODIS/Aqua
	Daytime image	suitable	not suitable	suitable
	Overpass time	13:48	-	13:36
	% clouds in the image	20.7%		0.0%
	Min/Max LST (K)	281.1/301.3		284.5/306.2
	Air temp. (^{o}C)*	18.96		19.46
3	Sensor type	MODIS/Aqua	MODIS/Aqua	MODIS/Aqua
	Daytime image	not suitable	suitable	not suitable
	Overpass time	-	13:24	-
	% clouds in the image		1.4%	
	Min/Max LST (K)		279.2/296.6	
	Air temp. (^{o}C)*		12.85	

* - Air temperature measured at S2 climate station.

Soil moisture measurements from four AMSR-E pixels have been used in this study. The footprint selected for the field study spreads out over one complete AMSR-E pixel (at EASE-grid column no. 1269 and row no. 449), covers about 75-80% of a second pixel (at column no. 1270 and row no. 449), and includes 40-50% of two other pixels (at column numbers 1269-1270 in row no. 450). The validation footprint therefore provided an opportunity to study the downscaled results from up to four AMSR-E pixels.

RNTI and VTCI indices are calculated for the selected dates from MODIS LST and EVI with 1.1 km resolution (see Chapter 6 for details of the computation procedure). The RNTI is a dryness index and it is therefore necessary to consider the residual ‘1-RNTI’ values for the spatial disaggregation of large-area soil moisture measurements. The VTCI values describe wetness conditions and no conversion was required. The downscaling approach involved calculating a weighting factor for each grid cell which is the ratio between the index value for that cell and the average of all index values across a given AMSR-E footprint. Multiplying the AMSR-E measured soil moisture value with this weighting factor yielded high-resolution soil moisture content values across a footprint. Accordingly, the soil moisture content computed for a given high-resolution pixel of RNTI (i.e. θ_{RNTIi}) is given by:

$$\theta_{RNTI_i} = \theta_{AMSR-E_j} \times \frac{(1 - RNTI_i)}{\frac{1}{n}\sum_{i=1}^{n}(1 - RNTI_i)} \qquad \textbf{(8-1)}$$

where $\theta_{AMSR\text{-}Ej}$ is the volumetric soil water content in the j^{th} AMSR-E pixel, n the number of high-resolution pixels within the j^{th} AMSR-E pixel and $RNTI_i$ the computed RNTI for high-resolution pixel i. This study considers n = 621 (the 25 km EASE-grid pixel contains 23 rows by 27 columns of 1.1 km pixels).

Similarly, the soil moisture content computed from a given high-resolution pixel of VTCI (i.e. θ_{VTCIi}) is given by:

$$\theta_{VTCI_i} = \theta_{AMSR-E_j} \times \frac{VTCI_i}{\frac{1}{n}\sum_{i=1}^{n}VTCI_i} \qquad \textbf{(8-2)}$$

where $VTCI_i$ is the computed VTCI for high-resolution pixel *i.*

8.4 RESULTS

8.4.1 COMPARISON OF DISAGGREGATED MEASUREMENTS WITH WHOLE DATA SET

Table 8-2 shows the daily averaged AMSR-E soil water contents used for the present study. The spatial distributions of AMSR-E soil water contents and field sampling sites during the selected dates are shown in Figure 8.1.

Table 8-2: Average AMSR-E SWC values (computed from daily ascending and descending paths, in $cm^3.cm^{-3}$) used for the disaggregation study. The four AMSR-E values used for the case studies are located under the column numbers 1269-1270 and row numbers 449-450. (Note: bold numbers used for case studies and all other numbers used for the regional maps)

Campaign	Day	EASE-grid row numbers	EASE-grid column numbers 1267	1268	1269	1270	1271
1	**3**	448	0.071	0.075	0.078	0.081	0.085
		449	0.071	0.074	**0.077**	**0.082**	0.091
		450	0.076	n.a.	**0.085**	**0.088**	0.101
		451	0.087	n.a.	n.a.	n.a.	0.121
		452	0.096	n.a.	n.a.	0.139	0.149
		453	0.102	n.a.	n.a.	0.142	0.145
2	**1**	448	0.113	0.111	0.116	0.115	0.123
		449	0.120	0.120	**0.121**	**0.124**	0.128
		450	0.132	0.137	**0.139**	**0.140**	0.131
		451	0.142	0.151	0.157	0.163	0.167
		452	0.144	0.150	0.160	0.186	0.168
		453	0.145	0.147	0.153	0.163	0.156
2	**3**	448	0.106	0.104	0.112	0.119	0.129
		449	0.112	0.115	**0.118**	**0.126**	0.129
		450	0.126	0.129	**0.133**	**0.137**	0.131
		451	0.138	0.144	0.143	0.148	0.159
		452	0.138	0.143	0.149	0.172	0.167
		453	0.133	0.139	0.147	0.159	0.150
3	**2**	448	0.114	0.107	0.098	0.100	0.118
		449	0.130	0.118	**0.111**	**0.113**	0.124
		450	0.146	0.136	**0.122**	**0.133**	0.139
		451	0.153	0.149	0.137	0.139	0.142
		452	0.159	0.153	0.152	n.a.	0.145
		453	0.165	0.158	0.156	n.a.	n.a.

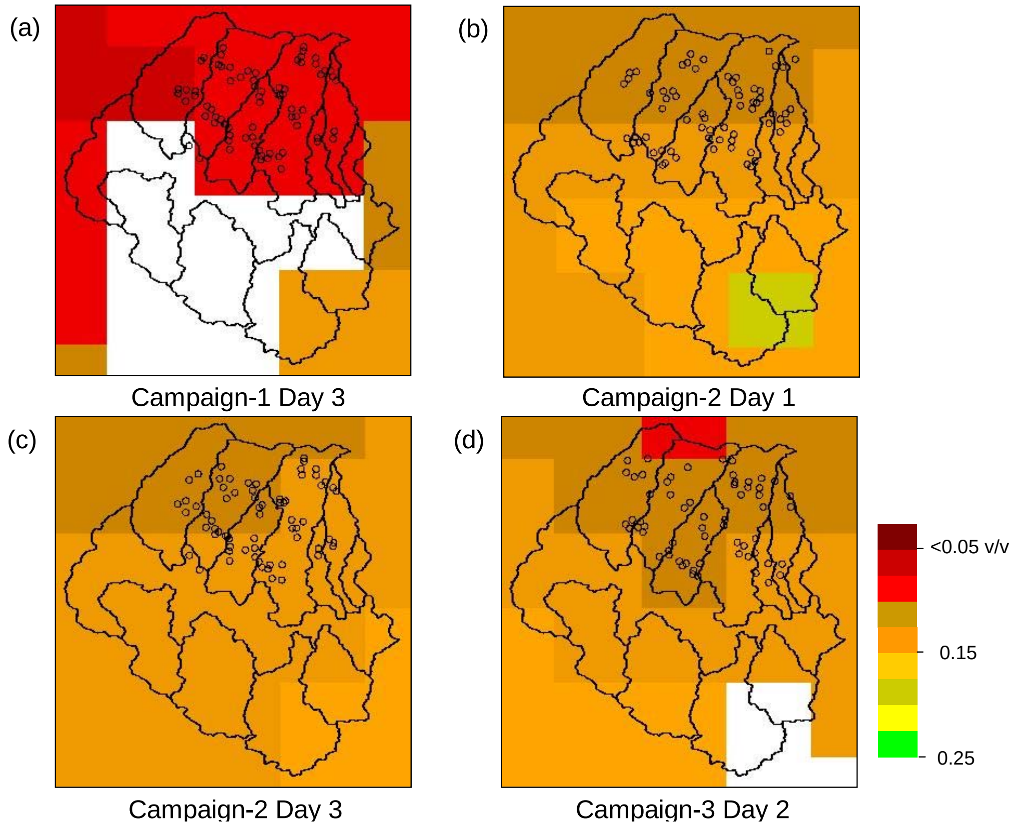

Figure 8.1: Average AMSR-E measured soil moisture ($cm^3.cm^{-3}$) across the Goulburn River catchment during: (a) Campaign 1 Day 3, (b) Campaign 2 Day 1, (c) Campaign 2 Day 3, and (d) Campaign 3 Day 2. Circles indicate field sampling locations.

Table 8-2 and in Figure 8.1 show that during the Campaign 1, the near-surface SWC within the case study area varied within a narrow range of 0.077 - 0.088 cm^3cm^{-3}. Campaign 2 was particularly interesting because there were two data sets and a rainfall event occurred during the campaign. On the first day of Campaign 2, the SWC of the case study area was between 0.121 - 0.140 cm^3cm^{-3} and by the third day these SWC values had slightly decreased to 0.118 - 0.137 cm^3cm^{-3}. During Campaign 2 there was a rainfall event of 0.2 mm, which occurred on day 2, but only in the northern part of the Goulburn River catchment. According to the AMSR-E soil moisture data, the effect of this 0.2 mm rain can be seen as an increase in SWC of approximately 0.001 - 0.006 cm^3cm^{-3} in the north-eastern part of the catchment. Soil moisture values in the other areas showed that the catchment was drying out. Finally, during Campaign 3 the near-surface SWC within the case study area varied from 0.111 - 0.133 cm^3cm^{-3}. Therefore, AMSR-E soil moisture values used in the case studies provided mainly two moisture status: a dry condition of 0.08-0.09 cm^3cm^{-3} (during Campaign 1 Day 3) and a slightly wetter condition of 0.12-0.14 cm^3cm^{-3} (during other three days).

The summary statistics for the four disaggregation case studies are shown in Table 8-3. Point scale soil moisture values measured over the 0-6 cm and 0-1 cm depths were used as indicative moisture contents. Thus, Table 8-3 compares the point scale soil moisture measurements (at two depths, 0-6 cm and 0-1 cm) with the disaggregated soil moisture data from 1.1 km^2 pixels (which are representative of the top 1 cm depth). In general, Table 8-3 indicates that both indices used in the disaggregation scheme provide reasonable estimates of moisture values. The average and the range of values of the downscaled moisture contents appear closer to the 0-1 cm moisture contents than the 0-6 cm moisture contents as expected. Except for Campaign 2 Day 1, the predicted soil moisture values were within +/- 0.05 $cm^3.cm^{-3}$ of the measured moisture content based on 0-1 cm measurements. During Campaign 2 Day 1, the predicted average soil moisture content was more than 0.05 $cm^3.cm^{-3}$ off the average 0-1 cm measured value. The higher difference between the measured and predicted moisture values may be due to the computational errors associated with cloud-contaminated images. The results however are encouraging because it is shown that implementation of a simple technique based on wetness (or dryness) indices computed at the high-resolution satellite footprint scale may be used to disaggregate the low-resolution near-surface moisture contents with some confidence.

Table 8-3: Summary statistics of measured point-scale soil moisture contents and the derived 1.1 km^2 scale soil moisture contents. (Note: *N* indicates the total number of point-scale values or total number of pixels used to compute the average moisture value from the measured or downscaled soil moisture respectively)

Campaign and day		**Measured soil moisture ($cm^3.cm^{-3}$)**		**Downscaled soil moisture ($cm^3.cm^{-3}$)**	
		0-6 cm	0-1 cm	RNTI-based	VTCI-based
1-3	Avg.	0.14	0.08	0.06	0.07
	Range	0.02-0.28	0.03-0.17	0.01-0.14	0.04-0.13
	N	76	65	75	75
2-1	Avg.	0.18	0.24	0.12	0.13
	Range	0.01-0.38	0.07-0.44	0.05-0.34	0.08-0.25
	N	65	64	65	65
2-3	Avg.	0.17	0.15	0.10	0.11
	Range	0.01-0.33	0.02-0.26	0.02-0.18	0.01-0.17
	N	71	71	71	71
3-2	Avg.	0.18	0.13	0.10	0.10
	Range	0.04-0.31	0.01-0.29	0.03-0.23	0.05-0.19
	N	62	63	63	63

Since a real comparison between the *in-situ* soil moisture measurements and satellite-derived disaggregated soil moisture data is difficult to make because of the difference in scale, estimates of different levels of errors between the disaggregated moisture contents and the measured moisture contents may assist in assessing the accuracy of predictions. Considering the considerable difference between the measurement scale (point scale) and the disaggregated (1.1 km^2) scale, allowing deviations of up to 0.05 cm^3cm^{-3} appears reasonable. As reported by Njoku (1999) the AMSR-E soil moisture measurements are expected to give an accuracy of ± 0.06 cm^3cm^{-3}. The present study has therefore considered three levels of deviations of ± 0.01, 0.03 and 0.05 cm^3cm^{-3} to assess the disaggregation results.

The error analyses are summarized in Table 8-4 and 8-5 for the RNTI and VTCI methods respectively. As seen in Table 8-4, for example, during Campaign 1 Day-3, approximately 71% (i.e. 46 (*n*) out of 75 (*N*) cases) of all RNTI based estimates are within ±0.05 cm^3cm^{-3} from the actual 0-1 cm measurements. In contrast, as seen in Table 8-5, VTCI based SWC estimates for the same day show that approximately 80% of data pairs (i.e. 52 out of 75 cases) are within ±0.05 cm^3cm^{-3} from actual 0-6 cm measurements. Considering 0-1 cm SWC values, the absolute values of deviations are ≤0.03 and ≤0.05 cm^3cm^{-3}. Thus, high resolution SWC values can be obtained at 55% to 80% of the time with the disaggregation approach based on VTCI method. With the RNTI approach, the possibility of obtaining actual SWC values takes slightly lower values between 46% and 71%.

Table 8-4: Comparison of absolute deviations of predicted SWC values based on RNTI approach and the measured SWC at 0-6 cm and 0-1 cm. (*n* = number of data pairs within the error level)

Day	Deviations from 0-6 cm SWC (in $cm^3.cm^{-3}$)			Deviations from 0-1 cm SWC (in $cm^3.cm^{-3}$)		
	≤0.01	≤0.03	≤0.05	≤0.01	≤0.03	≤0.05
Campaign-1 Day 3	4% *(n=3)*	11% *(n=8)*	20% *(n=15)*	17% *(n=11)*	46% *(n=30)*	71% *(n=46)*
Campaign-2 Day 1	10% *(n=6)*	21% *(n=13)*	32% *(n=20)*	3% *(n=2)*	10% *(n=6)*	15% *(n=9)*
Campaign-2 Day 3	1% *(n=1)*	15% *(n=11)*	28% *(n=20)*	11% *(n=8)*	24% *(n=17)*	38% *(n=27)*
Campaign-3 Day 2	3% *(n=2)*	16% *(n=10)*	31% *(n=19)*	8% *(n=5)*	27% *(n=17)*	46% *(n=29)*

Disaggregated AMSR-E soil moisture data should represent the soil water content in the top 0-1 cm soil layer. It was observed in the present study that the differences between the predictions and the measurements of SWC over 0-1 cm were smaller than the differences between predictions and measurements over 0-6 cm. Such good relationships have been observed during Campaign 1 Day 3, Campaign 2 Day 3 and Campaign 3 Day 2 (see Table 8-4 and 8-5). Approximately, 80%, 39%, and 56% of data pairs of VTCI based estimates were within ±0.05 $cm^3.cm^{-3}$ from actual 0-1 cm measurements during Campaign 1 Day 3, Campaign 2 Day 3 and Campaign 3 Day 2 respectively. During Campaign 2 Day 1 however, poor results (i.e. 15%) have been obtained with the VTCI method. On the other hand, approximately 71%, 38% and 46% of data pairs of RNTI based estimates were within ±0.05 $cm^3.cm^{-3}$ from actual 0-1 cm measurements during Campaign 1 Day 3, Campaign 2 Day 3 and Campaign 3 Day 2 respectively. During Campaign 2 Day 1 the RNTI method gave also poor results (i.e. 15%).

This result indicates that the VTCI method performed better than the RNTI method in soil moisture disaggregation schemes.

Table 8-5: Comparison of absolute deviations of predicted SWC values based on VTCI approach and the measured SWC at 0-6 cm and 0-1 cm. (*n* = number of data pairs within the error level)

Day	Deviations from 0-6 cm SWC (in $cm^3.cm^{-3}$)			Deviations from 0-1 cm SWC (in $cm^3.cm^{-3}$)		
	≤0.01	**≤0.03**	**≤0.05**	**≤0.01**	**≤0.03**	**≤0.05**
Campaign-1 Day 3	3% *(n=2)*	9% *(n=7)*	29% *(n=22)*	22% *(n=14)*	55% *(n=36)*	80% *(n=52)*
Campaign-2 Day 1	10% *(n=6)*	25% *(n=16)*	41% *(n=26)*	2% *(n=1)*	7% *(n=4)*	15% *(n=9)*
Campaign-2 Day 3	1% *(n=1)*	14% *(n=10)*	35% *(n=25)*	11% *(n=8)*	28% *(n=20)*	39% *(n=28)*
Campaign-3 Day 2	5% *(n=3)*	16% *(n=10)*	29% *(n=18)*	11% *(n=7)*	29% *(n=18)*	56% *(n=35)*

This result however, requires further discussion. The main purpose of a disaggregation scheme is to map the spatial pattern of soil moisture rather than comparing moisture values for two different scales (i.e. point measurements and 1.1 km2 estimates). Thus, it is also important to assess the moisture values at individual locations. Disaggregated AMSR-E near-surface soil moisture based on VTCI and measured 0-1 cm near-surface soil moisture values are shown in Figure 8.2. As seen in the figure, the agreement between the measured and disaggregated moisture contents is not convincing for VTCI based approach. Similar results were obtained between the computed and in-situ measurements when the RNTI approach was used to disaggregate AMSR-E (see Figure 8.3).

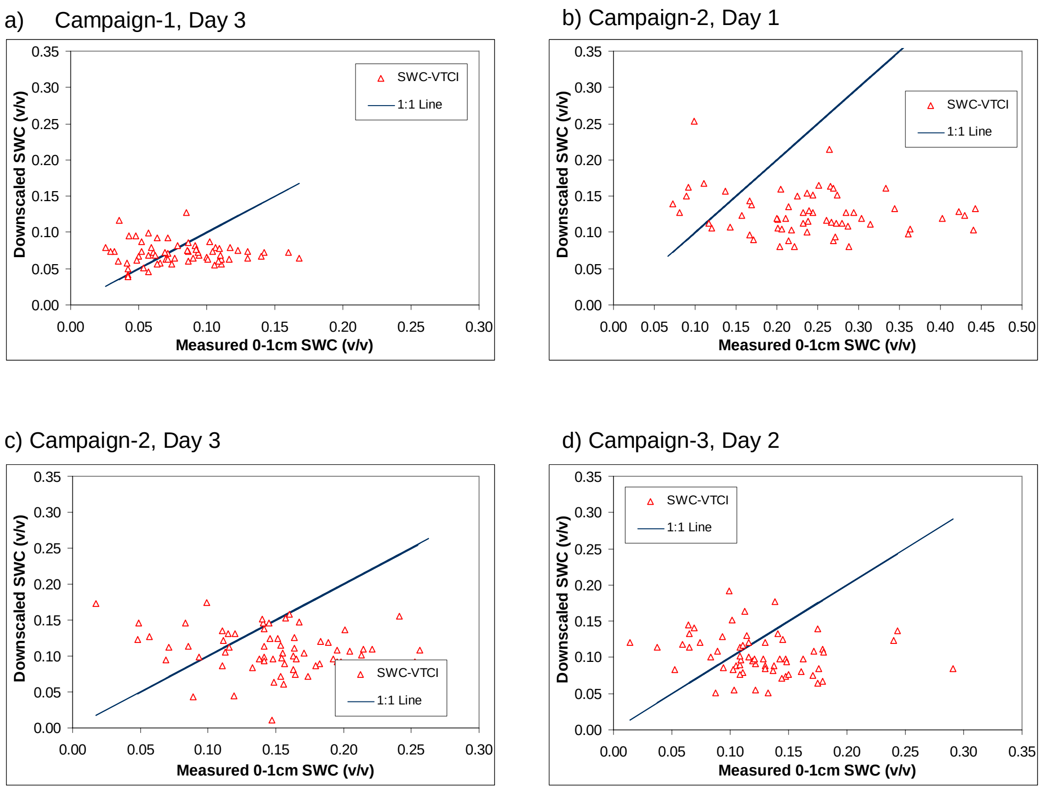

Figure 8.2: Comparison between measured point-scale 0-1 cm soil moisture content and the 1.1 km resolution estimates of soil moisture content based on VTCI for: a) Campaign 1 Day 3; b) Campaign 2 Day 1; c) Campaign 2 Day 3; and d) Campaign 3 Day 2.

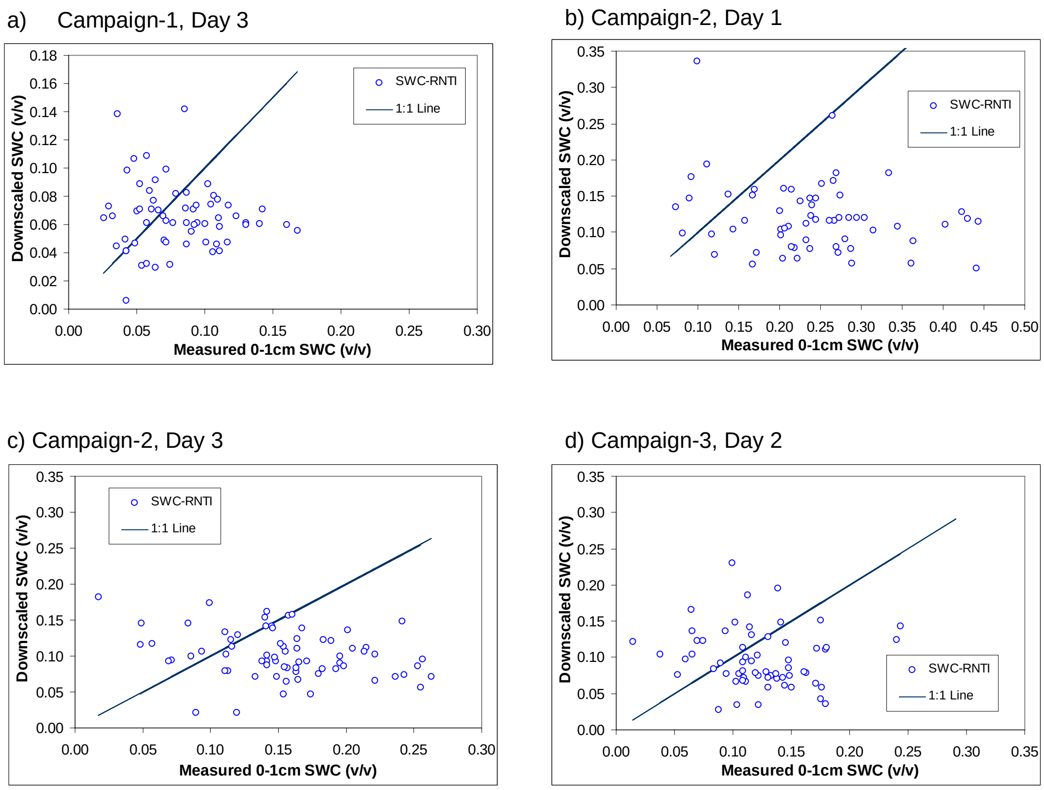

Figure 8.3: Comparison between measured point-scale 0-1 cm soil moisture content and the 1.1 km resolution estimates of soil moisture content based on RNTI for: a) Campaign 1 Day 3; b) Campaign 2 Day 1; c) Campaign 2 Day 3; and d) Campaign 3 Day 2.

Comparisons of disaggregated AMSR-E near-surface soil moisture based on VTCI and measured 0-6 cm near-surface soil moisture values are shown in Figure 8.4. As seen in the figure, the disaggregated moisture values compare poorly with the soil moisture in top 0-6 cm layer. Similar results can be seen when measured 0-6 cm near-surface soil moisture values are compared with the RNTI based moisture estimates (see Figure 8.5).

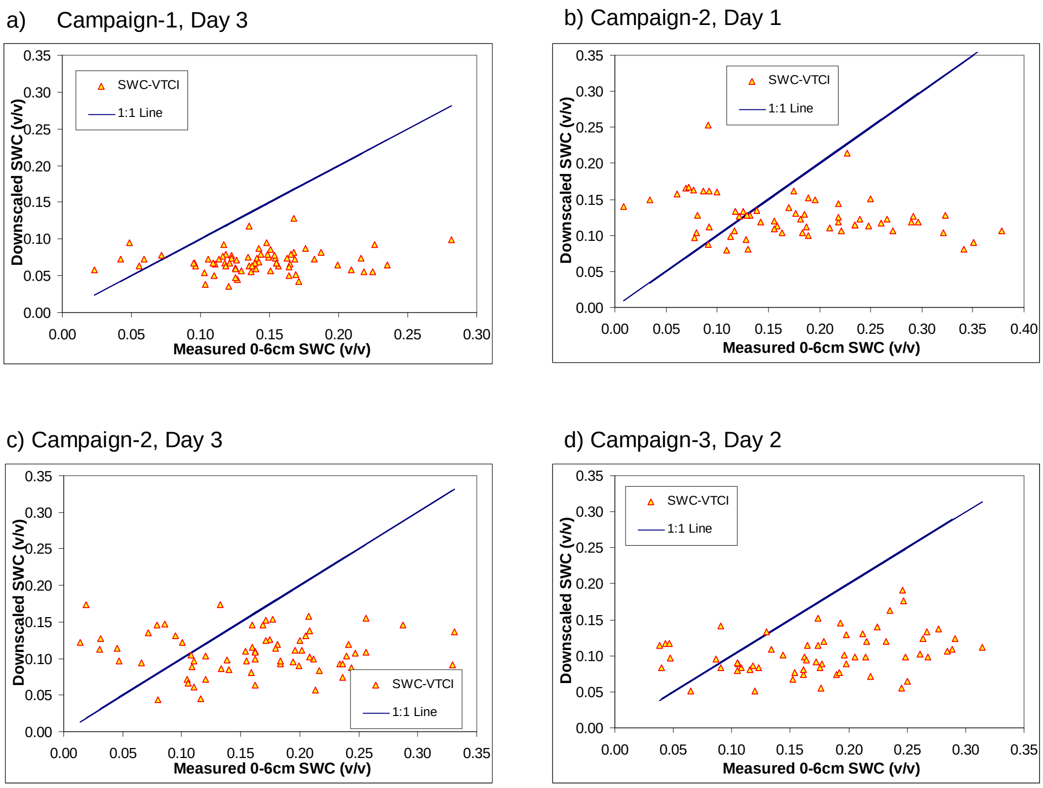

Figure 8.4: Comparison between measured point-scale 0-6 cm soil moisture content and the 1.1 km resolution estimates of soil moisture content based on VTCI for: a) Campaign 1 Day 3; b) Campaign 2 Day 1; c) Campaign 2 Day 3; and d) Campaign 3 Day 2.

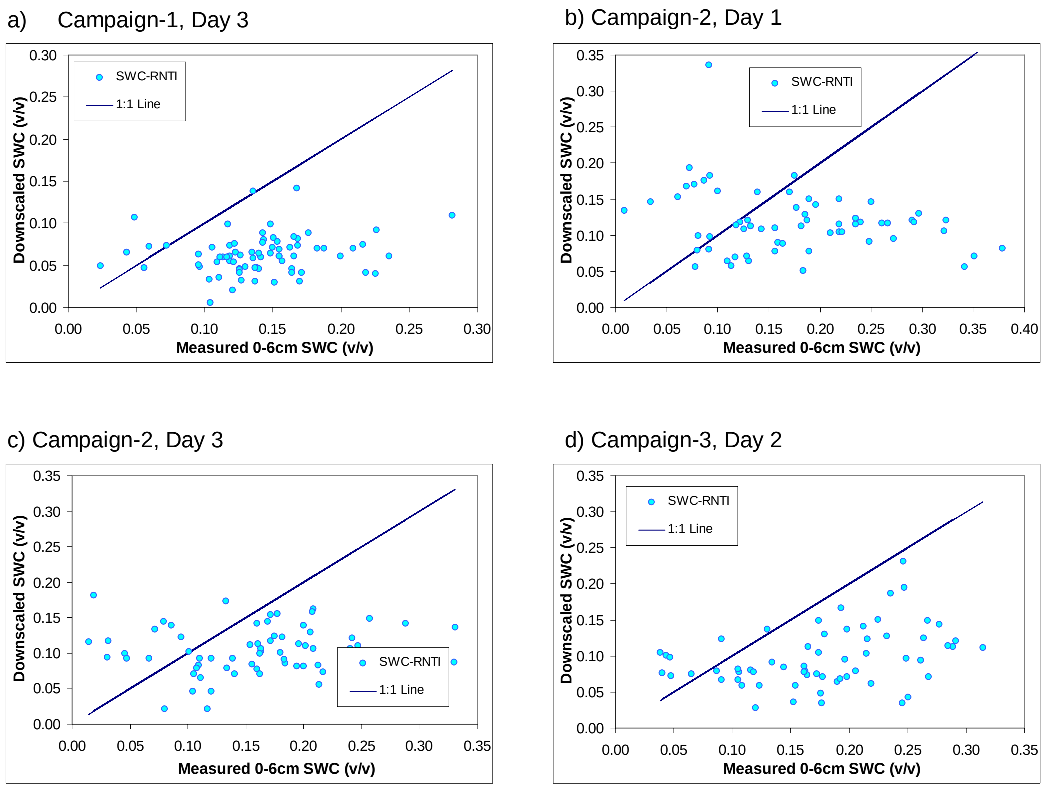

Figure 8.5: Comparison between measured point-scale 0-6 cm soil moisture content and the 1.1 km resolution estimates of soil moisture content based on RNTI for: a) Campaign 1 Day 3; b) Campaign 2 Day 1; c) Campaign 2 Day 3; and d) Campaign 3 Day 2.

These poor relationships between actual measurements and estimated SWC values are due to at least three main reasons. First, the vast difference between the scales of the data used in this study does not permit an ideal comparison. The original field measurements were made at the point scale, and hence it is obvious that one can never expect a perfect match between the point-scale measurements and the 1.1 km^2 scale predictions. Second, the presence of clouds in the image may lead to serious errors in the computation of indicators. Thus, it is not possible to have a strong relationship between the indicator and the actual soil water contents. For this reason, it is unlikely that strong relationships may be found between measured and estimated SWC values such as found during Campaign 2 Day 1 (see part (b) in Figures 8.2 to 8.5). Thirdly, the poor relationships between measured and predicted soil moisture may also be due to the use of land surface temperature (LST) in the disaggregation scheme. The diurnal course in solar radiation causes significant diurnal variations in land surface temperature. Thus, the use of instantaneous LST data may introduce errors in the comparison, especially if the soil moisture observation time differs significantly from the AMSR-E overpass time.

For practical reasons, it is difficult to overcome the problem of the significant difference between the scales of field measurements and predicted SWC values. To overcome the errors due to diurnal variation in LST, it is appropriate to consider a sub-set of the field measurements for comparison. Field measurements collected between 2 hours before and 1 hour after the Aqua-MODIS (and AMSR-E) overpass time have therefore been selected for further analysis. It was assumed that variation in LST during this period has least influence on the soil moisture observations made within the period whilst still providing sufficient data for the comparison. A summary of temperature observations during full campaign days and during the selected 3 hr periods is given in Table 8-6. It is clear from Table 8-6 that the shorter sampling period reduces the range of LST values.

Table 8-6: Average and range of soil temperature (^{o}C) values collected during the entire campaign day and during the period between 2 hours before and one hour after the MODIS and AMSR-E (on Aqua) overpass time.

Campaign and day		Measured soil temperature (^{o}C) whole day	selected 3 hr period
1-3	Avg.	29.38	33.30
	Range	17.1-43.0	21.8-42.9
2-1	Avg.	16.42	18.50
	Range	9.6-21.5	16.4-21.4
2-3	Avg.	14.37	18.56
	Range	5.5-26.3	10.9-26.3
3-2	Avg.	10.02	12.52
	Range	1.5-18.0	6.9-18.0

8.4.2 COMPARISON OF DISAGGREGATED MEASUREMENTS WITH SUB-SET OF DATA

The summary statistics based on the *in-situ* measurements collected during MODIS and AMSR-E overpass time for the four disaggregation case studies are shown in Table 8-7. In general, similar to the previous analysis (see Table 8-3) Table 8-7 indicates that both indices used in the disaggregation scheme provided reasonable estimates of moisture values. The average and the range of values of the downscaled moisture contents were closer to the 0-1 cm moisture contents than to the 0-6 cm moisture contents. The predicted soil moisture values were within ± 0.05 cm^3cm^{-3} of the measured moisture content for 0-1 cm during all case studies. Particularly, a significant improvement of measured 0-1 cm SWC value (from 0.24 to 0.18) during Campaign 2 Day 1 was observed. The obtained average and the range of SWC values during MODIS overpass time in Campaign 2 Day 1 were found to be closer to the measured average and the range of SWC value than when considering whole data set. It was also found that consideration of measurements collected during the overpass time resulted in a good match between measured (0.11 $cm^3.cm^{-3}$) and predicted SWC values (0.11 $cm^3.cm^{-3}$) as in Campaign 3 Day 2.

Consideration of SWC values during MODIS and AMSR-E overpass time is useful to explain the effect of sampling time on disaggregation. The effect on drying of the near-surface 0-1 cm soil layer can be explained by comparing the measured and predicted soil water contents, particularly during Campaign 2. The difference between the 0-1 cm measured SWC values on Day 1 and Day 3 during Campaign 2 was 0.03 $cm^3.cm^{-3}$. For the same period, the predicted SWC values based on the RNTI and VTCI methods showed a water content difference of 0.02 and 0.04 $cm^3.cm^{-3}$, respectively. It therefore appears that the downscaling methods adopted in the present study are capable of providing consistent results and hence the disaggregated results may be used for temporal analysis.

Table 8-7: Summary statistics of the measured soil moisture contents collected between 2 hrs before and one hour after the MODIS overpass time and the downscaled soil moisture contents.

Campaign and day		Measured soil moisture ($cm^3.cm^{-3}$)		Downscaled soil moisture ($cm^3.cm^{-3}$)	
		0-6 cm	0-1 cm	RNTI-based	VTCI-based
1-3	Avg.	0.14	0.07	0.07	0.08
	Range	0.05-0.28	0.03-0.12	0.04-0.14	0.06-0.12
	N	23	17	23	23
2-1	Avg.	0.15	0.18	0.13	0.14
	Range	0.01-0.35	0.07-0.31	0.07-0.19	0.09-0.17
	N	18	18	18	18
2-3	Avg.	0.16	0.15	0.11	0.10
	Range	0.01-0.32	0.05-0.26	0.02-0.16	0.01-0.16
	N	26	26	26	26
3-2	Avg.	0.16	0.11	0.10	0.11
	Range	0.04-0.29	0.01-0.24	0.03-0.15	0.05-0.15
	N	23	24	24	24

Allowing three levels of absolute deviations of ≤0.01, ≤0.03 and ≤0.05 $cm^3.cm^{-3}$ to assess the disaggregated results, Tables 8-8 and 8-9 summarize the results for the RNTI and VTCI methods respectively. As seen in Table 8-8, for example, during the Campaign 1 Day 3, approximately 65% (i.e. 11 (*n*) out of 23 (*N*) cases) of all RNTI based estimates are within ±0.05 $cm^3.cm^{-3}$ from the actual 0-1 cm measurements. In fact, this is a reduction (from 71%, see Table 8-4) when compared with the whole data set collected during the day. Apart from this 65% value observed for RNTI method during the Campaign 1 Day 3, all other three case studies with RNTI showed a significant improvement in the predicted SWC values. Similarly, as seen in Table 8-9, the VTCI based SWC estimates for the Campaign 1 Day-3 also shows that approximately 82% of estimates (i.e. 14 out of 23 cases) are within ±0.05 $cm^3.cm^{-3}$ from the actual 0-1 cm measurements. A similar improvement in VTCI approach is apparent in all four case studies. It is interesting to note that the RNTI based technique appears to be as successful as the VTCI based technique for downscaling SWC values.

Thus, use of field data collected closer to the MODIS overpass time strengthens the validity of the downscaling approaches used in the study.

Table 8-8: Comparison of absolute deviations of predicted SWC values based on RNTI approach and the measured SWC at 0-6 cm and 0-1 cm collected between 2 hrs before and one hour after the MODIS overpass time. (*n* = number of data pairs within the error level)

Day	Deviations from 0-6 cm SWC (in $cm^3.cm^{-3}$)			Deviations from 0-1 cm SWC (in $cm^3.cm^{-3}$)		
	≤0.01	≤0.03	≤0.05	≤0.01	≤0.03	≤0.05
Campaign-1 Day 3	13% *(n=3)*	13% *(n=3)*	30% *(n=7)*	6% *(n=1)*	41% *(n=7)*	65% *(n=11)*
Campaign-2 Day 1	6% *(n=1)*	17% *(n=3)*	17% *(n=3)*	0% *(n=0)*	17% *(n=3)*	22% *(n=4)*
Campaign-2 Day 3	0% *(n=0)*	15% *(n=4)*	35% *(n=9)*	12% *(n=3)*	31% *(n=8)*	50% *(n=13)*
Campaign-3 Day 2	4% *(n=1)*	13% *(n=3)*	35% *(n=8)*	8% *(n=2)*	33% *(n=8)*	58% *(n=14)*

Table 8-9: Comparison of absolute deviations of predicted SWC values based on VTCI approach and the measured SWC at 0-6 cm and 0-1 cm collected between 2 hrs before and one hour after the MODIS overpass time. (*n* = number of data pairs within the error level)

Day	Deviations from 0-6 cm SWC (in $cm^3.cm^{-3}$)			Deviations from 0-1 cm SWC (in $cm^3.cm^{-3}$)		
	≤0.01	≤0.03	≤0.05	≤0.01	≤0.03	≤0.05
Campaign-1 Day 3	9% *(n=2)*	17% *(n=4)*	43% *(n=10)*	12% *(n=2)*	53% *(n=9)*	82% *(n=14)*
Campaign-2 Day 1	6% *(n=1)*	11% *(n=2)*	22% *(n=4)*	6% *(n=1)*	11% *(n=2)*	22% *(n=4)*
Campaign-2 Day 3	0% *(n=0)*	12% *(n=3)*	38% *(n=10)*	12% *(n=3)*	38% *(n=10)*	46% *(n=12)*
Campaign-3 Day 2	4% *(n=1)*	17% *(n=4)*	30% *(n=7)*	17% *(n=4)*	33% *(n=8)*	54% *(n=13)*

The disaggregated AMSR-E near-surface soil moisture and measured 0-1 cm near-surface soil moisture values (collected closer to the MODIS overpass time) were also compared as was done for Figures 8.2 and 8.3. No significant improvement of the agreement between the computed values and the *in-situ* measurements of soil moisture was observed. Similarly, disaggregated AMSR-E near-surface soil moisture estimates and measured 0-6 cm near-surface soil moisture values during AMSR-E overpass time were also compared. Similar to the Figures 8.4-8.5, the disaggregated moisture values compare poorly with the soil moisture content in top 0-6 cm layer. These poor results appear to be mainly due to the great difference between the scales of the data used (i.e. field-measured point-scale SWC values against predicted 1.1 km^2 SWC values). At this point, it will be more appropriate to evaluate the predicted soil moisture patterns rather than considering SWC predictions at a relatively small number of locations.

8.4.3 PREDICTED MOISTURE PATTERNS

It is important to study the moisture patterns derived from the disaggregation schemes. Theoretically, soil moisture distribution in a catchment should relate to the antecedent rainfall patterns and variations in soil properties, vegetation, topography, and subcatchment boundaries. Thus, a moisture pattern in a catchment does not occur due to a random phenomenon but follows some level of organisation. As reported in Chapter 2 many studies have confirmed the spatial organization of soil moisture patterns.

Figures 8.6 - 8.9 show the predicted spatial variability in soil moisture on the four days selected. It is can be seen that there is a definite pattern in spatial variability of soil moisture that is related to the catchment properties such as vegetation pattern and rainfall (see Figure 8.10) and topography (see Figure 8.11). This variability could be the result of antecedent rainfall patterns and variations in soil properties, topography and subcatchment boundaries.

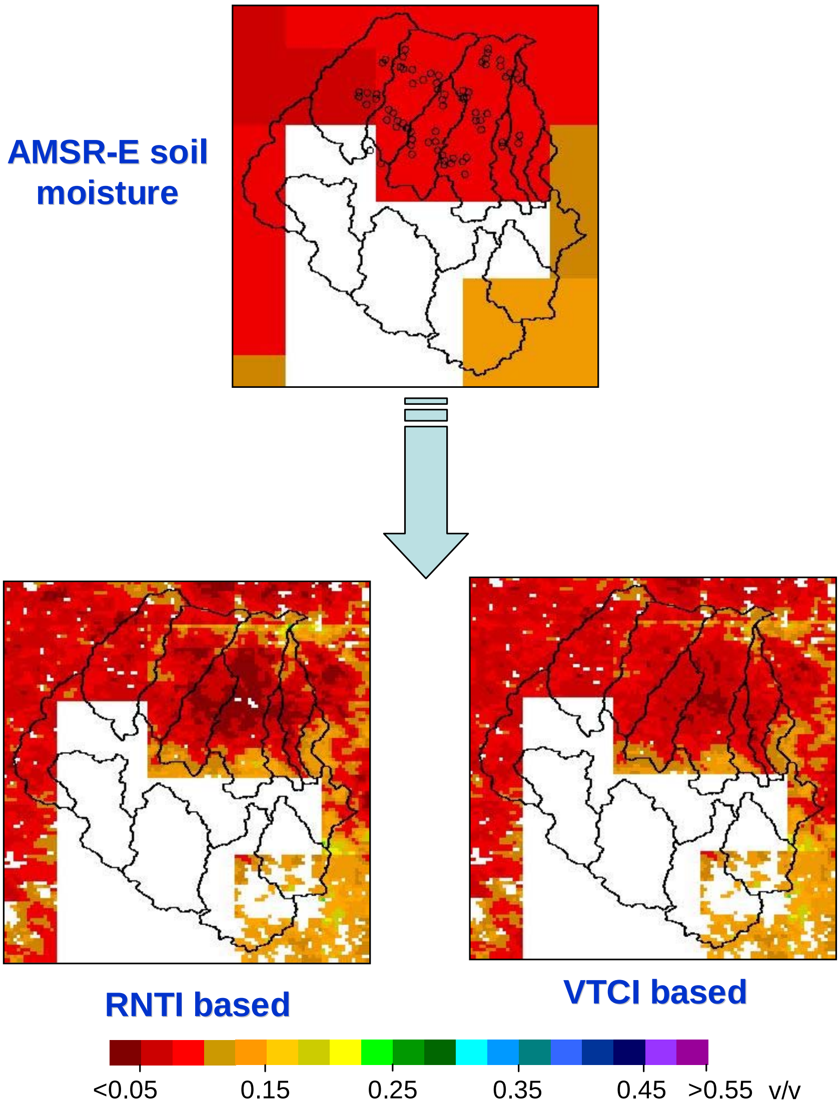

Figure 8.6: Disaggregated AMSR-E soil moisture measurements on day 313 in 2003 (i.e. day 3 in Campaign-1) based on RNTI and VTCI approaches. (Note – white patches are due to clouds and no soil moisture is computed)

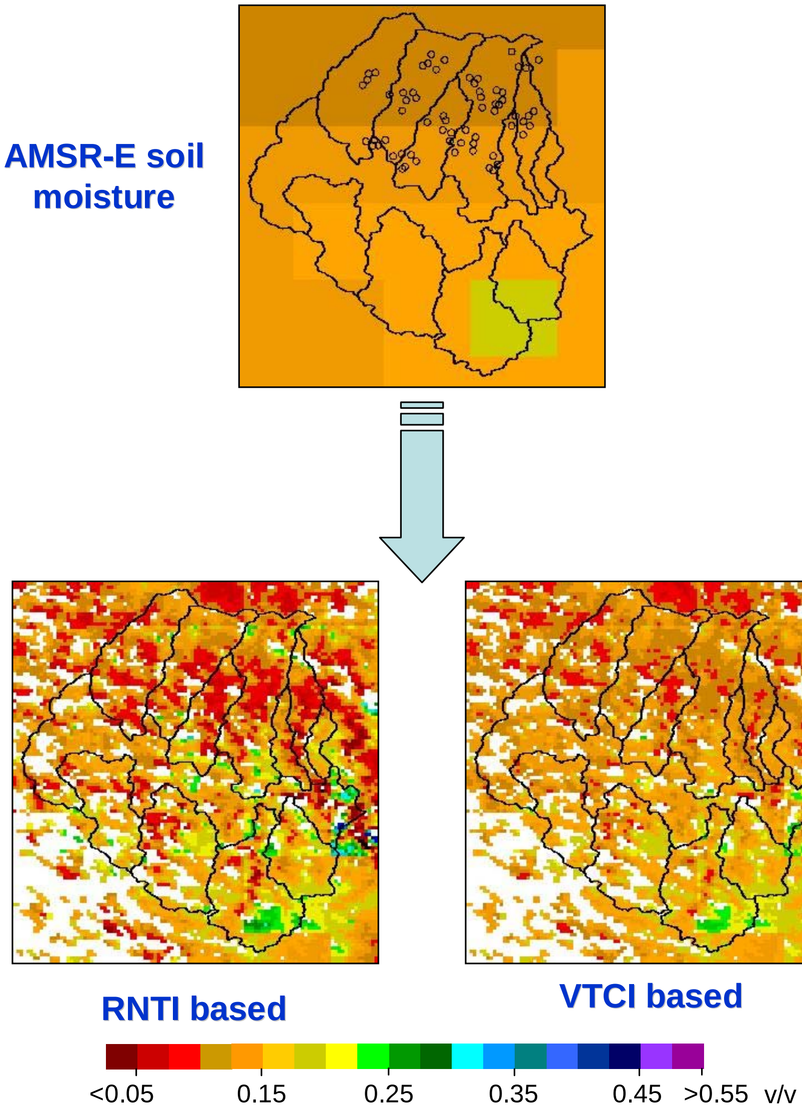

Figure 8.7: Disaggregated AMSR-E soil moisture measurements on day 122 in 2004 (i.e. day 1 in Campaign-2) based on RNTI and VTCI approaches. (Note – white patches are due to clouds and no soil moisture is computed).

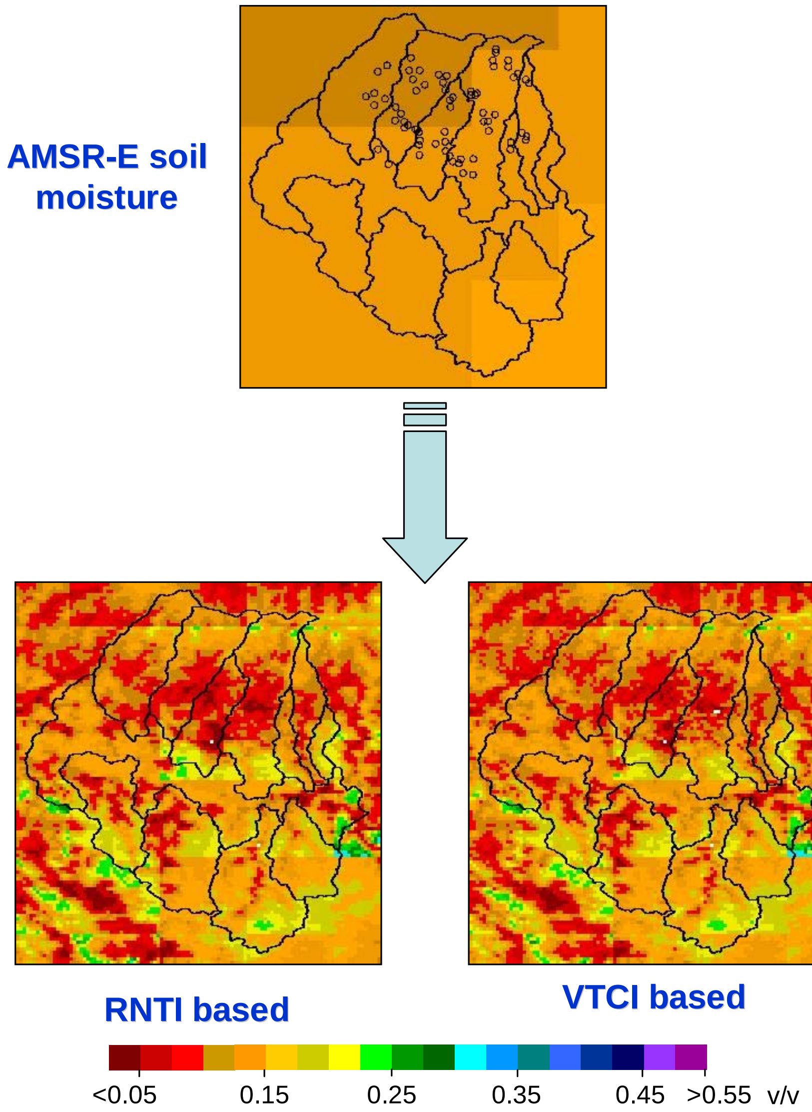

Figure 8.8: Disaggregated AMSR-E soil moisture measurements on day 124 in 2004 (i.e. day 3 in Campaign-2) based on RNTI and VTCI approaches.

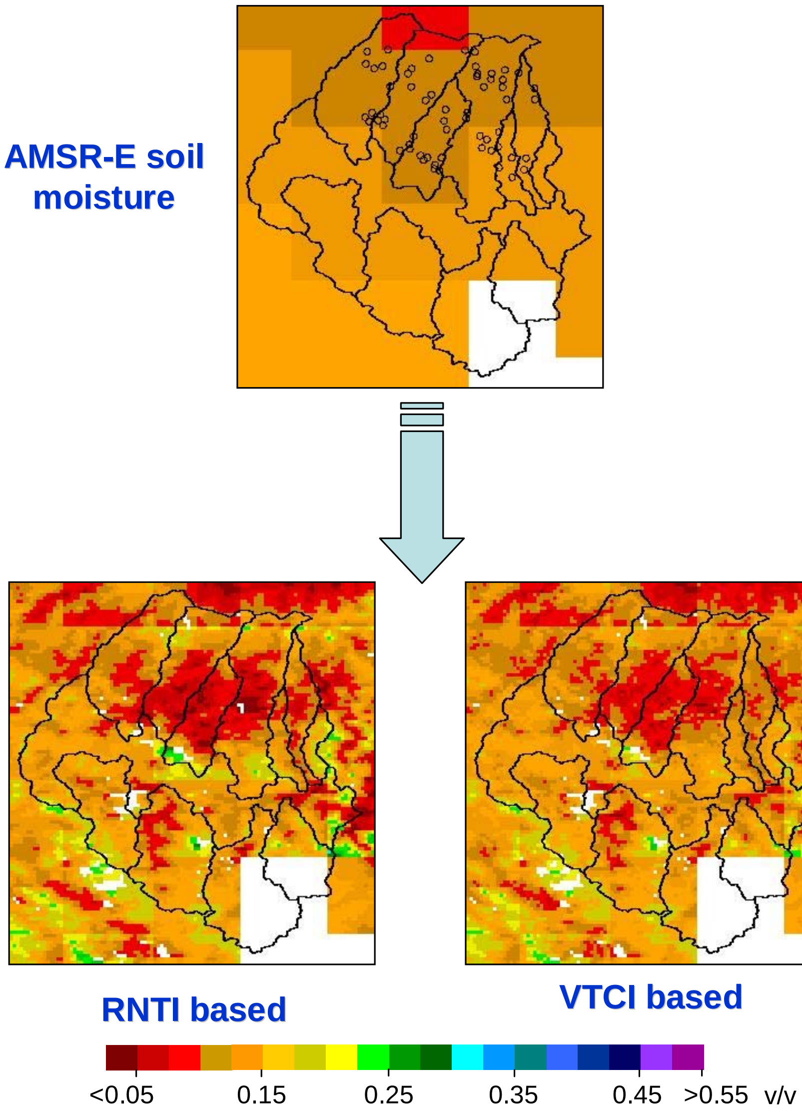

Figure 8.9: Disaggregated AMSR-E soil moisture measurements on day 190 in 2004 (i.e. day 2 in Campaign-3) based on RNTI and VTCI approaches. (Note – white patches are due to clouds and no soil moisture is computed).

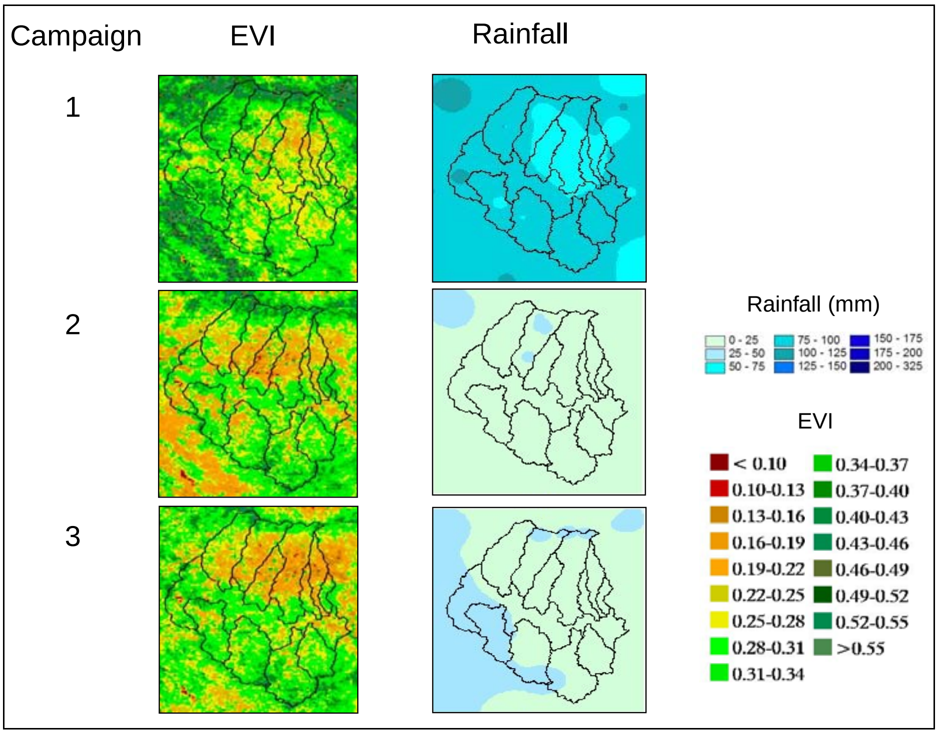

Figure 8.10: Enhanced Vegetation Index (EVI) and rainfall pattern in the previous month for the three field campaigns.

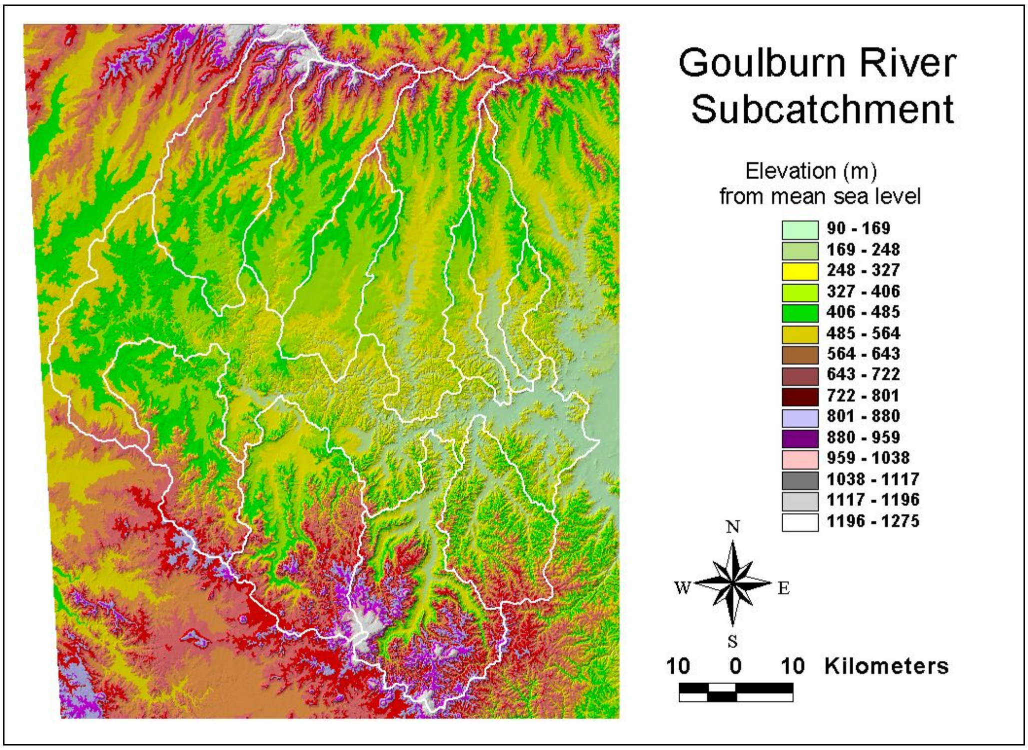

Figure 8.11: Topography of the Goulburn River subcatchment.

For the convenience of interpretation and evaluation of the predicted soil moisture patterns, the present study considers three main criteria. First, the study considers the relation between the vegetation health and soil moisture. It is well-known fact that healthy vegetation is associated with higher moisture values. Thus, use of a vegetation index such as Enhanced Vegetation Index (EVI) provides a means to assess the predicted soil moisture patterns. Second, antecedent rainfall across a catchment during the previous 3-5 days provides valuable information on potential SWC pattern in the catchment. Third, catchment topography may also be useful in obtaining some information on possible moisture patterns across a catchment. For example, valley bottoms are likely to be associated with higher moisture contents due to surface runoff which will be stronger following more rainfall in the previous 30 days as in the case of Campaign 1.

During Campaign 1, in general, vegetation across the catchment was more or less healthy (i.e. EVI exceed 0.25). The disaggregated moisture patterns across the catchment were near-uniform despite a generally lower moisture content. The vegetation indices during Campaign 2 showed less vegetation in the south-western and in north-central parts of the catchment. This pattern is clearly evident in the Figure 8.8 and lower SWC values are associated with these areas. Similarly, during Campaign-3, the north-central part of the catchment had less vegetation than the other areas. The disaggregated SWC maps during Campaign-3 (see Figure 8.9) showed more drier areas in the north-central part of the catchment. It can be therefore concluded that the disaggregated soil moisture patterns are linked to the natural vegetation pattern of the catchment.

As seen in Figure 8.10, three different rainfall patterns are available for interpretation of disaggregated SWC patterns. The highest rainfall was observed before Campaign 1. It can be seen from Figure 8.10 that this significant rainfall was experienced across the entire catchment. The disaggregated SWC during Campaign 1 (see Figure 8.6) did show a uniform distribution of soil moisture across the catchment. Rainfall before the Campaign 2 was very low but distributed evenly across the catchment. The disaggregated SWC map on Day 1 showed a near-uniform soil moisture pattern. The predicted SWC patterns for Day 3 however showed a patchy distribution pattern with some drier areas. As seen in Figure 8.10, the western part of the catchment received slightly higher rainfall than the other areas before the Campaign 3. The disaggregated SWC patterns during Campaign 3 showed some scattered wet areas in the western part of the catchment. This effect may be due to variations in the rainfall pattern. Hence, it may be concluded the disaggregated SWC patterns show broad agreement with antecedent rainfall patterns.

The main river of the catchment, i.e. the Goulburn River runs from west to east direction in the central part of the catchment. Naturally, the lowest elevations are found along the river course (see Figure 8.11) and it is obvious that these areas may show wetter conditions than the other parts of the catchment. The disaggregated SWC maps of Figures 8.7 to 8.9 indicate some wet patches (approximately moisture content of 0.25 $cm^3.cm^{-3}$) closer to the mouth area of the Goulburn River despite the lower moisture contents of the AMSR-E measurements (0.14-0.17 $cm^3.cm^{-3}$). It therefore appears that the disaggregated soil moisture patterns are linked to such dominant topographic features of the catchment.

Moreover, these disaggregated maps can show some significant patterns in the variations of moisture contents of AMSR-E. For instance, one can consider the soil moisture patterns within the catchment in Figures 8.7 to 8.9. It was note that the AMSR-E pixels within the catchment have different moisture contents. In the disaggregated map, a smooth transition from dry to wet condition is apparent. This confirms that the disaggregation procedures are capable of producing realistic seamless soil moisture distribution maps.

It is also noted that the disaggregated maps derived with the RNTI approach reveal more dry areas than the maps derived with VTCI. This is likely to be due to the fact that the RNTI approach only considers thermal behaviour at the land surface whereas the VTCI considers the entire root zone depth. The RNTI values computed in the present study used data collected from Aqua MODIS which senses the catchment between about 1.30-2.30 pm. Land surface temperatures can reach considerably higher values during this time due to surface drying. Thus, the high temperature areas can be interpreted as dry areas during the disaggregation process. This can also happen with the VTCI, but to a lesser extent, as it considers VI which reflects the entire root zone and the LST.

A border of approximately half the width of the AMSR-E pixel can be seen in disaggregated pattern and particularly in the top part of Figures 8-8 and 8-9. This is due to the use of partial AMSR-E pixels in the computation process. The spatial coverage of the MODIS data set used in the present study does not coincide with the AMSR-E pixels used in their entirety (see Table 8-2). For example, the MODIS data used in the study cover only part of the left column (number 1267) and part of the right column (number 1271) of the selected AMSR-E area. Similarly, the top (number 448) and the bottom row (number 453) of the AMSR-E data are not entirely covered by the MODIS data set. In order to derive a high-resolution soil moisture map for the entire catchment, these partially covered AMSR-E pixels were included. As a result, the disaggregated moisture patterns of the partial AMSR-E pixels did not always match perfectly with the disaggregated patterns of neighbouring AMSR-E pixels. These partial AMSR-E pixels are located completely outside the area considered for the present study. The estimated moisture patterns derived from these partial AMSR-E pixels have not been used for the comparisons.

The use of cloud contaminated images for the disaggregation can also introduce some errors in the predicted soil moisture patterns. For example, as seen in Figure 8.7 (and to a lesser extent in Figure 8.9) the presence of clouds prevents the prediction of soil moisture across the catchment and leaves some gaps. Thus, cloud-free images should preferably be used in any disaggregation method that employs the LST.

8.5 DISCUSSION

The disaggregation methods for high-resolution soil moisture determination described in this chapter involve the combined use of AMSR-E soil moisture and LST and VI from MODIS. This research has evaluated how the RNTI and VTCI indices may be used to disaggregate AMSR-E soil moisture data. The RNTI and VTCI indices adopt different approaches to describe soil wetness characteristics. While the RNTI based approach incorporates thermal inertia properties to determine soil moisture (see Section 6.4.3), the VTCI based approach incorporates the vegetation information in addition to the thermal inertia property as discussed in Section 2.3.5.2.3.

One of the objectives of the present study was to develop a disaggregation procedure which is simple, repeatable and does not require much time. As noted in Chapter 6, computation of the RNTI and VTCI indices is relatively straight-forward. The high-resolution LST and VI data from the MODIS sensor are reliable and available for the entire globe and can be downloaded free of charge. This provides an opportunity to apply high-resolution wetness indices for soil moisture disaggregation schemes. Additionally, the use of both MODIS and AMSR-E sensors from the Aqua satellite will reduce errors in the approach because both sensors observe the land surface simultaneously.

The techniques described here have their basis in surface energy balance considerations. As discussed in Chapter 2 and 6, the scatter diagrams between VI and LST such as used in the VTCI method are useful in describing soil wetness characteristics. The RNTI approach built upon the relationship between soil moisture and thermal inertia properties. The consideration of both VI and LST in the VTCI approach however is advantageous for soil moisture determination. Thus, it can be assumed that disaggregation schemes based on wetness indices have considerable potential and may provide a simple approach for the redistribution of soil moisture.

Catchment-scale high-resolution soil moisture maps created from AMSR-E measurements using the RNTI and VTCI methods reflect the soil moisture distribution across a catchment in a meaningful way. For instance, predicted soil moisture patterns appear to have some relationship with physical characteristics such as the vegetation pattern, rainfall distribution, catchment topography and location of major water courses. Additionally, they are also capable of mapping the transition of moisture contents between the adjoining AMSR-E pixels whose moisture values are significantly different. Thus, they provide a method to produce seamless soil moisture distribution maps.

Both disaggregation techniques studied in this thesis are capable of providing soil moisture predictions which can easily related with past rainfall distribution, vegetation pattern or topography.

The comparison between 1.1 km^2 scale near-surface soil moisture predictions (a type of instantaneous moisture estimates) with point-scale measurements collected over a long period always is hampered by concerns over the applicability of such a validation approach. The difficulty arises both in the estimation process as well as the measurements of *in-situ* soil moisture content. As discussed in Chapter 2, several issues are involved in soil moisture measurements. For example, microwave sensors measure soil moisture in the topmost soil layer where penetration depth varies from 1/10 to 1/4 of a wavelength. At 9.6 GHz of AMSR-E, this layer is up to 1 cm deep. As noted in Chapter 7, the penetration of microwave signals depends on soil moisture itself. It is this moisture content that is considered for the present disaggregation study. In view of this, it is difficult to determine firstly, the correct depth of soil samples and secondly, an accurate method which is efficient enough for collecting a large number of *in-situ* measurements to estimate the soil moisture. Soil moisture also changes very rapidly in the topmost soil layer as does the land surface temperature. In addition, there are practical problems in collecting accurate soil samples for the top 0-1 cm of soil. Many soil moisture studies, including the present study, use soil moisture measurements collected over 0-6 cm depth with convenient measuring tools such as the Theta probe or the Hydra probe. Furthermore, the spatial distribution of soil moisture depends on soil parameters that are not distributed homogeneously throughout the catchment. As a result, the average soil moisture computed from point measurements within a footprint does not necessarily give an accurate representation of the soil moisture across the footprint. In view of these uncertainties, no definite conclusion can be drawn from the comparison between *in-situ* point measurements and disaggregated soil moisture predictions from AMSR-E data. However, other approaches such as logical reasoning and interpretation of predicted patterns using catchment physical properties were found to be useful in the validation process.

It is also important to note that the distribution of soil moisture in a sub-humid environment is based on many variables with complex spatial interrelationships. The land surface temperature and vegetation information used in the present study however are the only freely available proxy variables for soil moisture disaggregation studies.

The proposed disaggregation schemes have some limitations. Catchment scale information like soil moisture is affected by biophysical and climatic factors as well as by technological constraints. For example, the signals from AMSR-E and MODIS may not be related to soil characteristics over the same vertical depth. As a result, their soil moisture estimates can differ. As described previously, AMSR-E measures soil moisture in the top 0-1 cm soil layer. On the other hand, wetness indices such as VTCI are based on vegetation indices and will reflect the soil wetness over the entire depth of the root-zone. It is therefore possible that the estimates of soil moisture using the above two methods are different. But in the approach outlined here, the VTCI concept is used to establish relations between soil moisture, temperature, and VI (in Chapter 6) and that information is used as a covariate to disaggregate soil moisture observations. This should have a minimal effect on the results of the disaggregation process employed here.

Cloud effects in the MODIS image pose another serious problem because they prevent the accurate estimation of LST. Accurate LST measurements are important for both indices used in the disaggregation methods. Incomplete coverage of LST across the catchment prevents accurate estimation of the boundary conditions for the indices. This is particularly true for the VTCI as the index values are entirely dependent on the accurate determination of the wet-edge and the dry-edge of the triangle used for the computation process. The RNTI on the other hand, is less affected by such boundary conditions but the use of the smaller number of high-resolution LST pixels in the disaggregation algorithm potentially leads to inaccurate predictions. This is also true for the VTCI approach. These inaccuracies may therefore lead to some uncertainty in the final result.

Both RNTI and VTCI based techniques appear to be useful for space-borne soil moisture estimation from satellite data. Further testing and validation of the proposed downscaling models should be conducted for a range of climatic and land surface conditions, if possible with use of high resolution soil moisture estimated from air-borne microwave radiometers and optical/IR data.

8.6 CHAPTER SUMMARY

This chapter has described two procedures that spatially distribute AMSR-E near-surface soil moisture measurements using information derived from other higher resolution images. The methodology discussed in this study uses thermal and visible imagery from MODIS to disaggregate AMSR-E soil moisture measurements. The methods are simple because they use surface wetness indices such as RNTI and VTCI derived from other radiometers. The use of these tools is demonstrated using field experiment data and AMSR-E 25 km scale soil moisture measurements which were downscaled into 1.1 km scale soil moisture products. The result demonstrates that the downscaling procedure can reveal the fine scale spatial distribution of soil moisture within a coarse resolution soil moisture observation although the actual validation of the method is difficult.

This study has demonstrated the ability of using remote sensing and GIS knowledge to redistribute AMSR-E soil moisture measurements using LST and vegetation indices derived from other sensors. The extraction and use of the wetness information from the LST-VI space for disaggregating large-area soil moisture values may be justifiable by considering that the LST-VI space encompasses the regional range of soil moisture conditions. In addition, the methodology presented in this chapter provides insight into the operational production of soil moisture fields from AMSR-E soil moisture products at spatial resolutions useful for a range of applications with freely available MODIS imagery.

CHAPTER NINE

9. DISCUSSION, CONCLUSIONS AND FUTURE DIRECTIONS

The primary objectives of this thesis were to develop methodologies to derive average soil moisture contents and distributions over large catchments from point scale observations and to disaggregate large-area soil moisture measurements from satellite microwave observations. The scaling approaches were to retain strong physical basis by using other dominant catchment-specific parameters, applicable at a range of scale, and do not require complex calibrations based on other ground-based soil moisture measurements. All scaling approaches presented in this thesis have been developed, applied, and validated in a field study conducted in the Goulburn River Catchment (6540 km^2) in New South Wales, Australia. This study used soil moisture measurements derived from point scale 0-30 cm and 0-90 cm observations as well as AMSR-E measurements of the top 0-1 cm soil layer.

Reliable estimates of soil moisture content in the top meter of the land surface at various spatial and temporal scales are important for a wide range of environmental studies. Accurate measurement of soil moisture is a difficult and time consuming process. The available techniques for assessing soil moisture content provide only two types of measurements. First, the *in-situ* techniques which can be used to measure soil moisture in a given location on a given time. Due to a small volume of soil used for the measurements, these techniques yield point scale moisture measurements but can also be used to measure the moisture throughout a soil profile using a number of sensors. Second, remote sensing techniques such as those based on the passive microwave approach can be used for soil moisture measurement across large scales. Microwave-based soil moisture measurements give soil moisture estimates over a large-area (e.g. 25 km x 25 km in the case of AMSR-E) but these measurements represent only the top 0-1 cm soil layer. For many environmental studies, such soil moisture data either at the point scale or for very large areas are not adequate.

A major problem that exists for hydrological modelling applications is the aggregation and disaggregation of soil moisture measurements across a range of spatial and/or temporal scales. Such a challenge occurs, for example, when field-scale behaviour must be determined from measured data collected from a limited number of point-scale measurements. The same difficulty arises when plot-scale soil moisture distributions have to be determined from large-scale AMSR-E measurements. The problems associated with soil moisture scaling can not be resolved by simple consideration of the differences in space or time scale, for several reasons. For example, many moisture dependent processes in hydrology are highly nonlinear. Consequently, the averaging of processes determined from a limited number of discrete point-scale samples may not reflect the accurate behaviour of the larger area. Similarly, obtaining a true estimate of field scale moisture content from a very large-area measurement remains as an illusive challenge. Hence, there is a need for developing upscaling and downscaling procedures that will allow us to move from one domain of interest to another while retaining the true properties of the medium at each scale.

Knowledge of the variation in spatial distribution of soil moisture rather than just average soil moisture content over a catchment may lead to understanding significant differences in the hydrological responses of the catchment. Soil moisture distributions may be generated from interpolating (or aggregating) point-scale measurements or disaggregating large-area measurements. The key question that must be answered in meaningful aggregation/disaggregation is how the problem of soil heterogeneity at different spatial (and temporal) scales affects the predictions and measurements. Two approaches have been considered in this thesis: (a) based on terrain characteristics and (b) using information collected from high resolution satellite-based sensors. These approaches however, may be expected to have some regional dependency as all the methods use site-specific characteristics as covariates for changing from one scale to another.

The conclusions of this thesis are based on studies covering six themes, namely: (i) evaluation of measured soil moisture values with single layer bucket models; (ii) identification of catchment average soil moisture measurement sites; (iii) predicting soil moisture distributions based on point-scale measurements and terrain characteristics; (iv) predicting soil moisture distributions based on point-scale measurements and remotely-sensed land surface characteristics; (v) field validation of AMSR-E soil moisture estimates; and (vi) disaggregation of large-area soil moisture measurements.

9.1 APPLICATION OF SINGLE LAYER BUCKET MODELS FOR SOIL MOISTURE PREDICTIONS

Soil moisture contents can be evaluated with simple hydrological models such as the single layer bucket model. These single layer bucket models are also useful for identifying systematic measurement errors due to poor calibration parameters of the sensors as well as any random errors. Simple bucket type models can be used to predict soil moisture values for virtually any soil depth considered for the bucket. In Chapter 4 this modelling technique has been employed for the evaluation of field measured soil moisture values over 0-30cm and over 0-90cm depths.

As discussed in Chapter 4, the application of single layer bucket models for balancing the inputs and outputs of water in the hillslope catchment confirmed that the soil moisture data collected during the study period are realistic. The predicted soil moisture values were found to be comparable with the measured soil moisture contents. Hence, soil moisture data collected during the study period could be used for other applications with some confidence.

The accuracy of the soil moisture data predicted with the bucket type water balance model depends on the quality of the input data. In this thesis, rainfall measurements were collected within the catchment using an automatic raingauge. All meteorological data required for the computation of actual evapotranspiration (ET_a) from the Penman-Monteith method were measured at the climate station located within the study catchment. The bucket size was determined from the actual soil moisture observations. Thus, the availability of such data provided an ideal basis for the model application whilst ignoring lateral water movement.

Moreover, the work described in Chapter 4 demonstrated that the soil moisture measurements collected at irregular intervals may assist in generating soil moisture trajectories over extended periods. With measurements of rainfall and estimates of actual evapotranspiration (ET_a) and soil water storage capacity, one can use a water accounting system based on the simple bucket type water balance model to generate soil moisture trends over longer time periods. This would provide a methodology for the scaling of soil moisture in the temporal domain. For instance, if intermittent soil moisture measurements are available for a catchment, it is possible to derive soil moisture evolution patterns for the monitoring locations by using simple bucket models with appropriate model parameters. However, the ET_a value remains a significant unknown.

The results also confirmed that the single layer (one-dimensional) bucket model has limited usefulness for hillslope-scale hydrological studies because it ignores seepage and percolated water as well as surface and sub-surface runoff/runon between adjacent buckets. It provides an estimate of soil moisture content over time by considering only rainfall inputs, evapotranspiration outputs and parameters such as soil water holding capacity. However, the model ignores the position in the landscape and any gain or loss of soil water from adjoining areas.

The results also showed that the use of a single moisture measurement at the beginning of a modelling period was not sufficient for accurate predictions of subsequent moisture contents over longer periods. Since water inputs from neighbouring buckets were not taken into account, moisture predictions were underestimated when run-on exceeded run-off. It has been demonstrated that the assimilation of measured root-zone moisture contents alone can alleviate this over/under estimation problem.

Simple bucket models may be of use if the soil moisture predictions are regularly updated with measured values. Chapter 4 shows a comparison of prediction errors using direct insertion of measurements into the model at one-week and two-week intervals. It can be concluded from this comparison that the collection of soil moisture data even at irregular intervals may be useful for assimilation into bucket type models to minimize prediction errors.

It was also noted that ignoring rainfall distributions within the catchment can introduce serious errors in the predicted moisture values. As discussed in Chapter 4, anomalies of rainfall distribution can occur even in small hillslope catchments such as the Stanley catchment (170 ha) used in the present study. Accurate rainfall measurements therefore are important in water balance modelling because they provide the main water inputs to the model.

It can be concluded that bucket type models provide simple approaches for soil moisture estimation at a range of scales provided suitable input data (rainfall, evaporation) can be obtained. Repeating the modelling for a larger number of sites across different regions would provide the basis for better understand the scaling behaviour of soil moisture in temporal domain.

9.2 IDENTIFICATION OF CATCHMENT AVERAGE SOIL MOISTURE MEASUREMENT (CASMM) SITES

In extensive areas, such as those studied in this thesis, it is of great interest to be able to identify which locations are representative of the mean soil moisture conditions as well as which locations are regularly drier or wetter sites. This study has demonstrated the appropriateness and usefulness of the temporal stability characteristics of the measurements which is based on the work of Vachaud *et al*. (1985).

When a catchment is regularly monitored for soil moisture content, locations can often be identified where the soil moisture is close to the average across the entire area as well as the soil is consistently wetter or drier than the catchment average. This phenomenon has been called the *time stability*, the *temporal stability*, or the *temporal persistence* in spatial patterns of soil water contents. The primary method for determining the temporal stability of a soil moisture field is the mean relative difference plot. This plot represents the ability of a particular soil moisture monitoring location to estimate the average over the catchment.

As pointed out by Starr (2005), temporal stability obviates frequent sampling of spatial variability. It also provides methods of finding the catchment average soil moisture monitoring (CASMM) sites and the range of moisture content in a given catchment. A CASMM site is the one which is closest to having a zero relative difference value and which has a low standard deviation value. Additionally, such a CASMM site preserves its position in wetness ranking. Note that it is difficult to set general reference values, of both relative difference and standard deviation to choose the representative station in a given network of stations.

The results of Chapter 5 show that it is possible to identify stations that are representative of the mean soil moisture content in a given catchment, regardless of scale, from a pre-established network of measuring stations. Three different scales (1.67 km^2, about 1000-1500 km^2 and about 6540 km^2) were considered and stations could be identified that yield mean moisture content at each scale. It was demonstrated that in order to select a representative site, approximately 12-15 months of monitoring data is required. Whilst smaller catchments (< 200 ha) require only shorter time records (12 months), larger catchments (>1000 km^2) require at least 15 months period. This period is necessary in order to capture the entire range of moisture conditions that usually associated with a complete seasonal cycle. Beyond such 12-15 month periods, monitoring of soil moisture content can be carried out at a smaller number of selected sites. Such findings may prove to be important for designing a long-term soil moisture measurement network at strategic locations.

It was observed in Chapter 5 that temporal stability patterns persisted over the entire two-year study period. The stations appeared to preserve their position in the wetness ranking regardless of the period considered, even under extreme conditions of soil moisture content. As a consequence, consistently "wet sites" and consistently "dry sites" in a catchment could be identified. It was also found that a strong correlation exists between mean soil moisture contents and the variance for the whole measurement range considered. It is important to identify locations with very high and very low soil moisture content because they can provide an insight into the range of moisture content in a catchment. Additionally, such sites can also be used to estimate the catchment average moisture value. It was noted that, in general, the difference between the extreme moisture contents was close to constant irrespective of the day of year.

It was also observed that temporal stability is more pronounced during dry periods. During the transition periods, soil moisture content varies across the catchment thus increasing the uncertainty about the temporal pattern. Furthermore, soil physical properties such as sand or clay fraction of the soil were also found to give an indication of the temporal stability characteristics. Soils with higher sand fraction are associated with greater temporal stability, whereas soils with high clay content show less temporal stability.

Temporal stability characteristics of soil moisture due to the mean variability are important for scaling applications. As demonstrated in this study, it is evident that moisture measurements at CASMM sites may be used at many scales across a catchment. Measured moisture content from a CASMM site can be used to represent the average moisture content at the hillslope scale (about 167 ha) as well as the entire catchment scale (about 6540 km^2). It was also found that the identification of CASMM site from point-scale data appears to have validity based on the wetness indices (e.g. VTCI) computed from MODIS data and may therefore have practical meaning at the 1.1 km pixel-level.

Based on the results from this study, two types of sampling procedures can be proposed for future soil water content monitoring programs. First, for existing permanent monitoring programs, time-stable locations must be identified that are representative of the soil moisture status of the catchment. This is useful in order to reduce the number of sampling sites to be maintained and for optimum allocation of limited resources. Second, in the case of non-permanent monitoring programs the sampling frequency must be considered as well as the number of sampling sites. For this purpose, a two-step approach can be adopted. The first step identifies the representative locations of the catchment. Then, in a second step, the number of sampling points can be reduced and resources allocated to increase the sampling frequency. This approach will help to collect more representative soil moisture fields at higher temporal resolution.

Temporal stability characteristics of soil moisture are also useful in validating remotely-sensed moisture measurements such as from AMSR-E (see Chapter 7). First, it may be used to identify suitable days for field campaigns. Based on the historical patterns of temporal stability, days with less soil moisture variability may be selected for field campaigns. The level of uncertainly in the estimations could probably be reduced if the temporal stability of soil moisture were considered in the field sampling design. Second, soil moisture measurements from a pixel-scale CASMM site are useful for evaluating temporal patterns of remotely sensed moisture contents. As demonstrated in Chapter 7, a CASMM site can be identified from a network of monitoring sites within the AMSR-E pixel. The measured soil moisture contents from such a site can then be used to evaluate the temporal pattern of AMSR-E soil moisture measurements.

It will be useful to study this method in a range of catchments from different geo-physical environments. Such studies would lead to better understanding of the temporal stability characteristics of soil moisture measurements under a range of climatic and geographical regions. Knowledge of temporal stability characteristics of soil moisture in different regions would assist in developing standardized guidelines for selecting sites for monitoring networks. Future studies should also include assessing the temporal stability characteristics of wetness indices so that regions with stable wetness patterns may be identified. This would also assist in the identification of possible locations for establishing monitoring sites. Adopting this approach, temporally stable sites whose moisture contents are always under- or over-estimates of the catchment average can also be identified. Inclusion of such sites in the monitoring program is important because they are useful in determining the range of moisture content within the catchment.

9.3 PREDICTING SOIL MOISTURE DISTRIBUTIONS BASED ON POINT-SCALE MEASUREMENTS AND TERRAIN CHARACTERISTICS

This thesis has investigated how topography and soil characteristics control the soil moisture distribution within a hill slope catchment. Chapter 4 has explored the upscaling of 0-30 cm point scale soil moisture measurements along a hillslope catchment based on topographic parameters.

A new wetness index called the Soil-adjusted Topographic Wetness Index (STWI) has been developed and used for up-scaling point-scale 0-30 cm (i.e. root-zone) soil moisture measurements. The traditional topographic wetness index (TWI) does only consider topography which is not sufficient to explain the variability in soil moisture. Thus, soil water storage capacity has been incorporated into the TWI to develop the STWI. The STWI of a given location varies with the capacity of the soil in that location to hold moisture and the propensity of that location to receive water from the upslope contributing areas. Thus, it describes the soil wetness characteristics in a given location in terms of the topographic position as well as soil properties in contrast to the traditional wetness index. Because soil type can significantly influence the water holding capacity of soil, it must be considered in any wetness mapping approaches.

Considering the 0-30 cm moisture measurements, Chapter 4 has demonstrated that the linear relationship between the amount of soil saturation and the STWI can provide a methodology to derive high resolution (5m grid) spatial patterns of moisture along a hillslope catchment. It was found that soil saturation ratio and STWI have a strong relationship (i.e. with higher R^2 values) during partially wet or partially dry periods and shows poorer relationships (with lower R^2 values) during prolonged wet or prolonged dry periods. This can be explained by noting that the spatial variation of soil moisture contents is generally higher during intermediate moisture contents than during extended dry or extended wet periods. For this reason, a methodology to explain the moisture variation during intermediate wet situation is more useful than during very wet or very dry periods. The relationship between the temporally variable soil saturation ratio on a given day and a location-specific intrinsic property such as STWI therefore provides a methodology to derive hillslope scale soil moisture distributions from a limited number of measurements.

It can therefore be concluded that the approach based on linking STWI and soil saturation may be used for generating high resolution soil moisture patterns in hillslope catchments if point-scale measurements and high resolution digital elevation data are available.

Further testing of the STWI approach for deriving wetness patterns should be undertaken in a range of different catchments under different wetness conditions with many soil types. Also, it will be useful to further investigate the effectiveness of soil depth information for such soil moisture scaling studies.

9.4 PREDICTING SOIL MOISTURE DISTRIBUTIONS BASED ON POINT-SCALE MEASUREMENTS AND HIGH RESOLUTION SATELLITE OBSERVATIONS

Three types of models for the generation of soil moisture patterns have been implemented in Chapter 6 based on the field measured soil moisture and MODIS data. These three types were: (i) LST and measured SWC, (ii) LST and NWDI, and (iii) combined use of LST and VI. The first set of methods was based on relationships between various forms of LST (e.g. daytime, nighttime, Δ LST, daytime LST-T_a, nighttime LST-T_a and regionally normalized temperature index (RNTI)) and field measured soil moisture measurements (SWC-based models). The second set of methods used relationships between all LST forms used in the first set and a normalized soil moisture index (NWDI-based models). The third type was based on the triangular-shape scatter diagrams as defined in the Vegetation-Temperature Condition Index (VTCI) between LST and vegetation indices, NDVI and EVI, over the catchment.

Regarding the first set of models, the regression models obtained with longer time periods were not realistic because weather changes over longer periods can mask the relationship between LST and SWC. Generally, a negative relationship existed between daytime LST and field measured moisture values.. The diurnal temperature variation gave a negative trend with SWC as well. It was also noted that the Daytime LST worked better in these models than did Nighttime LST or ΔLST. Comparing the daytime models, T_s–T_a appeared to produce better regression models than considering daytime LST only. This observation confirmed theoretical approaches taken by other researchers (Jackson *et al.,* 1981; Moran *et al.*, 1996). However, except for T_s–T_a, none of these models was convincing and they are not suitable for predicting catchments scale soil moisture patterns. It was also concluded that the use of non-normalised 0-30 cm SWC introduces serious errors in the predictions.

Land surface temperature is also influenced by other factors such as ground cover and soil type. In order to account for these effects, soil and vegetation factors were introduced into the LST-based SWC prediction models with the Regionally Normalised Temperature Index (RNTI). It was found that the RNTI holds a strong linear relationship with T_s–T_a which is independent of the season. This indicated that the RNTI also provided information on soil water status with a strong physical basis. The main advantage of the RNTI was the consistency of ranges obtained throughout the year. The correlation between soil moisture and RNTI was found to be negative. The computation of RNTI is simple and requires only satellite observations so that the RNTI is easier to compute than the T_s–T_a. RNTI based regression models can be applied to predict SWC. However, careful analysis of results revealed that predicted water contents are biased due to the residual effects of different soil types. This indicates that the water holding capacity of soil should be an important component in SWC prediction models.

Next, Chapter 6 considered the introduction of normalized soil water contents in the regression equations. For this purpose, a Normalized Water Deficit Index

(NWDI) was introduced which yielded significant improvement in the models, and particularly in those developed with daytime LST measurements. Thus, it was concluded that the NWDI more closely follows the variations of daytime LST measurements in LST-based regression models. The introduction of a soil related parameter such as saturated water content therefore improves the model predictions.

It was noted that RNTI-NWDI models can predict detailed soil moisture patterns. Reasonably good SWC predictions could be obtained when scaled variables were used for the independent variable as well as for the predicted variable in the regression equations. The use of dimensionless variables in the RNTI-NWDI model facilitates its use across a wide range of scales.

Nighttime LST measurements were considered inappropriate for soil moisture predictions. Because the soil moisture can be re-distributed during nighttime, the use of both nighttime and daytime information may potentially dampen the range of soil moisture values in the catchment. This effect may be more significant in wet to partially wet catchments than in very dry catchments.

It was found that a combination of LST and vegetation index (VI) was necessary for obtaining a more complete picture of the soil water distribution than was achievable by considering LST alone. The third set of models studied soil water predictions with LST and VI as combined in the VTCI approach. The catchment-scale SWCs derived with the VTCI method were similar to the measured water content at the CASMM site of the catchment. It was shown that the VTCI approach is capable of predicting the catchment average soil water content with an accuracy within ±0.03 cm^3 cm^{-3}.. Vegetation indices are thus more effective in predicting spatial and temporal patterns in soil moisture distribution the relative distributions of possible water stressed areas in a catchment and occurrences of water stressed periods better than by using LST measurements alone. This confirms that the consideration of soil and vegetation information is vital for accurate predictions from LST based models.

It is also important to note that all models were developed with a limited number of point scale *in-situ* soil moisture measurements for the top 0-30 cm (i.e. the root-zone) and remotely sensed LST measurements with 1.1 km^2 pixels. Considering the vast scale difference between these two variables, these models appear very encouraging for soil water content prediction. Hence, it may be concluded that the use of a limited number of *in-situ* soil moisture data in deriving the catchment scale moisture patterns appears feasible, particularly with RNTI-NWDI and VTCI-based models.

It may therefore be concluded that if regression models are to be used for extrapolating limited point-scale measurements across a catchment, one should use (a) normalized forms of LST and SWC or (b) consider both LST and VI as is done in the VTCI approach.

Future work should test the generality of the VTCI and RNTI approaches across different climatic regions and vegetation types. It is recommended that the wetness characteristics of sites should be studied before setting up any monitoring network in any future studies. This can be done entirely with public domain data such as MODIS derived LST and VI data. This would assist in identifying suitable locations for soil moisture monitoring in a large catchment. It would assist in the efficient allocation of limited monitoring devices based on the wetness behaviour of selected locations within a catchment. Potentially, this would also help to reduce the initial set-up cost, particularly in a large catchment.

The study reported in Chapter 6 found that it is possible to derive catchment scale SWC distribution maps with a sparse network of soil moisture monitoring sites. Such maps are not only useful for scaling studies and hydrological model applications but also for practical applications such as achieving maximum usage from limited water resources.

The use of a limited number of ground-based measurements in combination with remotely sensed observations will provide an economical way of collecting soil moisture related information across large catchments. Thus, remote sensing methodologies for soil moisture prediction will become an essential component in future soil moisture scaling approaches.

9.5 FIELD VALIDATION OF AMSR-E SOIL MOISTURE ESTIMATES

Chapter 7 has reported on the validation of AMSR-E soil moisture measurements with two approaches. The first approach was based on many point scale soil moisture measurements collected during three intensive field campaigns. The second approach compared the temporal evolution of AMSR-E soil moisture measurements with pixel-scale 0-30 cm moisture measurements collected with the ground-based monitoring network.

First, based on a large number of point scale observations, it was found that AMSR-E provides reasonable estimates of near-surface soil moisture content when compared with the averages of the point observations comprised within the AMSR-E pixel. A positive correlation was found between AMSR-E measured soil moisture and both 0-1 cm and 0-6 cm field measured values. However, AMSR-E moisture measurements did not exceed 15% (v/v) even at the higher measured soil moisture content of over 25% (v/v). The difference between AMSR-E near-surface measurements and the observed 0-1 and 0-6 cm soil moisture may be attributed to four factors. First, the field measured data did not provide perfect estimates of instantaneous surface moisture contents as measured by the AMSR-E in terms of the spatial extent and the depth. Second, collection of field measurements from the near-surface layer over 3-day period may introduce errors due to rapid drying of the surface layer. Third, past rainfall patterns can impact on the data. This is probably more so for 0-6 cm than for 0-1cm because the deeper layer can store more water and therefore its soil water content will reflect past rainfall better than the 0-1 cm layer. Finally, the effect of vegetation was not uniform across AMSR-E pixels. Vegetation may affect soil moisture distribution. Therefore, a perfect match between AMSR-E area values of near-surface soil moisture content and averages of ground-based point scale measurements over 0-1 and 0-6 cm may not always be possible. On the other hand, any inaccuracies of the soil moisture retrieval algorithm used by AMSR-E may also be contributed to this mismatch.

Microwave sensors measure soil moisture in the topmost soil layer where observation depth varies from 1/10 to 1/4 of a wavelength. At 9.6 GHz of AMSR-E, this penetration depth is up to 1 cm deep. The penetration of microwave signals depends on soil moisture itself. It is therefore difficult to determine firstly, the correct depth of soil samples and secondly, to arrive at an accurate method which is sufficiently efficient for collecting a large number of *in-situ* measurements. Soil moisture also changes very rapidly in the topmost soil layer as does the land surface temperature. In addition, there are practical problems in collecting accurate soil samples for the top 0-1 cm of soil. Often, many soil moisture studies, including the present study, use soil moisture measurements collected over 0-6 cm depth with convenient measuring tools such as the Theta probe. Besides, the spatial distribution of soil moisture depends on soil parameters that are not distributed homogeneously in the catchment. As a result, the average soil moisture computed from point measurements within a footprint does not necessarily give an accurate representation of the soil moisture across the footprint.

The 3-day field experiments described in Chapter 7 indicate that the use of a three-day period for the collection of near-surface soil moisture measurements to evaluate the AMSR-E measurements does not provide ideal conditions for validation studies. During field campaigns, the average daily differences between first and last observations in 0-1cm layer were found vary between -1.6% (v/v) to -3.3% (v/v). In situations where the surface is relatively wet and the climate is more favourable for rapid drying and hence rapid changes in wetness, it is advisable to consider shorter-duration field campaigns. This leads to the recommendation to conduct field campaigns preferably in the morning between 6 am and 9 am. During this time vertical gradients in near-surface soil moisture are smallest, resulting in the smallest discrepancies between observations and model predictions of near-surface soil moisture. Additionally, this is the time of day when near-surface soil moisture is most strongly coupled with the water status of the underlying soil.

The second approach for validating AMSR-E used soil moisture data from the permanent ground-based monitoring network. Continuous observations of 0-30 cm soil moisture made at the permanent network stations provided information on temporal patterns of soil moisture. Chapter 7 demonstrates the application of temporal stability characteristics of ground-based monitoring stations for validating AMSR-E measurements. Results showed that the AMSR-E soil moisture estimates are capable of mimicking temporal trends in land surface soil moisture reasonably well.

Comparisons between of 0-30 cm soil moisture measurements from a temporally stable monitoring site within a pixel and the day-time and night-time AMSR-E near-surface moisture values indicated that daytime values are better correlated with *in-situ* measurements than night time values. The lower correlation for night time values may be due to the variations caused by redistribution of soil moisture at night in the absence of evaporation. It is also possible that dew formation helps rewetting the surface layer, particularly at night time. Therefore, even when the 0-30 cm layer is generally dry, its thin surface layer may contain a slightly higher moisture level. This may explain in part the low correlation between night-time near-surface soil moisture measurements and the moisture contents of the 0-30cm deep layer. This analysis confirmed that 0-30 cm soil moisture measurements from a pixel-scale average soil moisture monitoring site indicate a positive relationship with the AMSR-E data. The results showed that it is possible to establish a site-specific empirical relationship to obtain area-averaged near-surface moisture content from 0-30 cm measurements. Such an analysis also helps to reduce the number of measuring points required for characterising soil moisture trends for a given AMSR-E pixel.

In the light of the above, it may be concluded that a permanent network of soil moisture measurement sites would be highly desirable when validating the soil moisture retrieval algorithm of AMSR-E. However, the 0-30 cm SWC values used in this thesis are not necessarily strongly related with AMSR-E near-surface measurements. Future studies therefore need to consider the continuous measurement of near-surface SWC values, preferably in the 0-1 cm to 0-6 cm depths for use in such an analysis. The Goulburn River catchment network has recently been upgraded with these measurements and it is therefore possible to implement such analysis in the near future.

The results suggest that changes to the AMSR-E soil moisture predictions algorithm may be needed in order to improve the accuracy of soil moisture retrieval.

The main problem in validating large-area moisture predictions is the absence of ground truth data at the appropriate scale. More studies are therefore needed to address this issue, whilst airborne sensors should also be considered for future validation studies.

No adequate techniques are currently available for *in-situ* validation of soil moisture measurements from satellite remote sensing such as from AMSR-E. Field campaigns must be carried out for a range of ecological and climatic regions in order to build a knowledge-base on validation approaches. Until they are fully validated, soil moisture data derived from satellite remote sensing should be used more for qualitative studies rather than for quantitative applications.

9.6 DISAGGREGATION OF LARGE-AREA SOIL MOISTURE MEASUREMENTS

In Chapter 8 two new methodologies have been developed for disaggregating large-scale AMSR-E soil moisture values into fields of 1.1 km x 1.1 km soil moisture values. The downscaling approach which was used retained a strong physical basis by using information from other satellites, it is applicable at a variety of spatial scales, and it does not require any form of calibration based on other ground measurements of soil moisture.

Two indices, RNTI and VTCI were used to disaggregate AMSR-E soil moisture data. The RNTI and VTCI indices adopt different approaches to describe soil wetness characteristics. While the RNTI based approach incorporates thermal inertia properties to determine soil moisture, the VTCI based approach incorporates the vegetation information in addition to the thermal inertia property.

The two disaggregation techniques studied in this chapter were found to be capable of providing soil moisture predictions which can readily be related to the dominant physical characteristics such as the vegetation pattern, catchment topography and major water courses as well as the distribution of recent rainfall.

The computation of RNTI and VTCI is relatively straight-forward. The high-resolution LST and VI data from the MODIS sensor are reliable and available for the entire globe and can be downloaded free of charge. Thus, computation of indices such as RNTI and VTCI from MODIS LST and VI data is cost-effective and achievable for many regions.

While the comparison of downscaled moisture patterns and field measured point-scale values gave plausible results, some differences were also observed. These differences occurred because microwave and visible/near infrared respond to different biophysical characteristics and energy sources. Additionally, visible/near infrared measurements of vegetation indices are typically reported as composites over time (15 days in the present study) because of frequent adverse atmospheric effects. Moreover, note that these comparisons were made with data obtained at two different scales: the point scale for measured values and the 1.1 km scale for downscaled values.

The disaggregation study reported in Chapter 8 was concerned with the top 0-1 cm soil layer which has a highly variable soil moisture content. The comparison between 1.1x1.1 km^2 scale near-surface soil moisture predictions based on instantaneous observations with point-scale measurements collected over a long period always was hampered by concerns over the applicability of such a validation approach. The difficulty arises both in the estimation process as well as in the measurements of *in-situ* soil moisture content. No definite conclusion could therefore be drawn from the comparison between *in-situ* point measurements and disaggregated soil moisture predictions from AMSR-E data.

Some limitations were identified in the above disaggregation schemes. Catchment scale information about soil moisture is affected by biophysical and climatic factors as well as by technological constraints. For example, the signals from AMSR-E and MODIS are not related to the same soil depth. As a result, their soil moisture estimates may differ. AMSR-E measures soil moisture in the top 0-1 cm soil layer. Wetness indices such as VTCI are based on vegetation indices and hence reflect soil wetness over the entire depth of the root-zone. For this reason, estimates of soil moisture using the above two methods may differ. However, the VTCI is used as a covariate to disaggregate soil moisture observations and effect on the final results are therefore expected to be relatively minor

This has been concluded that both RNTI and VTCI based techniques appear to be useful for the disaggregation of soil moisture estimates obtained with the AMSR-

E sensor. The research suggests that as long as one can use high resolution ancillary data as proxy indicators of surface wetness, the methodology can satisfactorily disaggregate soil moisture across spatial scales.

Further testing and validation of the above downscaling methods will need to be conducted for a range of climatic and land surface conditions and, where possible with the use of high resolution soil moisture estimated from air-borne microwave radiometers and optical/IR data.

9.7 CONCLUDING REMARKS

Despite the limitations of being able to measure soil moisture data at the proper scale, estimates of soil moisture averaged over small areas were compared with point-scale *in-situ* measurements, in order to interpret the results from soil moisture scaling studies. The issue of evaluating areal soil moisture predictions with a limited number of point-scale measurements however, will remain a serious issue for further discussion.

The benefits of this thesis include improved understanding of the scaling relationships of soil moisture in varied topography and in inherently spatially-variable soils. New scaling tools have been developed to upscale and downscale measured soil moisture from *in-situ* and passive microwave satellite respectively, which in the longer term may benefit both the scientific community and the general public. The scaled soil moisture values may be used in the study of hydrological behaviour of catchments at a variety of spatial scales, including plot, regional, and catchment scale, and temporally, at both inter-and intra-annual time scales.

Many possibilities exist for improving precision hydrological modelling when a parameter with a profound effect on model prediction such as soil moisture is found to be available at an appropriate scale. It is hoped that the issues discussed in this thesis will stimulate further research into the concepts of soil moisture scaling.

BIBLIOGRAPHY

Abuzar, M. and Al-Ghunaim, I., 1997. Spatial disaggregation of spectral data for haze assessment in an arid environment. *International Journal of Remote Sensing*, **18(8)**: 1693-1702.

Acock, B., and Allen L. H., 1985. Crop responses to elevated carbon dioxide concentrations. In: Strain B. R., and Cure, J. D. (Eds), *Direct effects of increasing carbon dioxide on vegetation.* Office of Energy Research, Department of Energy, Washington, 53–97.

Ahmad, M. D., and Bastiaanssen, W. G. M., 2003. Retrieving soil moisture storage in the unsaturated zone using satellite imagery and bi-annual phreatic surface fluctuations. *Irrigation and Drainage Systems*, **17**: 141-161.

Allen, R. G., Pereira, L. S., Raes, D., and Smith, M., 1998. Crop evapotranspiration - Guidelines for computing crop water requirements - FAO Irrigation and drainage paper 56, FAO, Roam. (Also available at http://www.fao.org/docrep/X0490E/x0490e00.htm#Contents)

Anctil, F., Mathieu, R., Parent, L.-E., Viau, A. A., Sbih, M., and Hessami, M., 2002. Geostatistics of near-surface moisture in bare cultivated organic soils. *Journal of Hydrology***, 260**: 30-37.

AS 1289.2.1.1-2005. Methods of testing soils for engineering purposes: Method 2.1.1, Soil moisture content tests - Determination of the moisture content of a soil – Oven drying method (standard method).

AS 1289 3.6.1-2005, Methods of testing soils for engineering purposes: Method 3.6.1, Soil classification tests - Determination of the particle size distribution of a soil – Standard method of analysis by sieving.

AS 1289 3.6.3-2003, Methods of testing soils for engineering purposes: Method 3.6.3, Soil classification tests - Determination of the particle size distribution of a soil - Standard method of fine analysis using a hydrometer.

Atkinson, P. M., and Lewis, P., 2000. Geostatistical classification for remote sensing: an introduction. *Computers and Geosciences,* **26**: 361-371.

Avissar, R., 1995. Scaling of land-atmosphere interactions: an atmospheric modelling perspective. In: Kalma, J. D. and Sivapalan, M. (Eds), *Advances in Hydrological Processes: Scale issues in hydrological modelling*. John Wiley & Sons Ltd, Chichester, 435-451.

Bárdossy, A., and Lehmann, W., 1998. Spatial distribution of soil moisture in a small catchment. Part 1: geostatistical analysis. *Journal of Hydrology,* **206**: 1-15.

Bastiaanssen, W. G. M., Pelgrum, H., Droogers, P., de Bruin, H. A. R., and Menenti, M., 1997. Area-average estimates of evaporation, wetness indicators and top soil moisture during two golden days in EFEDA. *Agricultural and Forest Meteorology*, **87(2-3)**: 119-137.

Becker, F., and Li, Z. L., 1990. Towards a local split window method over land surface. *International Journal of Remote Sensing,* **3**:17–33.

Beckett, P. H. T., and Webster, R., 1971. Soil Variability - A Review. *Soils and Fertilisers*, **34(1)**: p15.

Bernert, J. A., Eilers, J. M., Sullivan, T. J., Freemark, K. E., and Ribic, C., 1997. A quantitative method for delineating regions: an example for the western corn belt plains ecoregion of the USA. *Environmental Management* **21(3)**:405–420.

Beven, K. J., and Kirkby, M. J., 1979. A physically-based variable contributing area model of basin hydrology. *Hydrological Sciences Bulletin*, **24**: 43-69.

Beven, K. J., 1995. Linking parameters across scales: subgrid parameterizations and scale dependent hydrological models. In: Kalma, J. D., and Sivapalan, M. (Eds), *Advances in Hydrological Processes: Scale Issue in Hydrological Modelling*, Chichester, Wiley, 263-281.

Biftu G. F, and Gan, T., 1999. Retrieving near-surface soil moisture from Radarsat SAR data, *Water Resources Research*. **35**: 1569-1579.

Blöschl, G., and Sivapalan, M., 1995. Scale issues in hydrological modelling: a review. *Hydrological Processes*, **9(3-4)**: 251-290.

Blöschl, G., Grayson, R. B., and Sivapalan, M., 1995. On the representative elementary area (REA) concept and its utility for distributed rainfall-runoff modelling. *Hydrological Processes*, **9**:313-330.

Boegh, E., Soegaard, H., Hanan, N., Kabat, P., and Lesch, L., 1998. A remote sensing study of the NDVI-T_s relationship and the transpiration from sparse vegetation in the Sahel based on high resolution satellite data. *Remote Sensing of Environment*, **69(3)**: 224-240.

Buggman, H. K. M., 1997. Sensitivity of Forests in the European Alps to Future Climate Change, *Climate Research*, **8**:35-44.

Burrough, P. A., 1993. Soil variability: a late 20th century view. *Soils Fertilizers*, **56(5)**:529-562.

Campbell Scientific, Inc., 2002. *CS616 Water Content Reflectometer: Service Manual*. Logan, UT. CSI.

Capehart, W. J., and Carlson, T. N., 1997. Decoupling of surface and near-surface soil water content: A remote sensing perspective. *Water Resources Research*, **33(6)**: 1383-1395.

Carlson, T. N., 1986. Regional-scale estimates of surface moisture availability and thermal inertia using remote thermal measurements. *Remote Sensing Reviews*, **1**: 197-247.

Carlson, T. N., Dodd, J. K., Benjamin, S. G., and Cooper, J. N., 1981. Remote estimation of surface energy balance, moisture availability and thermal inertia. *Journal of Applied Meteorology*, **20**: 67-87.

Carlson, T. N., Gillies, R. R., and Perry, E. M., 1994. A method to make use of thermal infrared temperature and NDVI measurements to infer surface soil water content and fractional vegetation cover. *Remote Sensing Reviews*, **9**: 161-173.

Carlson, T. N., Gillies, R. R., and Schmugge, T. J., 1995. An interpretation of methodologies for indirect measurement of soil water content. *Agricultural and Forest Meteorology*, **77(3-4)**: 191-205.

Chandler, D. G., Seyfried, M., Murdock, M., and McNamara, J., 2004. Field calibration of water content reflectometers. *Soil Science Society of America Journal*, **68(5)**: Manuscript: S03-0163(1)**,** 9pp.

Chang, D. H., and Islam, S., 2003. Effects of topography, soil properties and mean soil moisture on the spatial distribution of soil moisture: A stochastic analysis. In: Pachepsky, Y.,Radcliffe, D. E., and Selim, H. M. (Eds), *Scaling methods in soil physics*, CRC Press, London, 193-225.

Charpentier, M. A., and Groffman, P. M., 1992. Soil moisture variability within remote sensing pixels. *Journal of Geophysical Research,* **97(D17)**:18,987–18,995.

Chauhan, N. S., Miller, S., and Ardanuy, P., 2003. Spaceborne soil moisture estimation at high resolution: A microwave-optical/IR synergistic approach. *International Journal of Remote Sensing,* **24(22)**:4599–4622.

Chen, J. H., Kan, C. E., Tan, C. H., and Shih, S. F., 2002. Use of spectral information for wetland evapotranspiration assessment. *Agricultural Water Management,* **55**: 239-248.

Choudhury, B. J., and Golus, R. E., 1988. Estimating soil wetness using satellite data. *International Journal of Remote Sensing,* **9**: 1251-1257.

Choudhury, B. J., Schmugge, T. J., Chang, A., and Newton, R. W., 1979. Effect of Surface Roughness on the Microwave Emission from Soils. *Journal of Geophysical Research,* **84(C9)**: 5699-5706.

Comegna, V., and Basile, A., 1994. Temporal stability of spatial patterns of soil water storage in a cultivated Vesuvian soil. *Geoderma,* **62(1-3)**: 299-310.

Cosh, M. H., Jackson, T. J., Starks, P., and Heathman, G., 2006. Temporal stability of surface soil moisture in the little Washita river watershed and its applications in satellite soil moisture product validation. *Journal of Hydrology,* **323(1-4)**: 168-177.

Cosh, M. H., Stedinger, J., R., and Brutsaert, W., 2003. Time changes in spatial structure of surface variability in the Southern Great Plains. *Advances in Water Resources,* **26(4)**: 407-415.

Czajkowski, K. P., Goward, S. N., Shirey, D., and Walz, A., 2002. Thermal remote sensing of near-surface water vapor. *Remote Sensing of Environment,* **79(2-3)**: 253-265.

De Jeu, R. A. M., 2003. Retrieval of land Surface Parameters using Passive Microwave Remote Sensing. PhD thesis, Vrije Universiteit, Amsterdam.

Department of Sustainable Natural Resources, 2003. Soil landscape map for Stanley. Unpublished map.

Diak, G. R., and Stewart, T. R., 1989. Assessment of surface turbulent fluxes using geostationary satellite surface skin temperatures and a mixed layer planetary boundary layer scheme. *Journal of Geophysical Research,* **94**: 6357-6373.

Dingman, S. L., 1994. *Physical Hydrology*. Macmillan Publishing Company, New York, 575pp.

Dobson, M. C., and Ulaby, F. T., 1986. Active microwave soil moisture research. *IEEE Transactions on Geoscience and Remote Sensing,* **GE**:2423-2436.

Dobson, M. C., Ulaby, F. T., Hallikainen, M. T., and El-Rayes, M. A., 1985. Microwave Dielectric Behaviour of Wet Soil - Part II: Dielectric Mixing Models. *IEEE Transactions on Geoscience and Remote Sensing ,* **GE-23(1)**: 35-46.

D'Odorico, P., Ridolfi, L., Porporato, A., and Rodriguez-Iturbe, I., 2000. Preferential states of seasonal soil moisture: The impact of climate fluctuations. *Water Resources Research,* **36(8)**: 2209-2219.

Dozier, J., and Wan, Z., 1994. Development of practical multiband algorithms for estimating land-surface temperature from EOS/MODIS data. *Advances in Space Research,* **14(3)**: 81-90.

Drusch, M., Wood, E. F., Gao, H., and Thiele, A., 2004. Soil moisture retrieval during the Southern Great Plains Hydrology Experiment 1999: A comparison between experimental remote sensing data and operational products. *Water Resources Research,* **40(W02504)**: 12.

Dunne, T., Moore, T. R., and Taylor, C. H., 1975. Recognition and prediction of runoff-producing zones in humid regions, Hydrological Sciences Bulletin **20(3)**:305-327

Eidenshink, J. C. and Faundeen, J. L., 1994. The 1 km AVHRR global land data set: First stages in implementation, *International Journal of Remote Sensing,* **15**:3443-3462.

Engman, E. T., 1990. Progress in microwave remote sensing of soil moisture. *Canadian Journal of Remote Sensing*, **16(3)**: 6-14.

Engman, E. T., 1992. Soil Moisture Needs in Earth Sciences. In: *Proc. International Geoscience and Remote Sensing Symposium (IGARSS),* 477-479.

Engman, E. T., and Chauhan, N., 1995. Status of microwave soil moisture measurements with remote Sensing. *Remote Sensing of Environment,* **51(1)**: 189-198.

Entekhabi, D., 1995. Recent advances in land-atmosphere interaction research. *Reviews of Geophysics,* **33**:995-1003.

Entekhabi, D., Nakamura, H., and Njoku, E. G., 1993. Retrieval of soil moisture by combined remote sensing and modeling. In: Choudhury, B. J., Kerr, Y. H., Njoku, E. G., and Pampaloni, P. (Eds), *ESA/NASA International Workshop on Passive Microwave Remote Sensing Research Related to Land-Atmosphere Interactions,* St. Lary, France, 485-498.

ESRI (Environmental Systems Research Institute, Inc.), 1996a. *Arcview GIS, Version 3.1,* Computer software. California.

ESRI (Environmental Systems Research Institute, Inc.), 1996b. *Arcview Spatial Analyst, Version 1.1,* Computer software. California.

Evett, S.R. 2002. Water and Energy Balances at Soil-Plant-Atmosphere Interfaces. In: Warrick, A. A. (Ed) *The Soil Physics Companion*, CRC Press LLC, Boca Raton, FL, 127-188.

Famiglietti J. S. and Wood E. F., 1995. Effects of spatial variability and scale on areally averaged evapotranspiration. *Water Resources Research*, **31**:699-712.

Famiglietti, J. S., Devereaux, J. A., Laymon, C. A., Tsegaye, T., Houser, P. R., Jackson, T. J., 1999. Ground-based investigation of soil moisture variability within remote sensing footprints during the Southern Great Plains 1997 (SGP97) Hydrology Experiment. *Water Resources Research,* **35(6)**: 1839-1851.

Famiglietti, J. S., Rudnicki, J. W., and Rodell, M., 1998. Variability in surface moisture content along a hillslope transect: Rattlesnake Hill, Texas. *Journal of Hydrology,* **210(1-4)**: 259-281.

Field, C. B., Jackson, R. B., and Mooney, H. A., 1995. Stomatal responses to increased CO2: implications from the plant to the global scale. *Plant Cell Environment* **18:**1214–1225

Flores, A. L., and Carlson, T. N., 1987. Estimation of surface moisture availability from remote temperature measurements. *Journal of Geophysics Research,* **92**: 9581-9585.

Foote, K. E., and Huebner, D. J., 2000. Database Concepts. Geographer's Craft Project, University of Colorado, Boulder. Retrieved on 21 June 2006 from the web site http://www.colorado.edu /geography/gcraft/notes/datacon /datacon.html.

Francis, C. F., Thornes, J. B., Romero Diaz, A., Lopez Bermudez, F., and Fisher, G. C., 1986. Topographic control of soil moisture, vegetation cover and land degradadation in a moisture stressed Mediterranean environment. *Catena*, **13**:211-225.

Friedl, M. A., and Davis, F. W., 1994. Sources of variation in radiometric surface temperature over a tall grass prairie. *Remote Sensing of Environment,* **48**: 1-17.

Gao, H., Wood, E. F., Drusch, M., Crow, W., and Jackson, T. J., 2004. Using a microwave emission model to estimate soil moisture from ESTAR observations during SGP99. *Journal of Hydrometeorology*, **5**:49– 63.

Gifford, R. M., 1992. Interaction of carbon dioxide with growth-limiting environmental factors in vegetation productivity: implications for the global carbon cycle. *Advances in Bioclimatology* **1**:24–58.

Gillespie, A. R., Rokugawa, S., Matsunaga, T., Cothern, J. S., Hook, S. J., and Kahle, A. B., 1998. A temperature and emissivity separation algorithm for advanced space borne thermal emission and reflection radiometer (ASTER) images. *IEEE Transactions on Geoscience and Remote Sensing*, **36**: 1113–1126.

Gillies, R. R., and Carlson, T. N., 1995. Thermal remote sensing of surface soil water content with partial vegetation cover for incorporation into climate models. *Journal of Applied Meteorology*, **34**:745–756.

Gillies, R. R., Carlson, T. N., Gui, J., Kustas, W. P., and Humes, K. S., 1997. A verification of the 'triangle' method for obtaining surface soil water content and energy fluxes from remote measurements of the Normalized Difference Vegetation Index (NDVI) and surface radiant temperature. *International Journal of Remote Sensing,* **18(15)**: 3145– 3166.

Glenn, N. F., and Carr, J. R., 2003. The use of geostatistics in relating soil moisture to RADARSAT-1 SAR data obtained over the Great Basin, Nevada, USA. *Computers & Geosciences*, **29(5)**:577-586.

Goetz, S. J., 1997. Multisensor analysis of NDVI, surface temperature and biophysical variables at a mixed grassland site. *International Journal of Remote Sensing,* **18(1)**: 71-94.

Gómez-Plaza, A., Alvarez-Rogel, J., Albaladejo, J., and Castillo, V. M., 2000. Spatial patterns and temporal stability of soil moisture across a range of scales in a semi-arid environment. *Hydrological Processes*, **14**: 1261-1277.

Goward, S. N., and Hope, A.S., 1989. Evapotranspiration from combined reflected solar and emitted terrestrial radiation: preliminary FIFE results from AVHRR data. *Advances in Space Research*, **9**: 239-249.

Goward, S. N., Xue, Y., and Czajkowski, K. P., 2002. Evaluating land surface moisture conditions from the remotely sensed temperature/vegetation index measurements. *Remote Sensing of Environment,* **79(2-3)**: 225-242.

Grayson, R. B., and Blöschl, G., 2000. Spatial processes, organization and patterns. In: Grayson, R. B., and Blöschl, G. (Eds), *Spatial Patterns in Catchment Hydrology: Observations and Modelling*. Cambridge University Press, 3-16.

Grayson, R. B., and Western, A. W., 1998. Towards areal estimation of soil water content from point measurements: time and space stability of mean response. *Journal of Hydrology*, **207(1-2)**: 68-82.

Grayson, R. B., Blöschl, G., Western, A. W., and McMahon, T. A., 2002. Advances in the use of observed spatial patterns of catchment hydrological response. *Advances in Water Resources,* **25(8-12)**: 1313-1334.

Grayson, R. B., Western, A. W., Chiew, F. H. S., and Blöschl, G., 1997. Preferred states in spatial soil moisture patterns: Local and nonlocal controls. *Water Resources Research,* **33(12)**: 2897-2908.

GSFC/NASA, 2003. MODIS technical specifications. Retrieved 30 June 2005, from http://modis.gsfc.nasa.gov/ about/specs.html.

Gupta, V. K., Waymire, E. and I. Rodriguez-Iturbe, 1986. On scales, gravity and network structure in basin runoff, In: Gupta, V. K., Rodriguez-Iturbe I., Wood E. F. (Eds), *Scale Problems in Hydrology*, Reidel, Dordrecht, 159-184.

Hallikainen, M. T., Ulaby, F. T., Dobson, M. C., El-Rayes, M. A., and Wu, L. K., 1985. Microwave dielectric behaviour of wet soil, Part I: Empirical models and experimental observations. *IEEE Transactions on Geoscience and Remote Sensing,* **GE-23(1)**: 25-34.

HCMT (Hunter Catchment Management Trust), 2003. Integrated catchment management plan for the Hunter catchment 2002, NSW Department of Land and Water Conservation. 62pp.

Hemakumara, H. M., Kalma, J. D., Walker, J. P., and Willgoose, G. R., 2004. Downscaling of low resolution passive microwave soil moisture observations. In: Teuling, A. J., Leijnse, H., Troch, P. A., Sheffield, J., and Wood, E.F. (Eds), *Proceedings of the 2nd international CAHMDA workshop on: The Terrestrial Water Cycle: Modelling and Data Assimilation Across Catchment Scales*, October 25-27, 2004, Princeton, NJ, 67-71.

Hu, Z., and Islam, S., 1997. Framework for analyzing and designing scale invariant remote sensing algorithms. *IEEE Transactions on Geoscience and Remote Sensing,* **35(3)**: 747-755.

Hu, Z., Islam, S., and Cheng, Y., 1997. Statistical characterization of remotely sensed soil moisture images. *Remote Sensing of Environment,* **61(2)**: 310-318.

Huete, A. R., 1988. A soil adjusted vegetation index (SAVI), *Remote Sensing of Environment,* **25**:295-309.

HVRF (Hunter Valley Research Foundation), 2005. *Hunter Region Yearbook: Newcastle and the Hunter Region 2005-2006*. Retrieved December 2005, from *http://www.hvrf.com.au /yearbook.htm.*

Idso, S. B., 1982. Non-water-stressed baselines: A key to measuring and interpreting plant water stress. *Agricultural Meteorology,* **27(1-2)**: 59-70.

Idso, S.B., Reginato, R. J., Jackson, R. D., and Pinter Jr., P. J., 1981. Measuring yield-reducing plant water potential depressions in wheat by infrared thermometry. Irrigation Science, **2(4)**: 205-212

Jackson, R. D., and Huete, A. R., 1991. Interpreting vegetation indices. *Preventive Veterinary Medicine*, **11**: 185-200.

Jackson, R. D., Kustas, W. P., and Choudhury, B. J., 1988. A reexamination of the crop water stress index. *Irrigation Science,* **9**: 309-317.

Jackson, R. D., Pinter Jr, P. J., Reginato, R. J., and Idso, S. B., 1986. Detection and evaluation of plant stresses for crop management decisions. *IEEE Transactions on Geoscience and Remote Sensing*, **24(1):** 99-106.

Jackson, T. J., 1993. Measuring surface soil moisture using passive microwave remote sensing. *Hydrological Processes*, **7**: 139-152.

Jackson, T. J., 1997. Soil moisture estimation using Special Satellite Microwave/Imager satellite data over a grassland region. *Water Resource Research*, **3**:1475–1484.

Jackson, T. J., and O'Neill, P. E., 1990. Attenuation of Soil Microwave Emissivity by Corn and Soybeans at 1.4 and 5 GHz. *IEEE Transactions on Geoscience and Remote Sensing*, **GE-28**: 978-980.

Jackson, T. J., and Schmugge, T. J., 1995. Surface soil moisture measurement with microwave radiometry. *Acta Astronautica*, **35(7)**: 477-482.

Jackson, T. J., and Schmugge, T. J., 1989. Passive microwave remote sensing system for soil moisture: Some supporting research. *IEEE Transactions on Geoscience and Remote Sensing,* **27(2)**: 225-235.

Jackson, T. J., Cosh, M. H., Zhan, X., Bosch, D. D., Seyfried, M. S., Starks, P. J., Keefer, T. O., Lakshmi, V. 2006. Validation of AMSR-E soil moisture products using watershed networks. In: *Proceedings of the International Geoscience and Remote Sensing Symposium*, July 31 - August 31, 2006, Denver, Colorado.

Jackson, R. D., Idso, S. B., Reginato, R. J., and Pinter Jr, P. J., 1981a. Canopy temperature as a crop water stress indicator. *Water Resources Research,* **17(4):**1133-1138

Jackson, T.J., Le Vine, D.M., Hsu, A.Y., Oldak, A., Starks, P.J., Swift, C.T., Isham, J.D., and Haken, M., 1999. Soil moisture mapping at regional scales using microwave radiometry: the Southern Great Plains Hydrology Experiment. *IEEE Transactions on Geoscience and Remote Sensing*, **37**:2136–2151.

Jackson, T. J., Schmugge, T. J., and Engman, E. T., 1996. Remote Sensing Applications to Hydrology: Soil Moisture. *Hydrological Sciences Journal,* **41(4)**: 517-530.

Jackson, T. J., Schmugge, T. J., and Wang, J. R., 1982. Passive microwave sensing of soil moisture under vegetation canopies. *Water Resources Research*, **18(4)**: 1137-1142.

Jackson, T. J., Schmugge, T. J., Nicks, A. D., Coleman, G. A., and Engman, E. T., 1981b. Soil moisture updating and microwave remote sensing for hydrological simulation. *Hydrological Sciences Bulletin,* **26(3)**: 305-319.

Justice, C. O., Vermote, E., Townshend, J. R. G., Defries, R., Roy, D. P., Hall, D. K., 1998. The moderate resolution imaging spectroradiometer (MODIS): Land remote sensing for global change research. *IEEE Transactions on Geoscience and Remote Sensing,* **36(4)**: 1228-1249.

Kachanoski, R. J., and De Jong, E., 1998. Scale dependence and the temporal persistence of spatial patterns of soil water storage. *Water Resource Research*, **24**: 85-91.

Kaihotsu, I., Yamanaka, T., and Koike, T., 2004. Current activities of the AMPEX AMSR/AMSR-E studies. *Proceedings of the 3rd International Workshop on Terrestrial Change in Mongolia, Tsukuba, Japan*, retrieved 20 December 2005 from http://www.suiri.tsukuba.ac.jp /bulletin/t5supple /t5supple_01.pdf.

Kaihotsu, I., Yamanaka, T., Oyunbaatar, D., Hirata, M., Oishi, K., Muramatsu, K., Miyazaki, S., Kondoh, A., and Koike, T., 2002. Preliminary ground-based observation for the soil moisture measurement validation of ADEOSII-AMSR/AMSR-E. *Proceedings of the 3rd Workshop on Remote Sensing of Hydrological Processes and Applications*, 1-6.

Kalma, J. D., Bates, B. C., and Woods, R. A., 1995. Predicting catchment-scale soil moisture status with limited field measurements. In: Kalma, J. D., and Sivapalan, M. (Eds), *Advances in Hydrological Processes: Scale Issues in Hydrological Modelling*, John Wiley and Sons, Chichester, 203-225.

Kawanishi, T., Sezai, T., Ito, Y., Imaoka, K., Takeshima, T., Ishido, Y., Shibata, A., Miura, M., Inahata, H., and Spencer, R. W., 2003. The Advanced Microwave Scanning Radiometer for the Earth Observing System (AMSR-E), NASDA's contribution to the EOS for global energy and water cycle studies, *IEEE Transactions on Geoscience and Remote Sensing*, **41(2)**: 184-194.

Kealy, P. S., and Hook, S. J., 1993. Separating temperature and emissivity in thermal infrared multispectral scanner data: Implications for recovering land surface temperatures. *Geoscience and Remote Sensing*, **31(6):**1155-1164.

Kerr, Y. H., Lagouarde, J. P., Nerry, F., and Ottle, C., 2004. Land surface temperature retrieval techniques and applications: case of AVHRR. In: Quattrochi, D. A., and Luvall, J. C. (Eds), *Thermal remote sensing in land surface processes*, CRC Press, Florida, USA, 33-109.

Kim, G., and Barros, A. P., 2002a. Space-time characterization of soil moisture from passive microwave remotely sensed imagery and ancillary data. *Remote Sensing of Environment*, **81(2-3)**: 393-403.

Kim, G., and Barros, A. P., 2002b. Downscaling of remotely sensed soil moisture with a modified fractal interpolation method using contraction mapping and ancillary data. *Remote Sensing of Environment*, **83(3)**: 400-413.

King, M., 2004. Moisture characteristics for soils in the Goulburn River Catchment as determined with the Tempe Pressure Cell. *Honours Thesis*, University of Newcastle, Newcastle, 59 pp.

Kirdiashev, K. P., Chikhlantsev, A. A., and Shutko, A. M., 1979. Microwave radiation of the earth's surface in the presence of vegetation cover. *Radio Engineering and Electronic Physics*, **24**:37–44.

Klemes V., 1983. Conceptualization and scale in hydrology. *Journal of Hydrology*, **5**:1-23.

Koike, T., Nakamura, Y., Kaihotsu, I., Davaa, G., and Matsuura, N., 2003. AMSR-E Soil moisture product validated at the CEOP Mongolia Reference site. *CEOP Newsletter*, **4:**6.

Kondoh, A., and Higuchi, A., 2001. Relationship between satellite-derived spectral brightness and evapotranspiration from a grassland. *Hydrological Processes*, **15(10)**: 1761-1770.

Laymon, C. A., Huntsville, A. L., Archer, F., Crosson, W. L., and Limaye, A., 2003. Soil moisture measurements and modeling for validating AMSR-E soil moisture products. *Paper presented at the 17th Conference on Hydrology, the Annual Meeting of the American Meteorological Society*, 9-13 February 2003, Long Beach, CA.

Le Toan, T., Davidson, M., Borderies, P., Chenerie, I., Mattia, F., Manninen, T., Borgeaud, M., 1998. Improved observation and modeling of bare soil surfaces for soil moisture retrieval. *Paper presented at the workshop on Retrieval of Bio- and Geo- physical Parameters from SAR Data for Land Applications, 21-23 October, 1998, ESTEC, The Netherlands.* Proceedings available at the web site http://conferences.esa.int/98c07/abstracts/A016.HTM

Lee, R., Kastens, L. A., Price, L. P., and Martinko, E. A., 2000. Forecasting corn yield in Iowa using remotely sensed data and vegetation phenology information. *Proceedings, International Conference on Geospatial Information in Agriculture and Forestry*, 10–12 Jan. 2000, Lake Buena Vista, FL. ERIM Int., Ann Arbor, MI.

Li, Z. L., and Becker, F., 1993. Feasibility of land surface temperature and emissivity determination from AVHRR data. *Remote Sensing of Environment*, **43**:67-85.

Li, F., and Lyons, T. J., 2002. Remote estimation of regional evapotranspiration. *Environmental Modelling and Software,* **17**: 61-75.

Li, J., and Islam, S., 2002. Estimation of root zone soil moisture and surface fluxes partitioning using near surface soil moisture measurements. *Journal of Hydrology,* **259(1-4)**: 1-14.

Li, L., Njoku, E. G., Im, E., Chang, P. S., and Germain, K. S., 2004. A preliminary. survey of radio-frequency interference over the U.S. in Aqua AMSR-E data. *IEEE Transactions on Geoscience and Remote Sensing*, **42**:380-390.

Li, X., Wang, J., and Strahler, A. H., 1999. Scale effects and scaling-up by geometric-optical model. *International Geoscience and Remote Sensing Symposium (IGARSS),* **3**: 1875-1877.

Liang, S., 2000. Inversion of land surface temperature and emissivity simultaneously from multispectral thermal infrared imagery. *Proceedings of 2000 International Geosciences and Remote Sensing Symposium (IGARSS)*, 24-28, July, Honolulu, Hawaii, Vol. VII, 3133-3135.

Liang, S., 2001. An optimization algorithm for separating land surface temperature and emissivity from multispectral thermal infrared imagery. *IEEE Transactions on Geoscience and Remote Sensing,* **39(2)**: 264-274.

Liang, X., Xie, Z., and Huang, M., 2003. A new parameterization for surface and groundwater interactions and its impact on water budgets with the variable infiltration capacity (VIC) land surface model. *Journal of Geophysical Research* **108(16)**, 8613, doi:10.1029/2002JD003090.

Liu, H.Q., and Huete, A.R., 1995. A feedback based modification of the NDVI to minimize canopy background and atmospheric noise. IEEE *Transactions on Geoscience and Remote Sensing,* **33**:457-465.

Luquet, D., Vidal, A., Dauzat, J., Begue, A., Olioso, A., and Clouvel, P., 2004. Using directional TIR measurements and 3D simulations to assess the limitations and opportunities of water stress indices. *Remote Sensing of Environment*, **90(1)**: 53-62.

Manaka, I. M., 2005. AMSR/AMSR-E data processing status at JAXA/EOC. *Joint AMSR Science Team Meeting at Hawaii, September 13-15*, 10p.

Martinez-Fernandez, J., and Ceballos, A., 2003. Temporal stability of soil moisture in a large-field experiment in Spain. *Soil Science Society of America Journal,* **67(6)**: 1647-1656.

Martinez-Fernandez, J., and Ceballos, A., 2005. Mean soil moisture estimation using temporal stability analysis. *Journal of Hydrology,* **312(1-4)**: 28-38.

Mätzler, C. and Standley, A., 2000. Relief effects for passive microwave remote sensing, *International Journal of Remote Sensing*, **21**:2403-2412.

McCabe, M. F., and Wood, E. F., 2006. Scale influences on the remote estimation of evapotranspiration using multiple satellite sensors. *Remote Sensing of Environment*, **105(4)**: 271-285.

McCabe, M. F., Gao, H., and Wood, E. F., 2005. Evaluation of AMSR-E-derived soil moisture retrievals using ground-based and PSR airborne data during SMEX02. *Journal of Hydrometeorology*, **6(6)**: 864-877.

McVicar, T. R., and Jupp, D. L. B., 1999. Using AVHRR Data and Meteorological Surfaces as Covariates to Spatially Interpolate Moisture Availability in the Murray-Darling Basin. *CSIRO Land and Water Technical Report No. 50/99,* Canberra, Australia.

McVicar, T. R., and Jupp, D. L. B., 2002. Using covariates to spatially interpolate moisture availability in the Murray-Darling Basin. *Remote Sensing of Environment,* **79(2-3)**: 199-212.

Merot, P., Crave, A., and Gascuel-Odoux, C., 1994. Effect of saturated areas on backscattering coefficient of the ERS-1 synthetic aperture radar: First results. *Water Resources Research*, **30(2)**:175-179.

Merz, B., and Plate, E. J. 1997. An analysis of the effects spatial variability of soil and soil moisture on runoff. *Water Resources Research,* **33**: 2909-2922

Mo, T., Choudhury, B. J., Schmugge, T. J., and Jackson, T. J., 1982. A model for microwave emission from vegetation-covered fields. *Journal of Hydrology*, **184**:101–129.

Mohanty, B. P., and Skaggs, T. H., 2001. Spatio-temporal evolution and time-stable characteristics of soil moisture within remote sensing footprints with varying soil, slope, and vegetation. *Advances in Water Resources*, **24(9-10)**: 1051-1067.

Mohanty, B. P., Skaggs, T. H., and Famiglietti, J. S., 2000. Analysis and mapping of field-scale soil moisture variability using high-resolution, ground-based data during the Southern Great Plains 1997 (SGP97) Hydrology Experiment. *Water Resources Research,* **36**: 1023.

Molenaar, M., 1998. An Introduction to the theory of spatial object modelling for GIS. Taylor & Francis.

Moore, I. D., Burch, G. J., and Mackenzie, D. H., 1988. Topographic effects on the distribution of surface soil water and the location of ephemeral gullies. *Transactions of the American Society of Agricultural Engineering*, **31**:1098–107.

Moran, M. S., Clarke, T. R., Inoue, Y., and Vidal, A., 1994. Estimating crop water deficit using the relation between surface-air temperature and spectral vegetation index. *Remote Sensing of Environment,* **49**: 246-263.

Moran, M. S., Rahman, A. F., Washburne, J. C., Goodrich, D. C., Weltz, M. A., and Kustas, W. P., 1996. Combining the Penman-Monteith equation with measurements of surface temperature and reflectance to estimate evaporation rates of semiarid grassland. *Agricultural and Forest Meteorology,* **80**: 87-109.

Narayan, U., and Lakshmi, V., 2005. A simple method for spatial disaggregation of radiometer derived soil moisture using high resolution radar observations, *Journal of Electromagnetic Wave Applications*, **19(13)**:1711-1719.

Nemani, R. R., and Running, S. W., 1989. Estimation of regional surface resistance to evapotranspiration from NDVI and thermal IR AVHRR data. *Journal of Applied Meteorology,* **28:**276-284.

Njoku, E. G., 1999. AMSR Land Surface Parameters: Surface Soil Moisture-Land Surface Temperature-Vegetation Water Content: Algorithm Theoretical Basis Document (Version 3.0), Jet Propulsion Laboratory, California Institute of Technology.

Njoku, E. G., and Entekhabi, D., 1995. Passive microwave remote sensing of soil moisture. *Journal of Hydrology,* **184**: 101-129.

Njoku, E. G. and Kong, J., 1977. Theory of passive microwave remote sensing of near-surface soil moisture. *Journal of Geophysical Research,* **82**:3108–3118.

Njoku, E. G., and Li, L., 1999. Retrieval of land surface parameters using passive microwave measurements at 6 to 18 GHz. *IEEE Transactions on Geoscience and Remote Sensing,* **37**: 79-93.

Njoku, E. G., Jackson, T. J., Lakshmi, V., Chan, T. K., and Nghiem, S. V., 2003. Soil moisture retrieval from AMSR-E (Advanced Microwave Scanning Radiometer). *IEEE Transactions on Geoscience and Remote Sensing,* **41(2)**: 215-229.

Norman, J. M., Divakarla, M., and Goel, N. S., 1995. Algorithms for extracting information from remote thermal-IR observations of the earth's surface. *Remote Sensing of Environment,* **51**: 157-168.

Nyberg, L., 1996. Spatial variability of soil water content in the covered catchment at Gardsjon, Sweden. *Hydrological Processes*, **10**: 89-103.

Or, D., and Wraith, J. M., 1999. Temperature effects on soil bulk dielectric permittivity measured by time domain reflectometry: A physical model. *Water Resources Research,* **35**:371-383.

Owe, M., De Jeu, R. M., and Walker, J., 2001. A methodology for surface soil moisture and vegetation optical depth retrieval using the microwave polarization difference index. *IEEE Transactions on Geoscience and Remote Sensing,* **39(8)**: 1643-1654.

Parde, M., Wigneron, J. P., Chanzy, A., Waldteufel, P., Kerr, Y., and Huet, S., 2003. Retrieving surface soil moisture over a wheat field: Comparison of different methods. *Remote Sensing of Environment,* **87(2-3)**: 334-344.

Parkinson, C. L., 2003. Aqua: An earth-observing satellite mission to examine water and other climate variables. *IEEE Transactions on Geoscience and Remote Sensing,* **41(2)**: 173-183.

Pellenq, J., Kalma, J. D., Boulet, G., Saulnier, G. M., Wooldridge, S., Kerr, Y., 2003. A disaggregation scheme for soil moisture based on topography and soil depth. *Journal of Hydrology,* **276(1-4)**: 112-127.

Peplenski, N., Ulaby, F., and Dobson, M., 1995. Dielectric properties of soils in the 0.3-1.3 GHz range. *IEEE Transactions on Geoscience and Remote Sensing,* **33**:803–807.

Perry, C. A., and Lautenschlager, L. P., 1984. Functional equivalence of spectral vegetation indices. *Remote Sensing of Environment,* **14**:169-182.

Price, J. C., 1980. The potential of remotely sensed thermal infrared data to infer surface soil moisture and evaporation. *Water Resources Research,* **16(4)**: 787-795.

Price, J. C., 1984. Land surface temperature measurements from the split window channels of the NOAA-7/AVHRR. *Journal of Geophysics Research,* **89**: 7231-7237.

Price, J. C., 1990, Using spatial context in satellite data to infer regional scale evapotranspiration. *IEEE Transactions on Geoscience and Remote Sensing*, 28:940–948.

Prihodko, L., and Goward, S. N., 1997. Estimation of air temperature from remotely sensed surface observations. *Remote Sensing of Environment*, **60(3)**: 335-346.

Qi J., Huete A. R., Kerr Y. J., and Sorooshian S., 1994. A Modified Soil Adjusted Vegetation Index, *Remote Sensing of Environment*, **48**:119-126.

Qiu, Y., Fu, B., Wang, J., and Chen, L., 2001. Soil moisture variation in relation to topography and land use in a hillslope catchment of the Loess Plateau, China. *Journal of Hydrology*, **240(3-4)**: 243-263.

Quesney, A., Le Hégarat-Mascle, S., Taconet, O., Vidal-Madjar, D., Wigneron, J.P., Loumagne, C., Normand, M., 2000. Estimation of watershed soil moisture index from ERS/SAR data. *Remote Sensing of Environment*, **72(3)**:290-303.

Ragab, R., 1995. Towards a continuous operational system to estimate the root-zone soil moisture from intermittent remotely sensed surface moisture. *Journal of Hydrology*, **173(1-4)**: 1-25.

Reichle, R. H., Entekhabi, D., and McLaughlin, D. B., 2001a. Downscaling of radio brightness measurements for soil moisture estimation: A four-dimensional variational data assimilation approach. *Water Resources Research*, **37(9)**: 2353-2364.

Reichle, R. H., McLaughlin, D. B., and Entekhabi, D., 2001b. Variational data assimilation of microwave radiobrightness observations for land surface hydrology applications. *IEEE Transactions on Geoscience and Remote Sensing*, **39(8)**: 1708-1718.

Reichle, R.H., Walker, J.P., Koster, R.D., and Houser, P.R., 2002. Extended versus ensemble Kalman Filtering for land data assimilation, *Journal of Hydrometerology*, **3**:728-740.

Reynolds, S. G., 1970. The gravimetric method of soil moisture determination Part III: An examination of factors influencing soil moisture variability. *Journal of Hydrology*, **11(3)**: 288-300.

Robinson, M., and Dean, T. J., 1993. Measurement of near surface soil water content using a capacitance probe. *Hydrological Processors*, **7**:77–86.

Rodhe, A., and Seibert, J., 1999. Wetland occurrence in relation to topography: a test of topographic indices as moisture indicators. *Agricultural and Forest Meteorology*, **98-99**: 325-340.

Rodriguez-Iturbe, I., 2000. Ecohydrology: a hydrologic perspective of climate-soil-vegetation dynamics. *Water Resources Research*, **36(1)**:3-9.

Roth, K., Schulin, R., Flühler, H., and Attinger, W., 1990. Calibration of time domain reflectrometry for water content measurement using a composite dielectric approach. *Water Resources Research*, **26(10)**: 2267-2273.

Rüdiger, C., Davidson, R. E., Hemakumara, H. M., Walker, J. P., Kalma, J. D., and Willgoose, G. R., 2003. Catchment monitoring for scaling and assimilation of soil moisture and streamflow. *Proceedings of the International Congress on Modelling and Simulation (MODSIM)*, Modelling and Simulation Society of Australia and New Zealand, Inc., Townsville, Australia, 14-17 July 2003, 1:386-391.

Rüdiger, C., Hemakumara, H. M., Jacobs, B., Kalma, K.D., Walker, J. P., Willgoose, G. R., Martinez, C., Hancock, G., Thyer, M., and Wells T., in review. The Goulburn River Experimental (GoRex) catchment data set, submitted to *Water Resources Research*.

Russo, D., and Jury, W.A., 1987. A theoretical study of the estimation of the correlation scale in spatially-variable fields: I. Stationary fields. *Water Resources Research,* **23**: 1257-1268.

Sabin, F. F., 1997. Remote Sensing: Principles and Interpretation (Third ed.), W.H. Freeman and Company, NY.

Sandholt, I., Rasmussen, K., and Andersen, J., 2002. A simple interpretation of the surface temperature/vegetation index space for assessment of surface moisture status. *Remote Sensing of Environment,* **79(2-3)**: 213-224.

Sano, E. E., Huete, A. R., Troufleau, D., Moran, M. S., and Vidal, A., 1998. Relation Between ERS-1 Synthetic Aperture Radar Data and Measurements of Surface Roughness and Moisture Content of Rocky Soils in a Semiarid Rangeland. *Water Resources Research*, **34(6)**: 1491-1498.

Schmidt, F., 2002. TOPOCROP.AVX, version 1.2. ArcView script file for deriving topographic indices from a DEM grid. Retrieved from web site http://arcscripts.esri.com/ on 7 July 2004.

Schmugge, T. J., 1998. Applications of passive microwave observations of surface soil moisture. *Journal of Hydrology*, **212-213(1-4)**: 188-197.

Schmugge, T. J., Jackson, T. J., and McKim, H. L., 1980. Survey of methods for soil moisture determination. *Water Resources Research,* **16(6)**: 961-979.

Schmugge, T. J., Kustas, W. P., Ritchie, J. C., Jackson, T. J., and Rango, A., 2002. Remote sensing in hydrology. *Advances in Water Resources,* **25(8-12)**: 1367-1385.

Schulze, R., 2000. Transcending scales of space and time in impact studies of climate and climate change on agrohydrological responses. *Agriculture, Ecosystems and Environment,* **82(1-3)**: 185-212.

Scott, C. A., Bastiaanssen, W. G. M., and Ahmad, M. D., 2003. Mapping spatio-temporal distribution of soil moisture throughout irrigated watersheds using optical and high resolution imagery. *ASCE Irrigation and Drainage Engineering*, **129(5)**: 326-335.

Sellers, P. J., Heiser, M. D., Hall, F. G., Verma, S. B., Desjardins, R. L., Schuepp, P. M., 1997. The impact of using area-averaged land surface properties -topography, vegetation condition, soil wetness- in calculations of intermediate scale (approximately 10 km^2) surface-atmosphere heat and moisture fluxes. *Journal of Hydrology*, **190(3-4)**: 269-301.

Sellers, P. J., Berry, J. A., Collatz, G. J., Field, C. B., and Hall, F. G., 1992. Canopy reflectance, photosynthesis, and transpiration. III. A reanalysis using improved leaf models and a new canopy integration scheme. *Remote Sensing of the Environment,* **42**:187-216.

Seyfried, M., 1998. Spatial variability constraints to modeling soil water at different scales. *Geoderma*, **85(2-3)**: 231-254.

Seyfried, M.S., and Murdock, M.D., 2001. Response of a new soil water sensor to variable soil, water content, and temperature. *Soil Science Society of America Journal*, **65**:28-34.

Seyfried, M.S., and Murdock, M.D., 2004. Measurement of soil water content with a 50-MHz soil dielectric sensor. *Soil Science Society of America Journal,* **68**:394-403.

Seyfried, M.S., and Wilcox, B.P., 1995. Scale and the nature of spatial variability: field examples having implications for hydrological modeling. *Water Resources Research*, **31(1)**: 173-184.

Sikorski, R. J., and Kealy, P. S., 2002. Land surface temperature: Visible/infrared imager/radiometer suit, Algorithm theoretical basis document. Raytheon Systems Company, Lanham, MD, 37p.

Singh, V.P. 1995. Watershed Modeling. In: Singh, V.P. (Ed), *Computer Models of Watershed Hydrology*, Water Resources Publications, Colorado, 1-22.

Sivapalan, M., and Jeevaraj, C. G. 1992. Scaling of hydrologic parameterizations: 2. Derivation of catchment scale runoff prediction equation from point-scale, processed-based description. *Report DE 614MS*, Centre for Water Research, University of Western Australia.

Sivapalan, M., Wood, E. F., 1986. Spatial heterogeneity and scale in the infiltration response of catchments. In: Gupta, V. K., Rodriguez-Iturbe, I., and Wood, E. F. (Eds), *Scale Problems in Hydrology*, D. Reidel, Dordrecht, 81-106.

Skøien, J. O., Blöschl, G., and Western, A. W., 2003. Characteristic space scales and timescales in hydrology. *Water Resources Research,* **39(10),** 1304, doi:10.1029/2002WR001736

Smith, R. C. G., and Choudhury, B. J., 1991. Analysis of normalized difference and surface temperature observations over southeastern Australia. *International Journal of Remote Sensing,* **12(10)**: 2021-2044.

Sobrino, J. A., Li, Z.-L., Stoll, M. P., and Becker, F., 1994: Improvements in the split-window technique for land surface temperature determination. *IEEE Transactions on Geoscience and Remote Sensing*, **32(2)**: 243-253.

Soil Moisture Equipment Corporation, 1996. Trase System 1 operating instructions. Soil Moisture Equipment Corporation, Santa Barbara, California, 54pp.

Srivastava, H. S., Patel, P., Manchanda, M. L., and Adiga, S., 2003. Use of multiincidence angle RADARSAT-1 SAR data to incorporate the effect of surface roughness in soil moisture estimation, *IEEE Transactions on Geoscience and Remote Sensing*, **41(7)**:1638-1640.

Starks, P. J., Heathman, G. C., Jackson, T. J., and Cosh, M. H., 2006. Temporal stability of soil moisture profile. *Journal of Hydrology*, **324**: 400-411.

Starr, G. C., 2005. Assessing temporal stability and spatial variability of soil water patterns with implications for precision water management. *Agricultural Water Management*, **72(3)**: 223-243.

Stenger, R., Barkle, G., and Burgess, C., 2005. Laboratory calibration of water content reflectometers and their *in-situ* verification. *Australian Journal of Soil Research*, **43**:607-615.

Steyaert, L. T., 1993. A perspective on the state of environmental simulation modeling. In: Goodchild, M. F., Parks, B. O., and Steyaert, L. T., *Environmental Modelling with GIS*. Oxford University Press, 16-30.

Story, R., Galloway, R. W., and Van de Graaff, R. H. M., 1963. Land systems of the Hunter Valley. In: Story, R., Galloway, R. W., Van de Graaff, R. H. M. and Tweedie, A. (Eds), *General Report on the Lands of the Hunter Valley*, *Land Research Series: No. 8,* CSIRO, Melbourne.

Su, Z., Troch, P. A., de Troch, F. P., Nochtergale, L., and Cosyn, B., 1995. Preliminary results of soil moisture retrieval from ESAR (EMAC 94) and ERS-1/SAR, Part II: Soil moisture retrieval. In: de Troch, F. P., Troch, P. A., Su, Z., and Cosyn, B. (Eds.), *Proceedings of the second workshop on hydrological and microwave scattering modelling for spatial and temporal soil moisture mapping from ERS-1 and JERS-1 SAR data and macroscale hydrologic modelling*, Institute National de la Recherche Agronomique, Unité de Science du Sol et de Bioclimatologie, France, 7-19.

Su, Z., and Troch, P. A., 1996. Soil surface parameters and radar backscattering. *Paper presented at the 21st General Assembly of the European Geophysical Society*, The Hague 6-10 May, 1996.

Sulebak, J. R., Tallaksen, L. M., and Erichsen, B., 2000. Estimation of areal soil moisture by use of terrain data. *Geografiska Annaler Series A,* **82(1)**: 89-105.

Svetlitchnyi, A. A., Plotnitskiy, S. V., and Stepovaya, O. Y., 2003. Spatial distribution of soil moisture content within catchments and its modelling on the basis of topographic data. *Journal of Hydrology,* **277(1-2)**: 50-60.

Tansey, K. J., Millington, A. C., Battikhi, A. M., and White, K. H., 1999. Monitoring soil moisture dynamics using satellite imaging radar in northeastern Jordan. *Applied Geography,* **19(4)**: 325-344.

Tayler, D., 2003. WXtrack. Satellite tracking software retrieved on October 20, 2003, from web site at http://www.satsignal.net/.

Thattai, D., and Islam, S., 2000. Spatial analysis of remotely sensed soil moisture data. *Journal of Hydrologic Engineering,* **5(4)**: 386-392.

Topp, G. C., Davis, J. L., and Annan, A. P., 1980. Electromagnetic determination of soil water content measurements in coaxial transmission lines. *Water Resources Research,* **16(3)**: 574-582.

Tsegaye, T. D., Crosson, W. L., Laymon, C. A., Schamschula, M. P., and Johnson, A. B., 2003. Application of a neural network-based spatial disaggregation scheme for addressing scaling of soil moisture. In: Pachepsky, Y., Radcliffe, D. E., and Selim, H. M. (Eds), *Scaling methods in soil physics*, CRC Press, New York, 261-277.

Turner, M. G., 1989. Landscape Ecology: The effect of pattern on process, *Annual Review of Ecology and Systematics*, **20**: 171-197.

Ulaby, F. T., Dubois, P. C., and van Zyl, J., 1996. Radar mapping of surface soil moisture. *Journal of Hydrology,* **184**: 57-84.

Ulaby, F. T., Moore, R. K., and Fung, A. K., 1981. Microwave remote sensing - Active and passive, Volume I: Microwave remote sensing fundamentals and radiometry. Artech House, Norwood, MA, 456pp.

Ulaby, F. T., Moore, R. K., and Fung, A. K., 1986. Microwave remote sensing - Active and passive, Volume III: From theory to applications. Artech House, Norwood, MA, 1097pp.

Vachaud, G., De Sillans, A. P., Balabanis, P., and Vauclin, M., 1985. Temporal stability of spatially measured soil water probability density function. *Soil Science Society of America Journal*, **49**: 822-828.

Valor, E., and Caselles, V., 1996. Mapping land surface emissivity from NDVI: Application to European, African, and South American areas. *Remote Sensing of Environment,* **57**: 167-184.

Van de Griend, A. A., and Engman, E. T., 1985. Partial area hydrology and remote sensing. *Journal of Hydrology*, **81**: 211-251.

Van de Griend, A. A., and Owe, M., 1994a. The Influence of polarization on canopy transmission properties at 6.6 GHz and implications for large scale soil moisture monitoring in semi-arid environments. *IEEE Transactions on Geoscience and Remote Sensing*, **32**:409–415.

Van de Griend, A.A. and Owe. M., 1994b. Microwave vegetation optical depth and inverse modelling of soil emissivity using Nimbus/SMMR satellite observations. *Journal of Meteorology and Atmospheric Physics*, **54**:225-239.

Van de Griend, A. A., Camillo, P. J., and Gurney, R. J., 1985. Discrimination of soil physical parameters, thermal inertia, and soil moisture from diurnal surface temperature fluctuations. *Water Resources Research*, **21**: 997-1009.

Van Pelt, R. S., and Wierenga, P. J., 2001. Temporal stability of spatially measured soil matric potential probability density function. *Soil Science Society of America Journal*, **65**: 668-677.

Voltz, M., 1997. Spatial variability of soil moisture regimes at different scales: Implications in the context of precision agriculture, In: Precision Agriculture: Spatial and Temporal Variability of Environmental Quality. Wiley Publishers, 18-30.

Walker, J. P., 1999. Estimating soil moisture profile dynamics from near-surface soil moisture measurements and standard meteorological data. *Unpublished PhD dissertation*, University of Newcastle, Newcastle.

Walker, J. P., and Houser, P.R., 2001. A methodology for initialising soil moisture in a global climate model: Assimilation of near-surface soil moisture observations. *Journal of Geophysical Research*, **106(D11)**:11761-11774.

Walker, J. P., Grayson, R. B., Panciera, R., Zhan, X., and Houser, P. R., 2003. AMSR-E soil moisture validation efforts in the Australian arid zone. *Paper presented at the AGU Fall meeting*, 8-12 December, San Francisco.

Walker, J. P., Willgoose, G. R., and Kalma, J. D., 2001. One-dimensional soil moisture profile retrieval by assimilation of near-surface observations: a comparison of retrieval algorithms. *Advances in Water Resources*, **24(6)**: 631-650.

Walker, G. R., and Zhang, L., 2002. Plot-scale models and their application to recharge studies. In: Zhang, L., and Walker, G. (Eds), *Studies in catchment hydrology: the basics of recharge and discharge*, CSIRO, 36pp.

Wallender, W. W., and Grismer, M. E., 2002. Irrigation hydrology: Crossing scales. *Journal of Irrigation and Drainage Engineering ASCE*, **128(4)**:203-211

Wan, Z., 1999. MODIS land surface temperature: Algorithm theoretical basis document (LST ATBD), LST calculations. Retrieved 20 May 2005 from web site at: http://modis.gsfc.nasa.gov/data/atbd/atbd_mod11.pdf.

Wan, Z., Wang, P., and Li, X., 2004. Using MODIS land surface temperature and normalized difference vegetation index products for monitoring drought in the southern Great Plains USA. *International Journal of Remote Sensing*, **25(1)**: 61-72.

Wan, Z. M., and Dozier, J., 1989. Land-surface temperature measurement from space: Physical principles and inverse modeling. *IEEE Transactions on Geoscience and Remote Sensing*, **27**: 268-278.

Wan, Z. M., and Dozier, J., 1996. A generalized split-window algorithm for retrieving land-surface temperature from space, *IEEE Transactions on Geoscience and Remote Sensing* **34**:892-899

Wang, C., Qi, J., Moran, S., and Marsett, R., 2004. Soil moisture estimation in a semiarid rangeland using ERS-2 and TM imagery. *Remote Sensing of Environment*, **90(2)**: 178-189.

Wang, J. R., 1983. Passive microwave sensing of soil moisture content: The effects of soil bulk density and surface roughness. *Remote Sensing of Environment*, **13**:329–344.

Wang, J. R. and Choudhury, B. J., 1981. Remote sensing of soil moisture content over bare field at 1.4 GHz frequency. *Journal of Geophysical Research*, **86**:5277–5282.

Wang, J. R., and Schmugge, T. J., 1980. An empirical model for the complex dielectric permittivity of soils as a function of water content. *IEEE Transactions on Geoscience and Remote Sensing*, **GE-18(4)**: 288-295.

Wang, P. X., Li, X. Gong, J. Y. and Song, C. 2001. Vegetation temperature condition index and its application for drought Monitoring. *IEEE 2001 International Geoscience And Remote Sensing Symposium (IGARSS)*, 9-13 July 2001, The University of New South Wales, Sydney, Australia.

Watson, K., 1992. Two-temperature method for measuring emissivity. *Remote Sensing of Environment*, **42**:117-121.

Weidong, L., Baret, F., Xingfa, G., Qingxi, T., Lanfen, Z., and Bing, Z., 2002. Relating soil surface moisture to reflectance. *Remote Sensing of Environment,* **81(2-3)**: 238-246.

Wen, J., Su, Z., and Ma, Y., 2003. Determination of land surface temperature and soil moisture from tropical rainfall measuring mission/microwave imager remote sensing data. *Journal of Geophysical research*, **108 (D2)**, 4038, doi:10.1029/2002JD002176.

Western, A. W., and Blöschl, G., 1999. On the spatial scaling of soil moisture. *Journal of Hydrology,* **217(3-4)**: 203-224.

Western, A. W., and Grayson, R. B., 2001. Soil moisture and runoff processes at Tarrawarra. In: Grayson, R., and Blöschl, G. (Eds), *Spatial Patterns in Catchment Hydrology: Observations and Modelling,* Cambridge University press, Cambridge, 209-246.

Western, A., and Seyfried, M.S. 2005. Calibration and temperature correction of a capacitance-based soil-moisture sensor. *Hydrological Processes,* **19**:3785-3795.

Western, A. W., Blöschl, G., and Grayson, R. B., 1998a. How well do indicator variograms capture the spatial connectivity of soil moisture? *Hydrological Processes*, **12(12)**: 1851-1868.

Western, A. W., Blöschl, G., and Grayson, R. B., 1998b. Geostatistical characterisation of soil moisture patterns in the Tarrawarra catchment. *Journal of Hydrology,* **205(1-2)**: 20-37.

Western, A. W., Blöschl, G., and Grayson, R. B., 2001. Toward capturing hydrologically significant connectivity in spatial patterns. *Water Resources Research*, **37**(1): 83-97.

Western, A. W., Grayson, R. B., and Blöschl, G., 2002. Scaling of soil moisture: a hydrologic perspective. *Annual Review of Earth and Planetary Science,* **30**: 149-180.

Western, A. W., Grayson, R. B., Blöschl, G., Willgoose, G. R., and McMahon, T. A., 1999. Observed spatial organization of soil moisture and its relation to terrain indices. *Water Resources Research,* **35(3)**: 797-810.

Wigneron, J. P., Calvet, J. C., and Kerr, Y., 1996. Monitoring water interception by crop fields from passive microwave observations. *Agricultural and Forest Meteorology,* **80(2-4)**: 177-194.

Wigneron, J. P., Calvet, J. C., Pellarin, T., Van de Griend, A. A., Berger, M., and Ferrazzoli, P., 2003. Retrieving near-surface soil moisture from microwave radiometric observations: current status and future plans. *Remote Sensing of Environment,* **85(4)**: 489-506.

Wigneron, J. P., Schmugge, T., Chanzy, A., Calvet, J. C., and Kerr, Y., 1998. Use of passive microwave remote sensing to monitor soil moisture. *Agronomie*, **18(1)**: 27-43.

Wilding, L.P., and Drees, L.R., 1983. Spatial variability and pedology. In: Wilding, L.P., Smeck, N.E., and Hall, G.F. (Eds), *Pedogenesis and Soil Taxonomy: I. Concepts and Interactions*, Elsevier Science, New York, 83-116.

Williams, R. D., and Ahuja, L. R., 2003. Scaling and estimating the soil water characteristic using a one-parameter model. In: Pachepsky, Y., Radcliffe, D. E., and Selim, H. M. (Eds), *Scaling methods in soil physics*, CRC Press, New York, 35-48.

Wood, E. F., 1995. Scaling behaviour of hydrological fluxes and variables: Empirical studies using a hydrological model and remote sensing data. In: Kalma, J. D., and Sivapalan, M. (Eds), *Advances in Hydrological Process: Scale Issues in Hydrological Modelling*, John Wiley and Sons Ltd., Chichester, 89-104.

Wood, E. F., 1997. Effects of soil moisture aggregation on surface evaporative fluxes. *Journal of Hydrology*, **190(3-4)**: 397-412.

Wood, E. F., 2004. Land surface modeling studies in support of Aqua AMSR-E validation. *Paper presented at the AMSR-E Science Team Presentations*, September 2004, Ft. Collins, CO.

Wood, E. F., Lettenmaier, D., and Zartarian, V., 1992. A land-surface hydrology parameterization with subgrid variability for general circulation models. *Journal of Geophysics Research*, **97**: 2717-2728.

Wood, E. F., Sivapalan M, and Beven K., 1990. Similarity and scale in catchment storm response. *Reviews in Geophysics*, **28**: 1–18

Woods, R., Sivapalan, M., and Duncan, M., 1995. Investigating the representative elementary area concept: an approach based on field data. In: Kalma, J. D., and Sivapalan, M. (Eds), *Advances in Hydrological Process: Scale issues in hydrological modelling*, John Wiley & Sons Ltd, Chichester, 49-70.

Wood, E. F., Sivapalan M, Beven K., and Band, L., 1988. Effects of spatial variability and scale with implications to hydrological modeling. *Journal of Hydrology*, **102**:29-47.

Wüthrich, M., 1997. In-situ measurement and remote sensing of soil moisture using time domain reflectometry, thermal infrared and active microwaves. *Unpublished PhD Thesis*, Naturwissenschaftlichen Fakultät der Universität Basel.

Zegelin, S., 1996. Soil moisture measurement. *Paper presented at the Field measurement techniques in hydrology*, April 1-4, 1996, Corpus Christi College, Clayton.

ANNEX-I

Sample data logger program used to collect SWC, soil temperature and rainfall

```
;Program name : MC_3S_RF
;{CR10}
;{CR500}
;Data logger program for three CS616 + T107

;This program logs 3 CS616s and Temperature sensor and write data to logger
;at 20 minute time intervals as the average of a reading taken every
;one minute.
;A pluviometer is also logged. It is scanned every 1 second so that each tip
;of the raingauge is logged as it occurs.

;Programmer: Manju Hemakumara
;Version & Date- Version 3.0 - 25 November 2003
;Last modification: change Time interval from 10 minutes to 20 minutes
;Previous modification - 28 March 2003

;LOG FILE- Day, Hour/Min, Battery Voltage, Soil T, period 1-3
;         Day,Hour/Min,Sec: Rain

;Sensor connections

;T107
;       Red   - SE1
;       Black - E1
;       Purple- AG
;       Clear - G

;CS 616
;       Red all   - 12V
;       Black all - GND
;       Green 1   - SE2
;       Green 2   - SE3
;       Green 3   - SE4
;       Orange all- C1

;Rain gauge - P1 and G

*Table 1 Program
  01: 60       Execution Interval (seconds)
```

```
1:  Batt Voltage (P10)
 1: 2        Loc [ Battery   ]

2:  Temp (107) (P11)
 1: 1        Reps
 2: 1        SE Channel
 3: 1        Excite all reps w/E1
 4: 1        Loc [ TSoil     ]
 5: 1.0      Mult
 6: 0.0      Offset

3:  Do (P86)
 1: 41       Set Port 1 High

4:  Period Average (SE) (P27)
 1: 3        Reps
 2: 4        200 kHz Max Freq @ 2 V Peak to Peak, Period Output
 3: 2        SE Channel
 4: 100      No. of Cycles
 5: 1        Timeout (units = 0.01 seconds)
 6: 3        Loc [ period_1  ]
 7: 1.0      Mult
 8: 0.0      Offset

5:  Polynomial (P55)
 1: 3        Reps
 2: 3        X Loc [ period_1  ]
 3: 6        F(X) Loc [ VWC_1     ]
 4: -0.0663  C0
 5: -0.0063  C1
 6: 0.0007   C2
 7: 0.0      C3
 8: 0.0      C4
 9: 0.0      C5

6:  Do (P86)
 1: 51       Set Port 1 Low

;every 20 minute write data to final storage area

7:  If time is (P92)
 1: 0000     Minutes (Seconds --) into a
 2: 20       Interval (same units as above)
 3: 10       Set Output Flag High (Flag 0)

8:  Real Time (P77)
```

```
 1: 0110     Day,Hour/Minute (midnight = 0000)

9:  Average (P71)
 1: 1        Reps
 2: 2        Loc [ Battery   ]

10:  Average (P71)
 1: 1        Reps
 2: 1        Loc [ TSoil     ]

11:  Average (P71)
 1: 3        Reps
 2: 3        Loc [ period_1  ]

*Table 2 Program
  02: 1        Execution Interval (seconds)

;Rainfall measurement (mm)

1:  Pulse (P3)
 1: 1        Reps
 2: 1        Pulse Input Channel
 3: 2        Switch Closure, All Counts
 4: 9        Loc [ Rain      ]
 5: .2       Mult
 6: 0.0      Offset

;Check if rainfall has occured

2:  IF (X<=>F) (P89)
 1: 9        X Loc [ Rain      ]
 2: 3        >=
 3: 0.2      F
 4: 10       Set Output Flag High

3:  Real Time (P77)
 1: 0111     Day,Hour/Minute,Seconds (midnight = 0000)

4:  Sample (P70)
 1: 1        Reps
 2: 9        Loc [ Rain      ]

*Table 3 Subroutines

End Program
```

Sample data logger program used at the Stanley climate station

```
;{CR10}
;
;         PROGRAM NAME:  SC_WETHR.CSI
;=============================================================
;    This program logs 2 heat flux plates, 8 soil temperature sensors,
;    relative humidity and air temperature,
;    atmospheric pressure, wind speed, pyranometer and net radiometer
;    at 20 MINUTES INTERVAL
;    as the average of a READING TAKEN EVERY 1 MINUTE
;    A pluviometer is also logged. It is SCANNED EVERY 1 SECOND
;    so that each tip of the raingauge is logged as it occurs.
;
;    LOG FILE:
;    Day,Hour/Min: Flux#1..2, S_Temp#1..8, RH, Air_Temp, Press, Wind ,
;     Net_Rad, Rn
;    Day,Hour/Min,Sec: Rain
;
;    PROGRAMMER:  Manju Hemakumara, University of Newcastle
;    LAST MODIFIED: 7/08/03
;=============================================================
;
; WIRING:
; Logger to Multiplexer connections
;     12V - 12V
;     G   - GND
;     C1  - RES
;     C2  - CLK
;     1H  - COM H1 (SE CHANNEL 1)
;     1L  - COM L1 (SE CHANNEL 2)
;     G   - SHIELD
;     C5  - COM H2
;     E1  - COM L2
;     G   - SHIELD
;
; Multiplexer Conections
;     Sets 1 and 2 - Heat Flux Plates (DIF measurements)
;                L1 - White
;                H1 - Black
;                    Clear to AG
;
;     Sets 3 to 8 - Soil Temp. Sensors, two per set (SE measurements)
;                 H1 - Red 1
```

```
;                L1 - Red 2
;                L2 - Black 1 + 2
;            SHIELD - Clear 1 + 2
;                    Purple to AG
;
; Logger Conections
;     RH and Air Temp
;         3H - Green(RH)
;         3L - Orange(Temp)
;         E2 - Yellow(Power control)
;         E3 - Black(Temp. exitation)
;         12V - Red
;         G - Clear
;         AG - White + Purple
;
;     Atmospheric Pressure
;         4H - Brown
;         4L - White
;         12V - Red
;         G - Black
;         C8 - Green
;         G - Clear
;
;     Net Radiometer
;         5H - Red
;         5L - Black
;         5L - AG (Jumper)
;         G - Clear
;
;     Pyranometer
;         6H - Red
;         6L - Black
;         AG - White
;         G  - Clear
;
;     Anemometer
;         P1 - Black
;         G - White + Clear
;
;     Tipping Bucket Raingauge
;         P2 - Blue
;         G - Brown
;
;     (Note: Pulse counting sensors must be in same execution table)

*Table 1 Program  ;READ SENSORS EVERY MINUTE
```

```
 01: 60.0      Execution Interval (seconds)

; CONFIGURE PORTS

1:  Set Port(s) (P20)
 1: 7997     C8..C5 = output/nc/nc/output
 2: 7747     C4..C1 = output/output/10ms/output

;=====================================================
; MEASUREMENTS FROM SENSORS CONNECTED TO MULTIPLEXER
;=====================================================
;ACTIVATE MULTIPLEXER

2:  Do (P86)
 1: 41       Set Port 1 High

;multiplexer clock -pulse control port 2
3:  Do (P86)
 1: 72       Pulse Port 2

;BEGIN SOIL HEAT FLUX MEASUREMENT LOOP

4:  Beginning of Loop (P87)
 1: 0        Delay
 2: 2        Loop Count

5:  Do (P86)
 1: 72       Pulse Port 2

6:  Excitation with Delay (P22)
 1: 1        Ex Channel
 2: 0        Delay W/Ex (units = 0.01 sec)
 3: 1        Delay After Ex (units = 0.01 sec)
 4: 0        mV Excitation

;SOIL HEAT FLUX MEASUREMENT INSTRUCTION (W/m^2)

7:  Volt (Diff) (P2)
 1: 1        Reps
 2: 3        ñ 25 mV Slow Range
 3: 1        DIFF Channel
 4: 1     -- Loc [ FLUX_1    ]
 5: 1        Mult
 6: 0        Offset

;END OF HEAT FLUX PLATE MEASUREMENT LOOP
```

```
8:  End (P95)

;BEGIN SOIL TEMPERATURE MEASUREMENT LOOP

9:  Beginning of Loop (P87)
 1: 0        Delay
 2: 4        Loop Count

10:  Do (P86)
 1: 72       Pulse Port 2

11:  Excitation with Delay (P22)
 1: 1        Ex Channel
 2: 0        Delay W/Ex (units = 0.01 sec)
 3: 1        Delay After Ex (units = 0.01 sec)
 4: 0        mV Excitation

12:  Step Loop Index (P90)
 1: 2        Step

;SOIL TEMPERATURE MEASUREMENT INSTRUCTION (DEG C)

13:  Temp (107) (P11)
 1: 2        Reps
 2: 1        SE Channel
 3: 1        Excite all reps w/Exchan 1
 4: 3     -- Loc [ S_TEMP_1  ]
 5: 1        Mult
 6: 0        Offset

;END OF SOIL TEMPERATURE MEASUREMENT LOOP

14:  End (P95)

;DEACTIVATE MULTIPLEXER

15:  Do (P86)
 1: 51       Set Port 1 Low
;==============================================================
; END OF MEASUREMENTS FROM SENSORS CONNECTED TO
MULTIPLEXER
;==============================================================

;APPLY FLUX PLATE CALIBRATION FACTORS
16:  Z=X*F (P37)
 1: 1        X Loc [ FLUX_1    ]
 2: 44.2     F
```

```
 3: 1        Z Loc [ FLUX_1    ]

17:  Z=X*F (P37)
 1: 2        X Loc [ FLUX_2    ]
 2: 48.7     F
 3: 2        Z Loc [ FLUX_2    ]

;=================================================
; MEASUREMENTS FROM DIRECTLY CONNECTED SESSORS
;=================================================

; RELATIVE HUMIDITY MEASUREMENT INSTRUCTION (%)
18:  Excite-Delay (SE) (P4)
 1: 1        Reps
 2: 5        ñ 2500 mV Slow Range
 3: 5        SE Channel
 4: 2        Excite all reps w/Exchan 2
 5: 15       Delay (units 0.01 sec)
 6: 2500     mV Excitation
 7: 11       Loc [ RH        ]
 8: .1       Mult
 9: 0        Offset

;AIR TEMPERATURE MEASUREMENT INSTRUCTION (DEG C)
19:  Temp (107) (P11)
 1: 1        Reps
 2: 6        SE Channel
 3: 3        Excite all reps w/Exchan 3
 4: 12       Loc [ AIR_TEMP  ]
 5: 1        Mult
 6: 0        Offset

;ATMOSPHERIC PRESSURE MEASUREMENT INSTRUCTION (kPa)
;Turn the sensor on
20:  Do (P86)
 1: 48       Set Port 8 High

;Delay 1s before taking measurement
21:  Excitation with Delay (P22)
 1: 1        Ex Channel
 2: 0        Delay W/Ex (units = 0.01 sec)
 3: 100      Delay After Ex (units = 0.01 sec)
 4: 0        mV Excitation

;Measure in Millibars
22:  Volt (Diff) (P2)
 1: 1        Reps
```

```
 2: 25       ñ 2500 mV 60 Hz Rejection Range
 3: 4        DIFF Channel
 4: 13       Loc [ PRESS    ]
 5: .184     Mult
 6: 600      Offset

;Convert to kPa
23:  Z=X*F (P37)
 1: 13       X Loc [ PRESS    ]
 2: .1       F
 3: 13       Z Loc [ PRESS    ]

;Turn the sensor off
24:  Do (P86)
 1: 58       Set Port 8 Low

;PYRANOMETER - INCOMING RADIATION Wm^2
25:  Volt (Diff) (P2)
 1: 1        Reps
 2: 22       7.5 mV 60 Hz Rejection Range
 3: 6        DIFF Channel
 4: 21       Loc [ Rn_Wm2    ]
 5: 200      Mult
 6: 0.0      Offset

;set negative values to zero

26:  IF (X<=>F) (P89)
 1: 21       X Loc [ Rn_Wm2    ]
 2: 4        <
 3: 0        F
 4: 30       Then Do

27:  Z=F (P30)
 1: 0.0      F
 2: 00       Exponent of 10
 3: 21       Z Loc [ Rn_Wm2    ]

28:  End (P95)

;NET RADIOMETER MEASUREMENT INSTRUCTION (W/m^2)
29:  Volt (Diff) (P2)
 1: 1        Reps
 2: 24       ñ 250 mV 60 Hz Rejection Range
 3: 5        DIFF Channel
 4: 15       Loc [ NET_RAD   ]
 5: 1        Mult
```

```
 6: 0       Offset

;Check if net radiation is positive or negative

30:  If (X<=>F) (P89)
 1: 15      X Loc [ NET_RAD   ]
 2: 3       >=
 3: 0       F
 4: 30      Then Do

;Apply the positive calibration and wind speed corrections
31:  Do (P86)
 1: 1       Call Subroutine 1

32:  Else (P94)

;Apply the negative calibration and wind speed corrections
33:  Do (P86)
 1: 2       Call Subroutine 2

34:  End (P95)

;=====================================================
; END OF MEASUREMENTS FROM DIRECTLY CONNECTED SESSORS
;=====================================================
;LOG AVERAGED READINGS OVER 20 MINUTES READING PERIOD
35:  If time is (P92)
 1: 0       Minutes (Seconds --) into a
 2: 20      Interval (same units as above)
 3: 10      Set Output Flag High

36:  Real Time (P77)
 1: 0110    Day,Hour/Minute (midnight = 0000)

37:  Average (P71)
 1: 2       Reps
 2: 1       Loc [ FLUX_1    ]

38:  Average (P71)
 1: 8       Reps
 2: 3       Loc [ S_TEMP_1  ]

39:  Average (P71)
 1: 1       Reps
 2: 11      Loc [ RH        ]

40:  Average (P71)
```

```
 1: 1       Reps
 2: 12      Loc [ AIR_TEMP  ]

41:  Average (P71)
 1: 1       Reps
 2: 13      Loc [ PRESS     ]

42:  Average (P71)
 1: 1       Reps
 2: 14      Loc [ WIND      ]

43:  Average (P71)
 1: 1       Reps
 2: 15      Loc [ NET_RAD   ]

44:  Average (P71)
 1: 1       Reps
 2: 21      Loc [ Rn_Wm2    ]

45:  Serial Out (P96)
 1: 71      SM192/SM716/CSM1

*Table 2 Program ;LOG THE TIPPING TIME OF PLUVIOMETER
  02: 1.0       Execution Interval (seconds)

;WIND SPEED MEASUREMENT INSTRUCTION (m/s)
;Note: All pulse readings must be done in the same table

1:  Pulse (P3)
 1: 1       Reps
 2: 1       Pulse Input Channel
 3: 21      Low Level AC, Output Hz
 4: 14      Loc [ WIND      ]
 5: .75     Mult
 6: .2      Offset

;RAINFALL MEASUREMENT INSTRUCTION (mm)

2:  Pulse (P3)
 1: 1       Reps
 2: 2       Pulse Input Channel
 3: 2       Switch Closure
 4: 20      Loc [ RAIN      ]
 5: .2      Mult
 6: 0       Offset

;LOG RAINFALL
```

```
;Check if rainfall has occured

3:  If (X<=>F) (P89)
 1: 20       X Loc [ RAIN      ]
 2: 3        >=
 3: 0.2      F
 4: 10       Set Output Flag High

4:  Real Time (P77)
 1: 0111     Day,Hour/Minute,Seconds (midnight = 0000)

5:  Sample (P70)
 1: 1        Reps
 2: 20       Loc [ RAIN      ]


*Table 3 Subroutines

;POSITIVE CALIBRATION AND WIND SPEED CORRECTIONS

1:  Beginning of Subroutine (P85)
 1: 1        Subroutine 1

;Calculate the wind speed correction factor
2:  Z=X*F (P37)
 1: 14       X Loc [ WIND      ]
 2: .2       F
 3: 16       Z Loc [ C         ]

3:  Z=X*F (P37)
 1: 16       X Loc [ C         ]
 2: .066     F
 3: 17       Z Loc [ A         ]

4:  Z=X+F (P34)
 1: 16       X Loc [ C         ]
 2: .066     F
 3: 18       Z Loc [ B         ]

5:  Z=X/Y (P38)
 1: 17       X Loc [ A         ]
 2: 18       Y Loc [ B         ]
 3: 19       Z Loc [ Corr_Fact ]

6:  Z=Z+1 (P32)
 1: 19       Z Loc [ Corr_Fact ]
```

```
;Apply positive zero wind calibration factor
7:  Z=X*F (P37)
 1: 15       X Loc [ NET_RAD   ]
 2: 9.16     F
 3: 15       Z Loc [ NET_RAD   ]

;Apply wind speed correction
8:  Z=X*Y (P36)
 1: 15       X Loc [ NET_RAD   ]
 2: 19       Y Loc [ Corr_Fact ]
 3: 15       Z Loc [ NET_RAD   ]

9:  End (P95)

;NEGATIVE CALIBRATION AND WIND SPEED CORRECTIONS

10:  Beginning of Subroutine (P85)
 1: 2        Subroutine 2

;Calculate the wind speed correction factor
11:  Z=X*F (P37)
 1: 14       X Loc [ WIND      ]
 2: .00174   F
 3: 17       Z Loc [ A         ]

12:  Z=X+F (P34)
 1: 17       X Loc [ A         ]
 2: .99755   F
 3: 19       Z Loc [ Corr_Fact ]

;Apply negative zero wind calibration factor
13:  Z=X*F (P37)
 1: 15       X Loc [ NET_RAD   ]
 2: 11.43    F
 3: 15       Z Loc [ NET_RAD   ]

;Apply wind speed correction
14:  Z=X*Y (P36)
 1: 15       X Loc [ NET_RAD   ]
 2: 19       Y Loc [ Corr_Fact ]
 3: 15       Z Loc [ NET_RAD   ]

15:  End (P95)

End Program
```

Annex – II: A. Monthly rainfall data (all SASMAS sites and BoM sites) in 2003.

Site_ID	Catchment	Name	Latitude	Longitude	Jan	Feb	Mar	Apr	May	Jun	Jul	Aug	Sep	Oct	Nov	Dec	Total
G1	Goulburn	Blue Wren Park	-32.3828	150.4894	20	109	8	66	2	34	32	95	7	86	65	64	584
K4	Krui	Pembroke	-31.9817	150.18	10	106	3	85	7	27	22	65	10	60	48	49	494
K6	Krui	Spring Hill	-31.8644	150.2061	17	165	4	133	16	29	38	122	18	78	51	103	774
S2	Krui	Stanley	-32.0958	150.1369	10	109	4	86	5	35	20	54	10	69	62	36	499
M1	Merriwa	Maram Park	-32.2417	150.3114													
M4	Merriwa	Kilwirrin	-32.0419	150.3964													
M7	Merriwa	The Echo	-31.8586	150.4672													
G4	Wollar	Cumbo	-32.4061	149.8822													
61075	Bow	Merriwa (Tunbridge)	-32.2229	150.2366	10	84	14	88	4	48	48	110	10	74	96	46	630
61287	Bow	Merriwa (Roscommon)	-32.1897	150.1728	10	86	10	87	6	48	17	110	7	75	89	43	588
61316	Bow	Merriwa (Mar-lea)	-32.0666	150.2326	15	93	20	87	3	31	20	99	11	72	51	46	548
62080	Bylong	Bylong (Heatherbrae)	-32.3580	150.0970	11	126	21	92	5	38	16	102	17	91	93	45	657
62100	Bylong	Nullo Mountain AWS	-32.7244	150.2290	17	161	30	72	39	66	46	144	10	95	99	64	842
62102	Bylong	Bylong (Bylong Road)	-32.5219	150.0811	9	138	25	66	2	43	24	125	11	75	123	27	665
62036	Goulburn	Ulan Post office	-32.2804	149.7425	9	112	40	118	1	51	27	131	12	104	120	34	759
61324	Hall	Gungal (Merryfields)	-32.2451	150.5130													
61002	Krui	Blackville (Krui Vale)	-31.8449	150.3410	22	75	9	132	43	48	16	117	19	83	77	128	769
61261	Krui	Merriwa (Bellview)	-31.9983	150.2420													
62015	Krui	Merriwa (Merry Vale)	-31.9273	150.2230	17	47	14	91	7	24	26	88	20	70	58	87	549
61040	Merriwa	Merriwa (Gummun Place)	-32.1388	150.3577	12	71	41	49	5	42	12	103	9	58	43	90	534
61073	Merriwa	Merriwa (Terragong)	-32.0780	150.3696	12	75	32	84	6	35	25	95	11	67	65	56	563
61400	Merriwa	Merriwa (Warra)	-32.1315	150.3639	11	59	26	80	7	43	19	89	7	58	41	90	530
62005	Munmurra	Cassilis Post office	-32.0067	149.9800	11	60	4	109	4	32	18	98	16	93	51	51	547
62009	Munmurra	Cassilis (Dalkeith)	-31.9963	149.9857	10	59	10	115	2	39	26	98	18	105	58	56	597
62032	Wollar	Wollar (Barrigan St)	-32.3592	149.9484	8	148	39	98	5	43	18	127	13	86	136	24	744
62056	Wollar	Wollar (Maree)	-32.4261	149.9535	8	189	42	89	8	49	24	131	13	70	145	41	809

Annex – II: A. Monthly rainfall data (all SASMAS sites and BoM sites) in 2003 continued.

Site_ID	Catchment	Name	Latitude	Longitude	Jan	Feb	Mar	Apr	May	Jun	Jul	Aug	Sep	Oct	Nov	Dec	Total
55006	Outside	Blackville Post office	-31.6414	150.2350	30	87	40	91	1	36	27	99	15	58	63	98	645
55017	Outside	Premer (Eden Moor)	-31.5711	149.7762	23	154	26	99	4	34	32	104	17	61	59	36	648
55025	Outside	Willow Tree (Highlands)	-31.7928	150.6730	0	23	6	79	71	50	32	105	28	57	20	136	606
55043	Outside	Willow Tree (Parraweena)	-31.7118	150.4135	28	96	21	99	2	48	20	92	19	95	62	115	695
55057	Outside	Willow Tree (Valais)	-31.7731	150.2856	15	60	38	89	4	25	25	121	15	76	41	138	646
55069	Outside	Yannergee (Dobroyd)	-31.4494	150.0247	18	64	28	88	2	32	28	82	8	61	49	50	510
55071	Outside	Premer Post office	-31.4568	149.9001	29	100	39	105	9	28	31	94	10	59	46	45	596
55248	Outside	Willow Tree (Kelverton)	-31.7249	150.5837	23	82	18	68	6	52	18	85	23	71	39	101	586
61007	Outside	Bunnan (Milhaven)	-32.0332	150.5836	10	98	13	71	19	24	30	91	9	67	92	61	585
61016	Outside	Denman (Palace Street)	-32.3885	150.6886	14	153	28	71	9	35	40	83	5	74	18	90	621
61065	Outside	Aberdeen (Rossgole)	-32.1402	150.7285	15	75	23	94	34	30	0	105	10	92	136	74	688
61086	Outside	Jerrys Plains Post office	-32.4972	150.9093	16	128	23	49	21	23	34	83	4	93	108	92	674
61130	Outside	Doyles Creek (Wood Park)	-32.5113	150.7968	17	169	17	40	6	21	31	87	3	89	87	55	623
61162	Outside	Howes Valley (Putty Rd)	-32.8446	150.8398	15	96	54	48	42	15	33	41	1	55	119	82	602
61168	Outside	Muswellbrook (Lindisfarne)	-32.3147	150.7552	16	75	47	35	4	38	22	85	5	82	109	48	566
61191	Outside	Bulga (South Wambo)	-32.6126	150.9761	15	128	44	0	26	0	36	64	1	62	87	84	545
61192	Outside	Muswellbrook (Spring Creek)	-32.2092	150.7365		77	32	62	19	29	37	87	6	88	106	52	594
61209	Outside	Putty Tea Rooms	-32.9614	150.6742	14	110	44	39	46	10	32	43	0	59	63	42	502
61215	Outside	Rylstone (Kelgoola)	-32.8722	150.2992	24	141	24	77	29	29	53	105	7	91	91	53	721
61306	Outside	Kars Springs (Welldun)	-31.8988	150.6580	13	88	21	104	19	38	32	91	20	106	76	102	710
61309	Outside	Milbrodale (Hillsdale)	-32.6881	150.9728	19	161	54	54	37	24	37	59	0	49	94	77	665
61334	Outside	Glen Alice	-33.0490	150.2327	12	86	39	66	13	27	26	67	4	61	90	64	555
61342	Outside	Bunnan (The Cuan)	-31.9863	150.6300	10	98	3	55	22	18	30	86	13	68	69	84	554
61352	Outside	Putty (Putty Valley Road)	-32.9687	150.6670	19	108	50	46	49	17	33	51	4	69	82	49	577
62013	Outside	Gulgong Post Office	-32.3634	149.5329	11	125	90	69	0	59	33	129	13	103	65	57	756
62017	Outside	Kandos Cement Works	-32.8647	149.9745	19	115	54	69	7	38	35	109	7	108	120	54	734

Annex – II: A. Monthly rainfall data (all SASMAS sites and BoM sites) in 2003 continued.

Site_ID	Catchment	Name	Latitude	Longitude	Jan	Feb	Mar	Apr	May	Jun	Jul	Aug	Sep	Oct	Nov	Dec	Total
62026	Outside	Rylstone (Ilford Rd)	-32.8079	149.9770	10	128	14	51	4	32	22	107	0	77	111	45	601
62035	Outside	Leadville (Moreton Bay)	-32.0792	149.6051	10	82	21	110	1	58	28	123	17	85	66	43	645
62062	Outside	Lue (Bayly St)	-32.6570	149.8376	10	319	42	33	9	57	35	114	17	95	84	54	867
62084	Outside	Budgee Budgee (Botobolar Vineyard)	-32.5008	149.7135	10	274	37	67	9	61	30	120	13	91	55	18	784
62104	Outside	Mudgee (Wandu-Too)	-32.5758	149.6790	9	224	45	71	5	54	29	109	14	86	100	52	797
64025	Outside	Coolah (Binnia St)	-31.8231	149.7200	14	43	9	105	2	46	33	106	18	110	74	51	612
		Average (within the GRC)		**(*n*=26)**	**12**	**104**	**20**	**91**	**9**	**40**	**25**	**105**	**12**	**78**	**79**	**59**	**634**
		Regional average		**(*n*=58)**	**14**	**112**	**28**	**78**	**14**	**36**	**28**	**97**	**11**	**78**	**78**	**65**	**638**

Annex – II: B. Monthly rainfall data (all SASMAS sites and BoM sites) in 2004.

Site_ID	Catchment	Name	Latitude	Longitude	Jan	Feb	Mar	Apr	May	Jun	Jul	Aug	Sep	Oct	Nov	Dec	Total
K6	Krui	Spring Hill	-31.8644	150.2061	98	132	77	26	31	32	54	55	53	90	75	213	936
K4	Krui	Pembroke	-31.9817	150.1800	57	81	29	22	35	18	43	47	19	57	23	157	588
S2	Krui	Stanley	-32.0958	150.1369	53	80	26	29	32	15	26	36	18	52	48	129	542
M7	Merriwa	The Echo	-31.8586	150.4672	124	128	55	12	44	27	64	57	52	67	97	242	968
M4	Merriwa	Kilwirrin	-32.0419	150.3964	80	81	38	13	26	14	36	49	13	67	34	185	636
M1	Merriwa	Maram Park	-32.2417	150.3114											34	143	
G4	Wollar	Cumbo	-32.4061	149.8822	40	90	9	12	44	38	62	43	47	68	57	111	620
G2	Widden	Widden Stud	-32.5258	150.3592	44	67	24	6	35	18	32	40	41	91	71	99	567
61075	Bow	Merriwa (Tunbridge)	-32.2229	150.2366	61	64	13	14	34	14	31	30	21	53	87	161	582
61287	Bow	Merriwa (Roscommon)	-32.1897	150.1728	80	85	18	25	30	21	27	31	23	59	49	99	547
61316	Bow	Merriwa (Mar-Lea)	-32.0666	150.2326	99	89	25	15	33	15	34	41	23	62	25	179	641
62080	Bylong	Bylong (Heatherbrae)	-32.3580	150.0970	61	97	19	11	49	22	37	33	39	50	74	103	594
62100	Bylong	Nullo Mountain AWS	-32.7244	150.2290	53	148	22	8	34	31	66	50	66	130	96	134	840
62102	Bylong	Bylong (Bylong Road)	-32.5219	150.0811	42	117	27	12	35	21	47	34	66	90	70	77	636
62036	Goulburn	Ulan Post Office	-32.2804	149.7425	46		11	13	55	33	56	39	41	85	62	134	
61324	Hall	Gungal (Merryfields)	-32.2451	150.5130					33	18	27	40	31	67	64	176	
61002	Krui	Blackville (Krui Vale)	-31.8449	150.3410	142	162	80	13	56	29	70	54	55	129	117	185	1093
61261	Krui	Merriwa (Bellview)	-31.9983	150.2420					30	19	44	44					
62015	Krui	Merriwa (Merry Vale)	-31.9273	150.2230	111	139	49	33	26	22	46	45	20	72	39	180	782
61040	Merriwa	Merriwa (Gummun Place)	-32.1388	150.3577	84	63	28	15	33	8							
61073	Merriwa	Merriwa (Terragong)	-32.0780	150.3696	88	113	40	12	28	16	31	53	14	84	31	145	655
61400	Merriwa	Merriwa (Warra)	-32.1315	150.3639	95	97	27	14	36	16	27	26		91	33		
62005	Munmurra	Cassilis Post Office	-32.0067	149.9800	106	93	21	14	46	8	30	22					
62009	Munmurra	Cassilis (Dalkeith)	-31.9963	149.9857	96	95	23	21	44	25	38	52	24	58	32	160	666
62032	Wollar	Wollar (Barrigan St.)	-32.3592	149.9484	63	137	14	12	48	30	42	40	45	67	55	110	664
62056	Wollar	Wollar (Maree)	-32.4261	149.9535	34						45	45	72	68	54		
55006	Outside	Blackville Post Office	-31.6414	150.2350	158	118	92	26	40	24	66	48	43	51	71	185	922
55017	Outside	Premer (Eden Moor)	-31.5711	149.7762	110	115	48	40	36	35	61	52	44	25	43	171	780

Annex – II: B. Monthly rainfall data (all SASMAS sites and BoM sites) in 2004 continued.

Site_ID	Catchment	Name	Latitude	Longitude	Jan	Feb	Mar	Apr	May	Jun	Jul	Aug	Sep	Oct	Nov	Dec	Total
55025	Outside	Willow Tree (Highlands)	-31.7928	150.6730	145	126	54	15	23	36	76	66	58	85	76	168	928
55043	Outside	Willow Tree (Parraweena)	-31.7118	150.4135	176	118	62	17	41	22	61	59	42	52	73	186	908
55057	Outside	Willow Tree (Valais)	-31.7731	150.2856	255	121	138	16	55	16	55	50	45	54	72	162	1039
55069	Outside	Yannergee (Dobroyd)	-31.4494	150.0247	87	139	54	26	39	22	49	44	25	32	71	199	786
55071	Outside	Premer Post Office	-31.4568	149.9001	112	167	49	28	31	26	23	43	32	16	64	191	781
55248	Outside	Willow Tree (Kelverton)	-31.7249	150.5837	151	95	64	0	54	17	71	46	54	73	75	171	871
61007	Outside	Bunnan (Milhaven)	-32.0332	150.5836	115	111	40	5	28	11	50	54	16	56	33	150	669
61016	Outside	Denman (Palace St.)	-32.3885	150.6886	106	101	34	3	32	15	20	43	32	88	65	167	706
61065	Outside	Aberdeen (Rossgole)	-32.1402	150.7285	77	87	42	7	32	16	42	59	22	103	39	164	691
61086	Outside	Jerrys Plains Post Office	-32.4972	150.9093	96	123	41	2	37	9	19	35	36	95	81	154	728
61110	Outside	Howes Valley Repeater	-32.8781	150.7911	53	107	56	4	10	5	14	27	35	119	78	87	595
61130	Outside	Doyles Creek (Wood Park)	-32.5113	150.7968	86	91	38	1	38		10	36	38	73	87		
61162	Outside	Howes Valley (Putty Rd)	-32.8446	150.8398	91	114	51	5	16	10	23	29	39	145	98	106	727
61168	Outside	Muswellbrook (Lindisfarne)	-32.3147	150.7552	108	85	31	2	33	8	22	71	31	73	62	119	644
61191	Outside	Bulga (South Wambo)	-32.6126	150.9761	132	162	55	1	28	6	14	30	34	120	90	125	798
61192	Outside	Muswellbrook (Spring Creek)	-32.2092	150.7365	73	106	46	0	36	4	28	50	17	78	175	128	740
61209	Outside	Putty Tea Rooms	-32.9614	150.6742	28	151	44	3	9	1	13	21	30	148	60	95	603
61215	Outside	Rylstone (Kelgoola)	-32.8722	150.2992	51	107	21	5	24	13	57	33	37	91	47	99	584
61306	Outside	Kars Springs (Welldun)	-31.8988	150.6580	125	130	60	7	23	19	53	57	32	28	76	141	751
61309	Outside	Milbrodale (Hillsdale)	-32.6881	150.9728	110	156	59	2	23	13	20	40	39	137	99	147	845
61334	Outside	Glen Alice	-33.0490	150.2327	36	64	12	2	27	14	47	24	29	89	58	99	502
61336	Outside	Putty (The Gibba)	-33.1583	150.6833	42	107	36	30	12	1							
61342	Outside	Bunnan (The Cuan)	-31.9863	150.6300	96	109	72	5	26	17		51	19	59	27	162	642
61352	Outside	Putty (Putty Valley Road)	-32.9687	150.6670	38	161	46	8	11	4	21	31	45	123	75	111	673
62013	Outside	Gulgong Post Office	-32.3634	149.5329	37	66	28	8	50	38	79	33	27	53	90	118	628
62017	Outside	Kandos Cement Works	-32.8647	149.9745	53	90	13	0	38	20	69	6	41	88	79	94	591

Annex – II: B. Monthly rainfall data (all SASMAS sites and BoM sites) in 2004 continued.

Site_ID	Catchment	Name	Latitude	Longitude	Jan	Feb	Mar	Apr	May	Jun	Jul	Aug	Sep	Oct	Nov	Dec	Total
62026	Outside	Rylstone (Ilford Rd)	-32.8079	149.9770	68	23	14	0	37		56	45	46	72	69	80	
62035	Outside	Leadville (Moreton Bay)	-32.0792	149.6051	71		20	23	59	40	48	45	24	53	53	131	
62062	Outside	Lue (Bayly St)	-32.6570	149.8376	24	80	14	5	36	39	64	41	44				
62084	Outside	Budgee Budgee (Botobolar Vineyard)	-32.5008	149.7135	61	119	11	4	55	31	66	40	41	57	72	99	657
62104	Outside	Mudgee (Wandu-Too)	-32.5758	149.6790	25	78	6	6	40	29	55	32	33	75	74	72	523
64025	Outside	Coolah (Binnia St)	-31.8231	149.7200	43	97	51	30	35	28	62	58	34	27	47	159	672
		Average (within the GRC)		**(*n*=26)**	**76**	**103**	**31**	**16**	**37**	**21**	**42**	**42**	**37**	**75**	**58**	**149**	**697**
		Regional average		**(*n*=60)**	**84**	**107**	**39**	**12**	**35**	**20**	**43**	**42**	**36**	**76**	**66**	**142**	**714**

Annex - III

CS 616 Calibrations

Site - G1

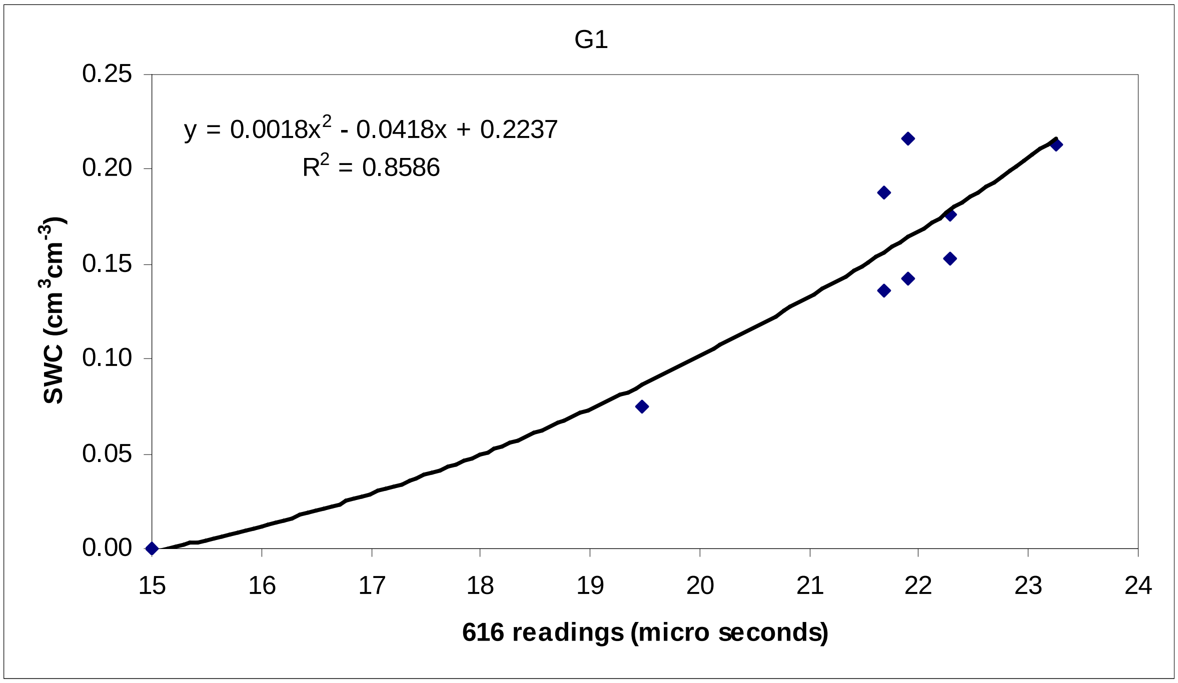


```
The regression equation is
G1-MC = 0.223 - 0.0417 G1-616 + 0.00178 G1-616**2

Predictor        Coef       StDev          T        P
Constant       0.2230      0.7238       0.31    0.768
616Ref       -0.04170     0.07817      -0.53    0.613
Ref**2       0.001781    0.002062       0.86    0.421

S = 0.03034     R-Sq = 85.8%     R-Sq(adj) = 81.0%

Analysis of Variance

Source             DF          SS          MS         F        P
Regression          2    0.033253    0.016627     18.07    0.003
Residual Error      6    0.005521    0.000920
Total               8    0.038775

Source        DF      Seq SS
616Ref         1    0.032567
Ref**2         1    0.000687

Unusual Observations
Obs      616Ref          MC         Fit    StDev Fit     Residual     St Resid
  9        15.0      0.0000     -0.0017       0.0302       0.0017         0.56 X

X denotes an observation whose X value gives it large influence.
```

Site - G2

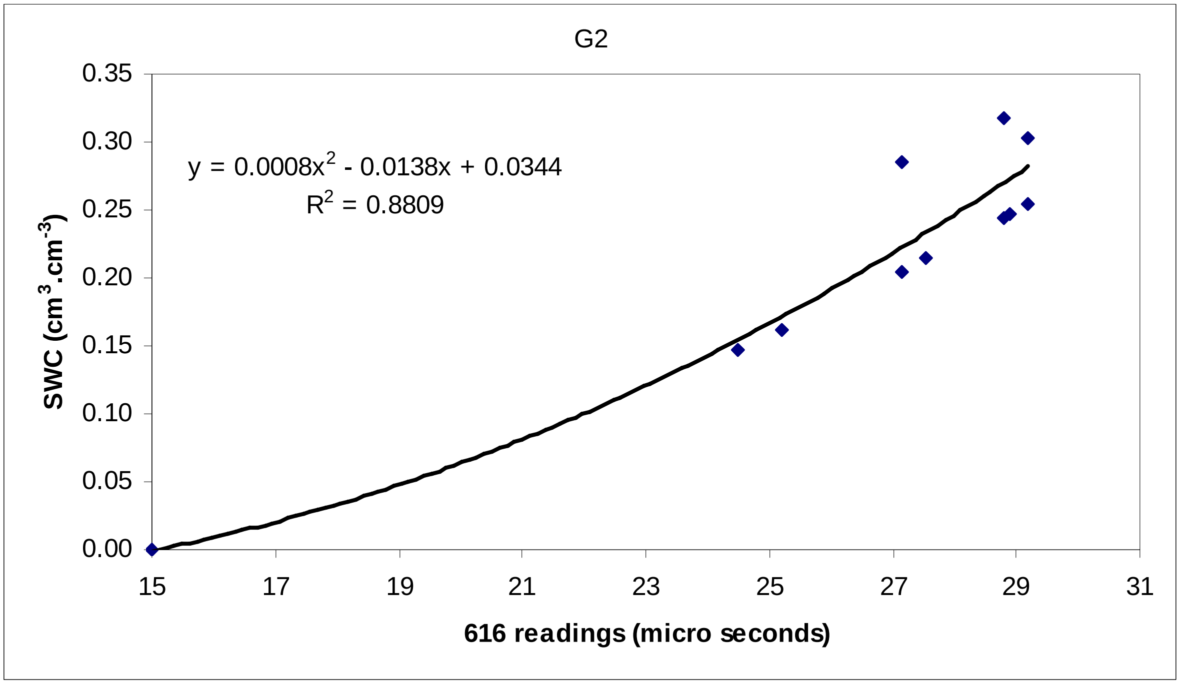


```
The regression equation is
G2-MC = 0.034 - 0.0138 G2-616 +0.000764 G2-616**

Predictor        Coef       StDev          T        P
Constant       0.0342      0.3146       0.11    0.916
G2-616       -0.01380     0.02966      -0.47    0.654
G2-616**    0.0007637   0.0006640       1.15    0.283

S = 0.03467     R-Sq = 88.1%     R-Sq(adj) = 85.1%

Analysis of Variance

Source             DF          SS          MS         F        P
Regression          2    0.071079    0.035540     29.57    0.000
Residual Error      8    0.009615    0.001202
Total              10    0.080694

Source       DF      Seq SS
G2-616        1    0.069489
G2-616**      1    0.001590

Unusual Observations
Obs     G2-616      G2-MC         Fit   StDev Fit    Residual    St Resid
 11       15.0     0.0000     -0.0010      0.0346      0.0010        0.60 X

X denotes an observation whose X value gives it large influence.
```

Site - G3

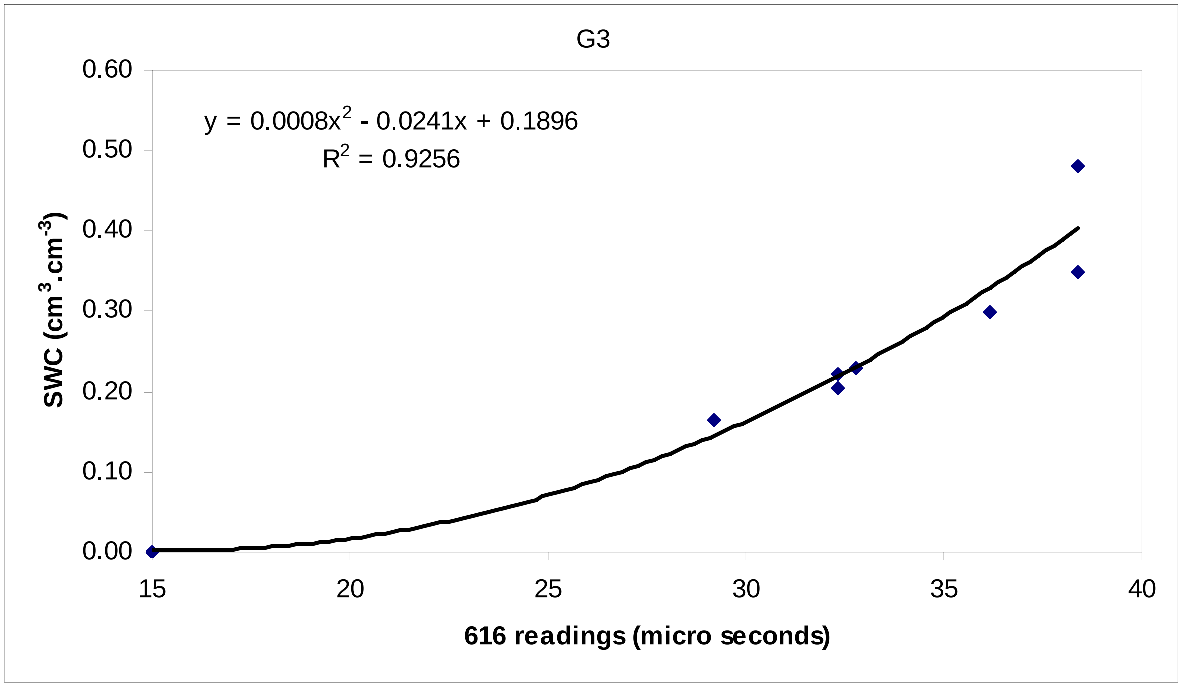


```
The regression equation is
G3-MC = 0.190 - 0.0241 G3-616 +0.000773 G3-616**

Predictor         Coef        StDev           T        P
Constant        0.1895       0.2087        0.91    0.406
G3-616        -0.02409      0.01660       -1.45    0.206
G3-616**     0.0007728    0.0003090        2.50    0.054

S = 0.04531     R-Sq = 92.6%     R-Sq(adj) = 89.6%

Analysis of Variance

Source            DF          SS          MS         F        P
Regression         2    0.127744    0.063872     31.11    0.002
Residual Error     5    0.010265    0.002053
Total              7    0.138009

Source       DF      Seq SS
G3-616        1    0.114902
G3-616**      1    0.012841

Unusual Observations
Obs      G3-616      G3-MC          Fit    StDev Fit     Residual    St Resid
  7        38.4     0.4800       0.4032       0.0291       0.0768       2.21R
  8        15.0     0.0000       0.0021       0.0452      -0.0021      -0.73 X

R denotes an observation with a large standardized residual
X denotes an observation whose X value gives it large influence.
```

Site - G4

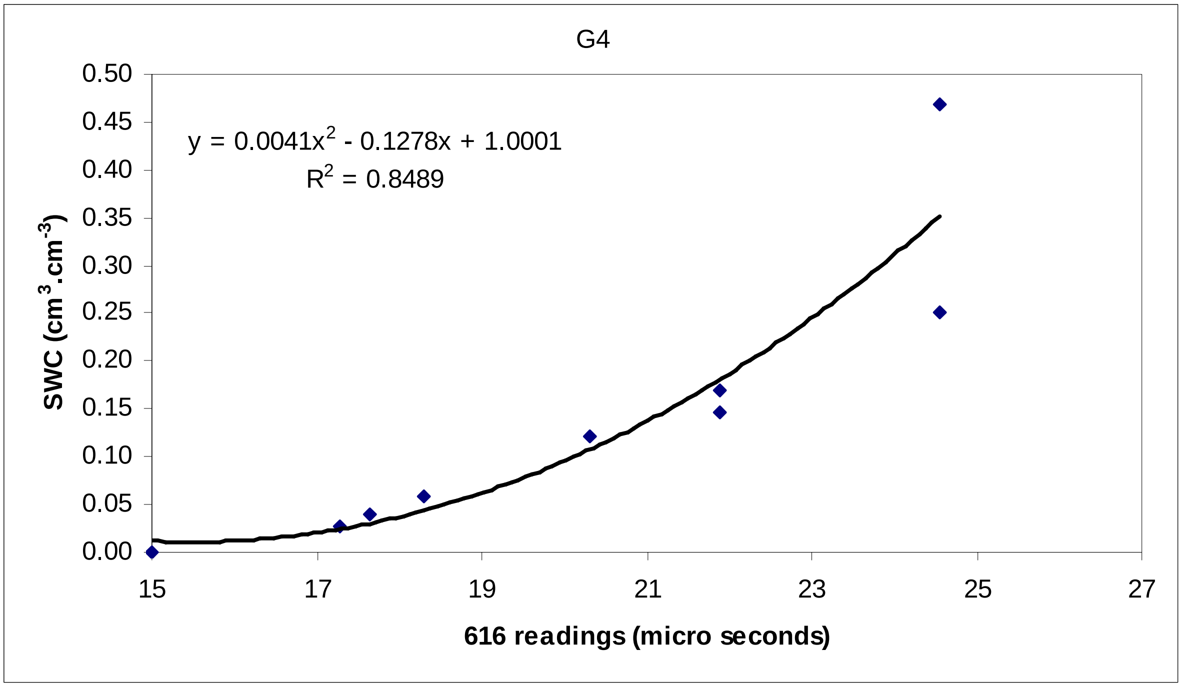


```
The regression equation is
G4-MC = 1.00 - 0.128 G4-616 + 0.00413 G4-616**

Predictor         Coef       StDev          T        P
Constant        1.0001      0.9862       1.01    0.350
G4-616        -0.12785     0.09960      -1.28    0.247
G4-616**      0.004131    0.002467       1.67    0.145

S = 0.06548     R-Sq = 84.9%     R-Sq(adj) = 79.8%

Analysis of Variance

Source             DF          SS          MS         F        P
Regression          2    0.144452    0.072226     16.85    0.003
Residual Error      6    0.025722    0.004287
Total               8    0.170174

Source       DF      Seq SS
G4-616        1    0.132432
G4-616**      1    0.012020

Unusual Observations
Obs      G4-616      G4-MC         Fit   StDev Fit    Residual     St Resid
  4        24.5     0.2507      0.3510      0.0442     -0.1003       -2.08R
  8        24.5     0.4680      0.3510      0.0442      0.1170        2.42R

R denotes an observation with a large standardized residual
```

Site - G5

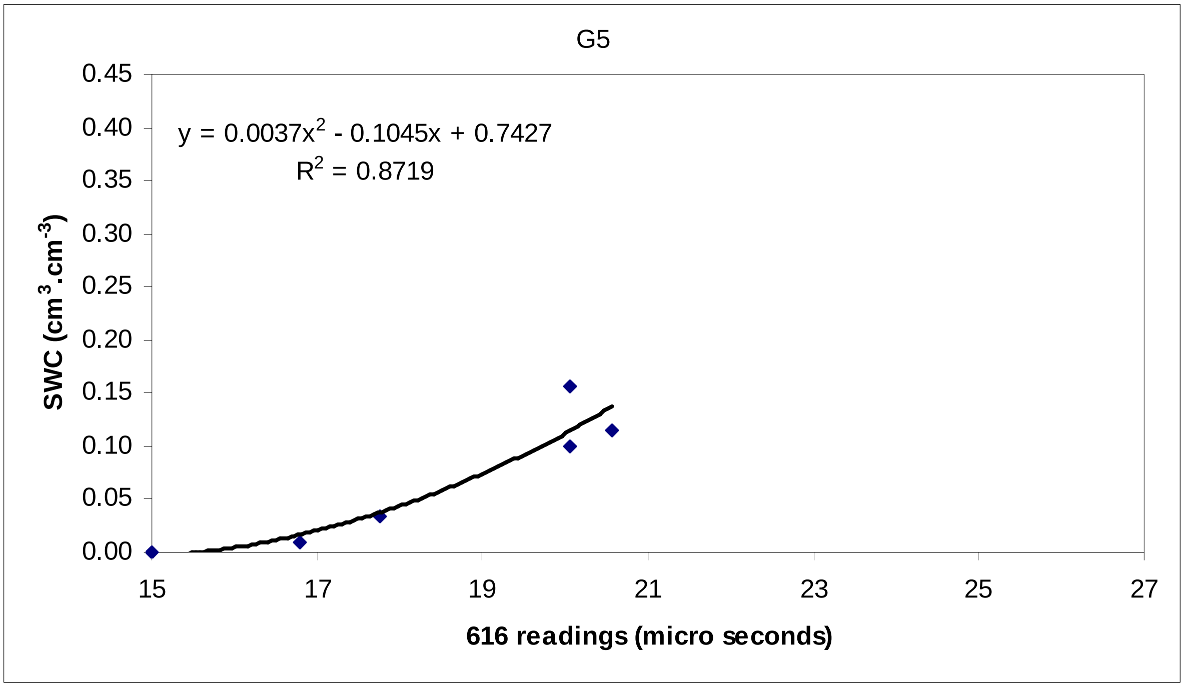


```
The regression equation is
G5-MC = 0.74 - 0.104 G5-616 + 0.00364 G5-616**

Predictor        Coef       StDev          T        P
Constant        0.740       1.290       0.57    0.606
G5-616        -0.1043      0.1456      -0.72    0.525
G5-616**     0.003644    0.004058       0.90    0.435

S = 0.02951     R-Sq = 87.2%     R-Sq(adj) = 78.6%

Analysis of Variance

Source             DF          SS          MS         F        P
Regression          2   0.0177631   0.0088816     10.20    0.046
Residual Error      3   0.0026131   0.0008710
Total               5   0.0203763

Source       DF      Seq SS
G5-616        1   0.0170610
G5-616**      1   0.0007021
```

Site - G6

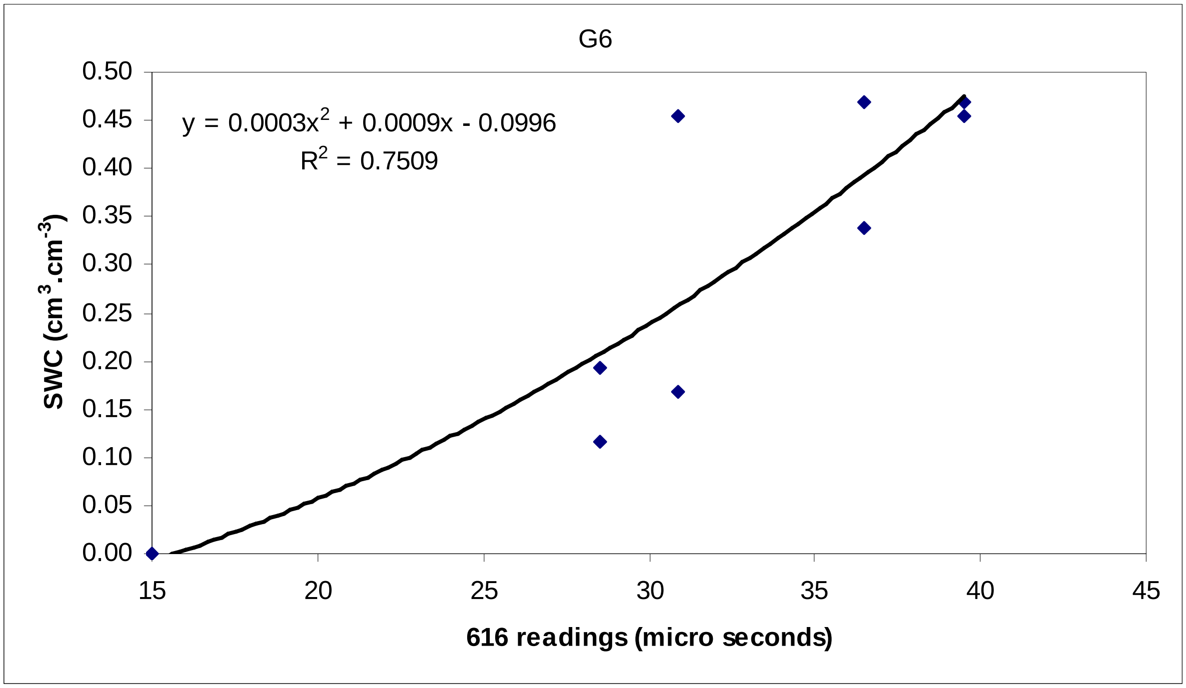


```
The regression equation is
G6-MC = - 0.099 + 0.0009 G6-616 +0.000344 G6-616**

Predictor         Coef        StDev          T        P
Constant       -0.0995       0.4238      -0.23    0.822
G6-616         0.00094      0.03129       0.03    0.977
G6-616**     0.0003440    0.0005542       0.62    0.558

S = 0.1037      R-Sq = 75.1%     R-Sq(adj) = 66.8%

Analysis of Variance

Source            DF          SS          MS         F        P
Regression         2     0.19434     0.09717      9.04    0.015
Residual Error     6     0.06446     0.01074
Total              8     0.25880

Source       DF      Seq SS
G6-616        1     0.19020
G6-616**      1     0.00414

Unusual Observations
Obs      G6-616      G6-MC         Fit   StDev Fit    Residual    St Resid
  7        30.9     0.4540      0.2574      0.0475      0.1966       2.13R
  9        15.0     0.0000     -0.0080      0.1032      0.0080       0.85 X

R denotes an observation with a large standardized residual
X denotes an observation whose X value gives it large influence.
```

Site - K1

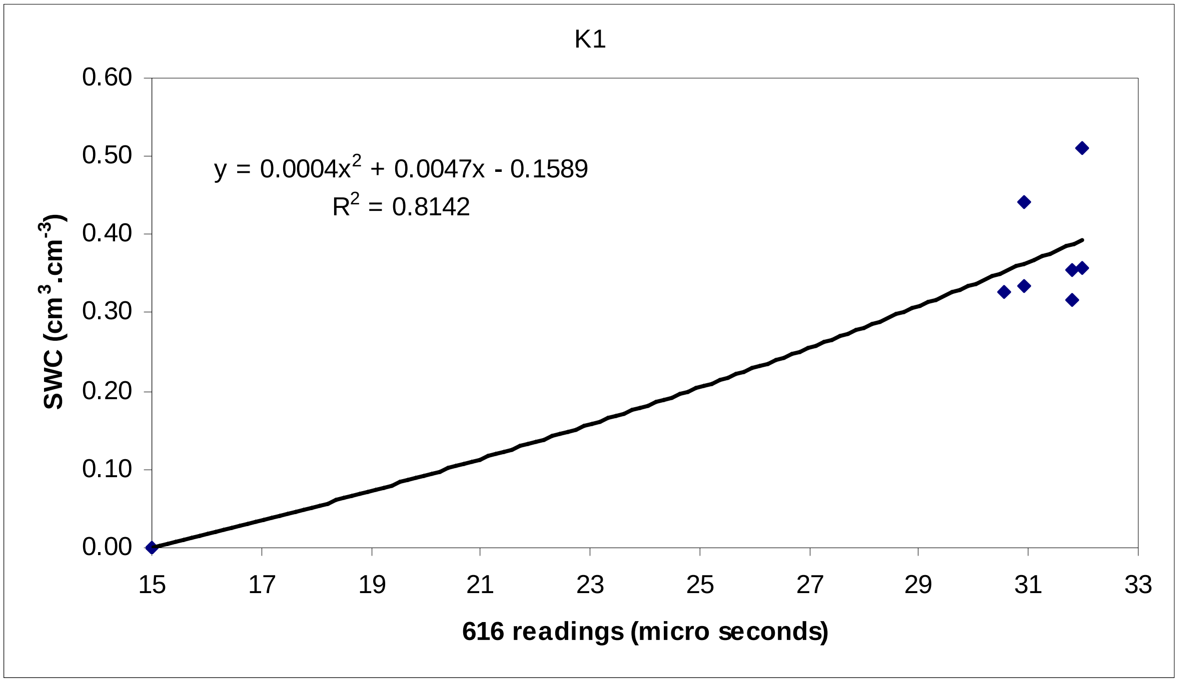


```
The regression equation is
K1-MC = - 0.16 + 0.005 K1-616 + 0.00039 K1-616**

Predictor         Coef        StDev          T        P
Constant        -0.159        1.546      -0.10    0.922
K1-616          0.0047       0.1507       0.03    0.976
K1-616**      0.000394     0.003234       0.12    0.908

S = 0.07604     R-Sq = 81.4%     R-Sq(adj) = 74.0%

Analysis of Variance

Source            DF          SS          MS         F        P
Regression         2    0.126657    0.063329     10.95    0.015
Residual Error     5    0.028909    0.005782
Total              7    0.155567

Source       DF      Seq SS
K1-616        1    0.126572
K1-616**      1    0.000086

Unusual Observations
Obs      K1-616       K1-MC          Fit    StDev Fit     Residual    St Resid
  8        15.0      0.0000       0.0000       0.0760      -0.0000       -0.07 X

X denotes an observation whose X value gives it large influence.
```

Site - K2

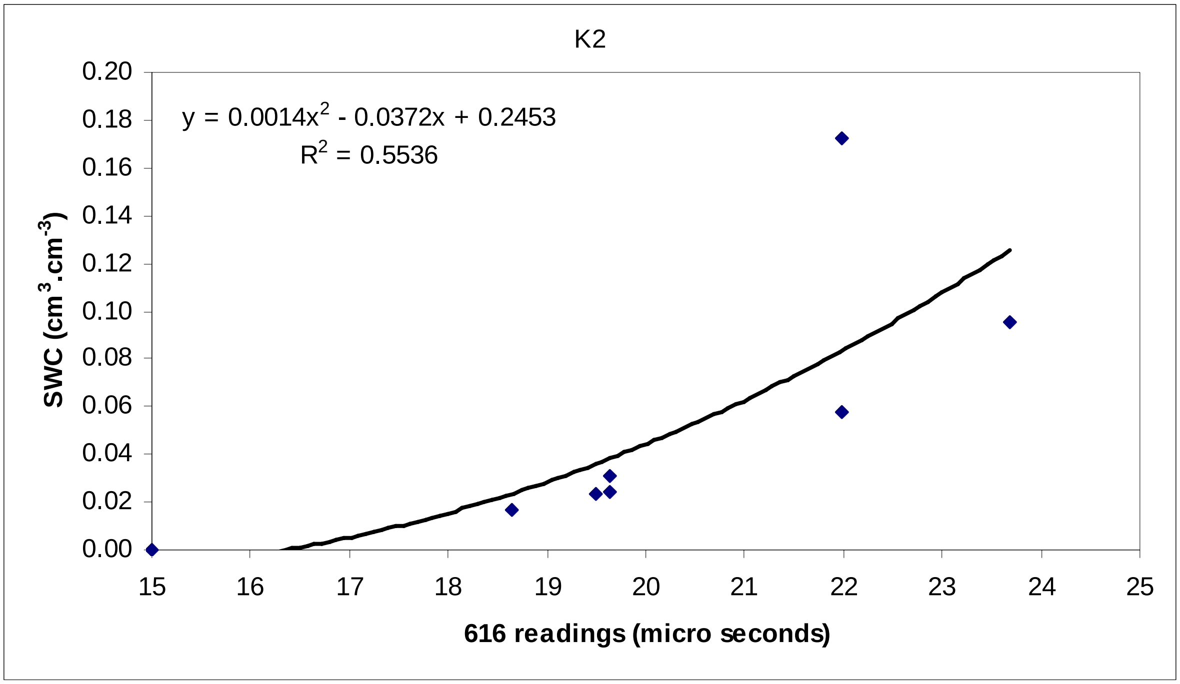


```
The regression equation is
K2-MC = 0.246 - 0.0372 K2-616 + 0.00136 K2-616**

Predictor        Coef       StDev          T        P
Constant       0.2455      0.7721       0.32    0.763
K2-616       -0.03722     0.08031      -0.46    0.663
K2-616**     0.001357    0.002068       0.66    0.541

S = 0.04456     R-Sq = 55.4%     R-Sq(adj) = 37.5%

Analysis of Variance

Source            DF          SS          MS         F        P
Regression         2    0.012315    0.006158      3.10    0.133
Residual Error     5    0.009929    0.001986
Total              7    0.022244

Source       DF      Seq SS
K2-616        1    0.011460
K2-616**      1    0.000856

Unusual Observations
Obs      K2-616      K2-MC         Fit   StDev Fit     Residual    St Resid
  6        22.0     0.1720      0.0833      0.0202       0.0887       2.23R

R denotes an observation with a large standardized residual
```

Site - K3

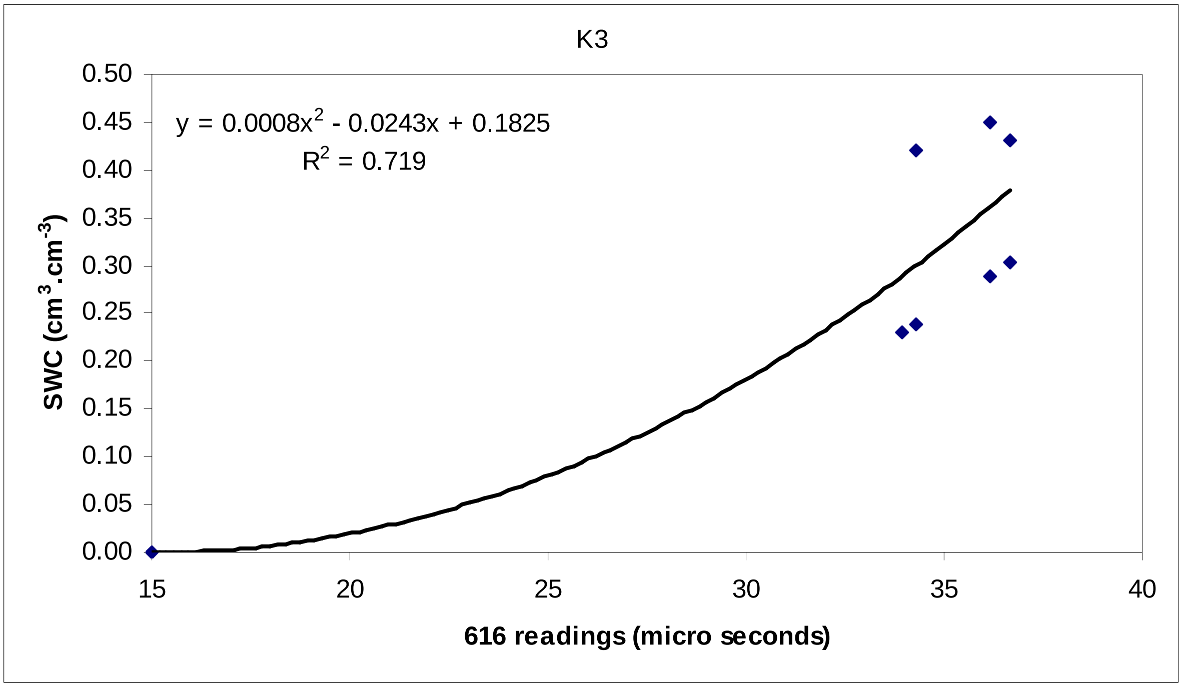


```
The regression equation is
K3-MC = 0.183 - 0.0243 K3-616 + 0.00081 K3-616**

Predictor          Coef        StDev          T        P
Constant         0.1825       0.8648       0.21    0.841
K3-616         -0.02431      0.07912      -0.31    0.771
K3-616**       0.000808     0.001548       0.52    0.624

S = 0.09264     R-Sq = 71.9%     R-Sq(adj) = 60.7%

Analysis of Variance

Source             DF          SS          MS         F        P
Regression          2    0.109825    0.054912      6.40    0.042
Residual Error      5    0.042913    0.008583
Total               7    0.152737

Source       DF       Seq SS
K3-616        1     0.107486
K3-616**      1     0.002339

Unusual Observations
Obs      K3-616       K3-MC          Fit    StDev Fit     Residual    St Resid
  8        15.0      0.0000      -0.0002       0.0926       0.0002        0.58 X

X denotes an observation whose X value gives it large influence.
```

Site - K4

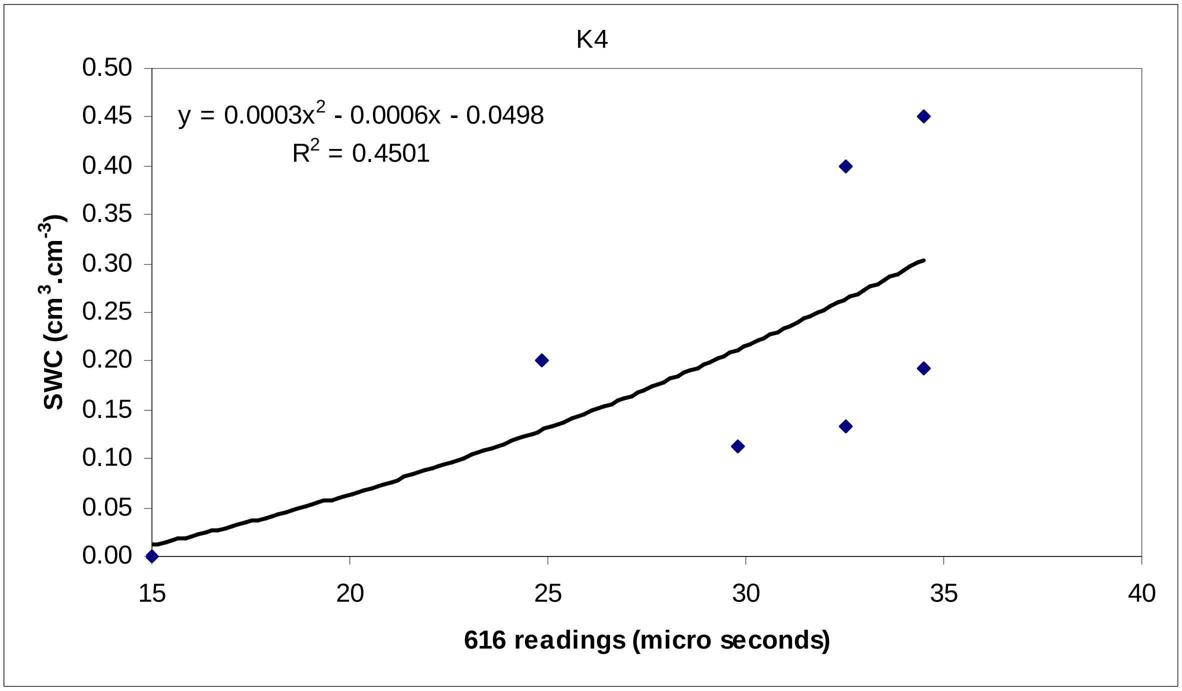


```
The regression equation is
K4-MC = - 0.050 - 0.0006 K4-616 + 0.00032 K4-616**

Predictor        Coef       StDev          T        P
Constant      -0.0498      0.9271      -0.05    0.960
K4-616       -0.00064     0.07963      -0.01    0.994
K4-616**     0.000316    0.001587       0.20    0.852

S = 0.1454      R-Sq = 45.0%     R-Sq(adj) = 17.5%

Analysis of Variance

Source            DF          SS          MS         F        P
Regression         2     0.06922     0.03461      1.64    0.302
Residual Error     4     0.08456     0.02114
Total              6     0.15378

Source       DF      Seq SS
K4-616        1     0.06838
K4-616**      1     0.00084
```

Site - K5

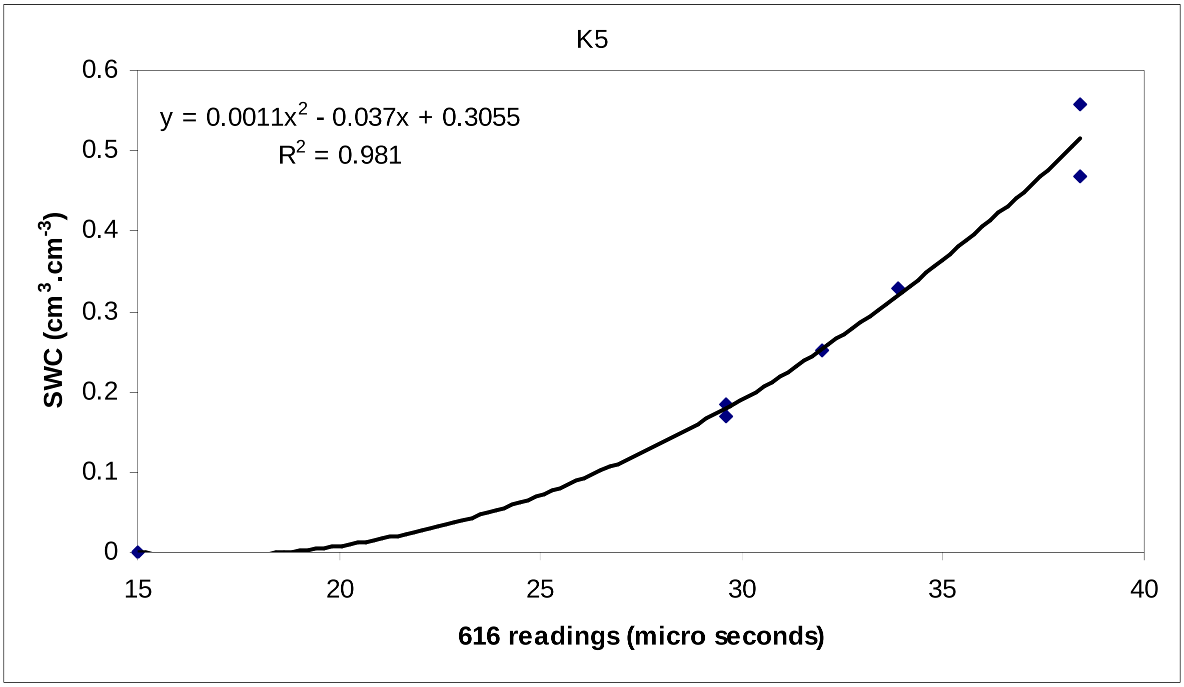


```
The regression equation is
K5-MC = 0.306 - 0.0370 K5-616 + 0.00110 K5-616**

Predictor        Coef       StDev          T        P
Constant       0.3055      0.1445       2.11    0.102
K5-616       -0.03695     0.01135      -3.26    0.031
K5-616**    0.0011036   0.0002102       5.25    0.006

S = 0.03199     R-Sq = 98.1%     R-Sq(adj) = 97.2%

Analysis of Variance

Source            DF          SS          MS         F        P
Regression         2     0.21162     0.10581    103.37    0.000
Residual Error     4     0.00409     0.00102
Total              6     0.21571

Source       DF      Seq SS
K5-616        1     0.18340
K5-616**      1     0.02822

Unusual Observations
Obs      K5-616      K5-MC          Fit    StDev Fit     Residual     St Resid
  7        15.0     0.0000      -0.0004       0.0319       0.0004       0.25 X

X denotes an observation whose X value gives it large influence.
```

Site - K6

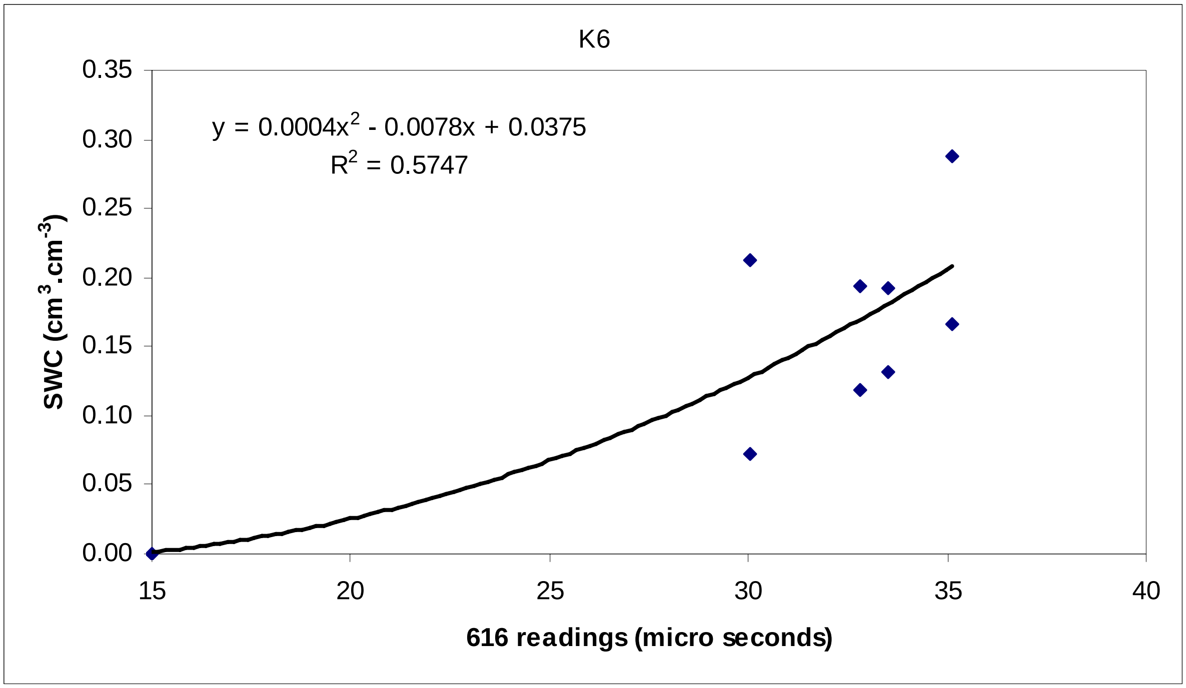


```
The regression equation is
K6-MC = 0.038 - 0.0078 K6-616 +0.000362 K6-616**

Predictor         Coef        StDev           T         P
Constant        0.0375       0.4215        0.09     0.932
K6-616        -0.00784      0.03732       -0.21     0.840
K6-616**     0.0003617    0.0007498        0.48     0.647

S = 0.06337     R-Sq = 57.5%     R-Sq(adj) = 43.3%

Analysis of Variance

Source             DF           SS           MS         F         P
Regression          2     0.032562     0.016281      4.05     0.077
Residual Error      6     0.024095     0.004016
Total               8     0.056657

Source       DF       Seq SS
K6-616        1     0.031627
K6-616**      1     0.000935

Unusual Observations
Obs      K6-616      K6-MC         Fit   StDev Fit    Residual    St Resid
  9        15.0     0.0000      0.0013      0.0633     -0.0013       -0.72 X

X denotes an observation whose X value gives it large influence.
```

Site - M1

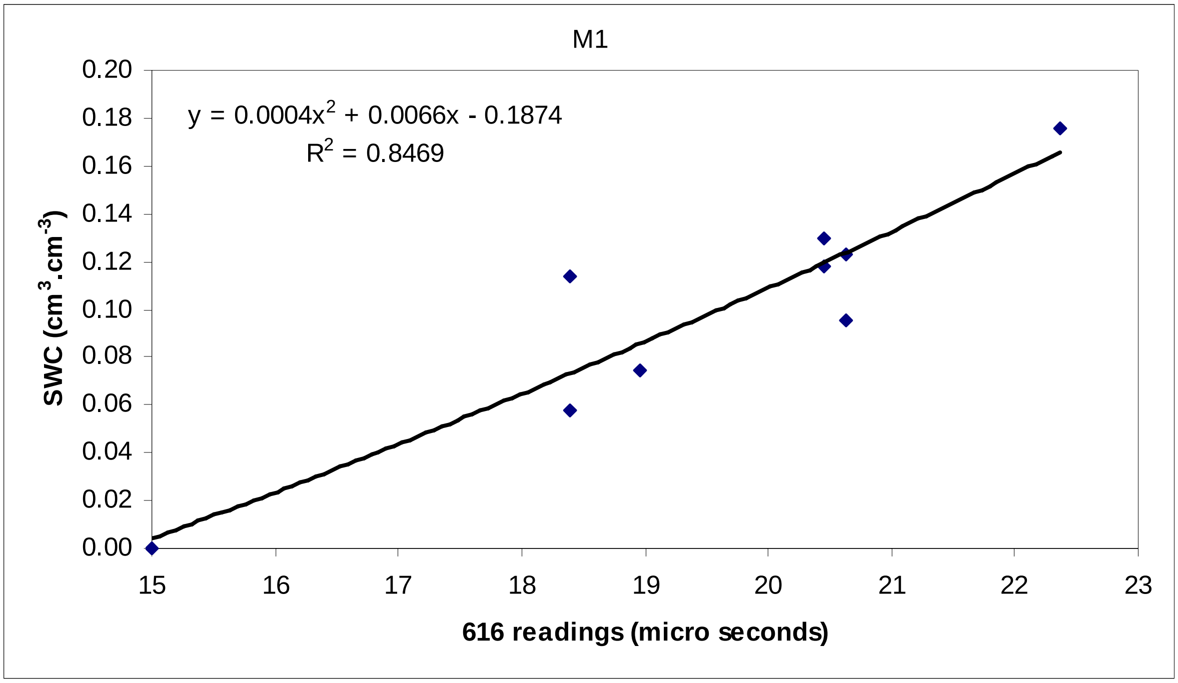

The regression equation is
M1-MC = - 0.187 + 0.0066 M1-616 + 0.00041 M1-616**

Predictor	Coef	StDev	T	P
Constant	-0.1874	0.5197	-0.36	0.731
M1-616	0.00660	0.05624	0.12	0.910
M1-616**	0.000411	0.001510	0.27	0.795

S = 0.02268   R-Sq = 84.7%   R-Sq(adj) = 79.6%

Analysis of Variance

Source	DF	SS	MS	F	P
Regression	2	0.0170703	0.0085351	16.60	0.004
Residual Error	6	0.0030854	0.0005142		
Total	8	0.0201557			

Source	DF	Seq SS
M1-616	1	0.0170321
M1-616**	1	0.0000381

Unusual Observations

Obs	M1-616	M1-MC	Fit	StDev Fit	Residual	St Resid
7	18.4	0.11400	0.07294	0.01116	0.04106	2.08R

R denotes an observation with a large standardized residual

Site - M2

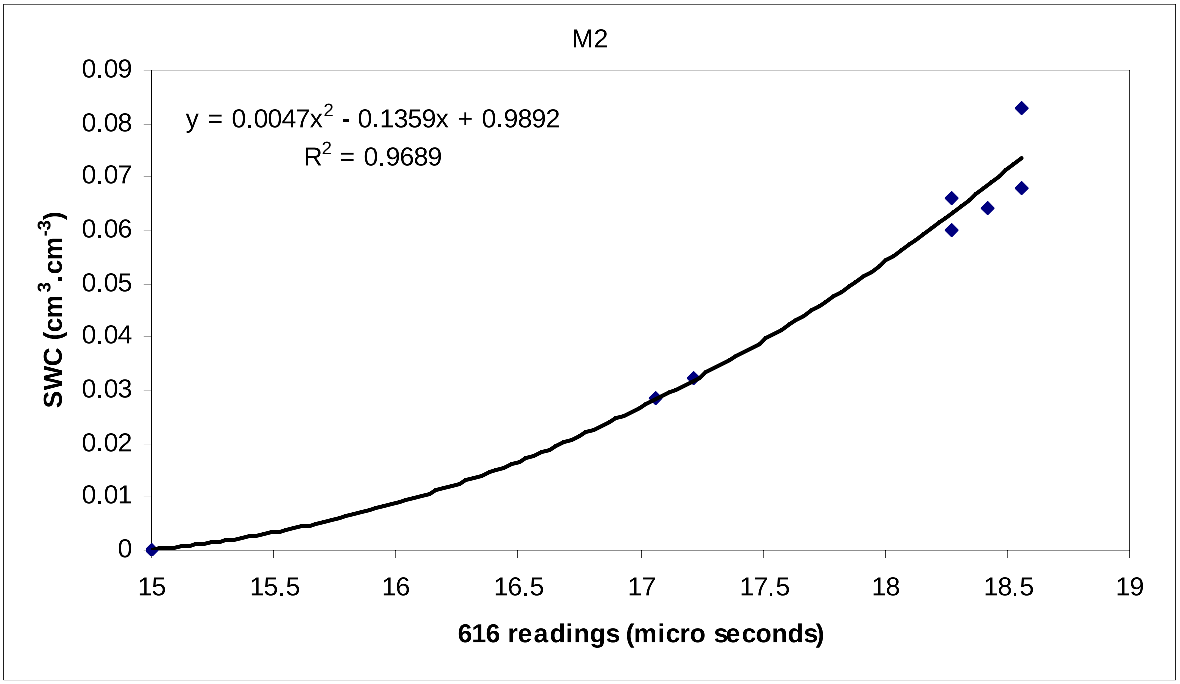


```
The regression equation is
M2-MC = 0.989 - 0.136 M2-616 + 0.00466 M2-616**

Predictor        Coef       StDev          T        P
Constant       0.9892      0.4820       2.05    0.095
M2-616       -0.13587     0.05747      -2.36    0.064
M2-616**     0.004662    0.001703       2.74    0.041

S = 0.005708    R-Sq = 96.9%     R-Sq(adj) = 95.6%

Analysis of Variance

Source            DF          SS          MS         F        P
Regression         2   0.0050703   0.0025352     77.82    0.000
Residual Error     5   0.0001629   0.0000326
Total              7   0.0052332

Source       DF      Seq SS
M2-616        1   0.0048263
M2-616**      1   0.0002440

Unusual Observations
Obs     M2-616      M2-MC         Fit   StDev Fit    Residual    St Resid
  8       15.0    0.00000     0.00011     0.00570    -0.00011       -0.37 X

X denotes an observation whose X value gives it large influence.
```

Site - M3

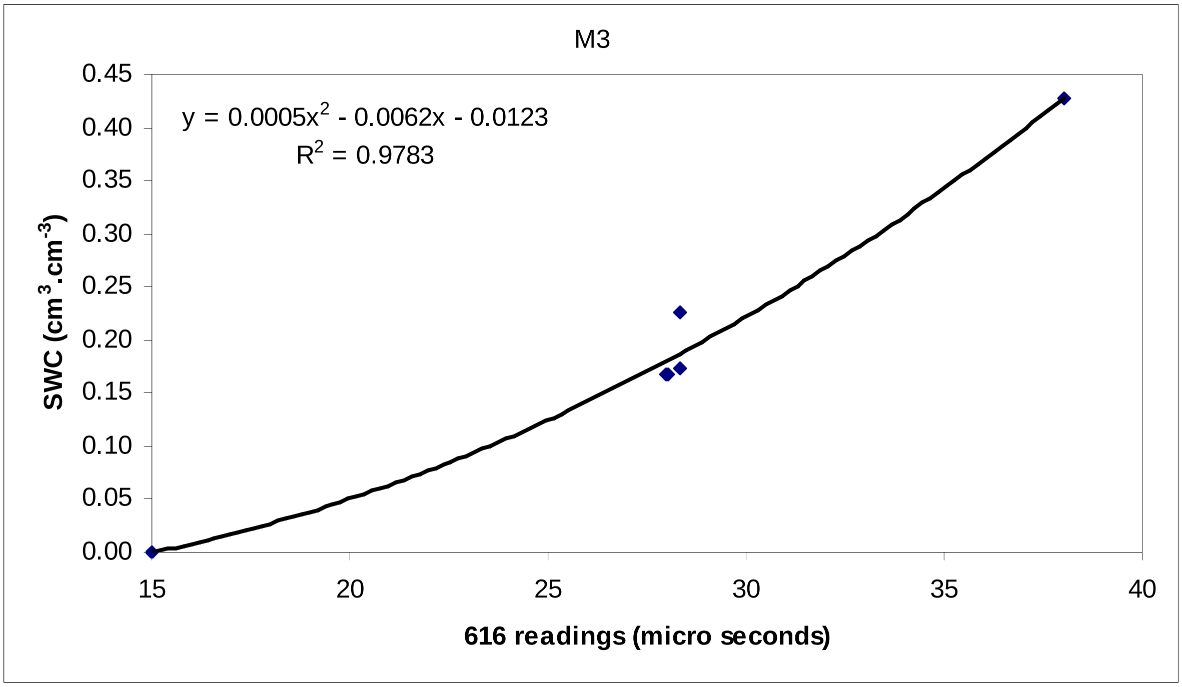


```
The regression equation is
M3-MC = - 0.012 - 0.00620 M3-616 +0.000467 M3-616**

Predictor          Coef        StDev            T         P
Constant        -0.0123       0.1192        -0.10     0.924
M3-616        -0.006204     0.009266        -0.67     0.551
M3-616**      0.0004670    0.0001756         2.66     0.076

S = 0.02618      R-Sq = 97.8%     R-Sq(adj) = 96.4%

Analysis of Variance

Source              DF           SS           MS          F         P
Regression           2     0.092776     0.046388      67.68     0.003
Residual Error       3     0.002056     0.000685
Total                5     0.094832

Source         DF       Seq SS
M3-616          1     0.087927
M3-616**        1     0.004849

Unusual Observations
Obs      M3-616       M3-MC          Fit    StDev Fit     Residual    St Resid
  4        38.0      0.4271       0.4276       0.0262      -0.0005      -1.00 X
  6        15.0      0.0000      -0.0003       0.0262       0.0003       1.00 X

X denotes an observation whose X value gives it large influence.
```

Site - M4

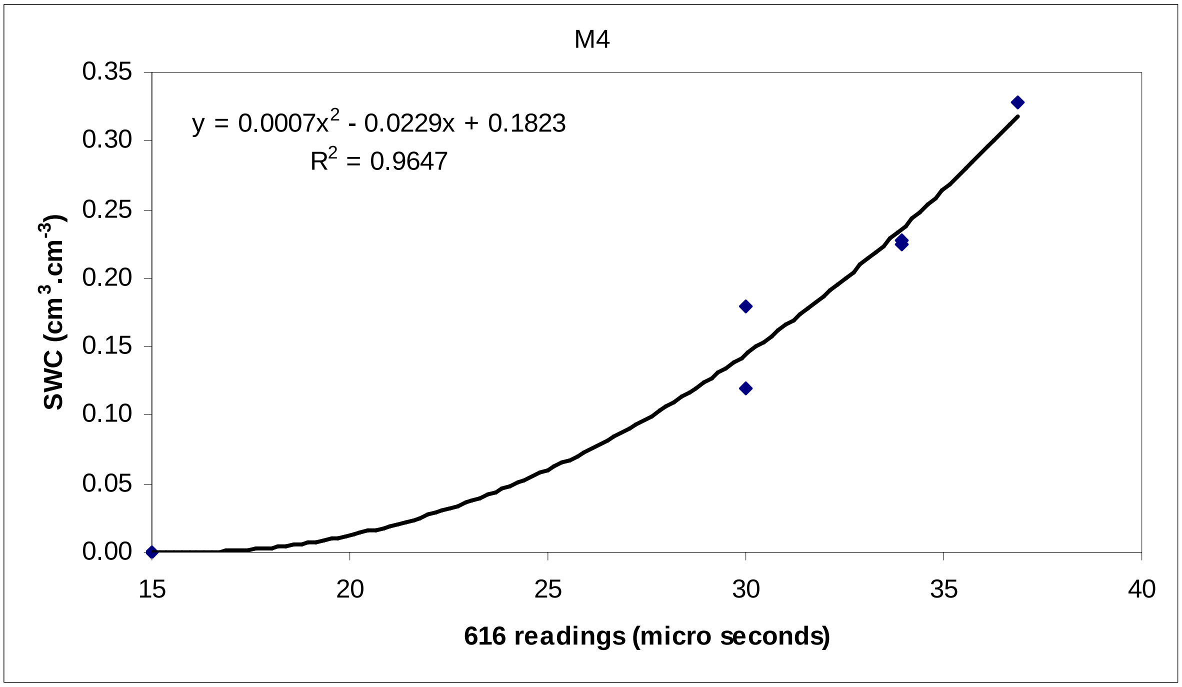


```
The regression equation is
M4-MC = 0.182 - 0.0229 M4-616 +0.000723 M4-616**

Predictor        Coef       StDev          T        P
Constant       0.1823      0.1599       1.14    0.337
M4-616       -0.02294     0.01378      -1.66    0.195
M4-616**    0.0007225   0.0002719       2.66    0.077

S = 0.02707     R-Sq = 96.5%     R-Sq(adj) = 94.1%

Analysis of Variance

Source            DF          SS          MS         F        P
Regression         2    0.060007    0.030003     40.95    0.007
Residual Error     3    0.002198    0.000733
Total              5    0.062204

Source       DF      Seq SS
M4-616        1    0.054834
M4-616**      1    0.005173

Unusual Observations
Obs     M4-616      M4-MC         Fit   StDev Fit    Residual    St Resid
  6       15.0     0.0000      0.0007      0.0270     -0.0007       -0.72 X

X denotes an observation whose X value gives it large influence.
```

Site - M5

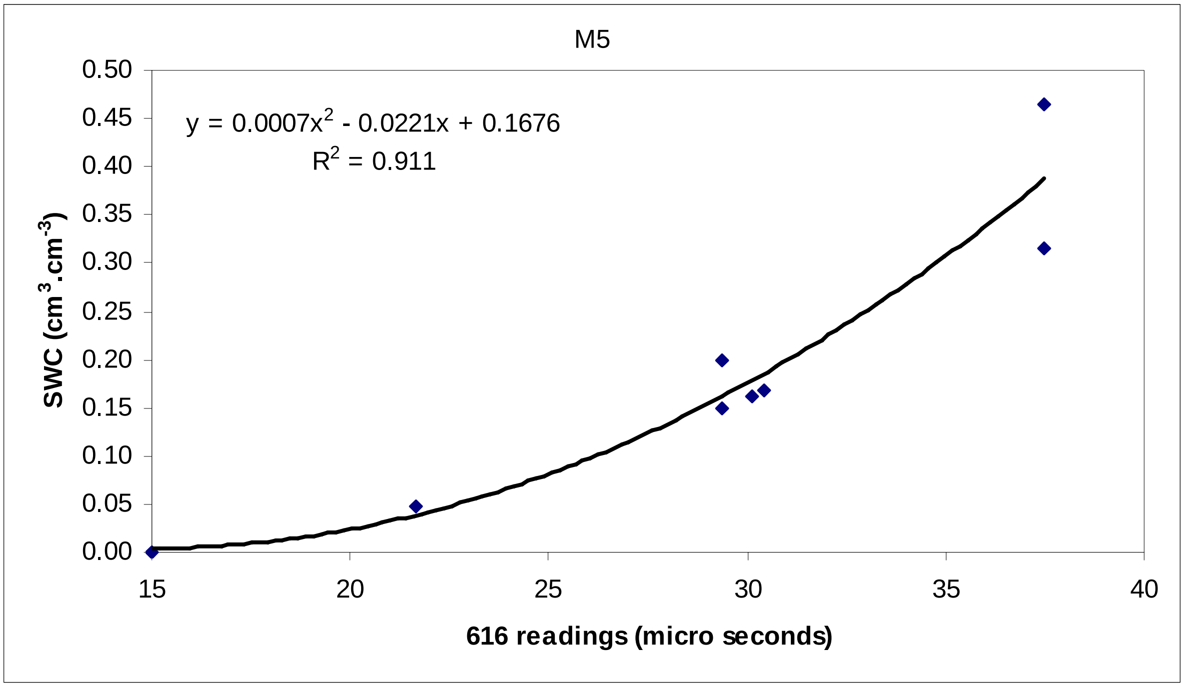


```
The regression equation is
M5-MC = 0.168 - 0.0221 M5-616 +0.000745 M5-616**

Predictor        Coef       StDev          T        P
Constant       0.1676      0.2355       0.71    0.508
M5-616       -0.02208     0.01827      -1.21    0.281
M5-616**    0.0007451   0.0003391       2.20    0.079

S = 0.05173     R-Sq = 91.1%     R-Sq(adj) = 87.5%

Analysis of Variance

Source            DF          SS          MS         F        P
Regression         2    0.136851    0.068426     25.57    0.002
Residual Error     5    0.013378    0.002676
Total              7    0.150229

Source       DF      Seq SS
M5-616        1    0.123934
M5-616**      1    0.012917

Unusual Observations
Obs     M5-616      M5-MC         Fit    StDev Fit     Residual    St Resid
  7       37.5     0.4640      0.3870       0.0359       0.0770       2.07R

R denotes an observation with a large standardized residual
```

Site - M6

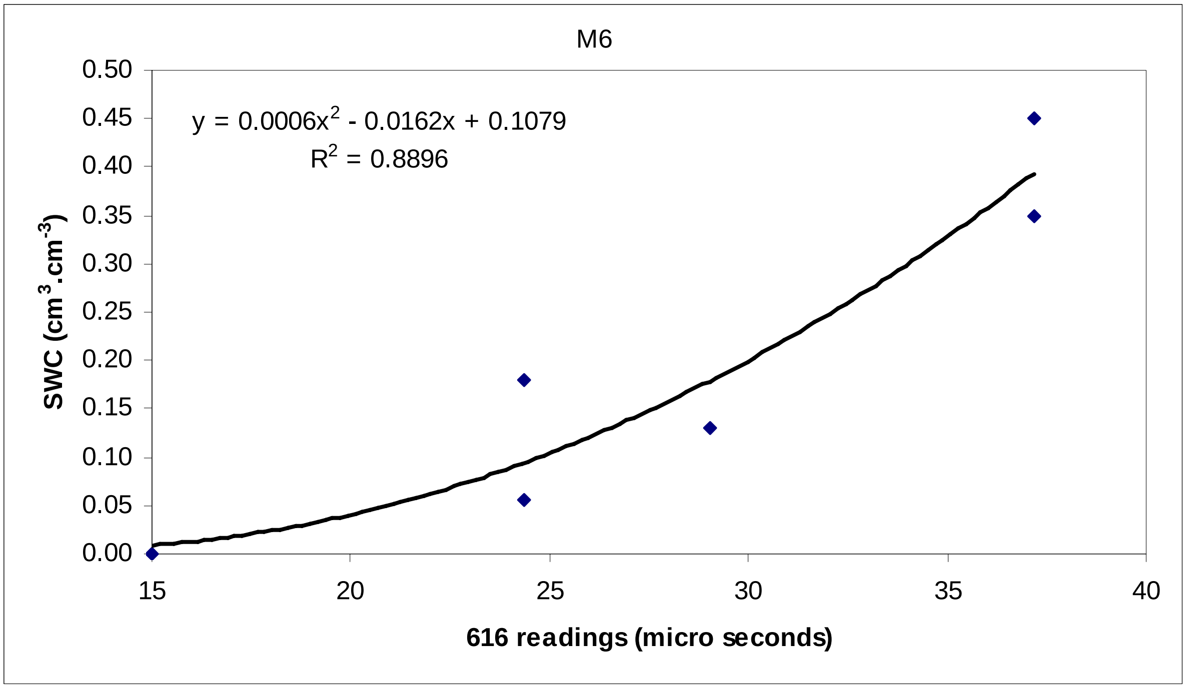


```
The regression equation is
M6-MC = 0.108 - 0.0162 M6-616 +0.000644 M6-616**

Predictor        Coef       StDev          T        P
Constant       0.1079      0.3741       0.29    0.792
M6-616       -0.01624     0.02906      -0.56    0.615
M6-616**    0.0006438   0.0005323       1.21    0.313

S = 0.07442     R-Sq = 89.0%     R-Sq(adj) = 81.6%

Analysis of Variance

Source            DF          SS          MS         F        P
Regression         2    0.133914    0.066957     12.09    0.037
Residual Error     3    0.016617    0.005539
Total              5    0.150531

Source       DF      Seq SS
M6-616        1    0.125812
M6-616**      1    0.008102
```

Site - M7

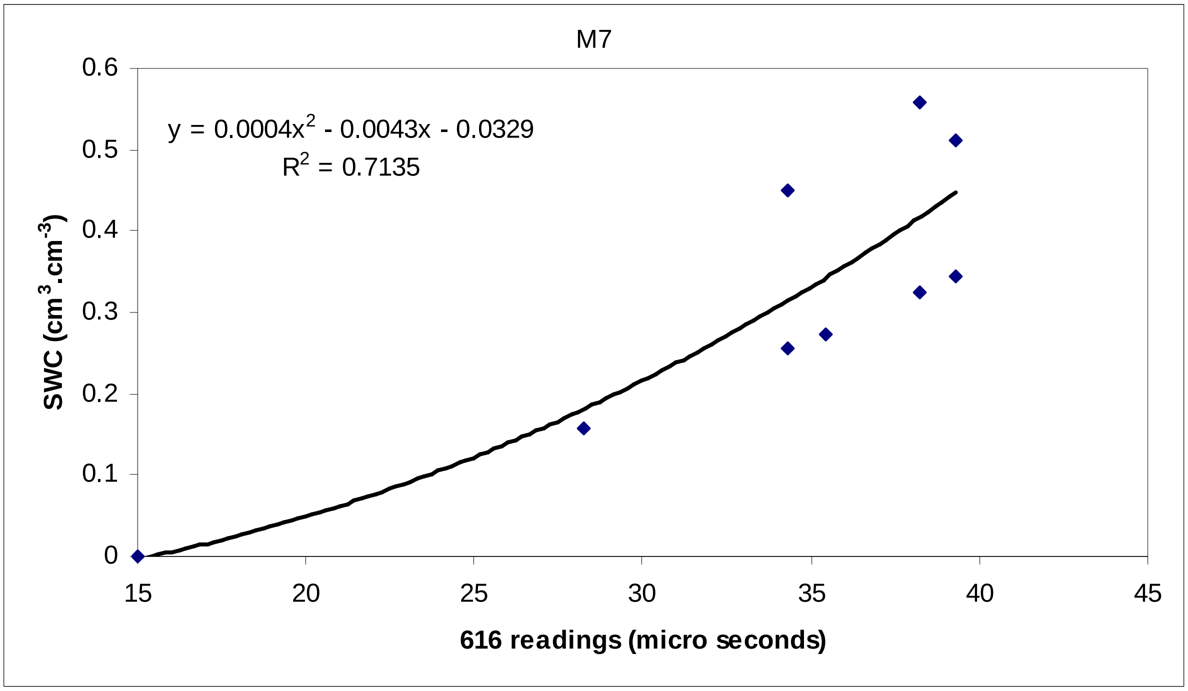


```
The regression equation is
M7-MC = - 0.033 - 0.0043 M7-616 +0.000421 M7-616**

Predictor         Coef        StDev          T        P
Constant       -0.0329       0.4998      -0.07    0.950
M7-616        -0.00433      0.03938      -0.11    0.916
M7-616**     0.0004207    0.0007120       0.59    0.576

S = 0.1084      R-Sq = 71.3%     R-Sq(adj) = 61.8%

Analysis of Variance

Source            DF          SS          MS         F        P
Regression         2     0.17554     0.08777      7.47    0.024
Residual Error     6     0.07050     0.01175
Total              8     0.24605

Source       DF      Seq SS
M7-616        1     0.17144
M7-616**      1     0.00410

Unusual Observations
Obs      M7-616       M7-MC          Fit     StDev Fit     Residual     St Resid
  9        15.0      0.0000      -0.0031        0.1079       0.0031        0.29 X

X denotes an observation whose X value gives it large influence.
```

Site - S1

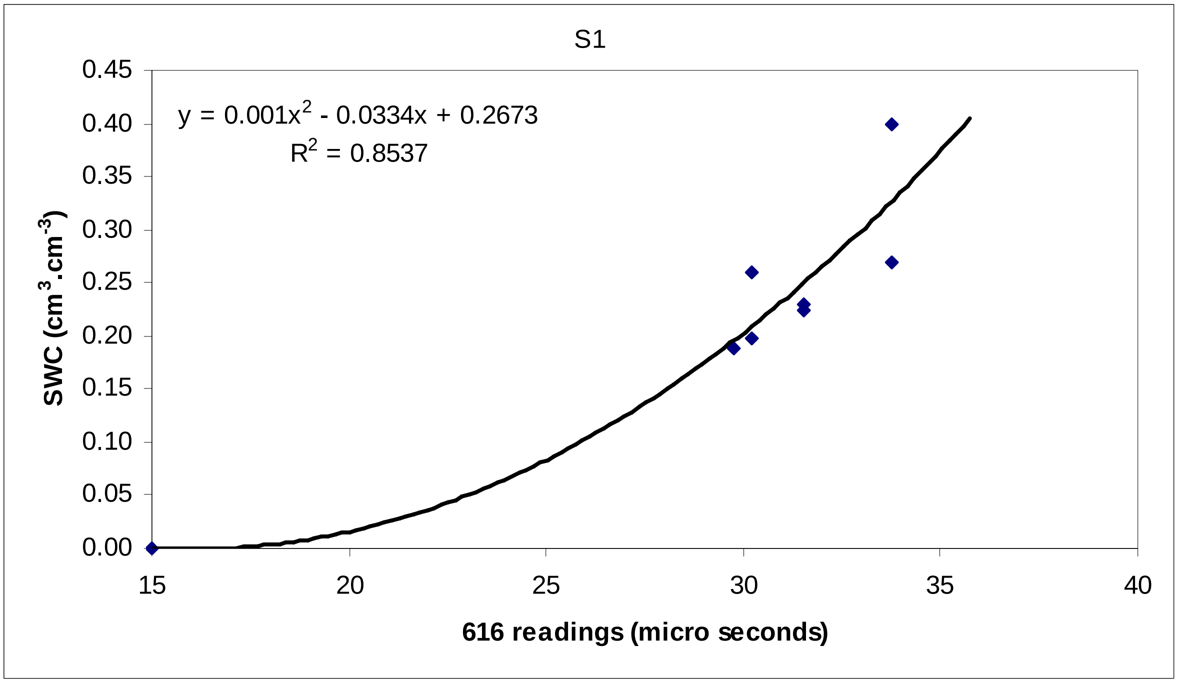


```
The regression equation is
S1-MC = 0.267 - 0.0334 S1-616 + 0.00104 S1-616**

Predictor        Coef       StDev          T        P
Constant       0.2673      0.3896       0.69    0.523
S1-616       -0.03342     0.03570      -0.94    0.392
S1-616**    0.0010423   0.0007441       1.40    0.220

S = 0.05028     R-Sq = 85.4%     R-Sq(adj) = 79.5%

Analysis of Variance

Source            DF          SS          MS         F        P
Regression         2    0.073783    0.036892     14.59    0.008
Residual Error     5    0.012642    0.002528
Total              7    0.086425

Source       DF      Seq SS
S1-616        1    0.068822
S1-616**      1    0.004961

Unusual Observations
Obs     S1-616      S1-MC         Fit    StDev Fit     Residual    St Resid
  8       15.0     0.0000      0.0005       0.0503      -0.0005       -0.61 X

X denotes an observation whose X value gives it large influence.
```

Site - S2

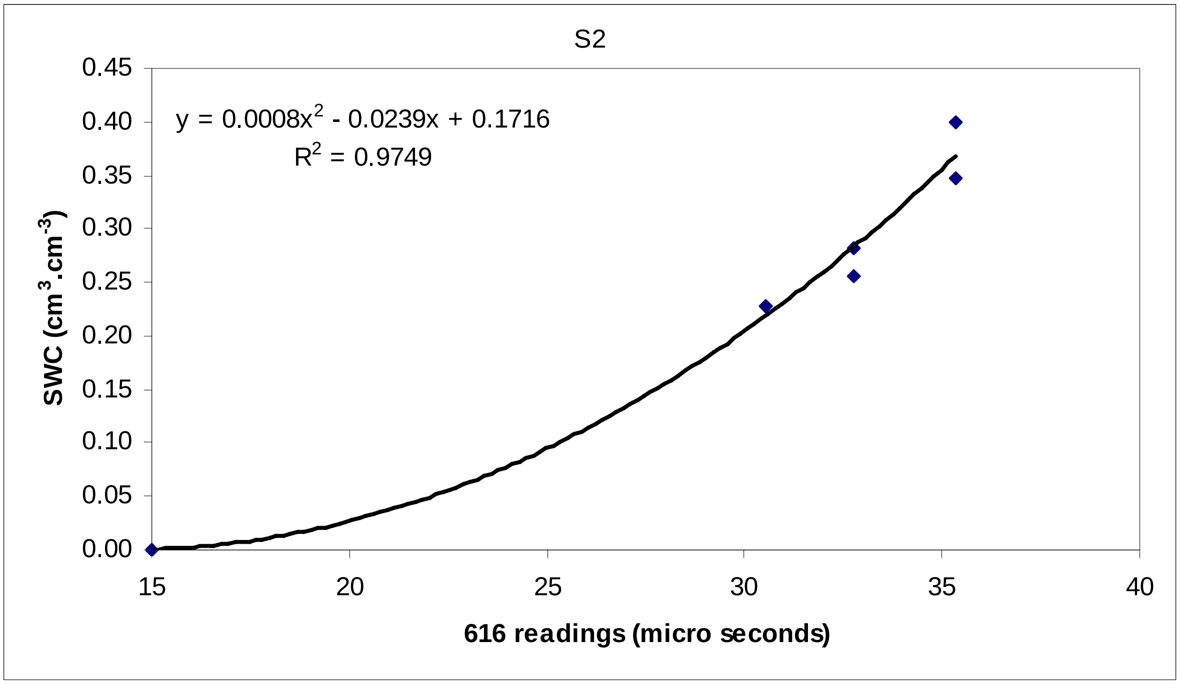


```
The regression equation is
S2-MC = 0.172 - 0.0239 S2-616 +0.000833 S2-616**

Predictor        Coef       StDev          T        P
Constant       0.1716      0.1665       1.03    0.361
S2-616       -0.02390     0.01482      -1.61    0.182
S2-616**    0.0008334   0.0002981       2.80    0.049

S = 0.02462     R-Sq = 97.5%     R-Sq(adj) = 96.2%

Analysis of Variance

Source            DF          SS          MS         F        P
Regression         2    0.094052    0.047026     77.59    0.001
Residual Error     4    0.002424    0.000606
Total              6    0.096476

Source       DF      Seq SS
S2-616        1    0.089316
S2-616**      1    0.004736

Unusual Observations
Obs     S2-616      S2-MC         Fit    StDev Fit     Residual    St Resid
  7       15.0    0.00000     0.00056      0.02461     -0.00056       -1.09 X

X denotes an observation whose X value gives it large influence.
```

Site - S3

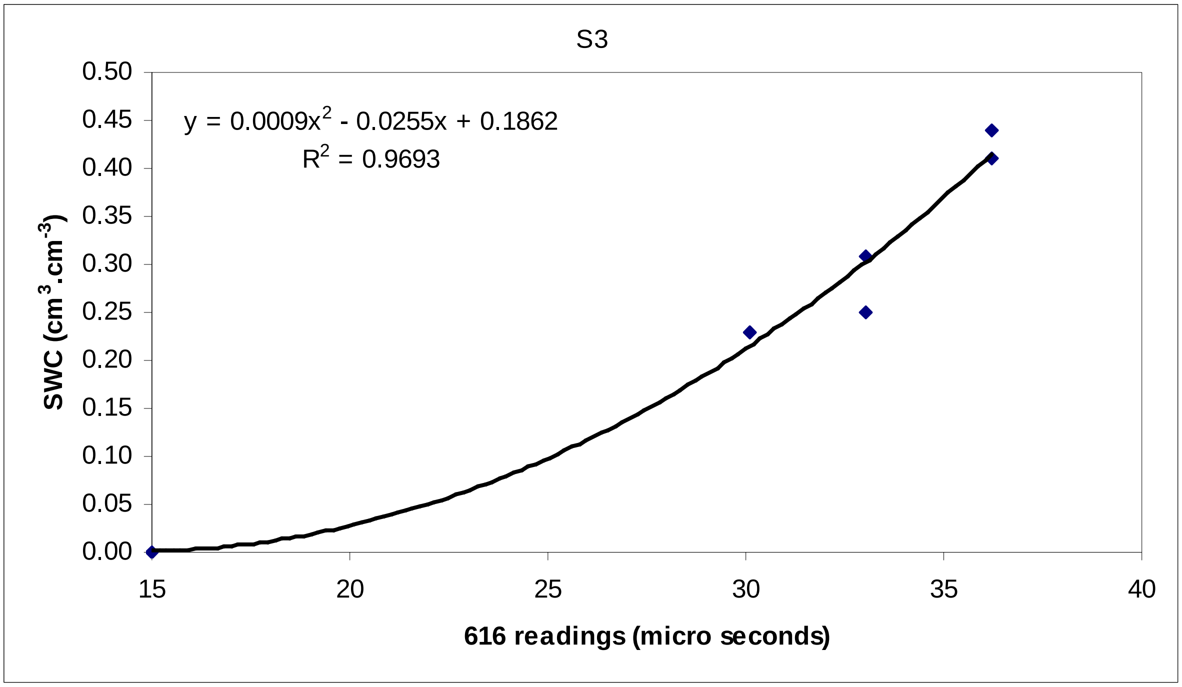


```
The regression equation is
S3-MC = 0.186 - 0.0255 S3-616 +0.000879 S3-616**

Predictor        Coef       StDev          T        P
Constant       0.1862      0.1789       1.04    0.357
S3-616       -0.02551     0.01532      -1.67    0.171
S3-616**    0.0008789   0.0003009       2.92    0.043

S = 0.03113     R-Sq = 96.9%     R-Sq(adj) = 95.4%

Analysis of Variance

Source            DF          SS          MS         F        P
Regression         2    0.122550    0.061275     63.22    0.001
Residual Error     4    0.003877    0.000969
Total              6    0.126427

Source       DF      Seq SS
S3-616        1    0.114282
S3-616**      1    0.008268

Unusual Observations
Obs     S3-616      S3-MC         Fit   StDev Fit    Residual    St Resid
  7       15.0     0.0000      0.0013      0.0311     -0.0013       -1.31 X

X denotes an observation whose X value gives it large influence.
```

Site - S4

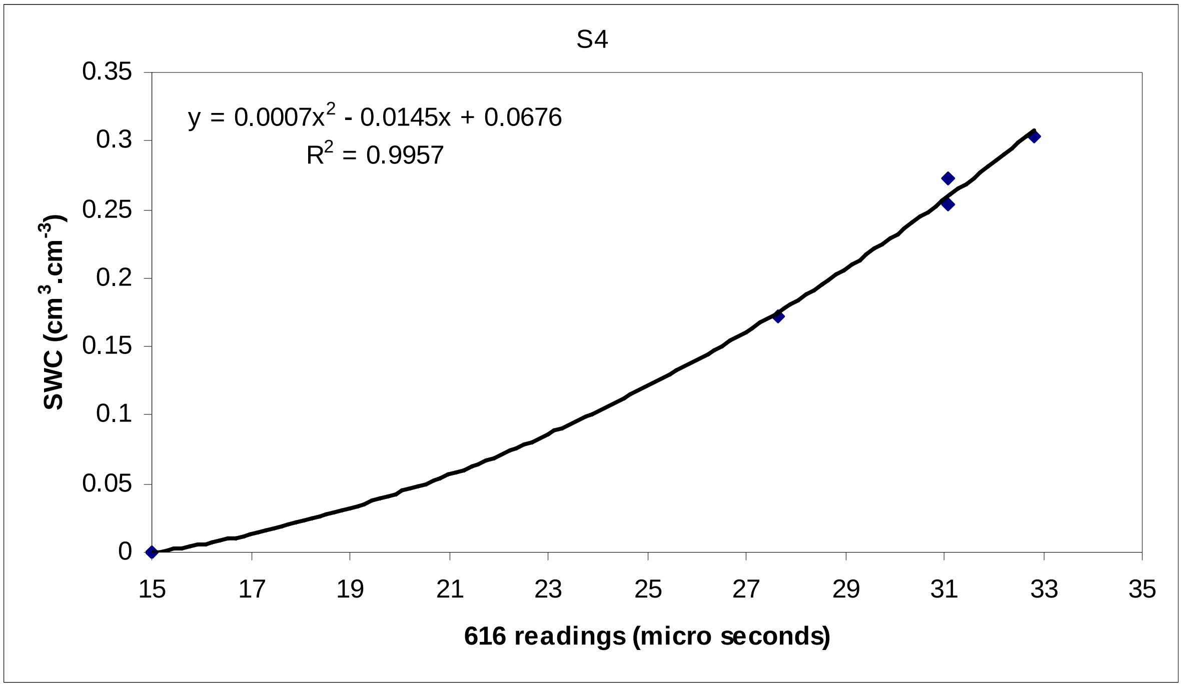


```
The regression equation is
S4-MC = 0.068 - 0.0145 S4-616 +0.000665 S4-616**

Predictor        Coef       StDev          T        P
Constant       0.0676      0.1096       0.62    0.600
S4-616       -0.01450     0.01030      -1.41    0.294
S4-616**    0.0006652   0.0002193       3.03    0.094

S = 0.01137     R-Sq = 99.6%     R-Sq(adj) = 99.1%

Analysis of Variance

Source            DF          SS          MS         F        P
Regression         2    0.059390    0.029695    229.87    0.004
Residual Error     2    0.000258    0.000129
Total              4    0.059649

Source       DF      Seq SS
S4-616        1    0.058201
S4-616**      1    0.001189

Unusual Observations
Obs     S4-616       S4-MC         Fit    StDev Fit     Residual    St Resid
  5       15.0    0.00000    -0.00024      0.01136      0.00024        0.80 X

X denotes an observation whose X value gives it large influence.
```

Site - S5

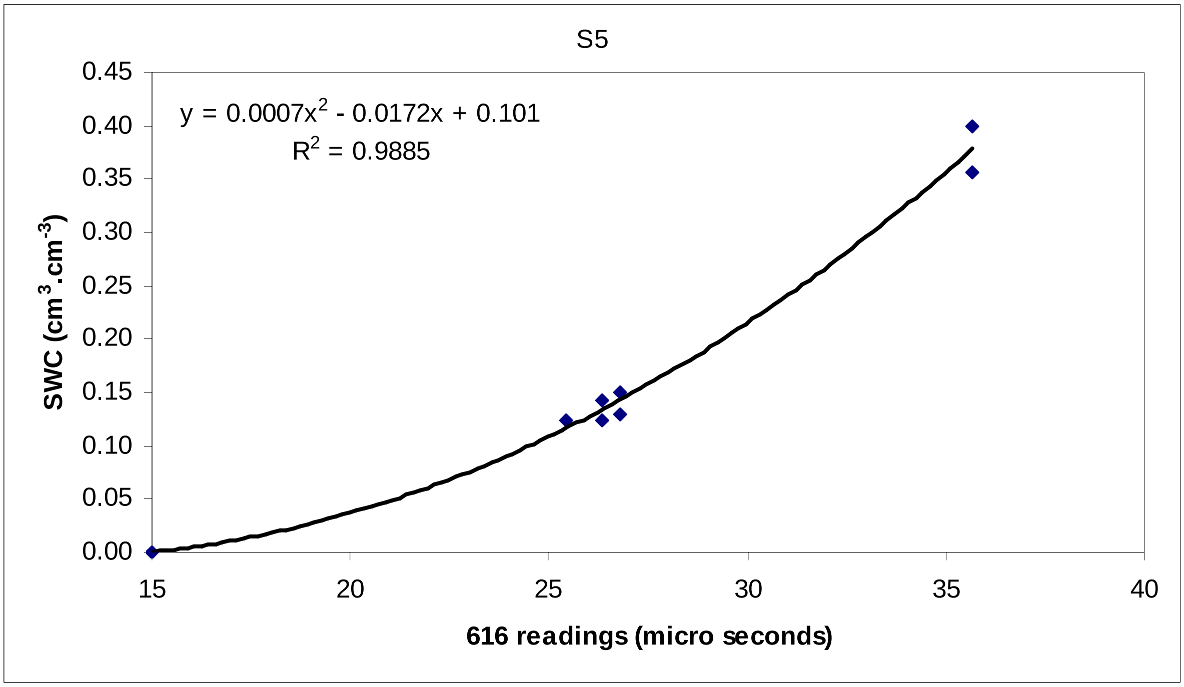


```
The regression equation is
S5-MC = 0.101 - 0.0172 S5-616 +0.000701 S5-616**

Predictor        Coef       StDev          T        P
Constant      0.10103     0.08127       1.24    0.269
S5-616      -0.017214    0.006283      -2.74    0.041
S5-616**    0.0007005   0.0001187       5.90    0.002

S = 0.01681     R-Sq = 98.9%     R-Sq(adj) = 98.4%

Analysis of Variance

Source            DF          SS          MS         F        P
Regression         2    0.121687    0.060843    215.31    0.000
Residual Error     5    0.001413    0.000283
Total              7    0.123100

Source       DF      Seq SS
S5-616        1    0.111845
S5-616**      1    0.009841

Unusual Observations
Obs     S5-616      S5-MC         Fit   StDev Fit    Residual    St Resid
  8       15.0    0.00000     0.00043     0.01679    -0.00043       -0.55 X

X denotes an observation whose X value gives it large influence.
```

Site - S6

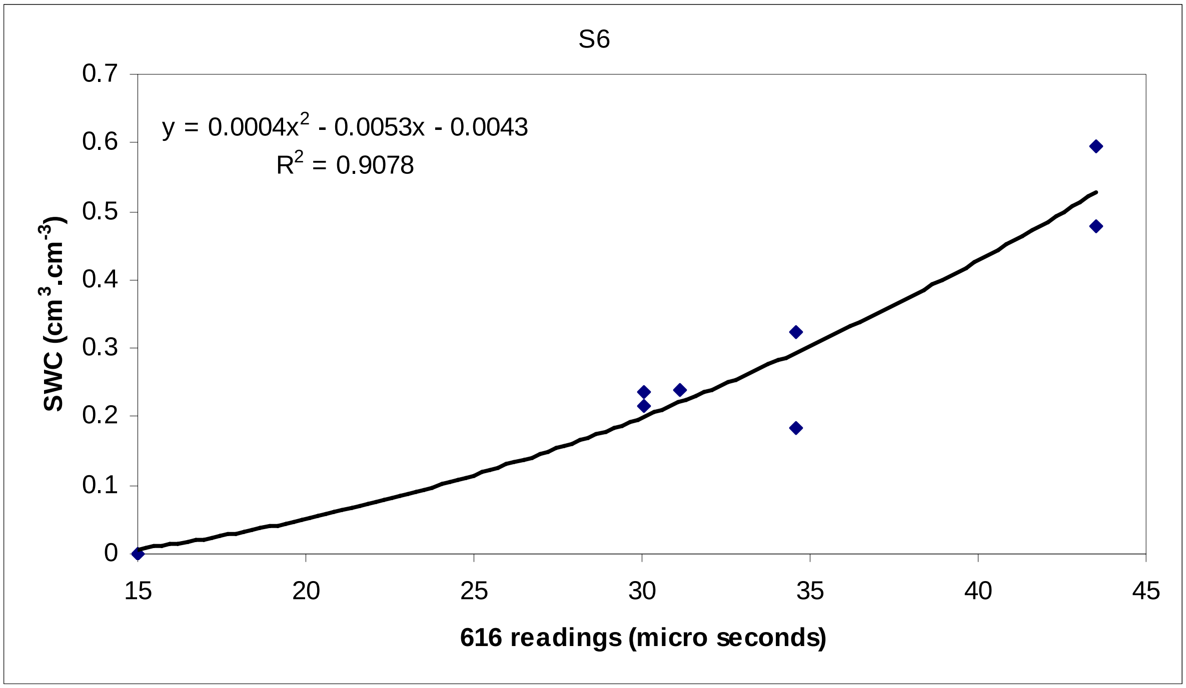


```
The regression equation is
S6-MC = - 0.004 - 0.0053 S6-616 +0.000402 S6-616**

Predictor        Coef        StDev          T        P
Constant      -0.0043       0.2270      -0.02    0.986
S6-616       -0.00528      0.01538      -0.34    0.745
S6-616**    0.0004022    0.0002523       1.59    0.172

S = 0.06590     R-Sq = 90.8%     R-Sq(adj) = 87.1%

Analysis of Variance

Source            DF          SS          MS         F        P
Regression         2     0.21373     0.10687     24.61    0.003
Residual Error     5     0.02171     0.00434
Total              7     0.23545

Source       DF      Seq SS
S6-616        1     0.20270
S6-616**      1     0.01104

Unusual Observations
Obs      S6-616      S6-MC          Fit    StDev Fit     Residual     St Resid
  8        15.0     0.0000       0.0069       0.0656      -0.0069      -1.06 X

X denotes an observation whose X value gives it large influence.
```

Site - S7

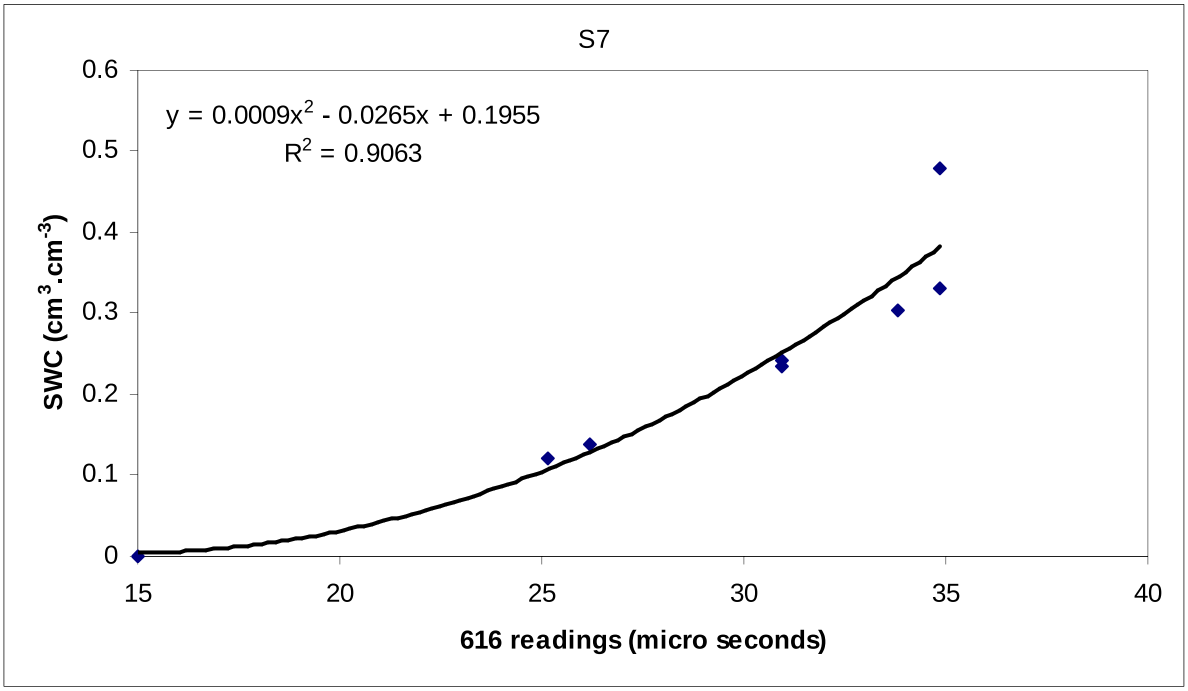


```
The regression equation is
S7-MC = 0.196 - 0.0265 S7-616 +0.000914 S7-616**

Predictor        Coef        StDev          T        P
Constant       0.1955       0.2952       0.66    0.537
S7-616       -0.02648      0.02431      -1.09    0.326
S7-616**    0.0009135    0.0004747       1.92    0.112

S = 0.05325     R-Sq = 90.6%     R-Sq(adj) = 86.9%

Analysis of Variance

Source             DF          SS          MS         F        P
Regression          2    0.137094    0.068547     24.18    0.003
Residual Error      5    0.014176    0.002835
Total               7    0.151269

Source       DF      Seq SS
S7-616        1    0.126595
S7-616**      1    0.010499

Unusual Observations
Obs     S7-616      S7-MC         Fit    StDev Fit     Residual     St Resid
  6       34.9     0.4790      0.3826       0.0312       0.0964        2.23R

R denotes an observation with a large standardized residual
```

ANNEX-IV

Frequency distribution of errors in the soil moisture predictions: SWC based models

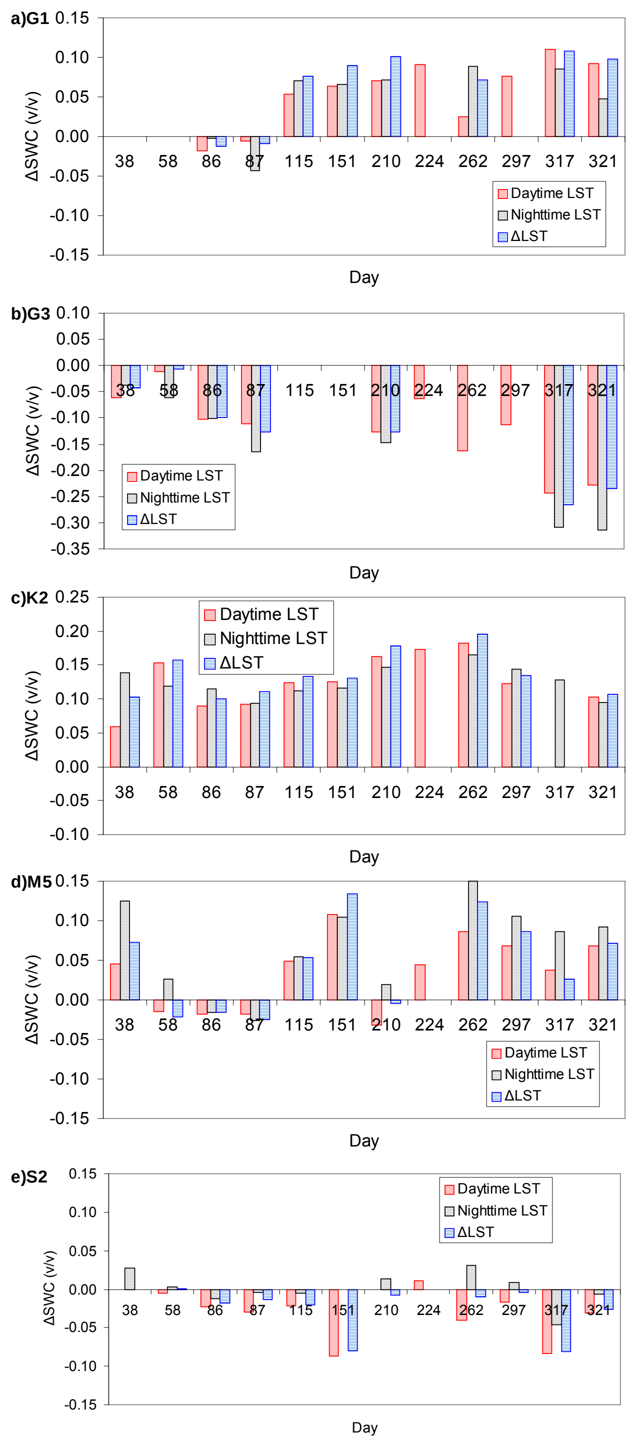

Frequency distribution of errors in the soil moisture predictions: SWC based models

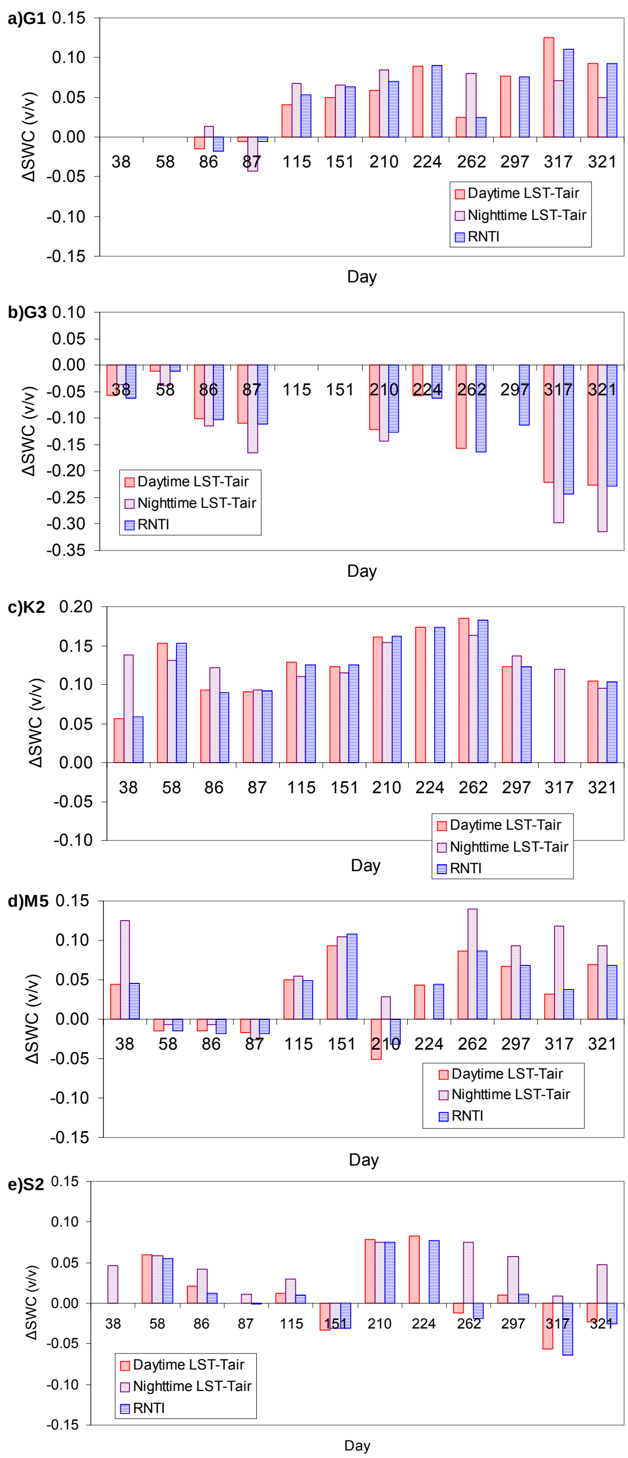

Frequency distribution of errors in the soil moisture predictions: NWDI based models

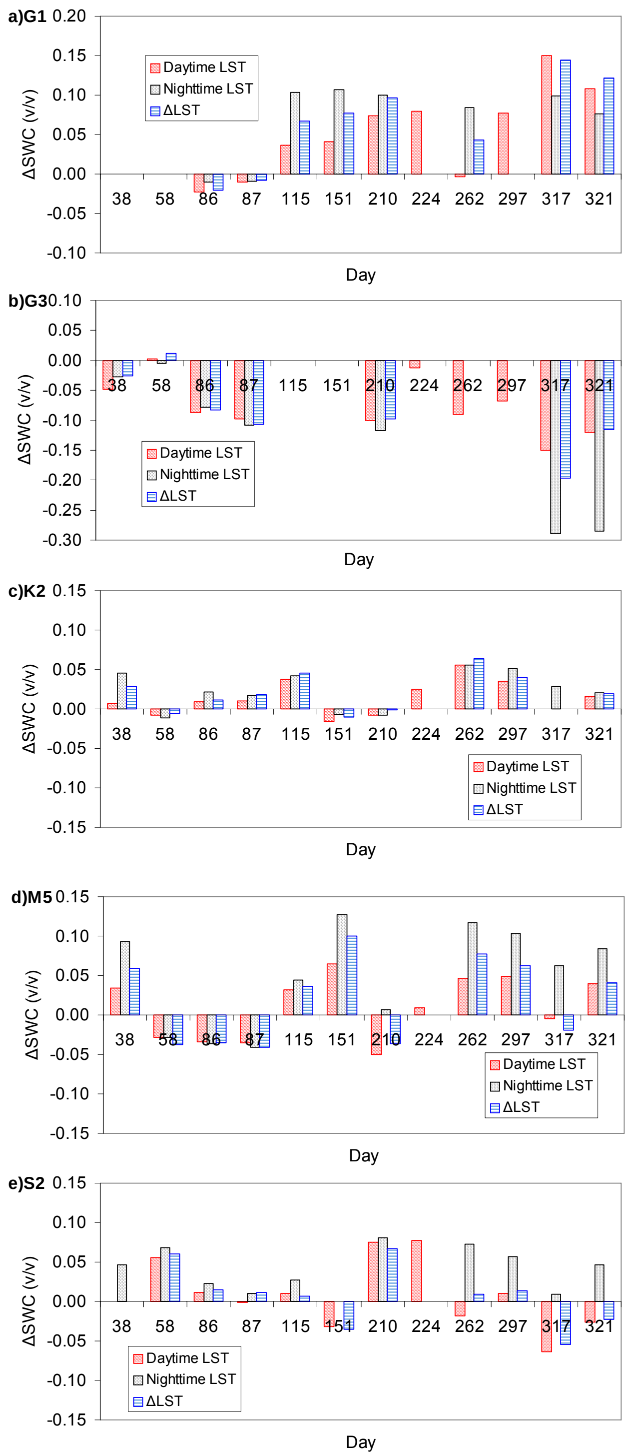

Frequency distribution of errors in the soil moisture predictions: NWDI based models

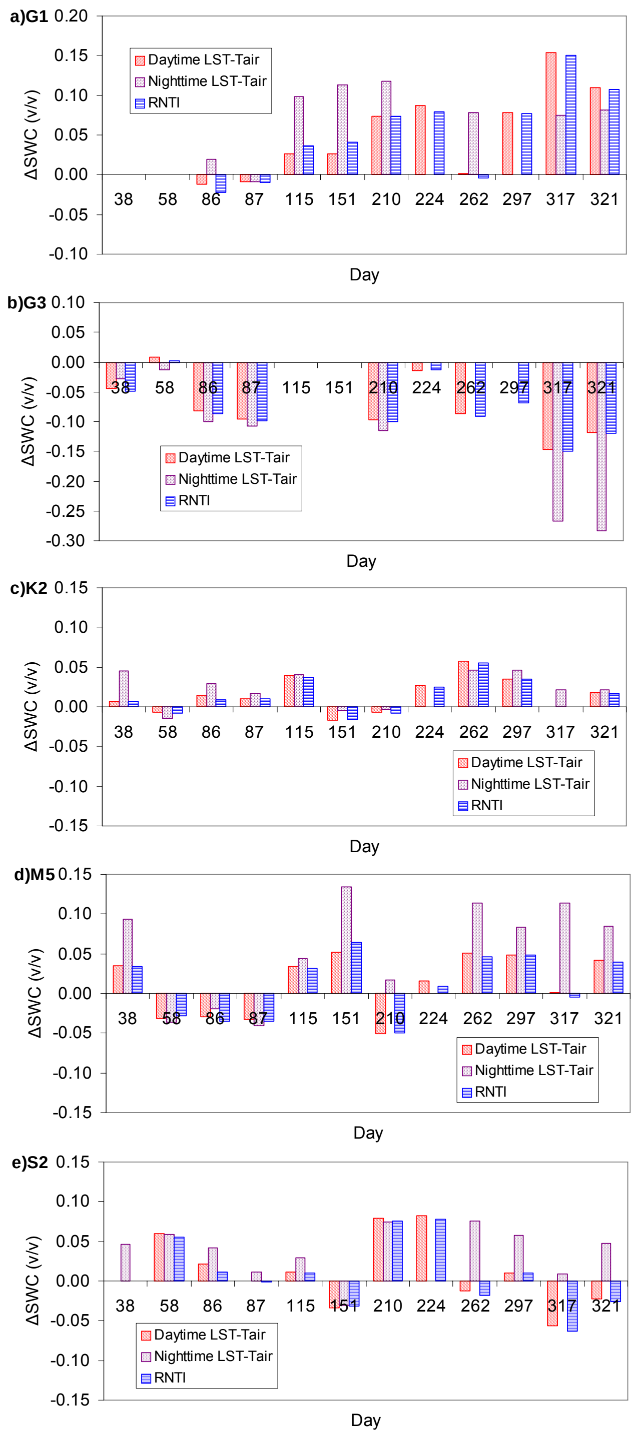

ANNEX-V

LST-VI scatter plots

LST and NDVI-2004

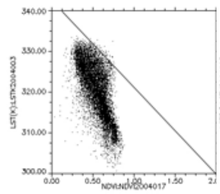
Day 003

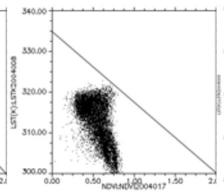
Day 008

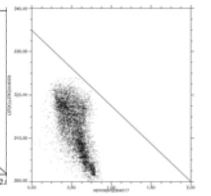
Day 009

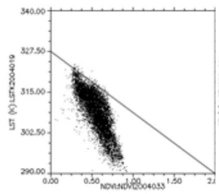
Day 019

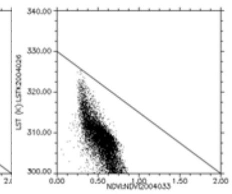
Day 026

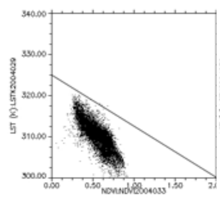
Day 029

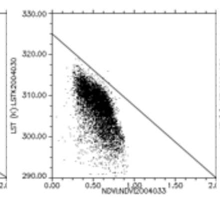
Day 030

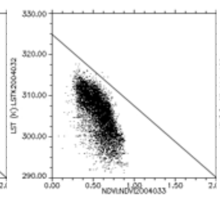
Day 032

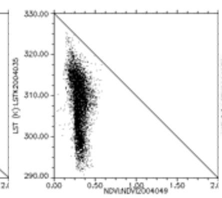
Day 035

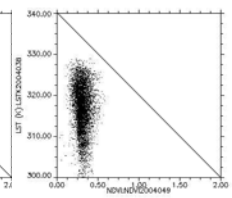
Day 038

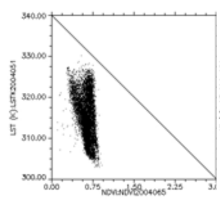
Day 051

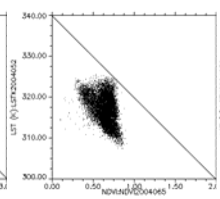
Day 051

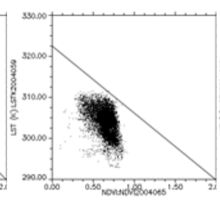
Day 059

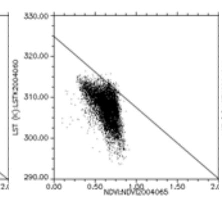
Day 060

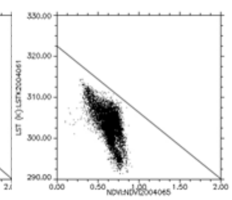
Day 061

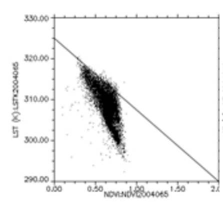
Day 061

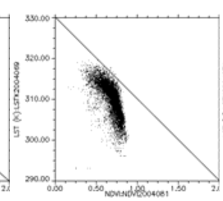
Day 069

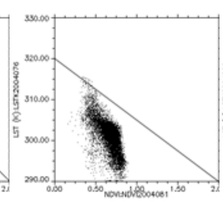
Day 076

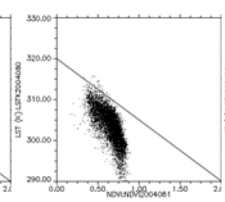
Day 080

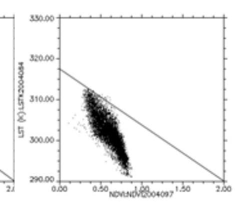
Day 084

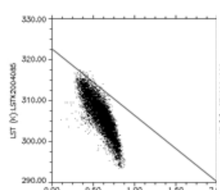
Day 085

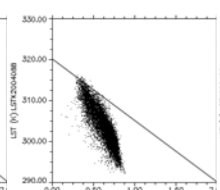
Day 088

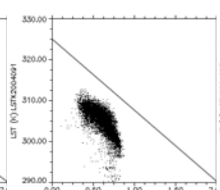
Day 091

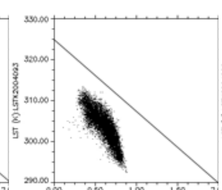
Day 093

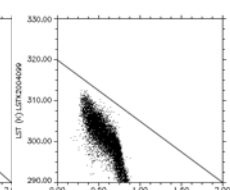
Day 099

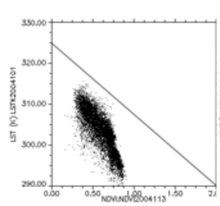
Day 101

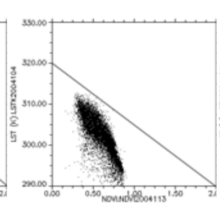
Day 104

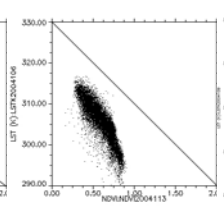
Day 106

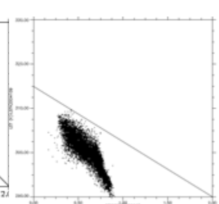
Day 003

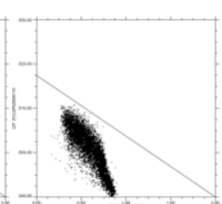
Day 110

LST and NDVI-2004

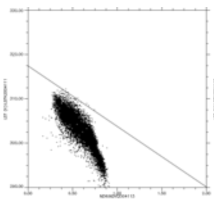

Day 111

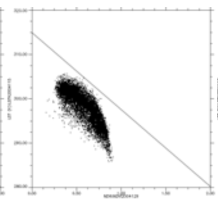

Day 115

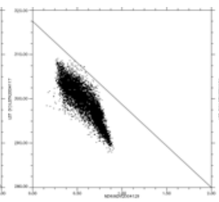

Day 117

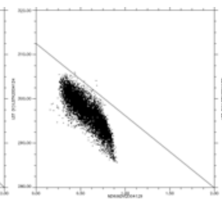

Day 124

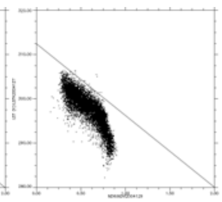

Day 127

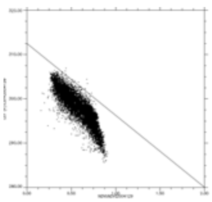

Day 129

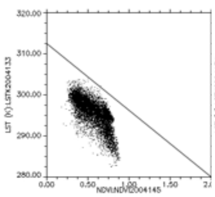

Day 133

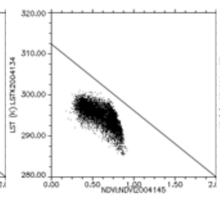

Day 134

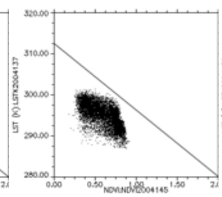

Day 137

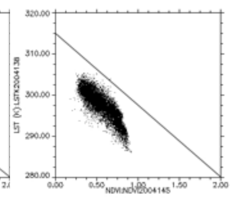

Day 138

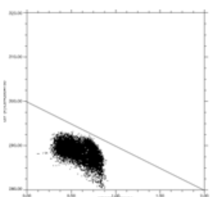

Day 150

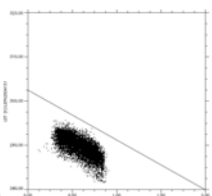

Day 151

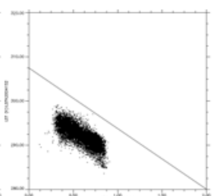

Day 052

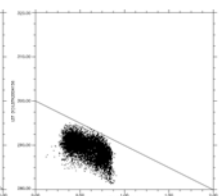

Day 056

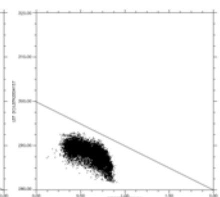

Day 057

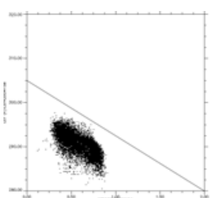

Day 158

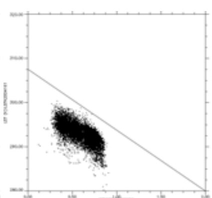

Day 161

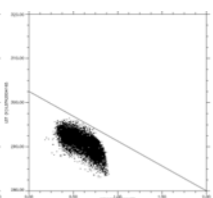

Day 165

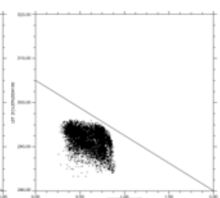

Day 166

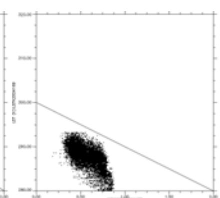

Day 169

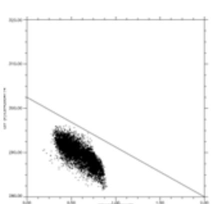

Day 174

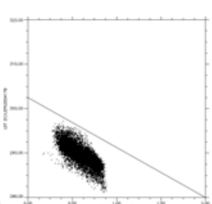

Day 179

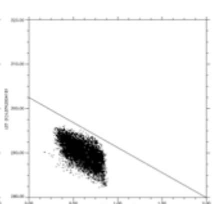

Day 181

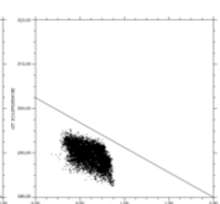

Day 182

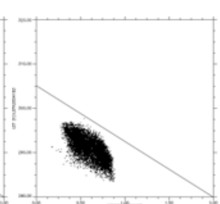

Day 183

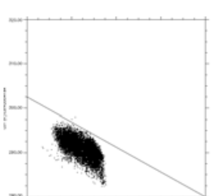

Day 184

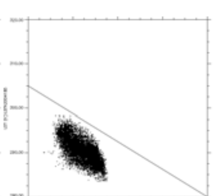

Day 185

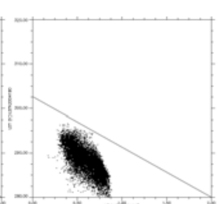

Day 190

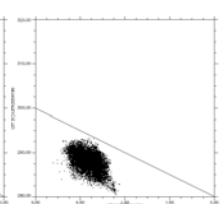

Day 196

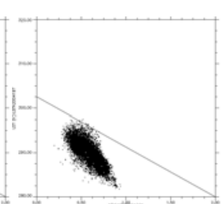

Day 197

LST and NDVI-2004

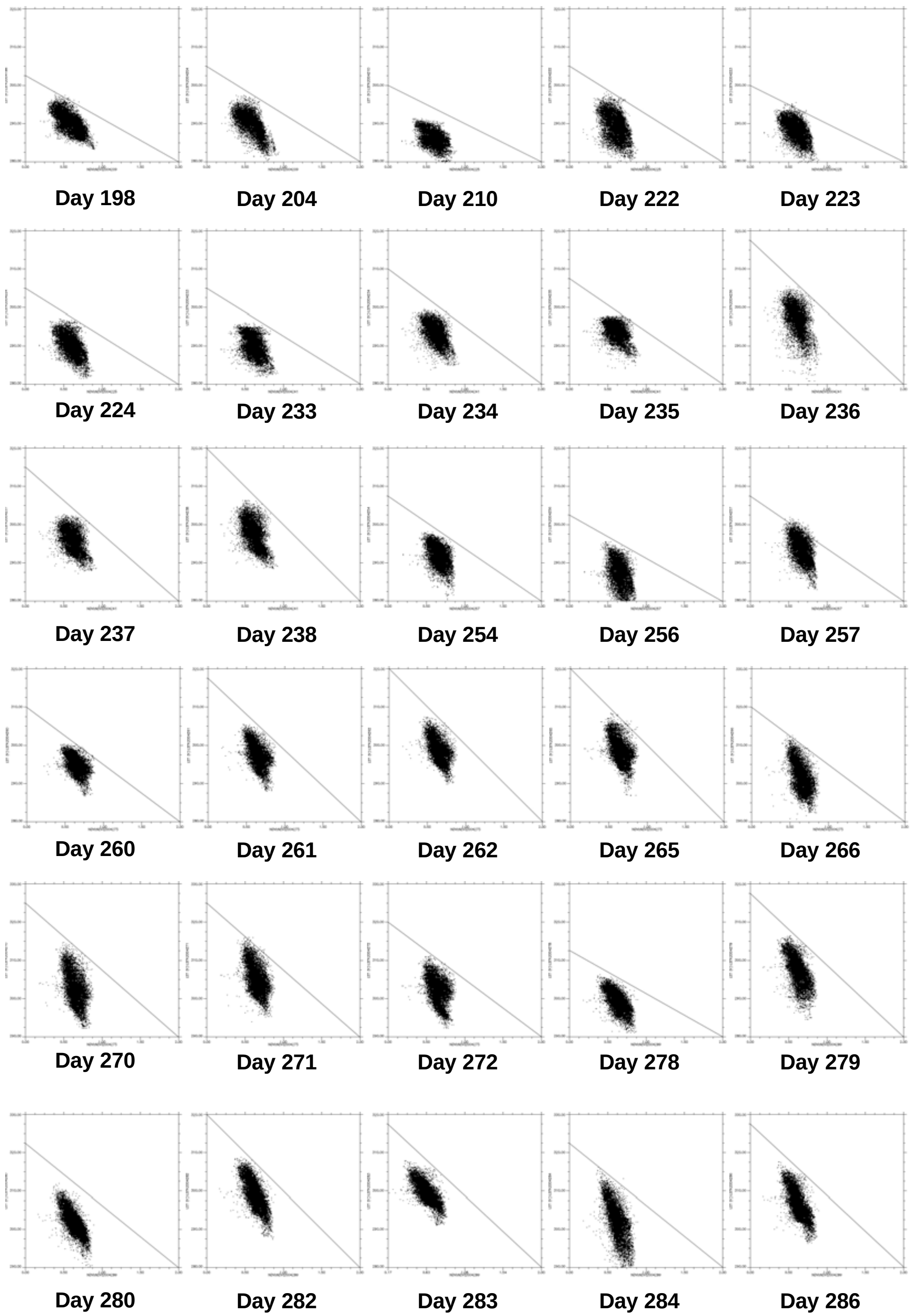

LST and NDVI-2004

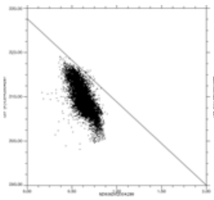
Day 287

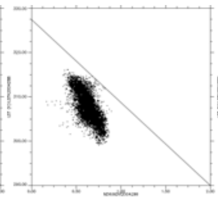
Day 288

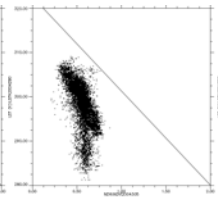
Day 290

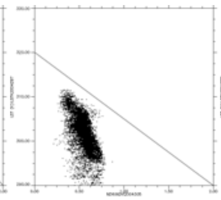
Day 297

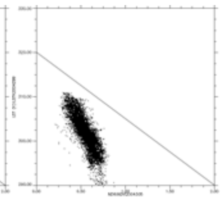
Day 299

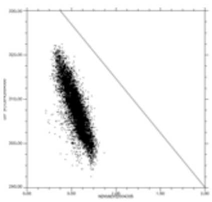
Day 300

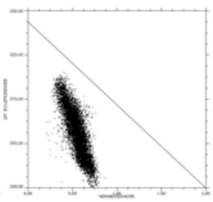
Day 302

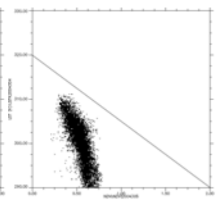
Day 304

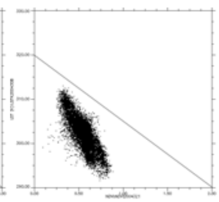
Day 308

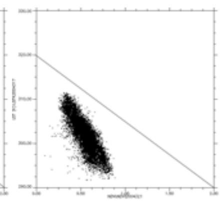
Day 317

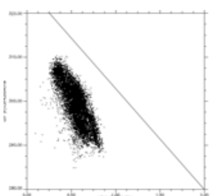
Day 318

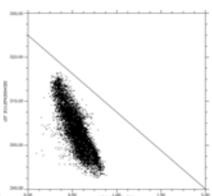
Day 320

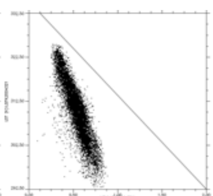
Day 321

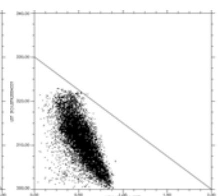
Day 331

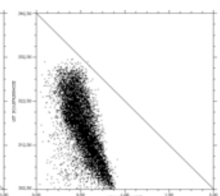
Day 332

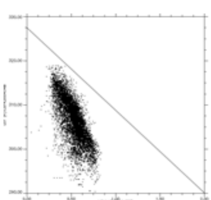
Day 348

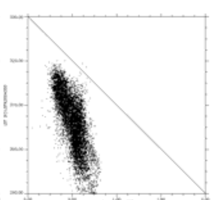
Day 350

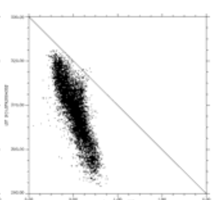
Day 352

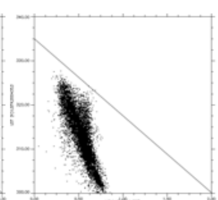
Day 353

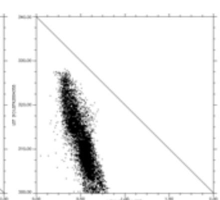
Day 355

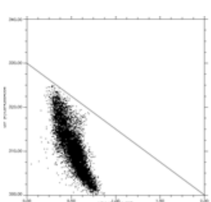
Day 356

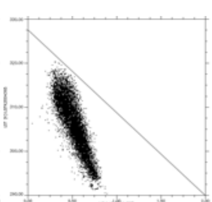
Day 365

LST and EVI-2004

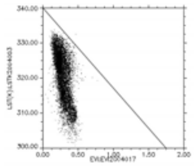
Day 003

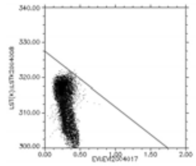
Day 008

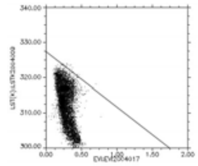
Day 009

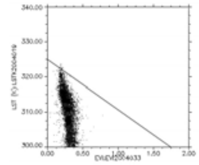
Day 019

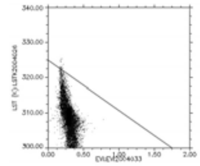
Day 026

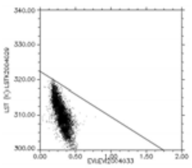
Day 029

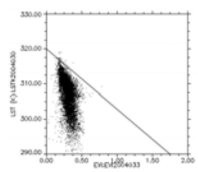
Day 030

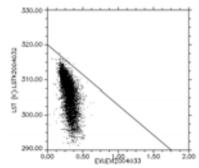
Day 032

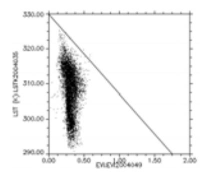
Day 035

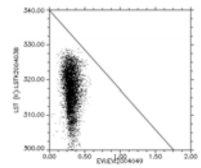
Day 038

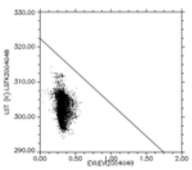
Day 048

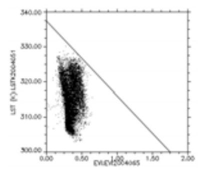
Day 051

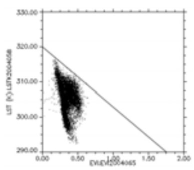
Day 058

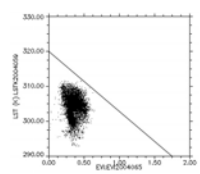
Day 059

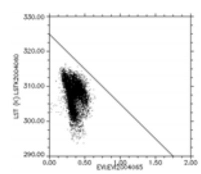
Day 060

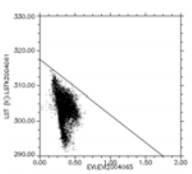
Day 061

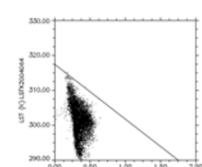
Day 064

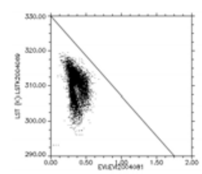
Day 069

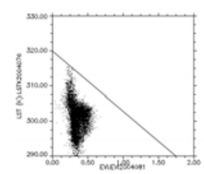
Day 076

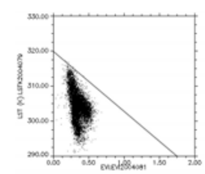
Day 079

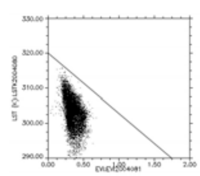
Day 080

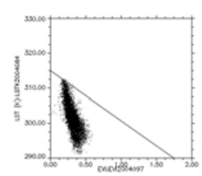
Day 084

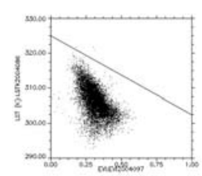
Day 086

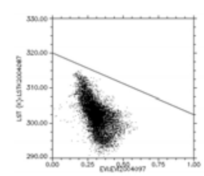
Day 087

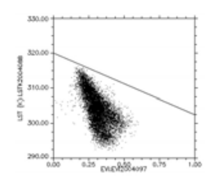
Day 088

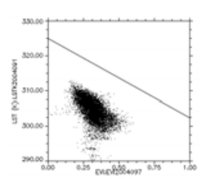
Day 091

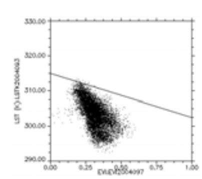
Day 093

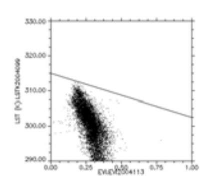
Day 099

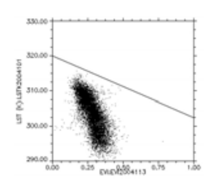
Day 101

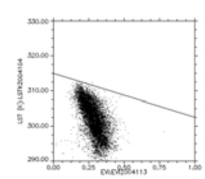
Day 104

LST and EVI-2004

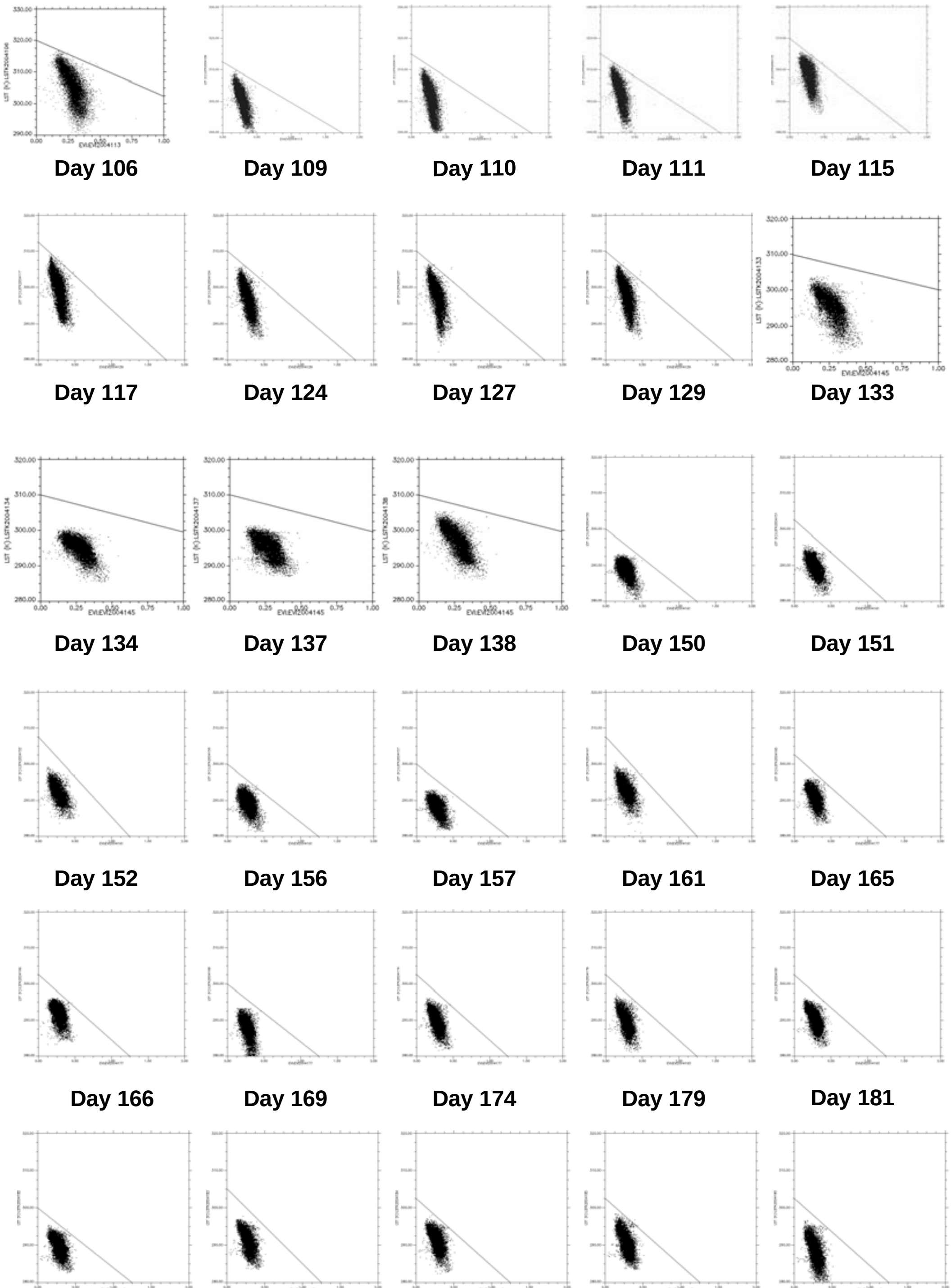

Day 106 **Day 109** **Day 110** **Day 111** **Day 115**

Day 117 **Day 124** **Day 127** **Day 129** **Day 133**

Day 134 **Day 137** **Day 138** **Day 150** **Day 151**

Day 152 **Day 156** **Day 157** **Day 161** **Day 165**

Day 166 **Day 169** **Day 174** **Day 179** **Day 181**

Day 182 **Day 183** **Day 184** **Day 185** **Day 190**

LST and EVI-2004

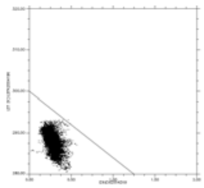
Day 196

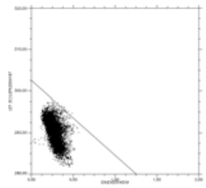
Day 197

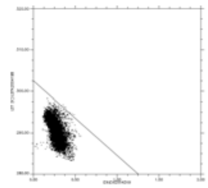
Day 198

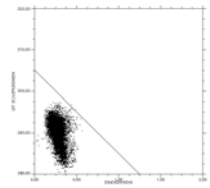
Day 204

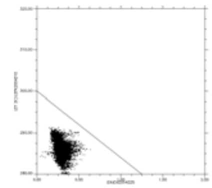
Day 210

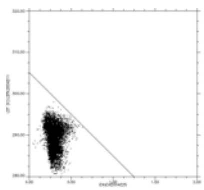
Day 211

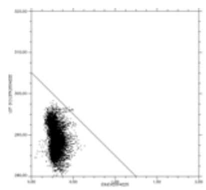
Day 222

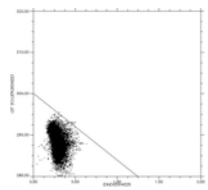
Day 223

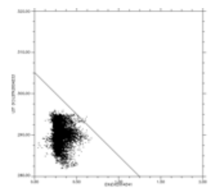
Day 233

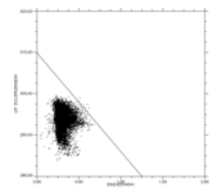
Day 234

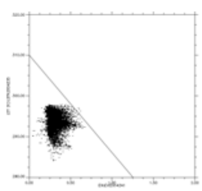
Day 235

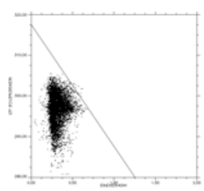
Day 236

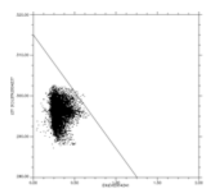
Day 237

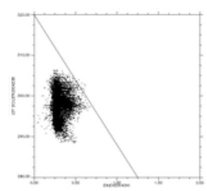
Day 238

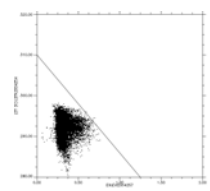
Day 254

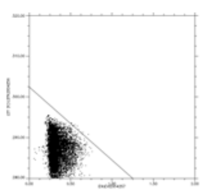
Day 256

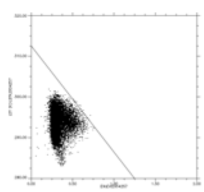
Day 257

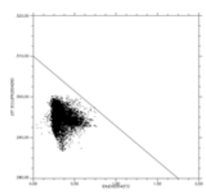
Day 260

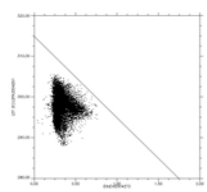
Day 261

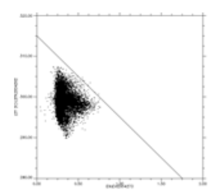
Day 262

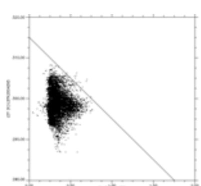
Day 265

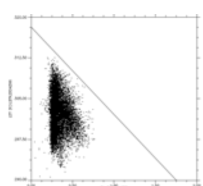
Day 266

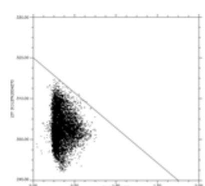
Day 270

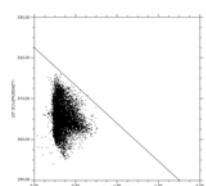
Day 271

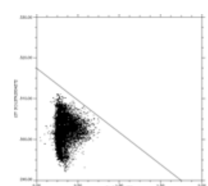
Day 272

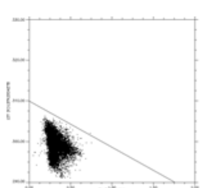
Day 278

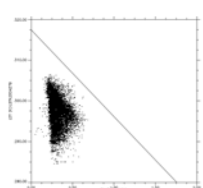
Day 279

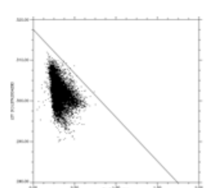
Day 280

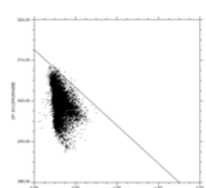
Day 282

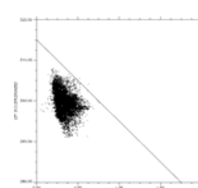
Day 283

LST and EVI-2004

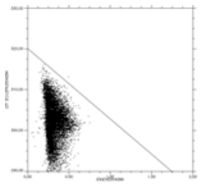
Day 284
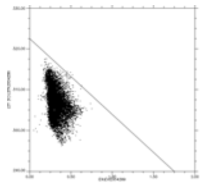
Day 286
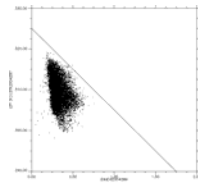
Day 287
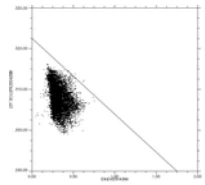
Day 288
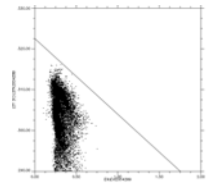
Day 289
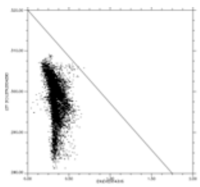
Day 290
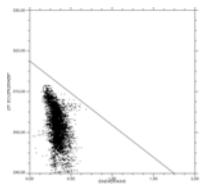
Day 297
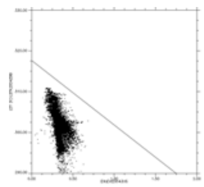
Day 299
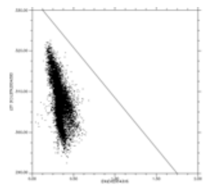
Day 300
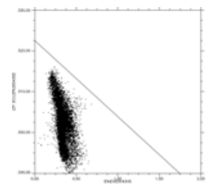
Day 302
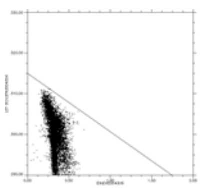
Day 304
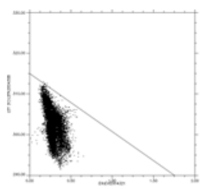
Day 308
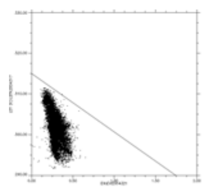
Day 317
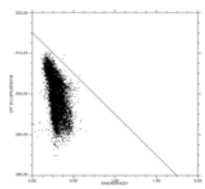
Day 318
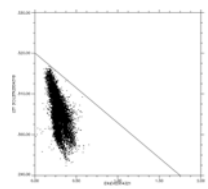
Day 319
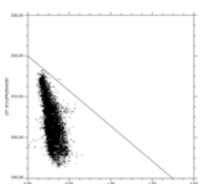
Day 320
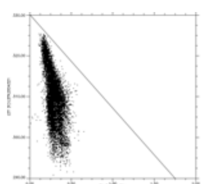
Day 321
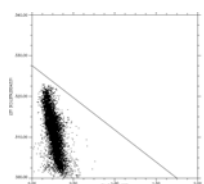
Day 333
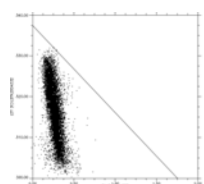
Day 332
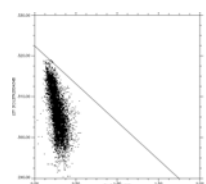
Day 348
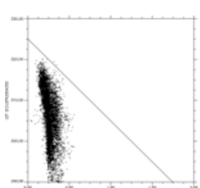
Day 350
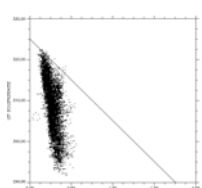
Day 352
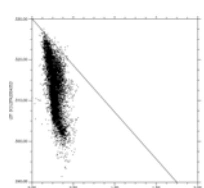
Day 353
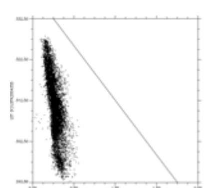
Day 355
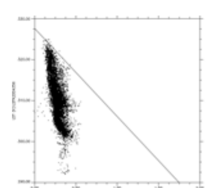
Day 356
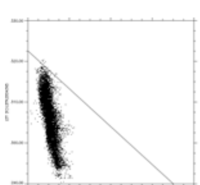
Day 365

ANNEX-VI

Regression equations used in LST based models

a) SWC models without test sites.

DOY	n	slope	Constant	R2	n	slope	Constant	R2
			Daytime LST				Daytime LST - Tair	
38	14	-0.010	0.614	0.374	14	-0.011	0.282	0.433
58	20	0.000	0.303	0.000	20	0.000	0.310	0.000
86	18	-0.008	0.496	0.082	18	-0.008	0.234	0.059
87	20	-0.010	0.487	0.106	20	-0.011	0.234	0.096
115	20	-0.015	0.600	0.085	20	-0.023	0.390	0.110
151	20	-0.012	0.503	0.026	20	-0.019	0.364	0.051
210	20	-0.024	0.683	0.124	20	-0.030	0.394	0.154
224	20	-0.012	0.535	0.051	20	-0.013	0.376	0.049
262	20	-0.023	0.912	0.166	20	-0.024	0.436	0.161
297	18	-0.009	0.491	0.176	18	-0.010	0.237	0.172
317	19	-0.014	0.667	0.178	20	-0.017	0.353	0.287
321	20	-0.005	0.419	0.087	20	-0.005	0.269	0.076
			Nighttime LST				Nighttime LST - Tair	
38	9	-0.005	0.272	0.020	9	-0.005	0.153	0.020
58	20	-0.084	1.339	0.349	20	-0.033	0.256	0.133
86	20	0.009	0.085	0.012	20	-0.015	0.143	0.044
87	18	-0.038	0.633	0.112	18	-0.038	0.074	0.112
115	20	-0.015	0.251	0.015	20	-0.017	0.091	0.019
151	20	-0.023	0.279	0.048	20	-0.022	0.160	0.033
210	20	-0.055	0.401	0.073	20	-0.046	0.193	0.061
224	0				0			
262	19	-0.033	0.402	0.134	19	-0.027	0.162	0.145
297	16	0.016	0.007	0.046	16	0.002	0.193	0.001
317	20	0.007	0.124	0.008	20	-0.013	0.160	0.017
321	20	-0.027	0.505	0.057	20	-0.026	0.121	0.050
			delta LST				RNTI	
38	9	-0.006	0.354	0.207	14	-0.313	0.384	0.374
58	20	0.006	0.186	0.024	20	0.006	0.308	0.000
86	18	-0.005	0.324	0.054	18	-0.245	0.330	0.082
87	18	0.007	0.027	0.034	20	-0.242	0.319	0.106
115	20	-0.010	0.400	0.045	20	-0.298	0.410	0.085
151	20	0.000	0.284	0.000	20	-0.169	0.402	0.026
210	20	-0.021	0.619	0.078	20	-0.333	0.572	0.124
224	0				20	-0.193	0.444	0.051
262	19	-0.005	0.391	0.016	20	-0.412	0.541	0.166
297	16	-0.007	0.340	0.106	18	-0.225	0.360	0.176
317	20	-0.011	0.442	0.175	19	-0.295	0.416	0.178
321	20	-0.005	0.333	0.067	20	-0.194	0.329	0.087

b) NWDI models without test sites.

DOY	n	slope	Constant	R2	n	slope	Constant	R2
		Daytime LST				Daytime LST - Tair		
38	14	0.020	-0.285	0.393	14	0.021	0.430	0.401
58	20	0.016	-0.180	0.045	20	0.011	0.257	0.016
86	18	0.021	-0.148	0.113	18	0.016	0.514	0.056
87	20	0.029	-0.282	0.214	20	0.031	0.473	0.173
115	20	0.048	-0.732	0.224	20	0.063	0.045	0.211
151	20	0.048	-0.462	0.136	20	0.064	0.145	0.184
210	20	0.045	-0.336	0.152	20	0.047	0.214	0.132
224	20	0.036	-0.325	0.131	20	0.032	0.193	0.083
262	20	0.070	-1.549	0.393	20	0.070	-0.050	0.338
297	18	0.027	-0.277	0.298	18	0.029	0.464	0.274
317	19	0.052	-1.155	0.488	20	0.052	0.119	0.394
321	20	0.022	-0.339	0.303	20	0.022	0.258	0.270
		Nighttime LST				Nighttime LST - Tair		
38	9	-0.002	0.680	0.001	9	-0.002	0.621	0.001
58	20	0.066	-0.446	0.071	20	0.061	0.463	0.153
86	20	-0.043	1.104	0.066	20	0.044	0.739	0.093
87	18	0.003	0.631	0.000	18	0.003	0.671	0.000
115	20	-0.023	0.746	0.009	20	-0.015	0.559	0.004
151	20	-0.030	0.413	0.026	20	-0.039	0.197	0.036
210	20	0.052	0.233	0.024	20	0.018	0.342	0.004
224	0				0			
262	19	0.028	0.351	0.026	19	0.053	0.663	0.156
297	16	-0.058	1.265	0.110	16	-0.011	0.567	0.004
317	20	-0.033	0.938	0.035	20	0.038	0.699	0.033
321	20	0.021	0.363	0.008	20	0.013	0.646	0.003
		delta LST				RNTI		
38	9	0.013	0.253	0.234	14	0.661	0.199	0.393
58	20	0.007	0.199	0.013	20	0.381	0.124	0.045
86	18	0.016	0.217	0.104	18	0.604	0.262	0.113
87	18	-0.002	0.701	0.001	20	0.712	0.215	0.214
115	20	0.040	-0.315	0.203	20	0.958	-0.119	0.224
151	20	0.025	-0.042	0.093	20	0.673	-0.060	0.136
210	20	0.045	-0.299	0.132	20	0.620	-0.130	0.152
224	0				20	0.580	-0.051	0.131
262	19	0.030	-0.272	0.140	20	1.272	-0.405	0.393
297	16	0.028	-0.002	0.306	18	0.655	0.102	0.298
317	20	0.041	-0.303	0.456	19	1.088	-0.233	0.488
321	20	0.022	-0.070	0.294	20	0.773	0.022	0.303

c) SWC models with all sites.

DOY	n	slope	Constant	R2	n	slope	Constant	R2
			Daytime LST				Daytime LST - Tair	
38	16	-0.011	0.688	0.442	16	-0.012	0.300	0.494
58	22	-0.003	0.411	0.005	22	-0.004	0.352	0.007
86	23	-0.009	0.526	0.101	23	-0.009	0.243	0.081
87	24	-0.010	0.498	0.106	24	-0.012	0.239	0.099
115	21	-0.017	0.643	0.101	21	-0.024	0.392	0.120
151	21	-0.019	0.617	0.063	21	-0.026	0.386	0.096
210	25	-0.027	0.715	0.158	25	-0.032	0.394	0.187
224	25	-0.018	0.647	0.122	25	-0.020	0.402	0.124
262	25	-0.030	1.121	0.266	25	-0.032	0.490	0.267
297	23	-0.011	0.556	0.234	23	-0.013	0.242	0.237
317	22	-0.019	0.818	0.242	22	-0.019	0.373	0.224
321	24	-0.010	0.608	0.248	24	-0.010	0.344	0.245
			Nighttime LST				Nighttime LST - Tair	
38	13	-0.005	0.259	0.016	13	-0.005	0.131	0.016
58	23	-0.084	1.333	0.335	23	-0.031	0.255	0.126
86	24	0.011	0.061	0.017	24	-0.010	0.154	0.046
87	22	-0.023	0.456	0.044	22	-0.023	0.114	0.044
115	21	-0.031	0.316	0.064	20	-0.002	0.147	0.001
151	21	-0.036	0.269	0.111	20	-0.028	0.114	0.140
210	25	-0.070	0.411	0.121	24	-0.071	0.091	0.132
224	0	-	-	-	0	-	-	-
262	23	-0.035	0.391	0.129	23	-0.029	0.137	0.151
297	19	0.011	0.047	0.021	19	-0.007	0.146	0.009
317	25	0.004	0.164	0.001	25	-0.015	0.146	0.037
321	25	-0.029	0.534	0.044	25	-0.025	0.124	0.029
			delta LST				RNTI	
38	13	-0.009	0.418	0.309	16	-0.366	0.421	0.442
58	23	0.002	0.268	0.003	22	-0.068	0.356	0.005
86	23	-0.006	0.345	0.073	23	-0.267	0.345	0.101
87	22	0.004	0.081	0.012	24	-0.248	0.325	0.106
115	21	-0.009	0.375	0.035	21	-0.334	0.429	0.101
151	21	-0.001	0.281	0.000	21	-0.263	0.460	0.063
210	25	-0.024	0.651	0.099	25	-0.368	0.593	0.158
224	0	-	-	-	25	-0.296	0.507	0.122
262	23	-0.007	0.421	0.027	25	-0.547	0.629	0.266
297	19	-0.008	0.344	0.116	23	-0.279	0.395	0.234
317	22	-0.014	0.506	0.200	22	-0.385	0.491	0.242
321	24	-0.009	0.470	0.220	24	-0.348	0.446	0.248

d) NWDI models with all sites.

DOY	n	slope	Constant	R2	n	slope	Constant	R2
			Daytime LST				Daytime LST - Tair	
38	13	0.020	-0.285	0.393	13	0.021	0.430	0.401
58	22	0.021	-0.398	0.119	22	0.019	0.153	0.076
86	23	0.020	-0.141	0.121	23	0.017	0.504	0.069
87	24	0.028	-0.276	0.209	24	0.031	0.466	0.172
115	20	0.056	-0.929	0.425	20	0.072	-0.002	0.397
151	22	0.064	-0.773	0.215	22	0.081	0.054	0.276
210	24	0.046	-0.344	0.172	24	0.048	0.211	0.155
224	25	0.042	-0.429	0.199	25	0.040	0.168	0.150
262	25	0.078	-1.762	0.484	25	0.078	-0.108	0.442
297	23	0.030	-0.369	0.354	23	0.033	0.462	0.337
317	21	0.059	-1.379	0.565	21	0.054	0.082	0.547
321	25	0.026	-0.510	0.437	25	0.026	0.193	0.414
			Nighttime LST				Nighttime LST - Tair	
38	9	-0.002	0.680	0.001	9	-0.002	0.621	0.001
58	23	0.066	-0.441	0.073	23	0.057	0.454	0.147
86	24	-0.044	1.116	0.071	24	0.034	0.717	0.132
87	22	-0.014	0.835	0.005	22	-0.014	0.622	0.005
115	22	0.009	0.614	0.001	22	0.009	0.697	0.001
151	22	-0.045	0.422	0.081	22	-0.050	0.144	0.092
210	24	0.065	0.225	0.040	24	0.035	0.407	0.013
224	0	-	-	-	0	-	-	-
262	23	0.028	0.385	0.024	25	0.002	0.477	0.000
297	19	-0.049	1.191	0.077	19	-0.001	0.631	0.000
317	24	-0.025	0.841	0.016	24	0.046	0.739	0.094
321	25	0.026	0.294	0.009	25	0.020	0.660	0.005
			delta LST				RNTI	
38	9	0.013	0.253	0.234	13	0.661	0.199	0.393
58	23	0.016	-0.018	0.085	23	0.521	0.018	0.119
86	23	0.016	0.211	0.113	23	0.590	0.260	0.121
87	22	0.002	0.623	0.000	24	0.700	0.212	0.209
115	20	0.043	-0.342	0.307	20	1.122	-0.211	0.425
151	22	0.038	-0.291	0.197	22	0.899	-0.235	0.215
210	24	0.048	-0.328	0.151	24	0.625	-0.136	0.172
224	0	-	-	-	25	0.682	-0.108	0.199
262	23	0.033	-0.321	0.166	25	1.409	-0.494	0.484
297	19	0.029	-0.010	0.321	23	0.735	0.056	0.354
317	21	0.045	-0.422	0.493	21	1.217	-0.348	0.565
321	25	0.025	-0.176	0.419	25	0.916	-0.083	0.437